

This document was produced
by scanning the original publication.

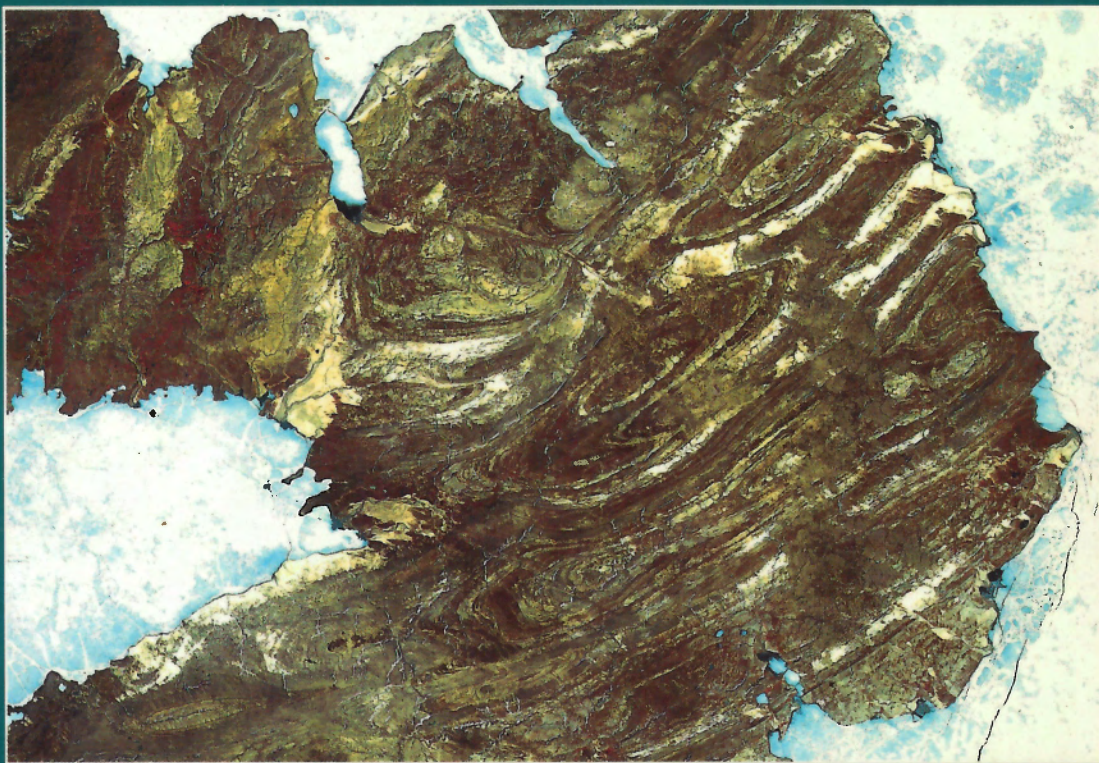
Ce document est le produit d'une
numérisation par balayage
de la publication originale.



GEOLOGICAL SURVEY OF CANADA
BULLETIN 472

**MELVILLE ISLAND'S SALT-BASED FOLD BELT,
ARCTIC CANADA**

J.C. Harrison



1995



Natural Resources Canada
Ressources naturelles Canada

Canada

GEOLOGICAL SURVEY OF CANADA
BULLETIN 472

**MELVILLE ISLAND'S SALT-BASED FOLD BELT,
ARCTIC CANADA**

J.C. Harrison

Contributions to subsurface mapping by T.A. Brent, and biostratigraphic
determinations by C.M. Henderson, A.C. Higgins, A.F. Lenz,
J.A. Jeletzky, D.C. McGregor, B.L. Mamet, A.D. McCracken,
D.J. McIntyre, B.S. Norford, A.W. Norris, G.S. Nowlan,
S. Pinard, T.P. Poulton, S. Turner, J. Utting,
T.T. Uyeno and J.H. Wall

1995

Available in Canada from

Geological Survey of Canada offices:

601 Booth Street
Ottawa, Canada K1A 0E8

3303-33rd Street N.W.,
Calgary, Alberta T2L 2A7

or from

Canada Communication Group - Publishing
Ottawa, Canada K1A 0S9

and through authorized bookstore agents
and other bookstores

A deposit copy of this publication is also available for reference
in public libraries across Canada

Cat. No. M42-472E
ISBN 0-660-15537-0

Price subject to change without notice

Cover Illustration

Surface expression of the salt-based fold belt on eastern and central Melville Island; part of LANDSAT-2 MSS image, track 60, frame 6/7 acquired July 19, 1981. Distributed with the authorization of the Canada Centre for Remote Sensing.

Critical readers

Rice University
P.O. Box 1892
Houston, Texas 77251
U.S.A.
A.W. Bally
H.G. Avé Lallemant
M. Talwani

Geological Survey of Canada
Institute of Sedimentary and Petroleum Geology
3303-33rd Street N.W.
Calgary, Alberta T2L 2A7
B. Beauchamp *L.S. Lane*
D.G. Cook *B.L. McLean*
T. de Freitas *R. Thorsteinsson*
A.F. Embry *H.P. Trettin*
J.G. Fyles

Author's address

J.C. Harrison
Geological Survey of Canada
Institute of Sedimentary and Petroleum Geology
3303-33rd Street N.W.
Calgary, Alberta T2L 2A7

PREFACE

Winter Harbour on Melville Island's south coast is an isolated and uninhabited spot that has great historical significance for Canada: it was the wintering site for voyages of discovery in the 19th century; the whole of the Arctic Islands were claimed for Canada on this spot in 1909; and the first exploratory well in the Arctic Islands was drilled here in 1961 by Dome Petroleum. The well was dry. However, this new frontier experience heralded 25 years of active oil and gas exploration in the western Arctic Islands that eventually led to the discovery of productive oil on nearby Cameron Island, large undeveloped gas fields on Melville Island's Sabine Peninsula, and the delineation of oil sand deposits in Triassic rocks of Sproule Peninsula.

Melville Island is notable for its sea cliffs and deep fiords; flat-topped uplands that represent an ancient erosion surface, now tilted to the east; small remnant ice caps; two photogenic evaporite diapirs on Sabine Peninsula; and a spectacular fold belt across the eastern part of the island that is readily visible on satellite images and from high flying aircraft.

This report deals with the structural geology and tectonic history of Melville Island's fold belt: the western part of the lower Paleozoic Franklinian Mobile Belt that is situated between flat-lying Cambrian to Devonian rocks of the Arctic Platform exposed to the south and post-orogenic Carboniferous to Tertiary strata of the Sverdrup Basin to the north.

Presented in this memoir is a 1:250 000 scale geological map covering the entire island (about 42 000 km²), seismic reflection profiles, structural cross-sections, and surface and subsurface studies including reports on biostratigraphy and newly discovered occurrences of base metal sulphides and coal. These data constitute an essential scientific base for the general understanding of salt-based fold belts, and for the evaluation and environmental management, by both government agencies and industry, of the contained economic mineral and fossil fuel resources.

Elkanah A. Babcock
Assistant Deputy Minister
Geological Survey of Canada

PRÉFACE

Le havre Winter est un lieu isolé et inhabité de la côte sud de l'île Melville, qui est d'une grande importance historique pour le Canada : ce fut là qu'hivernaient les explorateurs du XIX^e siècle; en 1909, tout l'archipel Arctique a été revendiqué pour le Canada à partir de ce lieu précis et c'est à cet endroit qu'en 1961 la Dome Petroleum forait le premier puits d'exploration dans l'archipel Arctique. Le puits était sec; cependant, cette nouvelle expérience en région pionnière marqua le début de 25 années d'exploration pétrolière et gazière active dans les îles arctiques occidentales. Ces travaux aboutirent à la découverte de gisements de pétrole dans l'île Cameron voisine et de vastes champs gazéifères dans la presqu'île Sabine de l'île Melville ainsi qu'à la délimitation de gisements de sable pétrolifère dans des roches triasiques de la presqu'île Sproule.

L'île Melville se distingue par ses falaises maritimes et ses fjords profonds; par ses hautes terres à sommet plat qui représentent une ancienne surface d'érosion, maintenant inclinée vers l'est; par de petites calottes glaciaires résiduelles; par deux diapirs évaporitiques remarquables dans la presqu'île Sabine; et par une ceinture orogénique spectaculaire traversant la partie est de l'île, visible sur les images-satellite et à partir d'aéronefs volant à haute altitude.

Le présent rapport porte sur la géologie structurale et l'histoire tectonique de la ceinture orogénique de l'île Melville : la partie occidentale de la ceinture mobile franklinienne du Paléozoïque inférieur qui se situe entre les roches horizontales du Cambrien-Dévonien de la Plate-forme de l'Arctique qui affleurent au sud et les couches post-orogéniques du Carbonifère-Tertiaire du bassin de Sverdrup au nord.

Le présent rapport contient une carte géologique à l'échelle de 1/250 000 couvrant toute l'île (environ 42 000 km²), des profils de sismique-réflexion, des coupes structurales ainsi que des études de la surface et de la subsurface, y compris des comptes rendus sur le biostratigraphie et les venues de sulfures de métal commun et de charbon découvertes récemment. Ces données constituent la base scientifique essentielle pour la compréhension générale des ceintures orogéniques à base de sel et pour l'évaluation et la gestion environnementale, par des organismes gouvernementaux et l'industrie, des ressources en minéraux et en combustibles fossiles de valeur économique qui y sont contenues.

Elkanah A. Babcock
Sous-ministre adjoint
Commission géologique du Canada

CONTENTS

1	Abstract
1	Résumé
2	Summary
3	Sommaire
 CHAPTER 1	
5	Introduction
5	Location and accessibility
6	Scope of study
6	History of geographic exploration
7	Previous work
9	Methods of data acquisition
9	General comments
9	Reflection seismic profiles
12	Physical features of Melville Island
12	Physiography
13	Glacial features
15	Potential field
15	Regional Bouguer gravity anomaly
18	Magnetic field
19	Stratigraphic successions (Precambrian(?) through Cenozoic)
21	Thermal maturity and metamorphic grade
 CHAPTER 2	
21	Precambrian(?) seismic stratigraphy and structure
21	General comments
22	Description of seismic units
22	Sub-Proterozoic(?) acoustic basement (Unit sAP)
24	Lower unreflective succession (Unit sP1)
24	Strongly reflective succession (Unit sP2)
24	Upper unreflective succession (Units sP3 and sP ϵ)
25	Precambrian(?) crustal structure and sedimentation
25	Structure on sub-Proterozoic(?) acoustic basement
25	Origin of the lower unreflective succession
25	Deformation of the highly reflective succession
26	Interpretation of the highly reflective succession
26	Structure of the upper unreflective succession
27	Interpretation of the upper unreflective succession
28	Summary of favoured geological models
29	Correlation and age of Precambrian(?) seismic units
29	Assumptions
29	Evidence
31	Regional implications
 CHAPTER 3	
32	Franklinian succession (Cambrian(?) through Devonian)
32	General comments
32	Franklinian paleogeography
32	Southern shelf
37	Deep water basin
37	Intrashelf basin and shelf rim
37	Intrashelf embayment
39	Offshore carbonate platforms
39	Middle and Upper Devonian clastic wedge

39	Description of seismic units
39	Seismic unit sC1A
41	Seismic unit sC1B
41	Seismic unit sC1C
43	Seismic unit sC2
43	Seismic unit sC3
45	Seismic unit sC4
45	Seismic unit sCO
47	Seismic unit sO
48	Age and correlation of Cambrian(?) and Lower Ordovician seismic units of the southern shelf
48	Assumptions
50	Evidence and regional implications
51	Description of formations (and other units)
51	Eleanor River Formation (OER)
52	Bay Fiord Formation (OBF)
57	Thumb Mountain Formation (OTM)
58	Irene Bay Formation (OIB)
59	Seismic unit OSC
60	Allen Bay Formation (OSA)
62	Cape Storm Formation (SCS)
62	Douro Formation (SD)
63	Barlow Inlet Formation (SBI)
64	Kitson Formation (DK)
65	Blue Fiord Formation (DBF)
69	Cape Phillips Formation (OSDCP, SDCP)
70	Canrobert Formation (OCR)
72	Ibbett Bay Formation (OIB1-SDIB5)
75	Blackley Formation (DB)
76	Cape De Bray Formation (DCB)
79	Weatherall Formation (DW)
82	Hecla Bay Formation (DHB)
84	Beverley Inlet Formation (DBI)
84	Parry Islands Formation (DPI)
86	Development of the Franklinian miogeocline and foredeep basin
86	General comments
87	Early(?) Cambrian through late(?) Middle Cambrian (550?-523? Ma)
90	Middle(?) Cambrian through late Arenig (523-480 Ma)
92	Late Arenig through early Ashgill (480-445 Ma)
94	Early Ashgill through Pridoli (447-410 Ma)
95	Lochkovian through early Eifelian (410-388 Ma)
98	Early Eifelian through late Givetian (388-375 Ma)
104	Frasnian and Famennian (375-355 Ma)
108	Onset of folding in Parry Islands Fold Belt

CHAPTER 4

109	Sverdrup Basin succession (Carboniferous through Paleocene) and younger cover
109	General comments
110	Description of formations (and other units)
110	Otto Fiord Formation (COF) and seismic graben fill (Unit SCGF)
112	Canyon Fiord Formation (CPC)
116	Belcher Channel Formation (PBC)
116	Great Bear Cape and Raanes formations (PGR; undivided in subsurface)
119	Hare Fiord and Trappers Cove formations (CPHT; undivided)
119	Sabine Bay Formation (PSB)
120	Assistance Formation (PA)
120	Degerbøls Formation (PD)

121	Trold Fiord Formation (PTF)
122	Van Hauen Formation (PVH)
122	Bjorne (TB) and Blind Fiord (TBF) formations
123	Schei Point Group (TS)
123	Heiberg Group (TJH)
124	Wilkie Point Group (JW)
125	Ringnes (JR), Awingak (JKA) and Deer Bay (JD, JKD) formations
127	Gabbro (KG)
128	Isachsen Formation (KI)
128	Christopher Formation (KC)
129	Hassel (KH) and Kanguk (Kk) formations
129	Eureka Sound Group (KTE, TSB)
130	Beaufort Formation (TB)
130	Quaternary (Q)
131	Summary of Carboniferous through Quaternary sedimentation
131	Early Carboniferous (Serpukhovian) through Early Permian (Artinskian)
131	Early Permian (Roadian) through Early Triassic
132	Middle Triassic through Middle Jurassic (Bajocian)
132	Middle Jurassic (Bathonian) through Early Cretaceous (Valanginian)
132	Early Cretaceous (Valanginian) through Paleocene
133	Neogene and Quaternary

CHAPTER 5

133	Overview of the structure of the Melville Island region
133	Field data acquisition and geological mapping
134	Overview of surface structure
138	Angular unconformities and peneplain surfaces
139	Sub-Carboniferous unconformity (Ellesmerian Orogeny)
139	Sub-Upper Permian unconformity (Melvillian Disturbance)
140	Sub-Lower Cretaceous unconformity
140	Sub-Neogene(?) unconformity (Eurekan Orogeny)
141	Sub-Quaternary unconformity
142	Structural cross-sections
142	Methods of construction
144	Description of cross-sections
144	Sections F and G
146	Section D
147	Section C
148	Section B
149	Section A
150	Section H
151	Section I
152	Section J
154	Section E
155	Structural domains
155	General comments
155	Arctic Platform (structural domain 1)
155	Parry Islands Fold Belt (structural domain 2)
158	Canrobert Hills Fold Belt (structural domain 3)
158	Deformation phases

CHAPTER 6

158	Thin-skinned deformation of the salt-based fold belt
158	General comments
160	The balancing problem
160	Description of the problem

160	Possible solutions
160	Solution 1: underthrust wedge (triangle zone)
162	Solution 2: volume redistribution (tectonic thickening)
163	Solution 3: volume loss (tectonic compaction)
164	Solution 4: syntectonic sedimentation
164	Approach to solutions
164	Folds
164	Scale and stratigraphic variation of folds
164	Principal tectonic transport directions
166	Asymmetry of second-order folds
169	Nonparallel folding in the Devonian clastic wedge
171	Faults
171	Distribution and recognition
172	Fold-oblique faults
173	Fold-perpendicular faults
173	Fold-parallel faults at surface
175	Subsurface thrusts
177	Nature of vertical linkages
178	Nature of lateral linkages
179	Spatial relation to folds
181	Temporal relation to folds
183	Kinematic analysis of conjugate thrusts
185	Towson Point Anticlinorium
188	Canrobert Hills region
192	Mechanical analysis of failure in the beam
199	Shear stress resulting in slip on the basal décollement
201	Deformation of the Bay Fiord Formation
201	Description
203	Welts: ductile rock bodies formed in compression
206	Ductility of evaporites
207	Deformation of the Cape De Bray Formation
207	Description
209	Mudrock welts of the Cape De Bray Formation
212	The "life history" of thin-skinned salt-based folds
212	The fold belt "family"
213	Fold belt inception
213	Embryonic folds
213	Birth of folds
213	Juvenile folds
213	Mature folds
215	Folds in "old age"
216	The end of folding
216	Discussion

CHAPTER 7

218	Superimposed deformation phases
218	Folding of the salt-based décollement system (D4)
218	Surface expression
219	Structural style of deformed Eleanor River Formation
221	Kinematic case histories
224	Late Paleozoic rifting (D5)
224	General comments
226	Kinematic case histories
233	Late Paleozoic inversion structures (D6)
233	General comments
233	Kitson Depression

239	Regional uplift during D6
239	Mesozoic tectonics (D7)
239	General comments
239	Mesozoic igneous activity
243	Extension faults and lineaments
247	Evaporite diapirs
251	Eurekan Orogeny (D8)
251	General comments
253	Kinematic case histories
255	Discussion
255	Recent seismicity and uplift (D9)

CHAPTER 8

258	Discussion and conclusions
258	D1: Precambrian rifting
260	Early(?)–Middle Cambrian thermal subsidence
260	D2: Mid(?)–Cambrian faulting
260	Late(?) Cambrian through Early Ordovician (mid-Arenig) subsidence
261	The Ordovician intrashelf basin and basin cover
261	The intrashelf embayment
261	The Devonian foredeep
262	D3: first phase of the Ellesmerian Orogeny
263	D4: second phase of the Ellesmerian Orogeny
263	D5: Sverdrup Basin rifting
263	D6: rift inversion (the Melvillian Disturbance)
264	D7: the Mesozoic igneous event
264	D8: the Eurekan Orogeny
265	D9: Neotectonic activity

CHAPTER 9

265	Economic geology
265	Economic minerals
265	Occurrences
265	Locality 1
266	Locality 2
267	Locality 3
267	Locality 4
268	Locality 5
269	Other localities
269	Exploration potential
270	Coal
271	Oil and gas
271	Gas pools and occurrences
272	Oil seeps, bitumen deposits and occurrences
273	Source beds
274	Exploration targets
274	Stratigraphic traps
274	Structural traps
275	Untested traps
275	Acknowledgments
276	References

Appendices

290	1. Acquisition parameters for reprocessed seismic data
295	2. Other sources for reprocessed seismic profiles
295	3. Reprocessing sequence and parameters
298	4. Paleontology reports

Figures

- 5 1. Index map of the Canadian Arctic Archipelago, showing the location of the study area
- 10 2. Geological provinces of the Arctic Islands
- 12 3. Locations of reflection seismic profiles, wells, and structural cross-sections, Melville Island
- 14 4. Seismic expression of the base of the permafrost reflector
- 14 5. Seismic expression of the downdip limit of permafrost
- 15 6. Sequence stratigraphic model
- 16 7. Correlation of sonic, density, lithological and various synthetic logs of the Panarctic et al. Sabine Bay A-07 well
- 17 8. Topography and bathymetry of the Melville Island area
- 19 9. Bouguer gravity anomaly map of the western Arctic Islands
- 20 10. Magnetic anomaly map of the western Arctic Islands
- 21 11. Schematic crustal-scale cross-section of the major rock successions of the Melville Island area
- 22 12. Precambrian(?) seismic stratigraphy, subsurface Dundas Peninsula
- 23 13. Precambrian(?) through Devonian seismic stratigraphy, southeastern Melville Island
- 25 14. Distribution of primary reflections (A) and preferred structural interpretation (B) of convex-shaped features above seismic unit sAP
- 26 15. Distribution of primary reflections (A) and preferred structural interpretation (B) of apparent tectonic thickening within unit sP2
- 26 16. Lithological model accounting for the seismic response of the highly reflective succession
- 27 17. Seismic expression and interpretation of a sub-Lower(?) Cambrian low-angle fault
- 28 18. Isopach map of the upper unreflective succession (sP3, sPC)
- 30 19. Suggested correlation of Precambrian lithostratigraphic units
- 31 20. Schematic, crustal-scale cross-section, Victoria Island to northwestern Melville Island
- 33 21. The Mackenzie dyke swarm and the distribution of post-plume sedimentary cover of late Middle and early Late Proterozoic age in northern Canada
- 34 22. The Franklin, Thule, and Hottah dyke swarms and the distribution of probable and possible post-plume sedimentary cover of late Late Proterozoic age in northern Canada
- 35 23. Generalized stratigraphic cross-section of the Franklinian Succession, northern Victoria Island to northwestern Melville Island
- 36 24. Lower Ordovician through Lower Devonian facies transitions of the Arctic Islands
- 38 25. Representative stratigraphy of the Ordovician to Devonian deep water basin, northwestern Melville Island
- 40 26. Representative stratigraphy of the Precambrian(?) to Devonian shelf rim stratigraphy and cover, west-central Melville Island
- 42 27. Representative stratigraphy of the Precambrian(?) to Devonian intrashelf basin, embayment and cover, central Melville Island
- 44 28. Representative stratigraphy of the Precambrian(?) to Devonian of the Towson Point carbonate platform and cover, northeastern Melville Island
- 46 29. Seismic expression and interpretation of Lower(?) Cambrian-incised valley fill
- 47 30. Part of seismic profile P1135 (Section I) displaying characteristic Cambrian(?) and Ordovician seismic stratigraphy
- 49 31. Suggested correlation of Cambrian(?) and Lower Ordovician seismic units
- 53 32. Correlation chart, Ordovician strata of Melville Island
- 54 33. Oblique airphoto of the Kitson River Inlier
- 55 34. Stratigraphy of the lower Bay Fiord Formation in the Panarctic et al. Sabine Bay A-07 well
- 56 35. Seismic expression and interpretation of the depositional limit of the evaporitic member of the Bay Fiord Formation, and the Upper Ordovician and Silurian carbonate bank, western Dundas Peninsula
- 57 36. Seismic expression and interpretation of the lower Bay Fiord Formation near its northern depositional limit
- 61 37. Correlation chart, Silurian strata of Melville Island
- 66 38. Correlation chart, Devonian strata of Melville Island
- 67 39. Vertical airphoto mosaic of Towson Point Anticlinorium

68	40. Seismic depositional facies of the Blue Fiord Formation
69	41. Aerial view of the contact between the Cape Phillips and Cape De Bray formations, McCormick Inlet area
71	42. Panoramic photograph of asymmetrical anticline on the north side of Ibbett Bay
71	43. Ripple crosslaminated sandstone and dolostone, Canrobert Formation
71	44. Matrix-supported breccia (debris flow) in the Canrobert Formation
73	45. Airphoto of a tight periclinal fold, northwestern Canrobert Hills
74	46. Hand specimens of the brown mudrock member of the Ibbett Bay Formation
76	47. Aerial view of Blackley Formation, northwestern Canrobert Hills
77	48. Panoramic view of clinoforms in the upper part of the Cape De Bray Formation, south shore of Ibbett Bay
78	49. Seismic stratigraphy of the Weatherall and Cape De Bray formations
78	50. Seismic stratigraphy of the Devonian clastic wedge
81	51. Vertical airphoto of a part of Beverley Inlet Anticline
83	52. Hand specimens of chert pebble conglomerate from the upper Hecla Bay Formation, Raglan Range
85	53. Vertical airphoto of Rea Point Anticline and Byam River Syncline
88	54. Arithmetic plot of southern shelf and shelf rim sediment accumulation rate plotted against time (550–355 Ma)
89	55. Isopach map of Lower(?) and Middle(?) Cambrian units sC _{1B} , sC _{1C} , sC ₂ and sC ₃
90	56. Palinspastic cross-section of seismic units sP _C through sC _{1C}
91	57. Palinspastic cross-section of seismic unit sC ₂
92	58. Palinspastic cross-section of seismic unit sC ₃
93	59. Isopach map of Middle(?) and Upper(?) Cambrian, and Lower Ordovician units
94	60. Palinspastic cross-section of units sC ₄ through sO, Eleanor River and lower Canrobert formations
95	61. Palinspastic cross-section of the Cornwallis Group and age-equivalent strata of the deep water basin
97	62. Paleogeography of late Arenig–early Llanvirn with isopachs of the halite facies
98	63. Isopach map of the Cornwallis Group and age-equivalent strata
99	64. Isopach map of the Cape Phillips Formation and age-equivalent strata
100	65. Palinspastic cross-section (NE–NW) of the Cape Phillips Formation
100	66. Phases of Silurian carbonate deposition on the southern shelf and shelf rim
101	67. Palinspastic cross-sections for Lochkovian through early Eifelian time
102	68. Deltaic lobes of the Hecla Bay Sequence, and locations through time of the shelf/slope break above the Cape De Bray Formation
103	69. Palinspastic cross-section for the early Eifelian and (part of the) middle Eifelian
104	70. Isopach map of the Hecla Bay Sequence
105	71. Palinspastic cross-sections of the Hecla Bay Sequence
106	72. Isopach map of the Beverley Inlet Sequence
107	73. Palinspastic cross-section of the Beverley Inlet and Parry Islands sequences
108	74. Isopach map of the Burnett Point and Cape Fortune members of the Parry Islands Sequence
110	75. Generalized stratigraphic cross-section of the Sverdrup Basin succession
111	76. Oblique aerial photograph of Colquhoun Dome
113	77. Correlation chart, Carboniferous through Holocene strata
114	78. Vertical airphoto of Tingmisut Lake area
115	79. Locally mappable units and members of the Canyon Fiord Formation
116	80. Polymictic breccia of lower Canyon Fiord Formation of Weatherall Depression
117	81. Surface expressions of Permian through Jurassic formations of the Sverdrup Basin succession on Melville Island
118	82. Stratigraphic section (E–W) of exposed Permian–Cretaceous formations
120	83. Coarse grained sandstone and chert-pebble conglomerate of Sabine Bay Formation
121	84. Cobble grade conglomerate of lower Troid Fiord Formation
122	85. Clast-supported conglomerate of the Bjorne Formation
125	86. Field photographs of the Hiccles Cove, Ringnes and Deer Bay formations, northwestern Melville Island

126	87. Field photographs of Middle Jurassic through Upper Cretaceous formations, Melville Island
135	88. Fold trends in the Franklinian Mobile Belt, western Canadian Arctic Islands
136	89. Oblique aerial photograph of the arcuate, easterly plunging fold belt of eastern Melville Island
138	90. Oblique aerial photograph of the southern portion of the Canrobert Hills fold belt, and part of Purchase Bay Homocline
140	91. Photographic views of the sub-Carboniferous angular unconformity
141	92. Photographic views of the sub-Permian angular unconformity
141	93. The sub-Cretaceous and sub-Tertiary unconformities on Melville Island
143	94. Cross-sections of the peneplain surface of Melville Island
144	95. Schematic geological relations between Isachsen, Christopher and Beaufort formations and various Quaternary gravels, central and eastern Melville Island
156	96. Paleozoic cratonic arches and basins, fold belts and accreted terranes of the northern Yukon, Canadian Arctic Islands and north Greenland
157	97. Stratigraphic distribution of detachments, thrust ramps and various scales of folding in the Franklinian Succession of Melville Island
161	98. Regional variations in bed length shortening of the medial rigid beam
162	99. Regional variations in bed length shortening of the upper rigid layer
163	100. Possible structural geometry of the Parry Islands Fold Belt, and similar triangle zone geometries of the Canadian Cordillera
165	101. Wavelength and frequency of fold types plotted as a function of stratigraphy
166	102. Outcrop-scale structures in the Weatherall Formation
167	103. Outcrop-scale structures in the Cape De Bray Formation
168	104. Outcrop-scale structures in the Blue Fiord Formation
169	105. Axial plane inclinations of surface anticlines and dip of subsurface thrusts plotted as a function of distance from the foreland
170	106. Meham River West Anticline, on a part of seismic profile P1763/1193
171	107. Beverley Inlet Anticline, on a part of seismic profile P1763/1193
172	108. Baldwin River Anticline and north half of Rea Point Anticline, on a part of seismic profile P2218
173	109. Sabine Bay Anticline, on a part of seismic profile P1192
174	110. Vertical airphoto of Robertson Point Anticline
176	111. Cape Providence Anticline and a second, unnamed anticline, on a part of seismic profile P1171, Section F
177	112. Cape Clarendon Anticline and another, unnamed anticline, on a part of seismic profile P1171, Section F
178	113. Robertson Point Anticline, on a part of seismic profile P1660, Section C
179	114. King Point East Anticline and Birch Point Syncline, on a part of seismic profile C75, Section A
180	115. Rea Point and Sabine Bay anticlines, seismic profile T8, Section D
181	116. Subsurface conjugate thrusts and other tectonic elements at the level of the Thumb Mountain Formation
182	117. Richardson Point Anticline, on a part of seismic profile C75, Section A
183	118. Vertically-linked thrust structures developed on a weak decoupling surface
184	119. Foreland- and hinterland-vergent duplexes developed on a weak decoupling surface
184	120. Mechanisms of displacement transfer in weak, basal detachment thrust systems
185	121. Temporal relations between folding and faulting: fault-bend folds and fault-propagation folds
186	122. Consett Head Anticline, south limb of Rea Point Anticline, and north limb of Byam River Syncline, on a part of seismic profile C75, Section A
187	123. Dealy Island Anticline, on a part of seismic profile P1763/1193, Section H
188	124. Beverley Inlet Anticline, on a part of seismic profile P1660, Section C
189	125. Stereonet plots for thrusts in the Thumb Mountain Formation
190	126. Geographic variation in attitude of the maximum principal stress axis (σ_1) determined from conjugate thrusts at the level of the Thumb Mountain Formation
191	127. Stereonet plots of kinematic indicators for the Towson Point Anticlinorium

192	128. Strike-slip faults and other kinematic elements, Weatherall Bay area
193	129. Sub-Middle Carboniferous geology of southern Sabine Peninsula
194	130. Outcrop- and hand-specimen-scale structures in the Canrobert and Ibbett Bay formations
196	131. Outcrop-scale structures in the Blackley Formation
197	132. Stereonet plots of kinematic indicators collected at numerous field stations in the Canrobert Hills
198	133. Giant cross-fibre calcite vein within the Ibbett Bay Formation
198	134. Stereonet plot of suggested principal compressive stress axes and associated structures of the Canrobert Hills region
199	135. Mohr's circle construction displaying maximum and minimum normal stresses and shear stresses at various pore fluid pressures for compressive failure in the beam
200	136. Schematic cross-sections of the salt-based thrust foldbelt and the eroded synorogenic clastic wedge
202	137. Burnett Point Syncline, on a part of seismic profile T4, Section C
203	138. Frequency histogram plot of tectonic thickness parameters (T') for the lower Bay Fiord Formation
204	139. External morphology of salt welts, shale welts and other ductile rock bodies formed in compression
205	140. Cape Phipps Anticline, on a part of seismic profile P1171, Section F
206	141. Progressive growth of a compound anticlinal welt by convergent thrusting
206	142. Halite vein filling in the core of the lower member of the Bay Fiord Formation
207	143. Minor folds and boudinage structures in core from the evaporitic Bay Fiord Formation
207	144. Tectonic breccia in core from the lower member of the Bay Fiord Formation
208	145. Possible internal geometries of anticlinal salt welts
209	146. Strengths of salt, and other common rock types
210	147. Vertical airphoto of clinoforms and other structures, Purchase Bay Homocline
211	148. Non-ductile internal geometries of synclinal welts in the Cape De Bray Formation
211	149. Vertical beds in the Weatherall Formation, north limb of Beverley Inlet Anticline, southeastern Melville Island
212	150. Near-surface structure of the Beverley Inlet Anticline
214	151. Schematic development of salt-based folds in six stages
218	152. Interference patterns produced by cross-folding
219	153. D3 and D4 fold trends of the Parry Islands Fold Belt as predicted from surface fold interference patterns
220	154. First- and second-order fold trends of the Canrobert Hills region, deduced from surface structural interference patterns
221	155. First-order fold axes of the Melville Island region and the trend of selected isopachs, facies, Bouguer anomalies, and deep-seated D1, D2, and D4 faults
222	156. Structure contour map (in two-way travel time) on the seismic stratigraphic top of the Eleanor River Formation
223	157. Nias Point Anticlinorium on a part of seismic profile P1654, Section I
224	158. Kinematic history of Dealy Island Anticline
225	159. Stereonet plot of kinematic data for the Kitson River Fault and inlier strata
226	160. Kinematic model illustrating the development of Purchase Bay Homocline
227	161. Late Paleozoic rift-related structures of northern Melville Island
228	162. Oblique aerial view of the Weatherall Depression in Spencer Range
229	163. Weatherall Depression and Spencer Range Uplift on a part of seismic profile P1921, Section E
230	164. Stereonet plot of poles to bedding planes and regional-scale normal faults, upper Paleozoic rocks, southern Sabine Peninsula
231	165. Kinematic model for the Paleozoic evolution of Spencer Range Anticlinorium, Spencer Range Uplift, and Weatherall Depression
232	166. Paleozoic kinematic history of McCormick Inlet Anticlinorium and eastern Raglan Range area
233	167. Paleozoic phases of deformation predicted for the Blue Hills structure
234	168. Geology and structure of the Kitson Depression and Raglan Range
238	169. Faults, folds and bedding attitudes of the Kitson Depression

239	170. A dipping outlier panel of Canyon Fiord Formation in horizontal tectonic contact with underlying and older Cape De Bray Formation
240	171. Ground and aerial views of Nisbet Point Fault in the Canrobert Hills
241	172. Vertical airphoto of the central parts of the Hawk Creek and Nisbet Point faults
242	173. Oblique panoramic view of a D3 syncline in the Blackley Formation, exposed in the hinge region of one of several D6 anticlines
242	174. Major tectonic elements of the southern Canrobert Hills region
243	175. Paleogeographic map of Melville Island area for late Early Permian time
244	176. Geological models to account for the sub-Upper Permian angular unconformity, northern Melville Island
245	177. Upper Jurassic-Lower Cretaceous gabbro dykes, extension faults and related magnetic anomalies
246	178. Seismic expression of Upper Jurassic-Lower Cretaceous gabbro sills and sheets
247	179. Field photographs of structures in the Hiccles Cove and Ringnes formations
248	180. Evaporite diapirs and other piercement structures of the Sverdrup Basin
249	181. Vertical airphotos of Barrow and Colquhoun domes
250	182. Line drawing of seismic profiles P2506 and P2507 adjacent to Vesey Hamilton Salt Wall
252	183. Tectonic elements of the Eurekan Orogeny, Melville Island area
253	184. Stereonet plots of (D8) kinematic elements and implied tectonic transport directions for Carboniferous and Lower Permian strata, southern Sabine Peninsula and Spencer Range
254	185. Stereonet plots of (D8) kinematic indicators and implied tectonic transport directions for the Tingmisut gabbro dykes
256	186. Kinematic elements of the Eurekan Orogen in the Canadian Arctic Islands
257	187. Recent earthquake epicentres (D9) of Melville Island region plotted on the Bouguer anomaly for land areas and on the isostatic anomaly for marine areas
259	188. Simplified correlation chart of the Melville Island region, with major geological events and tectonic transport directions, Precambrian to the Quaternary
267	189. Commodity occurrences map of Melville Island

Tables

18	1. Bounding and internal (within sequence) reflection patterns and interpreted bedforms
in pocket	2. Formations and seismic units, Melville Island
96	3. Phases of Silurian shallow-marine carbonate accumulations
127	4. Occurrence of gabbroic intrusive rocks in borehole-penetrated intervals of Sabine Peninsula
159	5. Deformation phases of the Melville Island region
251	6. Thinning of seismic stratigraphic units against Vesey Hamilton Salt Wall and calculated minimum rates of diapirism
266	7. Base metal and related economic mineral occurrences
268	8. Chemical analyses of Ordovician hydroxyapatite phosphorite
270	9. Coal deposits and major occurrences
271	10. Natural gas pools
273	11. Bitumen deposits and occurrences

MAP 1844A (1:250 000)

in pocket	Melville Island and adjacent small islands
-----------	--------------------------------------------

STRUCTURAL CROSS-SECTIONS AND SEISMIC PROFILES

in pocket	Section A: Little Point to Bradford Point
in pocket	Section B: Headwaters of Byam River to Domett Point
in pocket	Section C: Ross Point to Tingmisut Lake
in pocket	Section D: Chevalier Bay Syncline to west arm of Weatherall Bay
in pocket	Section E: St. Arnaud Hills to Vesey Hamilton
in pocket	Section F: Cape James Ross to Stony Pass Syncline
in pocket	Section G: Stony Pass Syncline to Sabine Bay
in pocket	Section H: Stony Pass to Hecla and Griper Bay
in pocket	Section I: Cape Edwards to Hecla and Griper Bay
in pocket	Section J: Bailey Point to Fitzwilliam Strait

MELVILLE ISLAND'S SALT-BASED FOLD BELT, ARCTIC CANADA

Abstract

Melville Island extends across the Cambrian through Devonian Arctic Platform and Franklinian Mobile Belt, and unconformable post-Devonian cover of the Sverdrup Basin. A revised geological map and seismic profiles provide insight into bedrock geology to depths exceeding 20 km. Possible Precambrian basement is identified at the deepest levels, as are three Proterozoic(?) seismic successions deformed and eroded prior to the Early(?) Cambrian. Cover includes a Cambrian(?) through Devonian shelf-margin wedge that increases in thickness northward to a maximum exceeding 10 000 m. The overlying Devonian clastic wedge (3000–4600 m) represents the depositional record of the ancestral Ellesmerian Orogeny, southerly directed deformation that eventually produced the exposed salt-based fold belt and terminated lower Paleozoic sedimentation. The fold belt is continuous downward with a bivergent, thrust-faulted interval with up to 15 per cent shortening, and a basal detachment at 5 km. Long-lived deep-seated thrusts and other faults terminate below the sub-salt décollement and lie within large anticlinoria near the present margin of the Sverdrup Basin. Ellesmerian deformation continues to the west where style is apparently related to slip on a mid(?)–Cambrian detachment. Six additional Devonian and younger phases of deformation are recognized.

Commodities of economic interest on Melville Island include natural gas, oil sand deposits, coal, showings of copper, lead and zinc sulphides, native sulphur, phosphorite and extensive subsurface rock salt.

Résumé

L'île Melville traverse la Plate-forme de l'Arctique et la ceinture mobile franklinienne (Cambrien-fin du Dévonien) ainsi que la couverture post-dévonienne discordante du bassin de Sverdrup. Une carte géologique révisée et des profils sismiques donnent un aperçu de la géologie du substratum rocheux jusqu'à des profondeurs dépassant 20 km. Aux niveaux les plus profonds se trouvent ce qui pourrait être un socle précambrien de même que trois successions sismiques protérozoïques(?) déformées et érodées avant le Cambrien précoce(?). La couverture comprend un biseau de marge de plate-forme s'échelonnant du Cambrien(?) à la fin du Dévonien qui s'épaissit vers le nord pour atteindre plus de 10 000 m. Le biseau détritique dévonien sus-jacent (3 000–4 600 m) représente les sédiments de l'ancienne orogénèse ellesmérienne, déformation orientée vers le sud qui a produit la ceinture orogénique à base de sel exposée et a mis fin à la sédimentation du Paléozoïque inférieur. La ceinture orogénique se confond vers le bas en un intervalle chevauché divergent dont le raccourcissement atteint jusqu'à 15 %, et en un décollement basal à 5 km. Des chevauchements profonds de longue durée et d'autres failles se terminent au-dessous du décollement sous le sel et se situent au sein de vastes anticlinoriaux près de la marge actuelle du bassin de Sverdrup. La déformation ellesmérienne se poursuit à l'ouest où le style est vraisemblablement lié au rejet sur un décollement du Cambrien moyen(?). Six phases de déformation additionnelles, dévoniennes et plus récentes, ont été dénombrées.

Les produits d'intérêt économique reconnus dans l'île Melville sont notamment du gaz naturel, des sables pétrolifères, du charbon, des indices de sulfures de cuivre, de plomb et de zinc, du soufre natif, de la phosphorite et de vastes zones souterraines de sel gemme.

Summary

Melville Island is situated on the Cambrian through Devonian Arctic Platform, correlative rocks of the Franklinian Mobile Belt, and unconformable post-Devonian cover of the Sverdrup Basin. Seismic profiles and a revised geology map provide insight into Melville Island bedrock structure to depths exceeding 20 km and spanning a billion years of earth history. Structures at the deepest levels include possible Precambrian(?) crystalline basement and three Proterozoic(?) seismic successions deformed and eroded prior to unconformable overlap by Lower(?) Cambrian strata. An extensive Cambrian through lower Middle Devonian (Eifelian) shelf-margin wedge underlies the entire region and is known to increase in thickness from 1200 m on northern Victoria Island to at least 10 000 m beneath central Melville Island, an intervening distance of 300 km. The conformable Middle and Upper Devonian clastic wedge (3000–4600 m) represents the depositional record of the ancestral Ellesmerian Orogeny, deformation that eventually terminated lower Paleozoic sediment accumulation after the mid-Famennian. Post-Franklinian strata of the Sverdrup Basin were deposited on the eroded and peneplained roots of Melville Island's salt-based fold belt. Sverdrup Basin strata in the area comprise rocks of Early Carboniferous (Serpukhovian) through late Paleocene ages. Together these sediments range from a feather edge in the south to at least 8000 m in thickness on northern Sabine Peninsula. A major unconformity separates scattered Plio-Pleistocene erosional remnants from all older rocks.

Southerly directed deformation associated with the latest Devonian or Early Carboniferous Ellesmerian Orogeny produced an arcuate, salt-based fold belt throughout the Parry Islands. This belt is 470 km in strike length from eastern Bathurst Island to central Melville Island and up to 230 km wide between the hinterland and the foreland limits of northern Melville Island and central Viscount Melville Sound. Ellesmerian deformation is also recognized farther west, where thin-skinned shortening appears to be related to slip on a mid(?)–Cambrian detachment.

Typical regional-scale folds of the salt-based fold belt have wavelengths of 12 to 17 km, axial planes that dip 80 to 90° north or south and axial plunge variation that is 0 to 6°. The surface fold belt is continuous downward with: an apparently ductile layer of Middle Devonian clinoformed basin-fill mudrocks, a seismically-imaged, folded and thrust-faulted interval in a competent beam of Ordovician to Middle Devonian shelf- and slope-facies carbonates and correlative basal mudrocks, and a basal detachment below a lower ductile layer of Middle Ordovician (Llanvirnian) evaporites at a depth of 5.0 to 5.8 km. Bed-length shortening measured on palinspastically restored sections is up to 28 km (15%). The deformation style is typical of a weak-based décollement system for which a near-horizontal compressive stress, transmitted through the beam, has facilitated slip on a near-horizontal detachment as well as the development of equally common southerly and northerly vergent thrusts in overlying strata. The thrusts, with individual offsets of up to 3.3 km, are concentrated below surface anticlines and are linked along strike by relayed and en echelon displacement transfer. Single thrusts and separate duplex thrust systems within individual anticlines are also stacked vertically and linked by relayed transferred slip between basal, intermediate and upper detachments.

Elements of a younger Ellesmerian deformation phase, recognized in surface cross-fold axes, have also been mapped within the folded sub-salt succession below 5 km. Thrusts that ramp up to the sub-salt décollement have produced large anticlinoria near the present margin of the Sverdrup Basin. These faults have been repeatedly reactivated since the Precambrian(?). Recognized deformation phases within and peripheral to the salt-based fold belt include: 1) N40–10°W-directed Middle(?) to Late(?) Proterozoic extension; 2) mid-Cambrian(?) extensional growth faulting; 3) thin-skinned salt-based shortening during the Ellesmerian Orogeny; 4) a partly coeval and partly younger phase of deep-seated, sinistral, transpressive inversion that reactivated older extensional structures; 5) northerly to northwesterly directed rifting of Sverdrup Basin in the Carboniferous; 6) inversion of the rift zone during the mid-Permian (Melvillian Disturbance); 7) Early Triassic through Albian diapirism of Carboniferous evaporites within the Sverdrup Basin only; 8) widespread gabbroic magmatic activity and N40–70°W-directed crustal extension between the Late(?) Jurassic and the Albian; 9) southwesterly directed sinistral transpressive adjustments and

open folding coeval with the mid-Tertiary Eureka Orogeny; and 10) a final phase of Plio-Pleistocene uplift and continuing intraplate seismicity.

Energy-related commodities of potential economic interest include natural gas trapped in Triassic and Jurassic sandstones, oil sands in the Lower Triassic, bituminous coal in the Upper Devonian and lignite in the Lower Cretaceous. Surface oil shows are also known in Devonian carbonates, Carboniferous conglomerates and carbonates, and Lower Cretaceous sandstones. Base metal occurrences include galena and sphalerite in lower Paleozoic basin-facies graptolitic mudrocks and correlative shelf carbonates, and chalcopyrite and other supergene copper minerals in Carboniferous redbeds. Other commodities include extensive deposits of subsurface rock salt (halite) and local occurrences of native sulphur, phosphorite, barite and fluorite.

Sommaire

L'île Melville se situe sur la Plate-forme de l'Arctique (Cambrien-fin du Dévonien), sur des roches corrélatives de la ceinture mobile franklinienne et sur la couverture post-dévonienne discordante du bassin de Sverdrup. Des profils sismiques et une carte géologique révisée donnent un aperçu de la structure du substratum rocheux de l'île Melville jusqu'à des profondeurs dépassant 20 km et correspondant à une période de l'histoire de la Terre s'échelonnant sur un milliard d'années. Aux niveaux les plus profonds se trouvent ce qui pourrait être un socle cristallin précambrien(?) et trois successions sismiques protérozoïques(?) qui ont été déformées et érodées avant d'être recouvertes en discordance par des strates du Cambrien inférieur(?). Un vaste biseau de marge de plate-forme du Cambrien-Dévonien moyen (Eifélien) se rencontre sous toute la région; il s'épaissit, passant de 1 200 m dans le nord de l'île Victoria à au moins 10 000 m sous le centre de l'île Melville, sur une distance de 300 km. Le biseau détritique concordant du Dévonien moyen et supérieur (3 000-4 600 m) représente les sédiments de l'ancienne orogénèse ellesmérienne, déformation qui a mis fin à l'accumulation de sédiments du Paléozoïque inférieur pendant le Famennien moyen. Les sédiments post-frankliniens du bassin de Sverdrup se sont déposés sur les racines érodées et pénéplanées de la ceinture orogénique à base de sel de l'île Melville. Les strates du bassin de Sverdrup dans cette région comportent des roches qui s'échelonnent du Carbonifère précoce (Serpukhovien) au Paléocène tardif. Ces sédiments, pris dans leur ensemble, forment au sud une bordure en biseau qui s'épaissit pour atteindre au moins 8 000 m dans le nord de la presqu'île Sabine. Une discordance majeure sépare les lambeaux d'érosion disséminés du Plio-Pléistocène de toutes les roches plus anciennes.

La déformation orientée vers le sud, associée à l'orogénèse ellesmérienne du Dévonien terminal ou du Carbonifère précoce, a produit une ceinture orogénique arquée à base de sel dans l'ensemble des îles Parry. Cette zone a 470 km de longueur parallèlement à sa direction depuis l'est de l'île Bathurst jusqu'au centre de l'île Melville, et jusqu'à 230 km de largeur entre l'arrière-pays et les limites de l'avant-pays dans le nord de l'île Melville et le centre du détroit de Viscount Melville. La déformation ellesmérienne est également reconnue plus à l'ouest, où le raccourcissement de couverture semble être lié au rejet sur un décollement du Cambrien moyen(?).

Les plis d'échelle régionale qui caractérisent la ceinture orogénique à base de sel présentent des longueurs d'onde variant entre 12 et 17 km, des plans axiaux plongeant entre 80° et 90° vers le nord ou le sud et un plongement axial allant de 0° à 6°. La ceinture orogénique superficielle se confond vers le bas en une couche vraisemblablement ductile de mudstones (Dévonien moyen) de remplissage de bassin de clinoforme, un intervalle plissé et chevauché que révèle des images sismiques et qui se trouve dans un faisceau compétent de roches carbonatées de faciès de plate-forme et de talus et de mudstones de bassin corrélatifs de l'Ordovicien au Dévonien moyen, et un décollement basal sous une couche ductile inférieure d'évaporites de l'Ordovicien moyen (Llanvirnien) à une profondeur de 5,0 à 5,8 km. Le raccourcissement des couches, mesuré sur des coupes palinspastiques, atteint jusqu'à 28 km (15 %). Le style de déformation est représentatif d'un système de décollement à base faible pour lequel une contrainte de compression quasi horizontale, transmise à travers le faisceau, a facilité le rejet sur un décollement quasi horizontal ainsi que la

formation de nombreux chevauchements à vergence sud et nord dans les strates sus-jacentes. Les chevauchements, dont le rejet horizontal transverse peut atteindre 3,3 km, sont concentrés sous des anticlinaux superficiels et sont reliés entre eux parallèlement à la direction par transmission ou transfert en échelon du rejet. Les chevauchements individuels et les duplex distincts au sein des anticlinaux individuels sont également empilés verticalement et sont reliés par un rejet transféré transmis entre les décollements basal, intermédiaire et supérieur.

Les éléments d'une phase de déformation ellesmérienne plus récente, reconnus dans les axes des plis transverses superficiels, ont également été cartographiés dans la succession plissée sous le sel à une profondeur supérieure à 5 km. Les chevauchements qui montent en pente jusqu'au décollement sous le sel ont produit de vastes anticlinoriaux près de la marge actuelle du bassin de Sverdrup. Ces failles ont été remobilisées à plusieurs reprises depuis le Précambrien(?). Les phases de déformation reconnues au sein et au pourtour de la ceinture orogénique à base de sel comprennent : 1) une distension orientée de 10 à 40° NW au Protérozoïque moyen(?)-tardif(?); 2) la formation de failles synsédimentaires par distension au Cambrien moyen(?); 3) un raccourcissement de couverture à base de sel durant l'orogénèse ellesmérienne; 4) une phase en partie contemporaine et en partie plus récente d'inversion de transpression senestre profonde qui a remobilisé des structures de distension plus anciennes; 5) un stade de rifting à direction nord à nord-ouest dans le bassin de Sverdrup au Carbonifère; 6) une inversion de la zone de fractures au Permien moyen (accident du Melvillien); 7) un diapirisme d'évaporites carbonifères du Trias précoce à l'Albien inclusivement, uniquement dans le bassin de Sverdrup; 8) une activité magmatique gabbroïque de grande étendue et une distension crustale orientée de 40 à 70° NW entre le Jurassique tardif(?) et l'Albien; 9) des ajustements de transpression senestres dirigés vers le sud-ouest et la formation de plis ouverts pendant l'orogénèse eurékienne au Tertiaire moyen; et 10) une phase finale de soulèvement et de sismicité intraplaque continue au Plio-Pléistocène.

Parmi les produits énergétiques offrant un intérêt économique potentiel, il y a le gaz naturel piégé dans les grès triasiques et jurassiques, les sables pétrolifères dans le Trias inférieur, le charbon bitumineux dans le Dévonien supérieur et le lignite dans le Crétacé inférieur. Des indices de pétrole ont également été relevés à la surface dans des roches carbonatées du Dévonien, des conglomérats et des roches carbonatées du Carbonifère et des grès du Crétacé inférieur. Les occurrences de métaux communs comprennent de la galène et de la sphalérite dans des mudstones graptolitiques de faciès de bassin et des roches carbonatées de plate-forme corrélatives du Paléozoïque inférieur, ainsi que de la chalcopryrite et d'autres minéraux de cuivre supergènes dans des couches rouges du Carbonifère. Il y a aussi de vastes gisements souterrains de sel gemme (halite) et des occurrences locales de soufre natif, de phosphorite, de barytine et de fluorite.

CHAPTER 1

INTRODUCTION

Location and accessibility

This account considers the bedrock geology, structural styles and tectonic evolution of a remote portion of Canada's western Arctic Islands (Fig. 1). Although the land areas of Melville Island provide natural geographic limits to this study, the adjacent bedrock beneath the inter-island channels is also of some interest. Melville Island occupies an area of 42 149 km² (16 275 mi²). Placed in the context of more familiar areas of the globe, Melville Island is larger than Switzerland and only marginally smaller than the Canadian province of Nova Scotia. The dominant feature of Melville Island's surface geology is a classic foreland fold belt that is widely exposed on the central

and eastern part of the island and is also known to be continuous beneath Byam Martin Channel, Byam Martin Island and most of adjacent Bathurst Island. The full 470 km length of this salt-based fold belt would stretch over the full extent of the better known Jura Fold Belt in the Swiss Alpine foreland. The exposed 230 km width of Melville Island's fold belt placed parallel to and over the Rocky Mountains of western Canada would stretch from Calgary in the foreland, across the entire foothills belt, the Front Ranges, the Main Ranges and beyond the Rocky Mountain Trench to nearly the summit of the Purcell Mountains.

Melville Island's long dimension is parallel to and near 75°30'N latitude. Five major peninsulas extend to the west like the fingers and thumb of a hand. Two of

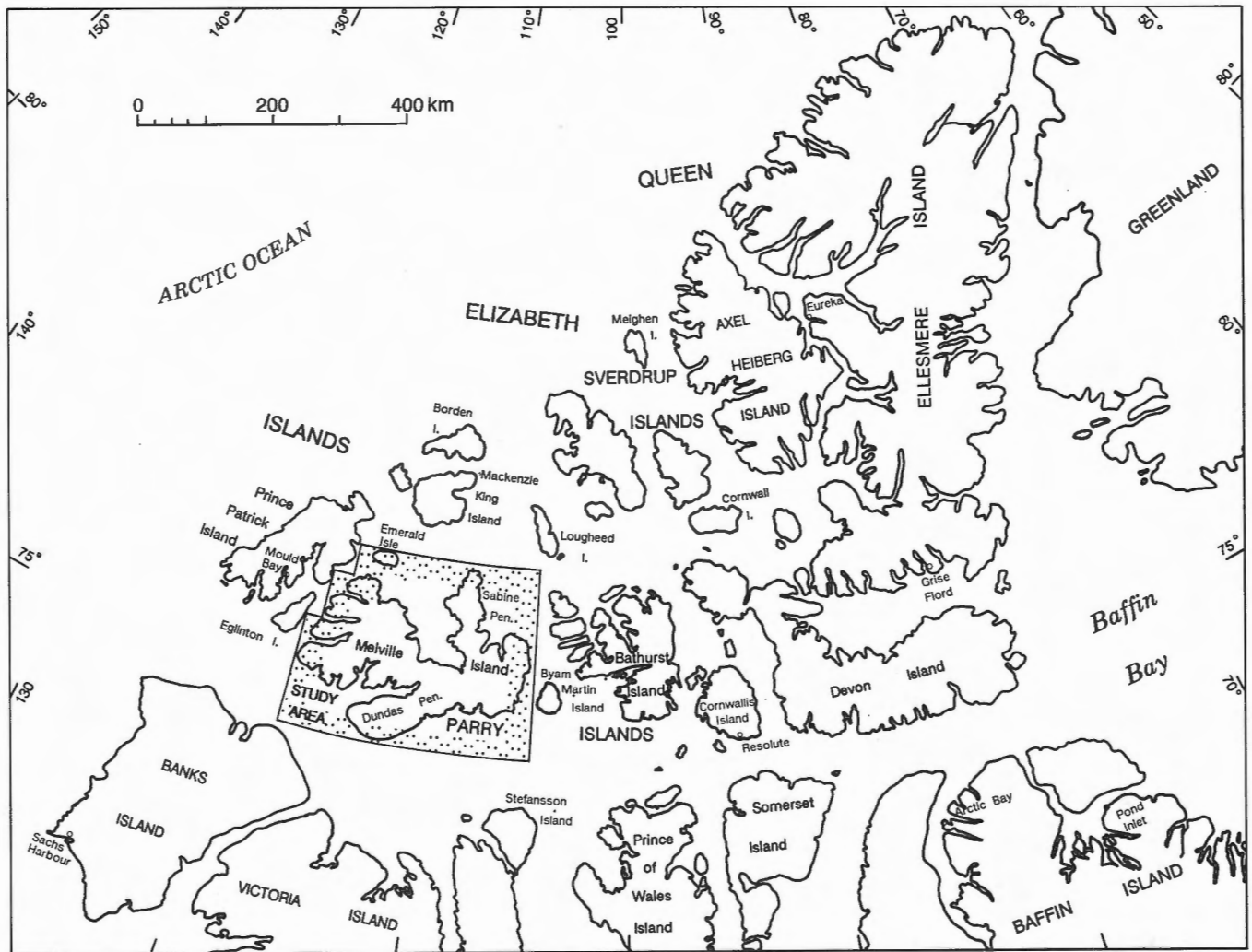


Figure 1. Index map of the Canadian Arctic Archipelago, showing the location of the study area.

these are named Sproule and Dundas peninsulas. A sixth landmass (Sabine Peninsula) extends north from the east end of the island. Smaller islands also included in this report are Emerald Isle and Vesey Hamilton Island.

There is no permanent settlement on Melville Island. A Canadian government weather and research station, occupied year round, is located 70 km to the west at Mould Bay on western Prince Patrick Island. The settlement of Resolute on Cornwallis Island, 310 km east of the closest part of Melville Island, is the nearest community served routinely by commercial aircraft from southern Canada. Resolute is also reached annually by ship from eastern Canada during the short period of open water in late summer and early fall. From Resolute, most of Melville Island is accessible by means of fixed-wing or rotary aircraft capable of landing on unprepared terrain.

Fieldwork for this report was conducted in 1984 and 1985. At that time, a gravel airstrip capable of receiving most large jet aircraft was maintained year round at the Rea Point exploration camp of Panarctic Oils Limited, and arrangements were made with Panarctic to transport field personnel and supplies directly by Boeing 737 aircraft from Edmonton, Alberta to Panarctic's Rea Point base. Declining exploration activity in the Arctic Islands led to the closure of the Rea Point facility in April, 1986. Most of the buildings remain on the site.

Scope of study

The range and quality of photographic, geological and geophysical data now available for Melville Island provide the tools for documenting what must be considered a world-class type area of foreland fold and thrust belts developed on salt. Regional and temporal variations in depositional facies for over 20 km of shallow- and mid-crustal strata representing over a billion years of earth history are evidenced in well and surface sections and a grid of 6 and 8 second industry-acquired seismic reflection profiles. Documentation of Precambrian through Recent sedimentation patterns, outlined in Chapters 2 through 4, form the descriptive basis for a new 1:250 000 scale bedrock geology map and ten regional structural cross-sections of the island (Chapter 5). Superbly exposed surface geology together with reflection profiles, (1400 line kilometres have been reprocessed for this project), have allowed for both a regional overview and also a locally detailed dissection of structural styles and deformation kinematics both within and on the periphery of the salt-based fold belt

(Chapter 6). A total of nine distinct phases of deformation are recognized: two preceding, two during and five following salt-based décollement tectonics. The earlier two phases, of probable Cambrian and Precambrian ages, are described in parts of Chapters 2 and 3. This ancient deformation has provided a deep-seated anisotropy, and therefore a direct or indirect influence on the style of all the later phases. The last six phases, outlined in Chapter 7, have overprinted the terminal Devonian main phase of décollement tectonics. Structural modifications of the salt-based fold belt by the younger events have been generally modest but each is sufficiently obvious to warrant the presentation of kinematic models for a variety of regional-scale structures. A geological history, presented in Chapter 8, attempts to synthesize the main depositional and tectonic highlights of the region and the options available for future research. Surface and shallow crustal structure are placed in an economic perspective with the description and tabulation (*in* Chapter 9) of all known base metal, mineral and energy-related commodity occurrences and some suggestions for future exploration.

History of geographic exploration

There is archaeological evidence of successive, permanent, prehistoric Inuit (Thule culture and older) settlements on Bathurst, Cornwallis and Victoria islands, all finally abandoned approximately 500 years ago (McGhee, 1978). The prehistory of Melville Island is limited to Dorset and pre-Dorset culture summer occupation sites (stone tent rings) around Bridport Inlet and Liddon Gulf. Thule culture temporary sites are also known from the Bridport Inlet region (P. Schlederman, pers. comm., 1992). From this evidence, it would appear likely that, between 3000 and 500 years ago, the island was periodically visited by hunting parties venturing outward from villages situated in the eastern and southern Arctic Islands.

Melville Island was first discovered by Europeans in September, 1819, during the course of an eminently successful voyage sponsored by the British Admiralty. William Edward Parry, the expedition leader and commander of the ships *HMS Hecla* and *Griper*, was commissioned to explore the western extent of Lancaster Sound, and if possible find, by this route, a Northwest Passage to the Pacific Ocean (Parry, 1821). Although the most desirable objectives were not attained on this voyage, there were fine weather and good sailing conditions in the previously uncharted inter-island channels running west from Baffin Bay. Parry and his crew were the first to sight Cornwallis, Bathurst, Byam Martin, Somerset and Banks islands as

well as Melville Island, on which they landed and subsequently named in honour of Viscount Melville, First Lord of the Admiralty.

After an ice-bound winter aboard ship, Parry, with a party of twelve men and hauling a cart, undertook an overland trek from Winter Harbour on the south coast to Nias Point on Hecla and Griper Bay. Land areas sighted to the north would later prove to be Sabine Peninsula, and the eastern end of Raglan Range (northwestern Melville Island). They returned to their ships by way of Bushnan Cove and Liddon Gulf. In August, Parry's expedition continued west by ship but found onward passage blocked by ice beyond Cape Dundas on western Dundas Peninsula.

Melville Island was more fully explored during the wide-ranging search for the ill-fated expedition led by Sir John Franklin between 1845 and 1848. The most significant geographic contributions were made by officers attached to the search ships of Capt. H.T. Austin in 1850–51 and of Sir Edward Belcher in 1852–53. This exploration, over land and sea ice, involved a series of separate man-hauled-sledge journeys led by Leopold M'Clintock and officers A.R. Bradford, G.F. Meham, R. Vesey Hamilton, G.H. Richards, and Sherard Osborn. Their efforts led to the charting of all the coasts of Melville Island, including Sabine Peninsula, and the additional discovery and charting of Emerald Isle, Eglinton and Prince Patrick islands (M'Clintock, 1857; British Parliamentary Papers, 1855; Belcher, 1855; Tozer and Thorsteinsson, 1964).

Melville Island was visited only periodically in the next hundred years. The most notable of these visits was a Canadian government-sponsored expedition travelling aboard the CGS *Arctic* and led by J.E. Bernier. Three scientific voyages were made by Bernier in the region between 1906 and 1910, including a winter spent in the ice at Winter Harbour in 1908–09 (Bernier, 1909, 1910, 1911). A plaque, which still exists, was laid by the expedition members at Winter Harbour on July 1, 1909 and claimed for Canada "the whole of the 'Arctic Archipelago', lying to the north of America from long. 60°W. to 141°W. up to 90°N."

Another well known explorer of the region and leader of the Canadian Arctic Expedition of 1913–18 was V. Stefansson. He is known to have wintered at Peddie Point on the south shore of Liddon Gulf in 1916–17 and, during the following spring, went on to explore by dog team large tracts of the far north-western Arctic (Stefansson, 1921). In 1929, a RCMP patrol led by Sgt. A.H. Joy, also travelling by dog team on the sea ice, reached and crossed Melville

Island during a wide-ranging reconnaissance mission through the central Arctic Islands (Tozer and Thorsteinsson, 1964; Taylor, 1964). Later, in 1944, Staff Sgt. A.H. Larsen, aboard the RCMP schooner *St. Roch*, made additional visits to the south coast of the island as part of a successful voyage through the Northwest Passage (Taylor, 1964).

The U.S.S. *Edisto* attempted to reach Winter Harbour in 1947 with the intention of setting up a joint Canada-U.S. weather station at the site. This mission failed and the station was constructed at Resolute (Zaslow, 1981).

Previous work

The earliest geological observations of Melville Island were made during Parry's voyage of discovery. Samples collected at the time were later described by König (1824). Bedrock was identified to include "fletz" sandstone with lesser "slate-clay", coal and ironstone. König also describes samples of igneous and metamorphic rocks, and limestones containing bivalves and trilobites. All of this material is now thought to have been collected from glacial drift.

From the notes and samples of M'Clintock's expeditions, Samuel Haughton (*in* M'Clintock, 1857) produced the first geology map of the Arctic Islands that included Melville Island. This map, which has five geological units, (two of them exposed on Melville) correctly identifies the easterly trending structural grain of rock units on the island and the widespread occurrence of sandstone and coal. Samples of this material collected at the time of the Franklin search expeditions were also commented on by Sir Roderick Impey Murchison (*in* Osborn, 1857) who was the first to suggest that the sandstone-bearing unit, although undated, could be the same age as the Devonian Old Red Sandstone of Britain.

J.G. McMillan accompanied Bernier's expedition of 1908–1909 and recorded many geological and structural observations during visits to the south coast of Melville Island (McMillan *in* Bernier, 1910). Dundas Peninsula was described as a tableland. Tilted strata were found between Cape Providence and Skene Bay, and on the south shore of Liddon Gulf. However, McMillan could find no evidence of folding and suggested that the tilted beds were associated with northeasterly trending fault blocks.

This was the sum of geological knowledge about Melville Island from 1909 to 1949. In fact Armstrong's

(1947) summary account of the geology of the region is almost exclusively based on Haughton's geology map of 1857 (*in* M'Clintock, 1857). Geological fieldwork shifted to the eastern Arctic Islands in the early 20th century. A northerly trending fold belt was proved to exist on Ellesmere Island as far south as Baumann Fiord by the cumulative field observations of Fielden and De Rance (1878), Schei (1903, 1904) and Bentham (1936, 1941). In 1950, Troelsen presented the first convincing evidence of two phases of Phanerozoic orogenic activity. The younger deformation was observed to affect Mesozoic strata. The older activity was linked to the Acadian-Caledonian deformation of Spitsbergen, Greenland, and northwestern Europe. Eardley (1948, 1951) guessed that the fold belt of Ellesmere Island might be linked to known deformation in the northern Yukon by way of Bathurst, Melville and Banks islands.

By 1950, two aerial photographic surveys of the Arctic Islands had been completed (Greenaway and Colthorpe, 1948; Dunbar and Greenaway, 1956). These first oblique and vertical (trimetregon) stereoscopic images convincingly established the existence of a major belt of folded rocks extending from eastern Bathurst Island to western Melville Island (Fortier and Thorsteinsson, 1953). The western limit of the fold belt remained uncertain: strata on Banks and Prince Patrick islands appeared to be largely flat lying. The age of the fold belt also remained to be determined. These and many other questions, including the potential for hydrocarbons (Fortier et al., 1954), were inspired by the photographs. Geological fieldwork on Melville Island was resumed after the opening of the weather station at Mould Bay. In 1954, E.T. Tozer made a spring and summer reconnaissance by dog-sled of the west side of the island, undertaking both geological mapping and stratigraphic studies. His collected rock samples contained fossil assemblages ranging from Ordovician through Cretaceous age (Tozer, 1956). He spent an additional three weeks the following year on the east end of the island, near Tingmisut Lake (Tozer, 1963a). The most complete survey of the northwestern Arctic Islands, including Melville, was completed by E.T. Tozer and R. Thorsteinsson in one field season of fine weather in 1958. Using a single engine Piper Super-Cub equipped to make unscheduled landings on the tundra, they were able to examine and report on all the major structural features and stratigraphic units exposed at the surface. Their very fine memoir and remarkably accurate 1:500 000 scale geology map is the most important single reference concerning the general geology of the western Queen Elizabeth Islands (Tozer and Thorsteinsson, 1964). These new data were integrated

into the summary accounts of Arctic Islands geology by Thorsteinsson and Tozer (1960, 1970), and Trettin (1972).

Interest by industry in the economic potential of the region began in 1959 (Jones, 1981). Most notable was the early work of J.C. Sproule and Associates Ltd. who conducted extensive photogeological studies and also sent out field parties to the area. Texaco, British Petroleum, Elf (Petropar) and Mobil were also very active in the region during the 1960s. The first exploratory well in the Arctic Islands was drilled near Winter Harbour in 1961 (Dome et al. Winter Harbour No. 1). In 1962, bitumen-impregnated oil sands were discovered in Triassic rocks of Sproule Peninsula. This area was later investigated by J.C. Sproule and Associates (unpublished data), and by Trettin and Hills (1966). Use of the seismic reflection technique by Panarctic Oils Limited began in this area in May, 1968. Reflection surveys supported by gravity and magnetic data were eventually used by Panarctic, Texaco, Chevron, Elf, Norlands, King Resources and other joint venture partners to evaluate the resource potential of the entire western Arctic Islands including the inter-island channels. To date there have been approximately 91 500 line kilometres of 6 to 8 second and some 10 second seismic reflection data acquired in the Arctic Islands (Brent, pers. comm., 1992). The seismic grid on Melville Island includes roughly 5000 line kilometres of reconnaissance-scale data in the southern and northwestern part of the island and an additional 10 000 line kilometres on Sabine Peninsula. An extensive seismic grid also exists in all marine areas around the island, although geophysical coverage in southern Viscount Melville Sound and M'Clure Strait is sparse. There have been 52 wells drilled in the map area. This has led to the discovery by Panarctic of three separate gas fields in the vicinity of northern Sabine Peninsula: the Drake Point, Hecla, and Roche Point fields. Together these accumulations contain 0.27 TCM (9.4 TCF) total undeveloped gas reserves (Panarctic, 1986; Waylett, 1979, 1990). Although studies have been undertaken to determine the feasibility of developing and shipping these reserves to southern markets by both land and sea routes, the fall of world gas prices in the mid-1980s, combined with a glut on the market of conventional gas, has led to a reduced interest in exploration activities on Melville Island, and throughout the Arctic Islands.

Most of the industry-acquired geophysical data remains unpublished. Representative seismic profiles of Melville Island's salt-based fold belt, and of diapiric features near Vesey Hamilton Island were published and interpreted by Fox (1983, 1985) and by Texaco

Canada Resources Ltd. (1983). Subsurface stratigraphy from wells, and contour maps based on the seismic data set are also presented by Fox and Densmore (1992). Regional syntheses of the industry-acquired geophysical data can be found in Daae and Rutgers (1975), Meneley et al. (1975), Henao-Londoño (1977), Stuart-Smith and Wennekers (1977), Hea et al. (1980) and Balkwill and Fox (1982). More recently, Kanasewich and Berkes (1988, 1990) have acquired and commercially reprocessed some 795 line kilometres of industry seismic data from eastern Melville Island and Sabine Peninsula. Their observations on Cambrian(?) and Proterozoic(?) seismic stratigraphy and structure represent a significant contribution to an improved understanding of subsurface geology. Some of their reprocessed lines have been reinterpreted and displayed for this report.

Devonian foreland basin siliciclastic rocks are the dominant component of the exposed succession of Melville Island's fold belt. The major contribution to numerous aspects of the stratigraphy, current nomenclature, sedimentology and paleogeography of this Arctic Islands-wide deposit is found in the comprehensive report of Embry and Klován, (1976). Other published sources on specific aspects of the Ordovician to Devonian strata are provided by McGregor and Camfield (1982), Goodbody (1988, 1993), Embry (1988a) and McGregor (1993). Notable refinements to the stratigraphy of the younger Sverdrup Basin succession of Melville Island since Tozer and Thorsteinsson (1964) include Nassichuk (1965, 1975), Beauchamp et al. (1989a, b), and Majid (1989) for the upper Paleozoic, and Embry (1982, 1983, 1984a, 1984b, 1984c, 1985a, 1985b, 1986, 1988b, 1991b, 1993) and Poulton (1993) for the Mesozoic. Refraction surveys interpreted by Overton (1972, 1982), and Forsyth et al. (1979) have added to an understanding of mid-crustal and deep crustal structure. A full aeromagnetic survey of the island was completed by the Polar Continental Shelf Project between 1962 and 1965. These results are published in 14 maps sheet at 1:125 000 scale, and on 14 additional maps at 1:126 720 (PCSP, 1965, 1987). The regional gravity field has been compiled and discussed by Sobczak and Overton (1984), and Sobczak and Halpenny (1990).

Results of fieldwork carried out in the 1980s on Melville Island can be found in a variety of publications, the most important being the multi-authored volume edited by R.L. Christie and N.J. McMillan (1993). Earlier preliminary publications that deal with different structural aspects of Melville Island area include Beauchamp et al. (1989a, b),

Harrison and Bally (1988), Harrison et al. (1985, 1991) and Harrison (1989, 1993). The current state of understanding of the geological and tectonic setting of Melville Island within the Arctic Islands is provided in Trettin (1989; Fig. 2) and the multi-authored DNAG volume on the Arctic Islands compiled by Trettin (1991). Virtually all the illustrations, data and ideas in the current publication have also been offered in the author's unpublished Ph.D thesis (Harrison, 1991). The present account should be considered an edited and somewhat condensed version of the thesis and reference to the earlier manuscript will not be made again.

Methods of data acquisition

General comments

Data acquired and integrated into this report include field observations synthesized onto a new geology map of Melville and adjacent smaller islands (in pocket), seismic profiles, interpretive structural cross-sections and restored sections, kinematic measurements, potential-field maps, and biostratigraphic data. Methods of geological mapping, cross-section construction and kinematic analysis are dealt with in Chapters 5 through 7. The potential-field maps (Figs. 9, 10) have been acquired from the Lithospheric Geophysics subdivision of the Geological Survey of Canada. Biostratigraphic determinations, listed in Appendix 4, have been compiled and selectively edited from mostly unpublished internal reports held at the Institute of Sedimentary and Petroleum Geology, Calgary. Aspects of field acquisition, digital reprocessing, and interpretation of seismic profiles illustrated in this report are summarized below.

Reflection seismic profiles

The industry reflection seismic profiles utilized for this report include primarily unmigrated paper copies of the original 4 to 6 second stacks obtained from the assessment reports presently held by the National Energy Board (formally the Canadian Oil and Gas Lands Administration). Important new insights into shallow and mid-crustal structure were also obtained from the reprocessing of 1418 line kilometres of reflection survey data. The extent and distribution of all these kinds of seismic data are illustrated in Figure 3. The field acquisition parameters for the reprocessed profiles are tabulated in Appendix 1 and the reprocessing steps are outlined in Appendix 3.

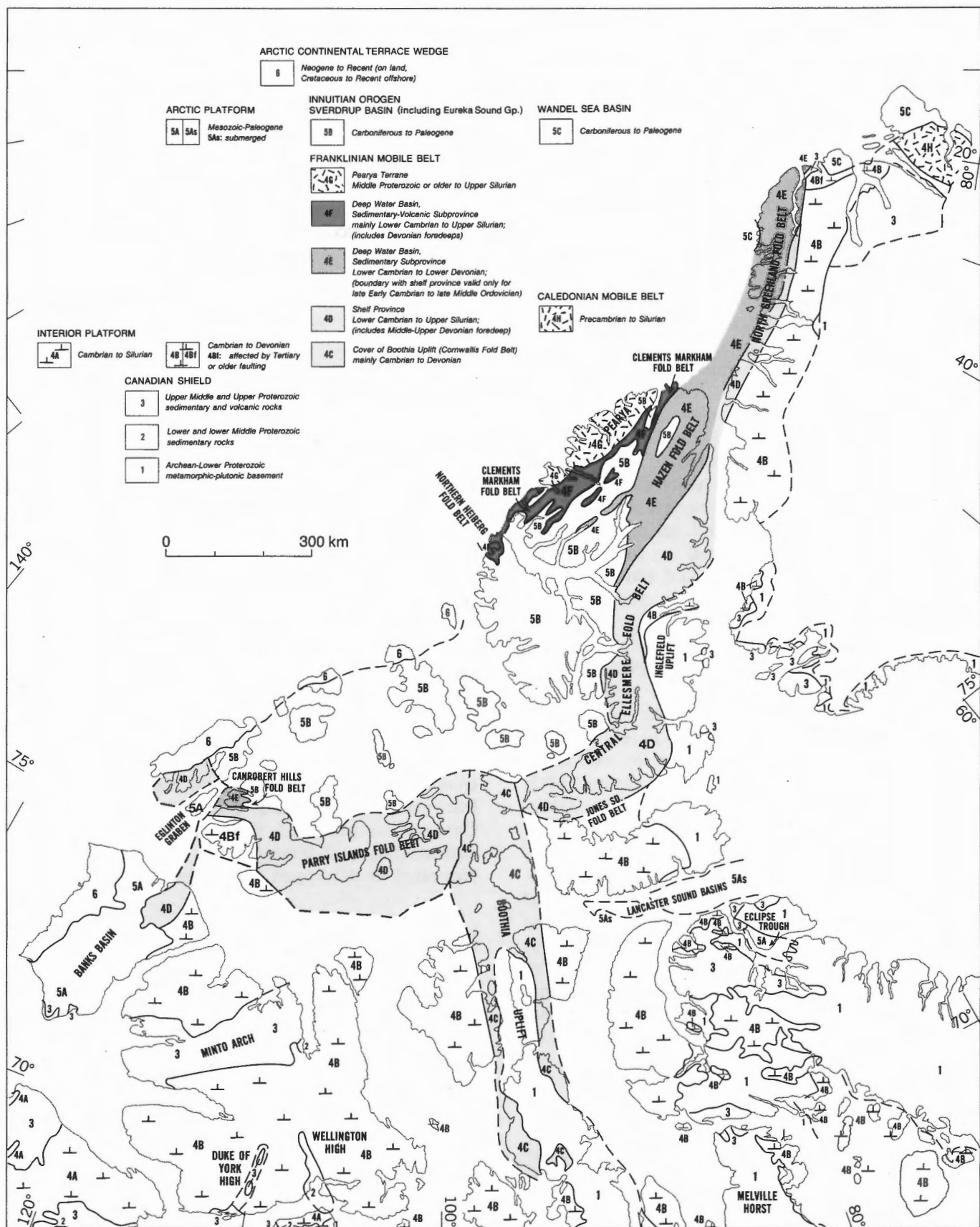


Figure 2. Geological provinces of the Arctic Islands. (Modified from Trettin, 1989.)

The advantages of seismic reprocessing include the migration of previously unmigrated data, display of the entire recorded section (to either 6 or 8 seconds), elimination of some types of linear coherent noise by filtering and deconvolution, digital merging of intersecting stacks to obtain a more regional view of subsurface structure, and the optimization of display parameters for publication. The benefits of the migration step are substantial and include collapsing of diffractions from laterally terminated reflectors and point diffractors, resolution of the shape and location of deep-focus synclines by eradication of "bow ties", and the displacement of dipping reflection segments into each of their correct subsurface locations.

In spite of these attempts to create a reliable manifestation of subsurface structure, interpretive pitfalls remain in the data. These pitfalls include: 1) the loss of signal strength with increasing distance and time beginning with the high frequency information (spherical divergence); 2) lateral variations in primary signal response as a result of field acquisition problems or complex subsurface structure; 3) overmigration hyperbolae; 4) residual diffractions; 5) velocity pull-up or sag due to lateral velocity variations higher in the section; 6) multiples; 7) variations in vertical exaggeration from top to bottom in the profiles as a result of changes in interval velocity as a function of depth of burial, rock porosity and density; and 8) reflector mismatch and polarity reversals between spliced profiles. Examples of the various interpretive pitfalls are tagged on the regional seismic profiles (Sections A to I) and explained in the accompanying marginal notes.

The effects of permafrost are apparently small (Figs. 4, 5). In some porous sandstone units it is possible to identify a base of permafrost reflection (Fig. 4; see also Fig. 122, Note 4). In other units having interlayered porous and impermeable layers, it is possible to detect the downdip limit of frozen porous layers (Fig. 5). Strong impedance contrasts are created between frozen, ice-filled layers and relatively dry and impermeable lenses. In these instances, the base of the permafrost can be drawn downdip, where the impedance contrast generated by the interstitial ice is no longer present. For a complete evaluation of current seismic data acquisition methods, processing procedures, and problems relating to geophysical artifacts, the reader is encouraged to obtain the appropriate references (Telford et al., 1976; Larner et al., 1983; Pieuchot and Sercel, 1984; and Yilmaz, 1987).

Vertical exaggeration on the illustrated profiles in this report ranges from approximately 0.9 for rocks

with interval velocities of 6.0 km s⁻¹ to 1.5 at 3.5 km s⁻¹. Most of the Cambrian through Lower Devonian rocks possess interval velocities in the range of 5.0 to 5.7 km s⁻¹. Vertical exaggeration of the corresponding seismic intervals is negligible. A representative listing of interval velocities and related vertical exaggerations is tabulated in Appendix 3.

The method of seismic stratigraphic analysis adopted in the present account follows from the techniques described initially by Mitchum and Vail (1977) and, more recently, by Vail (1987) and Van Wagoner et al. (1988). The fundamental seismic unit is the sequence (Fig. 6). By definition, a sequence is a generally conformable succession of strata bound above and below by unconformities and their correlative conformable surfaces. (The definitions of these and other sequence stratigraphic terms are summarized by Van Wagoner et al., 1987, 1988.) The upper and lower contacts separating sequences, the variation in seismic depositional facies and the internal boundaries between lowstand, transgressive and highstand seismic stratigraphic components (systems tracts) within each sequence can all be identified or inferred from the various bounding and internal reflection patterns as listed in Table 1. A more reliable interpretation of seismic profiles is provided by accurate correlation of reflectors to formational tops as mapped at surface and as intersected by a network of exploration wells.

Melville Island's seismic profiles have been converted from time to depth using interval velocities as obtained from the sonic logs of exploratory wells (located in Fig. 3 and the geology map, in pocket). These logs, used in combination with density logs and calculated synthetic seismograms, also permit the correlation of drilled formations to seismic units. An example of this technique applied to the Panarctic et al. Sabine Bay A-07 well is illustrated in Figure 7. Additional interval velocity data for Lower Ordovician and older units, presumed to exist below the deepest well penetrations, have been obtained from the interpreted refraction seismic profiles of Overton (1972). Interval velocities of selected near-surface stratigraphic units, including Devonian units lying in synclines within the fold belt, have been obtained from the normal moveout (NMO) correction during seismic data processing as provided by the Dix equation (Dix, 1955). Specific interval velocity values are listed with the seismic unit and formational descriptions (Chapters 2-4), in the marginal notes of Sections A to I, and on Figures 25 to 28 and Table 2 (in pocket).

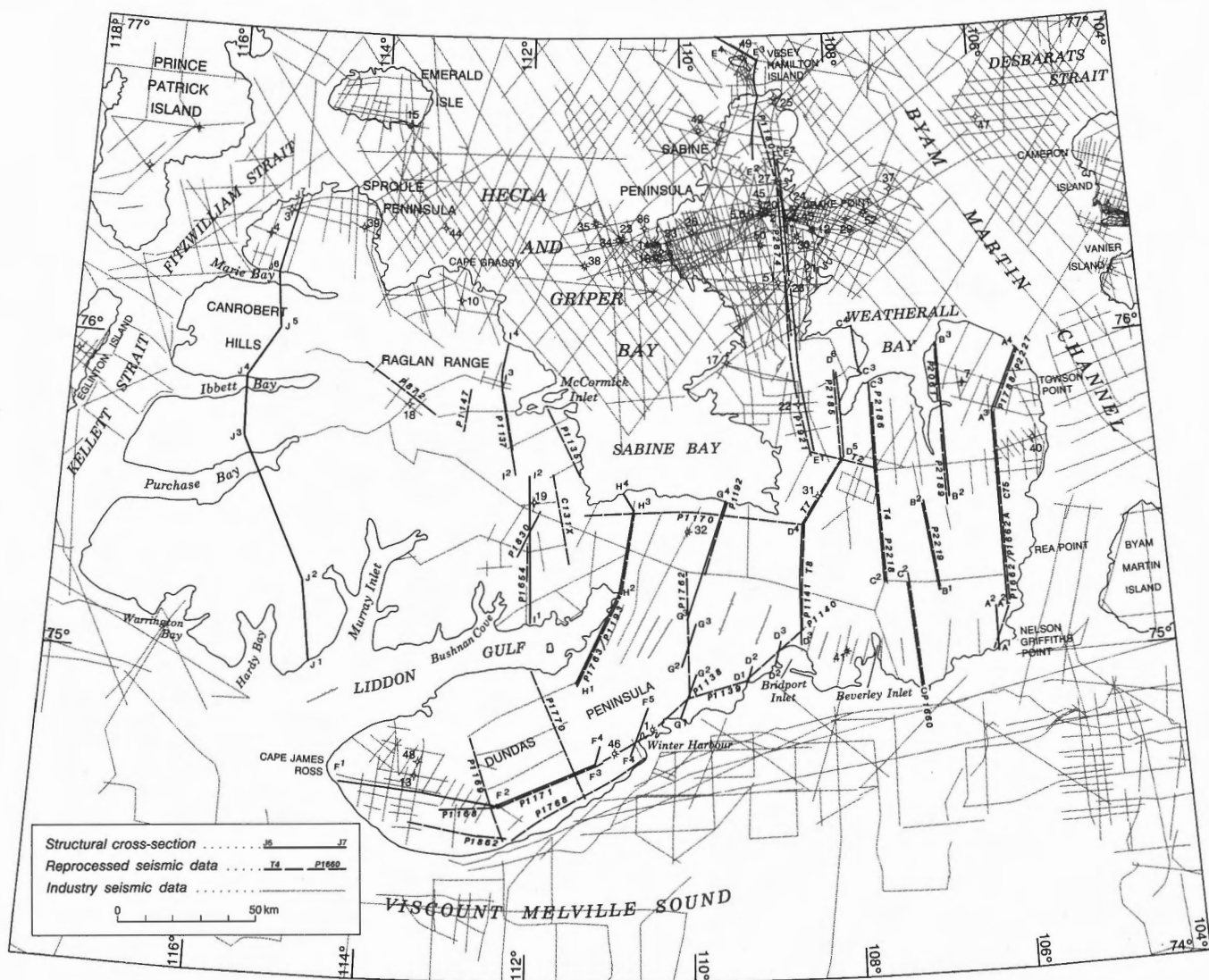


Figure 3. Locations of reflection seismic profiles, wells, and structural cross-sections, Melville Island.

Physical features of Melville Island

Physiography

Melville Island is physiographically divisible into lowlands, uplands, and dissected plateaux. The lowlands of Melville Island were defined by Hodgson et al. (1984) as all areas lying below the 100 m elevation contour (Fig. 8). This includes most of the northern capes and peninsulas and the smaller adjacent islands in Hazen Strait that are also included in this report (Emerald Isle and Vesey Hamilton Island). In the central part of the island, two northerly trending lowland corridors link Hecla and Griper Bay to Viscount Melville Sound. Coastal lowlands, locally up to 15 km wide, also fringe the eastern and southern shores of Melville Island, and the coasts of Hecla and Griper Bay as far north as McCormick Inlet. The

largest lowland areas in this region are associated with the drainage basins of the Sabine, Mecham, Byam and Baldwin rivers. The subdued topography of the coastal lowlands is continuous, with extensive shallow-marine areas (<200 m deep) that include southern Hecla and Griper Bay, Liddon Gulf, and Viscount Melville Sound east of Winter Harbour. In the western part of the island, lowlands are small and generally restricted to fan deltas and narrow bay-head braid plains. Bedrock outcrop is rare in all lowland areas. Good exposures are restricted to the incised convex banks of meandering river systems.

Dissected plateaux represent tablelands underlain by horizontal bedrock. The largest of these areas are found in the Blue Hills region west of Murray Inlet, where the plateau top stands at up to 775 m. The plateau is lower to the east and south, and lies at 300 m

SCHEDULE OF WELLS
(listed chronologically by completion date)

1	Dome et al Winter Harbour No. 1 A-09; T.D. 3823.1 m (09/61)
2	Panarctic Drake Point N-67; T.D. 2576.8 m (04/69)
3	Panarctic Sandy Point L-46; T.D. 2101.6 m (05/69)
4	Panarctic Marie Bay D-02; T.D. 1272.5 m (08/69)
5	Panarctic Drake Point L-67; T.D. 3252.5 m (09/69)
6	Panarctic Drake Point L-67A; T.D. 4119 m (03/70)
7	Panarctic Towson Point F-63; T.D. 1561.5 m (03/70)
8	Panarctic Homestead Hecla J-60; T.D. 3616.5 m (05/70)
9	Panarctic Drake Point K-67; T.D. 974.8 m (07/70)
10	Sun KR Panarctic Kitson R. C-71; T.D. 2766.1 m (11/70)
11	Panarctic Tenneco et al POR Drake Point F-16; T.D. 1478.3 m (05/72)
12	Panarctic Tenneco et al POR Drake B-44; T.D. 1396.0 m (09/72)
13	Panarctic Dome Dundas C-80; T.D. 3999.4 m (10/72)
14	Panarctic Tenneco et al POR Hecla F-62; T.D. 1219.2 m (11/72)
15	BP et al Emerald K-33; T.D. 3660.6 m (12/72)
16	Panarctic Tenneco et al Hecla I-69; T.D. 1456.6 m (02/73)
17	Panarctic Eldridge Bay E-79; T.D. 3048.0 m (03/73)
18	Panarctic Tenneco et al Zeus F-11; T.D. 949.1 m (05/73)
19	Panarctic Apollo C-73; T.D. 3665.2 m (05/73)
20	Panarctic et al Drake Point D-68; T.D. 5415.1 m (06/73)
21	Dome Arctic Venture Sherard O-54; T.D. 1228.3 m (10/73)
22	Dome Panarctic Texex Weatherall O-10; T.D. 2286.0 m (12/73)
23	Panarctic Tenn et al CS W. Hecla N-52; T.D. 938.8 m (03/74)
24	Panarctic POR Homestead Drake F-78; T.D. 1356.4 m (05/74)
25	Panarctic Hmstd POR N. Sabine H-49; T.D. 3811.5 m (05/74)
26	Panarctic et al Chads Creek B-64; T.D. 5036.2 m (06/74)

Facies change (defined, approximate)
Undetermined fault (defined, approximate; solid circle indicates downthrow side)
Strike slip fault (arrow indicates direction of movement)
Extension fault (defined, approximate)
Anticline (defined, approximate)
Syncline (defined, approximate)
Line of section

27	Panarctic Tenn et al Collingwood K-33; T.D. 2046.1 m (08/74)
28	Panarctic Dome et al Sherard Bay F-14; T.D. 1342.9 m (10/74)
29	Panarctic Gulf et al East Drake I-55; T.D. 1188.7 m (03/75)
30	Panarctic Tenn et al Drake D-73; T.D. 1360.9 m (04/75)
31	Texex King Point West B-53; T.D. 3126.6 m (09/75)
32	Panarctic et al Sabine Bay A-07; T.D. 5192.9 m (10/75)
33	Panarctic et al E. Hecla C-32; T.D. 1341.1 m (11/75)
34	Panarctic W. Hecla P-62; T.D. 1127.8 m (01/76)
35	Panarctic Tenn CS N.W. Hecla M-25; T.D. 1207.0 m (03/76)
36	Panarctic Tenn et al W. Hecla C-05; T.D. 1237.5 m (04/76)
37	Panarctic AIEG N.E. Drake P-40; T.D. 1295.4 m (02/77)
38	Panarctic S.W. Hecla C-58; T.D. 1219.2 m (04/77)
39	Panarctic AIEG et al Depot Island C-44; T.D. 2689.1 m (04/77)
40	Panarctic et al Richardson Point G-12; T.D. 3355.8 m (10/77)
41	Panarctic et al Beverley Inlet G-13; T.D. 4060.5 m (11/77)
42	Panarctic et al AIEG Roche Pt. J-43; T.D. 2881.9 m (01/78)
43	Panarctic Drake F-76; T.D. 935.7 m (03/78)
44	Panarctic Norcen AIEG et al Grassly I-34; T.D. 975.4 m (03/78)
45	Panarctic et al Drake Point K-79; T.D. 1725.2 m (05/78)
46	Dome Panarctic et al Hearne F-85; T.D. 501.8 m (10/78)
47	Panarctic Norcen AIEG Desbarats B-73; T.D. 330.6 m (02/79)
48	Dome Panarctic N. Dundas N-82; T.D. 4100.0 m (06/79)
49	Panarctic BP AIEG Vesey A-27; T.D. 890.5 m (06/80)
50	Panarctic et al Marryatt K-71; T.D. 5467 m (10/82)
51	Panarctic et al Sherard Bay F-34; T.D. 5449.3 m (10/83)
52	Panarctic et al East Drake L-06; T.D. 1300 m (02/85)

Erosional limit (defined, approximate)
Isopachs, in metres x 100
Data point
Spot thickness, in metres
Well with show of oil and gas
Well with show of gas
Well with show of oil
Gas well
Oil well
Dry well

Figure 3. (cont'd.)

on westernmost Dundas Peninsula. The plateau margins in these areas terminate in steep coastal cliffs, deeply incised canyons, and escarpment-associated talus fans. Bedrock is well exposed in these cliff areas, although the thickness of the stratigraphic section is limited by the horizontal attitude of the strata and the modest topographic relief (200–600 m). Steep topography continues into the offshore, with water depths rapidly reaching 200 to 400 m in eastern Kellett Strait, northern M'Clure Strait, and northern Viscount Melville Sound south of Dundas Peninsula.

Thicker rock sections on land are exposed in upland areas where bedrock has been either tilted or folded. Included here are all areas above the 100 m elevation contour on southern Sabine Peninsula, southeastern and central Melville Island east of Murray Inlet, Raglan Range and Canrobert Hills. In these regions, outcrops are found in incised river valleys or on hog-back ridges and cuestas. The most extensive area of well exposed bedrock occurs in the Canrobert Hills region, where differential erosion of tightly folded lower Paleozoic mudrocks and carbonates has produced up to 550 m of local relief.

Vegetation is limited to lowland sedge and grass meadows, and upland lichen, saxifrage and dwarfed willow tundra (Edlund, 1982). In upland areas above

about 400 m, the present erosion surface is entirely devoid of vegetation. Permanent though stagnant ice caps, presumably relicts of the latest Pleistocene glaciation, occur on high plateau surfaces south of Ibbett and Purchase bays, and some of the ancient drainage systems that dissect the upland surface of Raglan Range are partly or entirely filled with glacier ice. Small perennial banks of ice and snow are also common at lower elevations. Other surface materials between outcrop areas include vast expanses of frost-shattered felsenmeer, talus, and a patchy veneer of glaciogenic sediments, Pleistocene and Recent fluvial gravels, and raised strandline and deltaic deposits.

The plateau and upland surface of Melville Island represents a tilted, east-facing peneplain. The elevation of this surface ranges from a maximum of 775 m in the Blue Hills to less than 200 m in the southeastern part of the island. The age of the peneplain and a related question concerning the age of uplift and tilting of the peneplain is discussed in Chapter 5.

Glacial features

Glacial deposits, landforms and related aspects of the Pleistocene glacial history of eastern and central

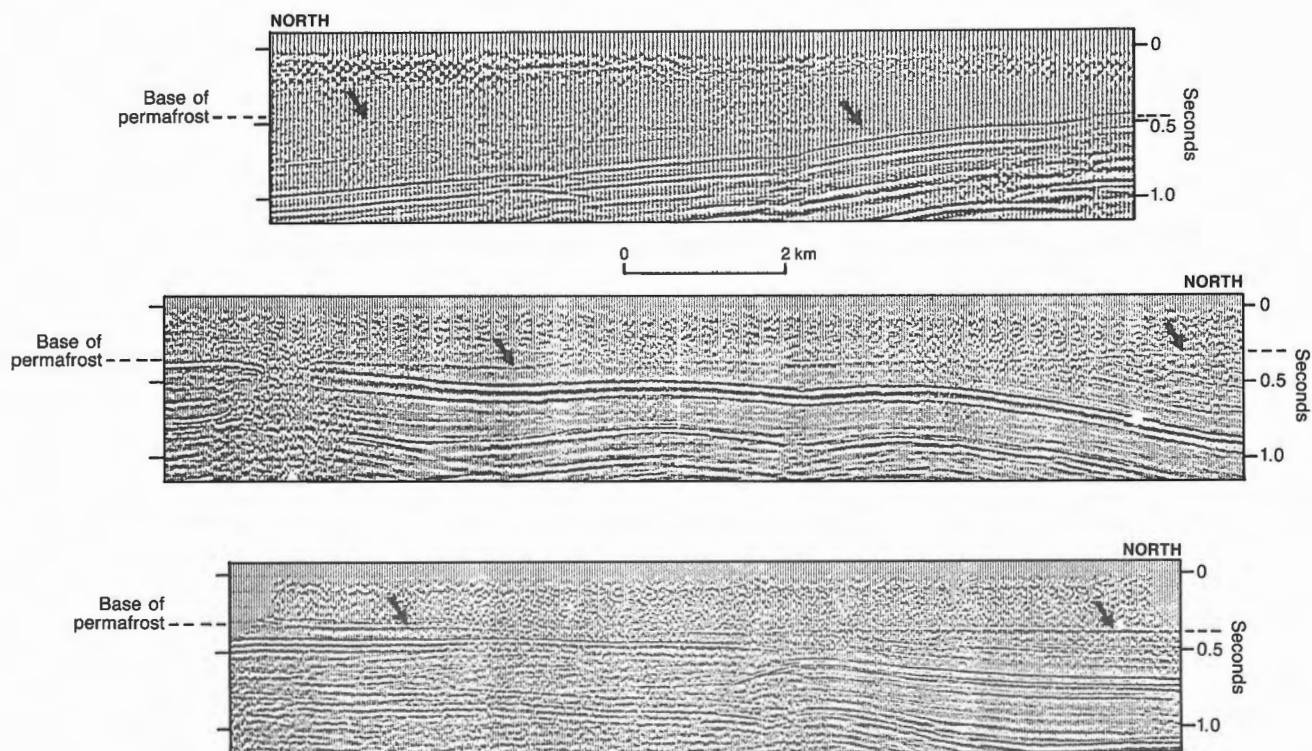


Figure 4. Seismic expression of the base of the permafrost reflector in the Lower Triassic Bjorne Formation at 300–400 ms. Indicated depth of permafrost is from 495 to 660 m below surface (at 3.3 km s^{-1}).

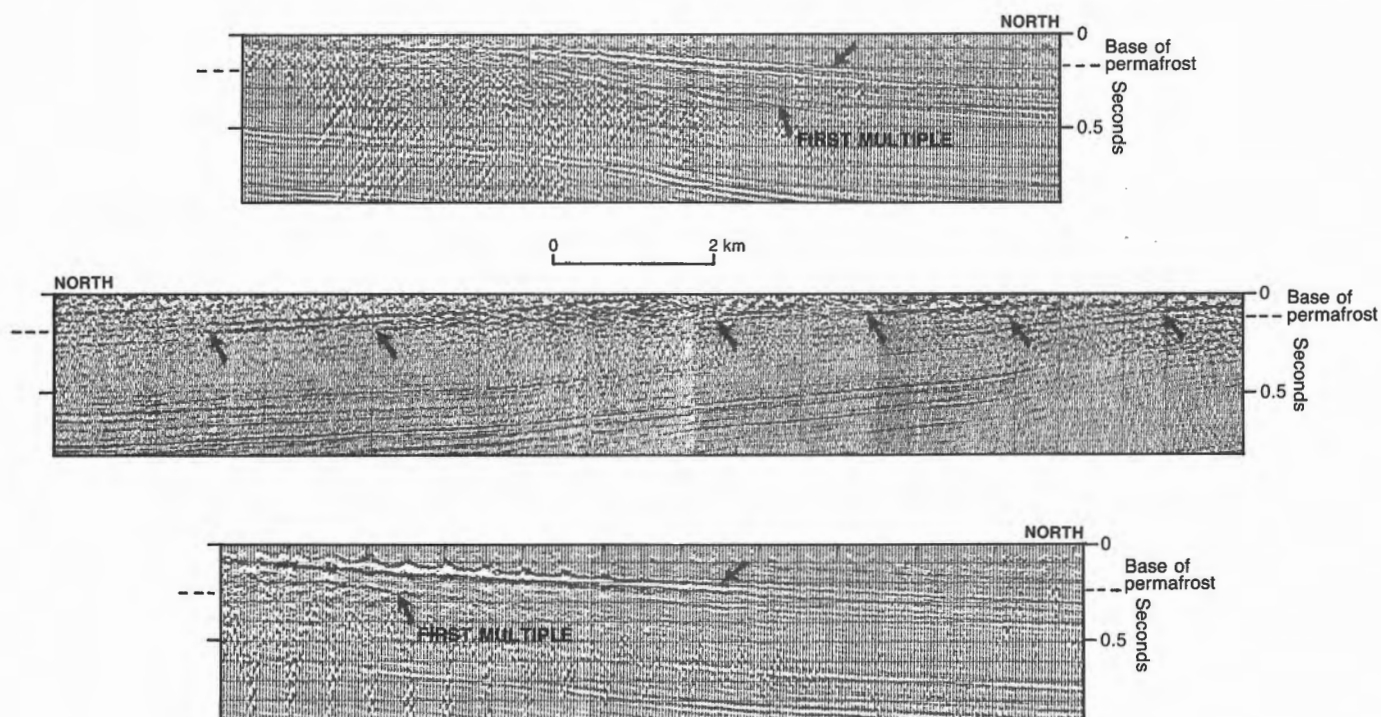


Figure 5. Seismic expression of the downdip limit of permafrost in the Christopher Formation, defined by downdip amplitude decay of porous frozen layer(s) imbedded in low-velocity mudrock. Amplitude fall-off is attributed to reduced velocity of the porous layer(s) in the unfrozen state below the base of permafrost. Indicated depth of permafrost is 230 ms or 380 m at 3.3 m s^{-1} .

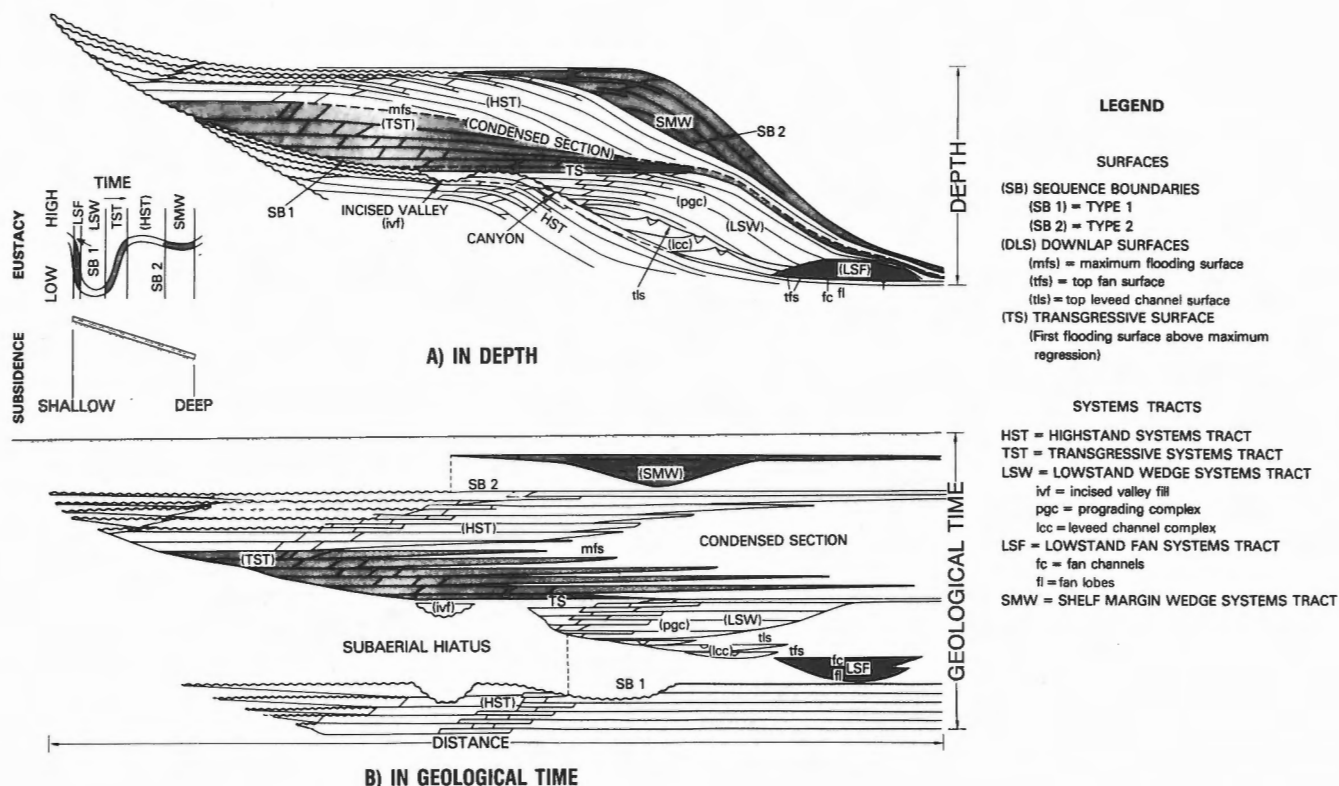


Figure 6. Sequence stratigraphic model. (From Haq et al., 1988.)

Melville Island are known from the field surveys of Barnett et al. (1975) and Hodgson et al. (1984), respectively. General features of Quaternary stratigraphy and chronology for the Melville Island region are reviewed by Hodgson (1989). The Late Wisconsinan retreat of ice from the Arctic Islands has been summarized by Dyke and Prest (1987). Stratigraphic and paleomagnetic study of Plio-Pleistocene deposits preserved on Banks Islands have allowed Barendregt and Vincent (1990) to recognize three full glacial/interglacial cycles of Early, Middle and Late Pleistocene ages in the southwestern Arctic Islands.

The extent to which the two earlier glaciations have affected Melville Island remains uncertain. However, evidence indicates that on at least four occasions during the later Pleistocene, lobes of the Laurentide Ice Sheet of northwestern Canada crossed Viscount Melville Sound and reached the southern edge of Melville Island. The depositional history of these ice lobe expansions and subsequent retreats is recorded in morainal and ice contact deposits of Dundas Peninsula, Liddon Gulf and Bridport Inlet areas (Hodgson et al., 1984). In addition to these later Pleistocene glacial advances from the southern mainland, widely scattered erratics of plutonic and metamorphic rocks testify to at least one complete and extensive glaciation of Melville Island, presumably

during Early or Middle Pleistocene time. At other times, the highland areas of the Blue Hills, Raglan and Baldwin Walker ranges supported small active ice caps that fed ice streams into the adjacent valleys.

The last retreat of the Laurentide ice (in the Late Wisconsinan) was accompanied by a postglacial marine advance in all coastal areas of the island. The maximum marine limit, which occurred at about 11 000 years bp, is indicated by the position above present sea level of raised strandline deposits. The magnitude of postglacial emergence ranges to more than 100 m in parts of eastern Melville Island.

Potential field

Regional Bouguer gravity anomaly

A Bouguer gravity anomaly map of part of the northern mainland and western Arctic Islands (including Melville Island), provided by the Earth Physics Branch of the Geological Survey of Canada, is shown in Figure 9 (see also Fig. 187). Areas of thick continental crust underlain by Precambrian shield are characterized by irregular strongly negative gravity anomalies in the -40 to -75 mgal range. The largest of

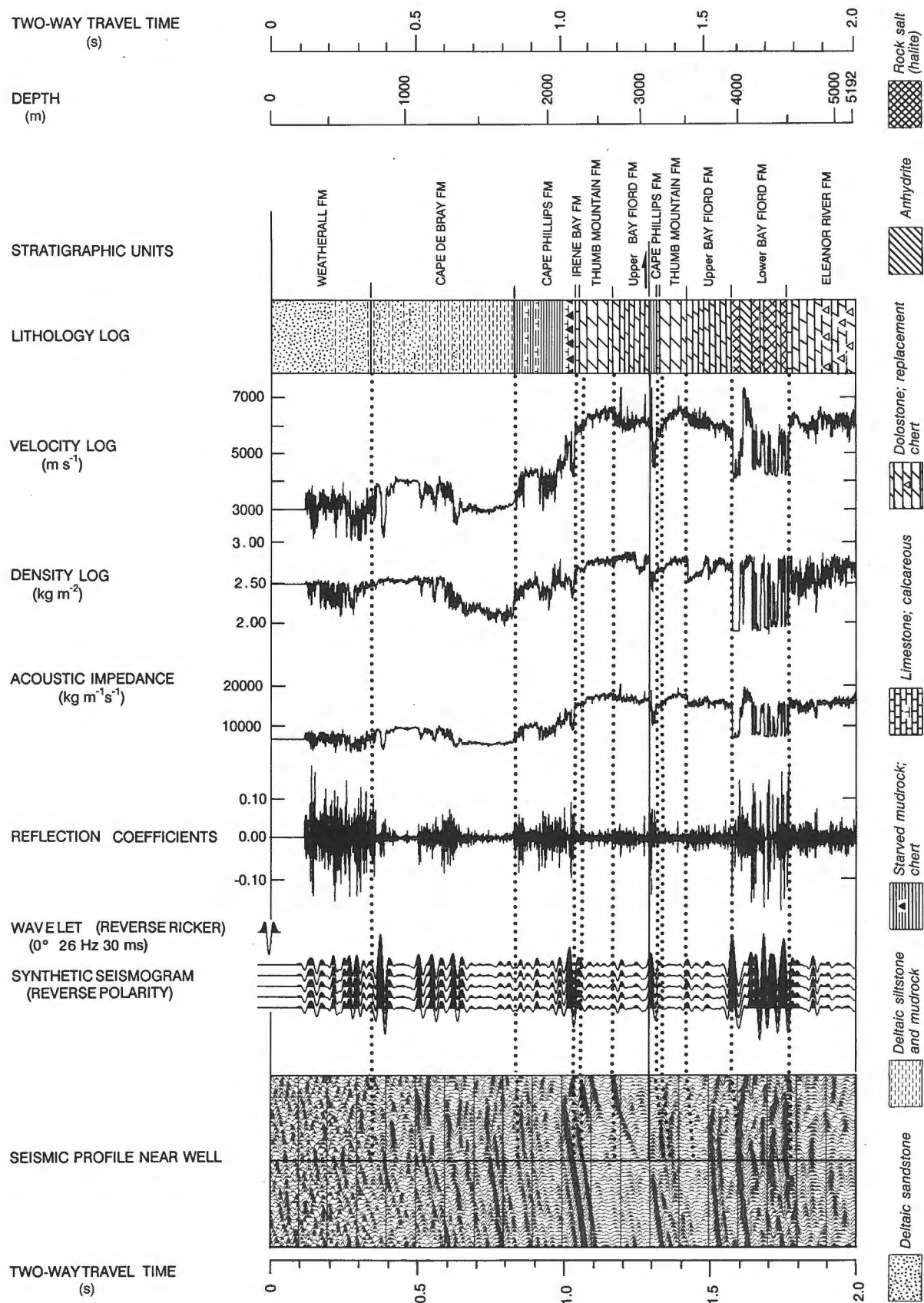


Figure 7. Correlation of sonic, density, lithological, and various synthetic logs of the Panarctic et al. Sabine Bay A-07 well with a nearby portion of reflection seismic profile P1192. The surface well location marked on P1192 has been projected 9.9 km east-southeast and down plunge from the actual well site.

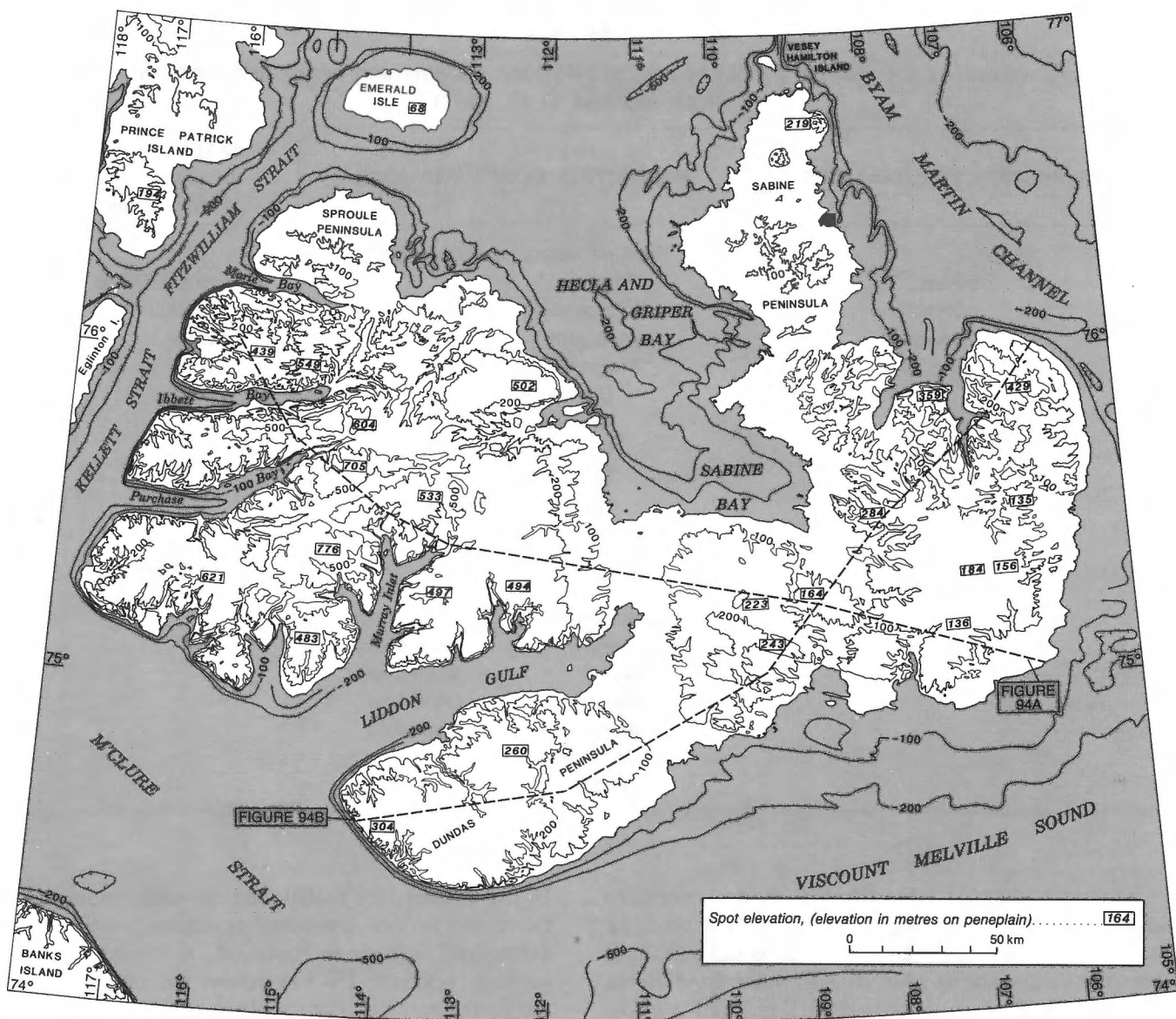


Figure 8. Topography and bathymetry of the Melville Island area.

these areas is located on the northern mainland, where Archean rocks of the Slave and Rae cratons, and Lower Proterozoic rocks of the Wopmay and Thelon orogenic belts are exposed at the surface (Hoffman, 1987, 1989). Northerly trending negative Bouguer anomalies of central and eastern Victoria Island and M'Clintock Channel indicate a northward continuation of Precambrian basement beneath thin Paleozoic cover in these areas. Northeasterly trending anomalies of northwestern Victoria Island also parallel Middle and Upper Proterozoic structural fabric as exposed in Minto Arch (Thorsteinsson and Tozer, 1962).

Moderately negative and positive (-30 to +10 mgal) northerly trending gravity anomalies over Boothia

Peninsula, and Prince of Wales and Cameron islands are spatially associated with areas of Tertiary-age uplift of basement and are parallel to the Proterozoic structural fabric exposed in Boothia Uplift. These northerly trends extend north of Barrow Strait along the axial trace of Boothia and Cornwall uplifts as far north as Cornwall Island in the central Sverdrup Basin (upper right corner of Fig. 9). In contrast, the northerly trending anomalies of Victoria Island are truncated by an easterly trending anomaly high (-10 to -30 mgal) located over southern Viscount Melville Sound, and a parallel low (-30 to -42.5 mgal) located over the northern part of the sound and southeastern Melville Island. The low continues to the northwest along the length of M'Clure Strait.

TABLE 1

Bounding and internal (within sequence) reflection patterns and interpreted bedforms
(from Mitchum et al., 1977)

REFLECTION TERMINATIONS	REFLECTION CONFIGURATIONS	EXTERNAL FORMS (of sequences and seismic facies units)
Lapout Baselap Onlap Downlap Toplap Truncation Erosional Structural Concordance (no termination)	Principal stratal configuration Parallel Subparallel Divergent Prograding clinoforms Sigmoid Oblique Complex sigmoid-oblique Shingled Hummocky clinoform Chaotic Reflection-free Modifying Terms Even Wavy Regular Irregular Uniform Variable	Sheet Sheet Drape Wedge Bank Lens Mound Fill

Most of Melville Island has a modest negative anomaly field (0 to -30 mgal; Fig. 187). Worth noting is a linear negative anomaly (-10 to -20 mgal) extending over the axial trace of Blue Hills Syncline from Hecla and Griper Bay to Warrington Bay, and weakly positive and negative anomalies (-5 to +12.5 mgal) over the topographically elevated Raglan Range, the western coasts of the island, the southern rim of Sverdrup Basin, and areas of uplifted and exposed Lower Devonian limestone around Weatherall Bay.

Magnetic field

A regional magnetic map of the northern mainland of Canada and part of the western Arctic Islands is displayed in Figure 10 (part of Geological Survey of Canada, Map 1255A, 1987). High amplitude, northeasterly trending anomalies located over the Thelon orogenic belt apparently extend from the mainland across Queen Maud Gulf, King William Island and M'Clintock Channel to Peel Sound near the west coast of Somerset Island (Hoffman, 1987, 1989).

In this respect, the gravity and magnetic anomalies in these areas are presumably caused by related anisotropic features in basement. A strongly negative anomaly (-300 to -750 nT) defines the eastern edge of the Slave Craton on the mainland east of the settlement of Bathurst Inlet. This ancient plate boundary (Hoffman, 1987, 1989) may also extend into the Arctic Islands along the trace of a similar negative anomaly (-300 to -400 nT) located over southern M'Clintock Channel and Prince of Wales Island.

The magnetic data for Victoria Island, although sparse, are not inconsistent with an extrapolated extension of the Slave Craton and Wopmay Orogen beneath Paleozoic and Proterozoic sedimentary cover. Most of the islands and channels north of Victoria and Banks islands are within an extensive magnetically featureless region (-225 to +25 nT); presumably an indication of the low susceptibility of sedimentary cover and the great depth to Precambrian crystalline basement. Magnetic spot highs, such as the one located west of Weatherall Bay are associated with exposed gabbro dykes. These and other local magnetic features of Melville Island region are discussed in Chapter 7.

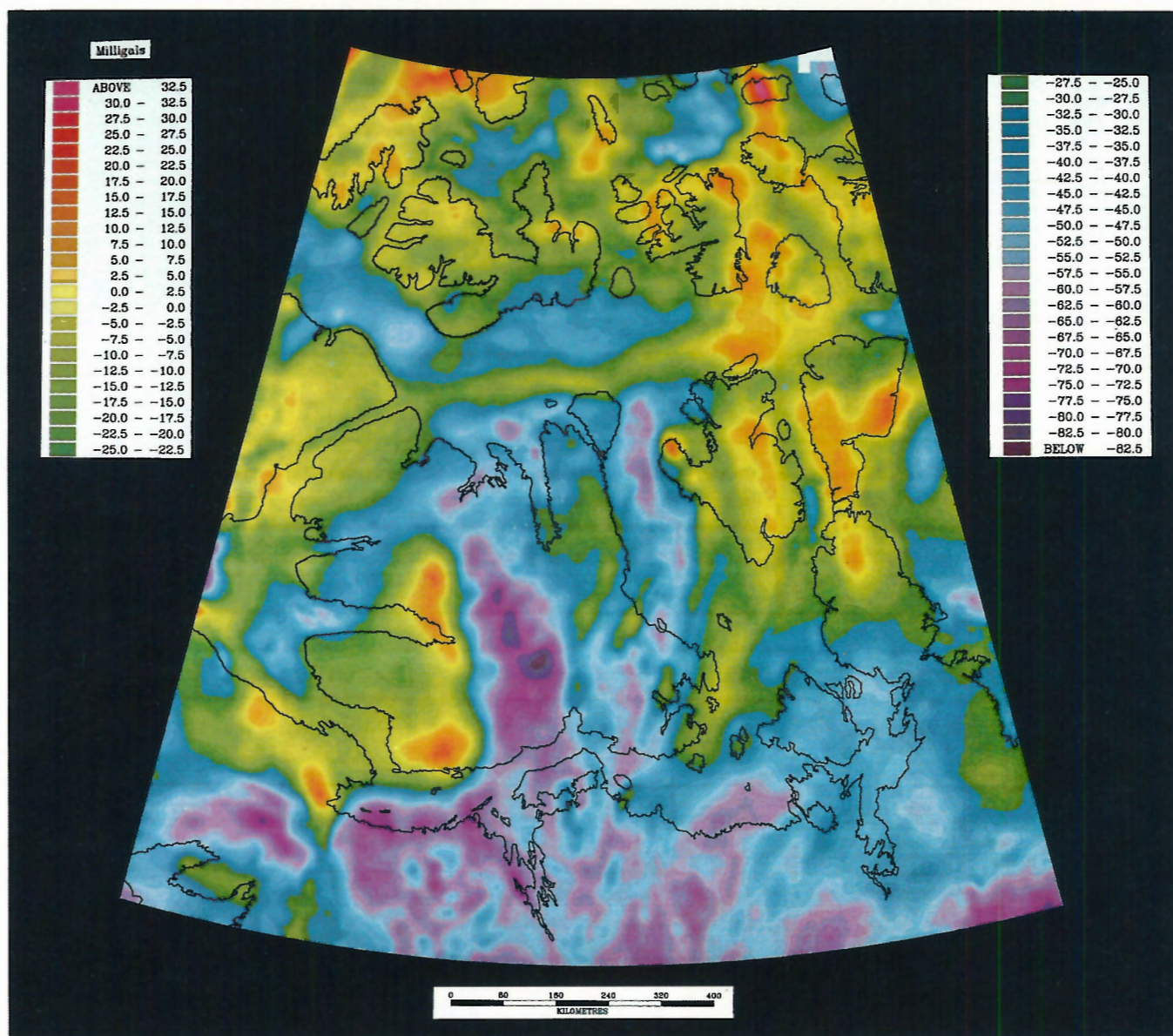


Figure 9. Bouguer gravity anomaly map of the western Arctic Islands. (Courtesy of the Lithospheric Geophysics Sector of the Geological Survey of Canada.)

Stratigraphic successions (Precambrian(?) through Cenozoic)

The stratigraphy of the Melville Island area is divisible into four major successions (Fig. 11; Table 2, in pocket). These include:

1. Approximately 24 to 29 km of strata defined by seismic above the Mohorovičić Discontinuity (Moho) and below a geophysically-defined sub-Cambrian(?) angular unconformity (Precam-

brian(?) seismic stratigraphy) that embraces a single seismic refraction unit and at least four coherent reflection packages.

2. Eight to thirteen kilometres of Cambrian(?) through Devonian strata (inclusive), including seismically-defined Cambrian(?) units, that were deposited in shelf, intrashelf basin and embayment, shelf rim, slope, deep water basin, and blanketing foredeep basin settings (Franklinian Succession).

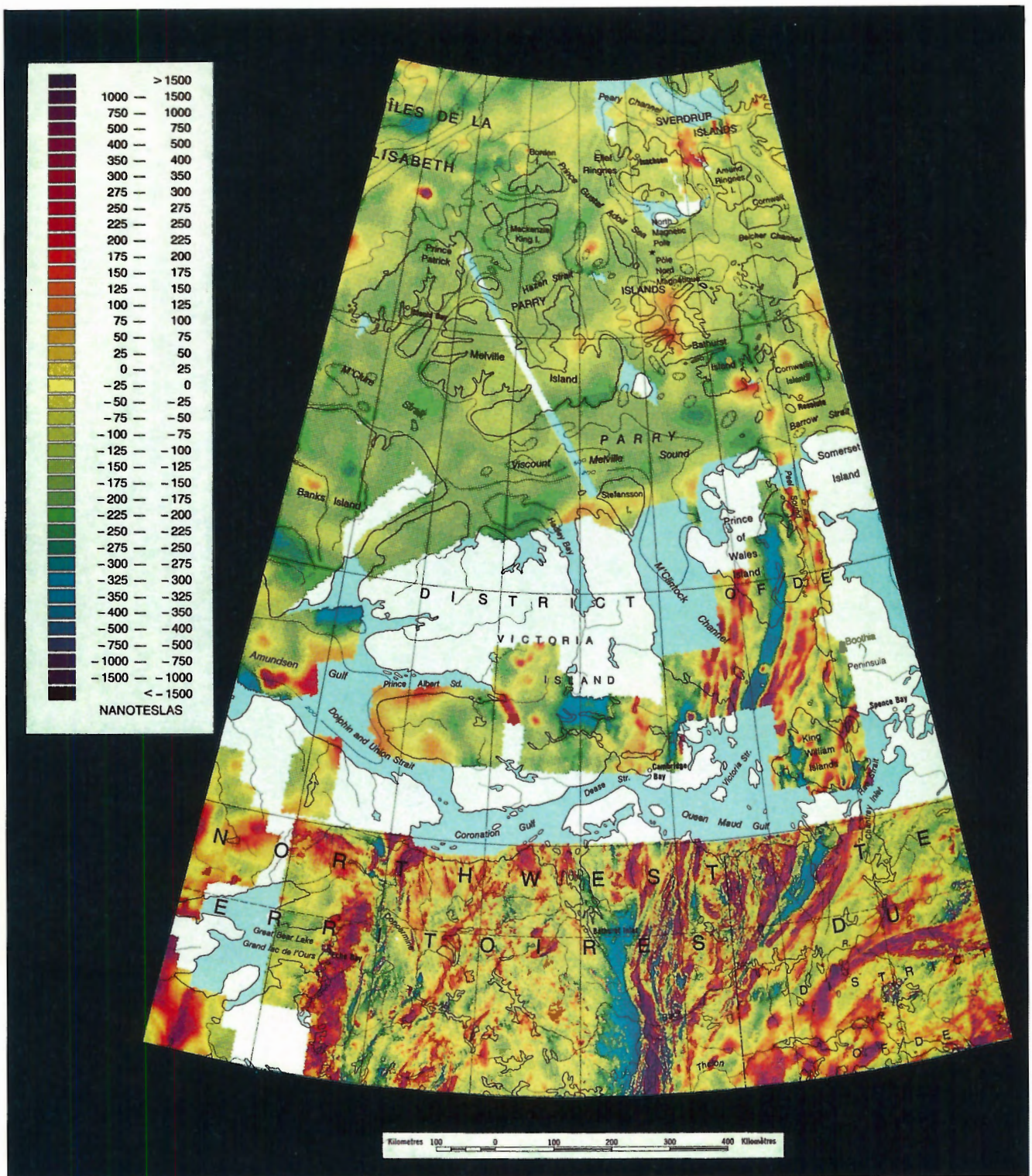


Figure 10. Magnetic anomaly map of the western Arctic Islands.
(Reproduced from Geological Survey of Canada, 1987.)

3. Two to at least seven kilometres of upper Paleozoic, Mesozoic and pre-Eocene Tertiary strata of the Sverdrup Basin and a thin and

discontinuous veneer (<200 m) of partly age-equivalent formations deposited on upturned and peneplained lower Paleozoic strata beyond the

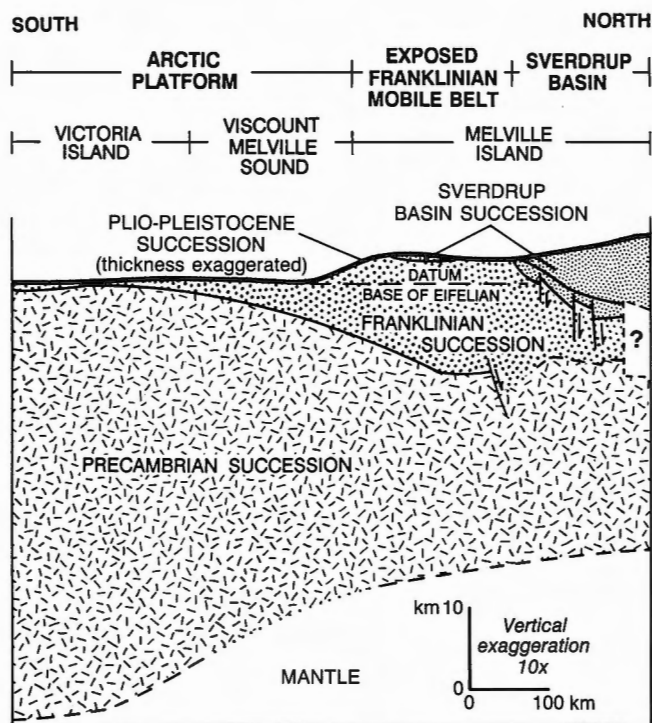


Figure 11. Schematic crustal-scale cross-section of the major rock successions of the Melville Island area.

Sverdrup Basin margin and preserved in outliers across southern Melville Island (Sverdrup Basin Succession).

4. Up to 110 m of Neogene(?), Pleistocene and Holocene gravels and finer surficial materials. Miocene-Pliocene strata are known only in isolated outliers in parts of central and south-eastern Melville Island.

Thermal maturity and metamorphic grade

Geographic variations of thermal maturity as a function of sediment age for the general Arctic Islands region have been reported by Henao-Londoño (1977) and Utting et al. (1989a). Detailed variations for strata of Melville Island have been obtained and interpreted by Gentzis (1990). Extensively preserved strata of Devonian age on Melville Island possess vitrinite reflectance values that range from 0.5% Ro at the surface to a maximum of 1.65% Ro at a depth of 3 km. This is in the normal range of oil generation or catagenesis for shallow sedimentary rocks (Tissot and Welte, 1984). Middle Ordovician rocks, intersected by exploratory wells at a depth of 5 km, possess vitrinite-equivalent reflectance values (measured on bitumen) of about 3.5% Ro. These data taken together point to paleotemperatures of 60–70°C at the surface, ranging to 185–195°C 5 km below surface. Estimated maximum paleogeothermal gradient for these rocks is close to 25 mK m⁻¹. By extrapolation, the transition from the metagenesis stage of burial metamorphism to the prehnite-laumontite facies of very low grade regional metamorphism would be expected to occur at about 4% Ro or 200°C and 5.5 km depth (Winkler, 1976; Tissot and Welte, 1984). Paleotemperatures at the presumed base of the Cambrian situated variably at 10 through 14 km below surface may have experienced temperatures of 300 to 400°C with the transition to greenschist facies metamorphism at 350°C and 12 km depth (Winkler, 1976).

Vitrinite reflectance ranges for younger sediments of Melville Island are 0.7–1.9% in the upper Paleozoic section, up to 1.0% Ro in the Triassic, and 0.3–0.5% Ro for Jurassic through Paleocene strata. Scattered wood fragments occurring in Neogene and younger sediments are not coalified.

CHAPTER 2

PRECAMBRIAN(?) SEISMIC STRATIGRAPHY AND STRUCTURE

General comments

Kanasewich and Berkes (1988, 1990) were the first to recognize a coherent seismic stratigraphy under a widespread, geophysically-defined angular unconformity that lies at 5 km below known Lower Ordovician rocks of southeastern Melville Island and

Dundas Peninsula. The seismic units that we propose differ somewhat from those recognized by Kanasewich and Berkes, who were inclined to name reflections rather than the geophysical space between reflectors.

In this report, four Precambrian(?) seismic successions are recognized (Figs. 12, 13; Section B, Note 5; Section F, Note 6). These include: 1) sub-Proterozoic(?) acoustic basement (Unit sAP); 2) a lower unreflective succession (Unit sP1); 3) a strongly

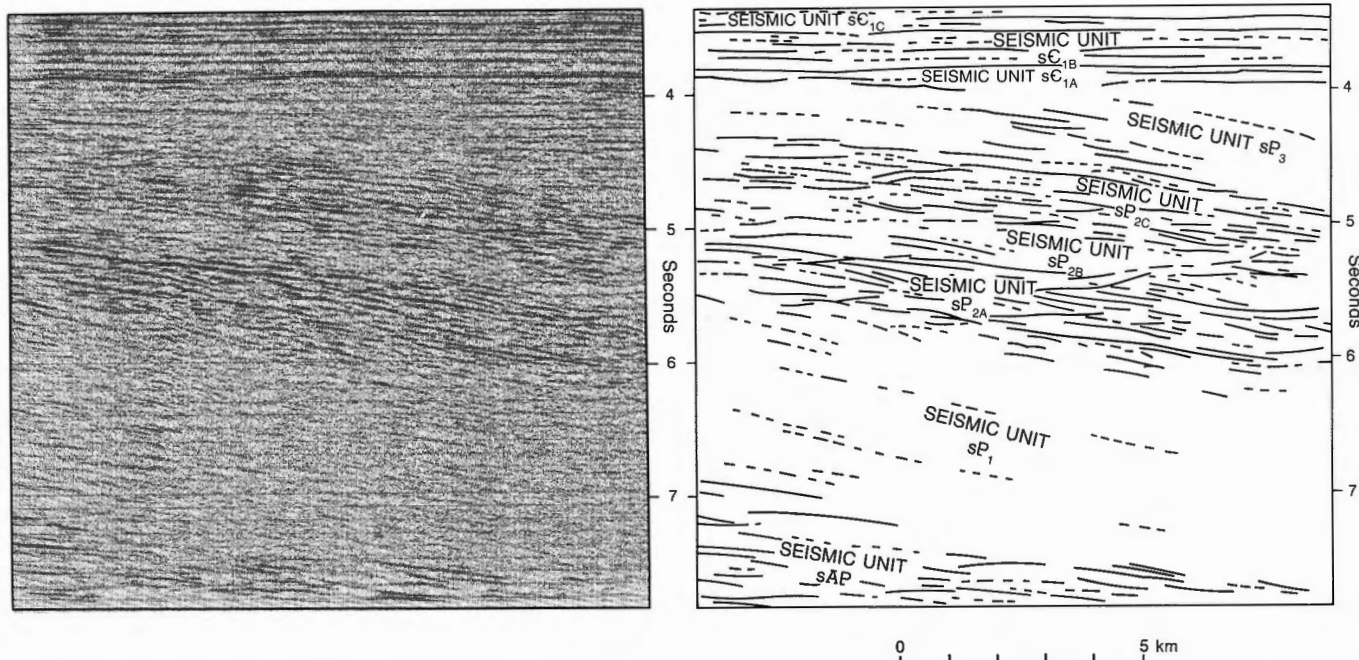


Figure 12. Precambrian(?) seismic stratigraphy, subsurface Dundas Peninsula; on a part of seismic profile P1168 (Section F). Vertical exaggeration is 0.88 for sAP through sP₂; 0.96 for sP₃ through sC₁.

reflective succession (Unit sP₂), locally divisible into three informal members (units sP_{2A}, sP_{2B} and sP_{2C}), and; 4) an upper, unreflective succession (units sP₃ and sP_C) overlain unconformably by a thick Cambrian(?) and younger package of seismic reflections. The interval velocity of units sAP, sP₁ and sP₂ is approximately 6.2 km s⁻¹. This corresponds to the velocity determined by Overton (1972) for an intermediate refraction layer above the Moho and below a mid-crustal discontinuity at 10 to 12 km. A slightly lower velocity is assumed for units sP₃ and sP_C (5.7 km s⁻¹), both of which are acoustically similar to incised valley fill (Unit sC_{1A}) at the base of the Cambrian(?) succession.

The term acoustic basement is reserved for that part of the seismic reflection data from which there has been no coherent response. As well as the aforementioned Precambrian(?) units, all of which can represent acoustic basement, an informal name (unit sP) is adopted to embrace nondiagnostic seismic data below seismic units believed to be part of the Cambrian(?) succession.

It is worth noting that all the supposed Precambrian units lie at depths in excess of 10 km, and that the maximum paleogeothermal gradient has been at least 25 mK m⁻¹ (as extrapolated from the known gradient in the upper 5 km of section). From this it can be

presumed that the minimum metamorphic grade of the youngest Precambrian rocks must be close to or within greenschist facies.

Description of seismic units

Sub-Proterozoic(?) acoustic basement (Unit sAP)

Location and distribution. Identified at and below 6.4 s on many seismic lines of Dundas Peninsula (Section F) and southeastern Melville Island (Sections B, C, D, G and H). Kanasewich and Berkes (1990) have also tentatively identified the reflection above this seismic unit at a depth of 9.5 to 10 s on several seismic lines of southern Sabine Peninsula.

Thickness. The imaged part of Unit sAP lies within the middle part of a seismic refraction layer above the Moho, which on central and western Melville Island occurs at a depth of 35 to 40 km (average 37 km; Overton, 1972). The maximum known thickness of Unit sAP on seismic reflection profiles is 1.3 s, or 4.1 km at 6.2 km s⁻¹. If the lower limit of Unit sAP is assumed to correspond to the refraction Moho Discontinuity, then Unit sAP has a total thickness of approximately 15 to 19 km. Thickness variations are attributed to structural irregularities imaged on the upper surface of the unit.

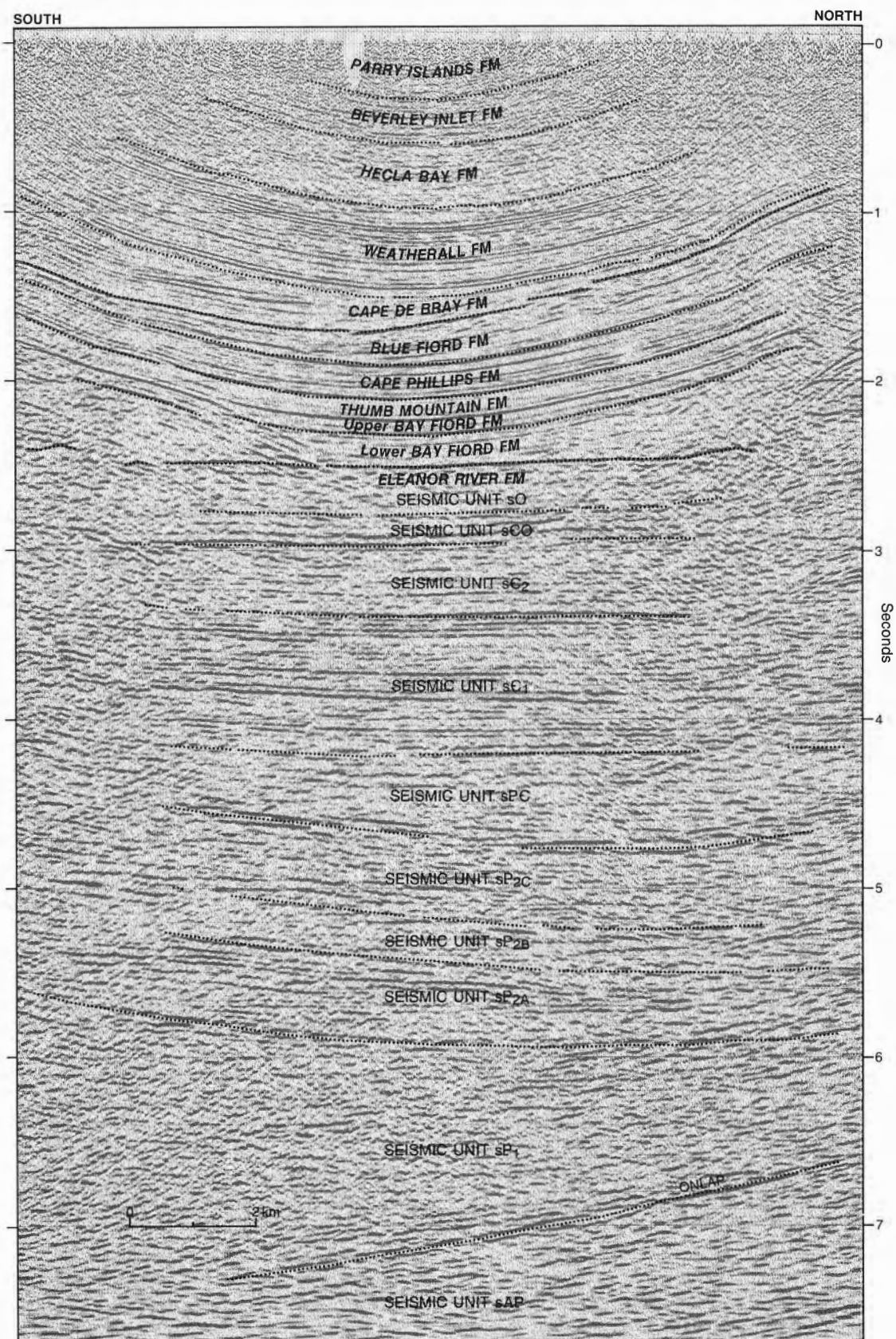


Figure 13. Precambrian(?) through Devonian seismic stratigraphy, southeastern Melville Island; part of seismic profile P2219 (Section B). Vertical exaggeration is approximately 0.85 at 5.0 s, 1.00 at 2.0 s and 1.50 at surface (see Appendix 3 for details).

Description. The reflector above Unit sAP is generally the lowest coherent primary feature on the seismic profiles. Seismic patterns from the internal part of sAP consist of short subhorizontal reflectors that may be simply a non-primary background noise response in the data.

Lower unreflective succession (Unit sP1)

Location and distribution. A widespread unit that underlies Dundas Peninsula and most (or all?) of eastern and central Melville Island at depths generally in excess of 5.3 s. It is below the limits of seismic resolution west of Liddon Gulf and north of latitude 76°N.

Thickness. Imaged thickness is 650 ms to 2.6+ s or 2.0 to 8.1+ km. Variations in thickness are due to structural relief on both the upper and lower contacts.

Description. Generally reflection free; strong internal reflection segments of uncertain lateral continuity can locally be observed within the unit such as at 6.0 to 6.2 s on P2219 (Section B), and at 6.8 to 7.0 s on P1140 (Section D). The basal contact is drawn above the persistent reflector that defines the upper surface of unit sAP. On seismic profile P2219 of Section B there is evidence of basal onlapping reflections above unit sAP (Fig. 13).

Strongly reflective succession (Unit sP2)

Location and distribution. A widespread seismic unit that has been identified at depth beneath much of eastern Melville Island and Dundas Peninsula.

Thickness. Undeformed thickness of sP2 beneath seismically conformable sP3 cover ranges from 1.3 s on Section F (4100 m at 6.2 km s⁻¹) to 1.4 s (4400 m) on Section B. Thinner intervals of sP2 are attributed to erosional truncation beneath the Cambrian(?). Unit sP2 also displays evidence of possible tectonic thickening to at least 2 s (6.2 km) on Sections D (Note 20) and F (Note 17).

Description. The unit is dominated by strong, discontinuous reflection segments. Some reflection segments within Unit sP2 display variations in attitude that cross the unit and members of the unit at oblique angles to the bounding contacts (Fig. 12; Section F,

Note 11). These reflection segments do not, however, crosscut the upper or lower contacts into the overlying or underlying units. The basal contact is apparently gradational on most seismic profiles. On P2219 of Section B (Note 9), the lower contact is marked by an apparent angular unconformity.

There are three locally identified members in sP2 (Figs. 12, 13). The lower part (sP2A) is 550 to 600 ms thick (1.7–1.9 km at 6.2 km s⁻¹) and comprises strong, discontinuous reflection segments. The middle part (sP2B) is a weakly reflective or reflection free unit 300 to 330 ms thick (900–1000 m). The upper part (sP2C; 450–500 ms or 1.4–1.6 km thick) again consists of strong, discontinuous reflection segments and can be mistaken for sP2A on some seismic profiles.

Upper unreflective succession (Units sP3 and sPC)

Location and distribution. Known to underlie the basal unit (sC1A) of the Cambrian(?) seismic succession in a saucer shaped erosional remnant beneath western Dundas Peninsula at and below 3.8 to 4.0 s (Section F). In this area, Unit sC1A and the younger units of the Cambrian(?) are readily distinguished from sP3. Strata partly age equivalent to Unit sP3 are also thought to be widely represented beneath the Cambrian(?) of central and eastern Melville Island. However, in these areas, sP3 and sC1A are both weakly reflective units and are necessarily mapped as a single undivided unit (sPC).

Thickness. Range is from 0 to 1.2 s for sP3 (0–3.4 km at 5.7 km s⁻¹) beneath Dundas Peninsula (Section F, Note 8). Unit sPC ranges to over 1.4 s (4.0 km) beneath parts of central Melville Island (Sections F and G). Thickness variations are the result of sub-Cambrian(?) structure and erosional truncation.

Description. Unit sP3 beneath Dundas Peninsula comprises uniformly weak and discontinuous internal reflection segments that parallel the lower contact with sP2 and are truncated upward by unit sC1A. Reflection-free internal patterns are also observed. Unit sPC is internally similar to sP3.

Basal contact. Lower contact of sP3 with sP2 is seismically gradational on P1171 (Section F). A strong, semi-continuous reflector marks the base of sPC on P2219 (Fig. 13; Section B). A low-angle normal fault or tilted apparent angular unconformity marks the base of sPC on P1660 (Section C), P1141 (Section D), and P1762 (Fig. 17; Section G, Note 9).

Precambrian(?) crustal structure and sedimentation

Structure on sub-Proterozoic(?) acoustic basement

The reflector above unit sAP is subhorizontal and, although commonly observed near the base of the recorded data (P1171, Section F), is continuous over distances up to at least 40 km. On P1168 (Section F; Fig. 12), this reflection is an inclined surface that is subparallel to tilted reflections from the base and top of sP2. On P2219 (Section B; Fig. 13), the reflector above sAP is also tilted but is inclined to angles steeper and apparently unrelated to reflection attitudes in sP2 and younger units. On P1660 (Section C) and on P2185 (Section D) the top sAP reflection appears to be offset. Perhaps the most distinctive top sAP reflection is the convex, pyramid-shaped surface at and below 6.5 s on P1763/1193 (Fig. 14; Section H, Note 9). The apex of a similar convex surface appears below CDP 300 on P1654 (Section I).

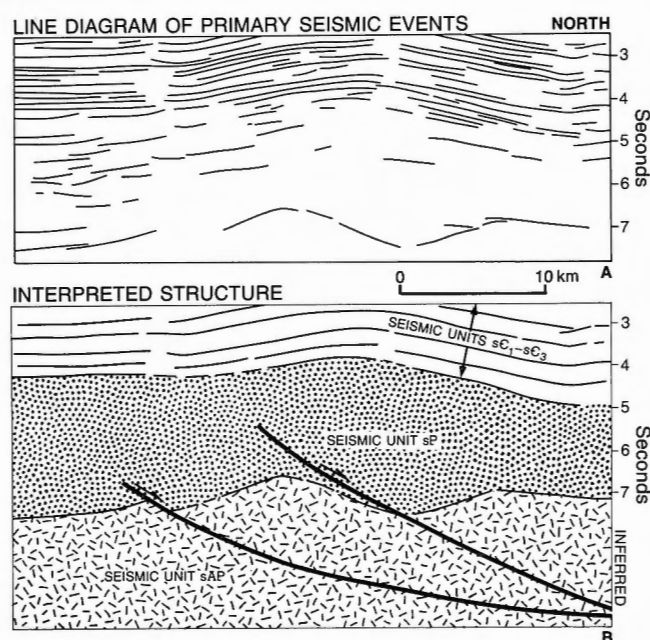


Figure 14. Distribution of primary reflections (A) and preferred structural interpretation (B) of convex-shaped tectonic features above seismic unit sAP on a portion of seismic profile P1763/1193 (Section H). Vertical exaggeration is approximately 0.87 below 5.0 s, and 0.96 above 5.0 s (see Appendix 3 for details).

The convex and offset reflection surfaces on Sections D, H and I are best explained by the structural model illustrated in Figure 14B; these features can be

produced by extensional faulting and block rotation. Rotated blocks of crystalline basement in this model are designed to resemble both the reflection surfaces on Section H and the block faulted patterns associated with crustal extension in young sedimentary basins such as are seen on the Bay of Biscay seismic profiles (Montadert et al., 1979).

Origin of the lower unreflective succession

The lower unreflective succession (sP1), sandwiched between the top of unit sAP and the base of the highly reflective succession (sP2) yields few clues to either its internal structure or composition. Thickness variations in the unit are generated by structural irregularities on both the upper and lower contacts (2.0 to 8.1 km at 6.2 km s⁻¹).

If the irregular surface above unit sAP is produced in part by extensional block faulting as illustrated in Figure 14B, then some thickness variations in sP1 can be attributed to syntectonic sediment accumulation in a half-graben setting. Additional variations in unit thickness may have been produced by a poorly imaged phase of post-sP1 deformation and erosion prior to overlap by younger Proterozoic(?) seismic units. Support for this proposal is provided on P2219 (Fig. 13; Section B): inclined but weak reflection segments in sP1 are truncated updip by an apparent angular unconformity below unit sP2A.

Deformation of the highly reflective succession

The contact between units sP1 and sP2 is apparently gradational on most seismic profiles. A key feature of seismic unit sP2 is its uniform thickness over distances of at least 40 km beneath Dundas Peninsula. The thickness of unit sP2 beneath parts of eastern Melville Island (P2219 of Section B; Fig. 13) is also remarkably similar to that observed on the Dundas Peninsula profiles, 190 km away. Departure from uniform thickness is attributed to widespread thinning of the top of the unit by erosion at the sub-sC_{1A} angular unconformity, and local tectonic thickening as noted on P1171 (Fig. 15A; Section F) and P1140 and 1141 (Section D).

The apparent localized thickening is here tentatively attributed to an inadequately understood phase of compressive deformation and associated thrust duplication involving part of the sP2 interval (Fig. 15B; Section F, Note 17). Although this model, it is believed, best fits the primary response of the data,

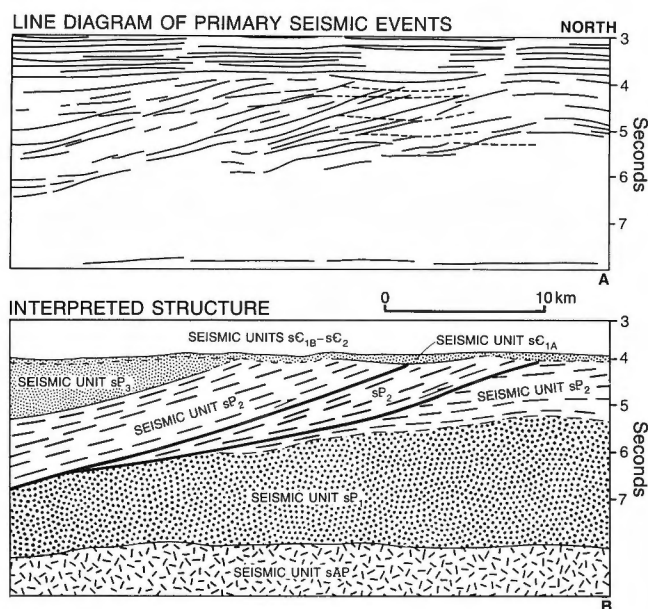


Figure 15. Distribution of primary reflections (A) and preferred structural interpretation (B) of apparent tectonic thickening within unit sP₂ as observed on a portion of seismic profile P1171 (Section F). Vertical exaggeration is approximately 0.85 below 3.8 s, and 0.92 above 3.8 s (see Appendix 3 for details).

these proposed compressional structures are not readily mapped onto adjacent seismic profiles.

Interpretation of the highly reflective succession

Scattered, low angle, crosscutting reflectors occurring within Unit sP₂ (but not in underlying and overlying units) are considered to be the seismic response from high-density intrusive sheets emplaced into lower density pre-existing host rocks (Fig. 12; Section F). The strong, subparallel, discontinuous reflection segments typical of sP₂ could be the acoustic image obtained from any one of a variety of rock successions containing large density contrasts and corresponding compositional variation. Possible assemblages might include: mafic volcanics and intercalated mudrocks; mixed felsic and mafic volcanics; mixed leucocratic and melanocratic schists and/or gneisses; or mixed metasediments. Also bearing on the interpretation is that this succession has been regionally metamorphosed to at least greenschist facies based on known paleo-geothermal gradients and the present depth of burial (see above, "Thermal maturity and metamorphic grade"). The regional continuity of unit thickness and feasibility of tripartite member correlation featured by the highly reflective succession is probably less likely in

a package dominated by volcanic flows or highly tectonized higher grade metamorphic rocks. This leaves the favoured interpretation, illustrated in Figure 16, that Unit sP₂ is a mixed metasedimentary succession intruded by igneous sheets.

Structure of the upper unreflective succession

The contact between the highly reflective succession (sP₂) and the upper unreflective succession (sP₃/sP_C) can be variously interpreted as a seismically conformable surface (Sections B and F), a tilted angular unconformity (Sections C and D) or a low angle (10–20°) northwesterly directed normal fault or southeasterly directed thrust with over 15 km of displacement (Fig. 17B; Section G). Unit sP₃ is in turn overlain with profound angular unconformity by flat-lying basal Cambrian(?) seismic unit sC_{1A}. Units sP₃ and sC_{1A} are acoustically similar and therefore may be lithologically similar. The channelized character and basal stratigraphic position of sC_{1A} above a widespread angular unconformity (see on) implies that sandstone and perhaps mudrocks and/or conglomerate

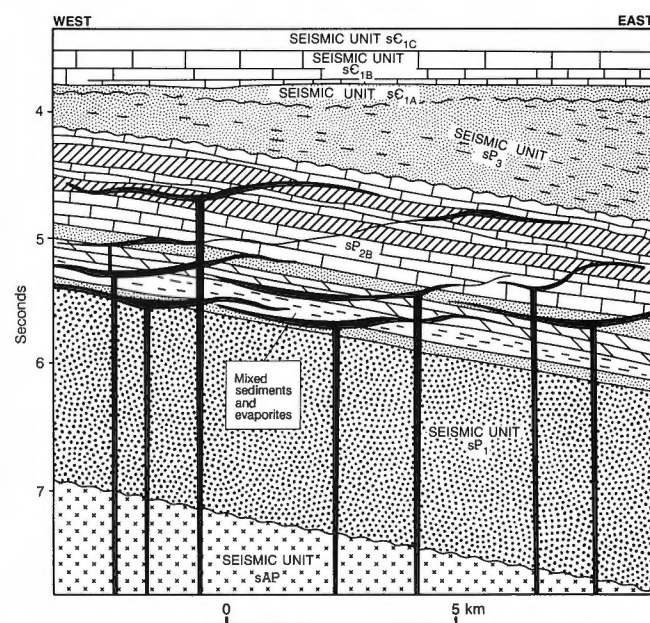


Figure 16. Preferred lithological model accounting for the seismic response of the highly reflective succession (sP₂) as observed on seismic profile P1168 (Section F; Fig. 12). Seismic unit sAP is assumed to represent crystalline basement, sC_{1A} and sP₃ (being acoustically similar) are thought to be lithologically similar terrigenous units, and sC_{1B} and sC_{1C} are interpreted as platform carbonates. Same vertical exaggeration as for Figure 12.

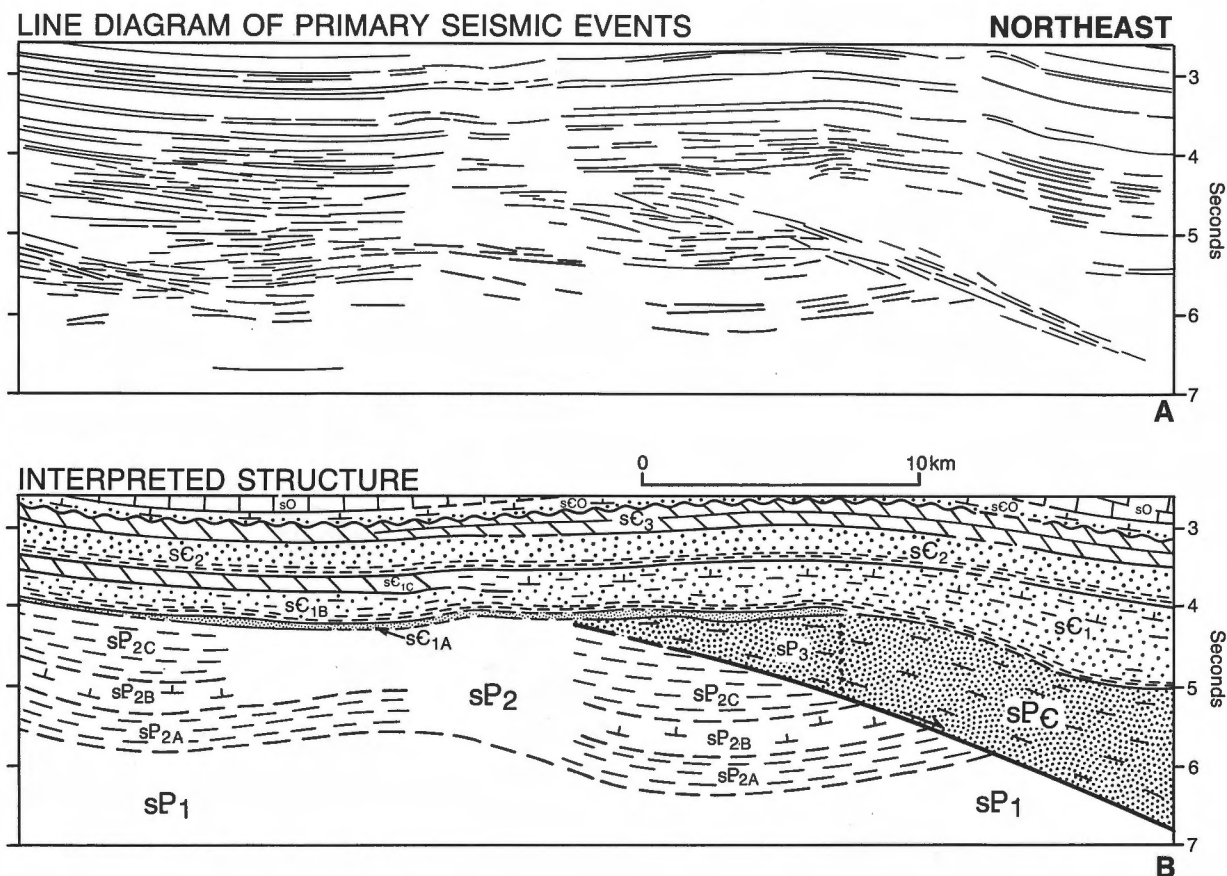


Figure 17. Seismic expressions (A) and interpretation (B) of a sub-Lower(?) Cambrian low-angle fault displacing sP₂ and older seismic units on a portion of seismic profile P1762 (Section G). Implied north-northwesterly directed displacement on the proposed normal fault is at least 15 km (see also Fig. 18).

are shared lithological components of sC_{1A} and sP₃ (Fig. 16). On many seismic profiles (Sections A through D and G), sC_{1A} is indistinguishable from sP₃. Under these circumstances, seismic unit sPc (sC_{1A} + sP₃) may include some basal Cambrian(?) beds in the upper part. Units sP₃ and sPc comprise mostly reflection-free material. An isopach map of these seismic units (Fig. 18) reveals three, indistinct, basin-shaped erosional remnants of significant size beneath a continuous blanket of Lower(?) Cambrian strata. Two of these Proterozoic(?) belts occur in the eastern part of the island and trend variably N50°E through N80°E. The trend and plunge on the axial keel of these features is west-southwesterly. The maximum imaged thickness (4.7 km) is at the western limit of seismic resolution. These partly eroded troughs are separated by a sub-Lower(?) Cambrian structural high over which sP₃ is thinned to about 1.2 km. A third erosional remnant, situated beneath western Dundas Peninsula, is more nearly ovoid in shape (axial trend N20°W) and contains up to 3.5 km of weakly stratified sP₃ bedrock. This third depression is partly separated from the

others by a westerly plunging arch. The upper unreflective succession (sP₃) is entirely absent on the imaged crest and northern flank of the arch beneath southeast Melville Island. In these areas, the arch is expressed by the subcrop of various members of the highly reflective succession (sP_{2A} through sP_{2C}) at the angular unconformity below Lower(?) Cambrian cover.

Interpretation of the upper unreflective succession

The structural setting of these Proterozoic(?) troughs remains highly speculative. Seismic profiles over the ovoid depression beneath Dundas Peninsula (Section F) indicate that the influence of subsidence extends at least to the base of unit sP_{2A}. Parallel tilt of the reflector above unit sAP (Fig. 12; line P1168, Section F) shows that unit sAP may be similarly affected by regional subsidence, although a more complex structural relief above unit sAP cannot be entirely ruled out.

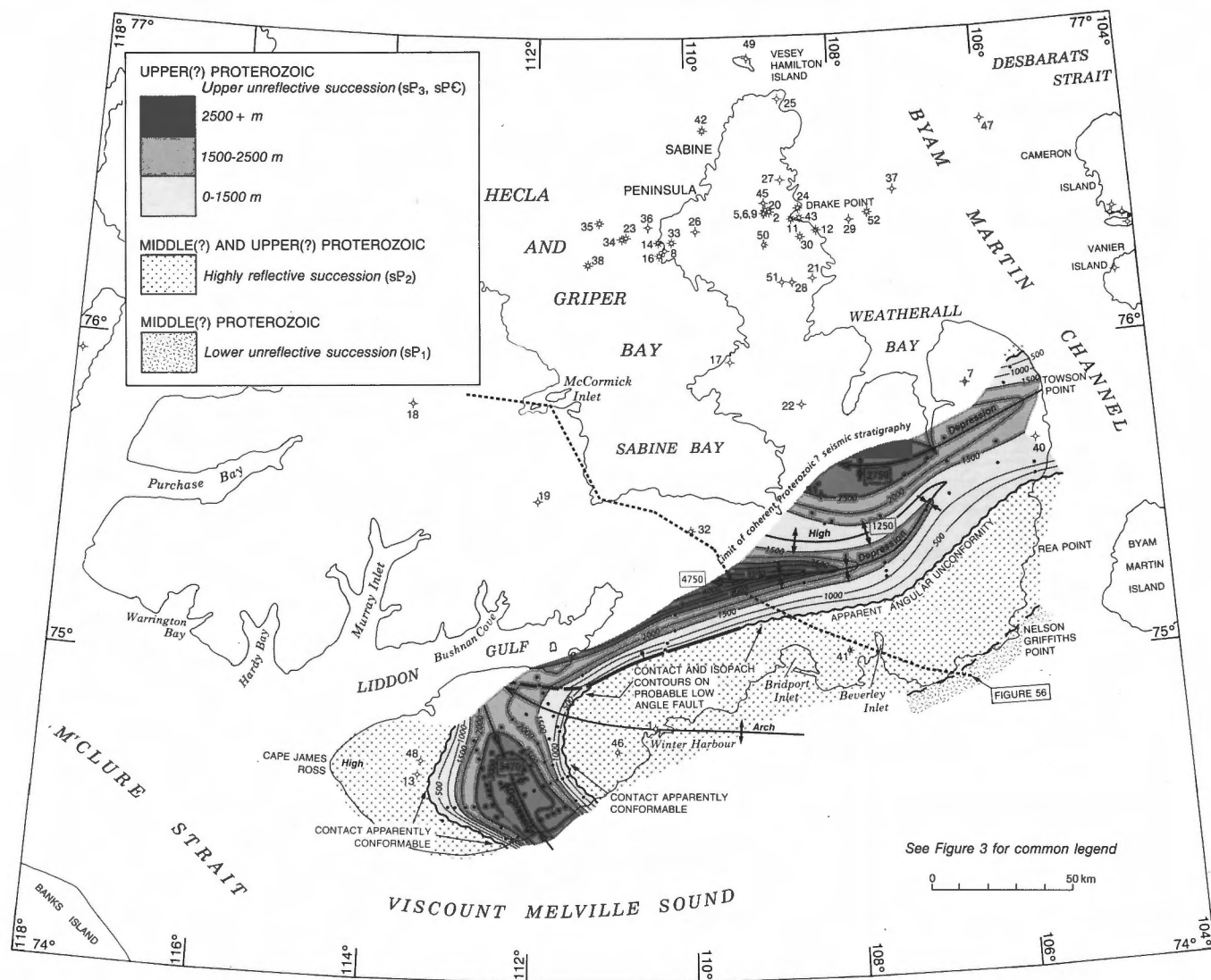


Figure 18. Isopach map of the upper unreflective succession (sP₃, sP_C). Depths have been calculated from two-way transit times using an interval velocity of 5.7 km s⁻¹. Contour interval is 500 m.

The evidence for placing a low-angle fault beneath sP_C along part of the northern flank of the Proterozoic(?) arch is moderately convincing (Fig. 17A); this fault can be mapped across two widely separated seismic profiles (P1763/1193 of Section H and P1762 of Section G), a minimum distance of 60 km. The structural model favoured on the cross-sections and Figure 17B is that this is an ancient normal fault that roots into block-faulted acoustic basement (sAP) and that the last phase of fault movement was responsible for some basin development during creation of the upper unreflective succession. Implied direction of extension is normal to isopachs and trough axes of Figure 18 or approximately N40°W through N10°W. Other mechanisms of trough formation and preservation can be visualized, including a late phase of long-wavelength, deep-seated folding prior to Cambrian(?) overlap. Whatever

kinematic model is accepted, it is suggested that this model should be also applicable to the long-wavelength folds of similar trend (N40°E through N75°E) and wavelength that have affected Middle and Upper Proterozoic rocks exposed below the sub-Lower Cambrian angular unconformity in the Minto Uplift of central Victoria Island (Thorsteinsson and Tozer, 1962).

Summary of favoured geological models

1. Unit sAP probably represents crystalline basement.
2. Structural features defined by the upper reflective surface of unit sAP may result from Bay-of-Biscay-type block rotation (Montadert et al., 1979)

during one or more phases of Precambrian lithospheric extension.

3. Unit sP₁ could represent an acoustically homogeneous metasedimentary assemblage that accumulated during one (early) phase of this Precambrian extension.
4. Unit sP₂ is probably a laterally extensive, mixed metasedimentary succession intruded by low-angle igneous sheets.
5. A phase of regional-scale subsidence and possibly coeval uplift (or folding) occurred during or after the accumulation of unit sP₃ but not later than a phase of widespread erosional truncation and peneplanation that preceded overlap by unconformable Lower(?) Cambrian cover.
6. The shape of one of three documented sub-Cambrian(?) depressions was influenced by a low angle possible normal fault with over 15 km of displacement. This fault is mapped over a distance of at least 60 km and at depth may root into unit sAP. The fault was apparently most active before overlap by Cambrian(?) unit sC₁. The implied direction of extension is N40°W through N10°W.
7. Unit sP₃ is acoustically (and therefore could be lithologically) similar to basal Cambrian(?) unit sC_{1A}: a unit of seismic incised valley fill, which undoubtedly consists of at least some basal transgressive sandstone with or without mudrock and conglomerate.
8. Greenchist facies is the lowest metamorphic grade for the youngest Precambrian rocks of subsurface Melville Island based on an extrapolation of paleogeothermal gradients of 25° mK m⁻¹ (in the top 5 km) and minimum 12 km depth of burial (upper 2 km now missing as a result of erosion).

Correlation and age of Precambrian(?) seismic units

Assumptions

Three assumptions have been adopted in order to facilitate correlation of the Precambrian(?) seismic stratigraphy of subsurface Melville Island. The first is that the widespread apparent angular unconformity below unit sC_{1A} represents the base of the Cambrian shelf succession. The validity of this assumption is discussed in more detail in the next chapter. The second assumption is that the nearest Precambrian outcrop belt (Victoria Island) is the most likely place to

encounter bedrock equivalents of Melville Island seismic stratigraphy. Finally, it is assumed that differences in internal reflection character between the various Proterozoic(?) successions are due to dramatic differences in lithological characteristics, which, in turn, are caused by dramatic changes in local or regional tectonics. This final assumption implies that the contacts separating Proterozoic successions represent either unconformity surfaces or conformable surfaces that are laterally equivalent to regionally significant unconformities elsewhere. Acceptance of these assumptions permits correlation of individual seismic successions with major unconformity-bound rock units (groups and supergroups) exposed throughout the Arctic Islands, Greenland, the Interior Platform, and Northern Cordillera.

Evidence

The preferred correlation and suggested age range of Precambrian(?) seismic units of Melville Island with exposed Proterozoic stratigraphy of Victoria Island and elsewhere is shown in Figure 19. This interpretation is not unlike that generally favoured by Kanasewich and Berkes (1990). Supportive evidence in favour of the proposed correlation includes five areas of similarity between the highly reflective succession (unit sP₂) of subsurface Melville Island and the Shaler Group of Victoria Island, including: 1) the Shaler Group is intruded by tholeiitic gabbro dykes and sheets (Thorsteinsson and Tozer, 1962; Christie, 1964), and Unit sP₂ can be interpreted as having been intruded by sheets; 2) thick, laterally continuous limestone formations occur in the medial part of the Shaler Group (Young, 1981), and the medial, reflection-free unit sP_{2B} is laterally continuous and could be interpreted as an interval of thick bedded carbonates more impervious to intrusive sills; 3) the thickness of Shaler Group sediments plus sills of central Victoria Island (4.0–4.3 km; Christie, 1964; Young, 1981) is essentially identical to the thickness estimate of unit sP₂ (4.1–4.4 km); 4) the sheet-like reflections in sP₂ do not continue upsection into younger units, and in this respect behave like the Graveyard sheets emplaced into the Shaler Group, which are the same age as and genetically related to the overlying basalts of the Upper Proterozoic Natkusiak Formation (Fahrig, 1987); and 5) the large variety of sedimentary rock types found in the Shaler Group (mudrock, limestone, anhydrite, and sandstone) could alone account for the large impedance contrasts in unit sP₂.

Assuming that the highly reflective succession is equivalent to the Shaler Group, then the lower unreflective succession (sP₁) could conceivably be correlated with one of several, low-grade sedimentary

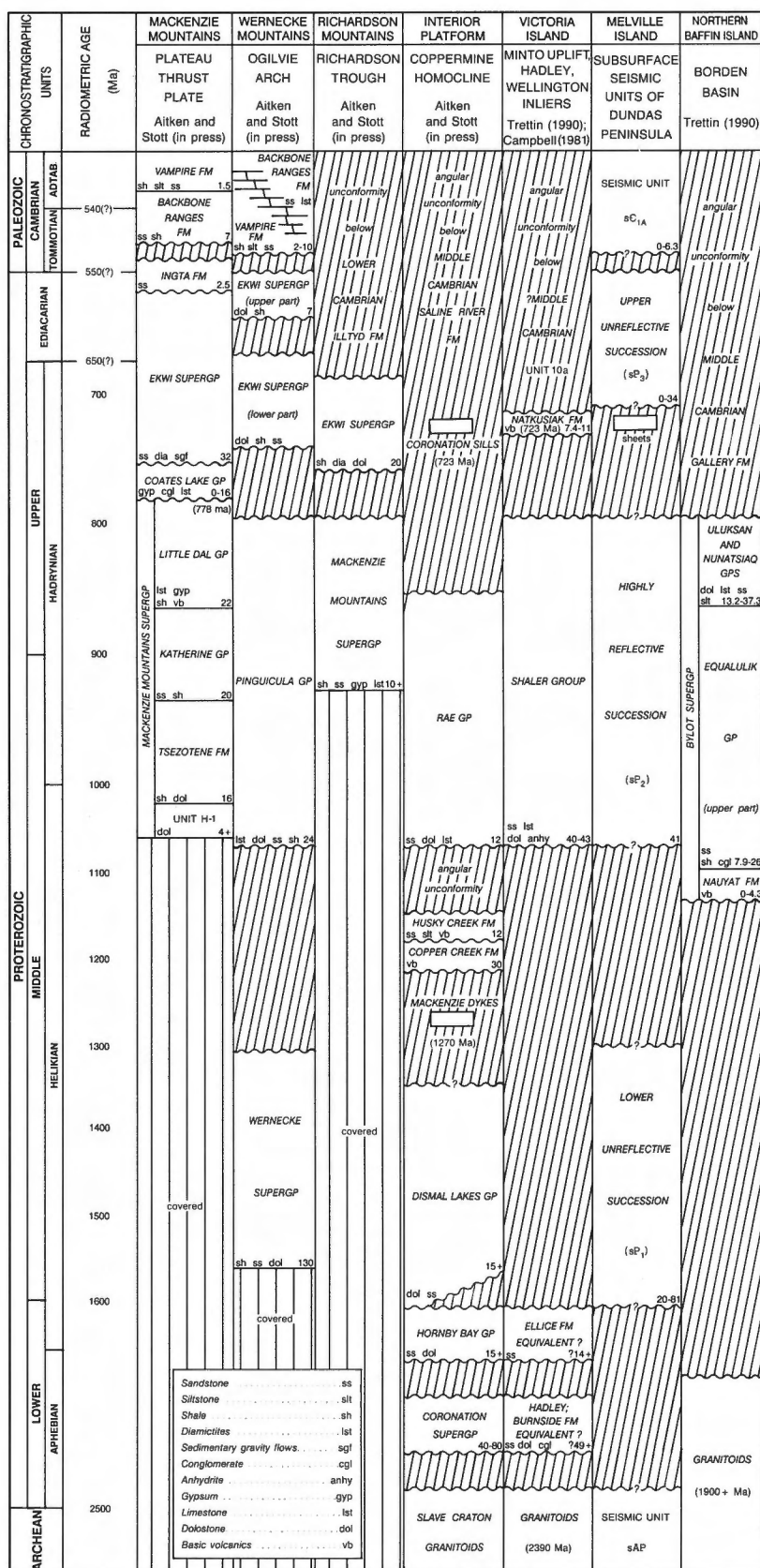


Figure 19. Suggested correlation of Precambrian lithostratigraphic units (Northern Cordillera and Arctic Islands), and Precambrian(?) to Paleozoic seismic stratigraphic units (Melville Island). Unit thicknesses are in metres ($\times 10^2$).

successions that underlie upper Middle and lower Upper Proterozoic rocks of northwestern Canada. These successions include either 1) the miogeoclinal belt of the Coronation Supergroup of the Wopmay Orogen (Lower Proterozoic; Hoffman et al., 1984), or 2) the Ellice Formation, Dismal Lakes and Hornby Bay groups of the lower Middle Proterozoic Amundsen Basin, including sub-Shaler Group strata exposed in the Hadley Bay inlier of northern Victoria Island (Baragar and Donaldson, 1973; Campbell, 1979, 1981) and equivalent Independance Fjord Group of North Greenland (Higgins, 1986). Similarly, unit sAP (acoustic basement) may be equivalent to either Archean granitoid basement of the Slave Craton (which nonconformably(?) underlies Lower Proterozoic sediments of Victoria Island and the Interior Platform) or Lower Proterozoic 1.7–1.9 Ga granulites as exposed on Boothia Peninsula, south-eastern Ellesmere Island and northwest Greenland.

For seismic Proterozoic(?) units sP₃ and sP_C, lying above the highly reflective succession, no volumetric equivalent of the Upper Proterozoic Natkusiak Formation (Victoria Island) is indicated. The Natkusiak Formation includes up to 1100 m of mafic volcanic flows and associated (very minor) volcanoclastic sediments (Dostal et al., 1986). The seismic

response from this sequence should yield two high-amplitude reflections; one from the top and one from the base (assuming seismic energy could penetrate the lower contact). Unit sP₃ is unlikely to be lithologically similar to the Natkusiak Formation because of its acoustic similarity to the basal unit of the Cambrian(?) succession (seismic unit sC_{1A}). The correlation proposed here is that sP₃ and most of unit sP_C is roughly equivalent to the quartzite, mudrock and tillite-dominated rocks of the Upper Proterozoic (Vendian) including the Petermann Series, Eleanore Bay and Tillite groups of central East Greenland (Higgins et al., 1981), the Campanuladal, Moraeneso and associated formations of Northeast Greenland (Higgins, 1986), and the Ekwi and Windermere supergroups of the northern and southern Cordillera, respectively (Aitken and Stott, 1991).

Regional implications

Schematic distribution of known Precambrian rocks of Victoria Island and seismic Precambrian units of Melville Island, together with the overlying Cambrian to Lower Devonian cover is illustrated in Figure 20. Depth to Moho estimates are compiled from refraction

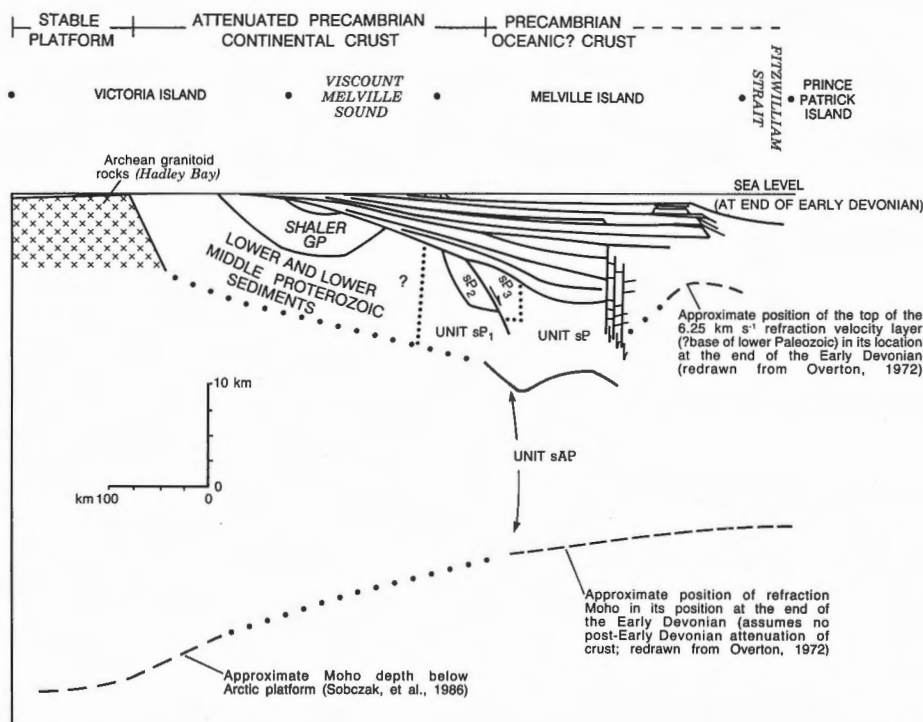


Figure 20. Schematic, crustal-scale cross-section, Victoria Island to north-western Melville Island, as it is believed to have appeared in the Early Devonian. The wedge-shaped array of formations below Melville Island and Viscount Melville Sound represents the Lower Cambrian through Lower Devonian part of the Franklinian succession, as illustrated in Figure 23.

data of Overton (1972) and modelled gravity profiles of Sobczak et al. (1986), and Sweeney et al. (1986). The implication of this cross-section is that presumed Archean granitoid basement and correlative unit sAP thins from 48 km to approximately 15 km over a distance of 350 to 400 km between northern Victoria Island and southern Melville Island. This apparent attenuation of basement to approximately 30 per cent of its full thickness can be attributed to extension during accumulation of Lower, Middle and Upper Proterozoic strata prior to widespread overlap by Lower Cambrian beds.

Two phases of seismically imaged extension in the Proterozoic interval can be correlated with two major crustal extensions of the Greenland and northwestern Canadian Shield. The first of these events (Fig. 21) produced the Mackenzie dyke swarm at 1267 ± 2 Ma (LeCheminant and Heaman, 1989), and an outpouring of tholeiitic volcanics including the Coppermine basalts of Amundsen Basin, the Nauyas Formation of Borden Basin (Jackson and Ianelli, 1981), and the Zig-zag Dal basalts above the Independence Fjord Group in North Greenland (Higgins, 1986). If seismic unit sP1 is equivalent to some or part of the Independence Fjord Group or pre-Coppermine Ellice Formation, Dismal and Hornby Bay groups, then first phase block

rotation of Archean and/or Lower Proterozoic granitoid basement (seismic unit sAP) during accumulation of sP1 may be indirect evidence for a phase of crustal extension in the early Middle Proterozoic preceding the Mackenzie thermal event. Subsequent accumulation of unit sP2 and deposition of correlative upper Middle and lower Upper Proterozoic strata (i.e., Shaler and Rae groups of Amundsen Basin; and Thule Group of Ellesmere and northwest Greenland) are viewed as the lithospheric response to post-plume thermal subsidence.

The second phase of crustal extension in the Canadian Arctic (Fig. 22) produced the Hottah and Franklin dyke swarms at 723 ± 3 Ma (Heaman et al., 1990; Fahrig and West, 1986), the Graveyard and Coronation gabbro sheets emplaced into the Shaler and Rae groups, the post-Shaler Natkusiak tholeiites of central Victoria Island, and the seismically imaged sheets emplaced into unit sP2 of Melville Island. Post-plume rift fill and associated glacioeustatic lowstand deposits may be represented by seismic units sP3 and sP4, and the equivalent exposed Vendian strata of Greenland and the Western Canadian Cordillera. The Late Proterozoic rifting phase was successful and led to widespread deposition of Lower Cambrian and younger Franklinian strata on a passively subsiding continental margin.

CHAPTER 3

FRANKLINIAN SUCCESSION (CAMBRIAN(?) THROUGH DEVONIAN)

General comments

This chapter presents a systematic description and interpretation of the Franklinian Succession of Melville Island, which includes 8 to 13 km of Cambrian(?) through Devonian strata deposited above a widespread angular unconformity that bevels geophysically-imaged units of Precambrian(?) age (Fig. 23). A generalized understanding of various seismic and bedrock units can be obtained by reference to Table 2 (in pocket) and to discussions of Franklinian paleogeography, unit correlation and regional interpretation.

Franklinian paleogeography

Named paleogeographic features of the Franklinian Succession in the western Arctic Islands, adopted from

Trettin et al. (1991) appear on Figures 23 and 24, and are described briefly below.

Southern shelf

The southern shelf is a northwesterly thickening miogeoclinal sedimentary prism that extends throughout the southern Arctic Islands with cratonward limits now defined by continuous outcrop of the Precambrian Shield (on Baffin Island and on the mainland south of Victoria Island). On Melville Island, the southern shelf comprises eight Cambrian(?) and Lower Ordovician seismic stratigraphic units (seismic units sE1A through sO) and eight Lower Ordovician through Upper Silurian, shallow-marine, mostly carbonate formations (including the Eleanor River, Bay Fiord, Thumb Mountain, Irene Bay, Allen Bay, Cape Storm, Douro and Barlow Inlet formations). The northern extent of the southern shelf has varied considerably through time. From the Cambrian(?) to

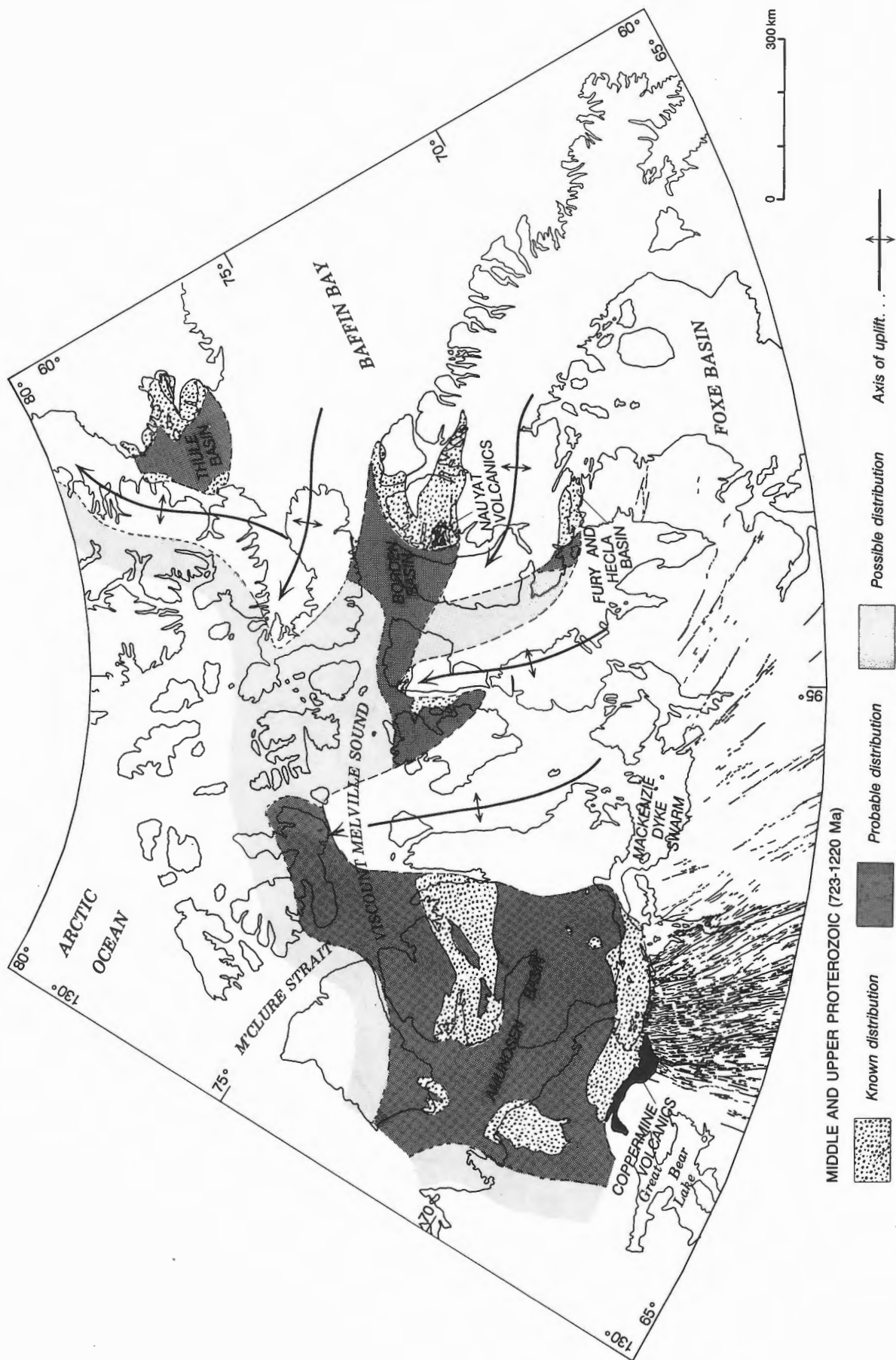


Figure 21. The Mackenzie dyke swarm, related plutonic igneous activity and the distribution of post-plume sedimentary cover of late Middle and early Late Proterozoic age in northern Canada. (Adapted from LeCheminant and Heaman, 1989.)

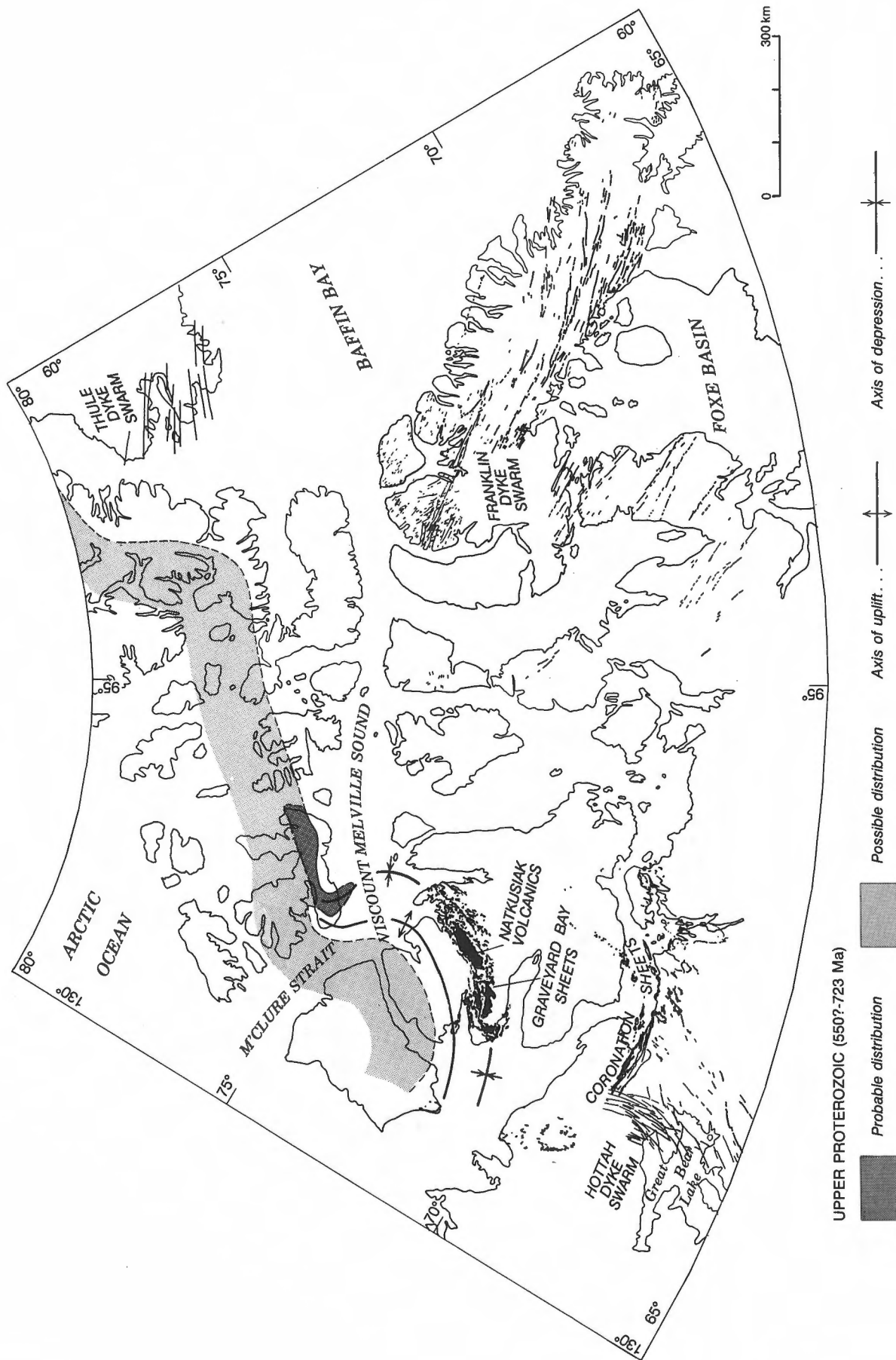


Figure 22. The Franklin, Thule, and Hottah dyke swarms, related plutonic igneous activity and the distribution of probable and possible post-plume sedimentary cover of late Late Proterozoic age in northern Canada. (Compiled from Fahrig and West, 1986; Fahrig, 1987; Nielsen, 1987; and Fig. 18.)

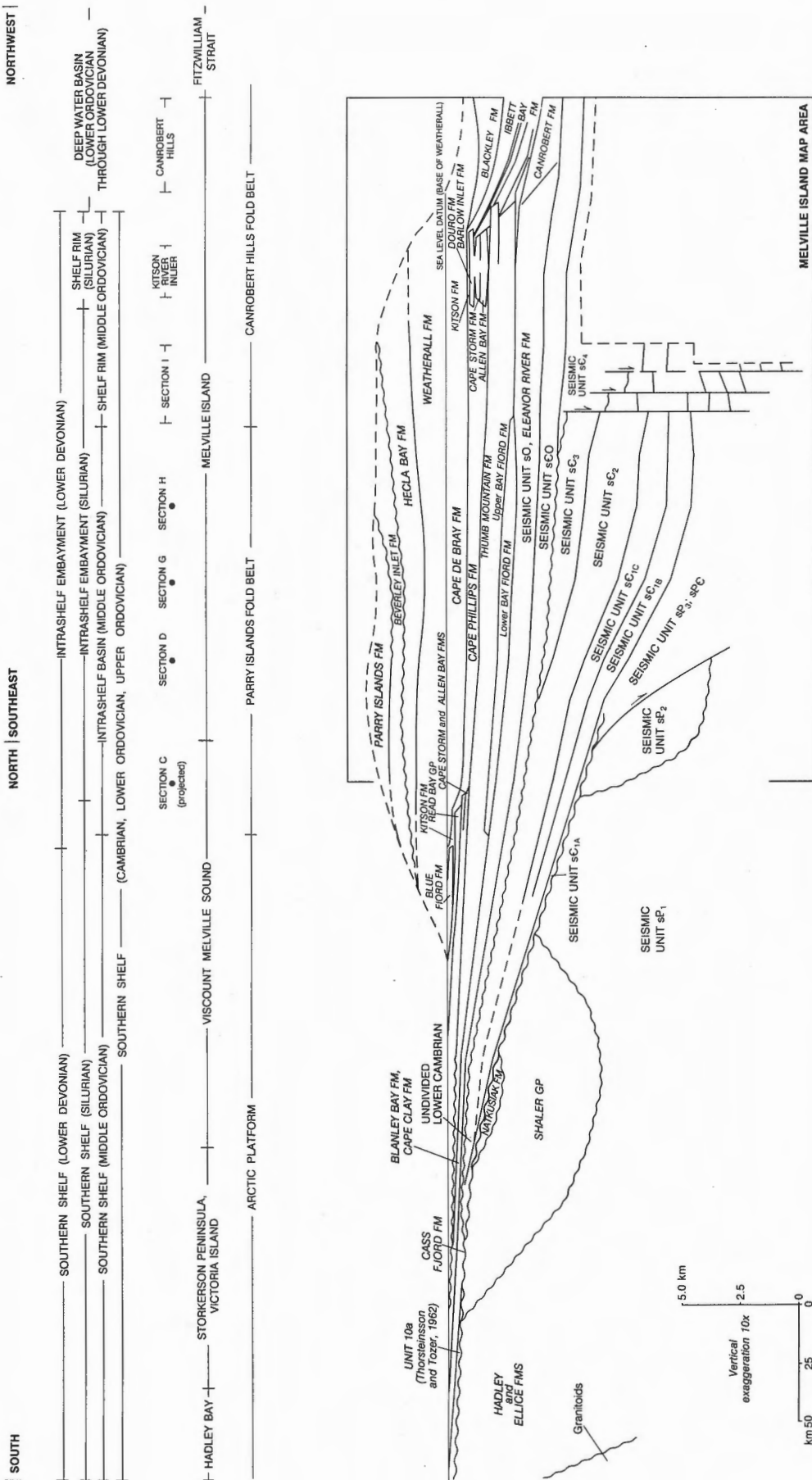


Figure 23. Generalized stratigraphic cross-section of the Franklinian Succession (Precambrian(?)–Devonian) from northern Victoria Island to northwestern Melville Island, displaying major lithostratigraphic and seismic stratigraphic units, facies transitions, geological provinces, and the location of the Melville Island map area. Note the distribution of these features with respect to the depth to the Moho (as shown on Fig. 20). Location of the line of section is shown on Figure 24.

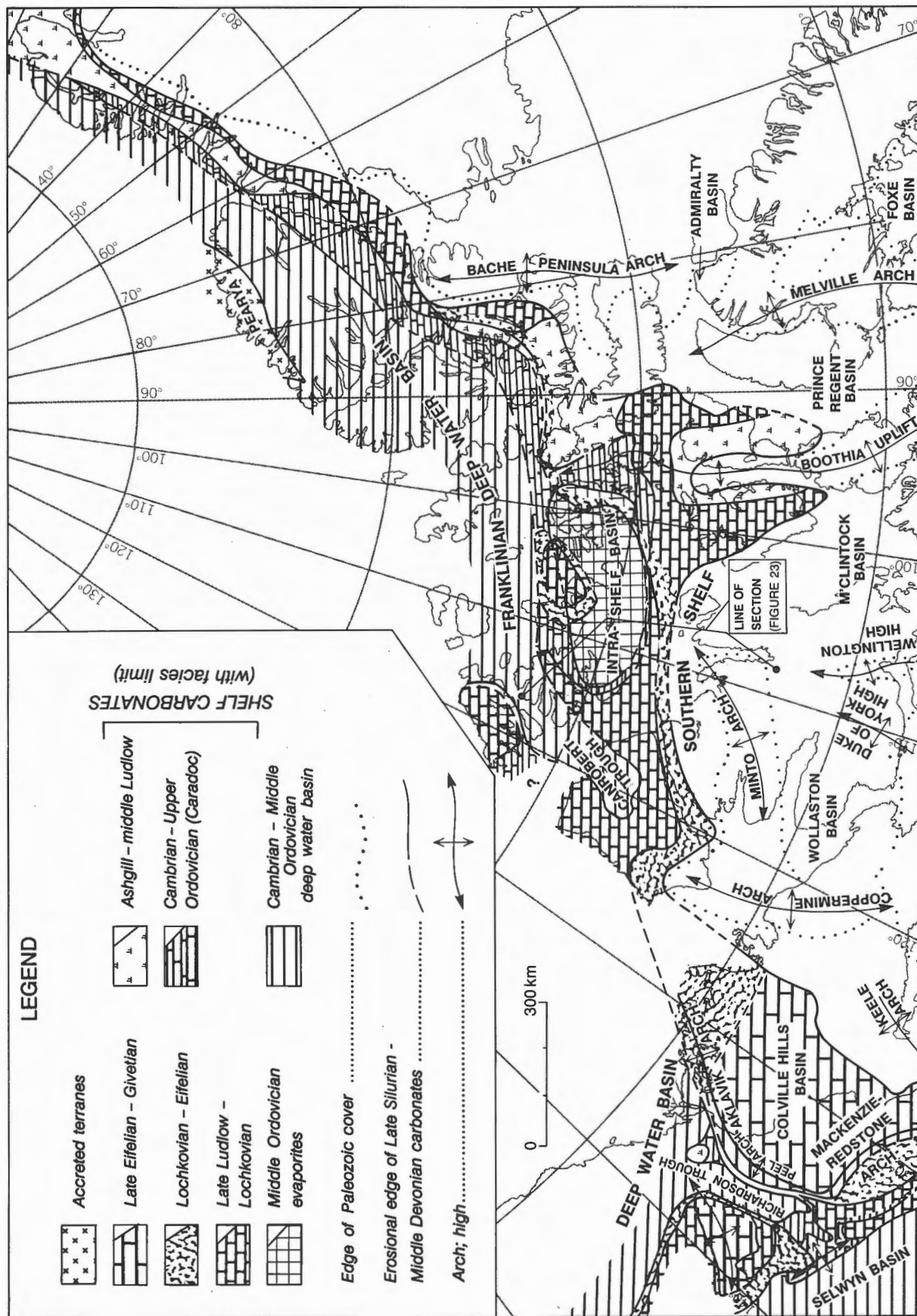


Figure 24. Lower Ordovician through Lower Devonian facies transitions of the Franklinian succession in the Arctic Islands (compiled from the interpretation of seismic profiles located on Fig. 3, together with paleogeographic maps of Brent, pers. comm., 1989; Kerr, 1974; Norris, 1985; and Trettin, 1989). Note the bifurcation of the deep water basin about the Prince Patrick carbonate platform, and the deep water trough (Canrobert Trough) beneath Eglinton and northern Banks islands.

the Early Ordovician and again in the Late Ordovician, the southern shelf was flanked on the northwest side by a deep water basin. In the Middle Ordovician, it was separated from the deep water basin by a shelf rim carbonate bank and evaporite-dominated intrashelf basin. The southern shelf reached its maximum width in the Early or Late Ordovician, then retreated episodically to the south from the latest Ordovician to the Early Devonian.

Important components of the southern shelf stratigraphy are reflection seismic units of Cambrian(?) and Early Ordovician age (named with a combination of letters and numbers prefixed with the letter 's'). The upper part of the highest seismic stratigraphic unit (seismic unit sO) has been drilled and includes strata of Early Ordovician age. The drilled section of unit sO has been assigned to the Eleanor River Formation by Goodbody (1993) and Fox and Densmore (1992). A key reference horizon used in describing the location and distribution of Cambrian(?) seismic units is the subhorizontal reflector marking the base of the Middle Ordovician Bay Fiord Formation evaporites, which is widely represented on most seismic profiles at $2.2 \pm .5$ below sea level datum.

Depth conversion of profiles that image the various drilled and exposed formations of the Franklinian Succession has been accomplished by judicious interpolation and application of sonic log interval velocities as described in Chapter 2 (Fig. 7). For depth conversion of seismic units sC1A through sO, a uniform interval velocity of 5.7 km s^{-1} has been applied. Choice of this velocity is based on two data sources. First, Overton (1972) identified a distinct seismic refraction unit in the subsurface of central and western Melville Island, the upper surface of which corresponds approximately to the top of the lower Paleozoic carbonate bank succession. The lower contact corresponds to a discontinuity at 10 to 12 km, which is assumed to be the unconformity at the base of the Paleozoic. Overton's refraction velocity estimate for this interval is 5.75 km s^{-1} . The second source of data for Cambrian and Lower Ordovician interval velocities is the Panarctic Deminex Cornwallis Central Dome K-40 well on Cornwallis Island (320 km east of Melville Island). Interval sonic velocities for 3063 m of Upper Cambrian and Lower Ordovician strata intersected by this well range from 4.7 to 6.4 km s^{-1} and have a weighted average sonic velocity of 5.4 km s^{-1} . Since this well was drilled on the axis of Boothia Uplift, it is possible that the lower Paleozoic strata in this area were never buried as deeply as those of subsurface Melville Island. Therefore the average velocity of 5.4 km s^{-1} is considered somewhat low for the corresponding Melville Island section.

Deep water basin

Traceable from northern Ellesmere Island to northwestern Melville and Eglinton islands, the deep water basin comprises a (once continuous?) belt of Cambrian through Devonian basin floor, basin rise, basin slope and basin fill sediments flanking the age-equivalent outer shelf sedimentary prism to the northwest (Fig. 24). Stratigraphic nomenclature unique to the deep water basin of northwestern Melville Island includes the Canrobert, Ibbett Bay and Blackley formations (Fig. 25).

The deep water basin diverges about a Silurian and older carbonate bank that underlies Prince Patrick Island. The principal deep water realm probably continues to the west, and a linear southerly trending arm of the deep water basin, identified on seismic reflection profiles of Eglinton Island, is presumably continuous across M'Clure Strait with a lower Paleozoic embayment that underlies and terminates on northern Banks Island. The deep water realm of Canrobert Hills and Sproule Peninsula lies in the mouth of the embayment. The term "Canrobert Trough" is therefore proposed to describe this linear embayment. It is worth noting that although less completely exposed at the surface, Canrobert Trough is comparable in size and orientation to Richardson Trough of the northern Yukon (Fig. 24).

Intrashelf basin and shelf rim

The centre of the intrashelf basin is defined by the paleogeographic limits of Middle Ordovician bedded salt (lower Bay Fiord Formation), a facies belt extending from eastern Bathurst Island to central Melville Island. The intrashelf basin is flanked some distance to the south by the southern shelf, and to the north by a peritidal carbonate barrier (dolostone facies of the Bay Fiord Formation) or shelf rim on the edge of the deep water basin. A schematic section through the units and formations of the southern shelf and shelf rim of western Melville Island is shown in Figure 26.

Intrashelf embayment

The intrashelf basin disappeared during the Middle Ordovician. Rapid subsidence of the basin combined with a continued regional-scale rise in relative sea level led at the end of the Ordovician to the development of a seaway or marine embayment of moderate water depth over the site of the pre-existing intrashelf basin. Limits of the embayment are defined by the

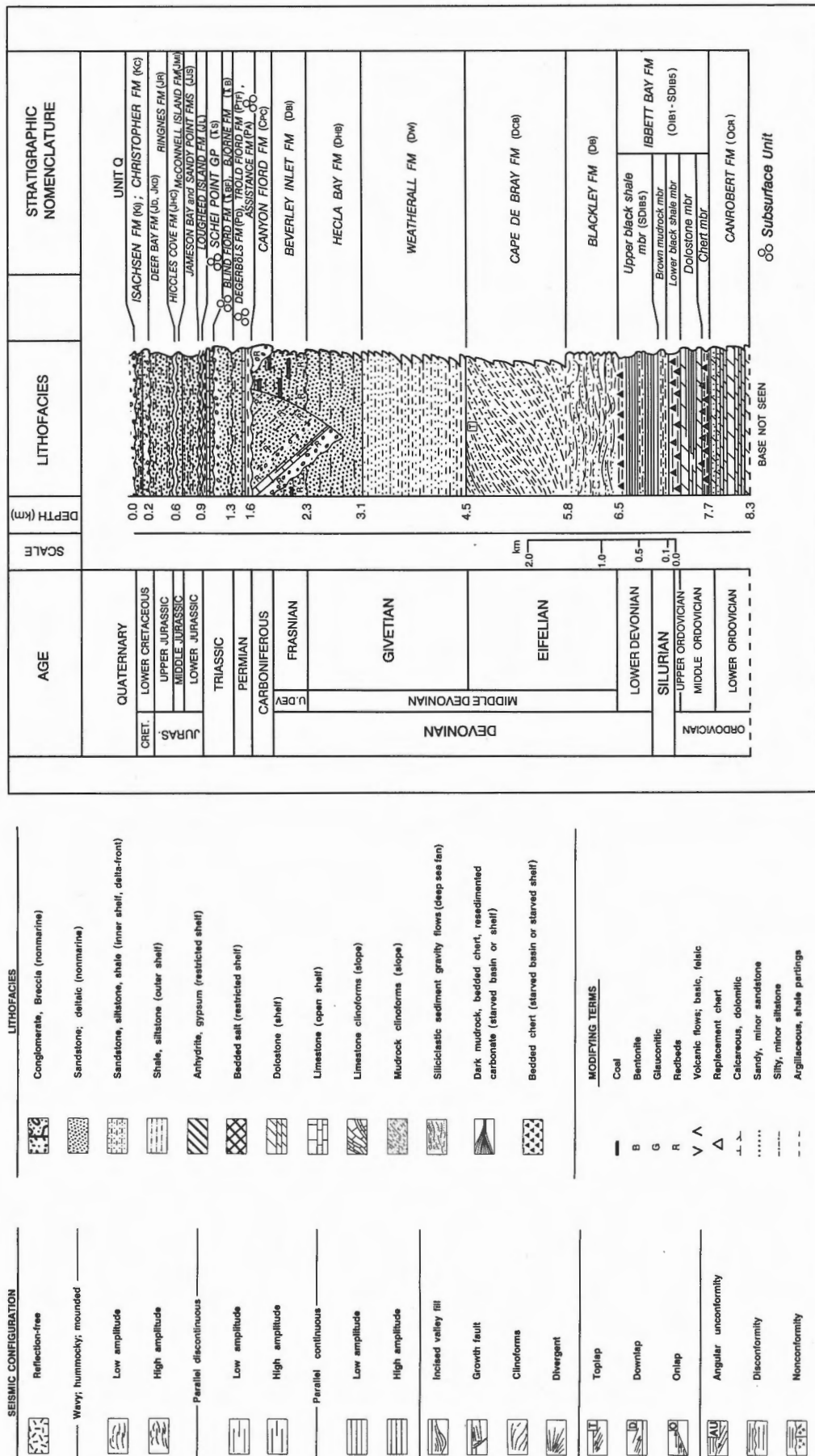


Figure 25. Representative stratigraphy of the Ordovician to Devonian deep water basin, Devonian clastic wedge, and Carboniferous to Cretaceous cover of Sverdrup Basin (Canrobert Hills and Sproule Peninsula), northwestern Melville Island. Thicknesses of the Canrobert, Ibbett Bay and Blackley formations are based on measured sections in Canrobert Hills. The thickness of the Cape De Bray Formation is based on a geometrical calculation. Thicknesses of the Weatherall, Hecla Bay and Beverley Inlet formations are from measured sections on Purchase Bay Homocline (south of Ibbett Bay). Thicknesses of Carboniferous through Cretaceous formations are based on surface, well, and seismic profiles of Sproule Peninsula. Note that in most of these areas, Carboniferous and Permian strata rest unconformably on lower Cape De Bray Formation and older strata.

paleogeographic distribution of two mudrock and resedimented carbonate formations: the Cape Phillips and Kitson formations. Strata of the Cambrian(?) through Lower Ordovician southern shelf, the Middle Ordovician intrashelf basin and the Upper Ordovician through Middle Devonian intrashelf embayment of southeastern Melville Island are shown in Figure 27.

Offshore carbonate platforms

Carbonate sedimentation persisted in two areas on the outer edge of the intrashelf embayment. These areas are not pinnacle reefs or mound-shaped biogenic buildups (although such features may occur) but extensive offshore banks. Each platform comprises a linked system of slope, shelf edge, reef and widespread back-reef seismic facies underlying areas measuring hundreds of square kilometres. In the northwest, the Raglan Range platform, 30 km wide at its narrowest point, is situated over a part of the Middle Ordovician shelf rim. This bank persisted as a site of shallow-marine sediment accumulation until it was drowned and buried by mudrock (Kitson Formation) in the Early Devonian. Distinct facies of the Allen Bay, Cape Storm, Douro and Barlow Inlet formations are recognized both on the southern shelf and in the Upper Ordovician through Upper Silurian strata of the offshore platform.

The Towson Point platform of northeastern Melville Island (coeval and probably continuous with the similar Bent Horn platform of Cameron Island area) also persisted as a shallow-marine carbonate bank into the Silurian but, after an Early(?) Devonian marine advance, continued to be the site of unrestricted carbonate deposition (Blue Fiord Formation) down to the latest Early Devonian or earliest Middle Devonian. The foundation strata of the southern shelf, the Ordovician to Devonian section of Towson Point platform, and representative younger formations in the Weatherall Bay-southeastern Sabine Peninsula area, are schematically depicted in Figure 28.

A third Silurian and older carbonate platform underlies Prince Patrick Island and is probably continuous with the southern shelf via M'Clure Strait and western subsurface Banks Island.

Middle and Upper Devonian clastic wedge

The depositional record of uplift and tectonic activity on the site of the deep water basin is preserved in the Middle and Upper Devonian clastic wedge. On Melville Island, this is a 3.3 to 4.6 km thick, siliciclastic- and

mudrock-dominated foreland succession that still blankets part of the southern shelf and most of the ancient intrashelf embayment, offshore carbonate platforms, Canrobert Trough and the southern fringe of the deep water basin (Figs. 23–28). The clastic wedge is widely exposed at the surface throughout most of Melville Island south of Sproule and Sabine peninsulas.

Embry (1988a, 1991a) distinguishes three unconformity-bounded sequences in the foreland basin succession of the Arctic Islands. The oldest of these is the Hecla Bay Sequence. On Melville Island, it comprises four diachronous formations, which, from the base include the Blackley, Cape De Bray, Weatherall, and Hecla Bay formations. Above this, the Beverley Inlet Sequence includes the Fram, Hell Gate and Nordstrand Point formations on Ellesmere and Devon islands (Embry and Klován, 1976). On Melville Island it comprises a single unit; the Beverley Inlet Formation. The Parry Islands Sequence is the youngest unconformity-bound package in the foreland basin and is also represented by a single formation (Parry Islands Formation) within which there are five locally mappable units.

Wherever possible, interval sonic velocities have been used to depth-convert seismic reflection profiles of the clastic wedge. However, some Middle and Upper Devonian formations were not drilled (because of their shallow structural position). Depth conversion of these profiles was accomplished by selective application of Dix interval velocities as calculated from optimal stacking velocities using the Dix equation (see above, Chapter 1).

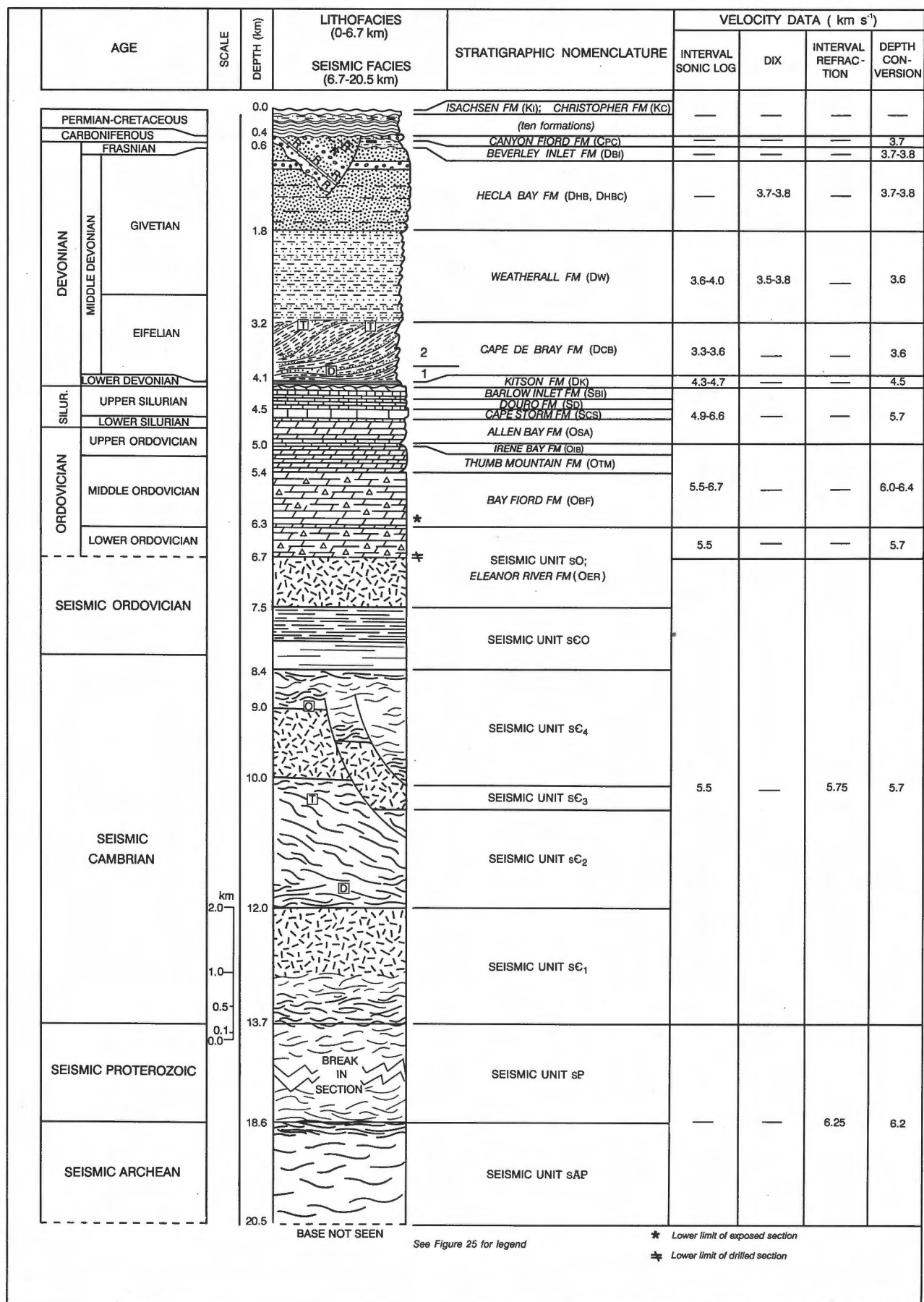
Description of seismic units

Seismic unit sC1A

Distribution. A seismically channelized unit identified in the subsurface of Dundas Peninsula and beneath many parts of southeastern Melville Island at depths of 1.2 to 1.7 s (3.4–4.8 km at 5.7 km s⁻¹) below the Bay Fiord Formation. In the northwest, seismic unit sC1A passes laterally into the upper part of acoustically similar, but much thicker, seismic unit sPC (Section G, Note 6).

Thickness. Ranges from 0(?) to 220 ms (or 0(?) to 630 m at 5.7 km s⁻¹). Local thickness variations of 80 to 160 ms (230 to 460 m) are observed.

Description. Basal onlapping and apparent toplapping reflections of variable amplitude (Fig. 29; Section F,



Note 9). Seismic fill can also be reflection free. Units encountered below sC1A include sP3 and the various members of sP2. The upper limit of these older units is defined by a dramatic truncation of their contained horizontal or dipping reflectors below sC1A. A weak basal reflection, commonly identified where sC1A overlies unit sP3, may also be absent locally. Where sC1A is indistinguishable from sP3, the two units are lumped together as unit sPc (Section G, Note 6).

Interpretation. The contact beneath sC1A is interpreted as a regionally significant angular unconformity (Figs. 16, 29). The weak basal reflection separating sC1A and what are thought to be Upper(?) Proterozoic clastic rocks of unit sP3 indicates that both units have similar densities and interval velocities. The additional occurrence of short, parallel, discontinuous internal reflections in sC1A, however, also argues for large lateral and vertical variation in lithofacies. The stratigraphic position of the unit above an irregular peneplain surface points to the likelihood of some coarse terrigenous sediment in these deposits. It is suggested that sC1A is a basal transgressive unit of mixed terrigenous lithofacies with variable thickness resulting from filling of a pre-existing erosional topography.

Seismic unit sC1B

Distribution. A tabular seismic unit known to underlie all parts of southeastern and central Melville Island at normal depths of 0.9 to 2.0 s (2.6–5.7 km at 5.7 km s⁻¹)

below the Bay Fiord Formation. The unit is up to 1.0 s deeper west of Hecla and Griper Bay and is beyond the limits of seismic resolution north and west of McCormick Inlet.

Thickness. Range is from a minimum of 180 ms (520 m at 5.7 km s⁻¹) in the southeast to a maximum of 400 ms (1100 m) in the northwest.

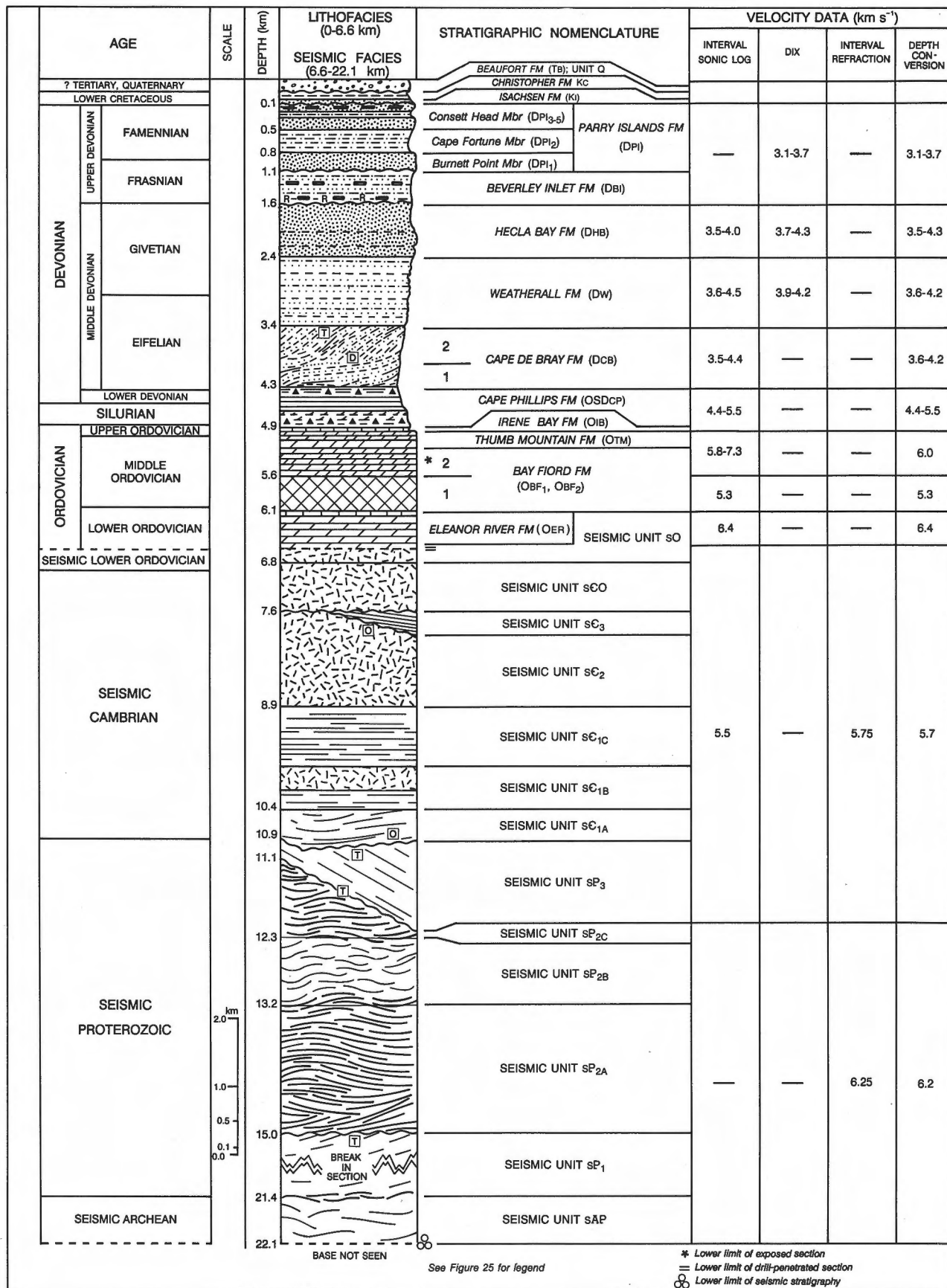
Description. Three gradationally linked seismic facies, which from southeast to northwest include: 1) a mildly reflective or unreflective facies 250 to 320 ms thick (710–910 m) with either weak parallel internal reflections or a reflection-free pattern grading to; 2) a thicker, moderately reflective facies with discontinuous reflection segments (320–400 ms or 910–1140 m thick); grading to 3) a strongly reflective but thinner facies with numerous strong reflection segments (about 320 ms or 910 m). Seismic facies 1 is present on Sections A and C. Facies 2 is widely represented on all of Sections A through G (Fig. 13). Facies 3 is present on Sections H and I (Fig. 30) where it underlies the lower of two, regionally persistent, reflection-free units (sC1C). A strong continuous reflector marks the base of sC1B where it overlies unit sC1A (Fig. 29A). Internal reflectors in sC1A below the lower contact locally display apparent toplap (P1662, Section A). Elsewhere, the lower contact is seismically gradational and is drawn at the base of the lowermost strong reflectors where sC1B overlies sPc or where reflections in sP2 are truncated updip. On many seismic sections, sC1B and sC1C are indistinguishable.

Interpretation. Unit sC1B is interpreted as comprising a lithologically mixed assemblage of outer shelf (facies 1) and slope-related (facies 2 and 3) deposits. The lower contact above sC1A is interpreted as a marine maximum flooding surface generated perhaps by the impedance contrast of laterally persistent mudrocks or carbonates lying on siliciclastics (Fig. 29C). The northwestward increase in internal impedance contrasts and thickness from facies 1 to facies 2 is equated with an increase in low velocity mudrock(?) in the section and a transition in depositional setting from outer shelf to upper basin slope. The thinning into facies 3 is believed to be associated with a slight depositional condensation of section, as might be expected in a lower basin slope setting.

Seismic unit sC1C

Distribution. A tabular seismic unit which everywhere overlies sC1B at normal depths of 0.9 to 1.6 s (2.6–4.7 km at 5.7 km s⁻¹) below the Bay Fiord Formation. The unit is up to 1.0 s deeper west of Hecla and Griper

Figure 26. Representative stratigraphy of the Precambrian(?) to Devonian shelf rim, Devonian clastic wedge, and Carboniferous through Cretaceous cover of Sverdrup Basin (Raglan Range and Cape Grassy areas), west-central Melville Island. Seismic stratigraphy is taken from seismic profile P1135 (Section I; Fig. 30). Ordovician through Lower Devonian lithostratigraphy is obtained from measured sections of the Kitson River Inlier and from the Zeus F-11 and Kitson River C-71 wells. The clastic wedge stratigraphy is taken from measured sections in Raglan Range and from seismic data. Thicknesses of Carboniferous to Cretaceous formations are based on the surface geology of the Cape Grassy area. The ten (undivided) formations in the interval between the Canyon Fiord and Isachsen formations are the Troid Fiord, Blind Fiord, Bjorne, Jameson Bay, Sandy Point, McConnell Island, Hiccles Cove, Ringnes, Awingak and Deer Bay formations.



Bay and is beyond the limits of seismic resolution north and west of McCormick Inlet.

Thickness. Ranges from 80 to 420 ms (or 240–1200 m at 5.7 km s^{-1}). The thinnest development of sC1C occurs on Section C (P1660) where it either feathers into sC1B or is nearly cut out below sC2.

Description. There are two gradationally linked seismic facies in sC1C, including 1) a reflective facies <100 to 300 ms thick (<250–850 m; Fig. 13) with strong, continuous, mildly divergent internal reflections; grading northwest to 2) a reflection-free facies 300 to 420 ms (850–1200 m) thick. The reflection-free facies of sC1C is fully developed on Sections H and I (Fig. 30) where it is the lower of two such units in the Cambrian(?) section. In this area, it overlies the strongly reflective facies of sC1B. The lower contact with sC1B is a strong, continuous reflection in the southeast and on Dundas Peninsula. Basal onlap patterns are observed at one location on line P1141 (Section D, Note 3). In the central and northwest part of the island, the basal contact is apparently gradational and is drawn above the highest strong reflections of sC1B.

Interpretation. Unit sC1C is interpreted as including transgressive and highstand deposits of heterogeneous inner shelf (seismic facies 1) and homogeneous outer shelf (facies 2) association. The basal contact with local onlapping reflectors is interpreted as a sequence boundary. The outer shelf facies of sC1C occurs

basinward of the same facies of sC1B. This is interpreted as indicating a significant basinward shift of facies belts during deposition of the younger unit.

Seismic unit sC2

Distribution. A widespread seismic unit that everywhere overlies sC1C at normal depths of 0.8 to 1.3 s (2.3–3.7 km at 5.7 km s^{-1}) below the Bay Fiord Formation. The unit is up to 1.0 s deeper on Section I and is beyond the limits of seismic resolution north and west of McCormick Inlet.

Thickness. Ranges from 350 to 860 ms (1000–2450 m).

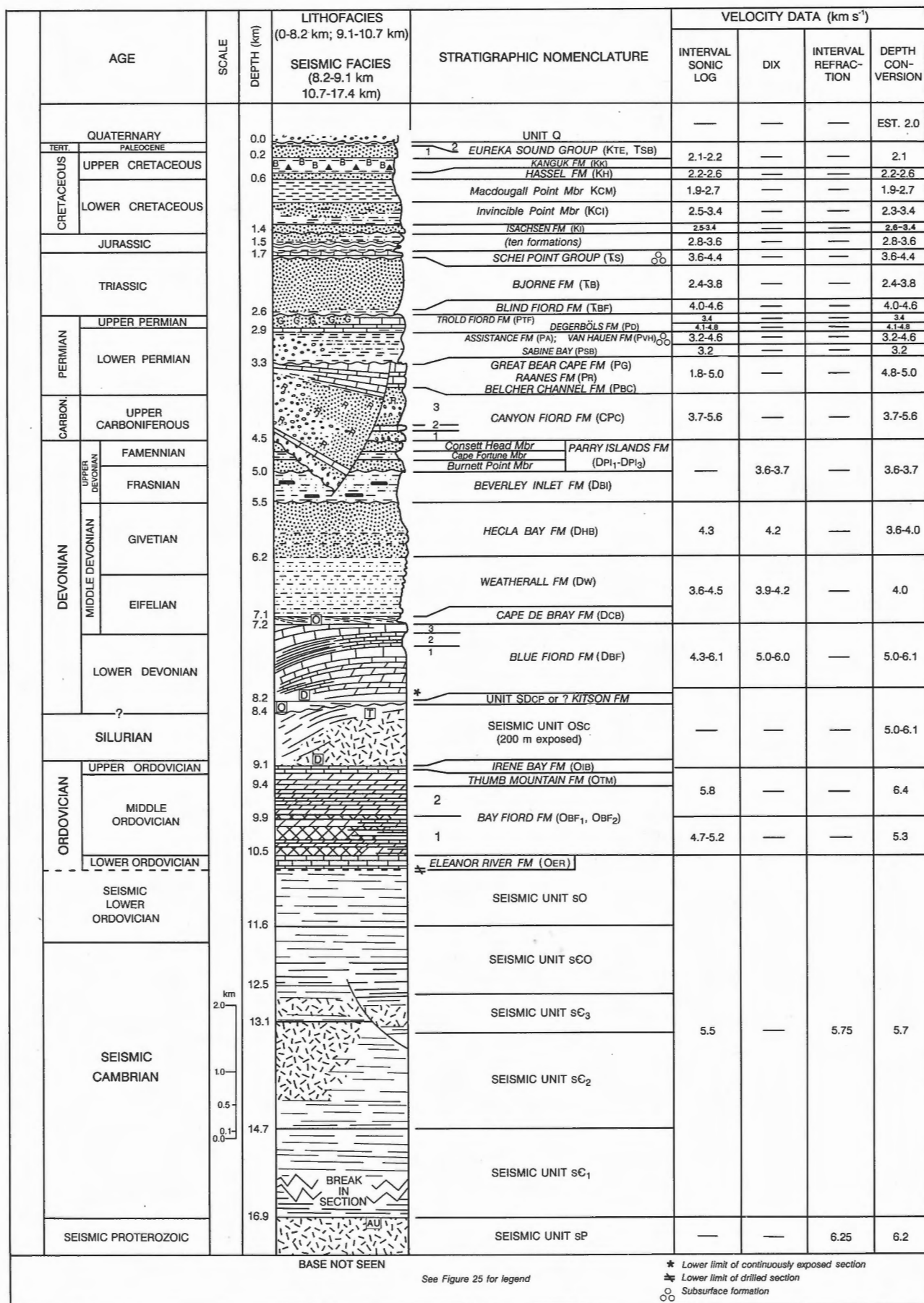
Description. There are two, gradationally linked seismic facies in sC2 including: 1) an extensive reflection-free facies in the southwest, 350 to 450 ms (1000–1300 m at 5.7 m s^{-1}) thick; grading into 2) a thicker, moderately reflective facies with discontinuous internal reflection segments of varying impedance contrast (450–860 ms; 1300–2450 m). Some of the thickening of sC2 is at the expense of underlying seismic unit sC1 (Section H, Note 5). Facies 2 of sC2 is best represented on part of P1135 of Section I (Fig. 30). Unit sC2 here underlies an extensive reflection-free facies of Unit sC3 and overlies a similar reflection-free facies of unit sC1C. The internal patterns in sC2 here display a downlapping and progradational seismic pattern with bottomset reflectors, clinoforms and topset reflectors (Section I, note 15). The basal contact is a universally strong and regionally traceable reflector.

Interpretation. Unit sC2 is interpreted as including transgressive and highstand deposits. Seismic facies 1 consists of an internally similar outer shelf assemblage that grades to clinoformed, acoustically variable basin-fill deposits of facies 2. In the southeast, the outer shelf facies is developed above the inner shelf facies of sC1C, and in the northwest the basin-fill facies of sC2 downlaps onto the outer shelf facies of sC1C. These observations indicate that a sequence boundary probably exists near the base of sC2 and that a major advance of relative sea level occurred at that time.

Seismic unit sC3

Distribution. A tabular unit that underlies Dundas Peninsula and central Melville Island. The top of the unit is normally found at 0.5 to 0.8 s (1.4–2.3 km)

Figure 27. Representative stratigraphy of the Precambrian(?) to Lower Ordovician seismic interval, Ordovician to Devonian intrashelf basin and embayment, Devonian clastic wedge, and Cretaceous to Quaternary cover, southeastern Melville Island. Seismic stratigraphy is based on seismic profiles in the vicinity of pin 5 on Section C. Lithostratigraphy of the Ordovician through Lower Devonian formations was obtained from the penetrated interval in the Sabine Bay A-07 well. The age and subdivisions of the Cape Phillips Formation were determined from measured sections on Middle Island and southeast of McCormick Inlet. The formations and members of the clastic wedge are from measured and traversed sections in the Meham River and Byam River synclines, north of Beverley Inlet. The Cretaceous and younger cover represents the stratigraphy of Meham River outlier.



deeper where it underlies Unit sC4 of Section I. It is below the depth of seismic resolution west and north of McCormick Inlet, is apparently overstepped by sC0 on P2218 of Section C (Note 8), and is absent on Sections A and B of eastern Melville Island (Fig. 13).

Thickness. The unit thickens progressively from a feather edge in the southeast to an imaged maximum of 480 ms (1370 m) in the northwest.

Description. There are two seismic facies in sC3, including: 1) a strongly reflective facies with modestly divergent internal reflections (which is found near the feather edge and in the thinner parts of the unit where it ranges from 0(?)–350 ms or 0(?)–1000 m in thickness); and 2) a thicker, reflection-free facies (350–480 ms or 1000–1370 m) found farther to the northwest beneath central Melville Island (Fig. 30). The lower contact is everywhere a persistent horizontal reflector. Onlapping reflection segments have been noted above the basal reflector on Section D (Note 4) and on Section I (Note 15).

Interpretation. The base of sC3 is at least locally interpreted as a sequence boundary. The strata

contained in sC3 are believed to include heterogeneous transgressive and highstand inner shelf (seismic facies 1) and more homogeneous outer shelf deposits (facies 2). The inner shelf facies of sC3 normally overlies the outer shelf facies of sC2. On Section I, the reflection-free outer shelf facies of sC3 overlies the basin-fill and clinoformed facies of sC2. These features of the unit, and the fact that sC3 is apparently overstepped shelfward by sC0, indicates that a major basinward retreat of the shelf margin occurred during the accumulation of sC3.

Seismic unit sC4

Distribution. The top of unit sC4 is found at 0.6 to 0.7 s (1.7–2.1 km at 5.7 km s⁻¹) below the Bay Fiord Formation and is limited in distribution to subsurface areas east and west of Hecla and Griper Bay. The unit is apparently overstepped shelfward (southward) by unit sC0 on P1830 and C131X of Section I (Note 11) and also on P1921 of Section E (Note 2). The unit is tentatively identified on disconnected seismic profiles beneath basin facies strata of Sproule Peninsula and Eglinton Island.

Thickness. Range in thickness is 0(?) to 1100 ms or 0(?) to 3100 m at 5.7 km s⁻¹. The unit displays large thickness increases (syntectonic growth) across seismically defined normal faults on P1135 (Section I, Note 17; Fig. 30).

Description. Internal seismic patterns include divergent internal reflections near the updip basin margin (southern) limit and variably disrupted weak and strong parallel reflections farther basinward (to the north). A strong, continuous reflector marks the basal contact. Basal onlap patterns are observed at the updip limit of the unit (Section I, Note 12; Section E, Note 2).

Interpretation. Unit sC4 is interpreted as a heterogeneous lithofacies that includes lowstand and transgressive deposits. The onlap patterns noted at the base are considered evidence for a sequence boundary beneath the unit.

Seismic unit sC0

Distribution. A widespread tabular seismic unit everywhere underlying the Eleanor River and Canrobert formations, and associated seismic stratigraphy (Unit s0). The upper contact of sC0 is encountered at depths ranging from 250 to 400 ms

Figure 28. Representative stratigraphy of the Precambrian(?) through Lower Ordovician seismic interval, Ordovician through basal Middle Devonian Towson Point carbonate platform, Devonian clastic wedge, and Carboniferous through Tertiary strata of southern Sverdrup Basin (southern Sabine Peninsula and Weatherall Bay areas) northeastern Melville Island. Seismic stratigraphy is based on seismic profiles P2185 (Section D) and P1921 (Section E). Lithostratigraphy of Ordovician through Lower Devonian formations is based on surface measured sections and some well data (Eldridge Bay E-79, King Point West B-53, Weatherall O-10). The clastic wedge data are from surface sections east of the east arm of Weatherall Bay. The stratigraphy of the Carboniferous through Lower Cretaceous formations is based on seismic profile P1921 (Section E) and associated wells (especially Sherard Bay F-34 and Marryatt K-71). Upper Cretaceous and Tertiary formations have been projected from northern Sabine Peninsula. The ten thin formations between the Schei Point Group and the Isachsen Formation are the Grosvenor Island, Maclean Strait, Loughheed Island, King Christian, Jameson Bay, Sandy Point, McConnell Island, Ringnes, Awingak, and Deer Bay formations.

SOUTHEAST

NORTHWEST

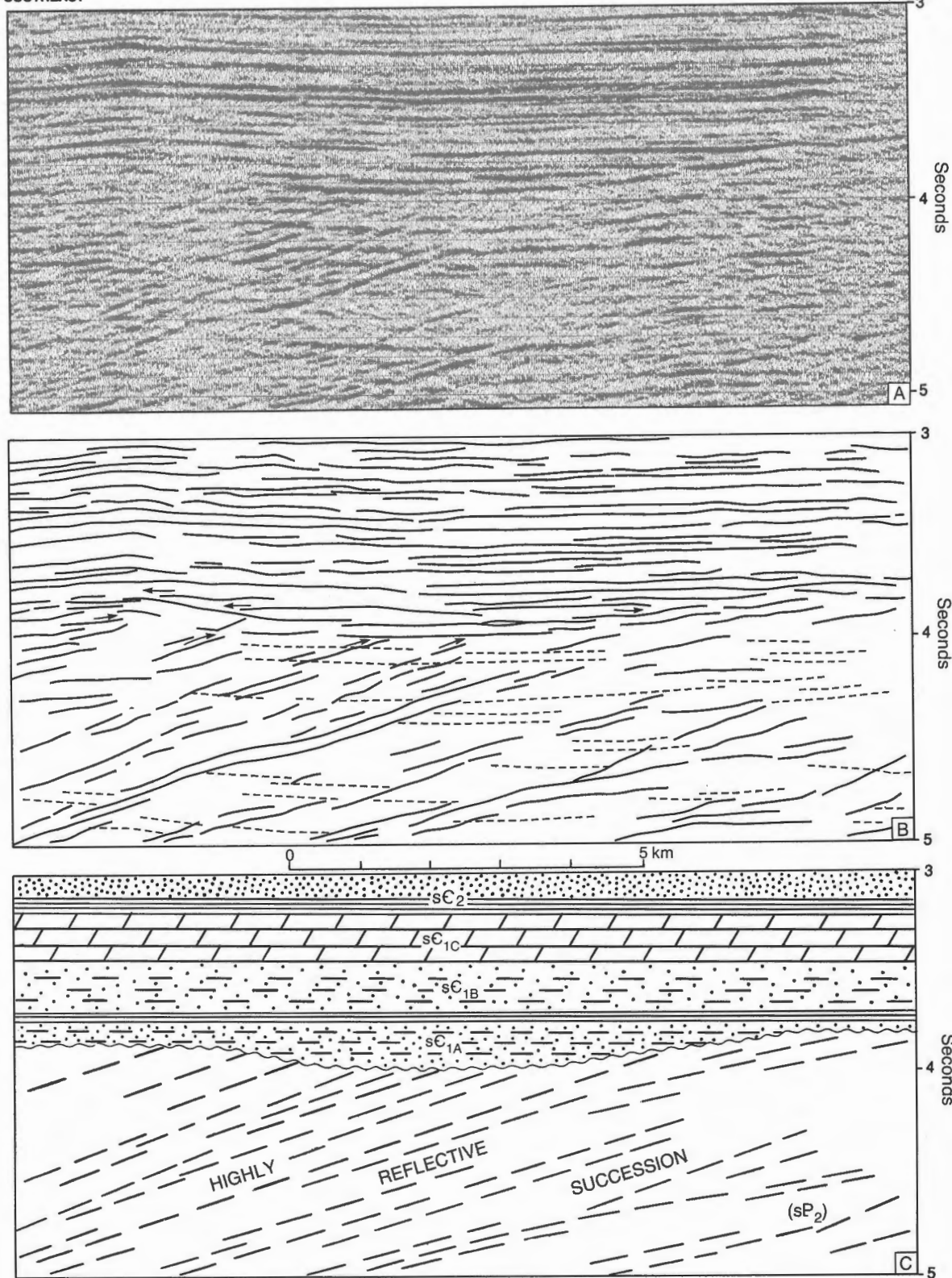


Figure 29. Seismic expression (A) and interpretations (B, C) of incised valley fill (unit sC_{1A}) at the base of the Lower(?) Cambrian on a portion of seismic profile P1171 (Section F). Structural relief suggested near the left side of these diagrams is attributed to velocity pull-up generated by velocity anisotropy higher in the section. Vertical exaggeration is approximately 0.85 below 3.8 s, and 0.92 above 3.8 s.

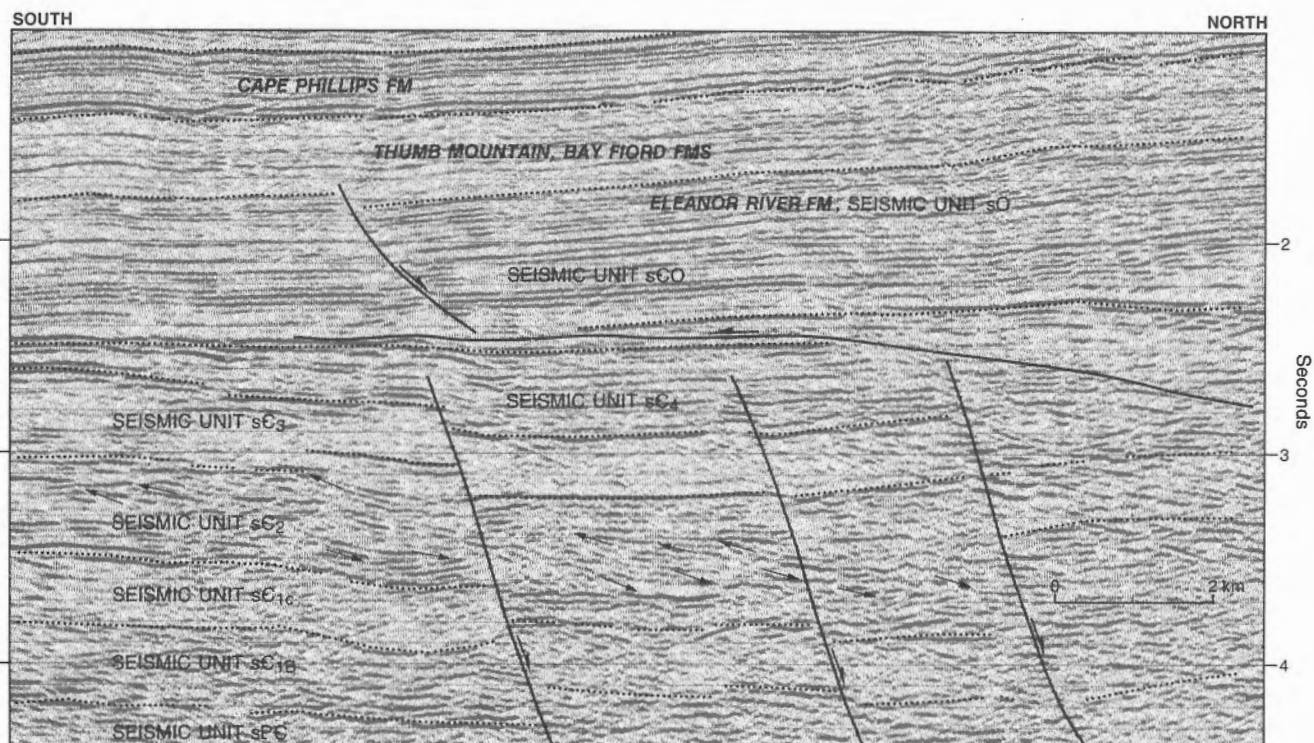


Figure 30. Part of seismic profile P1135 (Section I) displaying characteristic Cambrian(?) and Ordovician seismic stratigraphy. The Apollo C-71 well (located 18 km off section to the southwest) terminates in the upper part of the Bay Fiord Formation. Vertical exaggeration is approximately 0.96.

(750–1200 m at 6.0 km s⁻¹) below the Bay Fiord and Ibbett Bay formations.

Thickness. Increases progressively from 185 ms (530 m) in the southeast to a maximum of 390 ms (1110 m) in the northwest.

Description. Dominated internally by weak, parallel, continuous reflectors in the southeast (Fig. 13) where the unit overlies sE2 or sE3. In these areas the seismic expression of sEO is essentially identical to that of the overlying Unit sO, which is known to contain dolostone and limestone of the Eleanor River Formation. Seismic facies of sEO grade to strong continuous internal reflections in the central and northwestern areas (Section I; Note 11; Section D, Note 8; Fig. 30) and in the subsurface of southern Sabine Peninsula (Section E) where unit sEO overlies unit sE4. On Section I (P1135), the strong internal reflections of unit sEO are separated from the basal sEO reflector by a reflection-free subunit up to 185 ms (540 m at 5.7 km s⁻¹) thick. The lower contact of sEO is everywhere marked by a strong and continuous reflection above a variety of units (sE2, sE3 and sE4) two of which are progressively cut out by sEO toward the southeast (sE4 and sE3).

Interpretation. Unit sEO is interpreted as including transgressive and highstand deposits. The lower contact of sEO with sE4 is a possible maximum flooding surface and both units are believed to have accumulated within a common depositional sequence. The common basal sequence boundary is placed beneath sE4 where it is present, and beneath sEO where the latter overlies sE3 and sE2. Seismic facies 1 of sEO may include internally homogeneous platform carbonates similar to those in the overlying, seismically similar Eleanor River Formation and associated strata (Unit sO).

Seismic unit sO

Distribution. Seismic unit sO includes the drilled portion of the Eleanor River Formation in the upper part. This tabular seismic unit underlies the Bay Fiord Formation in all southern subsurface parts of the island. The unit, tentatively identified on disconnected seismic profiles of Sproule Peninsula and Eglinton Island may also extend beneath the Ibbett Bay and Canrobert formations of Canrobert Trough.

Thickness. Total thickness down to the seismically-defined lower contact ranges from 240 ms (720 m at 6.0 km s^{-1}) in the southeast, to 400 ms (1200 m) in the northwest. On Eglinton Island the unit is up to 530 ms thick (1500 m) but is again thinner beneath Sproule Peninsula (380 ms, 1100 m).

Description. In most areas, sO is a tabular seismic unit characterized internally by either weak, disrupted, parallel reflections or an internally reflection-free pattern (Fig. 13). A second seismic facies of uncertain areal extent is seen north of C131x on Section I (Note 14; see also Fig. 30). This facies consists of some strong, parallel internal reflections. On Sproule Peninsula and Eglinton Island, unit sO is reflection free. The basal contact features a low-amplitude but laterally continuous reflector in apparently conformable contact with seismic unit sCO.

Interpretation. Unit sO is interpreted as including open-marine shelf carbonates of intertidal and lesser subtidal origin. The known lower age range of the unit indicates a correlation of the drilled part of unit sO with similar carbonates of the Eleanor River Formation. The maximum known thickness of the Eleanor River Formation on Ellesmere Island is about 820 m (Trettin, 1990). Therefore, it seems likely that the seismic interval down to the sub-sO reflector also contains strata older than but acoustically similar to the Eleanor River Formation. This might include carbonate strata similar to the Tremadocian Blaney Bay Formation of Devon Island (Thorsteinsson and Mayr, 1987) or the Ninnis Glacier beds of Judge Daly Promontory (Trettin et al., 1991). The sub-sO reflector above sCO is tentatively correlated with the top or base of the Cape Clay Formation, a widespread Tremadocian dolostone unit with a high sonic velocity (6.4 km s^{-1}) and significant impedance contrast with overlying and underlying units as observed in the Panarctic Deminex Cornwallis Central Dome K-40 well of Cornwallis Island (Thorsteinsson and Mayr, 1987). The evaporitic Baumann Fiord Formation (Tremadoc; Trettin, 1990) of Ellesmere and Cornwallis islands may also be age equivalent to unit sO. Evaporitic layers interbedded with higher velocity carbonates could account for the more reflective facies of seismic unit sO on the northern part of Section I (Note 14).

Where unit sO underlies and is continuous with the slope facies resedimented carbonates of the Canrobert Formation, slope deposits are also interpreted as occurring in the typically reflection-free seismic facies of the unit.

Age and correlation of Cambrian(?) and Lower Ordovician seismic units of the southern shelf

Assumptions

Any attempt to correlate the Cambrian(?) and Lower(?) Ordovician seismic units of the southern shelf of subsurface Melville Island (for which no lithological or paleontological data are presently available), must take into account certain observations and assumptions.

The first observation concerns thickness variations in the Cambrian and Lower Ordovician of the Arctic Islands (summarized in Fig. 31). The closest known exposures of Cambrian strata, situated on northern Victoria Island, probably do not exceed 300 m in total thickness. The oldest strata in the area are isolated Lower Cambrian outcrops (near Glenelg Bay, northern Victoria Island) reported to contain a distinctive olenellid trilobite fauna (Thorsteinsson and Tozer, 1970; Thorsteinsson, pers. comm., 1990). More widespread though discontinuous, on Victoria Island is an upper Middle(?) and Upper Cambrian basal sandstone (Map Unit 10a of Thorsteinsson and Tozer, 1962) and a gradationally overlying succession of three Upper Cambrian through Lower Ordovician dolostone formations (410 m total; lower part of Map Unit 10b of Thorsteinsson and Tozer, 1962; Trettin et al., 1991).

Age-equivalent strata are equally thin on Somerset Island (Stewart, 1987) and Boothia Peninsula; the Cambrian (Upper Cambrian only?) and Lower Ordovician succession, represented by the Turner Cliffs and Ship Point formations (540 m of dolostone and lesser sandstone) lies unconformably on Proterozoic sedimentary rocks and older crystalline basement. In contrast to these thin successions of the exposed southern shelf, the same chronostratigraphic interval, 165 km to the north on Cornwallis Island, is dramatically thicker. More than 2100 m of Upper Cambrian strata (base not seen) and 2000 m of Lower Ordovician strata below the Bay Fiord Formation in surface sections and in the Cornwallis Central Dome K-40 well (Thorsteinsson and Mayr, 1987) is evident.

Figure 31. Suggested correlation of Cambrian(?) and Lower Ordovician seismic stratigraphic units of subsurface northwestern and southeastern Melville Island with Cambrian and Lower Ordovician surface formations of the central and eastern Arctic Islands (Thorsteinsson and Tozer, 1970; Mayr, 1978; Thorsteinsson and Mayr, 1987; Trettin, 1990; Trettin et al., 1991). Thicknesses in metres ($\times 10^2$).

RADIOMETRIC AGE		SYSTEM	SERIES	STAGE	MELVILLE ISLAND				VICTORIA ISLAND	CORNWALLIS ISLAND	SOMERSET ISLAND	ELLESMERE ISLAND	
COWIE et al. (1989)	PALMER (1983)				SUBSURFACE BLUE HILLS SYNCLINE		SUBSURFACE SOUTHEAST					BACHE PENINSULA	JUDGE DALY PROMONTORY
					Modified from Trettin, 1990								
473(?)	458	ORDOVICIAN	MIDDLE	LLANVIRN	BAY FIORD FM		BAY FIORD FM		strata possibly	BAY FIORD FM	BAY FIORD FM	eroded below Quaternary	BAY FIORD FM
			ARENIG	dol anhy 8.2-10.0		salt dol anhy 3.1-11.0				dol 1st anhy 5.2	sh 0.4		1st dol slt 5.8
			LOWER	ELEANOR RIVER FM	SEISMIC UNIT	ELEANOR RIVER FM	SEISMIC UNIT	absent		ELEANOR RIVER FM		ELEANOR RIVER FM	
			TREMADOC	dol 2.0+		dol 7.3+				SHIP POINT FM		3.0	
				not drilled	sO	not drilled	sO	BLANLEY BAY FM		BAUMANN FIORD FM		BAUMANN FIORD FM	
								CAPE CLAY FM		CHRISTIAN ELV FM		NINNIS GLACIER FM	
								CAPE CLAY FM		CAPE CLAY FM		CAPE CLAY FM	
510(?)	505	CAMBRIAN	UPPER	TREMPEALEAU	SEISMIC UNIT sC ₀		SEISMIC UNIT sC ₀		CASS FJORD FM		Upper		CASS FJORD FM
			FRANCONIAN	8.0-11.1		5.3-8.0		dol 2.1		sh 1st 7.4		TURNER	
								absent?		Lower		absent?	
			DRESDACHIAN	SEISMIC UNIT sC ₄				Map unit 10a		21.8+sh slt ss 14.4		CASS FJORD FM	
				70-31				ss				dol ss 3.4	
												1st slt 4.9	
												7.3-17.1	
			MIDDLE	SEISMIC UNIT sC ₃		SEISMIC UNIT sC ₃						CAPE WOOD FM	
				70-10								dol 1st 0.4	
												SCORESBY BAY FM	
523(?)		CAMBRIAN	LOWER		10-13.7						absent		
				topsets	SEISMIC UNIT sC ₂		unnamed, undivided		covered		above		four formations (undivided)
				clinoforms	SEISMIC UNIT sC ₂		10-13 thin				Proterozoic		DALLAS BUGT FM
				bottomsets	SEISMIC UNIT sC ₂						above		RAWLINGS BAY FM
				13-24	SEISMIC UNIT sC _{1C}		SEISMIC UNIT sC _{1C}				ss cgl 0.6		1.8
					8.5-12.0		2.5-8.5				absent		ELLA BAY FM
					9.1-11.4		7.1-9.1				above		KENNEDY CHANNEL FM
					SEISMIC UNIT sC _{1A}		70-6.3				Proterozoic		covered
					SEISMIC UNIT sP _C								
					SEISMIC UNIT sP ₃								
550(?)	570	EDIA-CARIAN											

See Figure 19 for legend

A similar thickening trend is observed on east-central Ellesmere Island, where Lower Cambrian through Lower Ordovician strata, 1370 m thick on Bache Peninsula, thicken progressively, over a distance of 225 km, to a maximum of 6500 m on Judge Daly Promontory (base not seen; Trettin et al., 1991; Trettin, 1990).

The first assumption to make therefore, is that the northward thickening of the Cambrian and Lower Ordovician succession of Ellesmere Island and the central Arctic Islands is a feature common to the entire lower Paleozoic shelf from Greenland to Melville Island, and that isopachs of this succession should be approximately parallel to the northeasterly trending shelf to deep water basin facies transition as indicated on the paleogeographic maps of Trettin (1989; see also Fig. 24).

Equally vital to the correct correlation of subsurface seismic units and distantly exposed formations are the ages of major unconformities in the Cambrian succession of the Canadian Arctic Islands and adjacent parts of the northern mainland. The most significant unconformity surface is the regional angular unconformity that places Lower Cambrian shelf-related strata on stratified Upper Proterozoic and older rocks. This relation is observed throughout the Arctic from North Greenland to Devon Island, throughout the southern Arctic Islands to Victoria Island, and in the Canadian Cordillera (Trettin, 1990; Aitken and Stott, 1991). It is therefore assumed that the angular unconformity beneath seismic unit sC1A of subsurface Melville Island corresponds to the angular unconformity beneath Lower Cambrian strata as observed elsewhere.

The next most significant unconformity in the Cambrian succession of Arctic North America is the disconformity beneath uppermost Middle Cambrian or lower Upper Cambrian (Dresbachian) strata. This corresponds to the unconformity beneath: 1) the Cass Fjord and Parrish Glacier formations of Ellesmere Island and northwest Greenland (Trettin, 1990; Kerr, 1967); 2) the Gallery and Turner Cliffs formations of Baffin and Somerset islands, respectively (Stewart, 1987; Trettin, 1969); Map Unit 10a of Victoria Island and; 4) the Saline River and Franklin Mountain formations of the Franklin and Mackenzie mountains and Mackenzie Platform (Aitken, 1991). In the Fairman Point area, on southern Ellesmere Island, the same major unconformity separates the Cass Fjord Formation, above, and regressive(?) quartz sand beds, below, that lie in the upper part of the lower Middle Cambrian, carbonate-dominated Cape Wood Formation (Trettin, 1990; Trettin et al., 1991; Mayr,

pers. comm., 1992). In each of these areas, all Lower Cambrian and most Middle Cambrian strata are overstepped by youngest Middle Cambrian and Dresbachian strata above the unconformity.

In a similar fashion, the sequence boundary beneath seismic units sC0 and sC4 is the second most significant unconformity in the Cambrian(?) seismic succession of Melville Island. Seismic unit sC3, which attains a maximum thickness of 480 ms (1370 m), appears to be entirely cut out to the southeast beneath the sub-sC0 unconformity. Therefore, the final stated assumption is that the unconformity below units sC0 and sC4 corresponds to the sub-upper Middle Cambrian unconformity documented in many ancient shelf areas of Arctic North America.

Evidence and regional implications

It follows from the above assumptions that Lower(?) and Middle(?) Cambrian seismic strata of Melville Island (seismic units sC1 through sC3) range from 2300 to more than 5600 m in combined total thickness. Comparable age-equivalent sections have been documented by Kerr (1967), Trettin (1990) and Long (1989a) on Judge Daly Promontory, where Lower and Middle Cambrian formations together exceed 4800 m (base not seen). Similarly, youngest Middle(?) Cambrian through Lower Ordovician units below the Bay Fiord Formation (seismic units sC4 through sO of subsurface Melville Island) range from 1200 to more than 5000 m thick. On Cornwallis Island, the same interval exceeds 4100 m (base not seen; Mayr, 1978; Trettin, 1990).

Several key features of the suggested unit by unit correlation (shown in Fig. 31) are worth noting:

1. Part or all of seismic unit sC1A (subsurface Dundas Peninsula and eastern Melville Island) may not have an exact time-equivalent counterpart elsewhere in the Arctic Islands, although the environment of deposition may have been similar to other basal Cambrian formations. The channelized and base onlapping character of the unit is consistent with it being a transgressive, lithologically mixed terrigenous deposit occupying and diachronously filling pre-existing depressions on an irregular sub-Lower(?) Cambrian erosion surface. Comparable strata may be represented by the covered basal beds of the Kennedy Channel Formation of northeast Ellesmere Island (Trettin et al., 1991), shelf facies Skagen Group of North Greenland (Surlyk and Ineson, 1987), the Backbone Ranges Formation of the Mackenzie

Mountains (Fig. 19) and the basal McNaughton Formation of the Gog Group, southern Rocky Mountains (Aitken, 1991; Aitken and Stott, 1991).

2. Three seismic units of moderate to strongly reflective character (sC1B, sC2 and sC4 of Fig. 30) are correlated with stratigraphic units on Ellesmere Island that are composed of mixed clastics, slaty mudrocks and proportionately variable carbonates; namely, the Kennedy Channel Formation, Ellesmere Group and lower Cass Fjord/Parrish Glacier formations (Kerr, 1967; Long, 1989a; Trettin et al., 1991).
3. In the subsurface of central Melville Island (seismic profile P1135; Fig. 30) two reflection-free Cambrian(?) units (sC1C and sC3) are correlated with two thick and massive bedded carbonate units of Judge Daly Promontory—the Ella Bay and Scoresby Bay formations, respectively (Kerr, 1967; Long, 1989a, b; Trettin et al., 1991).
4. Distinct depositional facies of sC2 on seismic line P1135 may correlate with the following formations of the Ellesmere Group of Judge Daly Promontory (formational descriptions from Kerr, 1967; Long, 1989a; and Trettin, pers. comm., 1992):
 - topset reflectors in upper sC2 = Kane Basin Formation (light to dark grey slate)
 - clinoform reflectors of sC2 = Rawlings Bay (quartzose sandstone, minor slate) and upper Ritter Bay (grey slate, lesser sandstone) formations
 - bottomset reflectors of sC2 = lower Ritter Bay (slate) and Archer Fiord (sandstone; basal pebbly sandstone) formations
5. The Scoresby Bay Formation and the cratonward equivalent Cape Wood Formation are known to be cut out by the Cass Fjord Formation of Bache Peninsula, southeastern and southern Ellesmere Island and Devon Island (Mayr, unpub. ms.; Thorsteinsson and Mayr, 1987). Similarly, the Scoresby Bay-equivalent seismic unit (sC3) is apparently cut out southeastward by the Cass Fjord-equivalent seismic unit (sC4) of Melville Island.
6. The great local thickness of lowstand unit sC4 is attributed in part to synchronous extension faulting (Fig. 30; Note 17, P1135 of Section I). If sC4 is age equivalent to some part of the lower Cass Fjord formation of Judge Daly Promontory,

southern Ellesmere and Cornwallis islands (variegated intertidal and subtidal carbonates and lesser quartz sandstone; Mayr, 1978; Thorsteinsson and Mayr, 1987; Trettin et al., 1991) and correlative Parrish Glacier Formation of central Ellesmere Island (Kerr, 1967; Nowlan, 1985), then the thick local accumulation of Upper Cambrian strata in the Arctic Islands may have been accompanied by widespread periodic exposure of the shelf and coeval tectonic instability.

7. The continuous and, commonly, high-amplitude reflector marking the base of unit sO is tentatively correlated with the impedance contrast from the top (or base) of the thin Cape Clay Formation (Mayr, 1978; Thorsteinsson and Mayr, 1987). In the Cornwallis Central Dome K-40 well, the Cape Clay Formation (90 m) has an interval velocity of 6.4 km s⁻¹ and is underlain and overlain by markedly slower carbonate formations (5.4 and 5.5 km s⁻¹, respectively).
8. Units sC4 and sO are internally reflection-free (or only weakly reflective) over large subsurface areas of Melville Island. This seismic facies of unit sO includes the Eleanor River Formation (shelf dolostone) and Canrobert Formation (resedimented slope carbonates) in the upper part. It is probably safe to conclude that the unreflective and weakly reflective facies of sC4 and sO are generated by lithologically homogeneous shelf- and slope-type carbonate strata and that Lower Ordovician evaporitic strata (such as the Baumann Fiord Formation of western Ellesmere and Cornwallis islands (Kerr, 1968; Mossop, 1979; Mayr, 1978; Thorsteinsson, 1988) are not substantially present in the Melville area.

Description of formations (and other units)

Eleanor River Formation (OER)

Type section. East-central Cornwallis Island (Thorsteinsson, 1958).

Distribution. Widely exposed at the surface throughout the eastern Arctic Islands, the Eleanor River Formation on Melville Island is known from three incomplete drill hole intersections including: 4461-TD 5192 m in the Panarctic et al. Sabine Bay A-07 well; 2316.5-TD 2764.5 m in the Sun KR Panarctic Kitson River C-71 well; and 2841-TD 3044 m in Panarctic Eldridge Bay E-79. Unit sO is the seismic unit that includes the drilled portion of the Eleanor River Formation in the upper part.

Sonic interval velocity. The sonic interval velocity ranges from 5.4 to 6.4 km s⁻¹.

Thickness. Maximum drilled thickness occurs in the Sabine Bay A-07 well (732 m).

Lithology. The Eleanor River Formation is the oldest of the five formations of the southern shelf of Melville Island for which lithological and biostratigraphic data are available. Common rock types in the drilled sections include light grey crystalline dolostone, argillaceous dolostone, and limestone. The dolostone in the Kitson River C-71 and Sabine Bay A-07 wells also contains some nodular replacement chert.

Basal contact. The base of the formation has not been penetrated by Melville Island exploratory wells.

Age and correlation. The Eleanor River Formation of Melville Island contains conodont assemblages of late Tremadoc and/or Arenig age (see reports of McCracken, and Barnes and Uyeno, Appendix 4). In the eastern Arctic Islands the Eleanor River Formation has been correlated with equivalent sections in Greenland that are known to range from the upper Tremadoc to the upper Arenig (Trettin, 1990; Nowlan, pers. comm., 1992). Correlation with the exposed part of the Canrobert Formation of Canrobert Hills is indicated (Fig. 32).

Interpretation. The Eleanor River Formation of Melville Island is interpreted as including unrestricted marine shelf carbonates of intertidal and lesser subtidal origin.

Bay Fiord Formation (OBF)

Type section. Near Irene Bay on west-central Ellesmere Island (Kerr, 1968).

Distribution. The Bay Fiord Formation is the lowest of the three formations that make up the Cornwallis Group. The distribution of the formation in the western Arctic Islands is based on scattered outcrops and drill hole intersections on Cornwallis and Bathurst islands. Four exploratory wells have penetrated the formation on Melville Island (3446–4461 m in the Sabine Bay A-07 well, 1485(?)–2316.5 m in the Kitson River C-71 well, 2101–2841 m in the Eldridge Bay E-79 well, and 3152–TD 3665 m in the Panarctic Apollo C-73 well). An incomplete surface section through the Bay Fiord Formation of the shelf rim is exposed in the lower 768 m of the Kitson River Inlier (Fig. 33) (Unit 1 of inlier section of Goodbody, 1993).

In the intrashelf basin, the Bay Fiord Formation is represented by the drilled interval in the Sabine Bay A-07 well.

Velocity and thickness. Interval velocity for Bay Fiord carbonates (OBF, OBF2) is 6.3 km s⁻¹. Bay Fiord evaporite member (OBF1) is 5.3 km s⁻¹. The computed restored-state (pre-deformational) thickness of these evaporites ranges from less than 120 m at the depositional limit to a maximum of 880 m. Northwesterly (downslope) thickening could be due in part to gravity-induced postdepositional and preorogenic creep of rock salt, common within the unit. Thickness of the carbonate-dominated upper member ranges from approximately 290 to 680 m.

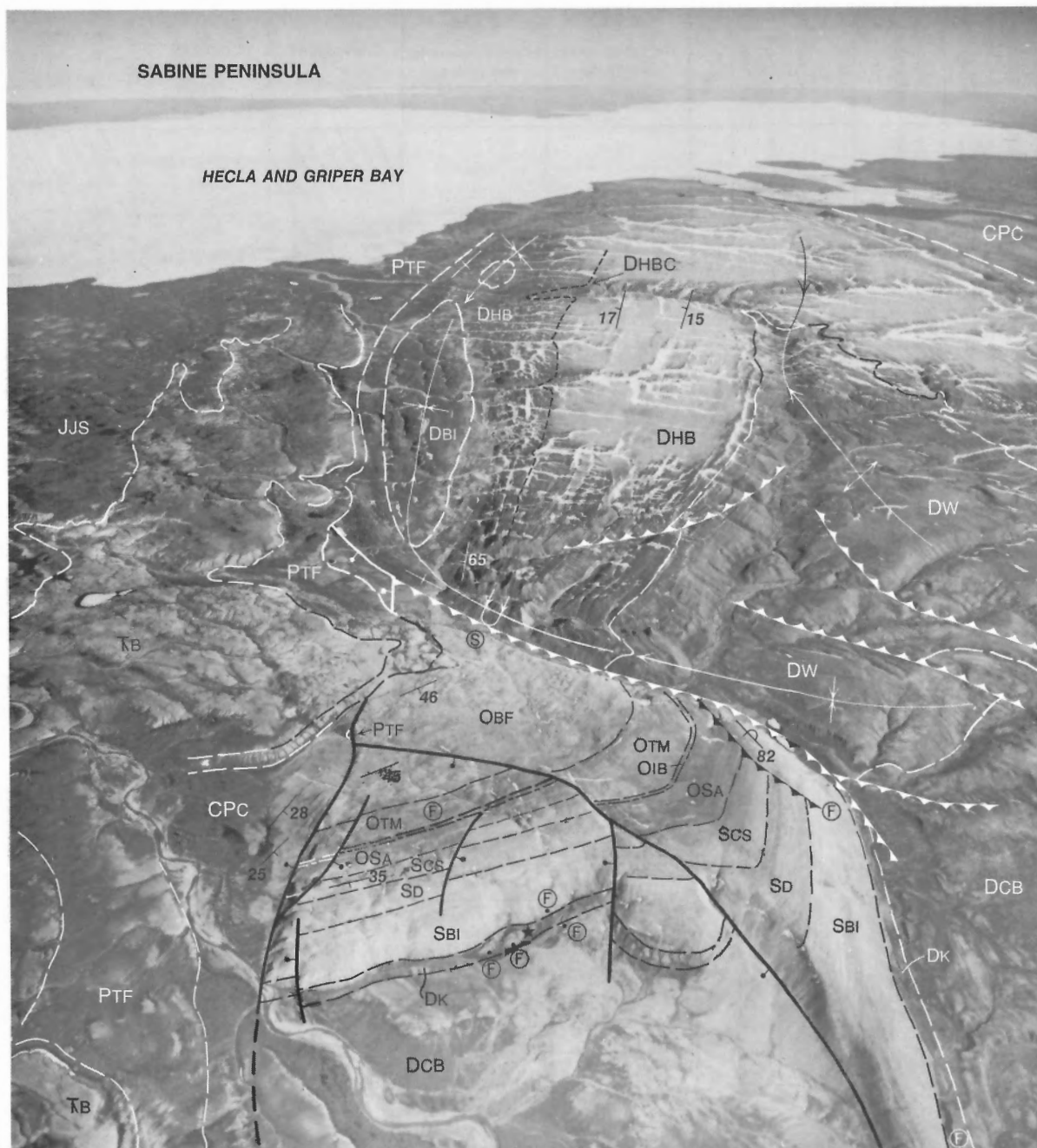
Lithology and seismic expression. The Bay Fiord Formation of the Middle Ordovician intrashelf basin (Figs. 23, 24) comprises variably argillaceous dolostone, halite, anhydrite, minor argillaceous limestone, siltstone and marl. Although only the evaporitic strata low in the formation have been included in the definition of the Bay Fiord Formation as described and mapped by Kerr (1974) and Fox and Densmore (1992), the definition adopted here matches that of Mayr (1980), and Thorsteinsson and Mayr (1987), who also include in the formation a succession of overlying, thin bedded, argillaceous dolostones.

Thus, two members of the Bay Fiord Formation are distinguished in the Sabine Bay A-07 well of Melville Island (Fig. 7). The lower member (OBF1), illustrated in Figure 34, is intersected at 3936 to 4461 m and consists of 42 per cent thick bedded rock salt (halite), 28 per cent anhydrite, and 30 per cent dolostone, with lesser interbeds of limestone and mudrock. Core has been drilled and collected from the lower member of the Bay Fiord Formation of the Dominion Explorers Canso et al. Caledonian R. J-34 well of Bathurst Island (Figs. 142–144). The halite layers tend to be an impure mixture of bedded halite with mudrock, carbonate and anhydrite partings. The halite is commonly very coarse crystalline, and the unit as a whole displays a variety of deformation textures.

The halite-rich lower member of the formation (OBF1) is a distinct and separate seismic unit of highly variable deformed-state thickness (Fig. 13). It is widely represented on seismic profiles of southeastern Melville Island and is bound above and below by very strong and strong, respectively, laterally continuous reflections. The base of the salt is also the fundamental detachment level in thin-skinned deformation in the area. Internally, the lower member consists of a chaotic or imbricated assemblage of reflection segments.

SYSTEM	SUB-SYSTEM	SERIES/STAGE	ABSOLUTE AGE (Ma)				GRAPTOLITE ZONES ARCTIC ISLANDS PROVINCE	CONODONT ZONES NORTH ATLANTIC PROVINCE	FORMATIONS AND MEMBERS		
			PALMER (1983)	HARLAND et al. (1989)	TUCKER et al. (1990)	Ma			CANROBERT HILLS	RAGLAN RANGE	McCORMICK INLET/CENTRAL MELVILLE ISLAND
ORDOVICIAN	SILURIAN	LLANDOVERY									
	LOWER SILURIAN										
	UPPER ORDOVICIAN	CINNCINNATIAN									
		MAYS-VILLAIN									
		EDENIAN									
		TREN-TONIAN									
	MIDDLE ORDOVICIAN	CHAMPLAINIAN									
		BLACK-RIVERIAN									
		CHAZYAN									
		LLANVRN									
	PART OF LOWER ORDOVICIAN	WHITEROCKIAN									
		TREMADOC (upper part)									
		ARENIG									
		CANADIAN									

Figure 32. Correlation chart, Ordovician strata of Melville Island. C, conodont collection; G, graptolite collection; M, shelly macrofauna. All significant fossil collections are listed in Appendix 4.



Geological contact
 Bedding attitudes (inclined, vertical, overturned) 16 / x x
 Minor fold (NV - north vergent, SV - south vergent) NV, SV 2
 Strike slip fault (T - toward, A - away) T A
 Extension fault
 Undetermined fault (solid circle indicates downthrow side)

Thrust or detachment fault
 Anticline (upright or inclined; overturned)
 Syncline (upright or inclined; overturned)
 Fossil location (GSC locality number) C-16903 • F
 Structural (kinematic) data site S
 Location of type section ★
 Exploratory well (abandoned, gas showing, oil showing) ✧ ✧ ✧

Figure 33. Oblique airphoto of the Kitson River Inlier (foreground) and Raglan Range (background). Location of the type section of the Kitson Formation is indicated with a star. OBF, Bay Fiord Formation; OTM, Thumb Mountain Formation; OIB, Irene Bay Formation; OSA, Allen Bay Formation; SCS, Cape Storm Formation; SD, Douro Formation; SBI, Barlow Inlet Formation; DK, Kitson Formation; DCB, Cape De Bray Formation; DW, Weatherall Formation; DHB, Hecla Bay Formation; DHBC, conglomerate in upper Hecla Bay Formation; DBI, Beverley Inlet Formation; CPC, Canyon Fiord Formation; PTF, Troid Fiord Formation; TB, Bjorne Formation; JJS, Jameson Bay and Sandy Point formations (undivided). NAPL photo. T4162-75.

PANARCTIC *et. al.*
SABINE BAY
A-07

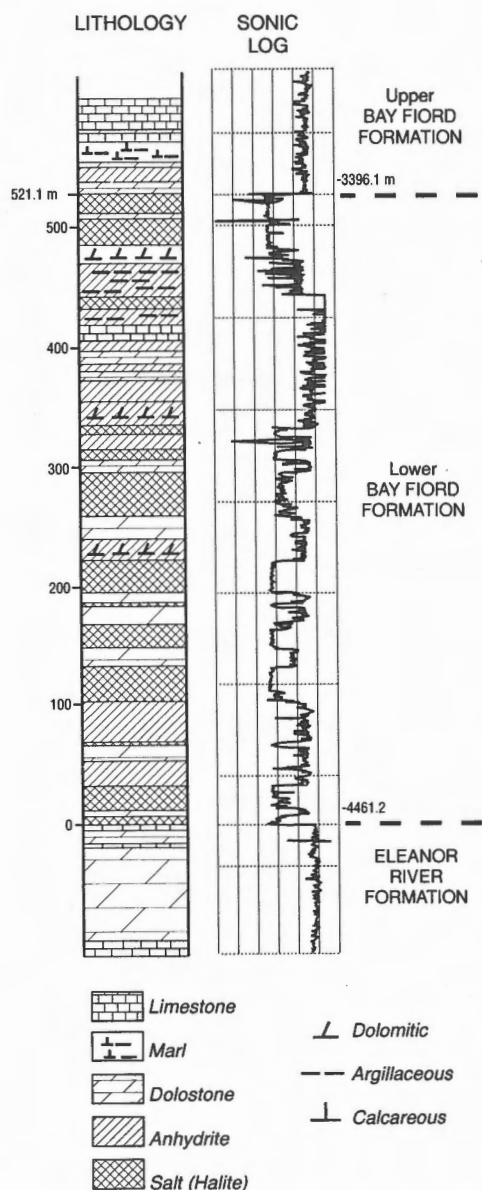


Figure 34. Stratigraphy of the lower Bay Fiord Formation in the Panarctic *et al.* Sabine Bay A-07 well (see also Fig. 7). Proportions of bedded rock salt, dolostone, and anhydrite are calculated to be 42%, 30%, and 28%, respectively.

The upper member (OBF2) is composed of dolostone, with minor marlstone and anhydrite. This member is everywhere a structurally competent succession and in this respect is similar to the overlying Thumb Mountain Formation. It is generally reflection free and seismically continuous with the Thumb

Mountain. There is a strong, laterally continuous internal reflector in the upper member of the Bay Fiord Formation (see Section A, Note 10 for an exception). Lithology and correlation of this marker into the Sabine Bay A-07 well remains undetermined.

The shelf rim facies of the Bay Fiord Formation, as exposed in the lower part of the Kitson River Inlier (Fig. 33) is represented by a continuous succession of yellowish to light grey weathering, light grey, medium to thick bedded cryptalgal laminated dolostones, minor skeletal dolostone and tectonic breccia. Subordinate diagenetic components include light coloured patchy replacement chert, quartz stockwork veinlets and a little vuggy porosity. Similar lithofacies occur in the Kitson River C-71 well.

The major feature of the Bay Fiord Formation of the shelf rim is the absence of the lower evaporitic member. Bay Fiord dolostones in the Kitson River C-71 well, which contain a typical Middle Ordovician conodont assemblage, conformably overlie a similar dolostone interval that contains a Lower Ordovician conodont assemblage typical of the Eleanor River Formation (Fig. 32; Appendix 4).

The regional transition from the southeastern evaporitic facies to the shelf rim dolostone facies of the Bay Fiord Formation is documented by correlative stratigraphic intervals in two wells located near the facies front (2338–2841 m in Eldridge Bay E-79 and 3423–TD 3665 m in Apollo C-73). These intervals, tentatively assigned to the lower member of the Bay Fiord Formation, consist of an intercalated and thinly interbedded succession of variably argillaceous limestone, dolostone and bedded anhydrite.

The depositional limit of the evaporitic (halite) facies of the lower Bay Fiord Formation is identified geophysically on P1168 of Section F (Note 13; Fig. 35), and on two seismic lines of Section I (Notes 6, 13; Fig. 36). The limit of the salt on Section F is marked by a gradual southwestward thinning of the seismically defined lower member approaching the interpreted depositional limit, and by a sudden tapering off of the bounding reflections at the facies front (Figs. 35A, B).

Approaching the northwestern facies front on Section I (Note 9; Fig. 36), thickening of the upper carbonate member is at the expense of a thinning to zero of the underlying evaporitic member. Irregularities on or near the upper contact of the evaporitic member have produced diffraction hyperbolae (Note 6). Absence of salt beyond the facies front is indicated by the absence of strong reflectors that underlie and overlie the salt facies elsewhere (Section I, Note 13).

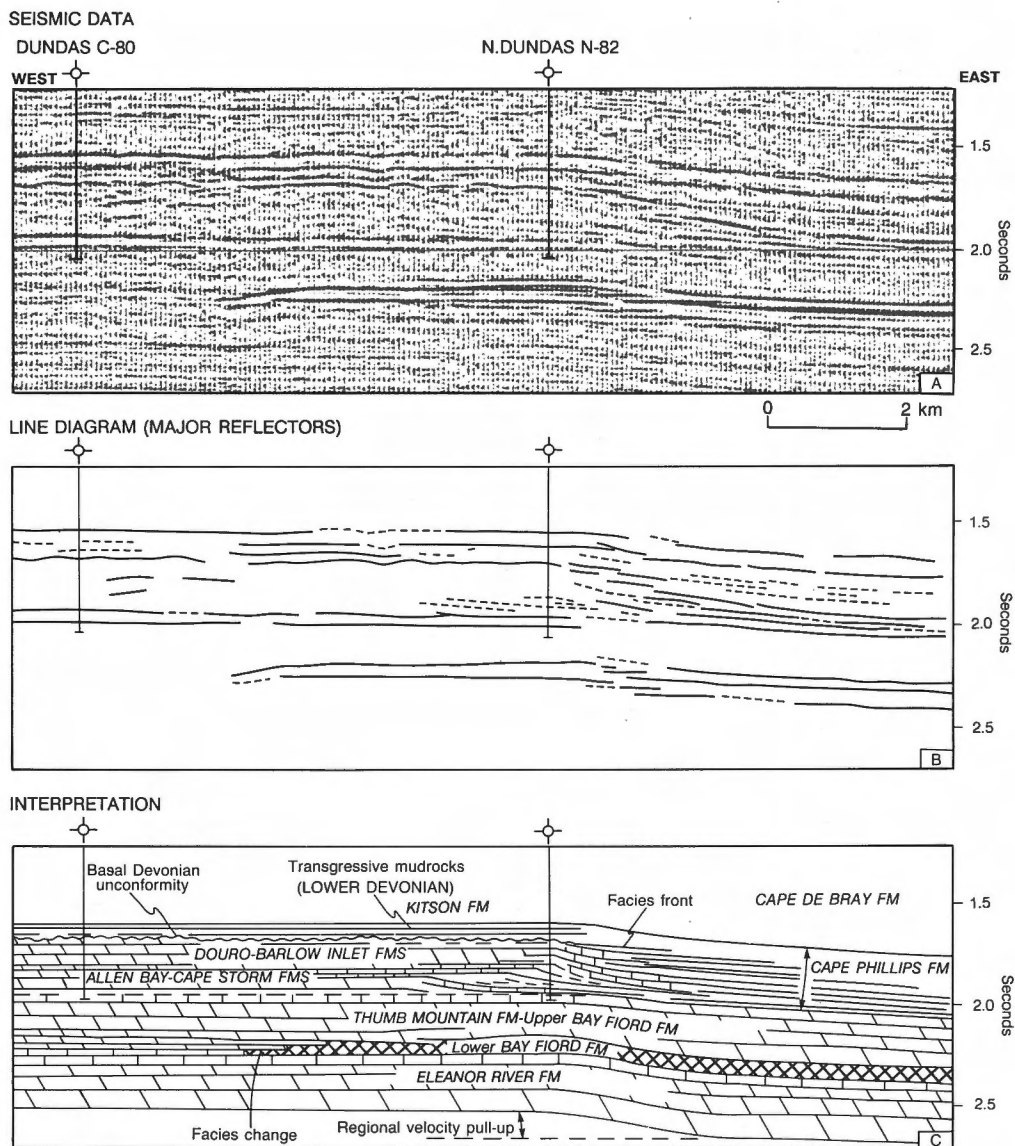


Figure 35. Seismic expression (A) and interpretation (B, C) of the depositional limit of the lower (evaporitic) member of the Bay Fiord Formation, and the Upper Ordovician and Silurian carbonate bank, western Dundas Peninsula (part of seismic profile P1168, Section F; Dundas C-80 and N. Dundas N-82 wells). A substantial horizontal velocity gradient probably exists in the 1.7 to 2.0 s interval.

Basal contact. The base of the formation is placed below the lowest common occurrence of evaporites. In the absence of evaporites, the lower contact is identified, consistent with biostratigraphic data, beneath a thin, argillaceous interval having a demonstrable response on gamma logs.

Age and correlation. The Bay Fiord Formation of Melville Island is approximately Whiterockian to Chazyian (late Arenig to Llandeilo) based on contained conodont assemblages (Fig. 32; reports of McCracken, and Barnes and Uyeno in Appendix 4). In the eastern

Arctic Islands and North Greenland, the Bay Fiord Formation and correlative strata range from the late Arenig through to the end of the Llanvirn (Trettin, 1990). The Bay Fiord Formation is correlated with the chert member of the Ibbett Bay Formation in Canrobert Hills.

The lower member of the Bay Fiord Formation of subsurface Melville Island is believed to correlate with Mayr's (1980) Unit 1 of the Bay Fiord Formation of Bathurst Island. The restricted-marine carbonates in the upper member correlate with Mayr's units 2

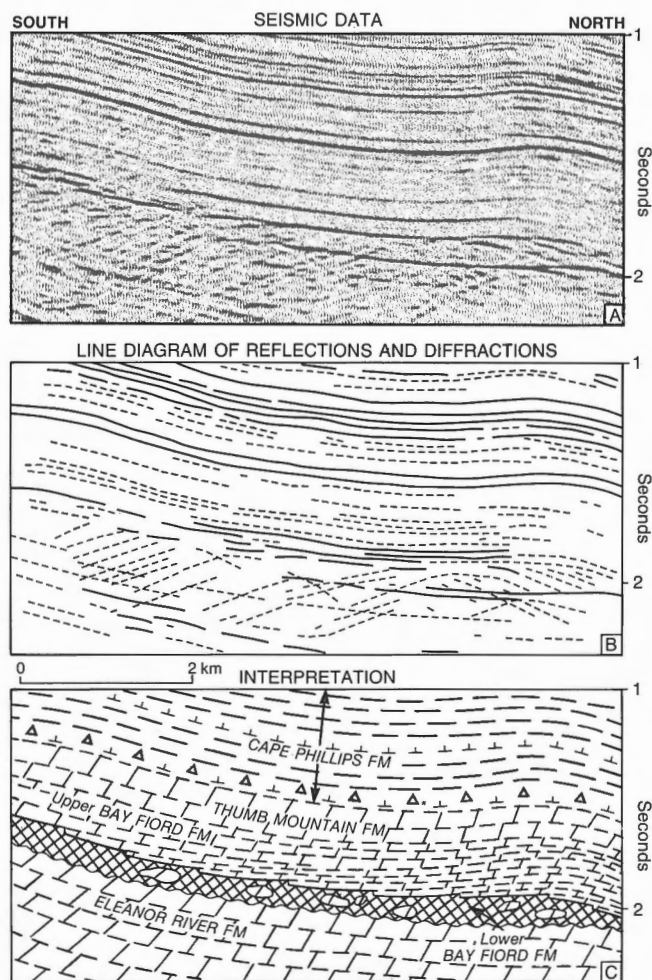


Figure 36. Seismic expression (A) and interpretations (B, C) of the lower Bay Fiord Formation near its northern depositional limit against the shelf rim, west-central Melville Island, on part of seismic profile C131X, Section I. In the centre of each figure the vertical exaggeration is approximately 1.4 at 1.0 s, 0.86 at 1.5 s, and 0.96 at 2.2 s.

through 5. The seismic marker in the middle of the upper member may eventually prove to correlate into the transgressive and normal (unrestricted) marine carbonates of Mayr's unit 3 of the Bay Fiord Formation.

Interpretation. The common occurrence of cryptalgal laminated, cryptocrystalline dolostone of low faunal diversity in the Bay Fiord interval of the Kitson River Inlier section indicates a prolonged history of intertidal carbonate accumulation on the shelf rim. Accumulation of the Bay Fiord evaporites of the intrashelf basin has been variously interpreted as occurring in either a supratidal shelf setting (Mayr, 1980) or in a shallow-restricted subtidal shelf environment (Packard

in Trettin et al., 1991). The lateral and vertical transition from the lower part to the upper part of the formation has been interpreted by Mayr (1980) as resulting from a gradual improvement in marine circulation. The fact that rates of sediment accumulation and subsidence were greater in the intrashelf basin than on the southern shelf and shelf rim tends to support the idea of a restricted subtidal setting for the evaporites in the lower member of the formation.

Pertaining to these theories are seismic stratigraphic features noted previously at the preserved limits of the evaporitic facies of the lower member of the formation (Figs. 35, 36). The apparently abrupt southwestward termination of the evaporitic member is attributed to a lateral facies transition from subtidal evaporites westward and cratonward into age-equivalent peritidal carbonates (Fig. 35C). There is no convincing evidence of syndepositional faulting along the facies front. Apparent structural relief on the Eleanor River Formation is a regional velocity (pull-up) anomaly induced by a Silurian carbonate to shale transition higher in the section; the Silurian carbonates (Allen Bay through Barlow Inlet formations) are 5.7 km s^{-1} whereas the equivalent shales (Cape Phillips) are 4.4 to 5.0 km s^{-1} .

On seismic profiles that cross the northwestern facies front noted previously, carbonates of the upper member thicken progressively at the expense of evaporites in the lower member and diffractions have been generated on or near the contact between the members (Fig. 36). These diffractions may be generated by tectonic rafts of carbonate embedded in the evaporites, and/or by the tectonically-truncated depositional limit of carbonate bedsets on the diachronous upper contact. The implication is that evaporites of the lower member in the intrashelf basin are probably age equivalent to dolostones low in the Bay Fiord Formation of the shelf rim. In conclusion, the available seismic profiles support the concept of a Middle Ordovician, subtidal, evaporite, intrashelf basin bound both shelfward and cratonward by peritidal facies belts.

Thumb Mountain Formation (OTM)

Type section. Thirty kilometres east-northeast of Irene Bay on west-central Ellesmere Island (Kerr, 1968).

Distribution. The Thumb Mountain Formation is the medial formation of the Cornwallis Group. On Melville Island, the formation is fully exposed in the Kitson River Inlier (Fig. 33) and is encountered in an

interval from 768 to 1164 m above the base of the inlier section (Unit 2 of Goodbody, 1993). Geometric calculations indicate that roughly 500 m of poorly exposed carbonates may also underlie the Cape Phillips and Irene Bay formations along the southeast shore of McCormick Inlet. This may include a complete section through the Thumb Mountain Formation (although the lower contact has not been identified). Additional isolated inland exposures occur on Middle Island. Complete sections through the Thumb Mountain Formation have been penetrated by the following wells: Apollo C-73 (2882–3152 m), Sabine Bay A-07 (2266–2617 m and 3147–3446 m; Fig. 7), Eldridge Bay E-79 (1801–2101 m) and Kitson River C-71 (1230–1485 m).

Velocity and thickness. Interval velocity ranges amongst the various drilled sections from 5.5 to 7.3 km s⁻¹. Also indicated is a regional velocity gradient decreasing to the north. Range of thickness based on surface and drill-hole data is 255 to 396 m. Seismic profiles indicate that the formation is thinnest in the southeastern part of the island (roughly 200 m).

Lithology and seismic expression. Variations in lithofacies between the three shelf and shelf edge facies belts are small. The following description therefore applies to the full areal extent of the formation east of the Canrobert Hills.

The formation consists principally of dolostone with minor dolomitic limestone and anhydrite. Weathering colours range from light to medium grey and brownish. The dolostones are medium bedded, microcrystalline and commonly contain cryptalgal lamination, bird's-eye textures, tectonic breccias and calcite veining. In the Apollo C-73, Beverley Inlet G-13 and N. Dundas N-82 wells, the lower part of the formation also contains accessory anhydrite and anhydritic dolostone. Fossiliferous limestone is encountered in the uppermost strata in the Beverley Inlet G-13, King Point West B-53 and N. Dundas N-82 wells.

On seismic reflection profiles (Fig. 13), the Thumb Mountain Formation is a tabular and uniformly reflection-poor or reflection-free seismic unit.

Basal contact. On geophysical logs, the lower contact is drawn above a break to uniformly higher sonic velocity and lower gamma-ray response in the Thumb Mountain; an indication of reduced argillaceous material and reduced porosity in the younger section. The lower contact as picked on well logs does not correspond to any observed seismic reflection, although the Thumb Mountain Formation is mar-

ginally faster than the upper part of the Bay Fiord Formation.

Age and correlation. Age of the formation based on long-ranging conodont assemblages is roughly Middle to Late Ordovician (Fig. 32; reports of McCracken in Appendix 4). Full age range of the formation in the eastern Arctic Islands is earliest Llandeilo through middle Caradoc (early Edenian). The Thumb Mountain Formation is approximately age equivalent to the dolostone member, and possible additional beds in the upper part of the chert member and lower part of the lower black shale member of the Ibbett Bay Formation of Canrobert Hills.

Interpretation. The Thumb Mountain Formation of Melville Island is interpreted as consisting primarily of restricted intertidal carbonates grading up into less restricted intertidal and subtidal carbonates. This trend is documented in three different wells by the upward decrease in accessory anhydrite and by the appearance of fossiliferous limestones and dolostones in the uppermost part of the formation.

Irene Bay Formation (OIB)

Type section. The Irene Bay Formation is the uppermost of the three formations of the Cornwallis Group. The type section is in the same location as the underlying Thumb Mountain Formation, near Irene Bay on Ellesmere Island (Kerr, 1968).

Distribution. At the surface, the formation has only been identified with certainty in the Kitson River Inlier (Fig. 33) at 1164 to 1201 m above the base of the inlier section (8 to 45 m above the base of Unit 3 of Goodbody, 1993). The Irene Bay Formation has not yet been found exposed in the McCormick Inlet area, although the age-equivalent strata on Middle Island probably lie in a covered interval below a ridge-forming fossiliferous dolostone considered to be a tongue of the Allen Bay Formation. The formation has been intersected by nine exploratory wells on Melville Island. A subsurface distribution similar to that of the Thumb Mountain Formation is indicated.

Velocity and thickness. Sonic interval velocity ranges from 5.8 to 6.4 km s⁻¹ in the south, and 5.0 to 5.1 km s⁻¹ where it has been intersected at a shallow depth beneath Sverdrup Basin (upper Paleozoic and Mesozoic) cover. Thickness is up to 46 m.

Lithology and seismic expression. In the Kitson River Inlier, the formation comprises thin bedded fossil-

iferous limestone with intercalated greenish mudstone partings. Large, solitary and colonial corals are common. The limestone beds are microcrystalline to cryptocrystalline and nodular with a rubbly weathering pattern. The unit weathers brown and greenish brown.

The Irene Bay Formation is generally too thin to be resolved as a distinct seismic unit. The formation is, however, situated in the vicinity of a strong reflection that marks the geophysical contact between Thumb Mountain Formation, below, and Cape Phillips and Allen Bay formations, above.

Basal contact. At the surface, the base of the formation is drawn below the lowest beds of recessive argillaceous limestone. In the subsurface, the base of the Irene Bay is marked by a deflection to high gamma and reduced sonic velocity response. This geophysical definition of the unit is similar to the one adopted by Mayr (1980) for the wells that intersect the Irene Bay Formation of Bathurst Island.

Age and correlation. The Irene Bay Formation in the Kitson River Inlier section contains a diverse assemblage of large, Late Ordovician (late Caradoc to early Ashgill), solitary and colonial corals—typical “Red River Fauna” as described by Elias (1981). Correlative strata also occur in the lower part of the lower black shale member of the Ibbett Bay Formation.

Interpretation. The Irene Bay Formation of the Kitson River Inlier is interpreted as including unrestricted subtidal strata deposited on a shallow, offshore carbonate platform. Deeper subtidal facies are probably present in the subsurface where the Irene Bay Formation is transitional into the Ibbett Bay Formation. The depositional environment of the Irene Bay within the intrashelf embayment region remains uncertain because of poor exposure of the critical interval. In the eastern Arctic Islands, the base of the Irene Bay Formation is a disconformity and has been interpreted as a regionally significant sequence boundary by Thorsteinsson and Mayr (1987).

Seismic unit OSC

Distribution. Unit OSC is a seismically defined unit of the southern shelf, shelf rim and Towson Point platform. It overlies the seismic interval correlated with the Cornwallis Group and underlies either the Kitson (DK) or Cape Phillips (SDCP) formations. Unit OSC and its depositional limit have been identified seismically in the subsurface of: 1) the Weatherall Bay region (Sections A–D); and 2) western Dundas

Peninsula (Section F; Fig. 35) and northwestern Melville Island between McCormick Inlet and Canrobert Hills.

Velocity and thickness. Interval velocity amongst the drilled sections ranges from 4.9 to 5.8 km s⁻¹. Maximum thickness in the Weatherall Bay and Dundas Peninsula areas is approximately 1000 m (5.4 km s⁻¹) and 1050 m (5.8 km s⁻¹), respectively. Minimum thickness is less than 200 m where the unit downlaps and thins into the age-equivalent beds of the Cape Phillips Formation.

Seismic expression. Internal seismic patterns are either chaotic or consist of weak subparallel reflection segments (Section A, Note 7; Section F, Note 7; Fig. 35). On four sections in the subsurface Weatherall Bay area, Unit OSC contains internal clinoform reflection segments that downlap southward onto the basal reflection above the Irene Bay reflector. These clinoforms are also locally truncated upward by apparent toplap (Section A, Note 7; Section B, Note 7; Section C, Note 10; Section D, Note 10). Thus, Unit OSC has a wedge-shaped downward convergent profile at its depositional limit. OSC on western Dundas Peninsula also terminates by downward convergence of the upper reflector into the lower part of the Cape Phillips. However, the wedging out of OSC in this area is toward the northeast. In the Raglan Range area, Unit OSC wedges out and downward to the east.

Basal contact. OSC is a tabular seismic unit with a strong, smooth and continuous lower bounding reflection. On P1168 (Section F) there are northerly progradational and downlapping reflectors above the basal contact near the facies transition to seismic Cape Phillips Formation.

Age and correlation. Unit OSC of the Raglan Range platform overlies the seismic interval equated with the Cornwallis Group (Bay Fiord, Thumb Mountain and Irene Bay formations) and is interpreted as being age-equivalent and stratigraphically equivalent to four distinct Upper Ordovician and Silurian carbonate formations exposed in the Kitson River Inlier section: the Allen Bay, Cape Storm, Douro, and Barlow Inlet formations (see on).

Drilled intervals of Unit OSC on the southern shelf on Dundas Peninsula contain a long-ranging conodont assemblage of Silurian age. Similarly, Silurian brachiopods have been collected from the Tingmisut Inlier (Tozer and Thorsteinsson, 1964), a dolostone outcrop on the west arm of Weatherall Bay that is probably equivalent to part of seismic unit OSC.

Allen Bay Formation (OSA)

Type section. South coast of Cornwallis Island (Thorsteinsson and Fortier, 1954)

Distribution. The Allen Bay Formation is a dolostone unit that is widely exposed on Cornwallis Island and throughout the eastern Arctic Islands (Thorsteinsson, 1988; Trettin, 1990). On Melville Island, the Allen Bay Formation is only fully exposed in the Kitson River Inlier section of Raglan Range platform (Fig. 33) in an interval from 1201 to 1578 m above the base of the section and 0 to 377 m above the Irene Bay Formation. This section includes the upper part of unit 3 and all of unit 4 of Goodbody (1993). The Allen Bay Formation is also intersected in the Dundas C-80 (3682–3899 m), N. Dundas N-82 (3790–3888 m), and Kitson River C-71 wells (792?–1230 m). It is suspected to occupy a stratigraphic position in the lower quarter of seismic Unit OSC and have a paleogeographic distribution comparable to OSC. On Middle Island, a ridge-forming, dark-coloured dolostone interval exposed in sea cliffs below the Cape Phillips Formation is considered a tongue of the Allen Bay Formation within the intrashelf embayment.

Thickness. Exposed and drilled sections of the Allen Bay Formation of the southern shelf and offshore platforms have a thickness range of 217 to 438 m. The formation is thinner in the N. Dundas N-82 well (98 m) where it is interpreted as being close to the facies change to age-equivalent basinal carbonates of the lower Cape Phillips Formation. The Allen Bay tongue on Middle Island is close to 40 m thick (lower contact covered).

Lithology. The Allen Bay Formation in the Kitson River Inlier section is divisible into three members. Member 1 (at 0 to 225 m above the Irene Bay Formation) consists of a thick bedded cliff-forming dolostone marker at the base (21 m thick) with silicified chain corals, crinoid fragments and some replacement chert. These beds are gradationally overlain by a less resistant, light grey to light brown weathering carbonate succession that includes crinoidal, medium bedded limestone (48 m) grading upsection into thick to massive bedded fossiliferous dolostone with brachiopod shell fragments and solitary corals (113 m), and an uppermost interval of cryptalgal laminated microcrystalline dolostone (43 m).

Member 2 of the Allen Bay Formation (225 to 320 m above the Irene Bay) is 95 m thick and consists of a dark grey weathering succession of medium and thick bedded dolostones. The basal contact is sharp. Brachiopods and solitary corals are common in the

lower part and decrease upsection. Cryptalgal lamination is common in the upper part.

Member 3 of the Allen Bay Formation is a 57 m thick recessive interval consisting of numerous thin interbeds of light to medium grey limestone and dolostone, with occasional large favositid and rugose corals. Oolitic limestone, algal dolostone and sedimentary breccia occurs in the uppermost beds of the member.

The Allen Bay tongue on Middle Island is a thick to massive-bedded, dark brown and dark grey fossiliferous dolostone with chalky white and vitreous brown chert nodules. These strata have a distinctly fetid and petroliferous odour. The macrofauna are especially abundant and diverse in the lower 18 m and include nautiloids, chain corals and solitary corals not unlike those found in the Irene Bay and lowest beds of the Allen Bay Formation in the Kitson River Inlier. Higher beds in the Middle Island section feature an accessory faunal assemblage of crinoid ossicles, brachiopods and scattered shell litter. All the exposed beds are tectonically brecciated and sealed with 15 to 25 per cent vein calcite, breccia matrix calcite and lesser barite void fill.

Age and correlation. The age of the Allen Bay Formation in the Kitson River Inlier section is approximately Ashgill to Wenlock (inclusive) as constrained by the age of faunas in the underlying Irene Bay Formation and as indicated by sparse conodont collections (Figs. 32, 37; reports of McCracken, Appendix 4). Full age range of the formation on the southern shelf in the eastern Arctic Islands is middle Ashgill through early Ludlow (Thorsteinsson and Mayr, 1987). These data indicate that the bulk of the Allen Bay Formation on the offshore platform of Melville Island is age-equivalent to basin facies strata that occur in the lower part of the Cape Phillips Formation of the intrashelf embayment as exposed on Middle Island, and in the upper part of the lower black shale member of the Ibbett Bay Formation of the deep-water basin in the Canrobert Hills.

Member 1 of the Allen Bay Formation has not yet yielded diagnostic fauna. However, it is bracketed in age by the late Caradoc to early Ashgill Irene Bay Formation below and Llandoveryan age of member 2 above. Members 1 through 3 closely resemble the lower, middle and upper members, respectively, of the Allen Bay Formation on Devon Island (Thorsteinsson and Mayr, 1987). The ages of the three members on Devon Island are respectively: 1) middle and late Ashgill, 2) Llandovery, and 3) Wenlock to early Ludlow.

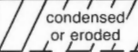


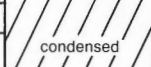
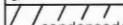
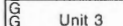
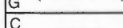

SYSTEM	SUB-SYSTEM	SERIES	STAGE	ABSOLUTE AGE (Ma)				GRAPTOLITE ZONES ARCTIC ISLANDS Melchin, 1989; Lenz and Melchin, 1990; Lenz, 1990	CONODONT ZONES WESTERN NORTH AMERICA Norford, Nowlan and Uyeno (pers. comm., 1992)	STRATIGRAPHIC UNITS							
				PALMER (1983)	COWIE et al. (1989)	HARLAND et al. (1989)	Ma			CANROBERT HILLS	RAGLAN RANGE	McCORMICK INLET MIDDLE ISLAND					
DEVONIAN				408	410	408.5	410	<i>uniformis</i>	<i>hesperius</i>				CAPE PHILLIPS FM				
SILURIAN	UPPER SILURIAN	PRIDOLI					<i>birchensis</i>										
							<i>transgrediens</i>										
							<i>bouceki</i>										
							<i>ultimus</i>	<i>eosteinhornensis</i>	G Upper black shale mbr (Lower part)								
		LUDLOW	LUD-FORDIAN		414	-	410.7										
								<i>parultimus</i>	<i>crispa</i>								
			GORSTIAN					<i>tenuis</i>	<i>latialata</i>	G Brown mudrock mbr							
								<i>linearis</i>	<i>siluricus</i>			C DOURO FM		Unit 3 (Middle part)			
		LOWER SILURIAN	WENLOCK	SHER-WOODIAN		421	424	424	<i>progenitor</i>	<i>ploeckensis</i>							
									<i>ludensis</i>	<i>crassa</i>							
				HOM-ERIAN					<i>testis</i>	<i>sagitta</i>							
									<i>perneri</i>	<i>patula</i>							
	LLANDOVERY		TELY-CHIAN					<i>rigidus</i>									
								<i>centrifugus</i>	<i>amorphognathoides</i>								
			AERONIAN		428	428	430.4		<i>sakmaricus</i>						Unit 3 (Lower Part)		
								<i>griestonensis</i>	<i>celloni</i>	G					Unit 2 (Upper part)		
	ORDOVICIAN		UPPER ORDOVICIAN	ASHGILL	GAMA-MONDIAN		448	445	443.1	<i>crispus</i>	<i>staurognathoides</i>	G					
										<i>turriculatus</i>		G					
					RICH-MONDIAN					<i>minor sedgwicki?</i>							
										<i>convolutus</i>	<i>kentuckyensis</i>						
		UPPER ORDOVICIAN		RHUDDANIAN					<i>curtus</i>								
									<i>cyphus</i>		G						
				ASHGILL					<i>acinaces</i>	<i>nathani</i>	G						
									<i>atavus</i>								

Figure 37. Correlation chart, Silurian strata of Melville Island. C, conodont collection; G, graptolite collection. All significant fossil collections are listed in Appendix 4. Base of Silurian from Tucker et al. (1990).

The Allen Bay tongue beneath the Cape Phillips Formation on Middle Island lies entirely within the *ordovicicus* Zone of the mid-Ashgill and is equated with the 21 m thick basal dolostone marker and possibly an unknown thickness of additional beds in the lower part of member 1 of the Allen Bay in the Kitson River Inlier section. A similar, readily-mappable, cliff-forming marker, well known to the author, occurs at the base of the formation and beneath the Cape Phillips throughout a wide area of the central and eastern Arctic Islands.

Interpretation. Bed thickness and internal features of the three Allen Bay members in the Kitson River section indicate that two third-order sequences are probably represented by the two lower members, respectively, with regressive subtidal strata in the lower part of each member grading upward into intertidal strata. Interdigitation of a variety of unrestricted intertidal carbonates is typical of member 3. The breccia beds at the top of the formation are interpreted as solution breccias generated during a period of subaerial exposure prior to overlap by the Cape Storm

Formation. The tongue of the Allen Bay Formation beneath the Cape Phillips Formation on Middle Island represents a deep, subtidal, carbonate facies that must be linked in the subsurface to Member 1 shallow subtidal and intertidal shelf carbonates of the surrounding platforms.

Cape Storm Formation (SCS)

Type section. Sea cliffs near Cape Storm, south coast of Ellesmere Island (Kerr, 1975).

Distribution. The Cape Storm Formation is a shelf carbonate unit of widespread distribution in the eastern Arctic Islands, where it commonly overlies the Allen Bay Formation (Kerr, 1975; Thorsteinsson and Mayr, 1987). On Melville Island, the Cape Storm Formation is only fully exposed in the Kitson River Inlier section (Fig. 33) in an interval from 1578 to 1714 m above the base of the section and 377 to 513 m above the Irene Bay Formation. This section includes all of unit 5 of Goodbody (1993). Carbonate strata age equivalent to the Cape Storm Formation have also probably been penetrated on western Dundas Peninsula. In the Dundas C-80 well, the Cape Storm interval based on gamma log character is picked at 3563 to 3682 m (11690–12080') below KB. In the N. Dundas N-82 well, the Cape Storm interval is at 3666 to 3790 m. The Cape Storm Formation is the second formation above the base of the correlative (seismic) Unit OSC and is interpreted as having a similar subsurface distribution.

Thickness. Thickness indicated by drilled and surface sections is 116 to 136 m.

Lithology. Unlike the correlative beds in the eastern Arctic Islands, the Cape Storm Formation in the Kitson River Inlier is a distinctive marker unit of resistant limestone. The lower contact is placed beneath the lowest thick limestone bed. Two members are distinguished. Member 1 (52 m) is a cliff-forming succession of yellowish to pale brown weathering, thick to massive bedded lime mudstone. Fossils are rare except in the basal few metres. Member 2 (84 m) is conformable with member 1. The upper member is distinguished primarily by its more uniformly thick bedding and reduced resistance to erosion. Weathering colours are similar. The interval assigned to the Cape Storm Formation in the Dundas C-80 well consists of unfossiliferous grey dolostone. The same interval in the N. Dundas N-82 well consists of a mixed succession of fossiliferous dolostone, chert and calcareous mudrocks.

Age and correlation. Age of the Cape Storm Formation is based on two separate ambiguous conodont collections obtained from the Kitson River Inlier section (Fig. 37; reports of McCracken in Appendix 4). The apparently older collection (middle Llandovery to early Wenlock) comes from above the younger one (middle Ludlow to Pridoli) collected at the base of the formation. With additional consideration of the faunal assemblages identified from overlying and underlying formations, the Cape Storm in this section could possibly range from the late Llandovery or early Wenlock to the middle Ludlow. The Cape Storm Formation in the eastern Arctic Islands is firmly dated within the *siluricus* Zone of the middle Ludlow (Thorsteinsson and Mayr, 1987). The correlation of the Kitson River Inlier section of the Cape Storm Formation with beds of the same name situated in the eastern Arctic is based on broad similarities of age, thickness, contact relations, and stratigraphic position. Lithological similarities are few. Detailed study of the inlier section may eventually lead to a different set of conclusions regarding regional correlation of these strata.

Interpretation. The Cape Storm Formation in the Kitson River section includes a normal unrestricted marine succession of shallow subtidal carbonates. The transition from intertidal and subaerially exposed conditions to shallow subtidal sedimentation and significant increase in bed thickness above the Allen Bay Formation is equated with a relative sea-level rise and a possible increase in sediment accumulation rate. The change in lithofacies in the Cape Storm interval between the two Dundas wells represents a north-easterly transition, consistent with local variation in seismic depositional facies, from an outer shelf to basin slope setting.

Douro Formation (SD)

Type section. The Douro Formation is the lowest of the formations that compose the Read Bay Group. The type section is near Prince Alfred Bay on Devon Island (Thorsteinsson, 1963; Thorsteinsson and Mayr, 1987).

Distribution. The Douro Formation overlies the Cape Storm Formation in many parts of the eastern Arctic Islands. In the Kitson River Inlier section (Fig. 33) of Melville Island, the Douro Formation is identified in a similar stratigraphic position at 1714 to 1868 m above the base and 513 to 667 m above the Irene Bay Formation. This interval is equivalent to unit 6 of

Goodbody (1993). Platform carbonate rocks that are believed to be age equivalent to the Douro Formation have also been intersected in the Dundas C-80 (3339–3563 m), and N. Dundas N-82 (3429–3666 m) wells. The Douro Formation is the third formation above the base of correlative seismic unit OSC and is interpreted as having a similar subsurface distribution.

Thickness. 154 to 237 m.

Lithology. In the Kitson River Inlier section, the Douro Formation includes 154 m of cyclically interbedded limestone and dolostone. The limestone is dark grey, thin bedded, rubbly fractured, and weathers to a medium brown and greenish brown colour. The dolostone beds are shades of light grey and can weather to light grey or off white colours. These two lithofacies are regularly interbedded with 18 limestone-dolostone couplets, making up the total formation thickness. Each couplet has an average and nearly uniform thickness of 8.5 m.

The Douro Formation is a dolomitic interval in the Dundas C-80 well. The formation comprises argillaceous limestone and calcareous mudrocks farther north in the N. Dundas N-82 well.

Basal contact. The lower contact with the Cape Storm Formation is sharp but apparently conformable. The contact is drawn below the lowest thin beds of recessive, dark coloured limestone. This contact is also easily identified in the Dundas C-80 and N. Dundas N-82 wells by a break to higher gamma-ray response and lower sonic velocity in the Douro Formation.

Age and correlation. The age of the Douro Formation in the Kitson River Inlier is constrained between middle and late Ludlow (Late Silurian) based on contained conodonts and the occurrence of additional Ludlow in the overlying Barlow Inlet Formation (Fig. 37; reports of McCracken, Appendix 4). The Douro Formation in the eastern Arctic Islands is firmly dated within the *siluricus* Zone of the middle Ludlow (Thorsteinsson and Mayr, 1987).

Interpretation. Deposition of the Douro Formation is interpreted as having occurred on a shallow, unrestricted marine shelf and offshore carbonate platform. Cyclicity is associated with shoaling upward carbonate sedimentation and harmonic fluctuations of relative sea level from shallow subtidal to intertidal. Cycle thickness may reflect approximate water depth range (0–8.5 m). The transition from dolostone to limestone and mudrock between the two Dundas wells

is interpreted as representing part of a northeasterly facies change of typical Douro Formation shelf carbonate to Ludlovian mudrock of the upper Cape Phillips Formation.

Barlow Inlet Formation (SBI)

Type section. Stream near central east coast of Cornwallis Island (Thorsteinsson and Uyeno, 1980).

Distribution. The Barlow Inlet Formation is the middle of three formations that make up the Read Bay Group of the eastern Arctic Islands. The formation is recognized in the upper part of the Kitson River Inlier (Fig. 33) at 1868 through approximately 2045 m above base of section (667–844 m above the Irene Bay Formation). The Barlow Inlet Formation is well exposed in two areas. The lower 70 to 100 m of the formation are found in an upland section at the north end of the inlier. Two incised stream bank exposures on the southeast and west sides of the inlier reveal additional sections up to 84 m thick from the medial and upper part of the formation. The Barlow Inlet Formation is equivalent to unit 7 of Goodbody (1993). Correlative shallow-marine carbonates have been intersected in the Dundas C-80 well (2883–3339 m), N. Dundas N-82 well (2955–3429 m), and Zeus F-11 well (625 – TD at 952 m). Ninety metres of crystalline dolostone exposed in sea cliffs of the Tingmisut Inlier could also be tentatively assigned to the Barlow Inlet Formation. The Barlow Inlet is the fourth and highest formation within seismic unit OSC. It is interpreted as having a similar subsurface distribution.

Thickness. In the Kitson River Inlier, 177 m. The upper contact with the Kitson Formation is nowhere exposed. A 4.5 m covered interval above the highest beds of the Barlow Inlet Formation are tentatively included in the Kitson Formation. Thickness in the three well sections ranges from 327 m to 474 m.

Lithology. The Barlow Inlet Formation in the Kitson River Inlier consists of two members of disproportionate thickness. The lower member is 22 m thick and consists primarily of light grey and yellowish brown weathering limestone. Beds are thin (1–10 cm) and sparsely bioclastic in the lower part, and range to thick bedded (50–100 cm), micritic and cliff forming in the upper part. The upper member of the formation is 155 m thick and consists of a series of (average) 3 m thick carbonate cycles. Weathering colours are variably light grey, light brown and greenish yellow, and

together these colours impart a finely striped pattern to exposed surfaces. From the base, each high-frequency cycle consists of rubbly fractured, bioturbated bryozoan limestone, resistant lime mudstone and yellowish to pale brown dolostone. The uppermost exposed beds of the upper member are represented by a partly talus covered dip slope ledge of light coloured dolostones.

The Barlow Inlet Formation is distinguished from the underlying Douro Formation by its lighter weathering colours, and greater resistance to erosion. Macrofauna are also more abundant in the Barlow Inlet and cycle thickness is more variable but thinner on average.

Light coloured dolostone is the dominant constituent of the Barlow Inlet Formation in the three drilled sections and in the isolated outcrop near Tingmisut Lake.

Age and correlation. Based on contained conodonts, the age of the Barlow Inlet Formation is Late Silurian (definitely Ludlow and probably Pridoli; see reports of McCracken, and Uyeno in Appendix 4). The full age range of the Barlow Inlet Formation in the type section on Cornwallis Island is from the *latialata* Zone of the late Ludlow to the *hesperius* Zone, which straddles the boundary between the Pridoli and the Lochkovian (Thorsteinsson and Uyeno, 1980). Lithofacies in the Melville Island section of the Barlow Inlet Formation are also not unlike those in the Drake Bay Formation of Prince of Wales Island, which has an age range that extends from the Ludlow to the Pragian (Thorsteinsson and Uyeno, 1980).

Interpretation. Deposition of the Barlow Inlet Formation is interpreted as having occurred on a shallow, unrestricted marine platform or offshore carbonate bank. Cyclicity is associated with shoaling-upward carbonate sedimentation and harmonic fluctuations of relative sea level from shallow subtidal to intertidal. Cycle thickness may reflect approximate water depth range (0–3 m). The lower member of the formation is interpreted as representing a single shoaling-upward cycle dominated by subtidal carbonate sedimentation. The base of the formation is apparently conformable with the Douro Formation. The transition from intertidal carbonates at the top of the Douro Formation to a thick interval of predominantly subtidal carbonates in the lower member of the Barlow Inlet Formation is interpreted as the result of a significant rise in relative sea level. Thus, the base of the Barlow Inlet Formation may be on or close to a low frequency third(?) order sequence boundary.

Kitson Formation (DK)

Type section. Near the Kitson River at the western end of Raglan Range within the upper part of the Kitson River Inlier (Tozer and Thorsteinsson, 1964). The Kitson Formation is nowhere fully exposed and is only understood from a minimum of four or five incomplete sections in this area (Fig. 33).

Distribution. The Kitson Formation, presently identified in parts of Melville Island and subsurface Banks and Prince Patrick islands, is the highest unit of the western shelf rim facies belt below the Middle and Upper Devonian clastic wedge. As well as the exposures in the Kitson River Inlier, the Kitson Formation is also correlated to drilled intervals in the Zeus F-11, Dundas C-80, and N. Dundas N-82 wells. The formation is believed to be widely represented in the subsurface of western Dundas Peninsula, and parts of western Melville Island between Raglan Range and Canrobert Hills where it corresponds to a single, thin seismic interval above seismic unit OSC. The seismic limit of the Kitson Formation is drawn above the shelf-slope break of the underlying unit OSC. Thicker, slope-related beds above the downward convergent portion of Unit OSC are considered to include both coeval and underlying older base-onlapping mudrocks laterally continuous with the Cape Phillips seismic interval.

Velocity and thickness. Interval velocity amongst the various wells ranges between 4.0 and 4.1 km s⁻¹. Thickness in the Kitson River Inlier is 62.5 to 89 m. Drilled intervals are 89 to 269 m thick.

Lithology and seismic expression. The Kitson Formation is a highly condensed and recessive-weathering interval of black, argillaceous limestone and mudrock. Two members are distinguished in the inlier section. The lower member has a thickness that ranges from a minimum of 11.5 m to a maximum of 27 m. It includes a highly recessive succession of thin bedded, black to dark brown weathering, argillaceous limestone and lesser calcareous mudstone. Bed thickness (5–30 cm) and ratio of mudrock to limestone vary considerably over short distances within age-equivalent intervals of the lower member. The most common limestone is a bioclastic and petroliferous variety with common crinoid ossicles, tentaculitids, bivalve and fish fragments. Mudrocks are fissile and locally graptolitic. No section has yet been found that exposes the lower contact above the Read Bay Group. The minimum covered interval across the lower contact is 4.5 m. The covered section is everywhere observed in

the lower part of the member, and limestone increases to the top of the member in several sections. If the covered interval is assumed to consist of a mudrock-dominated section within the Kitson Formation, then the thickness variations of the lower member may be an expression of pre-existing paleotopographic relief on a basal disconformity.

The upper member (62 m) is composed of black, fissile mudrocks with minor, thin, argillaceous limestone and occasional sandstone interbeds in the lower part. The lower contact is apparently conformable, although one conodont zone fauna (*pesavis*) has not been discovered (Fig. 38).

The Kitson Formation seismic interval is bound above and below by strong, continuous reflectors. Internally, the unit is weakly and discontinuously reflective, or reflection free. Although thinner, the Kitson Formation is continuous with and seismically similar to the Cape Phillips Formation (OSDCP, SDCP).

Basal contact. On the Dundas Peninsula seismic lines (Section F, P1168; Fig. 35), the basal reflection defines an irregular surface with up to 30 ms (60 m) of local relief. Similar reflection irregularities occur beneath the seismically-defined Kitson Formation of the western Raglan Range area. These irregularities are only observed on the basal reflection surface and are not mimicked by the upper contact, which is a smoother, more featureless reflector. Thus the basal irregularities are responsible for local variations in thickness of the lower part of the Kitson Formation and in the highest strata (Barlow Inlet Formation) at the top of seismic unit OSC.

Age and correlation. Middle Lochkovian through probably early Eifelian (Fig. 38; reports of T.T. Uyeno in Appendix 4). The lower member contains a middle Lochkovian conodont assemblage probably lying within the *eurekaensis* and *delta* zones. Full age range of the upper member, based on numerous precise conodont assemblages is from the *sulcatus* Zone of the Pragian through to the *patulus* or *costatus* zones in the latest Emsian to early Eifelian.

The Kitson Formation may be correlated with the upper 300 to 440 m of the Ibbett Bay, and the Cape Phillips formations. Less than 23 m of strata from the uppermost part of the Kitson Formation in the type area (which contains conodont zones from *gronbergi* to *costatus*) is age-equivalent to as much as 1250 m of Blue Fiord Formation carbonates in the Weatherall Bay area.

Interpretation. The Kitson Formation is interpreted as a platformal succession of strata deposited under conditions of prolonged submarine sediment starvation. Irregularities noted on the lower contact could have been created under shallow-marine conditions by small organic buildups (biostromes) on the upper surface of the underlying Barlow Inlet Formation. Alternatively, the basal contact may be a subaerial disconformity with erosional topography filled in by the onlapping Kitson Formation (Fig. 35). Depth of erosion (or height of reef growth) is at least as great as the height of the irregularities on the sub-Kitson Formation reflector (± 50 m).

The condensed or missing time interval evident in or below the basal metre of the upper member of the Kitson Formation is interpreted as being associated with a sequence boundary near this stratigraphic level and a major relative sea-level rise in late Lochkovian time.

Blue Fiord Formation (DBF)

Type section. Near Bird Fiord on southwestern Ellesmere Island (McLaren, 1963).

Distribution. The upper parts of the Blue Fiord Formation are exposed in Spencer Range between the two arms of Weatherall Bay and in the Towson Point Anticlinorium (Fig. 39; Tozer and Thorsteinsson, 1964; Goodbody, 1993). There are five well intersections (Towson Point F-63, Weatherall O-10, King Point West B-53, Richardson Point G-12, and Sherard Bay F-34). The extent and depositional limits of the equivalent seismic unit are readily defined on many seismic profiles of northeastern Melville Island.

Velocity and thickness. The interval velocity range amongst the various drilled sections, augmented in some areas by Dix interval velocities, is 5.0 to 6.2 km s⁻¹. The lowest velocities are encountered in the Towson Point and eastern Weatherall Bay areas, where the Blue Fiord Formation is thickest and closest to the surface. The thickest surface sections occur in Spencer Range, where the upper (approximately) 850 m of the formation are incompletely exposed. Thickness of well sections are as follows: King Point West B-53, 1009 m; Weatherall O-10, 831 m; Richardson Point G-12, 952 m +; Sherard Bay F-34, 179 m +. Stratigraphy of the Towson Point F-63 well is uncertain. Seismically defined thicknesses range from a maximum of 500 ms (1250 m at 5.0 km s⁻¹) to a negligible thickness where it grades basinward into the upper Cape Phillips Formation.

SYSTEM	SUB-SYSTEM	SERIES/STAGE	RADIOMETRIC AGE (Ma)				PALYNOMORPH ZONES Jaeger (1979), Murphy and Berry (1983) GRAPTOLITE ZONES Richardson and McGregor (1986)	CONODONT ZONES T.T. Uyeno and A.E.H. Pedder (pers. comm., 1992), Klapper and Johnson (1980), Sandberg and Dresson (1984)	BRACHIOPOD and DACRYOCONARID ZONES Crickmay (1966), Sartenaer (1969), Norris (1985)	STRATIGRAPHIC UNITS																																																																																																																																																																																																																																																																																																																																																																																																																																																																																																																																																																																																																																																																																																																																																																																																																																																																																																																																																																																																																																																																																																																																																																																																																																																																																																																																																																											
			PALMER (1983)	COWIE et al. (1989)	HARLAND et al. (1989)	Ma				CANROBERT HILLS	KITSON RIVER	McCORMICK INLET	WEATHERALL BAY																																																																																																																																																																																																																																																																																																																																																																																																																																																																																																																																																																																																																																																																																																																																																																																																																																																																																																																																																																																																																																																																																																																																																																																																																																																																																																																																																																								
										IBBETT BAY	RAGLAN RANGE	CENTRAL MELVILLE I.	BEVERLEY INLET																																																																																																																																																																																																																																																																																																																																																																																																																																																																																																																																																																																																																																																																																																																																																																																																																																																																																																																																																																																																																																																																																																																																																																																																																																																																																																																																																																								
CARBONIFEROUS																																																																																																																																																																																																																																																																																																																																																																																																																																																																																																																																																																																																																																																																																																																																																																																																																																																																																																																																																																																																																																																																																																																																																																																																																																																																																																																																																																																					
DEVONIAN	UPPER DEVONIAN	FAMENNIAN	360	355	362.5	355	<i>pusulites-lepidophyta</i>	<i>sulcata</i>																																																																																																																																																																																																																																																																																																																																																																																																																																																																																																																																																																																																																																																																																																																																																																																																																																																																																																																																																																																																																																																																																																																																																																																																																																																																																																																																																																													

See Figure 19 for legend

Figure 38. Correlation chart, Devonian strata of Melville Island. C, condont collection; G, graptolite collection; M, shelly macrofauna; P, palynomorphs. All significant fossil collections are listed in Appendix 4.

Lithology. Common surface rock types include variably fossiliferous and fenestral lime mudstone, and

microcrystalline dolostone. Weathering colours are shades of brown, light grey and greenish brown. Light



Figure 39. Vertical airphoto mosaic of Towson Point Anticlinorium. ★, location of the type section of the Weatherall Formation; DBF, Blue Fiord Formation; DCB, Cape De Bray Formation; DW, Weatherall Formation; DHB, Hecla Bay Formation. See also legend, Figure 33. NAPL photos. A16766-156, -158.

grey and dark grey calcareous dolostone is also present, especially in the lower parts of the Spencer Range section and in the oldest beds of the Towson Point structure. Limestones are faunally diverse and are noted to contain solitary and colonial corals, stromatoporoids, gastropods, crinoids, brachiopods, and trilobites. Three informal members of the Blue Fiord Formation are mappable around the Towson Point structure but have not been recognized with certainty in Spencer Range. From the base these include: 1) 275 m+ of coarse crystalline dolostone grading upsection into massive-bedded fossiliferous limestone ("Unit 1" of Goodbody, 1993); 2) 210 m of recessive, cyclically interbedded limestone and dolostone ("Unit 2" of Goodbody, 1993); and 3) 115 m of massive bedded limestone ("Unit 3" of Goodbody, 1993). Member 2, described above, is believed to pass laterally into a shale unit in the King Point West B-53, Weatherall O-10 and Richardson Point G-12 wells (91-260 m thick). The shale is bound below by thick limestones (121-432 m+ thick) and above by a similar, thick carbonate interval (429-603 m) that may correlate with members 1 and 3, respectively. In the Weatherall O-10 and King Point West B-53 wells, the lower member of the Blue Fiord Formation overlies Pragian(?) and older graptolitic- and tentaculitid-bearing mudrocks of the Cape Phillips Formation.

Seismic expression. The Blue Fiord seismic unit is bound below and above by continuous reflections. Internally, the unit consists of weak, parallel, disrupted reflections (Fig. 40). Near the southern seismic limit of

the unit, the uppermost weak internal reflectors pass into a region of much thicker, hummocky and internally chaotic reflections (Section C, Note 6). The upper reflection surface is also hummocky in character (Section B, Note 4; Fig. 13). The southern limit of the formation is marked by internal reflections that appear out of the chaotic reflection assemblage and converge and downlap onto the basal reflector. The unit as a whole also thins by downward convergence and downlap of the strong upper reflection (Section A, Note 8; Section B, Note 6; Section D, Note 6).

Age and correlation. Age of the Blue Fiord Formation on surface and subsurface northeastern Melville Island is based on conodonts and ranges from early Emsian (*dehiscens* or *gronbergi* zones) in member 1 to late Emsian or early Eifelian (possibly *patulus* Zone) in member 3 (Fig. 38; reports of Uyeno in Appendix 4). The lower age limit of the formation is unknown. Equivalent strata occur in the upper parts of the Kitson and Cape Phillips formations and in the upper part of the upper black shale member of the Ibbett Bay Formation. On southwestern Ellesmere Island, the Blue Fiord Formation near the type section ranges from early Emsian through late (not latest) Emsian or approximately upper *dehiscens* through *serotinus* conodont zones. Beds lying above *serotinus* on Ellesmere Island occur in the lower part of the Bird Fiord and Strathcona Fiord formations (Uyeno, 1990).

Interpretation. The highstand progradational character of the Blue Fiord Formation is indicated by the

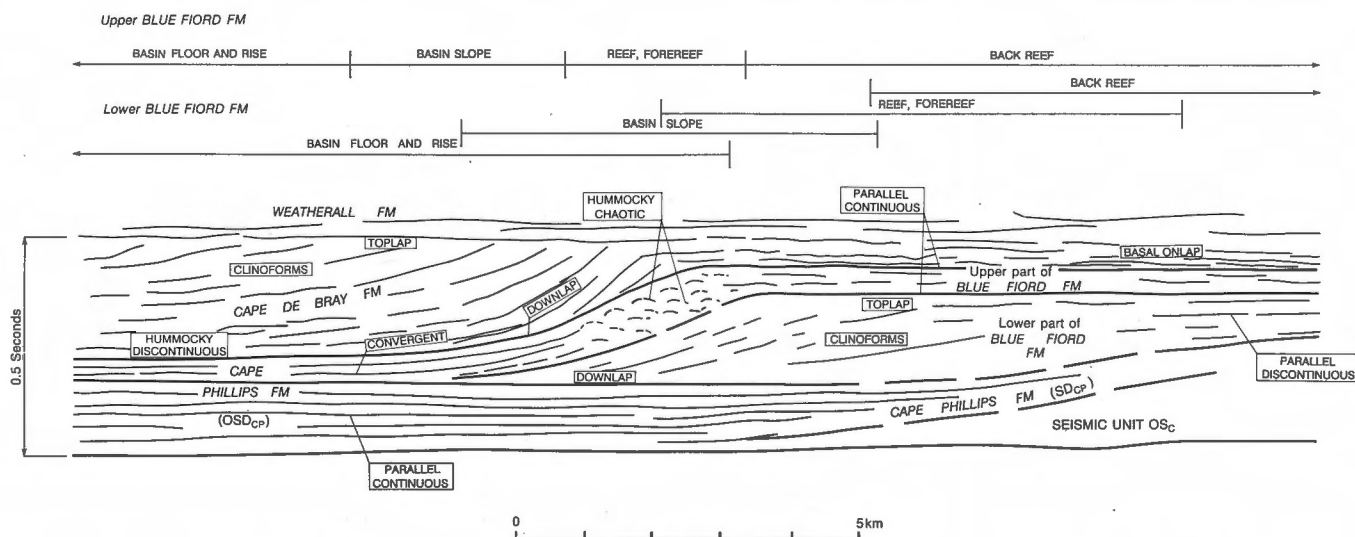


Figure 40. Seismic depositional facies of the Blue Fiord Formation, compiled from seismic profiles of Sections A through D (see also Figs. 13, 108). The seismic interval labelled "lower Blue Fiord" is approximately equivalent to Members 1 and 2 of the formation as described in the text. The "upper Blue Fiord" is equivalent to Member 3. Vertical exaggeration in the Blue Fiord interval at the centre of the figure is approximately 1.9.

downlapping reflections at the southern termination of the equivalent seismic interval. Internal seismic patterns (Fig. 40) indicate that the formation includes: 1) extensive shelf carbonates (weak, parallel, disrupted internal reflections); 2) shelf-edge carbonate buildups and proximal fore-reef facies carbonate debris aprons (hummocky upper reflection surface with chaotic internal patterns); and 3) lower slope to base-of-slope and rise facies layered carbonates and mudrocks (downward-converging and downlapping internal and bounding reflectors that emerge from in front of the bank-edge seismic facies).

The Blue Fiord Formation is interpreted as including two third(?) order depositional sequences. The lower sequence begins with lowstand and transgressive mudrocks of pre-early Emsian Early Devonian age as represented by parts of the Kitson Formation and by *Nowakia* and *Monograptus yukonensis*-bearing mudrocks of the upper Cape Phillips Formation and upper black shale member of the Ibbett Bay Formation. The thick bedded limestones of member 1 of the Blue Fiord Formation represent progradational strata associated with the highstand termination of this older sequence of the Blue Fiord Formation. A sequence boundary is placed near the top of member 1 within the *inversus* Zone of the mid-Emsian. Transgressive and especially highstand deposits of the younger sequence are represented by members 2 and 3, which may range from the mid-Emsian through the *patulus* or basal *costatus* zones of the early Eifelian.

Cape Phillips Formation (OSDCP, SDCP)

Type section. Northeastern Cornwallis Island (Thorsteinsson, 1958; Thorsteinsson and Kerr, 1968).

Distribution. Surface exposures are restricted in distribution to Middle Island and the south shore of McCormick Inlet. Evidence from drill holes and seismic profiles indicates that the formation underlies all of southeastern and central Melville Island. There are no complete surface sections of the Cape Phillips Formation represented on Melville Island. The lower 300 m of the formation is exposed in sea cliffs on the west end of Middle Island. The upper part of the formation, including some of the uppermost beds (Fig. 41), are exposed in stream bank exposures southwest of McCormick Inlet. The Cape Phillips Formation has been penetrated by eight exploratory wells.

Velocity and thickness. Average interval velocity amongst the various well intersections ranges from 4.0



Figure 41. Aerial view of the contact between the Cape Phillips (darker well bedded unit) and Cape De Bray (lighter weathering tones at top) formations, south shore of McCormick Inlet. Note the high, oblique minor faults, some filled with white calcite veins. ISPG photo. 3023-2.

to 5.5 km s⁻¹. There is also a strong vertical velocity gradient in the formation, which ranges from a maximum of 5.5 km s⁻¹ at the base to a minimum 4.0 km s⁻¹ at the top. The Cape Phillips Formation of the McCormick Inlet area has a thickness of approximately 600 m. Drilled thicknesses range from 513 to 800 m. Thickness based on depth conversion of the Cape Phillips seismic interval has a normal range (away from the surrounding carbonate platforms) of 420 to 980 m.

Lithology and seismic expression. The Cape Phillips Formation is a recessive, dark grey to black weathering unit consisting of platy to fissile, finely laminated, variably fetid and graptolitic mudrock with lesser, thin bedded, dark coloured limestone and chert (Melchin, 1987, 1989; Lenz and Melchin, 1990; Goodbody, 1993). Four informal members are distinguished in the Cape Phillips Formation of the McCormick Inlet area.

Below a probable conformable contact with the Cape De Bray Formation, these members, from top to bottom are:

4. Black, fissile, siliceous mudrock and black chert (60 to 75 m).
3. Fissile to platy, mostly noncalcareous or weakly calcareous, dark grey to black weathering mudrock. Monoserial graptolites are common except in the upper part. A concretionary limestone in the uppermost metre of the unit contains tentaculitids (360 m).

2. Laminated, medium grey to black limestone, radiolarian chert, graptolitic calcareous mudrock; numerous limestone concretions, common replacement chert; mudrock interbeds increasing to top (37 m).
1. Medium bedded, argillaceous, grey limestone; minor graptolitic mudrock partings (34 m).

The contact with the Allen Bay Formation appears to be conformable.

The Cape Phillips Formation is a distinct seismic unit consisting of many undisrupted, laterally continuous parallel reflections of moderate amplitude (Fig. 13). The basal reflector is very strong and corresponds to a 60 to 80 m thick interval that consists of the basinal tongue of the Allen Bay Formation, the Irene Bay, and upper contact of the Thumb Mountain Formation. The depositional limit of the Cape Phillips Formation is observed on seismic profiles P1788/2228 (Section A, Note 7), P2189 (Section B, Note 7), T4 (Section C, Note 10) and P1168 (Section F, Note 7; Fig. 35). The principal feature of this facies front is the progressive thinning from the base of the Cape Phillips (SDCP) seismic interval and a parallel increase in thickness of underlying seismic unit OSC. On P1168, the Cape Phillips Formation passes laterally into an acoustically similar but thinner interval assigned to the Kitson Formation. On the fringe of Towson Point platform (Sections A through C), the Cape Phillips seismic interval appears to onlap OSC at the base and to pass into the base of slope seismic facies of the Blue Fiord Formation at the top.

Age and correlation. Duration of deposition of the formation based on conodont and graptolite assemblages is mid-Ashgill (Richmondian) through early and possibly middle Eifelian (Figs. 32, 37). Age of the individual members in the McCormick Inlet and Middle Island sections is: member 1, mid-Ashgill; member 2, mid-Ashgill to late Llandovery (uppermost Ashgill through middle Llandovery beds are either highly condensed or absent); member 3, uppermost Llandovery through early Eifelian (Fig. 38); member 4, early and middle(?) Eifelian (reports of Lenz, McCracken, Norford, Norris, and Uyeno in Appendix 4).

The Cape Phillips Formation of Melville Island spans the age range of the Cape Phillips Formation of the type section (Ashgill to early Lochkovian) as well as younger mudrocks that in the eastern Arctic Islands have been assigned to other formations (Thorsteinsson, 1963; Trettin, 1990). Local correlations are shown on Figures 32, 37 and 38.

Interpretation. The Cape Phillips Formation represents a succession of starved basin floor, basin rise and lower basin slope mudrock and carbonate sediments that accumulated in deep water during the simultaneous accumulation to sea level of surrounding Ashgill through early Eifelian carbonate banks.

Canrobert Formation (OCR)

Type section. Between Blackley Haven and Ibbett Bay, southwestern Canrobert Hills (Tozer, 1956).

Distribution. The Canrobert Formation is exposed in the axial region of the larger anticlines of Canrobert Hills. Seismic reflection profiles indicate that it underlies younger cover of Sproule Peninsula and Eglinton Island.

Thickness. Up to 463 m (base not exposed). The base of the unit on seismic profiles is continuous with seismic unit sO. The latter thins northward from 530 ms (1500 m) on subsurface Eglinton Island to 380 ms (1100 m) on Sproule Peninsula.

Lithology and seismic expression. The exposed part of the formation is composed of thin bedded resedimented dolostone, arenaceous dolostone, dolosiltite, dolarenite, intraformational breccia and flat pebble conglomerate. Common weathering colours are shades of yellow and yellowish grey. The finer grained rock types show well developed parallel and ripple crosslamination. Bioturbation features are generally absent, although some horizontal traces have been observed. A weakly developed cleavage is locally evident (Fig. 130D).

The Canrobert Formation is at least locally divisible into three members, of which only the upper two are fully exposed (Fig. 42). A ledge-forming dolostone marks the upper part of the lower member in the reference section north of Ibbett Bay. It is overlain conformably by thin bedded dolostones and laminated dolosiltites. Bedding thickness increases and becomes increasingly resistant to erosion upsection. Flat laminated and ripple crosslaminated dolarenite (Fig. 43), breccia and intraformational conglomerate (along with the ubiquitous fine-grained carbonates) are common in the third and highest member. Breccia beds (Fig. 44) are composed of matrix-supported microcrystalline dolostone fragments. Some clasts have been selectively silicified. Chert occurs as either a complete clast replacement or as overgrowth rims of variable thickness on limestone or dolostone fragments. Clast composition resembles lithologies occurring above and below the conglomerate layers and also lithologies to

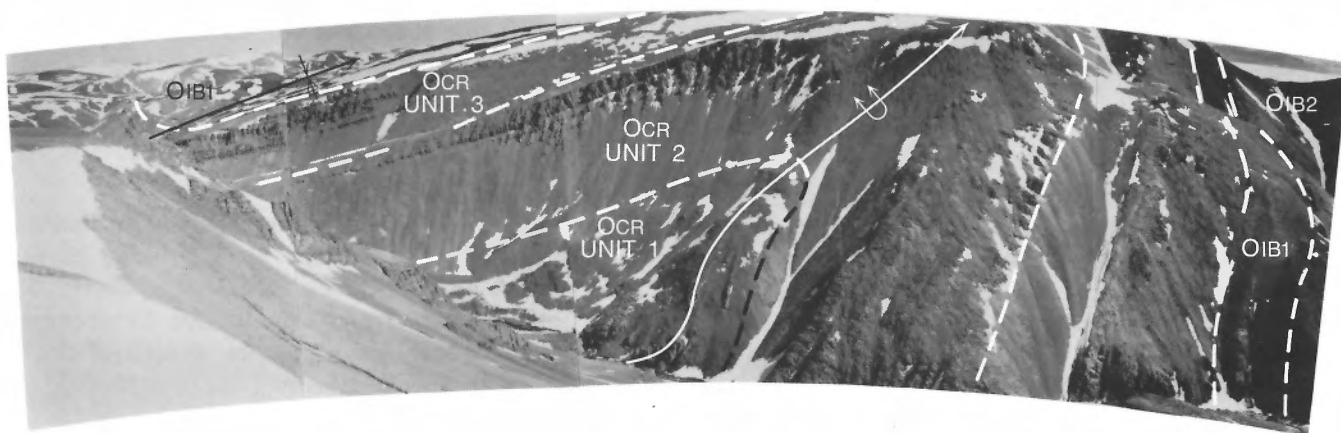


Figure 42. Panoramic photograph (view north) of an asymmetrical anticline on the north side of Ibbett Bay. The Canrobert Formation at this locality is 463 m thick (Robson, pers. comm., 1984). OCR, Canrobert Formation; Ibbett Bay Formation: OIB1, chert member, OIB2, dolostone member. ISPG photos. 2887-61 to 65.

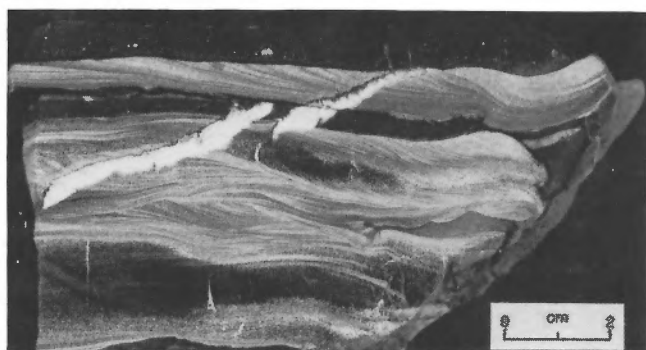


Figure 43. Ripple crosslaminated, dolomitic, fine grained sandstone and intercalated dolostone of the Canrobert Formation. ISPG photo. 3029-7.

be expected in the shelf environment. The matrix of conglomerates and breccias includes mud, carbonate micrite, and well rounded monocrystalline quartz grains to 0.7 mm. Near Nisbet Point, dolomitic, coarse grained quartz sandstones with similar, well-rounded quartz grains are also common in the upper informal member of the formation.

The seismic expression of the Canrobert Formation is reflection free and continuous downsection with seismic unit sO.

Age and correlation. Graptolite and supporting conodont collections indicate an age range from at least the *antiquus* Zone of the late Tremadoc to the *oncograptus* Zone of the late (not latest) Arenig age for the Canrobert Formation (reports of Norford, McCracken, and Lenz and Borré in Appendix 4). There have been no diagnostic fauna collected from the



Figure 44. Matrix-supported carbonate breccia (debris flow) in the Canrobert Formation. ISPG photo. 3874-5.

lower exposed beds. Presently available data indicate biostratigraphic equivalence with the Eleanor River Formation.

Interpretation. The common occurrence of finely laminated and crosslaminated carbonates and general absence of bioturbation suggests a low- to moderate-energy, deep water environment such as might be expected on the deeper part of a basin slope above the carbonate compensation depth. Quartz sand of terrigenous origin in the upper informal member of the formation indicates that cratonic source areas were exposed and actively being eroded at this time, and that siliciclastic sediments were bypassing the shelf, possibly as a result of a major drawdown of sea level. Breccias and intraformational conglomerates common in the upper part of the formation testify to instability of the shelf margin, perhaps as a result of above-wave-base erosional scouring of the upper slope. A major sequence boundary is placed near the contact between the Canrobert and Ibbett Bay formations.

Ibbett Bay Formation (OIB1–SDIB5)

Type section. Between Blackley Haven and Ibbett Bay, southwestern Canrobert Hills (Tozer, 1956). The Ibbett Bay Formation is everywhere divisible into five distinct members (Fig. 45). Each of these members fulfills the formal definition of a formation (including distinct and homogeneous internal characteristics, and regional mappability). For this reason it may eventually prove useful to raise the Ibbett Bay Formation to group status. The present account maintains the existing and familiar nomenclature; the five members have been given informal names based on the most common contained rock types.

Distribution. The Ibbett Bay Formation is exposed throughout the Canrobert Hills area of northwestern Melville Island. There are also inliers of the formation exposed in the coastal lowlands north of Marie Bay below Marie Heights. The northward continuation of the Ibbett Bay Formation beneath younger cover of Sproule Peninsula is also indicated by three well intersections (Panarctic Depot Island C-44, Panarctic Marie Bay D-02, and Panarctic Sandy Point L-46).

Seismic reflection profiles show that the formation probably underlies all parts of Sproule Peninsula and Eglinton Island but is not known to extend as far as Prince Patrick Island (Brent, pers. comm., 1988). Distribution in the subsurface of southwestern Melville Island is unknown.

Thickness. 1194.3 m

Upper black shale member (SDIB5), 562.3 m
Brown mudrock member (SIB4), 63.5 m
Lower black shale member (OSIB3), 191.5 m
Dolostone member (OIB2), 290 m
Chert member (OIB1), 87 m

Lithology. The major rock components, in decreasing order of importance, are: black, fissile, variably calcareous and dolomitic mudrocks; chert; dark coloured, laminated and thin bedded limestone and dolostone. Lithological properties of each of the five members are described below.

The *chert member* forms a distinctive, black rock band on upland surfaces. This, the lowest member of the Ibbett Bay Formation, consists of laminated black chert, with minor thin bedded and flat laminated dolostone and dolosiltite in the lower part. Common orange-brown pyritic dolostone concretions to 30 cm are found in some sections. Chert is thin bedded (3–5 cm) and weathers black or rusty brown. Radiolarians are present. The lower contact is conformable and placed above the highest bed of sedimentary breccia in the underlying Canrobert Formation.

The *dolostone member* is a cliff-forming unit that includes dark grey, argillaceous, microcrystalline dolostone, argillaceous limestone, calcareous mudstone, minor thin bedded black fissile mudrock, and chert. Dolostones, limestones and mudstones are medium to thick bedded and internally structureless or indistinctly laminated. An incipient cleavage is recognized in some exposures and in hand specimens (Fig. 130E). Weathering colours are medium to dark brown. The dolostone member is by far the most resistant rock unit of the Ibbett Bay Formation and can sometimes be confused with the Canrobert Formation when viewed at a distance. It is distinguished from the latter by its darker weathering colours, finer grain size, and stratigraphic position. It also commonly displays soft sediment deformation features such as slump structures and small, intraformational folds. In the southwestern exposures of this member, three units are distinguished, with cliff-forming, argillaceous dolostone common in the upper and lower units, and thin bedded, calcareous mudrock, chert and lesser carbonate in the intervening unit.

The *lower black shale member* is a black weathering, moderately recessive unit consisting of chert, flat-laminated black limestone and dolostone, and black, graptolitic mudrock. Chert beds are 2 to 15 cm thick, and locally contain radiolarians. It is the most common lithology in the lower part of the member. The carbonate beds are more abundant



Figure 45. Vertical airphoto of a tight pericline fold in the northwestern Canrobert Hills. This photograph demonstrates the mappability of the Canrobert Formation, the five members of the Ibbett Bay Formation, and the Blackley and Cape De Bray formations. OCR, Canrobert Formation; OSD1, Ibbett Bay Formation; (OIB1, chert member; OIB2, dolostone member; OSIB3, lower black shale member; SIB4, brown mud rock member; SDIB5, upper black shale member); DB, Blackley Formation; DCB, Cape De Bray Formation. See also legend, Figure 33. NAPL photo. A17719-55.

higher in the section and show varying degrees of silicification in the form of selectively replaced dark or light coloured chert. Primary sedimentary structures in carbonate beds include flat lamination, normal graded bedding and redeposited oolites. Minor vuggy porosity is partly infilled with calcite, fluorite and thermally degraded bitumen. The upper part of the member comprises recessive, black, fissile graptolitic mudrock, and minor argillaceous limestone.

The *brown mudrock member* includes blocky and slabby, fractured mudrock, dolomitic mudrock, silicified mudrock, and minor fissile mudrock (shale). Weathering colours are typically brown, dark brown, or yellowish brown. On fresh surfaces the blocky and slabby beds are light greenish grey and grey. The brown mudrock member is a resistant, ledge forming unit underlain and overlain by darker weathering and highly recessive mudrock of the enclosing members. Clinoform bedding up to several metres thick has been identified in cliff sections in the lower part of the member. Bedding thickness and resistance to erosion decrease upsection. The lower contact is sharp but apparently conformable. A common feature of mudrock slabs in the member is wavy and lenticular thin bedding and thick lamination (Fig. 46). Thin sections indicate that colour variation is due to an abundance of finely divided organic matter and not to grain size variation. The presence of horizontal feeding traces indicates that the intercalation of light and dark mudstone is probably produced from bioturbation.

The *upper black shale member* is the thickest and stratigraphically highest member of the Ibbett Bay Formation. It comprises siliceous and variably calcareous mudrock, with minor, orange-weathering siltstone and chert. The mudrock is variably pyritic, calcareous or dolomitic, and silty, highly recessive, typically platy and fissile and weathers either dark grey or black. Parting surfaces contain various secondary minerals including limonite, goethite, hydrozincite, gypsum, and calcite. Graptolites are common in the lower part of the member but are absent within 150 to 200 m of the upper contact. Half a dozen beds of orange-weathering pyritic black siltstone form a useful, laterally continuous, resistant-weathering stratigraphic marker in the middle part of the member. Olistoliths of buff-weathering, grey, crystalline dolostone up to several metres in size are scattered through the upper part of the member and concretions of orange-weathering, black, dolomitic and pyritic mudstone are observed in some sections. Thin bedded black chert with intercalated siliceous, fissile mudrock is common only in the upper 100 m of the member. The lower contact with the brown mudrock member is gra-

dational and generally drawn below the lowest beds of fissile, black mudrock.

Seismic expression. The seismic expression of the undivided lower four members of the Ibbett Bay Formation is one of horizontal continuous and parallel reflections. Member five is tabular and reflection free.

Age and correlation. The full age range of the Ibbett Bay Formation is Early Ordovician through approximately late Early or early Middle Devonian (Figs. 32,



Figure 46. Two hand specimens of intercalated light grey and dark grey mudrock of the brown mudrock member of the Ibbett Bay Formation. ISPG photos. 3874-1, -4.

37, 38; reports of Norford, Nowlan, McCracken, Lenz and Borré, in Appendix 4). The age of the chert member is based on contained graptolites and ranges from the *oncograptus* Zone in the late Arenig through the *tentaculatus* Zone in the Llanvirn. Beds of possible Llandeilo age may occur at the top. This member is age equivalent to all of the Bay Fiord and possible additional beds in the lowermost Thumb Mountain Formation of the shelf. The dolostone member is approximately Llandeilo in age but also contains older conodont assemblages. Unfossiliferous Caradocian strata could occur in the upper part. Equivalent rocks of the platform are represented by the lower and medial Thumb Mountain Formation. Graptolite assemblages from the lower black shale member range from Caradoc through late Llandovery. Correlative strata possibly include upper Thumb Mountain Formation, and definitely include the Irene Bay and lower Allen Bay formations. Wenlock and lower Ludlow fauna have not been collected from the lower black shale member. Graptolites of the *linearis* Zone in the brown mudrock member are middle Ludlow in age and correlative with parts of the Cape Storm, and Douro formations. Graptolites in the upper black shale member are middle Ludlow (*linearis* and *tenuis*) through late Pragian (*yukonensis*). The highest beds in the formation are not well dated but are probably not younger than late Emsian or early Eifelian (Appendix 4). The upper black shale member is equivalent to the Barlow Inlet, Kitson and Blue Fiord formations.

Interpretation. The Ibbett Bay Formation is a succession of basin floor, basin rise and lower basin slope deposits that record alternating periods of extreme sediment starvation during sea-level highstands on the shelf alternating with periods of more rapid deposition during times of sea-level lowstand. This comparatively thin formation spans the periods of deposition of the Bay Fiord, Thumb Mountain, Irene Bay and Cape Phillips formations, and the five or six shelf carbonate formations equivalent to the Cape Phillips Formation.

The chert member at the base of the formation was deposited under conditions of extreme sediment starvation; the 87 m of chert found in the member are age-equivalent to some 450 to 1000 m of shallow-marine dolostone and evaporite simultaneously deposited on the shelf. The dolostone member is roughly equivalent to the medial Thumb Mountain Formation. Thickness and sedimentation rate of the dolostone member are comparable to correlative strata on the shelf. Soft-sediment deformation, common within the member, may indicate significant above-wave-base erosional scouring of the shelf margin and

resultant sediment flow on the basin slope during a significant drawdown of sea level. Two sea-level minima of approximately Llandeilo and mid-Caradoc ages are indicated by the two resistant dolostone units occurring at the base and top of the member, respectively. The lower black shale member (191.5 m) is another highly condensed interval that corresponds to sea-level highstands and deep basinal starvation during the simultaneous deposition of the Irene Bay and Allen Bay formations (total 550 m). The base of the brown mudrock member is interpreted as a downlap surface resting on a diastem of Wenlock through early Ludlow age. Deposition of the brown mudrock member may indicate a significant drawdown of sea level and progradation of far-travelled silt and mud from an unknown terrigenous source. The gradational upper contact is believed to indicate a reduction in sediment supply, possibly resulting from a regional rise of relative sea level. The upper black shale member (562.3 m) displays lower sediment accumulation rates than equivalent shelf units for strata of Ludlow to Pridoli and Emsian age, but higher accumulation rates for strata of Lochkovian and Pragian age. These observations point to high relative sea levels in the Late Silurian and late Early Devonian, and low sea levels in the earlier part of the Early Devonian.

Blackley Formation (DB)

Type section. The Blackley Formation is the oldest unit contained within the Devonian clastic wedge of Melville Island. This deep water siliciclastic unit was first described as a member of the Weatherall Formation by Tozer and Thorsteinsson (1964). It was later raised to formational status by Embry and Klován (1976). The type section is situated 11 km northwest of Blackley Haven in the Canrobert Hills.

Distribution. The formation is exposed throughout the Canrobert Hills and along the north shore of Marie Bay. It is suspected, from seismic profiles, to underlie Sproule Peninsula, and Eglinton and Prince Patrick islands.

Velocity and thickness. The Blackley Formation on the north side of Ibbett Bay is approximately 700 m thick. Geometric calculations imply a thickness of about 1100 m near the south shore of Marie Bay.

Lithology and seismic expression. Rock types include interbedded very fine grained sandstone, siltstone and fissile mudrock arranged in fining-upward bed sets, each of which ranges from 10 cm to 2 m in thickness.

Goodbody (1993) has documented C-D-E and B-C-D-E Bouma sequences in bedsets of the Blackley Formation. Cleavage is well developed in some exposures (Fig. 131). Traversed sections of the formation along the north shore of Ibbett Bay indicate that the thickest sandstone beds are found in the upper (but not highest) part of the formation, and invariably display basal sole markings. Twenty-seven tool marks measured on eight bedding planes at a single locality near Blackley Haven indicate a unimodal sediment transport direction toward the northeast (N55°E). Clearly, these indicators must be measured at other localities to confirm this direction. Fresh surface colours are grey to dark grey. The weathered surface is medium grey or greenish grey, with resistant beds locally weathering to shades of brown and orange-brown. The Blackley Formation is more resistant to erosion than the underlying and overlying formations, and is readily identified from a distance by its characteristically striped pattern resulting from differential weathering of individual layers (Fig. 47).

Embry (1988a; pers. comm., 1988) has correlated the Blackley Formation with a subsurface seismic unit in the Prince Patrick Island area that has a wedge-shaped geometry in cross-section with internal and upper bounding reflections that converge downward and toward the south or southwest.

Basal contact. The lower contact of the formation is gradational with the underlying upper black shale member of the Ibbett Bay Formation. The lowest beds assigned to the formation are characterized by an interleaving of thin bedded, terrigenous sandstones with black fissile mudrock. These transitional beds



Figure 47. Aerial view of the Blackley Formation, northwestern Canrobert Hills. SD1B5, upper black shale member of Ibbett Bay Formation. ISPG photo. 2887-48.

account for a 10 m section on the north side of Ibbett Bay. However, transitional facies strata near the south shore of Marie Bay may be up to several tens of metres thick.

Age and correlation. The age of the Blackley Formation is not well constrained. Microflora of mid-Emsian to Eifelian age occur at 112 m above the base of the formation in a section near Ibbett Bay (reports of D.C. McGregor, Appendix 4). However the collection is sparse and poorly preserved, and the definitive Emsian spores may have been recycled. Spores from 547 m above the base are Eifelian, possibly mid-Eifelian. The youngest conodonts, from 30 m below the top of the underlying Ibbett Bay Formation, are not older than late Emsian (report of Uyeno in Appendix 4). The Blackley Formation probably has an age range from the early to middle Eifelian and would therefore be time equivalent to the lower Cape De Bray Formation of central and eastern Melville Island. It is also possible that the Blackley may be partly correlated with the upper part of the Blue Fiord Formation of northeastern Melville Island.

Interpretation. The Blackley Formation is interpreted as a deep water succession of southwesterly transported, siliciclastic sediment gravity flows. The gradational lower contact and thickening-upward feature of individual sediment gravity flows in the formation suggests that the formation is progradational and diachronous.

Cape De Bray Formation (DCB)

Type section. The Cape De Bray Formation was initially described as a member of the Weatherall Formation by Tozer and Thorsteinsson (1964). It was later raised to formational status by Embry and Klovan (1976). The type section is located 3.2 km south of Cape De Bray in the Canrobert Hills.

Distribution. The Cape De Bray Formation is a recessive, highly fissile siltstone and mudrock unit that variably overlies the Blackley, Kitson, Cape Phillips and Blue Fiord formations (Figs. 33, 39, 41, 45). A complete section through the Cape De Bray Formation is exposed on a north-flowing stream that empties into the southwest corner of McCormick Inlet. Incomplete cliff sections of the formation are well exposed along the south shore of Ibbett Bay. Complete sections of the formation have been penetrated by eight exploratory wells. The seismically-defined Cape De Bray Formation is believed to underlie nearly all parts of the island.

Velocity and thickness. Interval velocity ranges amongst the various wells from 3.5 km s⁻¹ in the southwest increasing to 3.9 km s⁻¹ in the northeast.

The formation ranges from less than 100 m in thickness where it overlies the Blue Fiord Formation to about 950 m where it overlies the Cape Phillips and Kitson formations. Restored (pre-deformational) thickness of the Cape De Bray in the Canrobert Hills area may be as much as 1300 to 1700 m.

Lithology. Non-fissile mudrocks with subordinate thin siltstone and very fine grained sandstone are the common rock types. In the upper part of the formation, these rock types are arranged in very thick coarsening-upward cycles, each cycle consisting of about 80 per cent mudrock and 20 per cent of the other constituents (Embry and Klován, 1976; Goodbody, 1993). The mudrocks are soft, intensely fractured, micaceous, abundantly silty and may have a little contained calcite. Plant fragments are abundant though minute. The formation weathers topographically very low and is uniformly monotone on upland surfaces when viewed at a distance. Weathering colours are dark grey and dark greenish grey. Bedding is commonly unidentifiable in the absence of siltstone and sandstone layers and can be entirely dominated by an incipient cleavage. Sandstones are thin bedded, fine to very fine grained and occasionally bioclastic. Sparse faunal remains are diverse and benthic in association. Cliff exposures of the Cape De Bray Formation on the south side of Ibbett Bay reveal large clinoforms in the upper part of the formation (Fig. 48).

Seismic expression. The Cape De Bray Formation is characterized seismically by the common occurrence of clinoform reflectors high in the formation (Figs. 13,

49, 50). Two informal seismic members are distinguished. The lower member features wavy or irregular and discontinuous, subparallel reflection segments. Individual segments can be correlated over distances ranging from a few hundred metres up to several kilometres. Also observed are chaotic, mounded (Section C, Note 11), and reflection free areas. The upper member of the Cape De Bray seismic interval includes sigmoidal and toplapping clinoforms (Fig. 49). The foreset reflections are most obvious in the upper part of the member but in some instances can be followed into bottomset reflections. The base of the upper member is drawn at the base of the steeply sloping segment of foreset reflectors where they can be traced into age-equivalent but shallower-dipping bottomset reflectors assigned to the lower member. Likewise, the upper contact is drawn where the clinoforms are apparently truncated by overlying topset reflectors. On some profiles, these topsets can be traced laterally into foreset reflections (Fig. 49; Section D, Note 5; Section G, Note 5; Section H, Note 4). In these cases, the upper contact of the formation has been shifted to the first topset reflector higher in the section.

Basal contact. The base of the Cape De Bray Formation is gradational and conformable with the underlying Blackley Formation in the Canrobert Hills. A sharp but apparently conformable contact also marks the base of the formation above the Cape Phillips and Kitson formations. In the Weatherall Bay area, the base of the Cape De Bray Formation above the Blue Fiord Formation is apparently conformable but is marked by a sharp transition from faunally diverse nonargillaceous limestone to overlying silty mudrocks and lesser, thin bedded bioclastic sandstone. On Cameron Island, there is drill-hole evidence of

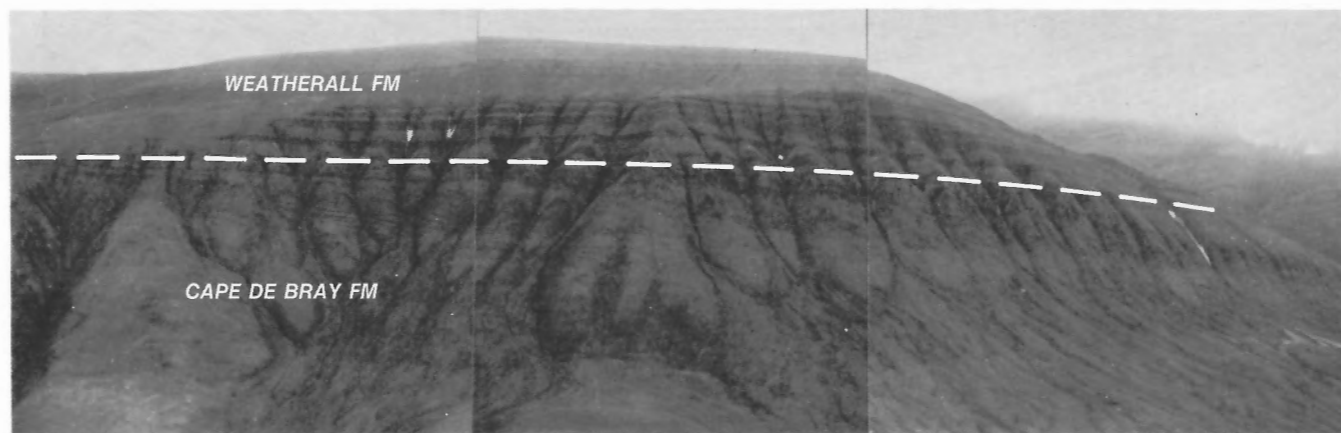


Figure 48. Panoramic view of large foreset beds (clinoforms) in the upper part of the Cape De Bray Formation, south shore of Ibbett Bay. The contact with the Weatherall Formation is placed above the foreset beds. ISPG photos. 2444-16, -17, -18.

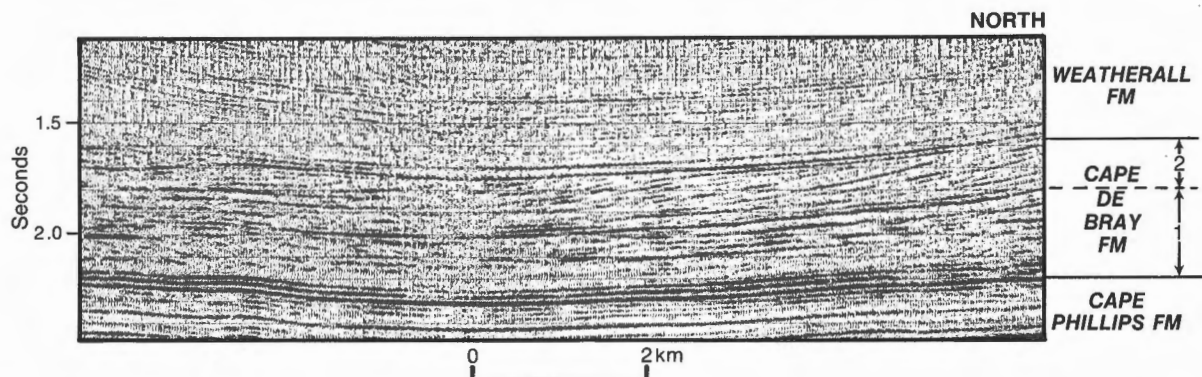


Figure 49. Seismic stratigraphy of the Weatherall and Cape De Bray formations for a part of profile P1138 (Sections F and G). Vertical exaggeration in the Cape De Bray interval is approximately 1.45. Note the diachronism of the contact between the Weatherall and Cape De Bray formations as defined by the stratigraphic position of the seismic shelf/slope break above the clinoform reflectors.

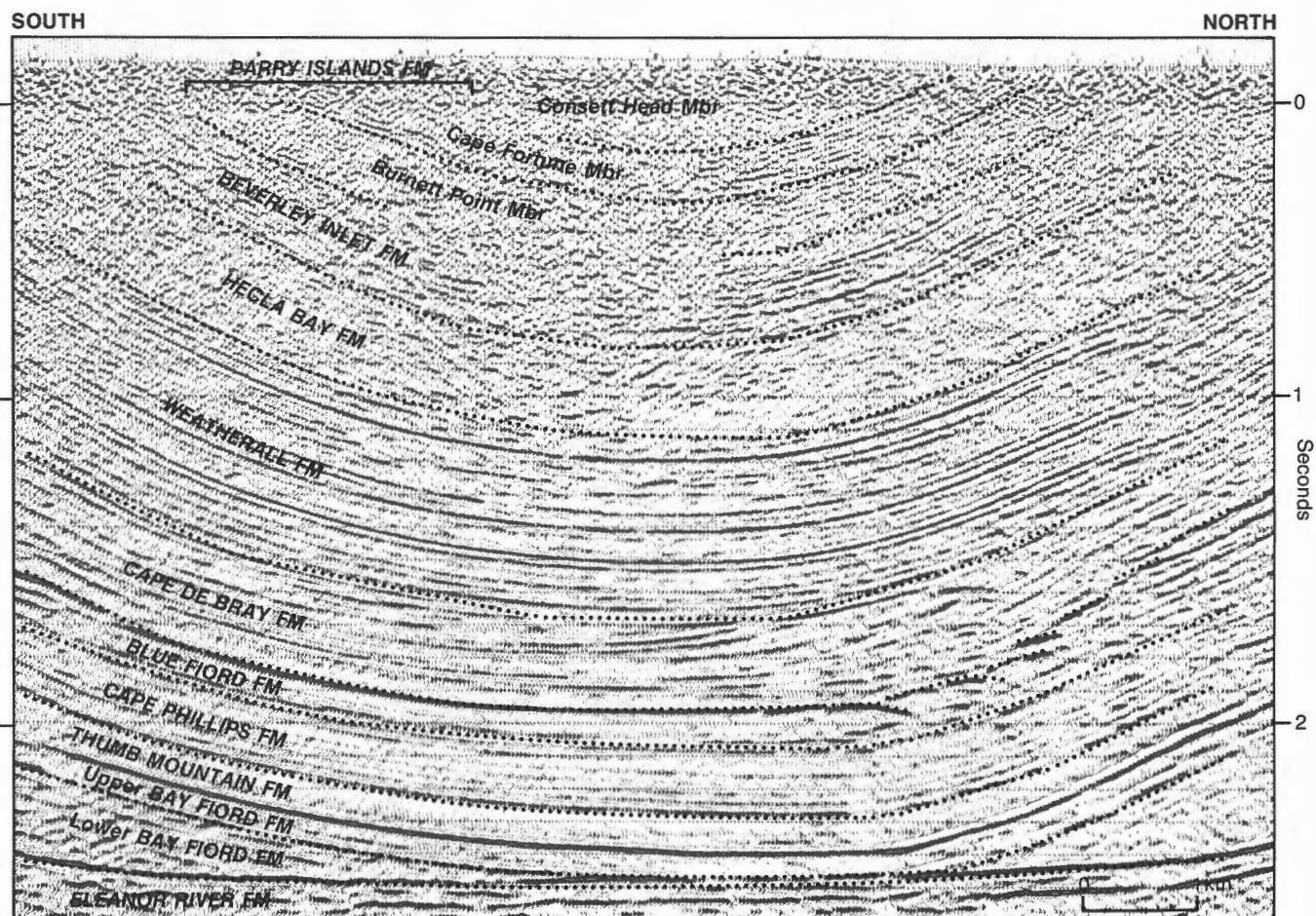


Figure 50. Seismic stratigraphy of the Devonian clastic wedge (Cape De Bray Formation to Consett Head Member of the Parry Islands Formation). Seismic data are taken from a portion of profile C75 (Section A), King Point East Syncline, eastern Melville Island. Vertical exaggeration in the middle of the figure is approximately 0.96 at 2.5 s, 1.22 at 1.5 s, and 1.5 at 0.5 s.

subaerial exposure and deep, karst-type erosion of the Blue Fiord Formation prior to overlap by the Cape De Bray (Waylett, pers. comm., 1988).

The seismically defined lower contact is a variably weak or strong, continuous parallel reflection above the Kitson and Cape Phillips seismic intervals and a strong continuous reflection above the Blue Fiord. Northerly to northeasterly onlapping reflection segments mark the base of the Cape De Bray above the Blue Fiord reflector (Section A, Note 8; Section C, Note 9; Section D, Note 9; Section E, Note 3).

Age and correlation. The age of the Cape De Bray Formation is based on contained spores and macrofauna, and conodont assemblages from the underlying and overlying formations (Fig. 38; reports of McGregor, Norris and Uyeno in Appendix 4; McGregor, 1993). In the Weatherall Bay area, the Cape De Bray Formation could range from the *serotinus* or *patulus* zones (late Emsian) to the *costatus* Zone (early Eifelian). Based on the occurrence of *costatus* in the uppermost Blue Fiord of adjacent Cameron Island (Mayr, 1980), the Cape De Bray over the Towson Point platform on Melville Island was probably deposited entirely during the span of the *costatus* Zone. In the central part of the island, the Cape De Bray Formation is early or middle Eifelian (within or above the *costatus* Zone) at the base, ranging through middle Eifelian (within or below the *kockelianus* Zone) at the top. In the Canrobert Hills-Ibbett Bay area, the formation has a probable age range of middle Eifelian below the base, ranging to middle or possibly late Eifelian at the top (within or below the *kockelianus* Zone). Palynomorph data require a late Eifelian age for the upper part of the Cape De Bray in all western areas, and seismic profiles point to the probability of some lower Givetian strata in the upper Cape De Bray beneath western Dundas Peninsula.

The Cape De Bray Formation of western and southwestern Melville Island is age equivalent to the Weatherall formation of eastern Melville Island, part of the Bird Fiord of Bathurst, Devon and southwestern Ellesmere islands, and part of the Strathcona Fiord Formation of central Ellesmere Island (Embry and Klován, 1976; Embry, 1988a; Goodbody, 1989; Uyeno, 1990).

Interpretation. The Cape De Bray Formation has been interpreted by Embry and Klován (1976) as a basin-fill succession. Seismic profiles confirm this and indicate that this deep water realm was a pre-existing intrashelf embayment previously occupied by condensed

mudrock of the Cape Phillips and Kitson formations. The lower contact of the Cape De Bray is interpreted as a downlap surface where it overlies starved basin sediments of the Cape Phillips and Kitson formations. The lower seismic member is a diachronous basin floor and basin rise succession that is linked proximally in the northeast to the basin slope (upper member), and also linked distally and to the southwest to age-equivalent starved basin and embayment plain sediments in the upper part of the subsurface Kitson Formation. This lower part of the Cape De Bray is dominated by mudrocks at the surface. The detrital components were deposited at very high accumulation rates in a deep water, marine setting featuring basin slopes of much less than 1°. It is therefore likely that mass flow processes were involved, especially the activity of silt-mud turbidites. Mounded and chaotic internal seismic patterns could also have been generated by syndepositional sediment gravity flows.

The contact between the two Cape De Bray seismic members is taken to be the base of slope and, thus, the upper member includes strata deposited on the slope. The foreset reflections are probably generated by shale on sandstone impedance contrasts that mark the base of progradational coarsening-upward and shallowing-upward cycles. The downslope fall off in impedance contrast of clinoform reflectors is believed to mark the normal downslope decrease in grain size of the coarsest fraction of each contained progradational cycle. Foreset reflectors that can be traced into bottomset reflectors imply a continuity of rock density contrasts and lithofacies contrast into the basin rise. This could be due to an interfingering of silt-mud turbidites with coarser grained sediment gravity flows. This interpretation is also consistent with the scattered occurrence throughout the formation of sandstones containing a diverse assemblage of allochthonous, shallow benthic marine macrofauna (trilobites, corals, brachiopods and bivalves). Onlap patterns at the base of the Cape De Bray Formation above the Blue Fiord Formation are interpreted as marking a sequence boundary that is correlated with the erosional interval above the Blue Fiord in the Cameron Island area. However, the onlap patterns at the base of the Melville Island Cape De Bray are undoubtedly marine in origin and generated in part by lateral onlap ("sidelap") and flooding of terrigenous sediment onto a continuously subsiding carbonate bank.

Weatherall Formation (DW)

Type section. The Weatherall Formation is a mixed siliciclastic succession first described and named by

Tozer and Thorsteinsson (1964). The type section is situated along a south-flowing stream 16 km east of the east arm of Weatherall Bay (Fig. 39). The term as used here is in the restricted sense proposed by Embry and Klovan (1976); this definition recognizes the Blackley and Cape De Bray beds as separate and distinct formations in their own right.

Distribution. The Weatherall Formation is widely exposed at the surface and underlies most of the southern part of the island. In the eastern part of the island, it is the most resistant to erosion of the formations that make up the Devonian clastic wedge and it therefore underlies the highest hills and ridges. There are two incomplete sections locally well exposed along several rivers north and east of Beverley Inlet (Fig. 51). Farther west, the overlying Hecla Bay Formation is most resistant to erosion. In these areas, the Weatherall Formation is mapped on the incised flanks of upland plateaux or in fringing hog-back ridges. The formation is well exposed on stream banks and in coastal cliff sections between McCormick Inlet and the west end of the island (Fig. 48). In the north, the formation has been removed by erosion prior to overlap by Carboniferous and younger cover. Complete sections of the formation have been penetrated by five exploratory wells.

Velocity and thickness. Sonic log and Dix interval velocities range from 4.3 km s⁻¹ in the east to 3.6 km s⁻¹ in the west. Formation thickness increases from approximately 750 m in the southeast to 1500 m in the west.

Lithology and seismic expression. The Weatherall Formation includes subequal proportions of very fine grained sandstone, siltstone and silty, fissile mudrock. All of the rock types contain concentrations of detrital green-brown biotite, muscovite, chlorite, coal fragments, and fine plant material on bedding plane partings. Subordinate components include ferruginous sandstone, and calcareous and fossiliferous sandstone with a wide variety of macrofauna including bivalves, brachiopods, crinoids, cephalopods, trilobites and corals. The rock types are normally arranged in thickening- and coarsening-upward cycles that are each 3 to 30 m thick. Several hundred cycles make up the bulk of the formation. Several longer period, lower frequency cycles have also been recognized by Goodbody (1993). Cycle thickness, maximum bed thickness and sandstone content of the formation all generally increase to the top. Weathering colours range from dark green in the mudstone layers through light green and brownish green in the siltstone and very fine grained sandstone beds, to yellowish brown and white in the thicker sandstone beds near the upper contact of

the formation. A combination of cyclically alternating beds of variable colour and resistance to erosion gives the Weatherall Formation a striped erosional pattern on upland surfaces.

The Weatherall Formation is a single coherent seismic unit characterized by parallel but disrupted and generally discontinuous weak reflections (Fig. 50).

Basal contact. The lower contact is drawn above upper slope facies mudrocks of the Cape De Bray Formation. This level is normally found below the first, thin, sandstone-dominated cycle. On the south side of Ibbett Bay, it is possible to locate the contact in coastal cliffs by identification of the shelf/slope break at the top of depositionally inclined and also top-truncated foreset beds in the upper Cape De Bray Formation (Fig. 48). The base of the Weatherall seismic unit is diachronous and is drawn on the topset reflection that defines the upper limit of top-truncated foreset reflections in the underlying Cape De Bray Formation (Fig. 49; Section D, Note 5; Section F, Note 10; Section G, Note 5; Section H, Note 4).

Age and correlation. The age range of the Weatherall Formation as defined by palynomorphs, conodonts, and macrofauna is: within the *costatus* Zone of the early Eifelian through to the earliest Givetian in the eastern part of Melville Island; middle Eifelian through middle Givetian in the central region; and middle to late Eifelian through late Givetian in the west (Fig. 38; reports of McGregor, Norris, and Uyeno in Appendix 4). The Weatherall Formation is markedly diachronous. Parts of the formation beneath central Melville Island are age equivalent to the upper Cape De Bray of the southwest and the lower Hecla Bay of the northeast. The Weatherall is also correlated with parts of the Bird Fiord and Strathcona Fiord formations of the central and eastern Arctic islands (Embry and Klovan, 1976; Embry, 1988a; Goodbody, 1989, 1993; Trettin, 1990; Uyeno, 1990).

Interpretation. The Weatherall Formation contains shallow-marine deltaic strata deposited in depositional environments that embrace the entire deltaic shelf region from the delta front and upper shoreface to the shelf/slope break (Embry and Klovan, 1976; Embry, 1988a). Shallow prodeltaic and clastic outer shelf lithofacies dominate thin, cyclical sediments in the lower part of the formation. Delta front and clastic nearshore depositional environments dominate in the upper part of the formation, with intertidal submarine channels accounting for some of the thicker and coarser sandstone units in the highest part of the formation (Goodbody, 1993). Seismic profiles support the biostratigraphic evidence that the shelf facies



Figure 51. Vertical airphoto of part of the Beverley Inlet Anticline. Mappable units include: formations of the Devonian clastic wedge (DW, Weatherall; DHB, Hecla Bay; DBI, Beverley Inlet and lower three members of Parry Islands Formation; DPI1, Burnett Point Member; DPI2, Cape Fortune Member; DPI3, DPI4, lower two units of the Consett Head Member), unconformable Lower Cretaceous (KI, Isachsen and Kc, Christopher formations) and disconformable outliers of possible Tertiary cover (TB?, Beaufort Formation). Photo contains the type section of the Hecla Bay, Beverley Inlet and Parry Islands formations (as indicated by stars). See also legend, Figure 33. NAPL photos. A16766-45, -46.

Weatherall Formation grades distally and to the southwest into age-equivalent slope facies strata of the Cape De Bray Formation.

Hecla Bay Formation (DHB)

Type section. The type section, defined and described by Tozer and Thorsteinsson (1964) and Embry and Klován (1976), is situated 11 km north-northwest of the head of Beverley Inlet on the south limb of the Robertson Point Anticline, Melville Island (Fig. 51).

Distribution. The Hecla Bay Formation is a prominent, light coloured unit mostly consisting of unfossiliferous quartz sandstone. It is widely exposed throughout the Parry Islands and also on western Devon and Ellesmere islands. It is also extensively preserved at the surface over most of Melville Island but has been removed by Carboniferous erosion in the north. Numerous incomplete sections of the Hecla Bay Formation are to be found in coastal cliffs around the southern and western parts of the island. There are also useful reference sections on the east arm of Weatherall Bay, and in incised stream valleys; one near Towson Point and the other east of Beverley Inlet. Four wells have intersected the formation on Melville Island.

Velocity and thickness. Sonic and Dix interval velocities increase from 3.7 km s⁻¹ in the west to 4.3 km s⁻¹ in the east. The maximum thickness range is from less than 200 m on western Dundas Peninsula to about 1300 m in areas north of Murray Inlet and west of Hecla and Griper Bay.

Lithology. In the eastern part of the island, the lower part of the formation comprises four or five very thick quartz sandstone intervals interbedded with lesser, greenish weathering, very fine grained sandstone and siltstone. The upper part of the formation is almost entirely white- to yellowish-weathering quartz sandstone that has a castellate erosional character presumably resulting from selective cementation. Primary sedimentary structures are well preserved and include mud rip-up clasts, planar bedding, planar cross-stratification, and scour surfaces resulting from channelling. Mineralogy includes subangular to subrounded fine and very fine grained monocrystalline quartz with greatly subordinate muscovite, feldspar, chert and polycrystalline quartz. The matrix includes quartz overgrowths, clay minerals and minor hematite.

West of Liddon Gulf and Hecla and Griper Bay, the Hecla Bay Formation is more resistant to erosion. Sandstones weather more readily into discrete, well

cemented beds that have been sculptured into cliffs, ledges and slabby talus fans. Weathering colours are shades of grey, yellow, yellowish brown, and reddish brown. The sandstones are also compositionally less well sorted and contain a higher proportion of detrital biotite, muscovite, chlorite, coal and carbonized plant material. Intercalated beds in all western sections of the formation include grey to greenish, very fine grained sandstone. As well as resistant, thick bedded, well cemented, fine to medium grained quartz sandstone, the Raglan Range section also includes a 30 m interval of normally graded chert pebble conglomerate and pebbly coarse grained sandstone (Figs. 33, 52). This distinctive marker unit (labelled 'DHBC' on the Melville Island map sheet and legend) is situated at approximately 170 to 200 m below the upper contact. Chert clasts in the conglomerate, ranging in size to several centimetres, display both compositional lamination and a pre-existing cleavage. The degree of wear associated with sediment transport ranges from highly angular to subrounded.

In the far southwestern part of the island, the Hecla Bay Formation consists of a single unit of orange-brown-weathering, massive bedded sandstone several hundred metres thick that is believed to be chronostratigraphically equivalent to the upper 200 m of section in Raglan Range. The Hecla Bay Formation in these cliff sections contains rare and sparse assemblages of marginal marine and brackish marine bivalves (reports of Norris, Appendix 4).

Southwestward thinning of the formation is also documented by surface geology and four well penetrations through the formation on Dundas Peninsula. In these sections, the typical sandstone lithofacies of the Hecla Bay Formation grades laterally into a mixed clastic facies assignable to the Weatherall Formation.

Seismic expression. On eastern Melville Island seismic sections, the Hecla Bay Formation forms a distinct and separate, reflection-free seismic unit (Figs. 13, 50). The lower contact is seismically gradational with the weak to moderately reflective Weatherall Formation. On Dundas Peninsula, and in all western areas, the Hecla Bay Formation features numerous weak and short, subparallel reflecting segments. In these areas, the bounding contacts cannot be seismically identified. On some seismic lines, the Hecla Bay Formation is geophysically indistinguishable from underlying and overlying units.

Basal contact. Drawn below the lowest massive sandstone bed above which white sandstone is the dominant lithology. The seismic base of the formation is gradational.

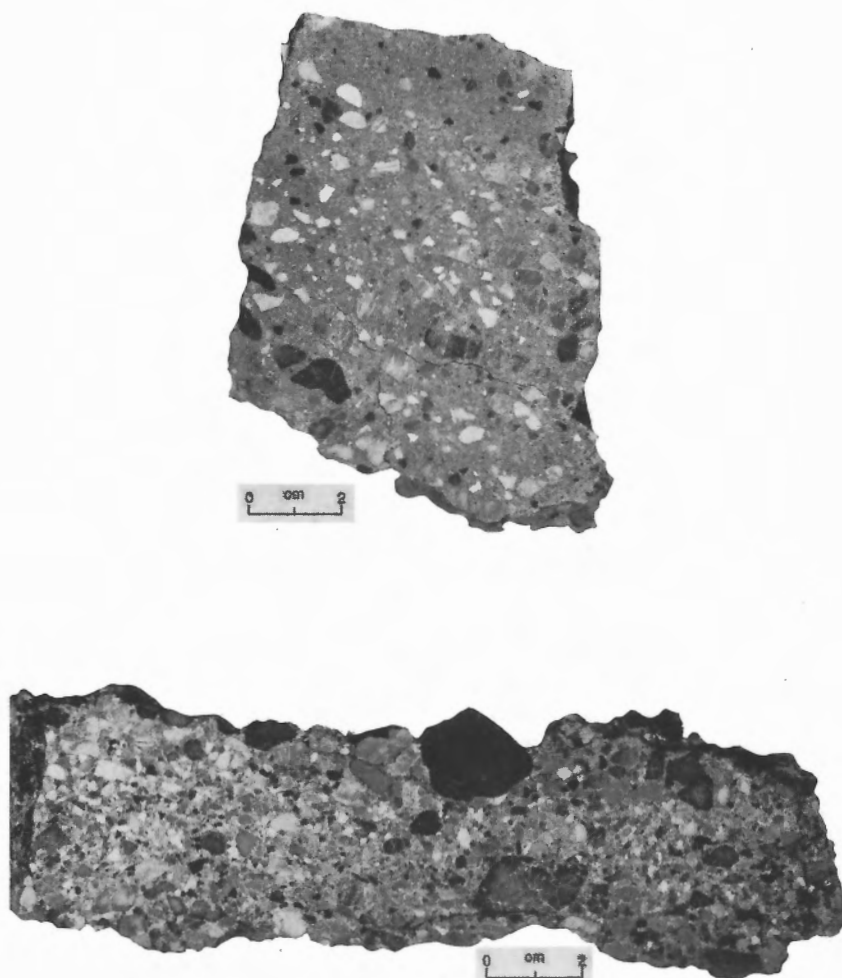


Figure 52. Hand specimens of chert-pebble conglomerate from the upper Hecla Bay Formation (DHBC), Raglan Range, northern Melville Island. ISPG photos. 3029-1, -10.

Age and correlation. The age of the Hecla Bay Formation is defined by contained palynomorph assemblages and also constrained by conodont and macrofaunal collections from the underlying and overlying formations. The base of the formation is early Givetian in Weatherall Bay area, middle Givetian in the central part of the island, and late Givetian in the west. The top of the formation is a disconformable surface that is close to the Givetian–Frasnian boundary (reports of McGregor and Norris, in Appendix 4). All but the youngest Hecla Bay Formation of eastern Melville Island is age equivalent to the medial and upper Weatherall Formation of western Melville Island.

Interpretation. The Hecla Bay Formation is interpreted as including terrigenous sediments of fluvial and deltaic association (Embry and Klován, 1976; Embry, 1988a). The eastern facies, as interpreted by Goodbody

(1993), includes distributary channel sands and interdistributary bay fill deposits in the lower part of the formation and stacked nonmarine braidplain channel sands in the upper part. The age-equivalent western facies consists almost entirely of delta mouth, brackish marine deposits that grade out into open-marine delta front and inner shelf sands of the Weatherall Formation. The conglomerates in the upper part of the formation in Raglan Range represent the most source-proximal facies in the formation. The extreme angularity of many clasts indicates a close spatial association with once tectonically uplifted areas to the north and/or northeast underlain by chert. Although grain size is not above about 2 cm, bedded basin-facies chert in the source area, similar to that presently encountered in the Ibbett Bay Formation, would be unlikely to yield cobble or boulder grade material because of the thin bedded nature of these rocks and the additional existence of closely spaced joints and cleavage.

Beverley Inlet Formation (DBI)

Type section. All the Devonian nonmarine and marginal marine siliciclastic strata above the Hecla Bay Formation in the Parry Islands were originally included in the Griper Bay Formation of Tozer and Thorsteinsson (1964). The latter unit was subsequently raised to "subgroup" status by Embry and Klovan, (1976) and divided into two regionally mappable formations separated by a disconformity. (The term "Griper Bay Subgroup", suggested by Embry and Klovan, is not used in this account.) The Beverley Inlet Formation is the lower of the two new formations. The type section is situated 10 km north-northeast of the head of Beverley Inlet, southeastern Melville Island (Fig. 51).

Distribution. The Beverley Inlet Formation is exposed at the surface throughout the Parry Islands. Similar age-equivalent strata occur on Prince Patrick and Banks islands. On Melville Island, the formation is common at the surface in synclines (eastern and central parts of the island; Fig. 53), and is also widely exposed in less deformed areas of Dundas Peninsula and the Blue Hills. The Beverley Inlet Formation has been intersected in the upper parts of three exploratory wells. There are excellent cliff sections through the formation around the southwestern coasts of the island.

Interval velocity. Dix interval velocities range from 3.3 km s⁻¹ and increase northeastward to 3.8 km s⁻¹.

Thickness. The thickness of the Beverley Inlet Formation ranges from 280 to 570 m where it is overlain by the Parry Islands Formation. In the central and southwestern part of the island, at least 750 m of strata are assigned to the Beverley Inlet Formation (top not seen).

Lithology and seismic expression. Dominant rock types in the formation include quartz sandstone, siltstone, lesser mudrock and minor coal. Medium bedded and cross-stratified, white to light green, fine and medium grained, detrital, micaceous and chloritic quartz- and chert-bearing sandstones are most common, and are normally interbedded in high-frequency fining-upward cycles with green to dark green planar laminated and ripple crosslaminated siltstones and silty micaceous mudrocks (Embry and Klovan, 1976; Goodbody, 1993). Accessory components include chert pebbles, plant and leaf fragments, coalified wood, phosphatic fish remains, brachiopods, and crinoids. Weathering colours are shades of light green, grey green, purple and red. The redbeds in the Beverley Inlet Formation are common only in the lower part of the formation.

The Beverley Inlet Formation is represented by numerous weak-to-moderate strength parallel but disrupted internal reflection segments (Figs. 13, 50).

Basal contact. The Beverley Inlet Formation everywhere disconformably overlies thick to massive bedded quartz sandstones of the Hecla Bay Formation. On some seismic reflection profiles, the lower contact is drawn above the lowest weakly reflective level below which is found, the (commonly) reflection-free Hecla Bay Formation.

Age and correlation. Macrofauna in the Beverley Inlet Formation are latest Givetian to early Frasnian in age (reports of Norris, Appendix 4). Palynomorph assemblages are early Frasnian through late Frasnian (McGregor, 1993; unpub. reports of McGregor; pers. comm., 1989). The Beverley Inlet Formation is age equivalent to the Fram, Hell Gate and Nordstrand Point formations of Ellesmere and Devon islands. It is also equivalent to the uppermost Weatherall Formation of Banks and Prince Patrick islands (Embry and Klovan, 1976; Embry, 1988a).

Interpretation. The Beverley Inlet Formation is a predominantly fluvial and nonmarine deltaic succession of strata in the eastern exposures. Brackish-marine deltaic environments dominate in the west and southwest (Embry and Klovan, 1976; Goodbody, 1993).

Parry Islands Formation (DPI)

Type section. The Parry Islands Formation is the upper of two marine and nonmarine siliciclastic formations that make up the "Griper Bay Subgroup" of Embry and Klovan (1976). The type section is situated 8 km north-northeast of the head of Beverley Inlet, southeastern Melville Island (Fig. 51).

Distribution. The Parry Islands Formation is exposed on Devon Island, Bathurst and adjacent small islands, and Prince Patrick Island. It is also preserved in the synclines of eastern Melville Island, where five distinct units have been recognized and mapped (Figs. 51, 53). The lower two units correspond to the Burnett Point (DPI1) and Cape Fortune (DPI2) members of Embry and Klovan (1976). The upper three units correspond to Embry and Klovan's (1976) Consett Head Member (DPI3–DPI5). Excellent exposures of the Burnett Point and Cape Fortune members, and the lower unit of the Consett Head Member occur in the vicinity of the type section (Fig. 51) and in coastal cliffs along the east arm of Weatherall Bay. The highest two units of the Consett Head are best exposed in Byam River Syncline, 20 to 25 km north of Beverley Inlet (Fig. 53).



Figure 53. Vertical airphoto of part of the Rea Point Anticline and Byam River Syncline. DW, Weatherall Formation; DHB, Hecla Bay Formation; DBI, Beverley Inlet Formation; DPI, Parry Islands Formation; DPI1, Burnett Point Member; DPI2, Cape Fortune Member; DPI3, DPI4, DPI5, three units of the Consett Head Member. See also legend, Figure 33. NAPL photos. A16766-40, -42.

Velocity and thickness. Dix interval velocities range from 3.3 to 3.7 km s⁻¹. The Parry Islands Formation attains a maximum preserved thickness of approximately 1100 m in Byam River Syncline. Thickness of the individual members are: Burnett Point Member (DPI1), 202–310 m; Cape Fortune Member (DPI2), 50–420 m; Consett Head Member (DPI3–DPI5), 380+ m. The thinnest development of the Burnett Point and Cape Fortune members occurs in northern outcrop areas near Weatherall Bay. The top of the Consett Head Member is everywhere eroded.

Lithology. Dominant rock types include quartz sandstone, siltstone, and silty mudrock with minor coal, pebbly sandstone, and fossiliferous sandstone. The Burnett Point Member is an off white to yellowish weathering, fine to medium grained quartz sandstone with pebbly sandstone and minor chert pebble conglomerate up to 2 m thick (observed by Embry and Klován, 1976) near the base of the formation in the Weatherall Bay area. The Cape Fortune Member consists of grey-green and medium green weathering, fine to very fine grained fossiliferous sandstone, siltstone, silty micaceous mudrock, and minor, argillaceous limestone. Macrofauna found in this member include brachiopods, bivalves, trilobites, crinoids and cephalopods. The lowest of the three units of the Consett Head Member is similar to the lowest member of the Parry Islands Formation and consists dominantly of white to yellowish weathering, medium to thick bedded, fine to medium grained quartz sandstone. The medial unit of the Consett Head Member is 65 m thick and gradationally overlies the lower unit. It primarily comprises recessive, medium grey weathering, dark grey fissile mudrock with occasional sideritic nodules. The second unit is in turn gradationally overlain by the highest unit, which consists of 65 m of white to yellowish weathering, fine to medium grained quartz sandstone. Thin intervals of grey, fissile mudrock and minor coal can be identified on the ground and on airphotos at two levels in the unit within Byam River Syncline. A third seam high in the unit includes, at one locality, 4 m of high-volatile bituminous B coal (see Chapter 9 for locality description and location).

Seismic expression. The Parry Islands Formation is represented by numerous weak to moderate strength, parallel but disrupted internal reflection segments. On seismic line C75 (Section A; Fig. 50), the Burnett Point Member is distinguished as a separate unreflective or very weakly reflective seismic subunit. In these circumstances, the base of the unreflective layer is on or near the base of the formation. However, individual members of the formation do not normally have

separate seismic characters and the lower contact above the Beverley Inlet Formation is then seen to be geophysically gradational (Fig. 13).

Age and correlation. The Parry Islands Formation is dated on palynomorph assemblages as late Frasnian through middle Famennian or early late Famennian. Two conodont assemblages of early Famennian (Lower–Middle *crepida*) and late Famennian (*Icriodus costatus*) ages occur in the type section of the Cape Fortune Member near Beverley Inlet (reports of Uyeno and Higgins, Appendix 4). The *crepida* Zone fauna are also associated with a diverse assemblage of chondrichthyan, ctenacanth, crossopterygian, lungfish, paleoniscoid and possible acanthodian teeth, scales and lepidotrichia (report of S. Turner, Appendix 4). A late (not latest) Famennian age is indicated for the Consett Head Member.

Interpretation. The Parry Islands Formation consists of a mixed siliciclastic succession deposited in a variety of fluvial, deltaic and shallow-marine settings (Embry and Klován, 1976). The gradational transition from fluvial Burnett Point Member through marine Cape Fortune Member marks a rise in relative sea level beginning at the base of the formation. Sandstones in the lower and upper units of the Consett Head Member are probably channelized delta front and/or delta plain deposits. The unfossiliferous medial shale unit and other mudrock and coal beds in the upper sandstone unit are probably lacustrine, interdistributary bay-fill and swamp deposits.

Development of the Franklinian miogeocline and foredeep basin

General comments

The following account of Precambrian(?) through Devonian tectonics and sedimentation in the Melville Island region is illustrated with a series of ten subsurface isopach maps and a series of vertically exaggerated stratigraphic cross-sections. Wherever possible, unit thicknesses determined from well intersections and surface measured sections have been used. Thickness variation has been additionally constrained by the locations of member and formational contacts established during regional geological mapping (maps attached). Most subsurface data, however, have been compiled from interpreted and depth-converted seismic reflection profiles (both time migrated and reprocessed data, and unmigrated data). Bearing in mind the errors unavoidably introduced

during depth conversion, interval velocity information is included in the captions of the map figures so that thickness data points can be (approximately) converted back into two-way travel times.

As previously discussed in Chapters 1 and 2, the oldest geological features in the western Arctic Islands are defined by north-trending Bouguer gravity and magnetic anomalies that betray the existence of north-trending Archean and Lower Proterozoic crystalline rocks of the Slave, Thelon and Wopmay orogens beneath the later Proterozoic and Paleozoic cover of Victoria Island, M'Clintock Channel, Prince of Wales, Cornwallis and Bathurst islands (Figs. 9, 10). The distribution of these deep-seated trends also favours the existence of Archean or Lower Proterozoic basement at great depth beneath Melville Island.

The Proterozoic seismic structural style described in this report is consistent with the regional geophysical evidence of Overton (1972) and Sobczak et al. (1986) that there has been substantial northwesterly thinning of the Precambrian crust in the western Arctic Islands. Seismic profiles and regional geological considerations support the presently held view that crustal attenuation was the result of two major thermal events and associated rifting phases. The first phase of rifting probably occurred in the early Middle Proterozoic and culminated with the emplacement of the Mackenzie thermal plume at about 1267 Ma. The first and second rifting phases are temporally separated by late Middle and early Late Proterozoic intracratonic deposition of the Shaler Group and the accumulation of a coeval seismic stratigraphic succession of subsurface Melville Island (sP2). The second phase of rifting occurred between the Franklin thermal event at about 723 Ma and the overlap of the entire Proterozoic succession by widespread post-rift continental margin cover in the Early Cambrian. This phase is now known to have produced a fundamental and long-lived northeast-trending plate-marginal anisotropy that has also influenced many subsequent depositional patterns and structural features of the Melville Island region.

The subsequent evolution of the Franklinian succession includes: 1) an Early(?) Cambrian through mid(?)–Silurian phase of trailing continental margin subsidence and sediment accumulation, probably driven by post-rift lithospheric cooling; and 2) a subsequent Late(?) Silurian through Famennian phase of enhanced downward flexure accompanied by Middle-Late Devonian foredeep sedimentation, presumably driven by plate margin tectonic loading. These two distinct phases of sedimentation are readily observed on the accompanying graph (Fig. 54) that

plots sediment accumulation rate on the southern shelf and shelf rim against absolute time.

The time interval between about 550(?) and 422 Ma is marked by a geometric fall in sediment accumulation rate. This undoubtedly corresponds to the post-rift thermally subsiding phase of evolution of the Franklinian continental margin. There are secondary peaks in accumulation rate of uncertain origin—on the shelf—the first between 472 and 464 Ma associated with deposition of Bay Fiord evaporites and carbonates in the Llanvirn, and the second between 421 and 410 Ma related to deposition of the combined Cape Storm, Douro and Barlow Inlet formations in the Ludlow and Pridoli. A period of widespread sediment starvation from 410 to 385 Ma preceded the main phases of foreland siliclastic sedimentation between 385 and 360 Ma.

Early(?) Cambrian through late(?) Middle Cambrian (550?–523? Ma)

Tectonically stable conditions mark the Early(?) Cambrian through late(?) Middle Cambrian pattern of sedimentation on the embryonic southern shelf and shelf margin (Fig. 55). Although these deposits completely blanket the Upper(?) Proterozoic rift deposits, the differential compaction of the older succession may account for the coincident parallelism of Proterozoic structural trends and Cambrian(?) isopachs (compare Figs. 18 and 55). Four seismic depositional sequences are recognized within the Early(?) Cambrian through late(?) Middle Cambrian time interval (Figs. 56–58). The oldest sequence includes transgressive incised valley fill (unit sC1A) and overlying highstand deposits (unit sC1B; Fig. 56).

The end of the Late(?) Proterozoic rifting phase, prior to deposition of these basal Cambrian(?) strata, produced widespread uplift of a rift-marginal arch beneath Dundas Peninsula, southeastern Melville Island, and Viscount Melville Sound(?) (Fig. 18). This uplift, possibly a thermal response to rifting, resulted in widespread erosion and channelling of the underlying highly reflective succession (unit sP2; Sections F and G). The earliest evidence of post-rift thermal subsidence is found in basal Lower(?) Cambrian deposits (seismic unit sC1A) that overstep erosional remnants of the Upper(?) Proterozoic and that are also seen to rest directly on Middle(?) Proterozoic seismic equivalents of the Shaler Group over the rift-marginal arch. Seismic depositional facies point to a mixed terrigenous lithofacies for these oldest Cambrian(?) sediments, deposited and preserved in

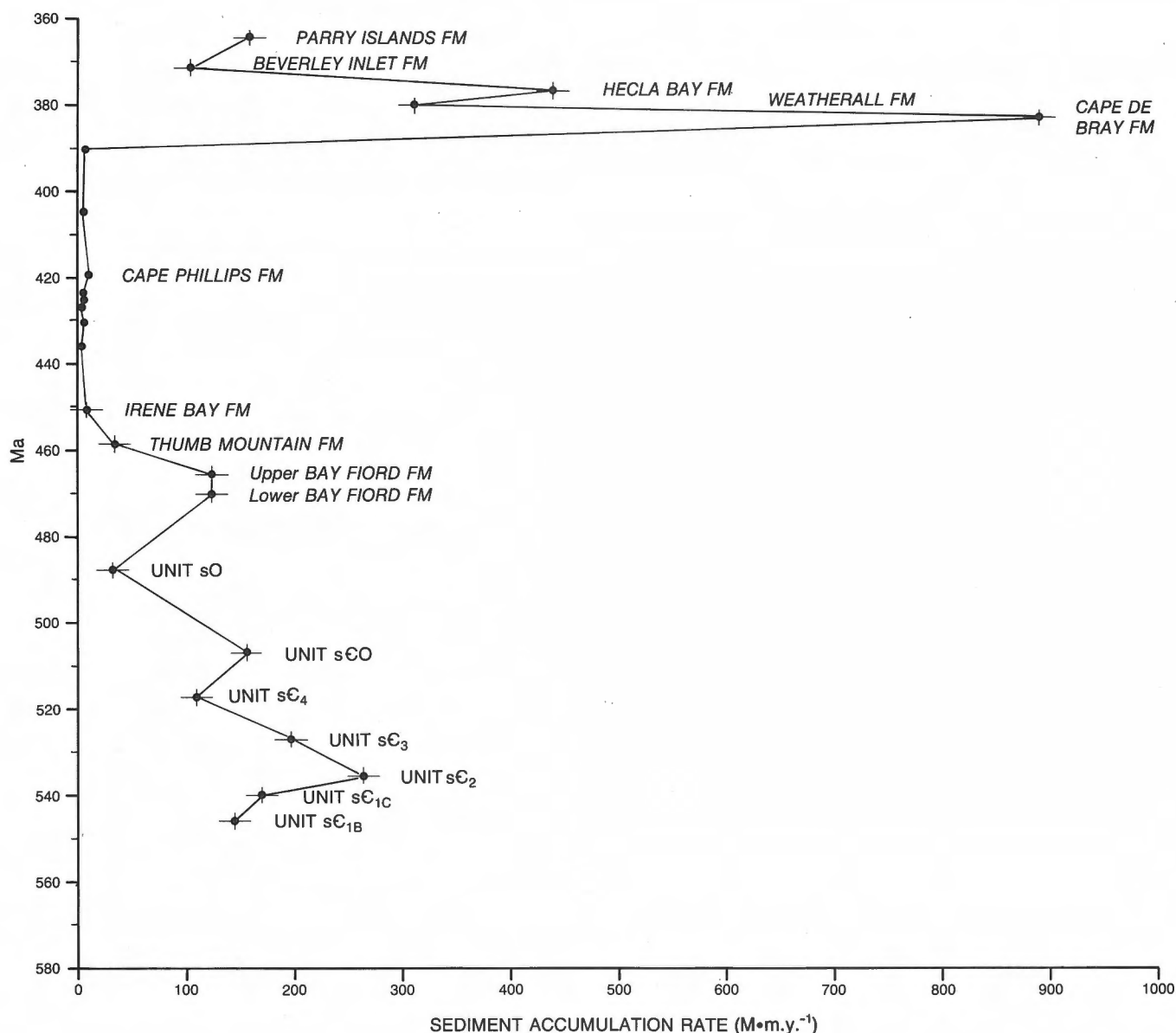


Figure 54. Arithmetic plot of the accumulation rate for southern shelf and shelf rim sediments plotted against time. This plot is intended to display the geometric decrease in accumulation rate on the Franklinian shelf from the Early(?) Cambrian to the Early Devonian, and the dramatic rise in deposition rate, beginning at about 388 Ma, associated with the progradation of the Middle and Upper Devonian clastic wedge.

paleotopographic lows on the post-Proterozoic(?) erosion surface (Fig. 29; Sections F, G). Subsequent valley fill is seen (on seismic profiles) as base-onlapping reflection segments that appear to progressively climb the margins of some channels.

The laterally continuous reflection above sC_{1A} is interpreted as a maximum flooding surface, separating coarse clastics below and, perhaps, mudrocks above. Three laterally linked seismic depositional facies in seismic unit sC_{1B}, tentatively correlated with the mixed

mudrock and siliciclastic Kennedy Channel Formation of northeastern Ellesmere Island, point to a fully established shelf-to-slope transition by this time in the Melville Island region: 1) a reflection-free outer shelf facies in the southeast above incised valley fill; 2) a thicker, moderately reflective upper slope facies overlying top-truncated reflectors within (undivided) Upper(?) Proterozoic to lowermost(?) Cambrian rift fill (sPC); and 3) a strongly reflective but thinner lower basin slope facies at the limits of seismic resolution in the northwest.

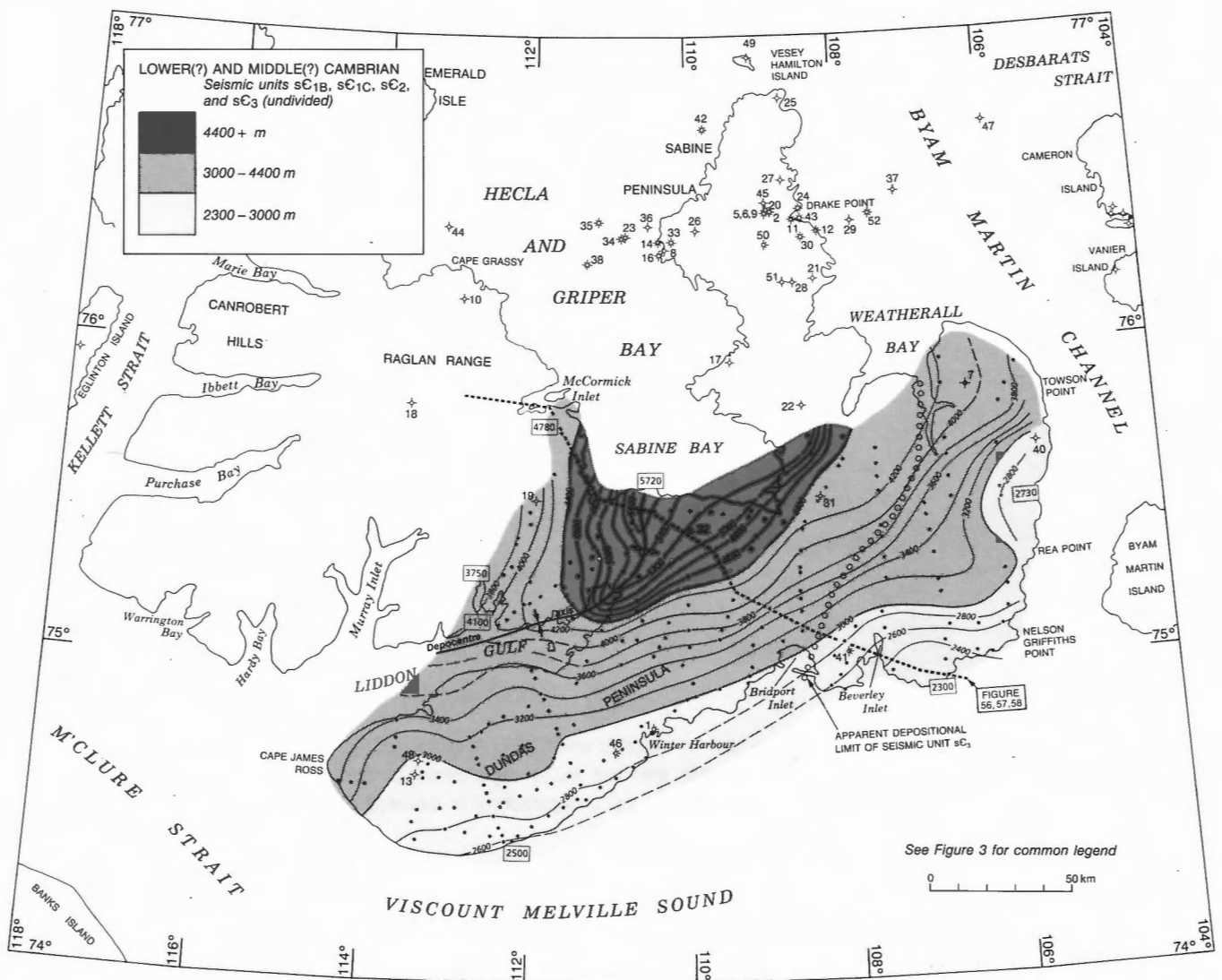


Figure 55. Isopach map of Lower(?) and Middle(?) Cambrian seismic units sC1B, and sC1C, sC2, and sC3. Interval velocity is 5.7 km s^{-1} . Also shown is the apparent depositional limit on the shelf of seismic unit sC3. The shelf/slope break at the end of deposition of unit sC3 is situated close to the depocentre axial line. The existence of deeper water facies is suspected northeast of the depocentre.

Local onlapping reflections define a sequence boundary at the base of unit sC1C; the latter considered the seismic stratigraphic equivalent of the Ella Bay Formation (dolostone) of Ellesmere Island. Above the lower contact, a significant northwesterly and basinward shift of facies belts is indicated. The inner shelf facies (high-amplitude continuous reflections) of sC1C overlies the outer shelf facies of sC1B, and the unreflective outer shelf facies of sC1C overlies slope deposits. Some thinning of the distal portion of the unreflective facies of sC1C may indicate either deposition in deeper water off the shelf edge, or shelf-edge erosion of sC1C prior to deposition of overlying strata.

Although onlap patterns are not seen at the base of unit sC2 (seismic equivalent of the mixed siliciclastic Ellesmere Group), significant deepening of relative sea level is indicated by a cratonward shift of seismic facies belts above sC1C (Fig. 57)—the unreflective outer(?) shelf facies of unit sC2 overlies inner shelf seismic facies of sC1C, and the slope facies of sC2 overlies the outer shelf of sC1C. The development of clinoforms in the distal portion of sC2 (Fig. 30) also points to a dramatic increase in accommodation for sediment on the shelf margin. The thickest sections of sC2 are situated approximately along the depocentre axis of Figure 55; this line also marks the approximate shelf/slope break position during the accumulation of unit sC2.

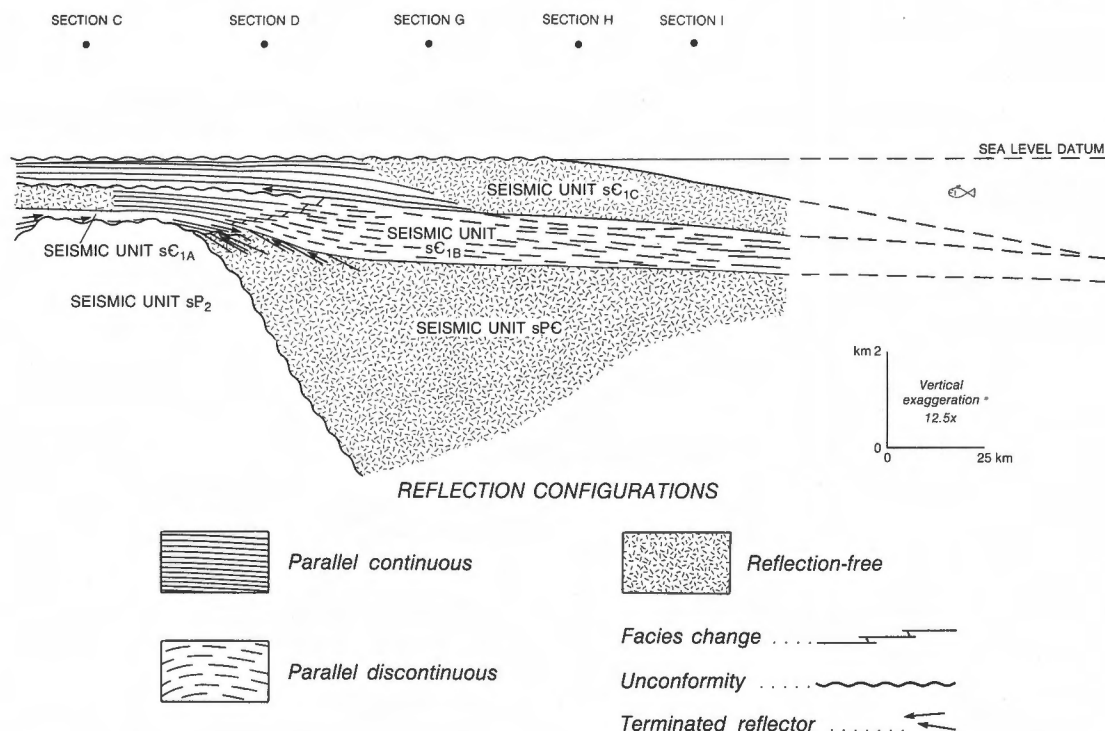


Figure 56. Palinspastic cross-section of seismic units sP_2 through sC_{1C} . The line of section is located on Figures 18 and 55. Note that the sC_{1B} depocentre is above a thick interval of Upper(?) Proterozoic rift fill (sPC) and the sC_{1C} depocentre is situated about 50 km basinward and to the northwest.

Unit sC_2 may be the seismic depositional record of a dramatic influx to the miogeocline of detrital material from distant tectonic highlands of late(?) Early Cambrian North America. Widening uplift of the craton after this time was accompanied by a substantial narrowing of the actively subsiding portion of the shelf (Fig. 58). A steep shelf gradient with narrow inner and outer shelf seismic facies belts persisted throughout the period of deposition of seismic unit sC_3 (seismically equated with carbonates of the Scoresby Bay Formation). Onlap patterns at the cratonward limit of sC_3 indicate progressive sea level rise during initial accumulation of the unit. However, the apparent absence of sC_3 over most areas of the pre-existing shelf, and the presence of a strongly reflective and mildly divergent inner shelf seismic facies of sC_3 stacked vertically above the unreflective outer shelf facies of sC_2 indicates a generally low relative sea level for much of sC_3 deposition.

Middle(?) Cambrian through late Arenig (523–480 Ma)

This time interval spans the accumulation of seismic units sC_4 through sO , and the lithostratigraphically

equivalent units that lie between the base of the Cass Fiord (Parrish Glacier) Formation of the central and eastern Arctic Islands and the top of the Eleanor River and Canrobert formations (Figs. 59, 60). The base of unit sC_4 is a regionally significant seismic sequence boundary marked by onlapping reflectors at the updip limit of the unit. This stratigraphic level marks the most extensive retreat of relative sea level until the late Arenig. The three seismic units and two formations above this unconformity have accumulated in two depositional systems: a lowstand tract during accumulation of sC_4 (equivalent to the Parrish Glacier Formation of Ellesmere Island); and transgressive and highstand tracts during deposition of the overlying units. The low relative sea level position during unit sC_4 deposition is indicated by the mappable line defining the apparent updip limit of the unit (Fig. 59). This line is situated 44 to 103 km basinward (northwest) of the cratonward limit of seismic unit sC_3 (compare Figs. 55 and 59), and 18 to 32 km basinward of the Early(?) Cambrian shelf edge! Widespread exposure and erosion of the shelf and shelf edge during sC_4 deposition may partly explain the very thick accumulation of sediment in the off-shelf realm. Steep shelf gradients would also allow craton-derived sand to bypass the shelf. The impact of growth faulting during

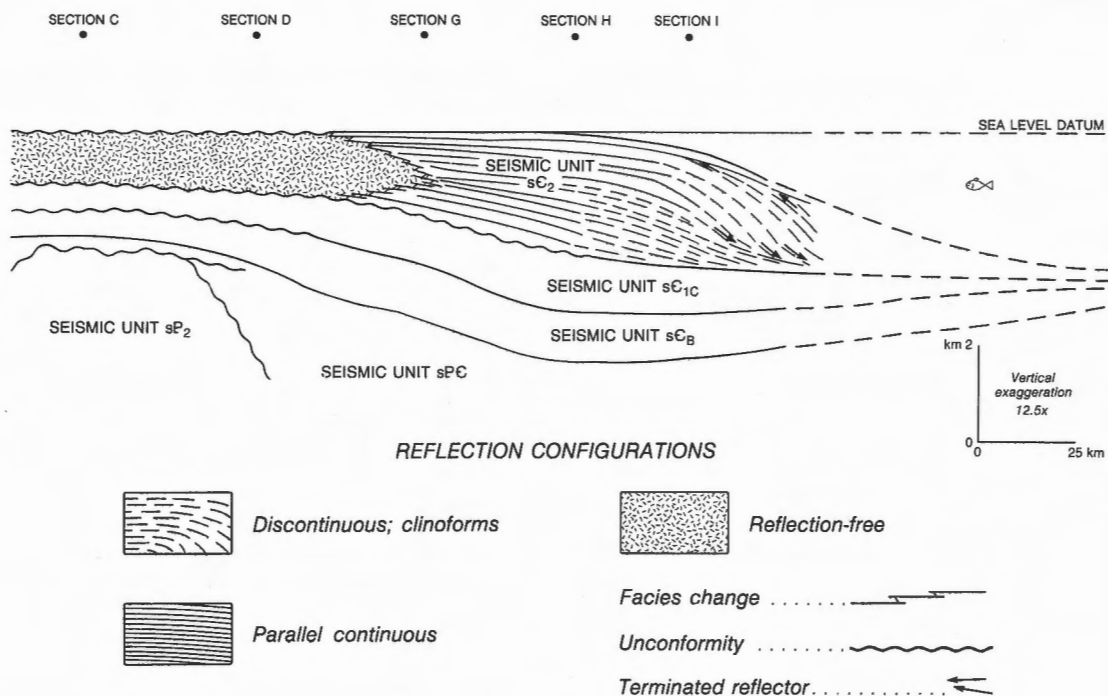


Figure 57. Palinspastic cross-section of seismic unit sC_2 . The line of section is located on Figure 55. Note that the sC_2 depocentre is situated about 25 km northwest and basinward of the sC_{1C} depocentre.

sC_4 deposition is also of great significance (Fig. 30); across several of these faults, there is a stepwise increase in unit thickness from 400 m to 3200 m over a distance of only 18 km. The strike of these growth faults is not known. However, it is possible that they are parallel to isopachs of the sC_4 - sO sequences as mapped on Figure 59. Worth noting in this respect is the coincident parallelism of: 1) Upper(?) Proterozoic structural trends (Fig. 18); 2) Early(?) to Middle(?) Cambrian isopachs (Fig. 55); 3) a variety of surface structural features of central Melville Island such as the axial trace of Blue Hills Syncline; and 4) a Bouguer gravity anomaly low over Blue Hills Syncline traceable from Hecla and Griper Bay southwest to Warrington Bay.

Unit sC_4 is succeeded conformably(?) by seismic units sCO (upper Cass Fjord Formation and Cape Clay equivalents) and sO (combined Blanley Bay/Ninnis Glacier, and Eleanor River formations). Unit sCO oversteps the cratonward limit of sC_4 , and also oversteps and appears to entirely cut out unit sC_3 . The depositional limits of sCO on the shelf are beyond the mapped area. A southeastern facies of the unit, characterized by weak, parallel, continuous reflections, is similar to that of the seismically-imaged Eleanor

River Formation (part of seismic unit sO) which, within the mapped area, consists of shallow-marine dolostone and limestone. The northwestern facies of sCO , characterized by strong, parallel, continuous internal reflections, could be generated by a carbonate-mudrock succession if the basinward limit of the facies is gradational with a progressively deeper water facies. This style of deposition is typical of a subsiding ramp. Alternatively, the northwestern facies could be a carbonate-evaporite succession if the basinward limit of this facies is barred by a shallow-marine sill.

Distribution and style of sedimentation during the accumulation of unit sO was similar to that of the southeastern facies of unit sCO . A weakly reflective seismic facies marked by continuous bounding reflection surfaces and parallel, discontinuous, internal reflection segments is common to all shelf facies of unit sO . A more reflective facies of unit sO in the subsurface west of Hecla and Griper Bay may include facies equivalents of the evaporitic Baumann Fiord Formation (Tremadoc) of Cornwallis and western Ellesmere islands. Farther to the northwest, the Eleanor River Formation is believed to be linked gradationally to age-equivalent slope facies resedimented carbonates, flat pebble conglomerates, and

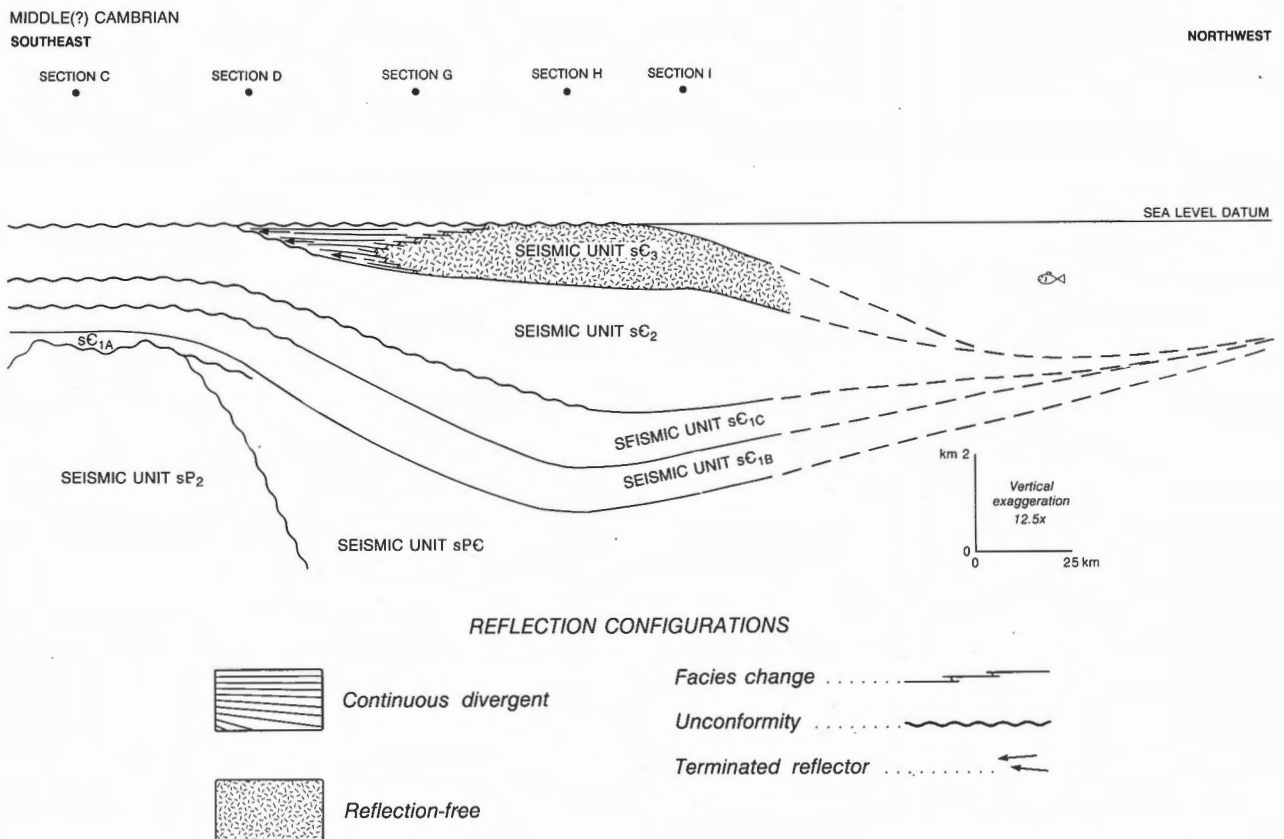


Figure 58. Palinspastic cross-section of seismic unit sC3. The line of section is located on Figure 55. Note that the sC3 depocentre is situated directly above the sC2 depocentre, although a sequence boundary and possible unconformity at the base of sC3 is implied by basal onlap patterns identified near the apparent updip limit of the unit.

carbonate breccias of the Canrobert Formation. Shelf-to-basin slope changes in water depth indicated on Figure 60 are somewhat schematic. The slope deposits of the Canrobert Formation were deposited below storm wave base but above the carbonate compensation depth.

Late Arenig through early Ashgill (480–445 Ma)

Progressive lowering of sea level during Arenig time is believed to have led to periodic termination of sediment accumulation on parts of the shelf during the late Arenig. At this time, quartz sand, presumably derived from exposed parts of the North American craton, was able to bypass the shelf and reach the deep water basin slope during the deposition of the upper informal member of the Canrobert Formation (Fig. 61). As sea level rose during latest Arenig and early Llanvirn, slope facies carbonates in the deep water basin gave way to deposition of chert (lower part

of the chert member of the Ibbett Bay Formation). Sediment accumulation rates fell to 10 m/m.y. by the early Llanvirn (see Table 3). It was during this time that a shallow-marine carbonate barrier developed on the northern rim of a newly established intrashelf basin (Figs. 62, 63). Upward growth of peritidal carbonates on the shelf rim was able to keep up with the progressive sea-level rise. The late Arenig relative sea-level rise, together with the maintenance of the shelf-rim carbonate sill, brought about widespread restricted-marine conditions in the intrashelf basin and subsequent accumulation of evaporites in the basin centre (lower Bay Fiord Formation). Rate of sediment accumulation within this basin (70–140 m/m.y.) was much higher than for corresponding strata of the shelf rim. The preferred structural model for the intrashelf basin subsidence does not include synchronous growth faulting. However, the N36°E- through N63°E-trending depositional limit of the evaporite facies against the shelf rim is nearly parallel to Upper(?) Proterozoic rift trends (Fig. 18), Cambrian(?) isopachs

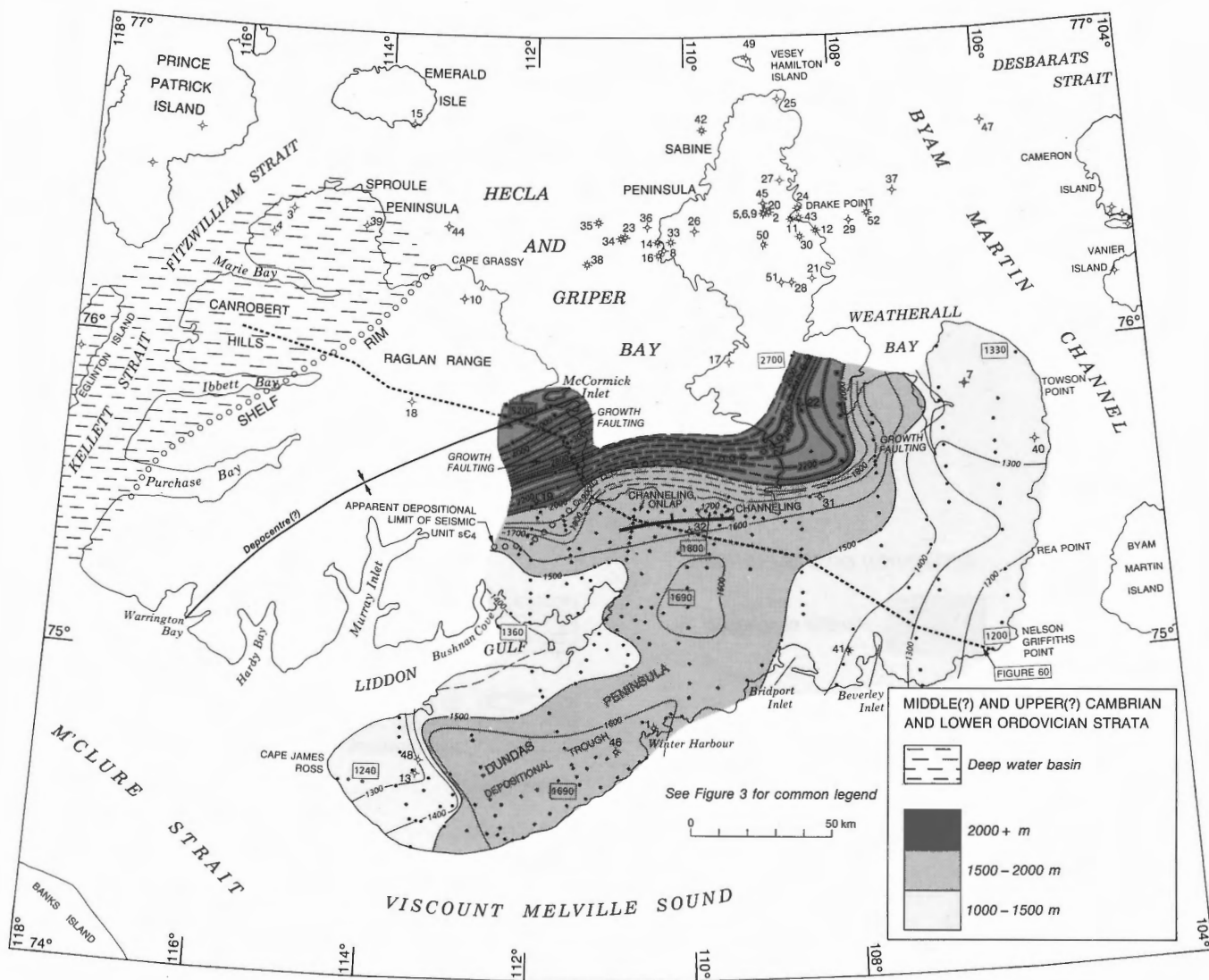


Figure 59. Isopach map of Middle(?) and Upper(?) Cambrian, and Lower Ordovician seismic units sC4, sC0, and sO and conformable strata of the Lower Ordovician Eleanor River Formation. The apparent depositional limit of seismic unit sC4, and a suggested depocentre axis (placed along the axial line of a negative Bouguer gravity anomaly; see Figs. 9, 187) are also shown.

(Figs. 55, 59) and regional gravity anomalies (Fig. 9) implying a continuing influence of deep structure on patterns of sedimentation.

Collapse of the shelf-rim barrier in the later Llanvirn brought to an end the accumulation of evaporites and the re-establishment of widespread, albeit semirestricted, peritidal carbonate sedimentation over the extinct intrashelf basin. These conditions persisted through the mid-Caradoc. Two relative sea-level minima are indicated during this time interval: the first in approximately the Llandeilo, during deposition of the lower cliff-forming carbonate tongue of the dolostone member of the Ibbett Bay Formation; the

second in the mid-Caradoc, during deposition of the upper carbonate tongue of the dolostone member.

The first evidence of a deeper water marine embayment on the shelf is found in late Caradoc strata. The development of the embayment was accompanied by a relative sea-level rise as indicated by: 1) falling sediment accumulation rate, and upward gradational transition to subtidal limestone and dark dolostone with increasing faunal diversity on the site of the embayment in the upper Thumb Mountain Formation; 2) upsection replacement of slope carbonates by chert in the lower black shale member of the Ibbett Bay Formation amid falling accumulation

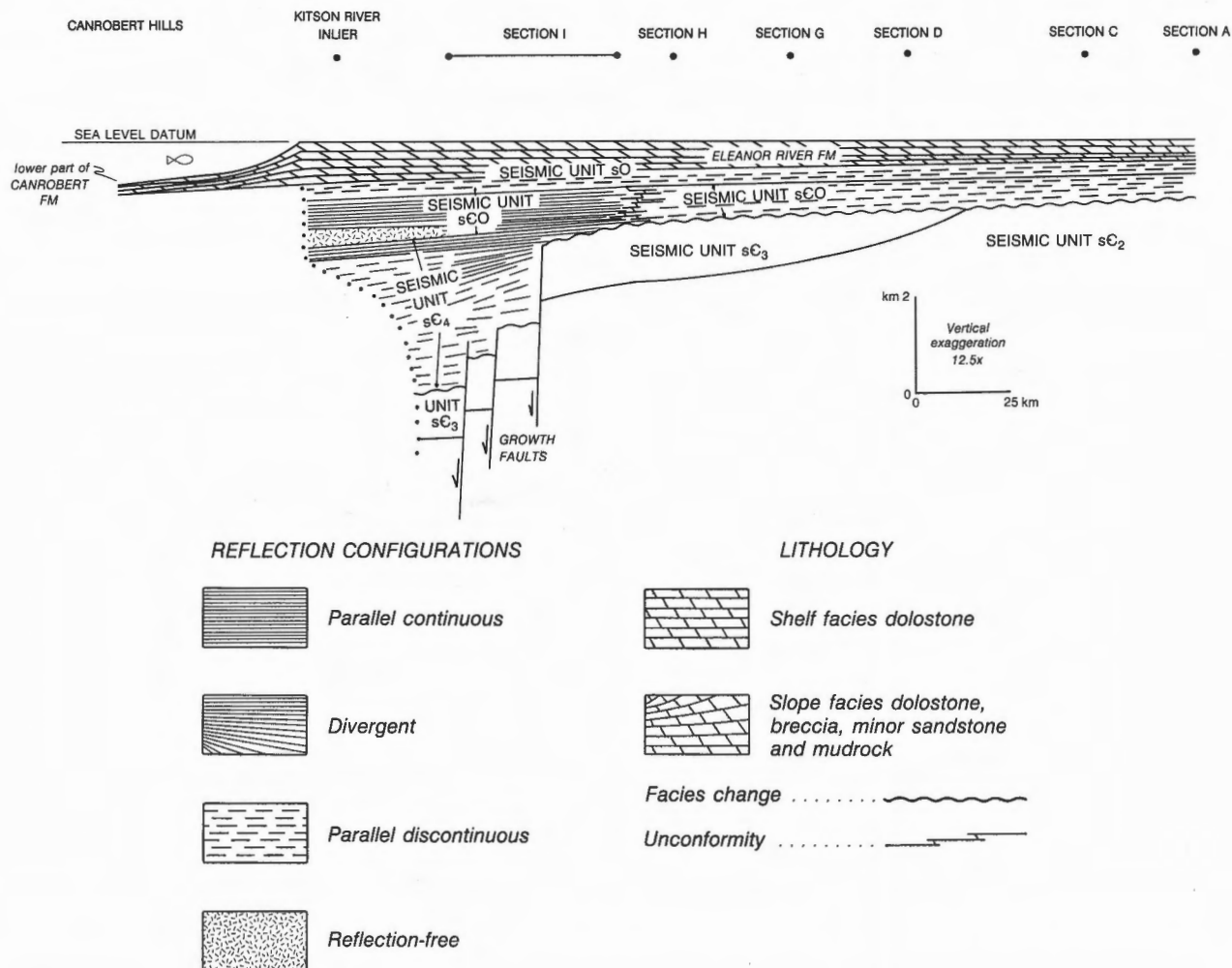


Figure 60. Palinspastic cross-section of seismic units sC4 through sO, and the Eleanor River and lower Canrobert formations. Note that the sC4 depocentre is at least 40 km northwest and basinward of the sC3 depocentre, and the Lower Ordovician shelf edge may be up to 40 km farther basinward still. Also worth noting is that unit sC0 oversteps sC4 and sC3, and lies with apparent unconformity on unit sC2 on a southeastern portion of the shelf.

rates in the deep water basin; and 3) continued deposition of intertidal dolostone amid rising accumulation rates on the shelf rim.

Early Ashgill through Pridoli (447–410 Ma)

The clear distinction of shelf, intrashelf embayment, and shelf-rim carbonate platforms was established early in the Ashgill; a time line corresponding to the base of the Allen Bay Formation. Once established, the position of facies fronts did not again change dramatically until the Early Devonian (Figs. 64, 65). The embayment extended over and beyond the region

previously occupied by the late Arenig–early Llanvirn intrashelf evaporite basin (compare Figs. 62 and 64). Unrestricted basin floor and rise mudrocks and argillaceous carbonates of the embayment (Cape Phillips Formation) testify to free circulation of open-marine waters with the deep water basin. Contributing to this circulation was a wide breach in the Lower–Middle Ordovician shelf rim (probably now located in the subsurface beneath Hecla and Griper Bay). The embayment has defined limits against shallow-water carbonate banks of subsurface Dundas Peninsula, western Raglan Range, and Weatherall Bay area. Isopachs of the Cape Phillips Formation also indicate probable continuity of the carbonate bank beneath the Blue Hills and western Liddon Gulf. The

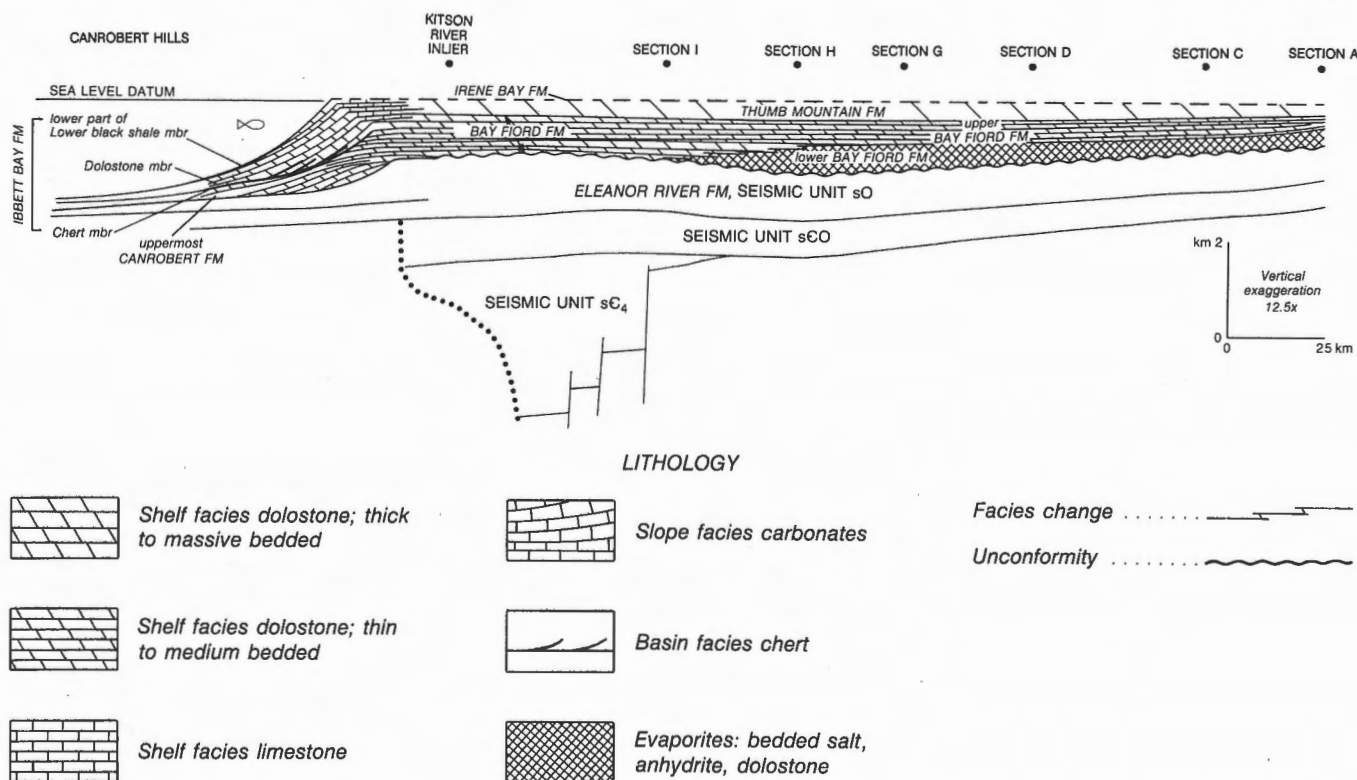


Figure 61. Palinspastic cross-section of the Cornwallis Group and age-equivalent strata of the deep water basin (late Arenig-early Ashgill). The line of section is located on Figure 63. Note that quartz sand in the upper Canrobert Formation may have reached the deep water basin, bypassing the shelf during a sea-level lowstand after (or late in) the period of Eleanor River Formation deposition. Deposition of salt in the intrashelf basin occurred during a period of sea-level rise and sediment starvation in the deep water basin.

overall depositional pattern through time was vertical accumulation of the carbonate banks to sea level and progressive deepening of the intrashelf embayment and deep water basin. Six significant phases are recognized in the construction of the Late Ordovician through Late Silurian shelf and offshore carbonate banks (Table 3; Figs. 65, 66). Long-term and accumulating shortfalls in sediment supply to the deep water realms point to a corresponding increase in maximum water depth in the intrashelf embayment from approximately 300 m in the early Ludlow, to about 750 m at the end of the Silurian.

The termination of Barlow Inlet (phase six) deposition is marked by a probable withdrawal of sea level off the shelf and shelf rim and the exposure and differential erosion of some unknown thickness of previously deposited shallow-marine carbonates. Minimum depth of erosion is indicated by the height of seismic irregularities on the erosion surface (Fig. 35); about 50 m for the southern shelf and 15 m for the shelf rim.

Lochkovian through early Eifelian (410–388 Ma)

The latest Silurian exposure of the shelf and shelf rim platforms was followed by a widespread Lochkovian submergence and a substantial southerly expansion of the intrashelf embayment. Depositional patterns in the Early Devonian and basal Middle Devonian are divisible into two distinct stages: 1) a Lochkovian through Pragian period of initially low but gradually rising relative sea level, when shelf areas were periodically or frequently submerged but sediment accumulation rates were higher in basinal realms than on the submerged shelves; and 2) an Emsian through early Eifelian phase of sea-level highstand characterized by sediment-starved basinal areas and a shallow offshore carbonate platform lying in deep water (Towson Point platform; Figs. 24, 64).

Surface stratigraphic sections through the Lochkovian and Pragian interval occur in the middle of the upper black shale member of the Ibbett Bay Formation, and in most of the Kitson Formation. Most

TABLE 3

Phases of Silurian shallow-marine carbonate accumulations

Phase	Age Range	Span (m.y.)	Formation Top	Thickness (m)	Rate (m/m.y.)
1	middle Ashgill through late Ashgill	6	1. above member 1 of Allen Bay Fm. 2. 13 m above base of unit 2 of Cape Phillips Fm. 3. about 80 m above base of lower black shale member of Ibbett Bay Fm.	204 45-55 <60	34 8.3 <10
2	early Llandovery through late Llandovery	8.5	1. above member 2 of Allen Bay Fm. 2. above unit 2 of Cape Phillips Fm. 3. est. 20 m below brown mudrock member of Ibbett Bay Fm.	90 21 110	11 2.5 13
3	latest Llandovery through earliest Ludlow	7	1. above member 3 of Allen Bay Fm. 2. lower part of unit 3 of Cape Phillips Fm. 3. above lower black shale member of Ibbett Bay Fm.	57 >29 20	8.1 >3.6 2.5
4	early Ludlow	3.5	1. above Cape Storm Fm. 2. lower part of unit 3 of Cape Phillips Fm. 3. above brown mudrock member of Ibbett Bay Fm.	136, 124 ? 63	39, 35 ? 18
5	middle Ludlow	3	1. above Douro Fm. 2. lower part of unit 3 of Cape Phillips Fm. 3. about 50 m above top of brown mudrock member of Ibbett Bay Fm.	147, 237 ? about 50	49, 79 ? 17
6	late Ludlow through Pridoli	5.5	1. above Barlow Inlet Fm. 2. middle of unit 3 of Cape Phillips Fm. 3. 200 m above base of upper black shale member of Ibbett Bay Fm.	204, 454 ? 100-200	37, 82 ? 22-30

of the same interval, situated in the upper part of unit 3 of the Cape Phillips Formation, has not been found because of poor exposure, and correlative subsurface beds beneath the Blue Fiord Formation of the Towson Point platform remain unidentified and undated. Nevertheless, black mudrock and lesser argillaceous limestone are common everywhere. Deep to very deep (sub-photoc) and sediment-starved conditions are indicated for all pre-existing (Silurian) shelf and offshore platform areas (Fig. 67). Sediment accumulation rates over the submerged northwestern shelf rim platform were less than 2 m/m.y. for nearly 18 m.y. (basal Lochkovian to base of *dehiscens* Zone of the early Pragian) and only rose to 6 m/m.y. in the late Pragian-early Emsian. In basinal areas, there are indications of higher accumulation rates (5-40 m/m.y.), especially in the deep water basin, where the rate of deposition of graptolitic mudrocks reached 46 m/m.y. during the Pragian.

Nevertheless, support for a southerly source of sediment provenance is provided by the isopach map of the Cape Phillips Formation and age-equivalent strata (Fig. 64). If the intrashelf basin were filled from the north, then isopachs of sediment deposited in the embayment should trend roughly east-west and should indicate increasing thickness in the direction of supply. However, embayment isopachs on Figure 64 parallel the southern and western shelf edges. Rate of sediment input was greatest near these shelf edges and maximum sediment starvation occurred in the embayment centre, near the base of the (future) Emsian-Eifelian offshore carbonate platform. This finding is perhaps not surprising, since exposures of the Cape Phillips Formation invariably include a significant component of shelf-derived carbonate material.

Sediment supply to the flooded shelf rim, the deep water basin and intrashelf embayment was still

generally low in the early Emsian. Conodonts collected from the oldest beds of the Blue Fiord Formation, however, indicate a new period of shallow-marine carbonate deposition beginning at about this time (prior to or within *gronbergi* Zone). The southern shelf edge had shifted southward to a newly established Emsian position situated in the subsurface north of Victoria Island beneath Viscount Melville Sound (Fig. 24). Within the map area, the distribution of shallow-marine carbonates is restricted to the Towson Point platform of northeastern Melville Island and adjacent subsurface areas as far east as Cameron Island (Figs. 24, 64). This region represents an offshore bank that apparently nucleated above a pre-existing

Silurian bank near the ancient rim of the intrashelf embayment. Carbonate sediments of the platform, composed of shallow-water shelf, shelf edge, slope and basin rise facies belts (Fig. 40) expanded upward and prograded outward into surrounding deep-water realms of the intrashelf embayment. Southerly and south-westerly progradation of the Towson Point bank edge during the Emsian and early Eifelian was up to 40 km. A significant feature of carbonate deposition at this time was the high sediment accumulation rate (140–260 m/m.y.), probably coincident with high rates of subsidence. Deposition of organically derived carbonate sediment was able to keep up with the relative sea-level rise. In contrast, the embayment, deep

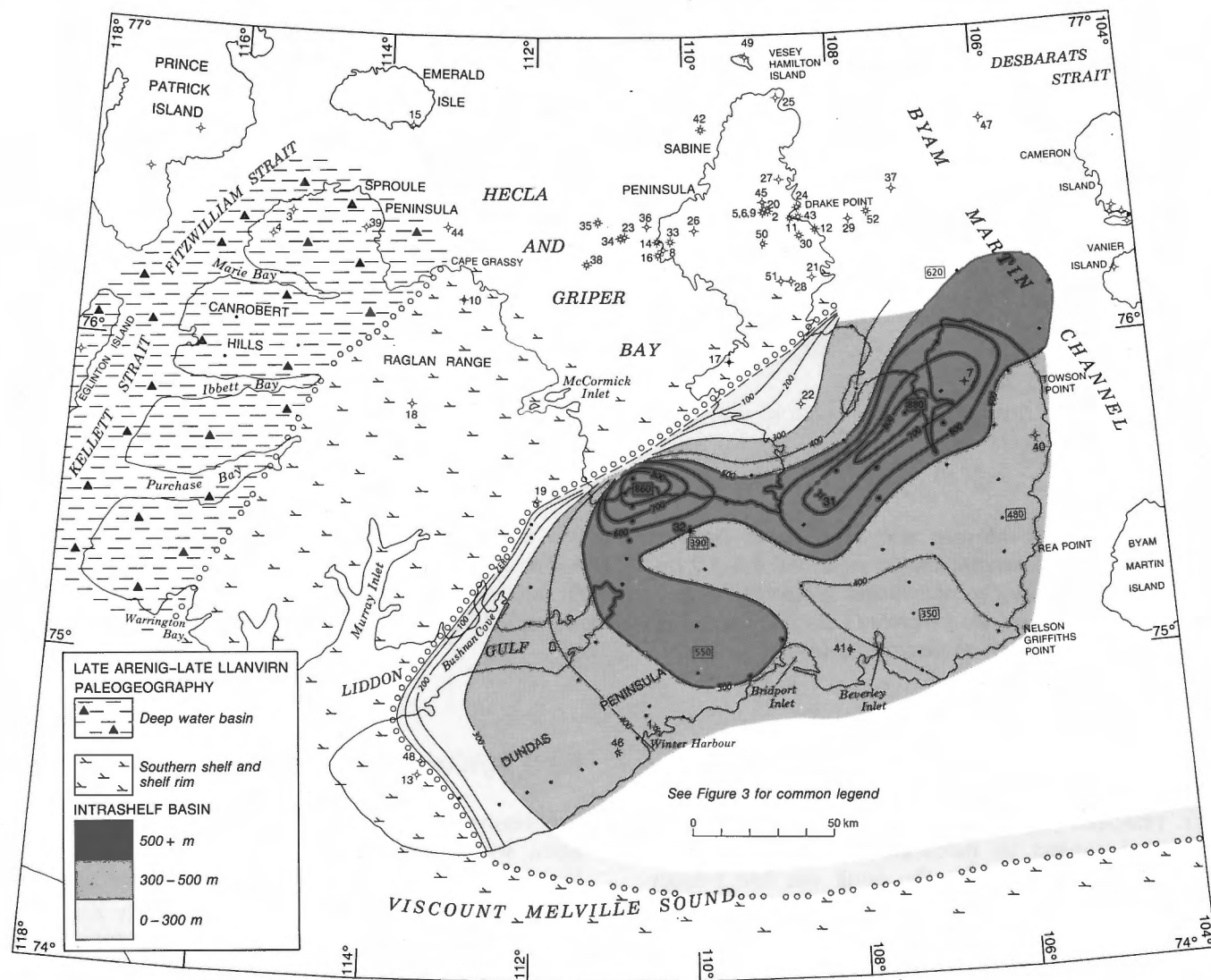


Figure 62. Paleogeography of late Arenig–late Llanvirn time with isopachs of the halite facies of the lower Bay Fiord Formation. Interval velocity, 5.3 km s⁻¹; based on 68 data points. Data were obtained from palinspastic restoration of the salt to its pre-deformation thickness and position (see restored cross-sections A through I).

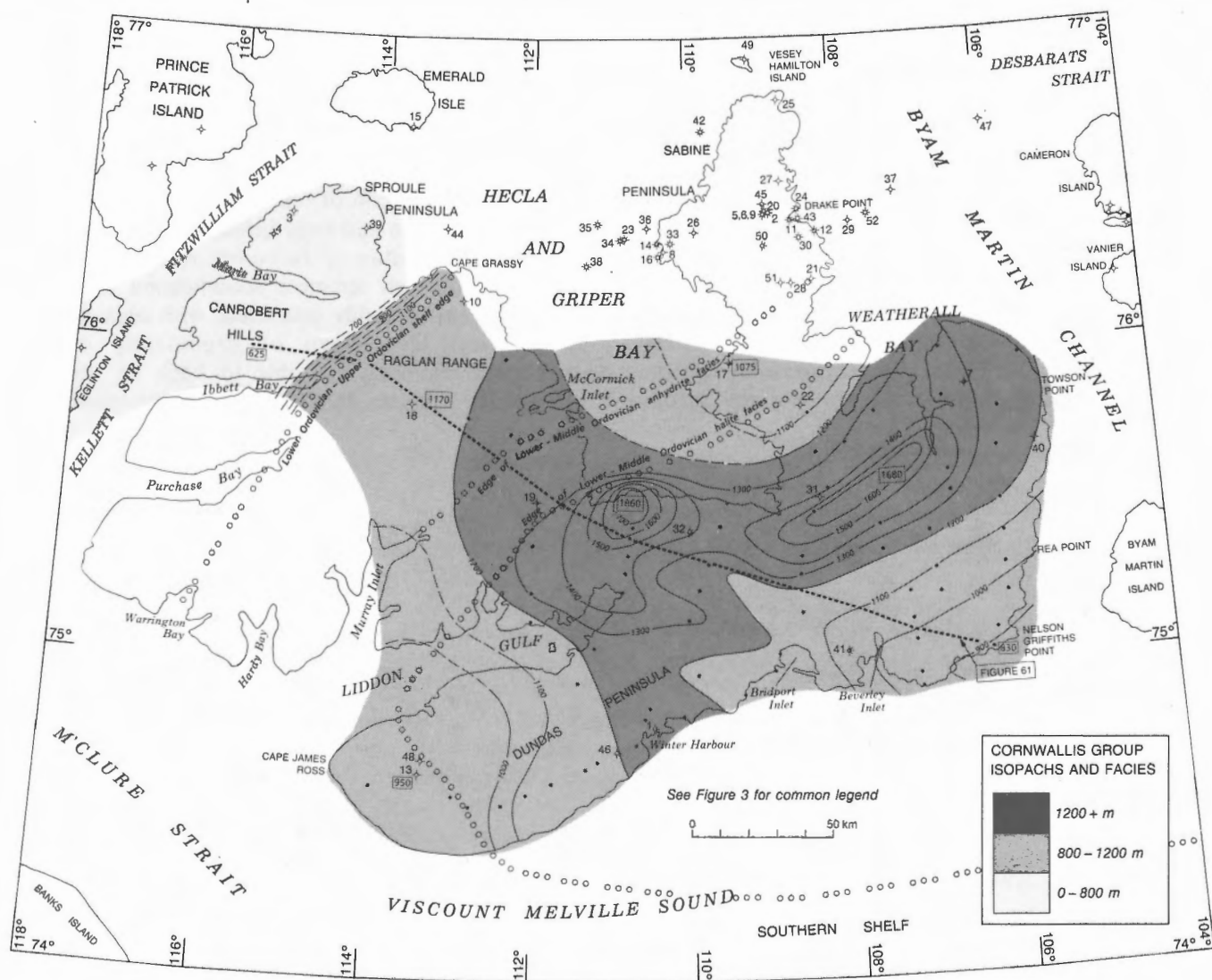


Figure 63. Isopach map and major facies boundaries of the Cornwallis Group and age-equivalent strata (late Arenig–early Ashgill). Interval velocities, 5.3–6.3 km s⁻¹; based on 73 data points. Note that the implied subsidence rate was greater in the intrashelf (evaporite) basin than on the shelf rim. Note also the parallel development of facies belts (this map), the interpreted Late(?) Cambrian depocentre (Fig. 59), the corresponding gravity anomaly (Figs. 9, 187), and Late(?) Proterozoic structures at depth (Fig. 18).

water basin, and drowned portions of the shelf rim, also probably affected by high subsidence rates, were far removed from terrigenous source areas and therefore subject to moderate or extreme sediment starvation (6–22 m/m.y.). The result was late Emsian–earliest Eifelian probable water depths of up to 1000 m in parts of the embayment. For the deep water basin, shortfalls in sediment accumulation (compared with the shelf rim) are recorded during the entire time interval from at least the late Arenig. Thus, water depths may have reached 2400 m on the lower slope of the deep water basin by the late Emsian (Fig. 67).

Early Eifelian through late Givetian (388–375 Ma)

Progressive filling of the Middle Devonian foredeep basin within the Melville Island area is shown on Figures 67 to 71. This phase of siliciclastic sedimentation spans the period of deposition of the Blackley, Cape De Bray, Weatherall and Hecla Bay formations (Hecla Bay Sequence of Embry, 1988a, 1991a, b). Burial of the deep water basin, drowned shelf rim, the Towson Point–Bent Horn platform, and the intrashelf embayment proceeded from at least two and possibly three directions (Fig. 68).

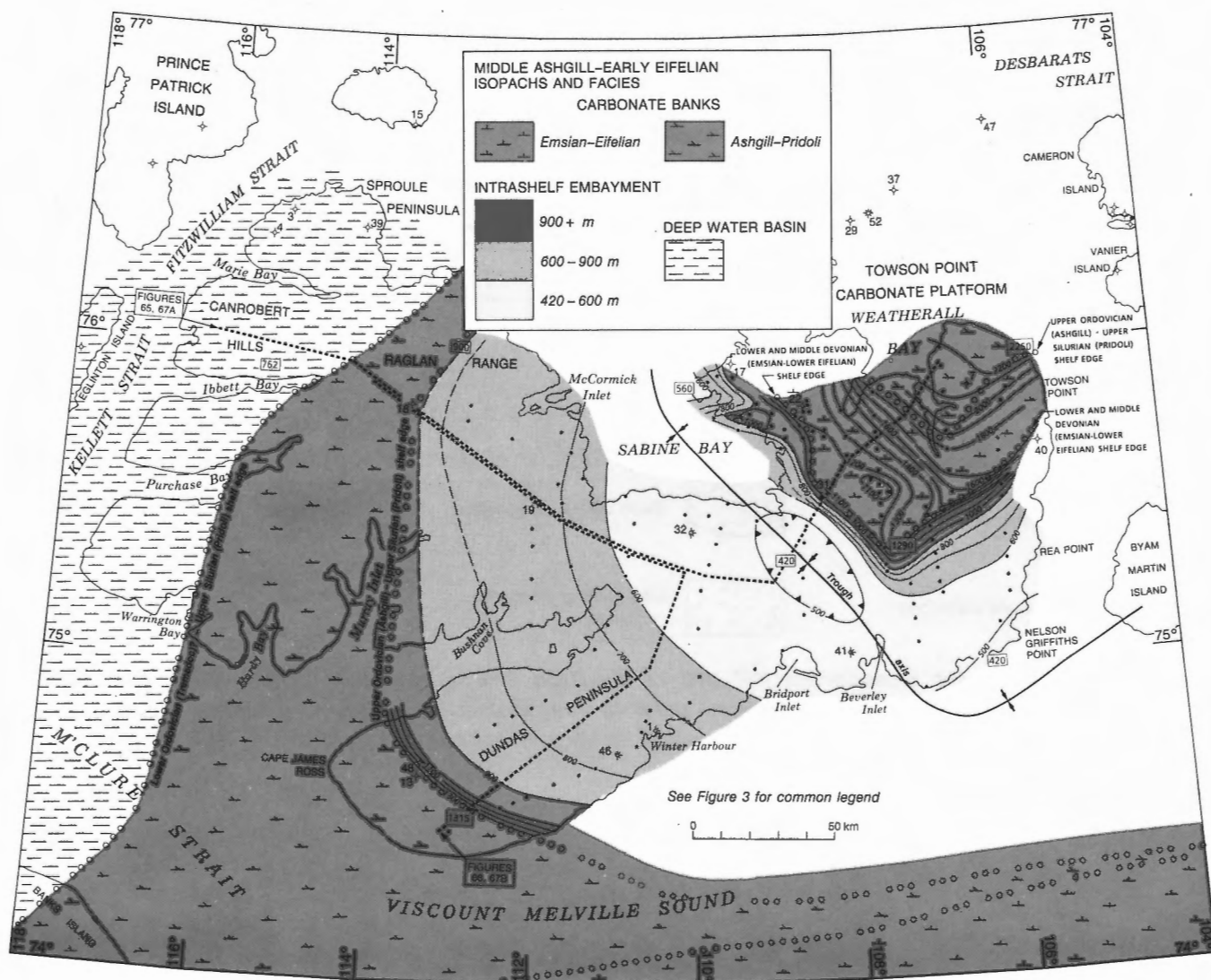


Figure 64. Isopach and paleogeographic map of the Cape Phillips Formation (middle Ashgill-early Eifelian) and age-equivalent strata of the deep water basin (medial Ibbett Bay Formation); shelf and shelf rim (Allen Bay, Cape Storm, Douro, Barlow Inlet and Kitson formations); and Towson Point carbonate platform (Blue Fiord Formation). Interval velocities, 4.3–6.0 km s⁻¹; based on 143 data points. Major shelf edge positions are also indicated. Note that the Emsian and Eifelian shallow-water carbonates occur only in the Weatherall Bay area, and that the Silurian and Ordovician shelf areas were part of a greatly expanded intrashelf embayment throughout the Early Devonian (see also Fig. 24).

Lobe 1. The first evidence in the western Arctic Islands of rising tectonic highlands within the ancient deep water basin appeared in the early, perhaps earliest, Eifelian, when siliciclastic sediment gravity flows of the Blackley Formation, transported from the northeast, reached the southwestern base-of-slope of the deep water basin of northwestern Melville Island. Since the lower contact of these deposits is gradational and therefore probably diachronous, it appears likely that the oldest sediment gravity flows, either within the

exposed belt of the Blackley Formation or to the northeast, are synchronous with deposition of the terminal phase of shallow-marine carbonate deposition on Towson Point platform (Fig. 67). However, biostratigraphic determinations do not establish firm proof of this relation. Published studies of sediment gravity flow deposits exposed in similar deep water basin settings of Greenland and Ellesmere Island indicate that progradation of these deposits spanned 44 m.y. and progressed from northeast to southwest

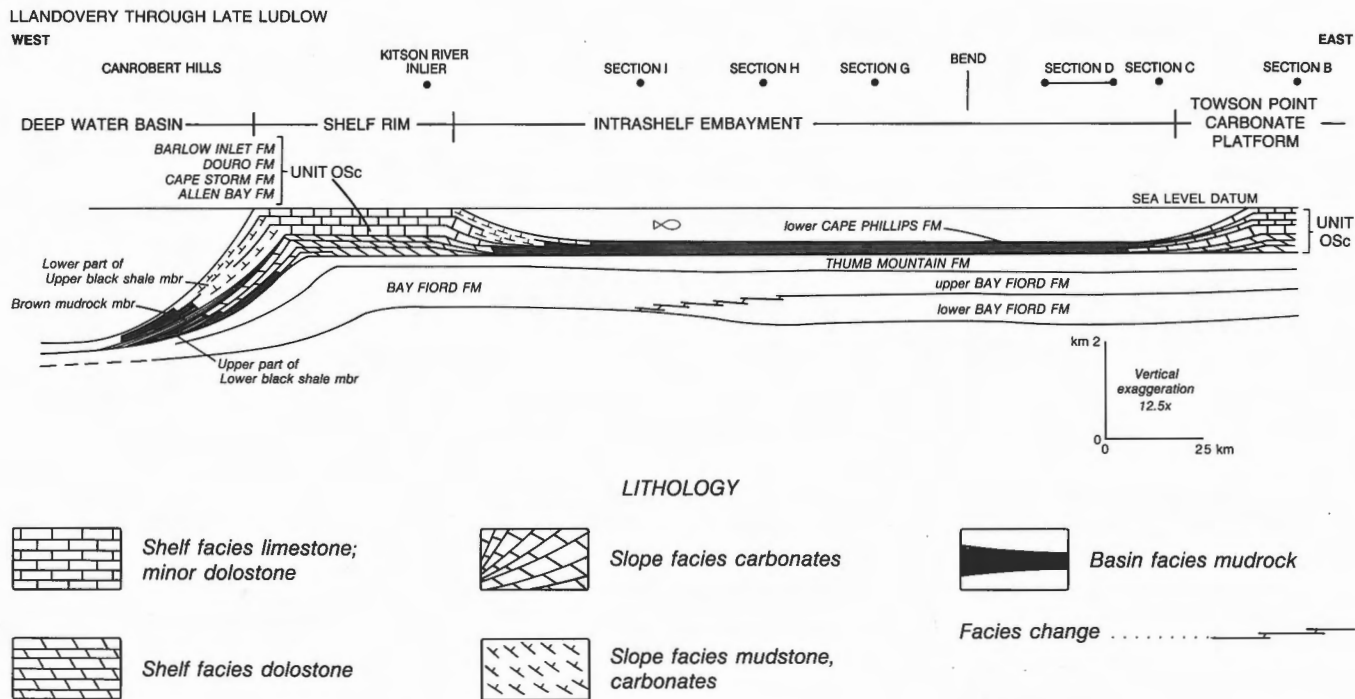


Figure 65. Palinspastic cross-section (NE-NW) of the Cape Phillips Formation (intrashef embayment) and age-equivalent strata of the shelf rim platforms and deep water basin. Line of section is located on Figure 64. Note that the interpreted water depth on the lower slope of the deep water basin was approximately 2000 m at the end of the Silurian.

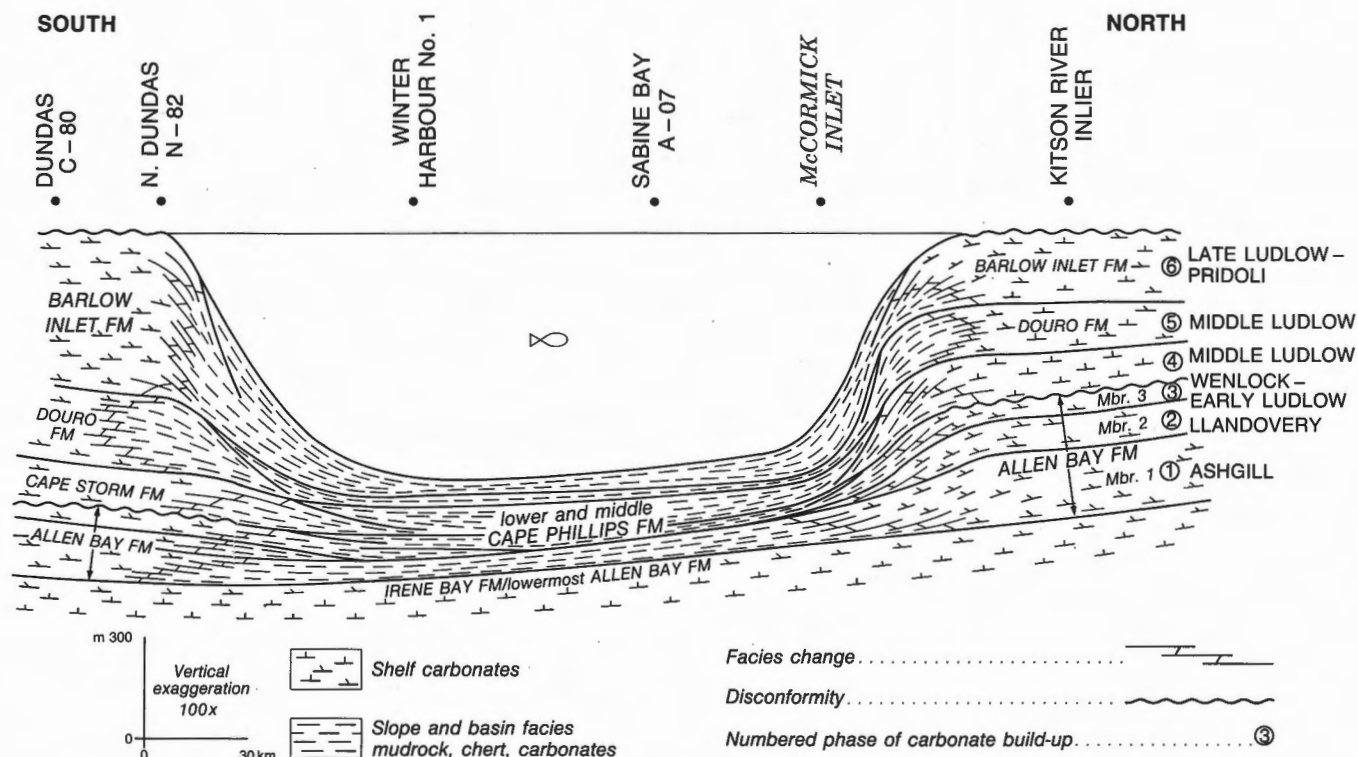


Figure 66. Sequential deposition of Late Ordovician through Late Silurian phases of shallow-marine carbonate on the southern shelf and shelf rim platform, and coeval sediment accumulation of the intrashef embayment. Line of cross-section is located on Figure 64.

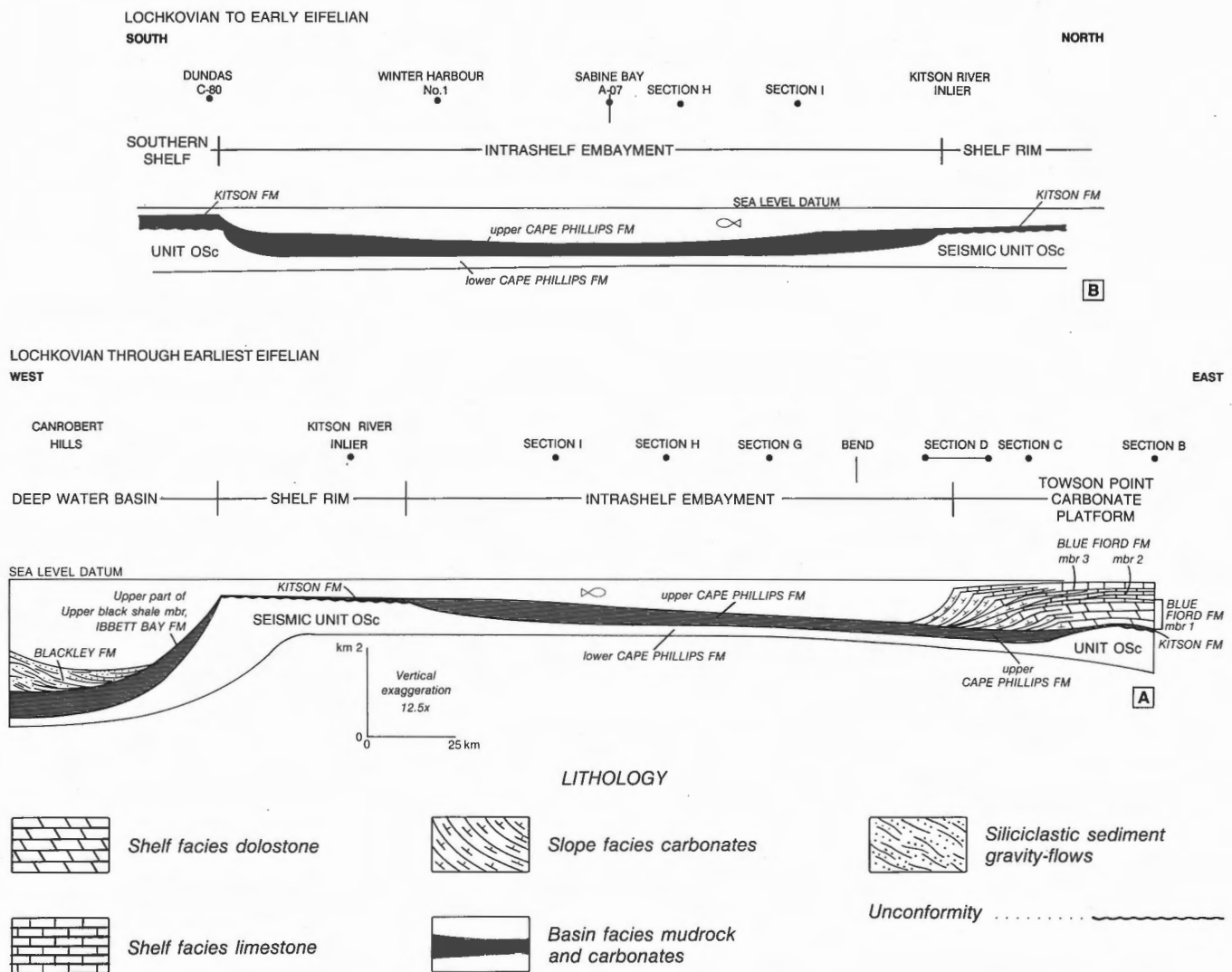


Figure 67. Palinspastic cross-sections for Lochkovian through early Eifelian time. **A.** Towson Point carbonate platform to the deep water basin. **B.** Southern shelf to the northwestern shelf rim. Lines of sections are located on Figure 64. Note that the Blue Fiord Formation (up to 1250 m of Emsian and lower Eifelian strata) is age equivalent to only about 18 m of section in the upper part of the Kitson Formation of the shelf rim. Note also that part of the lower Blackley Formation of the deep water basin may be partly age equivalent to the upper Blue Fiord Formation and upper Kitson Formation. OSc, Allen Bay through Barlow Inlet formations, undivided.

beginning in the late Llandovery in North Greenland, only reaching Melville Island area in the early Eifelian (Trettin, 1990; Trettin et al., 1991).

Lobe 2. Shallow-marine siliclastic sediments and embayment-fill mudrocks of the Cape De Bray Formation were first deposited on top of the Towson Point carbonate platform and along the easternmost axial line of the intrashelf embayment in the early Eifelian (within *costatus* Zone). Orientation of clinoforms within the Cape De Bray Formation indicate a S18°W through S51°W transport direction, influenced in part by the submarine paleotopography on the slopes of the platform. The preferred model is

that the oldest lobe 2 sediments were transported from the northeast and deposited in the deep-water moat lying along the southeast base-of-slope of the platform. The top of the platform at this time was either submerged and starved of sediment, or subaerially exposed as inferred from sub-Cape De Bray karst features in the Blue Fiord Formation of Cameron Island (Waylett, pers. comm., 1988). For the Melville Island portion of the Towson Point platform, there is no seismic or surface stratigraphic evidence for subaerial exposure. Subsequent flooding by Cape De Bray foredeep sediment of the southwest-facing surface of the platform progressed from the southeast by "sidelap" and from the southwest by simultaneous

submarine basal onlap and distal downlap onto the pre-existing platform slope and rise.

Lobe 3(?). There is the additional possibility of a third sediment lobe encircling the Towson platform in deep water from the northwest (Hecla and Griper Bay area) and sidelapping and onlapping onto the surface of the platform from this direction. Seismic profiles are sparse in the critical area and not conclusive on this matter.

By middle Eifelian time, these separate sediment lobes had completely filled the deep water basin, had covered the Towson Point carbonate platform, and

had coalesced into a single, southwesterly prograding clastic wedge within the intrashelf embayment. Filling of the embayment was accomplished within a 6 to 8 m.y. time interval between the early Eifelian and the early Givetian. The changing position of the siliciclastic shelf edge (corresponding to the diachronous contact between the Weatherall and Cape De Bray formations) as it migrated across the basin above basin-fill deposits is shown in Figure 68.

By the early Givetian, the break-in-slope between the siliciclastic shelf and embayment had migrated as far as western Dundas Peninsula and Blue Hills areas. Sediments of fluvial and delta-front association (Hecla

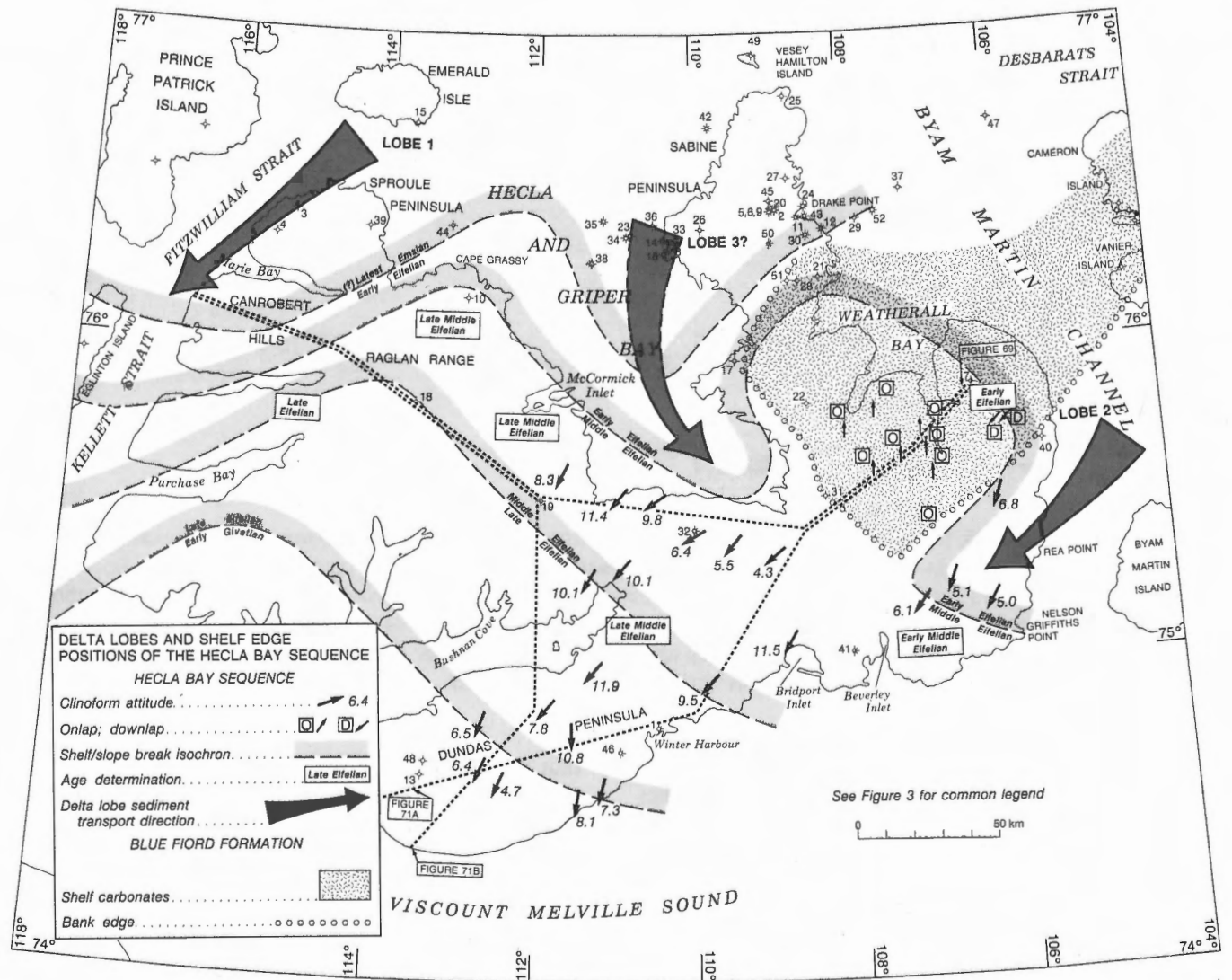


Figure 68. Deltaic lobes of the Hecla Bay Sequence, and the locations through time of the shelf/slope break above the Cape De Bray Formation. The early Eifelian through early Givetian shelf edge positions are deduced from biostratigraphic data, the attitude of seismic clinoforms (22 data points), and approximate bottom topography, as inferred from isopachs of the previously deposited rocks of the intrashelf embayment and Towson Point platform (see Fig. 64).

Bay Formation), which covered all of southwestern Ellesmere Island, Grinnell Peninsula and Bathurst Island, had simultaneously reached the Weatherall Bay region of Melville Island (Fig. 71A). Expansion of the marginal-marine and nonmarine facies belts across the project area continued throughout early, middle and late Givetian time. Angular chert pebbles appear in the youngest Givetian strata at 200 m below the top of the Hecla Bay Formation of northern Melville Island (Fig. 52). This event marks the earliest evidence in the western Arctic for the unroofing and erosion of previously uplifted deep water basin strata situated near by to the north or northeast.

Major features of the Eifelian and Givetian clastic wedge within the project area are shown on Figures 70 and 71. The thinnest development of this wedge (1700 m) is found over the underlying Towson Point platform of northeastern Melville Island. Basin-fill mudrocks of the Cape De Bray Formation in this area are not more than 100 m thick, indicating minimal water depth over the platform prior to the influx of siliciclastic sediment. A depocentre up to 2750 m thick is situated south of the platform over what was once a pre-early Eifelian embayment plain up to about 900 m deep. The extra sediment thickness here is attributed to this greater pre-existing water depth, and the additional compaction of the underlying Cape Phillips Formation

compared to adjacent platform carbonates. This westerly trending depocentre is linked to a much larger depocentre that extends from Raglan Range and Blue Hills Syncline west to Prince Patrick and Banks islands (Embry, 1988a). Maximum sediment thickness in the mapped portion of the western depocentre of Melville Island is about 3750 m. Extra thickness has developed principally in the Hecla Bay and Weatherall formations as a result of higher rates of tectonic subsidence of the pre-existing western shelf rim platform in the middle Eifelian to late Givetian.

Most of the upper part of the Eifelian–Givetian clastic wedge (upper Cape De Bray–Hecla Bay formations) of Sabine and Sproule peninsulas has been removed by post-Givetian pre-Bashkirian uplift and erosion. In the Canrobert Hills, minimum thickness of the eroded Eifelian and Givetian section is about 3.2 km (Fig. 71B). Total original thickness of the Eifelian and Givetian section over the deep basin must have been close to 5400 m as a result of a combination of extreme pre-Eifelian water depth (est. 2000 m+), differential compaction of underlying mudrocks and very high Middle Devonian rates of sediment supply. The north-to-south cross-section (Fig. 71B) reveals the gradual cratonward thinning of the Eifelian and Givetian interval—to a minimum of 2250 m on Dundas Peninsula. Reduction in formation thickness is most

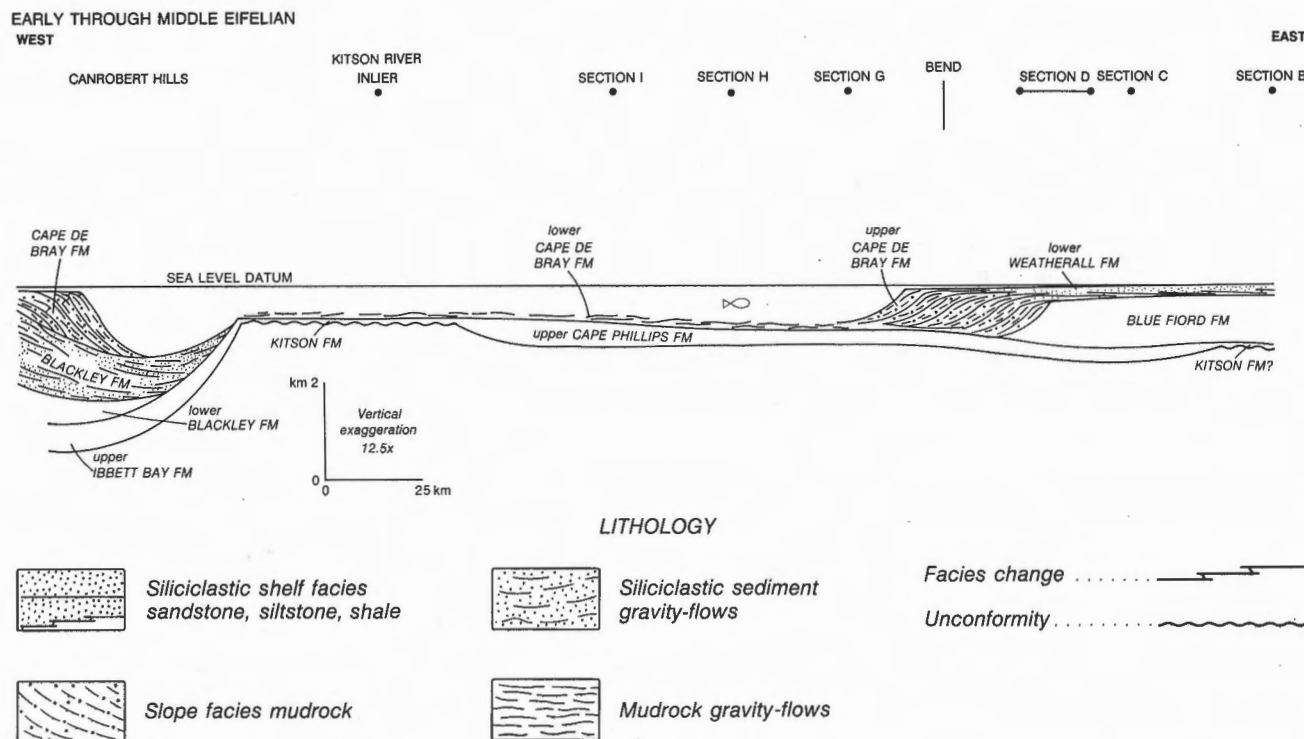


Figure 69. Palinspastic cross-section for the early Eifelian and (part of the) middle Eifelian Towson Point carbonate platform to the deep water basin. Line of section is located on Figure 68.

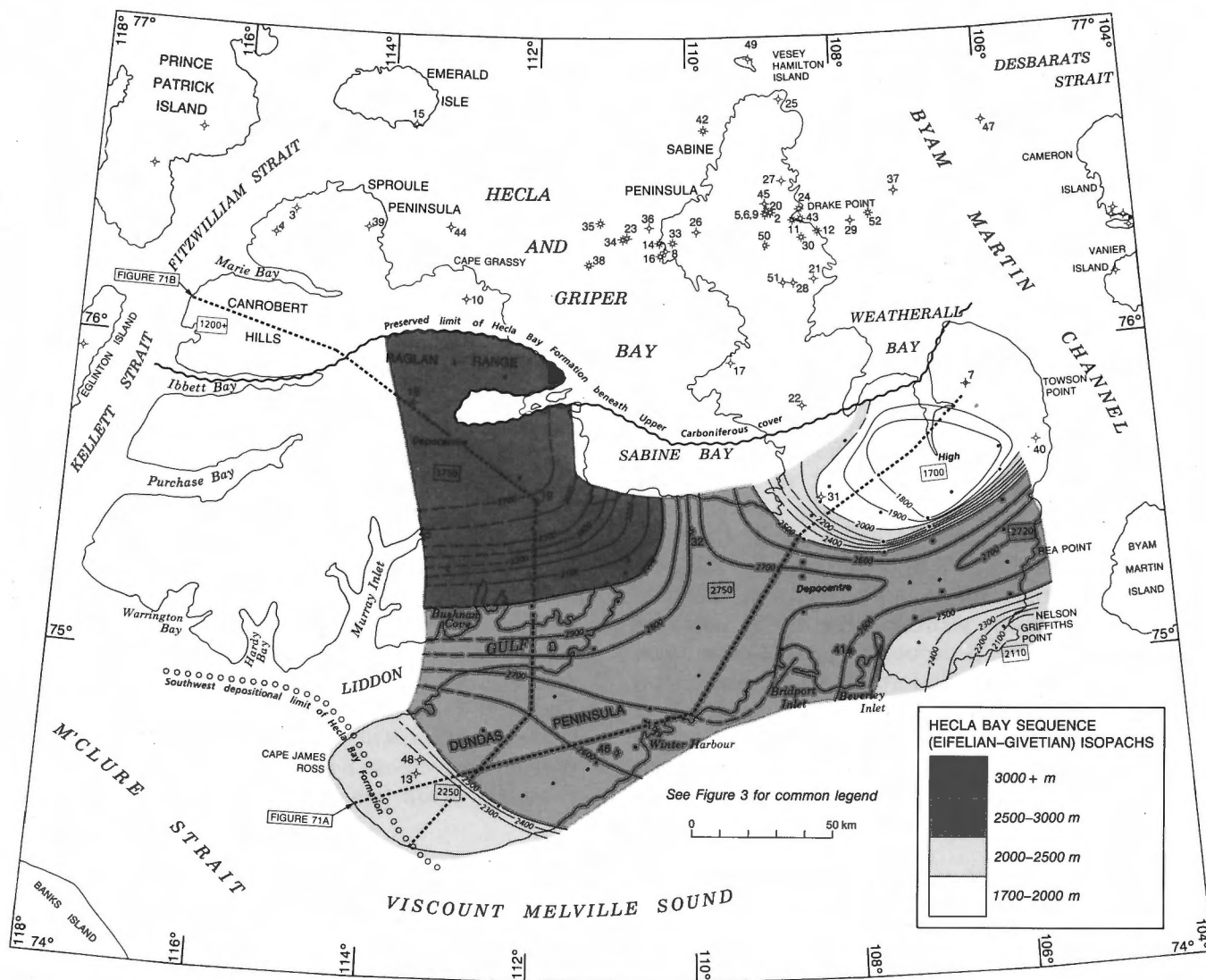


Figure 70. Isopach map of the early Eifelian through latest Givetian Hecla Bay Sequence (Blackley, Cape De Bray, Weatherall, and Hecla Bay formations). Interval velocities, 3.5–4.3 km s⁻¹; based on 65 data points. Thickness of the sequence over the deep water basin may once have been about 4800–5200 m, although only the lower 1200 m is now preserved north of Ibbett Bay (Blackley Formation, and lower Cape De Bray Formation).

evident in the deltaic and fluvatile Hecla Bay Formation, which ranges from a maximum of about 1500 m in the north to near zero in the south (and also west) where it grades laterally into the shallow-marine Weatherall Formation.

Frasnian and Famennian (375–355 Ma)

The Upper Devonian time interval spans the deposition of two disconformity-bounded fluvial, deltaic and nonmarine sequences: the Beverley Inlet and Parry Islands sequences of Embry (1988a). The thickest development of the older (Beverley Inlet) sequence occurs in the Schei Syncline of southwest Ellesmere

Island, where there are three contained formations with a combined thickness of about 2100 m (Fram, Hell Gate, and Nordstrand Point formations of Embry and Klován, 1976).

Within the project area, the Beverley Inlet sequence comprises a single formation: the Beverley Inlet Formation. Thickness variations are displayed on Figures 72 and 73. Two local sediment depocentres are indicated, including: 1) part of a major western depocentre containing more than 750 m of shallow- and marginal-marine siliclastic sediment (top not seen); and 2) a small eastern centre south of Weatherall Bay with over 600 m of beds. The eastern centre (defined by the 500 m isopach) is situated both over and north

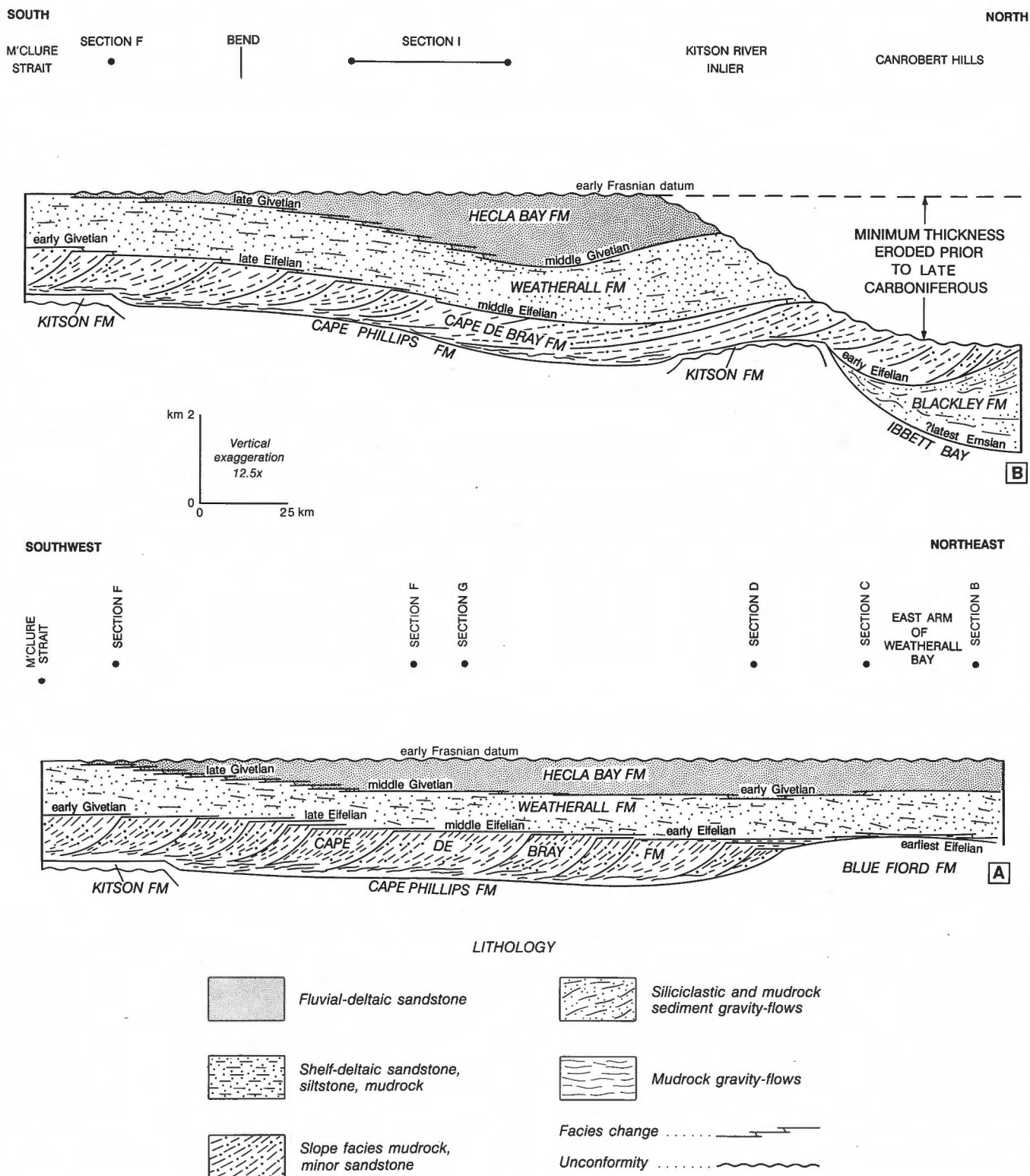


Figure 71. Palinspastic cross-sections of the Hecla Bay Sequence. **A.** Weatherall Bay to western Dundas Peninsula; **B.** western Dundas Peninsula to Canrobert Hills. Lines of section are located on Figures 68 and 70.

of one of the Eifellian–Givetian depocentres, and also stratigraphically above part of the Emsian–Eifellian carbonate platform (compare Figs. 64, 70 and 72). The

two Frasnian depocentres are separated by a depositional divide, where formation thickness is 400 to 500 m.

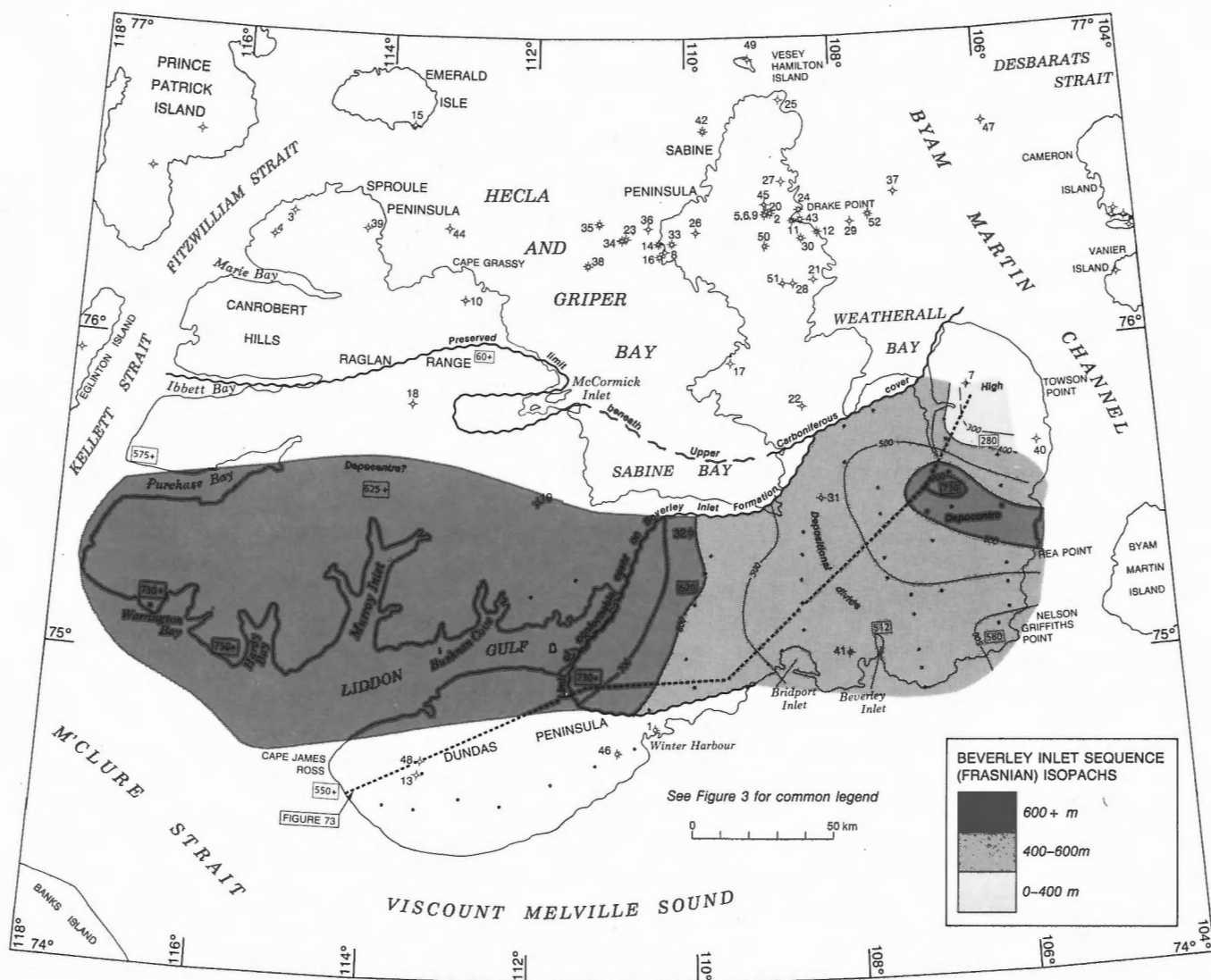


Figure 72. Isopach map of the Beverley Inlet Sequence (Beverley Inlet Formation; Frasnian). Interval velocities (DIX), 3.3–3.8 km s⁻¹; based on 66 data points.

Potentially more significant is a depositional minimum, on the southern edge of a possible structural high east of Weatherall Bay, where the Beverley Inlet Formation is locally less than 300 m thick. Reduced thicknesses for the Beverley Inlet Formation in this area have been obtained from the constraints imposed by the location of contacts established during regional mapping and the corresponding thickness implied by the dip of reflection segments in this interval on available seismic profiles (Sections A and B). For this reason, these thicknesses should not be considered as reliable as values obtained from well data or surface measured sections. Bearing in mind these limitations, it is possible to attribute local thinning of the Beverley Inlet Formation in the northeast to either: 1) syndepositional early to middle Frasnian uplift, or

2) postdepositional middle to late (not latest) Frasnian uplift prior to disconformable overlap by the Parry Islands Formation.

There is additional sedimentological evidence that the northeasterly thinning of the Beverley Inlet Formation may be postdepositional. In the Weatherall Bay area, Beverley Inlet beds are overlain by the Burnett Point Member of the Parry Islands Formation, and pebbly coarse sand occurs above a disconformity at the base of the Burnett Point Member in this area (Embry and Klován, 1976).

Thickness variations in the combined lower two members of the Parry Islands Formation (Burnett Point and Cape Fortune members) are displayed in

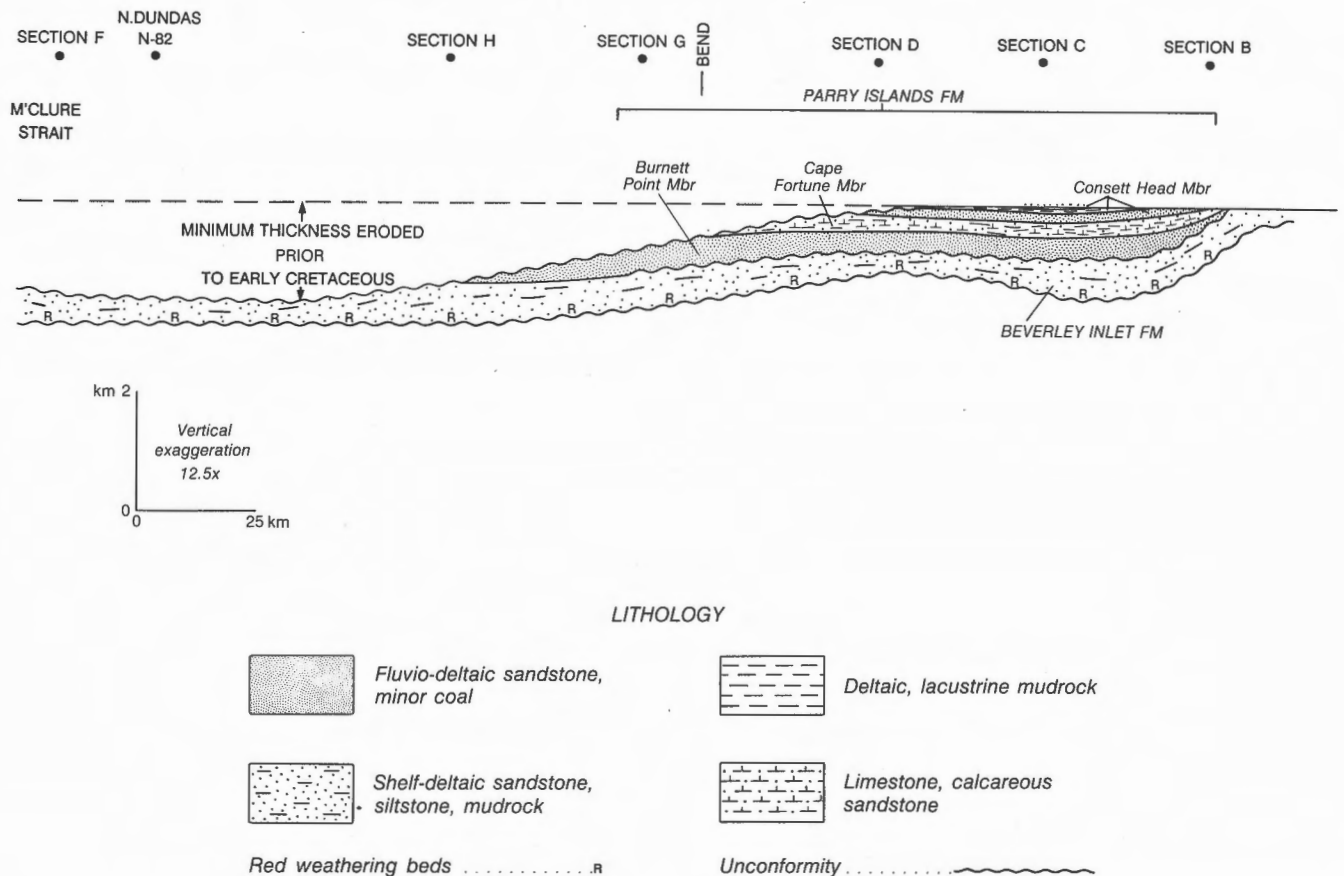


Figure 73. Palinspastic cross-section of the Beverley Inlet and Parry Islands sequences, Weatherall Bay to Dundas Peninsula. Line of section is located on Figures 72 and 74. The estimated thickness of the eroded section in the southwest is based on 1) subsidence rates and member thicknesses in the eastern depocentre, and 2) the westerly increasing thickness of the Beverley Inlet Formation and Burnett Point Member of the Parry Islands Formation as seen between sections D and H.

Figures 73 and 74. Worth noting is: 1) the depositional minimum east of Weatherall Bay, noted on the isopach map of the Beverley Inlet Formation, is also evident on the Parry Islands isopach map, indicating either a continued or renewed northeastern uplift; 2) a small Parry Islands depocentre to the south partly overlaps an underlying Beverley Inlet depocentre and is also stratigraphically above part of the Emsian-Eifelian carbonate platform (compare Figs. 64, 72 and 74); and 3) the Burnett Point Member appears to thicken to the west (Fig. 73). However, the entire Parry Islands Formation has been removed by one or more post-Devonian pre-Early Cretaceous phases of uplift.

Embry (1988a) has also provided evidence for the pre-existence of still younger pre-tectonic and syn-

tectonic strata of possible latest Devonian (latest Famennian) through Carboniferous (pre-late? Viséan or Namurian) age. First, coal and coalified organic matter in the Parry Islands Formation has thermal maturity values in the high-volatile bituminous range ($\%Ro > 0.55-0.60$ measured on vitrinite, Gentzis, pers. comm., 1987), whereas unconformable Lower Cretaceous cover contains coal of lignite rank. Second, chert pebbles and coarse cherty sand with a southern provenance, and reworked Tournaisian spores, are plentiful in Upper Carboniferous redbeds of the Canyon Fiord Formation of northern Melville Island. The thermal gap implied by the first observation may indicate a locally eroded post-Parry Islands cover sequence 2.5 to 3.0 km thick (Embry, 1988a). The gravel and chert found in the Carboniferous redbeds

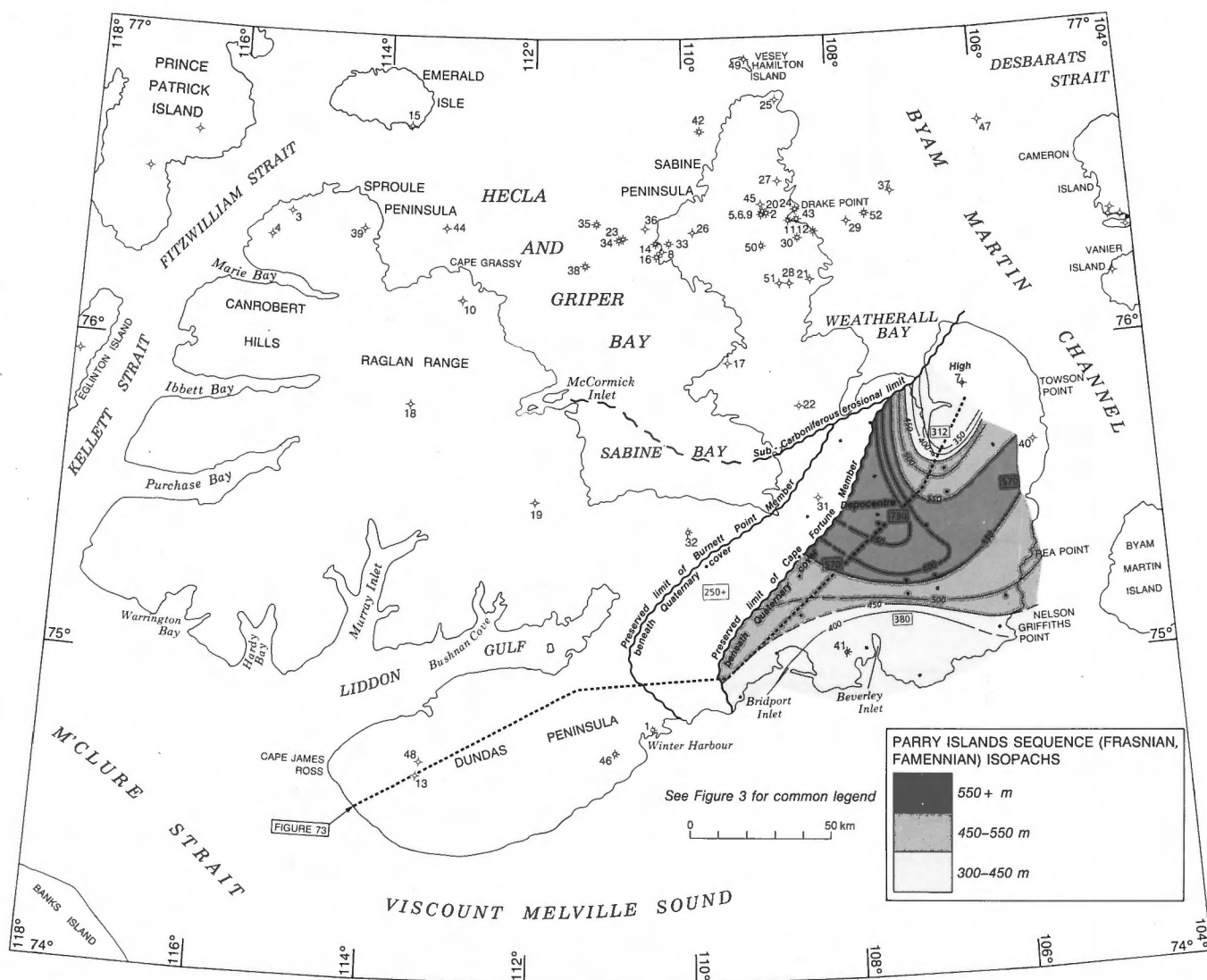


Figure 74. Isopach map of the Burnett Point and Cape Fortune members (combined) of the Parry Islands Sequence (upper Frasnian and Famennian). Interval velocities (DIX), 3.3–3.7 km s⁻¹; based on 32 data points.

could have only been derived from the eroded sequence since terrigenous material of this grade and abundance is not now found in the preserved Devonian section.

Onset of folding in Parry Islands Fold Belt

While the Middle and Upper Devonian clastic wedge provides abundant evidence of an actively eroding tectonic highland situated to the northeast, there is no evidence of thin-skinned deformation in Melville Island's salt-based fold belt prior to the early Givetian, and no likelihood of there having been any substantial folding prior to the latest Famennian. The absence of

folds in this belt prior to the early Givetian is indicated by the trend of seismic clinoforms. If the foreland folds of eastern Melville Island were actively forming prior to the early Givetian, then paleotopographic features created by these folds would have influenced sediment transport directions. In fact the Cape De Bray clinoforms are highly oblique to surface structure and are, therefore, probably older (compare Fig. 68 and geology map, in pocket).

Thin-skinned folding during the period from the early Givetian to the late Famennian is equally unlikely, because syntectonic strata of this age range should thin over anticlinal crests. Apart from selected

features attributable to differential compaction thinning of the Cape De Bray Formation over some foreland anticlines (Section F), truly convincing syndepositional sediment accumulation is observed nowhere on any of the numerous available seismic profiles. While a case can also be made for local uplift of the Towson Point carbonate platform in the Frasnian and Famennian, as discussed above, there is no reason to kinematically link this uplift to the formation of other structures in the fold belt.

This leaves the traditional view of the timing of mid-Paleozoic foreland folding in the southeastern and southwestern Arctic Islands (as first proposed by Tozer and Thorsteinsson, 1964)—that it began after deposition of the youngest-preserved Devonian strata affected by folding (upper sandstone unit of the Consett Head Member, Parry Islands Formation: late (not latest) Famennian), but prior to deposition and overlap by the youngest post-tectonic deposits (late Viséan; Utting et al., 1989b).

CHAPTER 4

SVERDRUP BASIN SUCCESSION (CARBONIFEROUS THROUGH PALEOCENE) AND YOUNGER COVER

General comments

Post-orogenic late Paleozoic through Cenozoic tectonic phases have also affected and, to some extent, obscured the structural style of Melville Island's salt-based fold belt. The nature and timing of these superimposed deformations are partly known through patterns of post-Devonian sedimentation and syndepositional tectonism as documented on seismic profiles and in the course of mapping. Therefore, in order to place these younger tectonic phases in true spatial and temporal perspective, a systematic description of stratigraphic units occurring within the post-Devonian succession is presented. These strata have been deposited mostly north of the exposed fold belt within the Sverdrup Basin. Erosional remnants of widespread Lower Cretaceous, Neogene and Quaternary formations have also been preserved on the peneplained roots of the salt-based folds.

The depositional record of the Sverdrup Basin across northern Melville Island (Fig. 75) includes a Carboniferous through upper Lower Permian rift succession, and a higher Permian through Paleocene succession displaying variations on a pattern of passive subsidence driven by lithospheric cooling (Stephenson et al., 1987). The upper Paleozoic succession of the Sverdrup Basin includes rift-related nonmarine and shallow-marine formations exposed at the surface (Canyon Fiord, Great Bear Cape, Sabine Bay, Assistance, lowermost Degerbøls and Trolld Fiord formations), age-equivalent shallow-marine strata entirely masked by younger cover (emended Belcher

Channel, Raanes and upper Degerbøls formations), rift-axial marine mudrock formations beneath cover (emended Hare Fiord, Trappers Cove and Van Hauen formations), and rift-axial evaporites locally exposed in piercement diapirs (Otto Fiord Formation). Also assigned to this succession is a seismic unit (sCGF) tentatively interpreted to include strata age-equivalent to the Otto Fiord and/or Borup Fiord formations. Useful summary papers concerning the upper Paleozoic stratigraphy of Melville Island and the Arctic Islands region in general include Tozer and Thorsteinsson (1964), Thorsteinsson (1974), Nassichuk (1975), Beauchamp et al. (1989a, b), Davies and Nassichuk (1991), and Beauchamp and Henderson (1994).

The surface strata of the Mesozoic and Tertiary Sverdrup Basin sequence include the Bjorne and Lougheed Island formations, the Jameson Bay, Sandy Point, McConnell Island and Hiccles Cove formations of the Wilkie Point Group, the Ringnes, Awingak and Deer Bay formations (previously assigned to the abandoned Mould Bay Formation of Tozer, 1956), the Isachsen, Christopher, Hassel, and Kanguk formations, and two formations of the Eureka Sound Group (Expedition and Strand Bay formations). Stratigraphic units overstepped and entirely covered by the surface formations include the Blind Fiord Formation, the entire Schei Point Group (undivided), and three formations of the Heiberg Group (Grosvenor Island, McLean Strait and King Christian formations). Recent summary papers concerning the Mesozoic stratigraphy of the Arctic islands region can be found in Embry (1991b, 1993).

Details of the upper Paleozoic through Tertiary geology and structure of the Sverdrup Basin region of

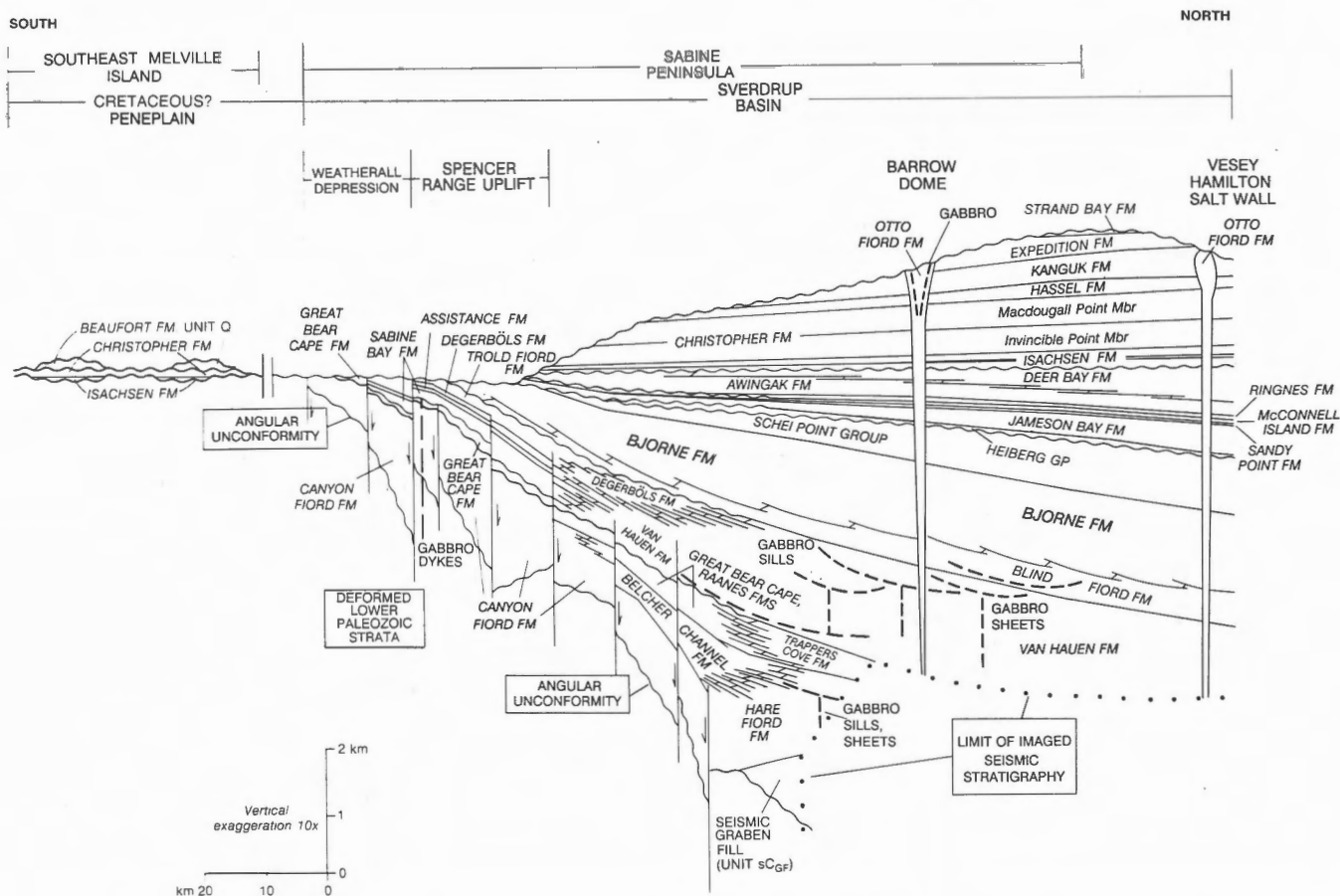


Figure 75. Generalized stratigraphic cross-section of the Sverdrup Basin succession, southeastern Melville Island to northernmost Sabine Peninsula.

Melville Island are beyond the scope of this report. Therefore the following formation descriptions serve merely to introduce the reader to only the most fundamental geological features. Alternate sources of information are also listed. Thickness ranges, lithology, seismic expression and interval sonic velocity ranges are displayed in Table 2 (in pocket). Biostratigraphic determinations are compiled in Appendix 4.

Description of formations (and other units)

Otto Fiord Formation (COF) and seismic graben fill (Unit sCGF)

References (Otto Fiord Formation). Thorsteinsson (1974); Nassichuk (1975); Nassichuk and Davies (1980); Balkwill and Fox (1982); Fox (1983).

Description. Evaporitic rocks exposed in piercement diapirs of the Sverdrup Basin, including two on Sabine

Peninsula (Barrow and Colquhoun domes; Figs. 76, 181) of northern Sabine Peninsula, have been assigned to the Otto Fiord Formation by Thorsteinsson and Tozer (1957). Marine seismic surveys within the Melville Island map area have also defined the shallow parts of other piercement structures reaching the sea floor, including two diapirs east of Cape George Richards in Byam Martin Channel, two diapirs west of Roche Point in Hazen Strait and a piercement salt wall near Vesey Hamilton Island (Figs. 180, 182; Section E; Balkwill and Fox, 1982; Fox, 1983).

The Otto Fiord Formation in the exposed diapirs consists of variably deformed anhydrite and gypsum with tectonic "rafts" of more competent sediments. Weathering colours range from shades of grey and white to light green and red. The rafts, up to 150 m in length, display a more coherent internal stratigraphy, believed to be a relict of the primary depositional layering of the formation. Rock types in these transported blocks include phylloid algal limestone, dark grey crystalline dolostone, quartz sandstone, dark



Figure 76. Oblique aerial photograph of Colquhoun Dome [Otto Fiord Formation (CoF)] and intruded strata of the Kanguk Formation (Kk), and Expedition (KTE) and Strand Bay (TSB) formations of the Eureka Sound Group. View is to the east with Cameron Island just visible on the horizon (upper right). Circled F, Cretaceous–Tertiary boundary microflora. See also legend, Figure 33.

calcareous mudrock, bedded gypsum and anhydrite. Some of the impure carbonate rocks have been altered by contact metamorphism in the contact aureole of intrusive gabbro bodies (unit KG) found within the diapirs. In addition to the above lithological mix, rock salt (halite) is believed to exist in abundance at a shallow depth below the exposed carbonate/sulphate cap rock. This belief derives from the fact that 3600 m of salt have been penetrated in the Imperial, Panarctic Dome et al. Hoodoo L-41 well drilled on the flanks of Hoodoo diapir, south central Ellef Ringnes Island (Nassichuk and Davies, 1980; Davies, 1975). Evidence for and timing of movement of Otto Fiord diapirs is reviewed in Chapter 7.

Seismic profiles available to date fail to image the stratigraphic roots of these diapirs. In the marginal areas of the basin, rift fill successions are correlated with the Canyon Fiord and younger formations. However, seismic graben fill (unit sCGF of Section E) near and below the Panarctic et al. Marryatt K-71 well appears to contain pre-Hare Fiord Formation strata that may prove to be age equivalent to the evaporites in the diapirs, Borup Fiord (Namurian redbeds of Thorsteinsson, 1974) or Emma Fiord (late Viséan lacustrine mudrock and carbonate) formations.

Age. Ammonoids and brachiopods collected and described by Nassichuk (1975) and J.L. Carter (*in* Nassichuk, 1975) from carbonate rafts in the Barrow Dome evaporites are late Early and early Late Carboniferous in age (early Namurian through Bashkirian; Fig. 77; see also Appendix 4 and Fig. 181B for fossil localities). According to Nassichuk (1975), ammonoids in the vicinity of the type section of the Otto Fiord Formation are Morrowan (Bashkirian) and also possibly Atokan (early Moscovian).

Canyon Fiord Formation (CPC)

References. Troelsen (1950); Thorsteinsson (1974); Utting (1985); Beauchamp (1987); Majid (1989); Riediger and Harrison (1993).

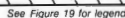
Description. The Canyon Fiord Formation is a proximal redbed sandstone, siltstone and conglomerate formation widely exposed on the eastern and southern margin of the Sverdrup Basin. On Melville Island, surface exposures occur on southern Sabine Peninsula (Fig. 78), in Spencer Range, north and south of Raglan Range, in outliers north and east of Canrobert Hills, and in several inliers along the north shore of Marie Bay. In the subsurface, the Canyon Fiord Formation is suspected to underlie most of Sproule Peninsula, southern Hecla and Griper Bay (where it locally

outcrops on the sea floor), and Sabine Peninsula at least as far north as the Sherard Bay F-34 well. Maximum thickness of the formation indicated by surface sections and seismic profiles is at least 1790 m on southern Sabine Peninsula, and over 1800 m in surface sections east of the Canrobert Hills. Thickness implied by seismic profiles across a Canyon Fiord-filled depression beneath Permian and younger cover north of Raglan Range may be up to 3200 m.

The three informal members of the formation on western Ellesmere Island (described by Beauchamp, 1987) are also locally recognized on Melville Island (Fig. 79) and here include:

3. Upper clastic member. Up to 1670 m of red, orange and light green weathering sandstone, siltstone, and clast- and matrix-supported conglomerates; minor impure nonmarine mudrock and limestone.
2. Middle limestone member (CCL). Zero to ninety metres of yellow weathering, also hematite stained, bioclastic limestone, sandy limestone and lesser quartzose sandstone (common solitary and colonial corals, crinoids, brachiopods, fusulinids and small forams).
1. Lower clastic member. Zero to one hundred sixty metres of yellow or red weathering, coarse grained, quartzose and cherty sandstone, calcareous sandstone, clast- and matrix-supported conglomerate and breccia.

Introduced clast compositions in the conglomerates include, in decreasing abundance: black or variegated, commonly laminated chert; variably micaceous, very fine and fine grained quartz sandstones; variably fossiliferous and cryptalgal limestone; dolostone; and mudrock. Intraclasts include some well rounded variegated chert ranging to pebble grade, and cobbles of chert pebble conglomerate and chert pebbly coarse grained sandstone. Clasts of polycrystalline quartz identified in thin section are internally fractured and even mylonite textured. The sandstone clasts are derived from the Weatherall Formation and younger strata of the Devonian clastic wedge. The carbonate clasts resemble the Blue Fiord Formation of the Towson Point area (Fig. 80) and the Ordovician through Silurian formations of the Kitson River inlier. The mudrocks resemble those occurring in the Ibbett Bay and Cape Phillips formations. The dark coloured chert is similar to that found in the Ibbett Bay Formation. However, Embry (1991) has suggested that most of the Canyon Fiord black and variegated chert has been derived from pre-existing chert pebble con-



113



Figure 78. Vertical airphoto of Tingmisut Lake area. Star indicates the approximate location of the type section of the Sabine Bay Formation. OSC, unnamed Silurian dolostone; CPC, Canyon Fiord Formation; PG, Great Bear Cape Formation; PSB, Sabine Bay Formation; PA, Assistance Formation; PD, Degerbøls Formation; PTF, Troid Fiord Formation; TB, Bjorne Formation; KG, Cretaceous gabbro. See also legend, Figure 33. NAPL photo. A16763-54, -55.

glomerate formations of Famennian–Tournaisian age hypothesized to once lie within the salt-based fold belt. Calcite-cemented sandstone nodules are exceedingly common throughout the formation. These may have formed in caliche deposits near minor intraformational disconformity surfaces.

The lower contact of the Canyon Fiord Formation is everywhere marked by a major angular unconformity, which places the lower clastic member on upturned Franklinian strata of Ordovician through Devonian age. On Sabine Peninsula, the upper contact is probably unconformable with the Great Bear Cape Formation at the surface (Figs. 81A, B) and gradational with the emended Belcher Channel Formation

in the subsurface. Basinward, the upper part of the upper clastic member grades into the subsurface Belcher Channel and Hare Fiord formations (Fig. 75; Majid, 1989).

On seismic sections, the Canyon Fiord Formation is represented by discontinuous, high-amplitude reflections that diverge downdip (Section E, Note 4). These primary depositional patterns are influenced in part by extensional growth faults that divide the belt of outcropping and subcropping Canyon Fiord Formation into a series of sub-basins, half-grabens, and intra-basinal uplifts. Syntectonic basins exposed at the surface include Weatherall Depression (south of the St. Arnaud Fault of southern Sabine Peninsula;

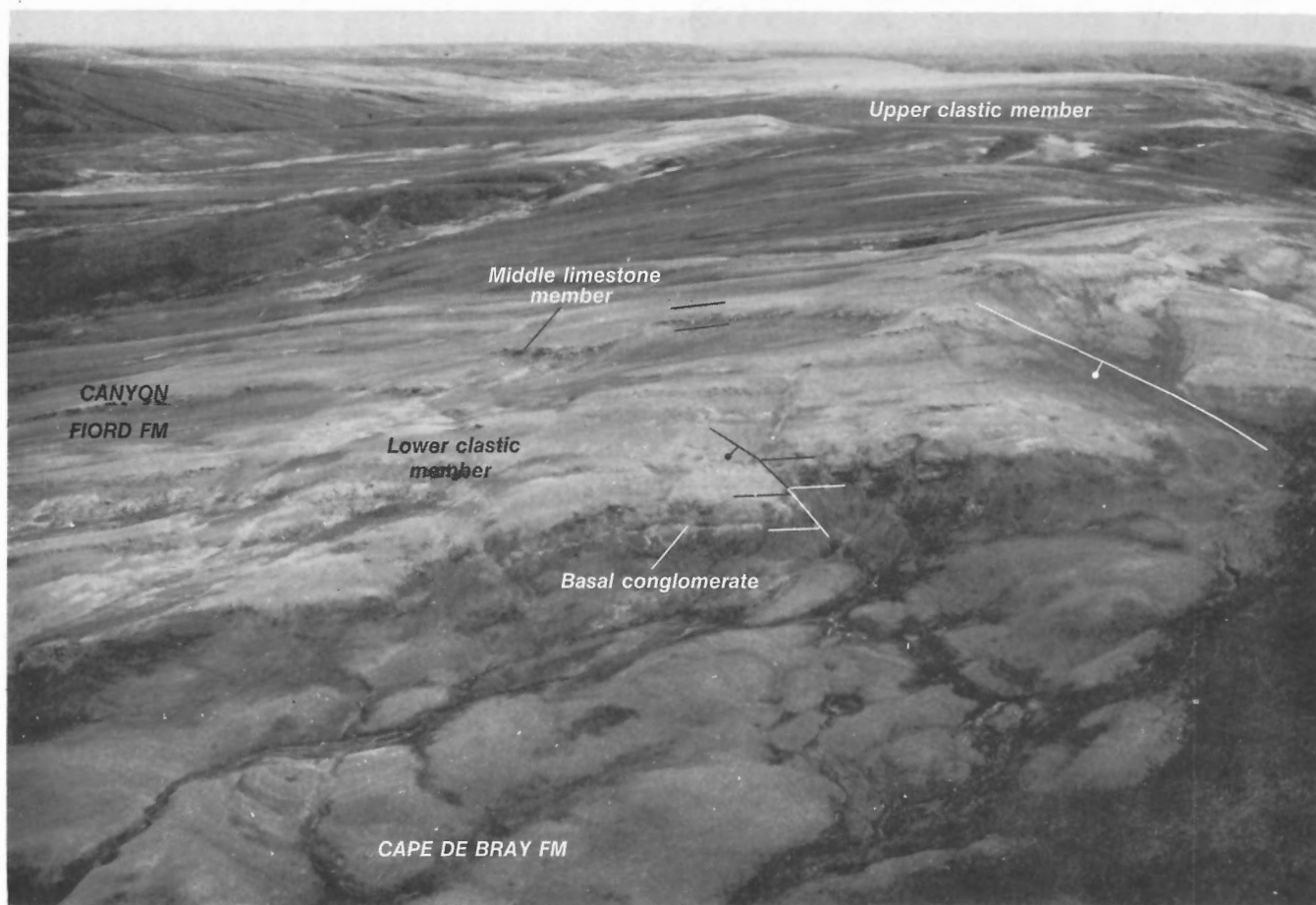


Figure 79. Locally mappable units and members of the Canyon Fiord Formation, northwestern Melville Island. At this location the basal conglomerate unconformably overlies the Cape De Bray Formation (Eifelian). ISPG photo. 2997-5.

Sections C, D and E), McCormick Depression (south of Raglan Range; Section I), and Kitson Depression (extensively exposed between Canrobert Hills and Raglan Range and also continuing beneath Upper Permian and younger cover north and northeast of Raglan Range as far north as the Kitson River C-71 well; Fig. 33; north end of Section I).

In the Canrobert Hills region, the Canyon Fiord Formation is also folded and otherwise deformed. On the north side of Marie Bay and throughout the subsurface of Sproule Peninsula, the variably eroded and peneplained roots of these folds are overlapped by the Troid Fiord (Upper Permian; Wordian) and Bjorne (Lower Triassic) formations (Section J).

Age. The lower clastic and middle limestone members of Melville Island contain Bashkirian and Moscovian foraminifera (Fig. 77; reports of Mamet and Pinard, Appendix 4), and Moscovian fusulinids (Tozer and

Thorsteinsson, 1964). The upper clastic member contains definite early and late Moscovian and (at one locality only) possible Gzhelian to early Asselian conodonts, Moscovian foraminifera, and Moscovian through Sakmarian palynomorph assemblages (reports of Henderson, Mamet, Pinard and Utting, Appendix 4; Utting, 1985, 1989). Strata of latest Carboniferous (Kasimovian–Gzhelian) age are not known with certainty in the exposed Canyon Fiord Formation. The existence of a major intraformational disconformity spanning the Carboniferous–Permian boundary is suspected. If present, it is probably situated high in the southern Sabine Peninsula exposures, where Moscovian redbeds are apparently continuous with additional redbeds in the uppermost Canyon Fiord Formation. The Canyon Fiord redbeds contain Early Permian (late Asselian and/or early Sakmarian) palynomorphs at 11 m below middle and late Artinskian strata of the Great Bear Cape Formation.

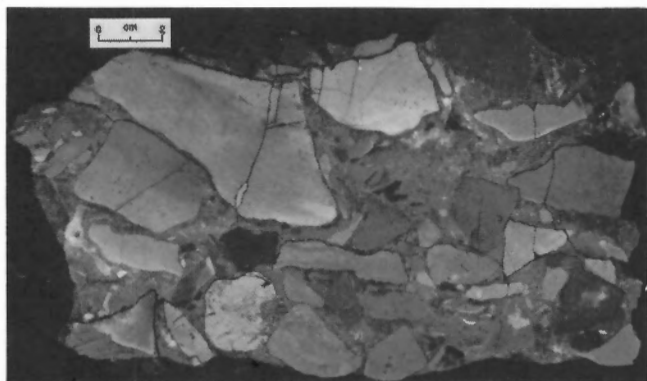


Figure 80. Polymictic breccia of sample from the lower Canyon Fiord Formation in Weatherall Depression, comprising various Lower Devonian limestone and dolostone clasts derived from the Blue Fiord Formation (presently exposed to the north in Spencer Range). ISPG photo. 3029-5.

Belcher Channel Formation (PBC)

References. Harker and Thorsteinsson (1960); Thorsteinsson (1974); Beauchamp (1987); Majid (1989); Utting (1985, 1989); emended by Beauchamp et al. (1989b) and Beauchamp and Henderson (1994). The Belcher Channel Formation, as utilized in the present account, is identical to the emended definition proposed by Beauchamp and Henderson (1994). It includes only the Asselian and Sakmarian part of the Belcher Channel Formation as described by Thorsteinsson (1974) for exposures on Ellesmere and Devon islands, and excludes strata of Artinskian age now assigned to the Raanes and Great Bear Cape formations.

Description. In the Sabine Peninsula area, Majid (1989), Utting (1989) and Beauchamp and Henderson (1994) have identified the emended Belcher Channel Formation in drilled intervals of the Chads Creek B-64, Marryatt K-71, and Sherard Bay F-34 wells of Sabine Peninsula. The sonic log interval velocity is 4.8 to 4.9 km s⁻¹ and the thickness ranges up to at least 567 m. The Belcher Channel Formation in these wells is a mixed unit of arenaceous limestone, argillaceous limestone, mudrocks, and quartzose sandstone. Laterally, the formation passes shelfward into the upper part of the upper clastic member of the Canyon Fiord Formation, and basinward into the upper part of the emended Hare Fiord Formation (Fig. 75). The Belcher Channel is also apparently conformable with the underlying upper clastic member of the Canyon Fiord Formation, although the existence of uppermost Carboniferous (Gzhelian-Kasimovian) beds remains in

doubt. The corresponding Belcher Channel seismic interval is characterized by numerous, high-amplitude, slightly divergent, and laterally continuous internal and bounding reflections, resulting, presumably, from the interlayering of limestone and lower velocity siliciclastic strata. At the depositional limit of the formation, the associated reflectors converge, downlap and lose amplitude as they pass into age-equivalent beds of the upper Hare Fiord Formation (Section E, Note 5).

Age. Early Permian foraminifera and palynomorphs (Asselian and/or Sakmarian) occur in the Belcher Channel Formation as intersected by the Sherard F-34 well (Fig. 77; Utting, 1989; report of Mamet in Appendix 4). Age-equivalent microflora occur in a mudrock interbed 11 m below the top of the exposed Canyon Fiord Formation on southwest Sabine Peninsula. The age of the emended Belcher Channel Formation on Ellesmere Island, defined by contained conodont assemblages, ranges from early Asselian through late Sakmarian (Henderson, 1988; Beauchamp and Henderson, 1994).

Great Bear Cape and Raanes formations (PGR; undivided in subsurface)

References. Beauchamp and Henderson (1994); unnamed "A" formation of Beauchamp et al. (1989b). The Raanes and Great Bear Cape formations represent a distinctive and widespread couplet of limestone formations on Ellesmere Island (Beauchamp and Henderson, 1994). These beds are also recognized on Melville Island. The surface exposures on southern Sabine Peninsula, previously correlated with the Belcher Channel Formation by Nassichuk (1965) and Thorsteinsson (1974) are here assigned to the Great Bear Cape Formation (PG). Both Raanes and Great Bear Cape formations have been intersected by boreholes during exploratory drilling on southern and central Sabine Peninsula. However, no attempt has been made to distinguish the two in the present study.

Description. In outcrop, the Great Bear Cape Formation transgressively and disconformably overlies the upper clastic member of the Canyon Fiord Formation. These beds form an obvious, resistant, light brown and greenish brown weathering ledge (Figs. 78, 81A, B). The thickness range is 10 m to about 90 m in outcrop. Westward, the Great Bear Cape Formation is inferred to be cut out beneath the Sabine Bay Formation on the sea floor of Hecla and Griper Bay (Fig. 82). To the north in the subsurface, the combined Raanes and Great Bear Cape formations thicken to a maximum of 195 m in the Marryatt K-71

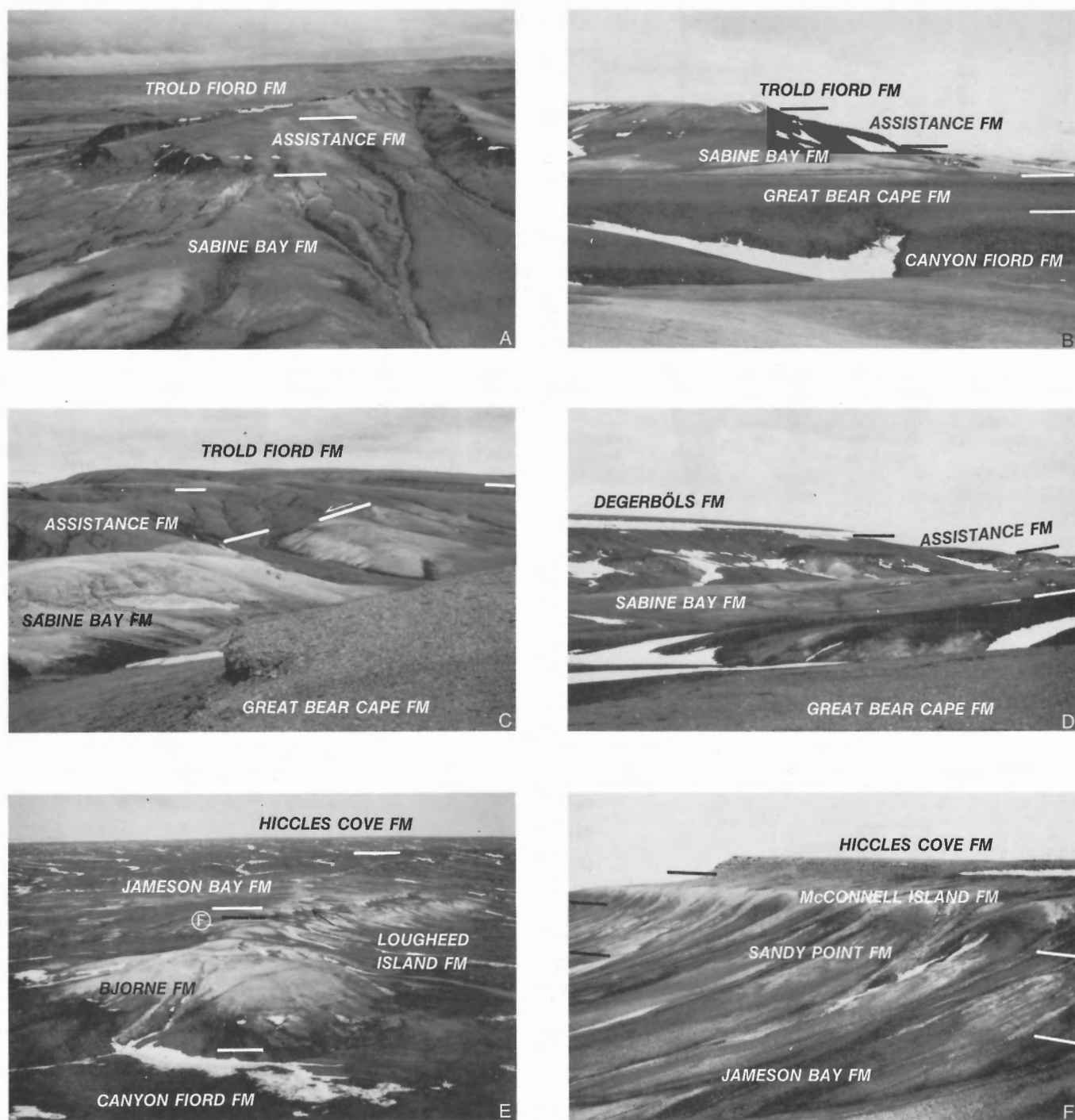


Figure 81. Surface expressions of Permian through Jurassic formations of the Sverdrup Basin succession on Melville Island. Circled F, fossil locality. **A, B.** Uppermost Canyon Fiord Formation through Trolld Fiord Formation in the southwestern St. Arnaud Hills. **C.** Trolld Fiord Formation strata faulted against strata of the Sabine Bay Formation, which in turn is in fault contact (extensional) with the Canyon Fiord and Great Bear Cape formations, in the southern St. Arnaud Hills. The two visible faults represent shallow, northerly dipping conjugates of the Tingmisut Fault situated 7 km to the north. **D.** Great Bear Cape through Degerbøls formations exposed north of Tingmisut Lake (see also Fig. 78). This photo was taken close to the type section of the Sabine Bay formation (120 m thick at this locality). **E.** Bjorne through Hiccles Cove formations, north side of Marie Bay. The late Sinemurian ammonoid *Echioceras* sp. was collected by Tozer and Thorsteinsson (1964) near the indicated fossil locality (see under Loughheed Island Formation in Appendix 4). **F.** Formations of the Wilkie Point Group at Marie Heights. ISPG photos. 2887-4, -70; 2912-4, -8, -13; 3023-5.

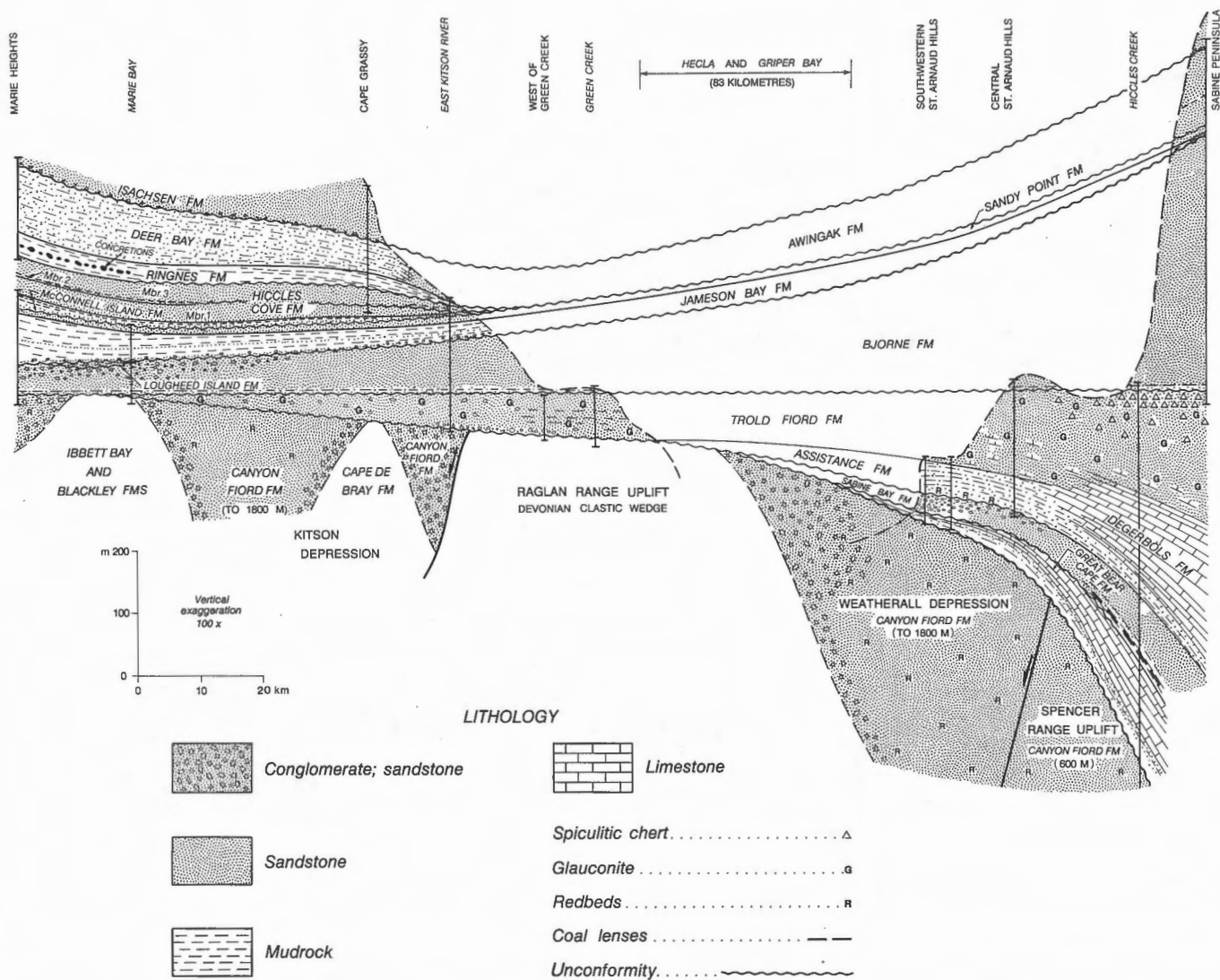


Figure 82. Schematic east-west stratigraphic section of the exposed Permian through Cretaceous (pre-Valanginian) formations above the Canyon Fiord Formation, Marie Bay to central Sabine Peninsula, via the southwestern St. Arnaud Hills and Tingmisut Lake areas. Note that, for display purposes, the distance across Hecla and Griper Bay has been intentionally narrowed. Otherwise, the horizontal scale and vertical exaggeration are approximately correct (as indicated at lower left).

well (near the basinward facies transition to Trappers Cove Formation).

The lowest beds of the exposed Great Bear Cape Formation include 3 m of yellow weathering calcareous sandstone with numerous *Zoophycos* traces and vertical escape burrows. These beds grade upward into thin and medium bedded, pebbly, arenaceous limestones. The medial part of the formation, exposed in a section situated 0.6 km north of Tingmisut Lake (Fig. 78), contains a quartz sandstone-dominated interval overlain by an upper resistant ledge of wackestone and packestone. The contained fauna in all

sections include crinoids, productid and spiriferid brachiopods, gastropods, fenestellid bryozoans, fish teeth and fragments, fusulinids and small forams. The highest beds (exposed in the headwaters of Hiccles Creek northwest of Tingmisut Lake; Fig. 78) are recessive limestones with interbedded arenaceous rocks.

On seismic profiles of Sabine Peninsula, the combined Great Bear Cape and Raanes interval is characterized by one or more high-amplitude reflections that gradually diverge in a northerly (basinward) direction. Where the Raanes and Great Bear Cape

formations conformably overlie the Belcher Channel, the two seismic intervals are acoustically identical. At the basinward limit of the Raanes and Great Bear Cape limestones, near the Marryatt K-71 well (Section E, Note 5), the strong internal reflections abruptly converge northward and downward into a condensed interval corresponding to the seismic interval equated with the Trappers Cove Formation.

Age. The Great Bear Cape Formation exposed on Melville Island has yielded conodont assemblages of middle and late Artinskian age (conodont zones 7 to 9 of Henderson, 1988; see also Fig. 77 and reports of Henderson, Appendix 4). On southwestern Sabine Peninsula, 15 m of strata separate upper Asselian-lower Sakmarian mudrocks in the upper part of the Canyon Fiord Formation and lower Artinskian limestones in the lowermost Great Bear Cape Formation. A disconformity is therefore inferred to occur at the base of the Great Bear Cape that cuts out the upper part of the Canyon Fiord, emended Belcher Channel and possibly also the Raanes Formation toward the Sverdrup Basin margin.

Hare Fiord and Trappers Cove formations (CPHT; undivided)

References (Hare Fiord Formation). Thorsteinsson (1974); Majid (1989); Utting (1989); emended by Beauchamp and Henderson (1994).

References (Trappers Cove Formation). Beauchamp and Henderson (1994); unnamed "B" formation of Beauchamp et al. (1989b).

Description. The undivided Hare Fiord and Trappers Cove formations are a succession of dark-coloured siltstone, mudrock, dark limestone and chert exposed in parts of Ellesmere and Axel Heiberg islands, and also suspected to underlie all axial portions of the Sverdrup Basin. The emended Hare Fiord is laterally equivalent to the medial and upper Canyon Fiord Formation and the emended Belcher Channel Formation. The overlying Trappers Cove Formation is equivalent to the Raanes and Great Bear Cape limestones of the shelf (Beauchamp et al., 1989b; Beauchamp and Henderson, 1994). Majid (1989) has assigned to the Hare Fiord Formation an interval in the lower part of the Drake Point D-68 well (4685 m; T.D. 5416 m). This interval also includes, in the upper part, basin facies rocks of the Trappers Cove Formation (Beauchamp and Henderson, 1994). On seismic reflection profiles (of Sabine Peninsula north of MacDougall and Marryatt points), the combined Hare Fiord and Trappers Cove formations comprise an

interval of subparallel reflections above either acoustic basement or seismic unit sCGF (Section E). Sonic log interval velocity is 4.4 to 5.0 km s⁻¹ in the D-68 well. Full thickness of the seismically imaged formations near the southern depositional limit is approximately 1380 to 1850 m (this could include an unpenetrated seismic interval laterally equivalent to the Otto Fiord Formation).

Age. The Hare Fiord Formation in the Drake D-68 well contains an early Permian palynomorph assemblage similar to that found in the Belcher Channel Formation (Fig. 77; Utting, 1989). Ammonoids at the base of the Hare Fiord Formation in the type section on Ellesmere Island are early Moscovian (Nassichuk, 1975). The probable age range of the emended Hare Fiord Formation of Melville Island is Moscovian through Sakmarian. The subsurface Trappers Cove Formation is laterally gradational with the limestone-dominated Raanes and Great Bear Cape formations; the latter contains an Artinskian conodont assemblage.

Sabine Bay Formation (PSB)

References. Tozer and Thorsteinsson (1964); Thorsteinsson (1974); Majid (1989).

Description. The Sabine Bay Formation is a distinctive off-white, yellow and yellowish brown weathering quartzose sandstone unit exposed across southern Sabine Peninsula. The type section is located 1.6 km northwest of Tingmisut Lake (Figs. 78, 81A-D). In outcrop, thicknesses range from 19 m in the southwest to about 120 m in the vicinity of the type section (Fig. 82). In the subsurface, the Sabine Bay Formation has been intersected in three wells, including the Hecla J-60 well near MacDougall Point, northwestern Sabine Peninsula. In southwestern Sabine Peninsula, the Sabine Bay Formation disconformably overlies the lower and older beds of the Great Bear Cape Formation. In this area the Sabine Bay Formation consists of uncemented coarse and medium grained sandstone with lenses of pebbly sandstone and clast-supported chert pebble (pebbles to 3 cm; Fig. 83). Neptunian dykes occur in some sections. The coarser grained beds are selectively cemented with calcite, and metre-scale calcareous sandstone concretions are also present. Toward the northwest, the Sabine Bay Formation appears to gradationally overlie the Great Bear Cape Formation. However, the contact lies on a recessive dip slope and is not known to be exposed. The sandstones are mostly fine grained, and in the lower part, are intercalated with weakly compacted carbonaceous sandstone, siltstone and minor coal and limestone. A thickening- and coarsening-upward



Figure 83. Intercalated coarse grained, pebbly sandstone and chert-pebble conglomerate of the Sabine Bay Formation, southwestern St. Arnaud Hills. ISPG photo. 3023-3.

pattern is also seen in the sections north of Tingmisut Lake. Cliff-forming sandstone with some cemented beds occurs near the top of the formation (Figs. 78, 81D). The Sabine Bay Formation grades basinward and to the northeast into the lower part of the (sub-surface) Van Hauen Formation (Fig. 75; Section E).

Age. Marine faunas in the Sabine Bay Formation include brachiopods, *Zoophycos* burrows and (rare) ammonoids (Fig. 77). Based on an occurrence of *Sverdrupites* sp., in the lower part of the type section, Nassichuk (1970; pers. comm., 1992) would consider the Sabine Bay Formation on Melville Island to be Roadian. Henderson (1988) has also suggested a late Early Permian age for the Sabine Bay Formation based on the additional occurrence of a distinctive conodont assemblage collected from basal marine beds in a section on west-central Ellesmere Island.

Assistance Formation (PA)

References. Thorsteinsson (1974); Nassichuk and Wilde (1977); Nassichuk (1970).

Description. The Assistance Formation on Melville Island is a thin (15–54 m) but widespread unit of weakly compacted and recessive, greenish grey and dark grey weathering, variably glauconitic and argillaceous, fine grained sandstone and siltstone with thin ledges of dusky red weathering pebbly mudstone in the upper part (Figs. 78, 81A–D, 82). Marine macrofauna, including gastropods, bryozoa, conularids, and especially brachiopods are exceedingly abundant in the formation, and in some areas, these fossils have weathered out into a veritable felsenmeer carpet of finely preserved and unbroken specimens.

On southern Sabine Peninsula and in northwestern Spencer Range, the Assistance Formation transgressively and disconformably overlies the Sabine Bay Formation. Red weathering beds on the lower contact testify to subaerial exposure and oxidation. Borehole sections and seismic profiles indicate that the Assistance Formation grades northward into the lower part of the Van Hauen Formation (Section E).

Age. Based on the occurrence of ammonoids and other macrofauna, Nassichuk (1970) has suggested a late Early Permian (Roadian) age for the Assistance Formation (see also Appendix 4).

Degerbøls Formation (PD)

References. Thorsteinsson (1974); the following description also embraces “Unit A” of Nassichuk (1965).

Description. The Degerbøls Formation of Melville Island is here considered to include the limestone formation that overlies the Assistance Formation north and west of Tingmisut Lake, southeastern Sabine Peninsula (Figs. 78, 81D; “Unit A” of Nassichuk, 1965) as well as subsurface limestones of southern and central Sabine Peninsula that are laterally equivalent to the Trolld Fiord Formation and which have been intersected by the Hecla J-60 and Sherard F-34 wells.

The Degerbøls Formation in outcrop includes about 130 m of fossiliferous limestone. The limestone is a readily mappable, cuesta-forming unit. Outcrops of the middle part of the formation (on Hiccles Creek) are grey and greenish grey weathering, medium bedded

and abundantly fossiliferous. Fauna include numerous brachiopods, fenestellid bryozoans, trilobite fragments, bivalves, echinoderms, sponge spicules, some small forams and *Zoophycos* burrows. The lower contact with the Assistance Formation is covered by felsenmeer. The Degerbøls Formation is absent south of the St. Arnaud Fault (Fig. 82). Age-equivalent strata are either cut out by or undergo facies changes into the Troid Fiord Formation. In the subsurface, the Degerbøls Formation overlies either the Assistance or lower Van Hauen formations (Section E). It attains a maximum thickness of 720 m in the Hecla J-60 well.

Seismic profiles display a laterally gradational contact with the entire Troid Fiord seismic interval as indicated by an observed increase in internal and bounding reflection amplitudes passing into the limestone-dominated facies. Slightly divergent reflections seen in the southern portion of the Degerbøls seismic interval pass into sigmoidal clinoforms at the distal (northward) limit of the unit, where at least three carbonate units downlap and prograde into the upper Van Hauen interval.

Age. The Degerbøls Formation as exposed on Sabine Peninsula contains a conodont assemblage of late Roadian to early Wordian (probably late Roadian) age (Fig. 77; report of Henderson in Appendix 4). The younger subsurface Degerbøls, an age-equivalent facies of the Troid Fiord Formation, is entirely Wordian.

Troid Fiord Formation (PTF)

Reference. Thorsteinsson (1974).

Description. The Troid Fiord Formation, exposed across northern Melville Island and (on Sabine Peninsula), includes up to 230 m of bright green glauconitic sandstone, spiculitic chert, minor limestone and clast-supported chert pebble conglomerate. The sandstones are commonly peloidal, bioturbated and variably intercalated with spiculitic chert. In the lower part of the formation, gastropods and decimetre-size productid and spiriferid brachiopods are found weathering out on the surface in some exposures.

The Troid Fiord Formation gradationally overlies the Degerbøls Formation north and west of Tingmisut Lake. The formation thins and progressively oversteps older and older strata to the south and west (Fig. 82). It is 130 m thick on southwestern Sabine Peninsula where it conformably overlies the Assistance Formation, and is less than 60 m thick where it rests

with angular unconformity on folded Carboniferous and Devonian rocks of northwestern Melville Island (Fig. 33). A section examined north of Raglan Range contains several thin conglomerate layers within 5 m of the basal unconformity (Fig. 84). Clasts (up to cobble grade) are composed of fine-grained sandstone, presumably derived from Devonian sandstone formations (situated to the south) that must have been exposed to erosion at this time.

In the subsurface, the Troid Fiord seismic interval (interval velocity of 3.4 km s⁻¹) reaches a maximum thickness of approximately 250 m near the facies transition to Degerbøls Formation.

Age. The lower part of the Troid Fiord Formation on Melville Island contains a Wordian (middle? Wordian) conodont assemblage. Contained palynomorphs are also unlike those found in either the underlying Roadian and overlying lower Triassic formations (Fig. 77; reports of Henderson, and Utting in Appendix 4).



Figure 84. Cobble-grade conglomerate of the lower Troid Fiord Formation, at a section west of Green Creek on the north side of Raglan Range. Sandstone clasts were presumably derived from Devonian siliciclastic formations presently exposed to the south. ISPG photo. 2887-69.

Van Hauen Formation (PVH)

References. Thorsteinsson (1974); Majid (1989); Utting (1989).

Description. The Van Hauen Formation of Melville Island is a subsurface unit intersected in exploratory wells of central and northern Sabine Peninsula. It is also assigned to a seismic interval that is laterally equivalent to the basin margin Permian formations above the Great Bear Cape Formation. Dominant rock types encountered in the formation include dark coloured mudrocks, siltstone and spiculitic chert. The seismic expression is reflection free in the lower part, and, in the upper part, one of continuous internal and bounding reflections of low to moderate amplitude that gradually diverge basinward.

The Van Hauen Formation, penetrated by boreholes, is between 558 and 1085 m thick. The equivalent seismic interval appears to become progressively thicker north of the deepest borehole penetrations.

Onlap patterns observed in the Van Hauen seismic interval serve to divide the formation into five members (Section E, Note 6; Majid, 1989). Integration of borehole picks and seismic reflection profiles indicates that 1) the base of the formation correlates with the top of the Artinskian Great Bear Cape Formation on the shelf; 2) the reflection-free lower member of the Van Hauen is laterally equivalent to the Sabine Bay and Assistance formations; 3) the thin second member (from the base) is equivalent to the Degerbøls Formation as exposed at the surface; and 4) that the three upper Van Hauen members are equivalent to (and also younger? than) separate progradational carbonate members of the upper Degerbøls Formation.

Age. Palynomorph assemblages occurring in borehole-penetrated sections of the Van Hauen Formation of Sabine Peninsula are found in the Roadian through Wordian formations of the basin margin (Utting, 1989). This correlation is also indicated by reflection seismic profiles (Section E). It has also been suggested by Beauchamp et al. (1989b) that the upper Van Hauen Formation on western Ellesmere Island and elsewhere, may locally be gradational with the overlying (Griesbachian) Blind Fiord Formation. If true, the Van Hauen may also contain a depositional record of post-Wordian through pre-Griesbachian sedimentation (Fig. 77). There is no biostratigraphic evidence available from anywhere in the Arctic Islands that would support this reasonable proposal.

Bjorne (TB) and Blind Fiord (TBF) formations

References. Tozer (1961, 1963b); Tozer and Thorsteinsson (1964); Trettin and Hills (1966); Embry (1986); Utting (1985, 1989).

Description. The Bjorne Formation is exposed across northern Melville Island and has been intersected by numerous boreholes down dip to the north. The thickness ranges from a minimum of about 50 m on Sproule Peninsula to as much as 1345 m in the subsurface of Sabine Peninsula (Figs. 75, 82). Rock types include medium and coarse grained quartzose sandstone, siltstone, minor carbonaceous sandstone, mudrock and clast-supported conglomerate. Sedimentary structures include reverse- and normal-graded bedding, planar and trough cross-stratification. Weathering colours include shades of orange, red, buff, and green. Conglomerate is especially common in outcrops on Sproule Peninsula, where well-rounded cobble- and boulder-grade clasts are seen in some sections. Clast types include cemented quartzose sandstone and chert (Fig. 85).

At the surface, the Bjorne Formation disconformably overlies the Trold Fiord Formation in most areas, but on Sproule Peninsula it cuts out the Permian section and rests directly on strata of Carboniferous and older age. In the subsurface, the Bjorne Formation gradationally overlies the Blind Fiord Formation. Separate members of the Bjorne Formation are recognized by Trettin and Hills (1966) on northwestern Melville Island. Other members have been described



Figure 85. Clast-supported conglomerate of the Bjorne Formation, near the head of Marie Bay on Sproule Peninsula. ISPG photo. 2887-25.

and named by Embry (1986) from scattered well logs throughout the Sverdrup Basin and also outcrops in the eastern Arctic Islands. There has been no attempt to map subdivisions of the Bjorne Formation at the present scale of study.

The Blind Fiord Formation (Tozer, 1963b) is the distal, age-equivalent facies of the Bjorne Formation and comprises grey-green siltstone and grey mudrock. It has not been recognized with certainty at the surface. In the subsurface, the Blind Fiord Formation lies variably on the Troid Fiord, Degerbøls and Van Hauen formations, and is up to to 230 m thick in the Drake D-68 well. The seismic upper contact of the formation is marked by a series of diachronous reflection segments that young to the north (Section E, Note 9).

Age. The exposed lower Bjorne Formation and basal Blind Fiord Formation as penetrated by boreholes of Sabine Peninsula have both yielded palynomorph assemblages typical of those also found in the Griesbachian sections of east Greenland and Svalbard (Fig. 77; Utting, 1985, 1989). Many diagnostic ammonoid species have been collected and described by Tozer (1965) from the Blind Fiord Formation of Ellesmere and Axel Heiberg islands. All Early Triassic stages from the Griesbachian through the Spathian are represented.

Schei Point Group (KS)

References. Embry (1984a, 1984c); Schei Point Formation of Tozer (1961).

Description. The Schei Point Group comprises shallow-marine formations of Middle and Late Triassic age (Murray Harbour, Roche Point, Hoyle Bay, Pat Bay and Barrow formations of Embry, 1984a), all of which in the Melville Island area are known only from subsurface data sources. As well as containing quartz sandstones and mudrocks, the Schei Point Group also comprises two intervals of limestone, both of which are characterized on seismic records by strong, laterally continuous reflections (Gore Point Member of the Roche Point Formation and the Eden Bay Member of the Hoyle Bay Formation; Embry, 1984c). Where present, the Schei Point Group disconformably and conformably overlies the Bjorne Formation. Sonic interval velocities increase northward and basinward from 3.6 to 4.4 km s⁻¹. Thicknesses indicated by boreholes and seismic profiles range to approximately 750 m within the map area (Fig. 75).

The Schei Point Group grades northward and basinward into the mudrock-dominated Blaa Mountain Group (not known in Melville Island area).

Age. Ammonoids and bivalves collected from the Schei Point Group type section on Ellesmere, and other correlative exposures on Axel Heiberg and adjacent small islands are Anisian through Norian in age (Tozer, 1961). The two limestone members in the Schei Point Group are late Ladinian and/or Carnian for the Gore Point Member and Carnian for the Eden Bay Member (Tozer, 1961, 1963b; Embry, 1984c).

Heiberg Group (TJH)

References. Tozer and Thorsteinsson (1964); Embry (1982, 1983, 1993); Poulton (1993); Johannessen and Embry (1989). The Heiberg Group as proposed by Embry (1983) and as described below includes the lower half of the Lower Jurassic (Sinemurian) Borden Island Formation of Tozer and Thorsteinsson (1964). It also probably contains Upper Triassic subsurface beds that correlate with part of the Heiberg Formation in the type section at Buchanan Lake on Axel Heiberg Island as first described by Souther (1963).

Description. The Heiberg Group is an Upper Triassic to Lower Jurassic deltaic sandstone and mudrock-dominated succession that is widespread throughout the Arctic Islands. Widespread, thick exposures are also found in the Tertiary fold belt of western Ellesmere and Axel Heiberg islands. In the western Arctic Islands, including Melville Island, exposures are limited to thin and discontinuous intervals around the Sverdrup Basin margin and to sections penetrated by exploratory wells.

Four subsurface formations of the northern Melville Island region and Emerald Isle are identified on borehole logs and cuttings by Embry (1993) and Johannessen and Embry (1989). From the base these include the Grosvenor Island (mudrock with basal oolitic ferruginous sandstone), Maclean Strait (sandstone), Loughheed Island (mudrock) and King Christian (sandstone) formations. A maximum combined thickness of 138 m is encountered in the Emerald K-33 well. On Melville Island, these formations are thickest in the North Sabine H-49 well (78 m). Disconformities are recognized at the base of the Heiberg Group and at several additional levels within the succession. The base of the Grosvenor Island Formation is also a readily identifiable reflection on seismic profiles where these beds overlie the Schei Point Group (Section E, Note 8). Southward

in the subsurface, the Grosvenor Island Formation cuts out the entire underlying Schei Point Group. Likewise, the entire Heiberg Group thins toward the basin margin. The Loughed Island oversteps the Grosvenor Island and McLean Strait formations and the King Christian Formation is progressively cut out by the overlying Wilkie Point Group.

Outcrops of the Heiberg Group, situated on northwestern Melville Island only, are limited to definitely one, but probably several, disconformity-bound erosional remnants (up to several metres thick) of the Loughed Island Formation (JL) that lie between the Bjorne and Jameson Bay formations (Figs. 81E, 82; Embry, 1993; Poulton, 1993).

Age. The Melville Island outcrops of the Loughed Island Formation contain the late Sinemurian ammonoids *Echioceras* sp. and *E. aklavikense* Frebold (Fig. 77; Frebold, 1960, 1975; Poulton, 1993; Appendix 4). Tozer (1961) has collected and described bivalve assemblages from the upper part of the Heiberg Group exposed on Ellesmere and Axel Heiberg islands. These fauna include species of *Monotis*, *Oxytoma* and *Melagrinnella* considered by Tozer (ibid.) to be probably late Carnian or early Norian ranging to late Norian in age. Four palynomorph biozones identified by Suneby and Hills (1988) in the Heiberg Formation of the eastern Arctic Islands span Norian through early Toarcian ages. Similar unpublished palynomorph data are also available for the subsurface Heiberg Group of the western Arctic Islands (Embry, pers. comm., 1992). The full age range for the Heiberg Group of subsurface Melville Island is considered to be Norian through late Sinemurian (Embry, 1993).

Wilkie Point Group (JW)

References. Embry (1984b, 1991, 1993); Poulton (1993); Wilkie Point Formation of Tozer (1956).

Description. The Wilkie Point Group is divided into four formations (Embry, 1984b) all of which are recognizable and, for the most part, are mappable on northwestern Melville Island.

The oldest strata of the Wilkie Point Group are assigned to the Jameson Bay Formation (JJ). The section at Marie Heights (Figs. 81E, F) includes approximately 50 m of recessive, greenish grey mudrock, siltstone, and glauconitic sandstone. Ammonoids, belemnoids, silicified wood, and phosphatic concretions are all common accessory components. Embry (1984b, 1993) has widely correlated two separate but laterally extensive marker beds within the

formation: the lower marker, a horizon of oolitic ironstone and phosphatic nodules above the Intrepid Member; the upper, a ledge-forming ironstone separating the Cape Canning Member below, and the Snowpatch Member above.

The Jameson Bay Formation is gradationally overlain by the Sandy Point Formation (JS). At Marie Heights, the latter includes 6 m of burrowed, glauconitic and ferruginous quartz sandstone. These are recessive, compacted but mostly uncemented, off-white weathering beds, locally exposed on incised slopes where the formation is supported by resistant ledges lying in the lower part of the overlying McConnell Island Formation (Fig. 81F).

At Marie Heights, the McConnell Island Formation (JMI) is exposed on several escarpment faces beneath cemented basal beds of the lower Hiccles Cove Formation. The McConnell Island also underlies a broad, north-facing dip slope to the north and east. At Marie Heights there are two members in the McConnell Island, each of approximately equal thickness. The lower member includes 12 m of interbedded ferruginous sandstone, lesser uncemented sandstone and mudrock. The cemented beds are represented in three or four brown, rubbly-weathering ledges that are easily recognizable on aerial photographs by their striped pattern against darker recessive layers. The upper member at Marie Heights comprises 8 m of recessive, brownish grey, bioturbated mudrock. This section also includes calcite-cemented sandstone concretions (to 1.5 m). The formation is not practically mapped east of Sproule Peninsula because of reduced thickness in this direction of the upper member.

Sandstone is the dominant sediment in two of the three members of the overlying Hiccles Cove Formation (JHC). The lower member at Marie Heights comprises approximately 40 m of orange weathering, fine grained, selectively cemented sandstone (Figs. 81F, 86B, 87A). Common accessory components include decimetre-scale Inoceramid casts, phosphatic nodules, bone fragments, and silicified wood. The middle member includes up to 5 m of recessive grey mudrock, siltstone, and very fine grained sandstone (Fig. 87A). The third and highest member of the Hiccles Cove Formation near Marie Heights and throughout Sproule Peninsula is represented by a 70 m thick interval of white to off-white, thick bedded, castellate weathering, medium grained quartz sandstone (Figs. 86A, B). Stratal features include planar beds, planar crossbeds and rip-up clasts (to about 30 cm).

Combined thickness of the four formations of the Wilkie Point Group ranges from a few metres to 185 m



Figure 86. Field photographs of the Hiccles Cove, Ringnes and Deer Bay formations, northwestern Melville Island. **A.** Conformable contact between the castellate weathering upper member of the Hiccles Cove Formation and the Ringnes Formation. **B.** The lower part of the Hiccles Cove Formation, faulted against strata of the upper Hiccles Cove Formation and the Ringnes Formation. Medial shale member of the Hiccles Cove Formation is absent in this area and the upper sandstone member lies disconformably on the lower sandstone member. Conformable Deer Bay Formation strata are visible on the skyline. Faunal lists for fossil localities in the Ringnes (GSC locs. C-134291–95) and Deer Bay (GSC loc. C-134300) formations are noted in Appendix 4. ISPG photos. 2887-34, -60.

at surface, to 330 m in the northern subsurface (Figs. 75, 82). Most of this thickness occurs in the Jameson Bay Formation. The Sandy Point Formation is everywhere represented by only a few metres of section and is therefore not separated from the underlying Jameson Bay Formation at the present scale of mapping. A disconformity beneath the Jameson Bay Formation cuts out the Heiberg Group in the shallow subsurface. A significant disconformity also separates the Sandy Point and McConnell Island formations, and a third disconformity occurs between the lower and medial members of the Hiccles Cove Formation (Fig. 86B). Eastward, in the outcrop belt of Sproule Peninsula, the lower sandstone member of the Hiccles Cove Formation is progressively cut out to the southeast beneath the medial shale member. On the East Kitson River, the medial Hiccles lies unconformably on the Sandy Point Formation (Fig. 87A). The Hiccles Cove Formation is entirely absent in all surface and subsurface areas of Sabine Peninsula.

Age. On northwestern Melville Island, the Jameson Bay Formation contains Toarcian and Aalenian foraminifera and ammonoids of late Pliensbachian, probable Toarcian, and early Aalenian ages (Fig. 77). Early Aalenian ammonoids occur in the Sandy Point Formation on southern Sabine Peninsula. The lower part of the McConnell Island Formation contains early Bajocian ammonoids at Marie Heights. The middle member of the Hiccles Cove Formation contains early Bathonian to early Callovian dinoflagellates and

miospores, and an early Callovian ammonoid of the genus *Cadoceras* (reports of Davies, Poulton, and Wall in Appendix 4).

Ringnes (JR), Awingak (JKA) and Deer Bay (JD, JKD) formations

References. Balkwill, Wilson and Wall (1977); Souther (1963); Heywood (1957); Balkwill (1983). All three formations were assigned to the Mould Bay Formation (abandoned) of Tozer, 1956.

Description. The Ringnes, Awingak and Deer Bay formations are each clearly separable and individually mappable units on Sabine Peninsula and northwestern Melville Island. In outcrop, the Ringnes Formation disconformably overlies the Hiccles Cove Formation on northwestern Melville Island and overlies the Sandy Point on Sabine Peninsula. The Ringnes Formation is represented by up to 30 m of black, recessive, carbonaceous and micaceous shale (Figs. 86, 87A). In the thickest exposed sections (on Sproule Peninsula), the Ringnes also contains large, calcite-cemented siltstone concretions (to 1 m) in the middle part of the formation, and fragments of silicified wood, marine vertebrate bone, and bivalves throughout. The Ringnes Formation grades upward into either the Deer Bay Formation (Fig. 86B) or the laterally equivalent Awingak Formation (Fig. 87A). The Deer Bay includes

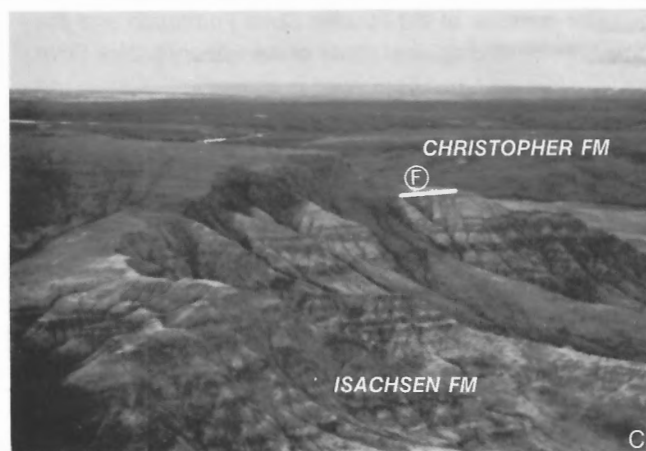
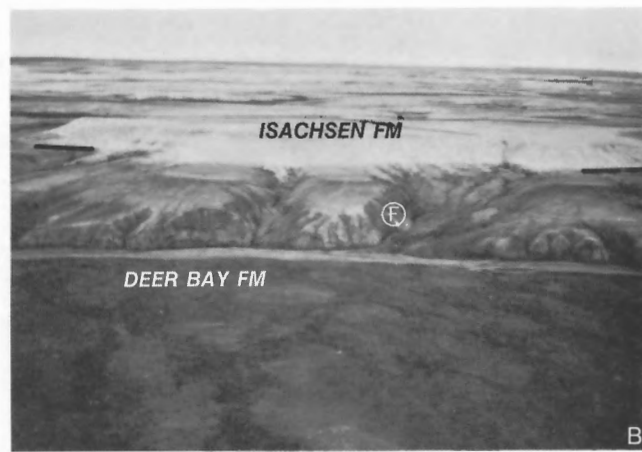
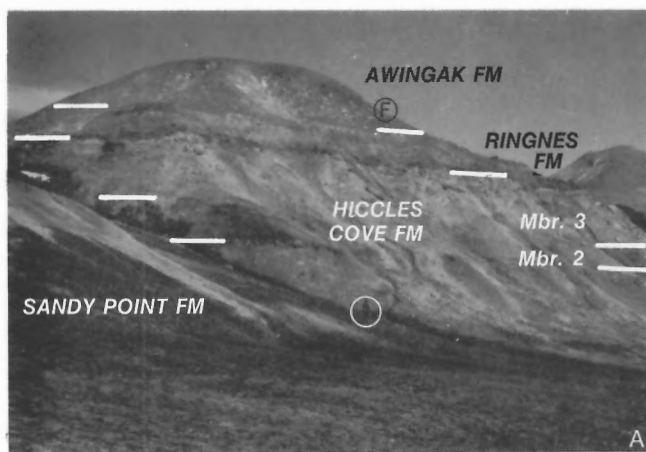


Figure 87. Field photographs of Middle Jurassic through Upper Cretaceous formations on Melville Island. Circled F, fossil locality. **A.** Jurassic section on the East Kitson River. Very thin Ringnes Formation strata (Oxfordian–Volgian) disconformably overlie the upper member of the Hiccles Cove Formation, and strata of the medial Hiccles Cove Formation (Callovian) disconformably overlie strata of the Sandy Point Formation (Aalenian). GSC fossil loc. C-127435 in the Awingak Formation is indicated (see Appendix 4). Base of Hiccles Cove to top of section is 31 m. Circled individual for scale. **B.** Disconformable contact between the Isachsen and Deer Bay formations, 8.6 km southeast of Sandy Point on Sproule Peninsula. GSC fossil loc. C-128829 in the upper Deer Bay Formation is indicated. The Deer Bay section exposed here is about 40 m thick. **C.** Conformable contact between the Isachsen and Christopher formations, 4.4 km southeast of Cape Grassy. GSC fossil loc. C-128178 in the lower Christopher is indicated. The Christopher Formation in this section is 12 m thick. **D.** Upper Christopher Formation strata and complete Hassel (80 m), and Kanguk formations, east-northeast of Chads Point, central Melville Island. Note the light coloured lower member and dark upper member of the Kanguk Formation. GSC locs. C-128849, 128851 in upper member are indicated. ISPG photos. 2887-1, -10, -30, -35.

50 to 294 m of interbedded greenish-grey weathering siltstone and very fine grained cemented and unce-mented sandstone arranged in numerous coarsening-upward cycles. Scaphopods, bivalves and ophiuroids are common. The Awingak Formation (up to 241 m) is composed of yellow weathering, fine grained, compacted or selectively cemented quartzose sandstone with scattered microscopic foraminifera, echinoid

spines, sponge spicules and plant debris. The transition from Awingak to age-equivalent Deer Bay Formation occurs at the surface near the Kitson River well (northwestern Melville; Fig. 82) and in the subsurface of Sabine Peninsula.

On the Sabine Peninsula seismic profiles, the Ringnes, Awingak and Deer Bay formations together

represent a distinct seismic interval bound above and below by laterally continuous reflectors (Section E, Note 7). This interval diverges northward as the formations thicken into the basin to a combined maximum of approximately 600 m on northern Sabine Peninsula.

Beyond the Sverdrup Basin, the Awingak Formation also occurs in fault-bounded outliers in the extreme southwestern part of the island (Comfort Cove and Cape Russell). In these areas the Awingak Formation includes up to 170 m (upper contact not seen) of sandstone, pebbly sandstone and minor mudrock and conglomerate (to cobble grade). The base of the formation disconformably overlies the (Upper Devonian) Beverley Inlet Formation.

Age. Dinoflagellate and foraminifera assemblages collected from the Ringnes Formation range from Oxfordian through Volgian in age (Fig. 77; report of Wall in Appendix 4). This overlaps the age range of the Awingak Formation on Axel Heiberg Island (Wall, 1983). The Awingak Formation near Comfort Cove on southwesternmost Melville Island contains a large and diverse bivalve assemblage that firmly dates the formation as Early Volgian. The Awingak Formation on the East Kitson River is also Volgian (reports of Jeletzky and Poulton, in Appendix 4). Similarly, the youngest exposed beds of the Deer Bay Formation on Sproule Peninsula are also Volgian as indicated by contained foraminifera (report of Wall, Appendix 4). Dinoflagellates in the upper part of the Deer Bay Formation in the Sandy Point L-46 well include *Lithodinia(?)* sp. B., which occurs within dinoflagellate Oppel zone N of Early Cretaceous (Berriasian) age (Davies, 1983, 1985).

Gabbro (KG)

References. Balkwill and Fox (1982); Tozer and Thorsteinsson (1964).

Description. Igneous rocks of gabbroic composition have been identified: 1) within a series of three, dextral, en echelon dykes intruding Canyon Fiord and Great Bear Cape formations east of Tingmisut Lake, southeastern Sabine Peninsula (Fig. 78); 2) as discontinuous cone sheets and irregular bodies intruding Otto Fiord Formation evaporites of Barrow and Colquhoun domes, northern Sabine Peninsula (Fig. 181); and 3) in borehole-penetrated intervals of the Chads Creek B-64, Drake Point D-68, Marryatt K-71, and Sherard Bay F-34 wells (Majid, 1989; compiled on Table 4). In addition to the above occurrences, sills and intrusive sheets (some intersected by exploratory wells) can also be identified on numerous reflection profiles of southern and central Sabine Peninsula (Section E). The sills follow bedding planes in the Hare Fiord, Trappers Cove and Van Hauen formations, and are also seen to cut upsection at shallow angles (0-30°) through seismically defined sedimentary layering. The Tingmisut Lake dykes are also part of a much larger swarm of subsurface dykes defined by a series of linear magnetic anomalies that extend from central Melville Island in the south to Isachsen Peninsula of northwestern Ellef Ringnes Island in the north (see also Chapter 7 and Balkwill and Fox, 1982).

Age. Balkwill and Fox (1982) quote isotopic ages of 123 ± 6 Ma (approximately Barremian-Aptian) for a gabbro sample collected from the Tingmisut dykes, and 131 ± 6 Ma (Hauterivian-Barremian) and

TABLE 4
Occurrence of gabbroic intrusive rocks in borehole-penetrated intervals of Sabine Peninsula

Well	Interval (m)	Intruded formation	Intruded rock types
Chads Creek B-64	3401-3453	Van Hauen (upper)	chert, siltstone
	4435-4451	Van Hauen (lower)	siltstone
Drake Point D-68	4681-4767	Trappers Cove	siltstone
	4883-4946	Hare Fiord (upper)	mudrock
Marryatt K-71	4507-4561	Van Hauen (lower)	siltstone
Sherard F-34	3500-3533	Van Hauen (lower)	mudrock

152 ± 6 Ma (Oxfordian–Volgian) for borehole-penetrated gabbro bodies of Sabine Peninsula (radiometric technique not quoted). Paired normal faults, spatially and kinematically linked to the emplacement of the subsurface sills of Sabine Peninsula are observed on reflection seismic profiles (Section E) to die out upsection in growth-faulted Christopher Formation (Albian).

On Axel Heiberg and northwestern Ellesmere islands, Embry and Osadetz (1988) have identified tholeiitic volcanic flows interstratified with sandstones of the Paterson Island (Barremian) and Walker Island (Aptian) members of the Isachsen Formation, as well as below and at a level equivalent to the Kanguk Formation (latest Albian through Campanian in this area). Bentonite is also common in the upper part of the Kanguk Formation of Sabine Peninsula.

Isachsen Formation (KI)

References. Heywood (1957); divided into three members by Embry (1985b).

Description. The Isachsen Formation is widely exposed on northwestern Melville Island and in a narrow belt extending across southern Sabine Peninsula. The formation also occurs in three outliers of southeastern Melville Island (geology map, in pocket). In the northern belt, the Isachsen Formation consists of 90 to 200 m of white to light yellow weathering, coarse to fine grained quartzose sandstone, siltstone and minor mudrocks, and coal. The formation is loosely consolidated and uncemented at the surface. Nevertheless, the formation is moderately resistant to erosion. The basal section, where it overlies the Awingak or Deer Bay formations, is represented by a low escarpment (Fig. 87B). The Isachsen Formation in outcrop and on borehole logs of southern Sabine Peninsula is divisible into three members. These include, from the base: the Paterson Island Member (KIP, white weathering coarse grained sandstone with clast-supported chert pebble conglomerate at the base); the Rondon Member (KIR, siltstone and mudrocks); and the Walker Island Member (KIW, fine to medium grained sandstone, carbonaceous sandstone and minor coal; Fig. 87C). In the Sverdrup Basin area, the base of the Isachsen Formation is a major unconformity. Erosional features, including channelling, are observed on some seismic profiles, and reflections generated by sandstone-on-shale impedance contrasts in the underlying Deer Bay Formation are cut out southward beneath the sub-Isachsen surface (Section E, Notes 7, 8).

Beyond the Sverdrup Basin, the Isachsen Formation has overstepped the entire underlying Carboniferous

through sub-Aptian Lower Cretaceous succession. The base of the formation is a major angular unconformity on which the basal conglomerate and sandstone of the Isachsen Formation are seen to variably overlie folded strata of Middle and Late Devonian ages (Hecla Bay, Beverley Inlet and Parry Islands formations; Fig. 51). The Isachsen Formation in the southeast includes up to 23 m of coarse and medium grained quartzose sandstone (in part pebbly), lignite coal, clast-supported cobble conglomerate, siltstone and minor mudrock. The coal seams in the outliers are laterally extensive and locally up to several metres thick. In one section located near a proximal depositional limit along the southern edge of the Bridport outlier, the entire Isachsen Formation interval is cobble grade clast-supported conglomerate. The general depositional setting for the Isachsen Formation in the outliers is one of transgressive sandstone-dominated channel fill occupying erosional depressions on the post-Devonian peneplain surface.

Age. The Paterson Island Member of the Isachsen Formation has failed to yield reliable biostratigraphic material, although dinoflagellates extracted from composited samples of cuttings from the lower part of the formation in the Sandy Point L-46 well have an extended age range between middle Valanginian and Barremian (Fig. 77; Davies, 1985; E.H. Davies, pers. comm., 1992). The Rondon Member of the Isachsen Formation on southern Sabine Peninsula contains a late Barremian to early Aptian foraminifera assemblage. Foraminifera in the Isachsen Formation of northwestern Melville Island (Cape Grassy) and southeastern Melville Island (Mecham and Beverley Inlet areas) are generally dated as late Early Cretaceous (Barremian, Aptian and/or Albian). On the Sverdrup Basin margin and beyond the Sverdrup Basin, the base of the formation is mostly post-Hauterivian, and in the absence of the Rondon Member, may be entirely Aptian (reports of Wall in Appendix 4).

Christopher Formation (KC)

References. Heywood (1957); divided into two locally mappable members by Embry (1985b).

Description. The Christopher Formation is widely exposed throughout central Sabine Peninsula (570–960 m thick) and on Emerald Isle. Extensive outliers also occur on northwestern and southeastern Melville Island, where up to 75 and 73 m of section, respectively, are preserved beneath disconformable Cenozoic cover. The Christopher Formation gradationally overlies the Isachsen Formation in most areas and consists of recessive black and dark grey weathering mudrocks, minor siltstone and ripple crosslaminated very fine

grained sandstone (Fig. 87C). Bioturbation is common and all three rock types can be found intercalated and interlaminated. On Sabine Peninsula, the formation is divisible into two members. The Invincible Point Member (KCI) below, comprising interbedded, laminated and ripple crosslaminated sandstone, siltstone and shale; and the MacDougall Point Member (KCM) above, which is darker, more recessive and consists almost entirely of black mudrocks with common ferruginous ironstone concretions.

On southeastern and central Melville Island, there are numerous exposed riverbank sections where the Christopher conformably overlies the Isachsen Formation and where the latter occurs in erosional depressions on the peneplained salt-based fold belt. In addition, a thin, flat-lying veneer (to 10 m) of Christopher Formation also oversteps the Isachsen Formation and in these circumstances is widely preserved, lying directly on the eroded roots of the folded Devonian siliciclastic formations. These intervals of Christopher Formation possess a relatively uniform thickness but are composed internally of unstratified grey to dark grey mud. These deposits are almost universally represented in cryogenically disturbed incised stream bank slopes, the upper surfaces of which include erosional remnants of the Beaufort Formation and an ubiquitous litter of embedded glacial erratics.

Age. The Christopher Formation, where it overlies the Isachsen Formation on the Mecham River (southeastern Melville Island) contains foraminifera and ostracodes of probable early Albian age (Fig. 77). Similarly, the thin but extensive Christopher Formation, where it lies directly and unconformably on the folded Devonian, contains at two localities a diagnostic assemblage of Albian forams and dinoflagellates (Wall, pers. comm., 1992; McIntyre, pers. comm., 1992). Typical Christopher Formation exposed at Cape Grassy has yielded a general late Early Cretaceous foraminifera fauna (report of Wall in Appendix 4).

Hassel (KH) and Kanguk (KK) formations

References. Heywood (1957); Souther (1963); Tozer and Thorsteinsson (1964).

Description. The Hassel and Kanguk formations are restricted in distribution on Melville Island to central and northern Sabine Peninsula. The Hassel Formation (Fig. 87D) includes 80 to 220 m of recessive, loosely compacted, but uncemented, medium and coarse grained quartzose sandstone, variably pebbly and

carbonaceous. The Hassel Formation gradationally overlies the Christopher.

The Kanguk Formation (370 m on northern Sabine Peninsula), although consisting principally of shale and mudrock, is more resistant to erosion. Two informal members of the Kanguk are distinguished on central Sabine Peninsula (Fig. 87D): 1) a lower grey weathering, platy, siliceous shale with intercalated spiculitic fissile chert and common radiolarians, foraminifera, siliceous sponge spicules, fish fragments and teeth, and rare diatoms; and 2) an upper dark grey, brownish grey and greenish grey fissile mudrock unit with numerous yellow interbeds of bentonitic clay. The lower contact of the Kanguk Formation was not observed. The medial contact between the two members of the Kanguk, represented by a topographic bench, is sharp but appears conformable.

Age. The Hassel Formation has not been dated on Melville Island. The probable age range, based on fossil collections from elsewhere in the Sverdrup Basin, is late Albian to Cenomanian (Thorsteinsson and Tozer, 1970; Wall, 1983). The upper informal member of the Kanguk Formation on central Sabine Peninsula contains a Late Cretaceous (Coniacian to Campanian) assemblage of radiolarians and diatoms (report of Wall in Appendix 4). In the eastern Sverdrup Basin, ammonites, bivalves and especially forams identified from the Kanguk Formation have a full age range from the Turonian to the Late Campanian (Wall, 1983).

Eureka Sound Group (KTE, TSB)

References. Troelsen (1950); Rahmani and Hopkins (1977); raised to group status by Ricketts (1986) and subdivided by him into four mappable units that from the base include the Expedition, Strand Bay, Iceberg Bay, and Buchanan Lake formations. A competing stratigraphy for a revised Eureka Sound Group in the Arctic Islands that includes six formations defined primarily on the basis of contained lithofacies has also been proposed by Miall (1986).

Description. The base of the Eureka Sound Group exposed in a stream bank section west of Colquhoun Dome has been described by Rahmani and Hopkins (1977) as conformable and gradational with the underlying Kanguk Formation, and is placed below the first appearance of grey sand in the section. Two units of the Eureka Sound Group on northernmost Sabine Peninsula are here tentatively assigned to Rickett's (1986) Expedition and Strand formations (Fig. 76). The Expedition Formation (KTE) on Sabine Peninsula, also broadly similar to Miall's (1986) Mount Bell and Vesle

Fiord formations, includes some 230 m of planar laminated and trough cross-stratified, white weathering quartzose sandstone with common slightly coalified wood, twigs, fossil cones and logs. The overlying Strand Bay Formation (TSB), similar to Miall's Mount Lawson Formation, consists of grey-brown and dark grey mudrock with quartz sandstone interbeds occurring in the uppermost exposures. About 50 m is preserved below unconformable Quaternary and Holocene cover. The contact between the two formations of the Eureka Sound Group is sharp but apparently conformable.

Age. The Expedition Formation on Sabine Peninsula contains the Maastrichtian-Paleocene boundary (as dated by palynomorphs; Fig. 77) in a sandstone interval situated approximately 20 m above the base of the formation (Rahmani and Hopkins, 1977). The age of the Expedition Formation in the vicinity of the type section at Strand Fiord on Axel Heiberg Island ranges from Campanian or Maastrichtian at the base through Early Paleocene (Ricketts, 1986).

The Strand Bay Formation on Sabine Peninsula contains rare specimens of Paleocene(?) foraminifera including *Cyclamina* sp. and *Trochammina* sp. (Wall, pers. comm., 1987) and a fine assemblage of Late Paleocene palynomorphs (report of McIntyre in Appendix 4). The palynomorph ages are entirely younger than the early to middle Paleocene mudrocks of the type section Strand Bay on Axel Heiberg Island, and instead appear to indicate a mudrock facies that is age equivalent to sandstones assigned by Ricketts (1986) to the lower part of his Iceberg Bay Formation.

Beaufort Formation (TB)

References. Tozer (1956); correlative deposits on Melville Island assigned to Beaufort Formation by J.G. Fyles (in Tozer and Thorsteinsson, 1964).

Description. The Beaufort Formation is a north-west-dipping and thickening wedge-shaped sand deposit of the Arctic Coastal Plain widely exposed on Banks, Prince Patrick, Brock, Borden, Ellef Ringnes and Meighen islands. Outliers, possibly correlated with the Beaufort Formation, are also found on central and eastern Melville Island. Typical occurrences are within steep-sided and stream-dissected flat-topped hills occurring individually or in clusters, and commonly overlying more extensive deposits of the Christopher Formation. These hills may represent the erosional remnants of a blanket deposit once continuous with the Arctic continental terrace wedge.

Several exposures examined by the author include deposits up to tens of metres thick of clast-supported, stratified gravel containing well-rounded pebble and cobble grade clasts to 60 cm in a coarse sand- or void-filled matrix. Clast compositions comprise locally derived Devonian sandstones and coal as well as far-travelled materials such as clasts of granite and gneiss derived from the Precambrian Shield, Paleozoic limestone, white laminated chert and dolostone. The Beaufort Formation of the Arctic Coastal Plain is often recognized by the common occurrence of uncoalified wood and peat layers. Isolated occurrences of wood and peat are also known from the outliers on Melville Island (Fyles, pers. comm., 1991).

Uncertainty exists in the discrimination of Beaufort Formation outliers and Quaternary ice-contact deposits of central Melville Island and Dundas Peninsula as described and mapped by Hodgson et al. (1984). Part of the confusion lies in the common steep-sided shape of the outliers and the similar grade and composition of the contained gravels. In addition, centimetre-scale marine bivalve fragments and angular erratics (up to 2 m) of obvious glacial origin are commonly found littering the surface of both the Quaternary and Beaufort deposits.

Age. The occurrence of uncoalified wood in the Beaufort Formation outliers of Melville Island points to the existence of either continuous or localized forest cover, a condition that may have ended as late as the Late Pliocene or Early Pleistocene in this part of the Arctic Islands (Funder et al., 1985). The oldest pre-orogenic deposits (situated on northern Sabine Peninsula) are Late Paleocene. Matthews et al. (1987) pointed out that the flora occurring in the Beaufort Formation *sensu stricto* of Prince Patrick Island are similar to and not younger than the early Late Pliocene of Meighen Island. However, they do not rule out the possibility of older Beaufort Formation on Prince Patrick Island. The Beaufort-like outliers on Melville Island are probably Pliocene. However, since these deposits lie outside the known belt of Eureka deformation, the possible age range could fall anywhere between the Late Cretaceous and the Early Pleistocene.

Quaternary (Q)

References. Barnett et al. (1975); Hodgson et al. (1984); Hodgson (1989).

Pleistocene and Holocene deposits include modern and ancient fluvial and deltaic deposits, marine sediments and marine-modified bedrock on raised

beach terraces, weathered bedrock as colluvium, talus fans or felsenmeer, varved marine or lacustrine silt, till, and peat. These materials, forming a variable and generally thin veneer over bedrock, have been ignored in mapping except where the nature of bedrock cannot be determined with confidence because of either complex structural relations or widespread cover. Land areas of mapped Quaternary cover include the islands in Hecla and Griper Bay, and the delta emptying into Sherard Bay on the east side of Sabine Peninsula. Also considered to be Quaternary is stratified, flat-lying, post-orogenic cover on the inter-island channel floor, and incised valley fill observed on seismic profiles to unconformably overlie tilted and eroded Kanguk Formation near Vesey Hamilton Island (Fig. 182). Maximum indicated thickness of these offshore deposits is 110 m (or 110 m at 2 km s⁻¹). A similar flat-lying veneer of post-orogenic cover occurs on the floor of M'Clure Strait southwest of Cape Russell at a water depth of nearly 500 m.

Age. Marine and marginal marine Quaternary deposits are primarily associated with the most recent Pleistocene (Late Wisconsinan) glaciation and with post-Late Wisconsinan flooding and subsequent uplift and emergence of low relief areas of the island. On Dundas Peninsula and coastal southeastern Melville Island, Quaternary deposits also include tills of probable Early and/or Middle Pleistocene, and Early Wisconsinan ages (Hodgson et al., 1984; Hodgson, 1989; Vincent, 1989). Far-travelled erratics of central and northern Melville Island, and the offshore seismic Quaternary deposits near Vesey Hamilton Island are probably Early and/or Middle Pleistocene in age because the Late Pleistocene continental ice sheet is not known to have extended north of Dundas Peninsula and coastal southern Melville Island.

Summary of Carboniferous through Quaternary sedimentation

Aspects of the deformation of the Sverdrup Basin succession are dealt with in Chapters 7 to 9. The following paragraphs summarize the major tectonic adjustments of the basin and its margin in the Melville Island area as revealed by depositional facies belts. These adjustments occurred 1) prior to Early Carboniferous rifting; 2) after the Melvillian Disturbance in the late Early Permian (which marks the end of the late Paleozoic rifting phase of the Sverdrup Basin); 3) after the Early Jurassic, when thermal subsidence of the Sverdrup Basin about east-west lines gave way to some sublongitudinal facies belts influenced by the onset of rifting parallel to the Arctic continental margin; 4) after a mid-Early

Cretaceous marine expansion marking the end of the previous rifting phase; and 5) prior to inversion of the western Sverdrup Basin during the mid-Tertiary Eurekan Orogeny.

In general, all formations deposited after the late Paleozoic phase of rifting are observed to thicken and fine progressively in a northerly direction (Fig. 75; Sections E and J). Proximal siliciclastic formations (sandstone, mudrock and lesser conglomerate) occur in the outcrop belt, while Permian and lesser Upper Triassic limestone occur within important subsurface stratigraphic intervals of central Sabine Peninsula. Northerly facies changes from sandstone and limestone to mudrock and chert occur in the subsurface Permian (Asselian through Artinskian, and Roadian–Wordian) of northern Sabine Peninsula. Limestone is absent above the Triassic. Proximal (south) to distal (north) facies changes in siliciclastic strata dominate the Jurassic and younger formations of the Sverdrup Basin. Departures from this pattern are summarized below with emphasis on observations collected from surface geology.

Early Carboniferous (Serpukhovian) through Early Permian (Artinskian)

The onset of Sverdrup Basin rifting in the Melville Island region predates the deposition of Namurian and Bashkirian evaporites of the Otto Fiord Formation, now only exposed in diapiric structures of Sabine Peninsula and adjacent offshore areas. Division of the rift margin into local depocentres and intrabasinal uplifts (horsts) characterized the period of deposition of the Canyon Fiord Formation from the Bashkirian through the Sakmarian (Fig. 161). Conodont biostratigraphy points to rapid rift-related subsidence and sediment accumulation during the Moscovian (75–120 m/m.y.) and lower rates from the Asselian through the Artinskian (max. 40–45 m/m.y.).

Early Permian (Roadian) through Early Triassic

The saucer-shaped configuration of the post-rift Sverdrup Basin dates to the late Early Permian (Roadian) when rift-marginal Canyon Fiord sub-basins were folded and inverted during the Melvillian Disturbance. In the subsurface of central and northern Sabine Peninsula, sediment accumulation rates rose progressively from the Roadian (max. 120 m/m.y. for the lower Van Hauen) through the Early Triassic (max. 260 m/m.y. for the Blind Fiord and Bjorne formations).

In the basin marginal belt of southern Sabine Peninsula, Roadian sedimentation included proximal facies conglomerate and coarse cherty sands derived from the Canyon Fiord Formation and redeposited in a southwesterly derived clastic wedge of the Sabine Bay Formation that fringed the mid-Early Permian uplifted region of northwestern Melville Island (Fig. 175). Preserved Roadian through Paleocene strata document subtle changes in the shape and tectonic forces acting on the Sverdrup Basin. In the outcrop belt, Roadian through Lower Triassic strata are thickest on southern Sabine Peninsula. Tracing these strata in outcrop, the Sabine Bay Formation of Sabine Peninsula progressively cuts out the Great Bear Cape Formation between Hiccles Creek and southwestern St. Arnaud Hills (Fig. 82). All Lower Permian formations are also cut out to the west beneath Upper Permian Trolld Fiord Formation. Cobble conglomerate containing Devonian sandstone clasts occurs in a proximal facies of the Trolld Fiord Formation west of Green Creek on the north flank of the Raglan Range. Likewise, the Bjorne Formation (Lower Triassic) cuts out the Upper Permian section toward the northwest and is thinnest and most proximal to sediment source areas in the northwesternmost exposures of Sproule Peninsula. Conglomerate clasts in the Bjorne Formation north of Marie Bay are also derived from southerly terrains underlain by Devonian sandstone. Westward thinning of the Bjorne Formation is attributed to a combination of reduced Early Triassic sediment accumulation rates on the most proximal portions of the basin margin, and erosion beneath unconformable Lower Jurassic cover.

Middle Triassic through Middle Jurassic (Bajocian)

Middle Triassic through Lower Jurassic (Hettangian) strata are confined to the subsurface of Sabine and Sproule peninsulas while Sinemurian through Bajocian strata also occur in a thin interval of mudrock, sandstone, and intervening unconformities exposed across northern Melville Island (Lougheed Island, Jameson Bay, Sandy Point and McConnell Island formations). Low sediment accumulation rates characterize most of the time interval, with starved offshore marine conditions in all areas for all of latest Triassic (Rhaetian) through Middle Jurassic (Bajocian) time. In general, the thickness and proportion of sand in the section increase to the northeast out of the map area. Accumulation rates range from a Middle Triassic maximum of 25 m/m.y. through a latest Triassic–Early Jurassic minimum of 5 m/m.y., rising again to 20 m/m.y. during the Middle Jurassic. Thickness and

accumulation rates are much higher near the depocentre of the so-called Late Triassic–Early Jurassic Heiberg delta complex (Embry, 1982) of the central Sverdrup Basin (western Axel Heiberg Island).

Regional thickness and facies patterns of subsurface Middle Triassic through Middle Jurassic formations are summarized in Embry (1991, 1993), and Johannessen and Embry (1989). In contrast to the outcropping Lower Permian through Lower Triassic succession, the oldest and thickest Jurassic sections are exposed in the northwest (near Marie Heights on Sproule Peninsula).

Middle Jurassic (Bathonian) through Early Cretaceous (Valanginian)

Modest sediment accumulation rates in the west began with deposition of the McConnell Island Formation in the Bathonian (3 m/m.y.) and continued through the period of deposition of the Hiccles Cove (4 m/m.y.), Ringnes (3 m/m.y.) and Deer Bay (17 m/m.y.) formations (Bathonian through Volgian). New sources of siliciclastic sediment are recognized in the Bathonian and Callovian deltaic wedges of the Hiccles Cove Formation, which are thickest and most proximal to source on westernmost Sproule Peninsula at the west end of the island. A third westerly derived deltaic wedge is represented by Volgian strata of the Ringnes, Awingak, and Deer Bay formations. Outcropping Volgian sections are thickest in the northwest and most proximal to source (coarse sand and conglomerate) in outliers near Comfort Cove in the southwest. A widespread depositional hiatus spans the pre-Valanginian Early Cretaceous.

Early Cretaceous (Valanginian) through Paleocene

The Isachsen and conformably overlying formations were deposited both within the Sverdrup Basin depocentre and beyond it. During this time interval, siliciclastic and mudrock sediment accumulation rates within the depocentre of northern Sabine Peninsula were moderate for Barremian to Aptian (max. 16 m/m.y.) and Cenomanian through Paleocene (max. 15–25 m/m.y.) times and very high during the Albian (100 m/m.y.).

A Barremian to earliest Albian near depositional limit of the Isachsen Formation is defined by proximal conglomerates exposed in the southernmost outcrops

of the Bridport Inlet outlier. The Christopher Formation (Albian deltaic mudrock) conformably overlies the Isachsen in the three outlier areas of central and southeastern Melville. The Christopher also oversteps the Isachsen and, over a wide area of eastern Melville Island, rests directly on folded Devonian "basement". Mudrock and sandstone accumulation was possibly continuous from the Aptian through to the Maastrichtian during deposition of the Isachsen, Christopher, Hassel and Kanguk formations of central and northern Sabine Peninsula. Deltaic Maastrichtian sandstone is also apparently continuous with lower Paleocene strata in the lower part of the Expedition Formation of northern Sabine Peninsula, although an unrecognized depositional hiatus in sandstone is likely across the Cretaceous/Tertiary boundary.

A western Sverdrup Basin depocentre became separated from other basins of the eastern Arctic during part of Maastrichtian and Paleocene time by exposure of Cornwall Arch; a northerly trending high centred on Amund Ringnes and Cornwall islands (Balkwill, 1983; Miall, 1986). Cornwall Arch became inactive in the Early Eocene (McIntyre and Ricketts,

1989). Quartz sands deposited over the hinge of Cornwall Arch at this time are entirely younger than prodeltaic mudrocks of the Strand Bay Formation of northernmost Sabine Peninsula. Tertiary sedimentation in the western Sverdrup Basin was terminated by regional uplift and related tectonic effects of the culminating mid-Tertiary phase of the Eurekan Orogeny.

Neogene and Quaternary

Post-orogenic Pliocene(?) deposits of the Arctic continental terrace wedge are represented by outliers of the Beaufort Formation on eastern and central Melville Island that contain preserved remains of uncoalified wood and peat. The preserved extent of this once widespread and potentially continuous deposit of the Arctic continental terrace has been much reduced by Pleistocene and Holocene exposure and fluvial dissection. The Quaternary stratigraphic record includes evidence of at least three glacial advances of Early and/or Middle Pleistocene, and Early and Late Wisconsinan (Late Pleistocene) ages.

CHAPTER 5

OVERVIEW OF THE STRUCTURE OF THE MELVILLE ISLAND REGION

Field data acquisition and geological mapping

The 1:250 000-scale geology map prepared for this study (in pocket) has been compiled from pre-existing maps (both published and unpublished), interpreted aerial photographs, aerial reconnaissance and ground traverse observations, and interpreted seismic reflection profiles.

Fundamental data incorporated into the present work were obtained from Tozer and Thorsteinsson's (1964) geology map of the Western Queen Elizabeth Islands published at a scale of 1:500 000. The geology of Sabine Peninsula was redrafted from a 1:125 000-scale unpublished preliminary map compiled by H.R. Balkwill, with additional observations added during the present phase of field activities in the area. Geology of part of the outcrop belt exposed along the north shore of Marie Bay was obtained from unpublished field maps of H.P. Trettin, simplified

versions of which appear in Trettin and Hills (1966). Unpublished photogeology maps of the island (1:60 000 scale), prepared by J.C. Sproule and Associates Limited, were also available to the writer and were occasionally consulted.

Fieldwork included the interpretation of a complete set of vertical aerial photographs (1262 stereoscopic pairs), aerial reconnaissance mapping by helicopter, and related data acquisition during foot traverses. Structural measurements and kinematic data were collected with a damped Brunton compass. The magnetic north pole in 1985 was situated off the southeast coast of nearby Loughheed Island at 77°N, 103°W. At that time, magnetic declination varied from 50°E through 68°E across the report area and substantial corrections for geographic location and diurnal variation (1–2°) were required. The inclination of the magnetic field increases eastward across the island from 87.5° to 89°. Compass use proved wholly unreliable near gabbro bodies, such as those exposed near Tingmisut Lake, which contain up to 10 per cent titanomagnetite. Kinematic data collected in such areas

were obtained by triangulation against local topographic features.

Overview of surface structure

Reference to the geology map of Melville Island (in pocket) is essential for a full understanding of the following overview of exposed structure. The major surface structural domains of Melville Island, previously classified and described by Tozer and Thorsteinsson (1964) include: 1) areas of undeformed lower Paleozoic strata exposed on Dundas Peninsula, 2) faulted areas of the Blue Hills in the southwestern part of the island, 3) regions of folded lower Paleozoic strata (eastern, central and northwestern Melville Island) and 4) relatively undeformed upper Paleozoic through Tertiary strata of the southern Sverdrup Basin exposed across the northern peninsulas.

The outstanding structural feature of Melville Island is the 200 km wide belt of linear, harmonic, sub-latitudinal folds exposed throughout the eastern half of the island (Fig. 89). The regional trend of these salt-based folds defines the western half of a foreland deformation arc that faces south on its convex side and is continuous across Byam Channel, Byam Martin Island, and Bathurst Island terminating against the west side of Boothia Uplift on eastern Bathurst Island (Fig. 88). On aerial photographs, the folds are outlined by alternating light and dark units. The light-coloured rocks include Silurian and Devonian carbonate units (Barlow Inlet? and Blue Fiord formations), and quartz sandstone units of the Devonian clastic wedge (Hecla Bay Formation and the Burnett Point Member and upper and lower units of the Consett Head Member of the Parry Islands Formation). The darker weathering units include the uppermost Cape De Bray, Weatherall, and Beverley Inlet formations, the Cape Fortune Member and medial mudrock unit of the Consett Head member within the Parry Islands Formation. Together all these surface units represent about 3 km of section repeatedly exposed at the surface by folding and subsequent erosion. Carbonate formations are in fact quite rare and only exposed in three areas around Weatherall Bay. These areas include the outcrops of Tingmisut Inlier, Spencer Range Anticlinorium and Towson Point Anticlinorium (geology map, in pocket; Figs. 39, 78).

Fault systems associated with the harmonic folds of eastern Melville Island include fold-parallel reverse faults with low sinuosity and relatively small displacement, fold-orthogonal normal and indeterminate faults, and various small oblique faults of uncertain

transport direction. Towson Point Anticlinorium is also associated with a system of easterly striking sinistral strike-slip faults and at least one high-sinuosity thrust fault that places Blue Fiord Formation carbonates on (younger) Cape De Bray mudrock and sandstone. Some of the faults associated with the Towson Point structure appear to continue across Weatherall Bay into Spencer Range and southern Sabine Peninsula, where the deformed rocks are mostly late Paleozoic in age.

The folds of eastern Melville Island continue to the southeast and east beneath Viscount Melville Sound and Byam Channel (Fig. 88). However, to the southwest on Dundas Peninsula, where salt at depth is transitional into anhydrite and carbonate, surface folds are seen to die away across strike by gradual loss of amplitude (see geology map in pocket and Fig. 88). The folds also die away to the west along strike above the western and northwestern limit of underlying salt. Disappearance of surface folds west of Liddon Gulf and Hecla and Griper Bay is associated with increased fold wavelength, reduced fold amplitude, and increased deformation by faulting. This transitional region at the edge of the salt-based fold belt also features a change in structural style and trend. Linear folds evolve westward into an en echelon set of doubly plunging anticlines (periclines). The dominant structural trend changes fairly abruptly from N70°W to variably N65–85°E. Nias Point Anticlinorium, situated within this transitional area, is characterized by a mix of these fold trends and a complex pattern of mostly fold-parallel faults, and oblique faults having a sinistral sense of offset.

The sinistral and oblique faults continue to the west, beyond the region of obvious folding, into a region of generally flat-lying, or tilted and faulted strata of southwestern Melville Island (Blue Hills Fault Belt of Tozer and Thorsteinsson, 1964). This area lies outside the salt-based fold belt where underlying rocks at the level of the salt probably lie in shelf carbonate facies. Differential erosion of exposed Hecla Bay and Beverley Inlet formations has readily permitted the identification of major and minor fault systems. Northerly and northeasterly-striking extension faults are also common in the Blue Hills, especially along the southwest coast where the Hecla Bay and Beverley Inlet formations and disconformable outliers of the Awingak Formation (Volgian) are all locally tilted and offset.

A distinct region of folded Paleozoic strata is also evident in the northwest, in a narrow, westerly trending belt extending from Hecla and Griper Bay to Kellett Strait (geology map, in pocket). Periclinal folds of

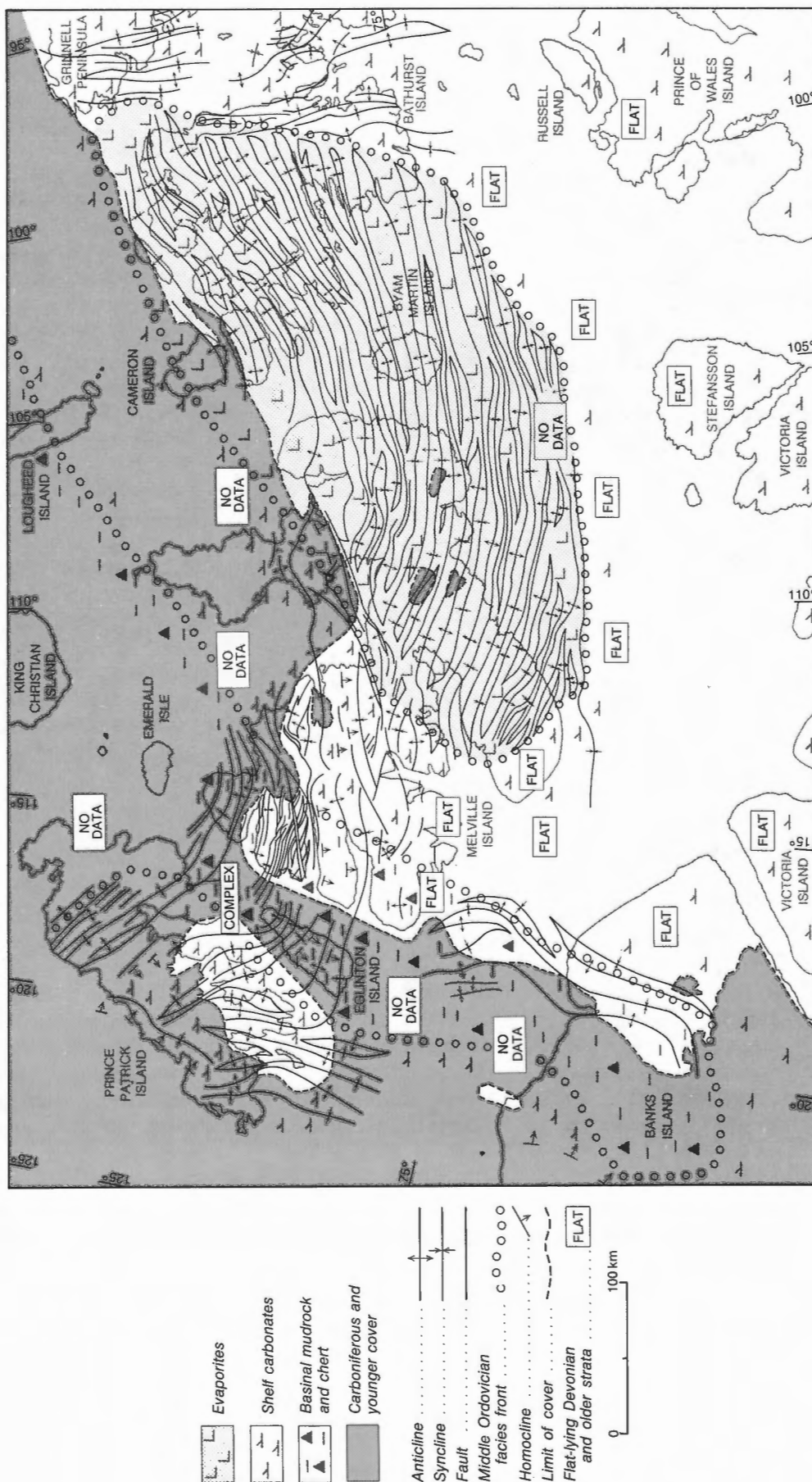


Figure 88. Fold trends in the Franklinian Mobile Belt of the western Canadian Arctic Islands. Structural trends of Viscount Melville Sound and M'Clure Strait are based on a reinterpretation of marine seismic reflection surveys and assessment reports of Baxendale (1972; for Magnorth Exploration Management Ltd.) and Norlands (1974, 1976). Banks Island data are based on assessment reports of Panarctic Oils Limited (van der Houwen and Schwartz, 1983) and Elf Oil Exploration and Production Ltd. (Beauchamp, 1974). Byam Channel and Byam Martin and Bathurst islands data are from Kerr (1974) and from unpublished 1:1 000 000 scale compilation maps by A.V. Okulich (pers. comm., 1990). Structural features of Fitzwilliam Strait and Eglinton and Prince Patrick islands are taken from Harrison et al. (1988) and Harrison and Brent (1991).



Figure 89. Oblique aerial photograph of the arcuate, easterly plunging fold belt of eastern Melville Island. Major folds (from right to left) include Robertson Point Anticline, Byam River Syncline, and Rea Point Anticline. The perpendicular fault pairs in the foreground that cross the eastern end of Sabine Bay Anticline are also spatially associated with linear aeromagnetic anomalies thought to represent unroofed Lower(?) Cretaceous mafic dykes (similar to those exposed near Tingmisut Lake; see also Figs. 78 and 177).

varying scale, and other structural culminations have exposed the Thumb Mountain and Cape Phillips formations in McCormick Inlet area (McCormick Inlet Anticlinorium), Bay Fiord through Kitson formations

in the faulted Kitson River Inlier (Fig. 33), and Canrobert through Ibbett Bay formations of the Canrobert Hills and southern Sproule Peninsula areas. It has long been recognized that rocks age equivalent to

the Bay Fiord evaporites are exposed at the surface in the Canrobert Hills and are found there in chert and graptolitic mudrock facies. Tozer and Thorsteinsson (1964) pointed out that the depth-to-detachment in this region must necessarily lie at some unknown depth in rocks of Early Ordovician, Cambrian or older age. Regional-scale uplift of all Canrobert Hills folds has brought to the surface older beds of the Blackley and Cape De Bray formations now preserved in exposed synclines. Folding has also produced overturning of strata in some parts of the Canrobert Hills, particularly in the front range north of Ibbett Bay, and while folding is most intense in Devonian and older rocks, the Canyon Fiord Formation has also been folded about east-west lines. Limits of folding in the Canrobert Hills are defined by: 1) sinistral en echelon folds of the Blackley Formation that die out upsection and also plunge to the southeast into the Cape De Bray Formation, 2) tight folds that plunge to the west beneath Kellett Strait, and 3) the distribution of Upper Permian and overlying unconformable cover.

The southern limit of folding and uplift against the Blue Hills fault belt is also defined by the south-facing Purchase Bay Homocline, which is exposed along the peninsula between Ibbett and Purchase bays. From the air (Fig. 90), Purchase Bay Homocline comprises sublatitudinal hog-back ridges with low-lying Cape De Bray Formation along the south shore of Ibbett Bay, Weatherall Formation (snow free) at intermediate elevations, and Hecla Bay Formation underlying the ice-covered axial high of the peninsula. Farther south, the Beverley Inlet Formation lies at the upper exposed limit of the homocline on a dissected dip slope north of Purchase Bay (geology map, in pocket). The homocline terminates to the east against Blue Hills Syncline and McCormick Inlet Anticlinorium, and to the west, where it is covered by the waters of Kellett Strait and unconformable Cretaceous cover of Eglinton Graben. Maximum structural relief on the homocline is approximately 7 km.

Major faults in the northwest include: the Kitson River Fault (a reverse fault with up to 6 km of stratigraphic separation across the faulted north end of Kitson River Inlier); the compressive, south-dipping Ibbett Bay Fault and associated splays, with up to 8.6 km of displacement in the Cape De Bray Formation and Weatherall formations of Purchase Bay Homocline; and two dextral wrench faults of the central Canrobert Hills (Nisbet Point and Hawk Creek faults) each displaying up to 2.5 km of lateral offset. Orthogonal normal faults and fold-parallel faults (some contractional) are also exceedingly common throughout the Canrobert Hills. Some of these also

displace the Canyon Fiord Formation. Only the largest faults are shown on the geology map (in pocket).

In contrast to the relatively intense deformation experienced by lower Paleozoic strata, the Sverdrup Basin succession remains nearly flat lying (Figs. 81, 86, 87). This is particularly true of Upper Permian and younger strata that possess bedding attitudes of less than 5° on the northern peninsulas. Carboniferous and Lower Permian strata, however, commonly dip at 0–30°. Upper Paleozoic strata are also affected by several phases of faulting and at least one period of folding. Worth noting is a 'klippe' of Canyon Fiord Formation situated 20 km east of the head of Ibbett Bay (geology map, in pocket; Fig. 169, Note 4; Fig. 170). Tilted strata in this outlier are truncated down-dip and on all sides by a horizontal detachment fault that places younger strata over older.

On southern Sabine Peninsula, the intensity of deformation appears to die out gradually upsection and to the north into the Trolld Fiord and Bjorne formations. West of Hecla and Griper Bay, folds and associated structures are mostly restricted to the Canyon Fiord Formation beneath a sub-Upper Permian angular unconformity.

Although Upper Permian and younger rocks are nearly flat lying, exposures are not entirely free of deformation. Broad folds outlined at the surface by Cretaceous and Paleocene strata on Sabine Peninsula include the Marryatt Point and Murray Harbour synclines and the intervening Drake Point Anticline (geology map, in pocket). Also worth noting in this area are two piercement diapirs; others are known in offshore areas of Byam Channel and Hazen Strait (west of Vesey Hamilton Island; Figs. 177, 180).

The Permian and younger rocks of northwestern Melville Island are represented in a simple northerly dipping homocline. The small, doubly plunging Marie Heights Anticline is situated near the updip limit of the homocline on the north shore of Marie Bay. Oil sand deposits are known from numerous exposures of the Bjorne Formation on the periphery of this structure, and all along the outcropping Lower Triassic belt as far east as Kitson River (Trettin and Hills, 1966; see also Chapter 9).

Faults in the post-Carboniferous succession are a mix of: 1) westerly striking normal and wrench faults that mostly die out upsection below the base of the Bjorne Formation (with one exception on Sproule Peninsula), and 2) N- through N45°E-striking normal faults that mostly die out upsection in the Christopher Formation.

Angular unconformities and peneplain surfaces

Angular unconformities and related peneplain surfaces serve to date the end of both major orogenic events

and lesser structural adjustments. In the Melville Island area, Phanerozoic angular unconformities occur:

1. Below the Canyon Fiord Formation (Ellesmerian Orogeny).

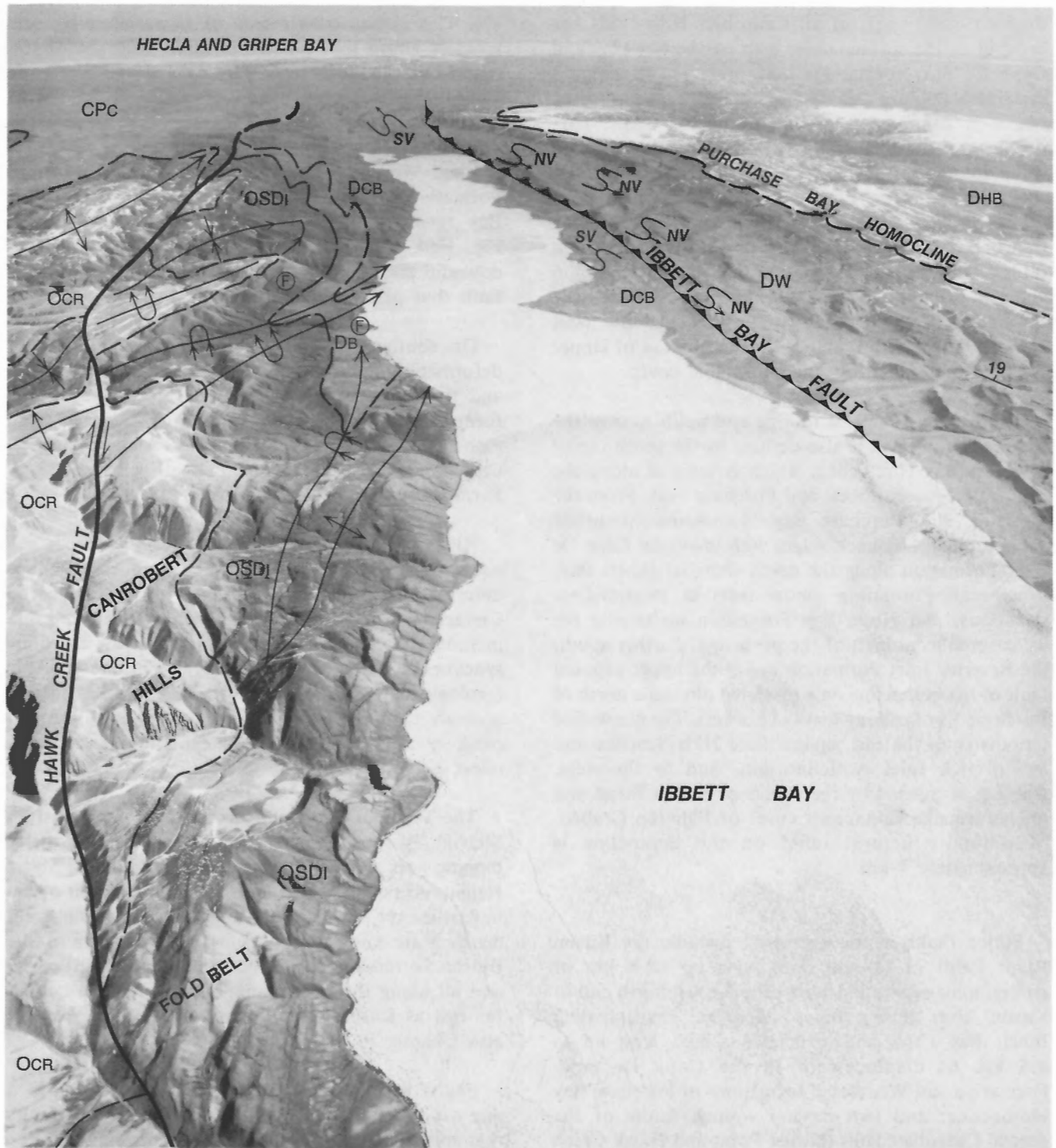


Figure 90. Oblique aerial photograph of the southern portion of the Canrobert Hills (left) fold belt, and part of Purchase Bay Homocline. Mesoscopic folds are labelled either south-vergent (SV) or north-vergent (NV). OCR, Canrobert Formation; OSDI, Ibbett Bay Formation; DB, Blackley Formation; DCB, Cape De Bray Formation; DW, Weatherall Formation; DHB, Hecla Bay Formation; CPC, Canyon Fiord Formation.

2. Below the Troid Fiord and Bjorne formations of Sproule Peninsula (Melvillian Disturbance).
3. Below outliers of the Isachsen and Christopher formations on southeastern Melville Island.
4. Below Beaufort Formation outliers (Eurekan Orogeny).
5. Below Quaternary and Holocene gravels.

In addition, faulted Volgian strata of the Awingak Formation rest with pronounced disconformity on Frasnian Beverley Inlet Formation in several small areas near Cape Russell and Comfort Cove, southwesternmost Melville Island.

Sub-Carboniferous unconformity (Ellesmerian Orogeny)

The Ellesmerian Orogeny is the term that Thorsteinsson and Tozer (1970) applied to the Arctic Islands-wide deformation that occurred during the time interval separating the youngest Devonian rocks involved in folding (mid-Famennian) and the oldest known post-orogenic cover (late Viséan; Utting et al., 1989b). Constraints on the beginning and end of Ellesmerian deformation vary from place to place depending on the age of the pre- and postorogenic rocks associated with each given structure. The timing constraints for the Ellesmerian Orogeny of Melville Island are summarized below.

On southern Sabine Peninsula and in Spencer Range, the lower clastic member of the Canyon Fiord Formation (Bashkirian-Moscovian) unconformably overlies broadly folded and tilted rocks of Silurian through Late Devonian (Frasnian) age within Spencer Range Anticlinorium (Sections C-E). Angularity of the unconformity ranges from 0 to 30°. Over the anticlinal hinge, the Canyon Fiord Formation generally overlies the Blue Fiord Formation; most of the Devonian clastic wedge has been removed during a pre-Late Carboniferous erosion cycle. The youngest preorogenic rocks on the south limb of Spencer Range Anticlinorium are middle Famennian in age (Consett Head Member of the Parry Islands Formation).

In McCormick Inlet area, the lower clastic member of the Canyon Fiord Formation lies with angular unconformity on folded mid-Ordovician (Thumb Mountain Formation) through middle Eifelian (Cape De Bray Formation) strata of McCormick Inlet Anticlinorium (Section I; Figs. 91C, D). The youngest conformable preorogenic rocks on the flanks of the

McCormick Inlet structure are mid-Frasnian (Beverley Inlet Formation).

North of western Raglan Range, the Canyon Fiord Formation is in fault contact with Lower Ordovician and younger strata of the Kitson River Inlier. Breccias in the Canyon Fiord Formation contain angular clasts of Ordovician to Silurian formations indicating exposure and erosion of rocks of this age during the Carboniferous.

East of Canrobert Hills, the lower clastic member of the Canyon Fiord Formation lies variably on Lower Devonian (Pragian?) through Middle Devonian (Givetian) strata (upper Ibbett Bay through lower Weatherall formations). Throughout the northern Canrobert Hills and north and south of Marie Bay, the Canyon Fiord Formation overlies folded rocks of pre-Givetian age. Angularity of the unconformity ranges to 90° (Figs. 91A, B). Seismic reflection profiles of Sproule Peninsula indicate that the Canyon Fiord Formation also rests unconformably on the lower part of the Ibbett Bay Formation, the Canrobert Formation, and even pre-Canrobert section assigned to Upper(?) Cambrian through Lower Ordovician seismic units sO and sEO.

Sub-Upper Permian unconformity (Melvillian Disturbance)

Thorsteinsson and Tozer (1970) applied the name Melvillian Disturbance to folded areas of northwestern Melville Island underlain by deformed Canyon Fiord Formation and unconformably overlain by the Troid Fiord Formation (Wordian). Strata assigned to the Troid Fiord Formation indeed rest variably on tectonized strata of Devonian, Carboniferous, and possibly Early Permian age in a belt running west from Hecla and Griper Bay as far as the head of Marie Bay (Figs. 33, 92A, B). Angularity of the unconformity ranges to 40° and may locally reach 60° in the subsurface. Structures presumably related to the same deformation unconformably underlie the Bjorne Formation along the entire north shore of Marie Bay. Seismic reflection profiles of Sproule Peninsula and northwestern Hecla and Griper Bay (Fig. 168) also indicate the effects of the Melvillian Disturbance in these areas. On Sabine Peninsula, the regional uplift associated with the Melvillian Disturbance is recorded by the disconformity that, toward the southeast, progressively cuts out the (Artinskian) Great Bear Cape Formation. The depositional record of the disturbance is preserved in proximal marine sandstones and chert pebble conglomerates of the Sabine Bay Formation (Roadian; Figs. 82, 83, 175; see also Chapter 7).



Figure 91. Selected examples of the sub-Carboniferous angular unconformity. **A.** Tilted Canyon Fiord Formation strata resting with pronounced angular unconformity on nearly vertical beds of the Blackley Formation. **B.** Detail of the unconformable contact between the Canyon Fiord and Blackley formations. **C.** The angular unconformity between basal conglomerate of the Canyon Fiord Formation and weathered shales of the upper Cape Phillips Formation, south edge of McCormick Depression, (exposure is on a tributary situated 5 km southwest of McCormick Inlet). **D.** Low-angle angular unconformity between the Canyon Fiord and Cape De Bray formations, west end of McCormick Depression, and 20 km west of McCormick Inlet. ISPG photos. 2887-1, -2, -6, -18.

Sub-Lower Cretaceous unconformity

Flat-lying outliers of Lower Cretaceous Isachsen and Christopher formations overlie the folded and peneplained roots of Middle and Upper Devonian strata throughout an extensive area of central and eastern Melville island (Figs. 51, 93A, 94, 95). The youngest preorogenic rocks are mid-Famennian strata of the Cape Fortune Member of the Parry Islands Formation. The oldest postorogenic strata are probably not older than Barremian and not younger than Late Albian (Appendix 4). While it is likely that the sub-Cretaceous folds were created during the Ellesmerian Orogeny (latest Devonian through early

Carboniferous), the stratigraphic relations described here do not rule out the possibility of some compressive deformation during the time interval between the Carboniferous and the pre-Isachsen Early Cretaceous.

Sub-Neogene(?) unconformity (Eurekan Orogeny)

In the eastern Arctic Islands, a regionally extensive angular unconformity separates Miocene and younger strata above from folded and commonly thrust faulted middle Eocene and older strata below (Balkwill, 1978; De Paor, et al., 1989). During the same time interval,

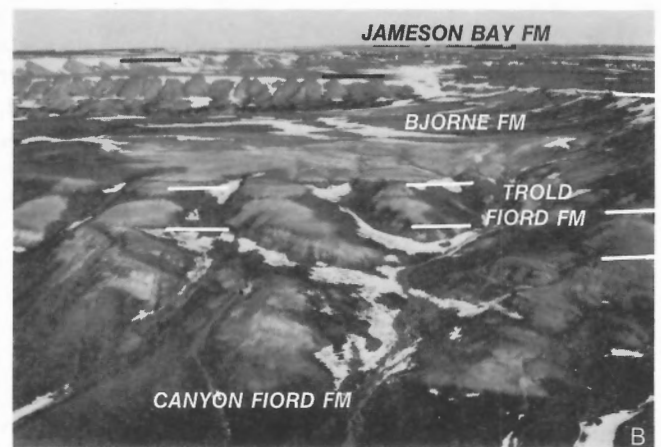


Figure 92. The sub-Permian angular unconformity in northwestern Melville Island. **A.** Two angular unconformities (on the west bank of the Kitson River, 4 km west of Kitson River Inlier); the Canyon Fiord Formation cuts out the Weatherall Formation, and the Canyon Fiord Formation is in turn cut out beneath flat-lying strata of the Trolld Fiord Formation. **B.** Detail of the angular unconformity between tilted strata of the Canyon Fiord Formation and flat-lying strata of the Trolld Fiord, BJORNE, and Jameson Bay formations (13 km west of Kitson River). ISPG photos. 2887-27, -66.

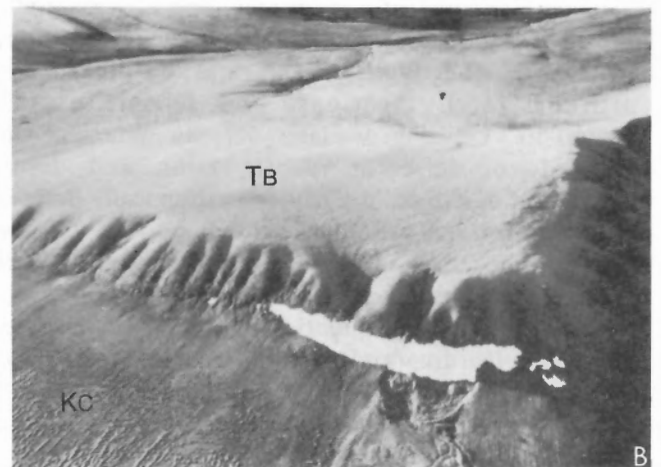
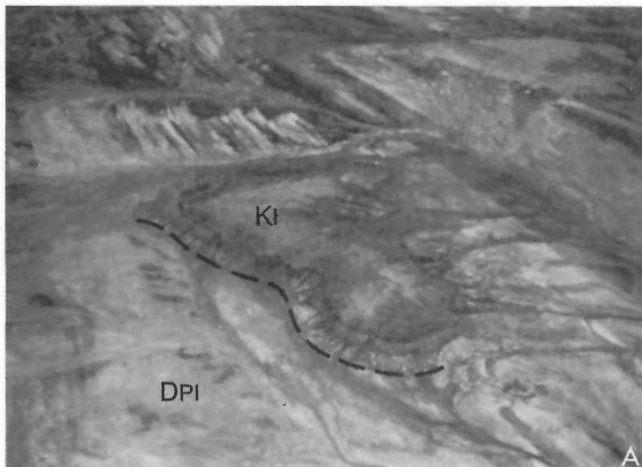


Figure 93. The sub-Cretaceous and sub-Tertiary unconformities on Melville Island. **A.** The sub-Lower Cretaceous angular unconformity between flat-lying outliers of the Isachsen Formation (KI), above, and folded and peneplained Devonian strata (DPI), below, Beverley Inlet area. **B.** Erosional remnants of the Beaufort Formation (TB) lying disconformably on dark coloured strata of the Christopher Formation (KC), eastern Melville Island. ISPG photos. 3152-2, 3896-2.

broad folds and piercement diapirs deformed Upper Paleocene Strand Bay Formation and all underlying units on Melville Island. The oldest post-Eurekan and post-Paleocene cover rocks are erosional remnants of the Pliocene(?) Beaufort Formation of central and eastern Melville Island (Fig. 93B). In this region, the Beaufort Formation disconformably overlies flat-lying and essentially undeformed Isachsen and Christopher formations (Figs. 93B-95). The tectonic significance of the erosional hiatus across the sub-Beaufort disconformity is limited to differences in thermal

maturity of contained organic matter. The Isachsen Formation contains lignite to subbituminous grade coal and has maximum vitrinite reflectance (%Ro) values of 0.37 to 0.49 Ro_{max}. (Goodarzi et al., 1993). In contrast, fossil wood in the Beaufort Formation is uncoalified.

Sub-Quaternary unconformity

Lower and/or Middle Pleistocene till, Upper Pleistocene tills, Upper Wisconsinan marine mudrocks

and gravels, raised beach and other periglacial deposits unconformably overlie folded and uplifted upper Paleocene and older strata of northern Melville Island, and uplifted and dissected Pliocene(?) and older deposits of southern Melville Island (Figs. 94, 95).

Structural cross-sections

Methods of construction

Ten regional structural cross-sections (Sections A through J, in pocket), have been constructed from the integration of surface geology and seismic reflection profiles. Wherever possible, the cross-sections are drawn perpendicular to structural grain while still taking full advantage of all available data sources. Many sections are intentionally coincident with seismic profiles (Fig. 3). The construction of each deformed-state section involved initial projection of all types of data onto the line of section including a topographic profile, stratigraphic contacts, large structural features (fold axes and faults), fault and bedding plane attitudes, well locations, and seismic profile shotpoints. Utilizing available velocity data and the methods of reflector identification and depth conversion described in Chapter 1, seismically defined structural features were then plotted, starting with the near-surface units and working downward. This process also involved the inclusion of borehole formation tops, extrapolation to depth of surface-mappable features and extrapolation to surface of seismically defined structures.

Fundamental thrust belt rules were applied in the construction of all sections. These rules include: 1) thrusts cut upsection in the direction of transport and tend to die out in folds; 2) competent bed thickness remains constant or varies in a systematic fashion consistent with all available well, surface, and seismic data; 3) a concentric style of folding is assumed unless evidence to the contrary is presented; 4) most major faults are listric in shape and tend to flatten downsection onto either an intermediate or through-going bedding plane detachment; 5) cut off angles of thrusts are steepest in strata of greatest competence; 6) older rocks are usually thrust over younger rocks; 7) rock is neither created nor destroyed by deformation; and 8) most important, the deformed-state cross-section should be palinspastically restorable. Other general rules applied to thrust belts, especially those rules concerned with vergence, kinematics and relative timing of fault movement, probably do not apply to the salt-based fold belt of Melville Island. Deformation kinematics are fully treated in Chapters 6 and 7.

To verify fault trajectories, primary depositional thickness variations, and interpreted structural style, a palinspastically-restored section has been constructed to accompany each deformed-state section. The balancing and restoration method began with the placement of a pin line through undeformed strata in the foreland and the placement of intermediate pins at intervals of approximately 12 km along each deformed-state section. The intermediate pins, generally located along the axes of synclines, merely serve to divide the cross-sections into smaller, more manageable blocks and do not imply that strata are undeformed at these points.

The fundamental techniques applied to completion of the structural cross-sections and restored sections are bed length balancing of rigid units and area balancing of ductile units. Bed length balancing is generally suited to concentrically folded units of competent character that retain primary depositional thickness in the deformed state. When successfully applied, bed lengths, measured along formational contacts, are identical on both the structural cross-section and the accompanying restored section. Where data permit, a series of formational contacts may be measured and, between the same set of pin lines, should all be of equal length on both restored- and deformed-state sections. Where slip on any given detachment cannot be dissipated by folding between adjacent pin lines, the excess slip is then carried backward and allowed to accumulate or dissipate elsewhere in the hinterland of the fold belt. Ductile units do not maintain constant deformed-state thickness. For these rock layers, cross-sectional areas are measured and restored to an identical area that also matches the restored length of intervening competent units.

Starting at the foreland pin (at pin 1 of Sections F and J), unit bed lengths and areas in the present study were measured between pin lines with the aid of a Lasico Model 1280 graphic digitizer. Conformable units of structurally competent character were iteratively line length balanced to within ± 0.1 km per pin line separation length. This has resulted in a cumulative error of ± 0.6 to ± 0.9 km per cross-section. Bed-length-balanced horizons on Sections A through I include unit seismic tops above Cambrian(?) units sC1A through sC0, and stratigraphic tops above the Eleanor River Formation, lower and upper members of the Bay Fiord Formation, Thumb Mountain, Cape Phillips (or seismic unit OSc), and Blue Fiord formations. On Section J, additional bed-length-balanced horizons include stratigraphic tops above the Canrobert Formation, the dolostone, lower black shale and upper black shale members of the Ibbett Bay Formation, and the Blackley Formation.

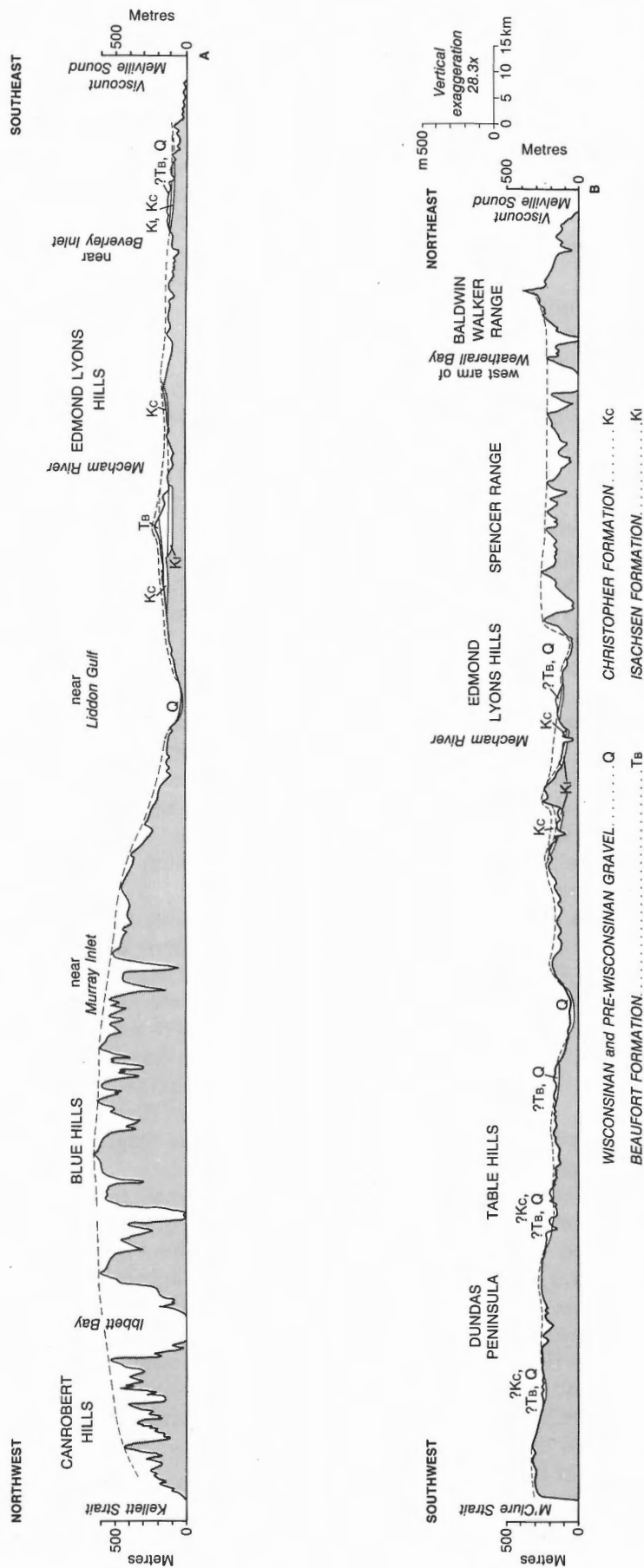


Figure 94. Cross-sections of the peneplain surface on Melville Island. Distribution of Wisconsinan (upper Quaternary) and pre-Wisconsinan gravels of the Dundas Peninsula and Liddon Gulf area has been taken from Hodgson et al. (1984). Lines of section are located on Figure 8.

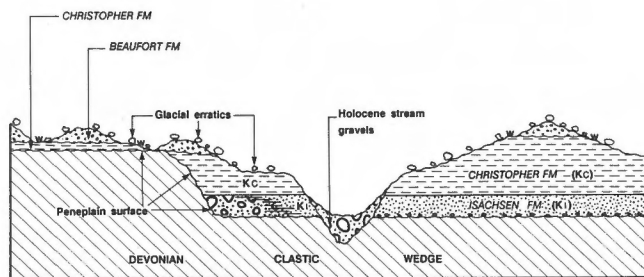


Figure 95. Schematic geological relations between the Isachsen, Christopher, and Beaufort formations and various Quaternary gravels deposited on the peneplained salt-based fold belt in central and eastern Melville Island. W, uncoalified-wood localities.

Other units of variable deformed-state thickness and reduced competency were area balanced and restored to a line length equal to that of the competent units involved in the same deformation. Area-balanced units include the lower member of the Bay Fiord Formation, and Cape De Bray Formation on Sections A through I and the upper part of seismic unit sC4, the Blackley, Cape De Bray and lower Weatherall formations on Section J. For Sections A through I, it has also been necessary to area balance the siliciclastic formations of the Devonian clastic wedge that lie above the Cape De Bray Formation. This method of restoration assumes that the magnitude of horizontal shortening was identical amongst all affected competent and ductile units. These and other assumptions relating to section balancing and restoration are introduced in the discussion of the individual cross-sections to follow, and are explored in detail in Chapter 6.

Description of cross-sections

The ten presented cross-sections are labelled from east to west, with Section A¹A⁴ located along the east coast of the island and Section J¹J⁷ located near the west coast. For the purpose of organized description, Sections F and G will be described first. These two sections together document a typical profile through the salt-based fold belt starting on an undeformed portion of the Arctic Platform at the southwest end of Section F. The eastern cross-sections (D through to A), considered next, begin within the fold belt at the south end and proceed north to the edge of the Sverdrup Basin. The periclinal folds typical of the western limit of the salt-based portion of the fold belt are seen on Sections H and I. These cross-sections are described after Section A. The quality and distribution of seismic

profiles are limited at the west end of the island. Nevertheless, major variations in structural style are evident in Blue Hills Fault Belt, Purchase Bay Homocline and the fold belt of Canrobert Hills and subsurface Sproule Peninsula. These structures have been interpreted on Section J. Deformed lower Paleozoic strata also extend under the Sverdrup Basin cover of Sabine Peninsula. These features and other structures related to the development of the southern margin of the Sverdrup Basin are introduced on Section E.

Sections F and G: Cape James Ross (on M'Clure Strait) to Sabine Bay (near Reid Point)

The combined length of Sections F and G is 203.5 km. The sections are generally perpendicular to structure except at the southwest end of Section F, where a significant obliquity to structure was deemed necessary in order to faithfully follow available seismic profiles (which in this area are all similarly oblique to structure). In order to remain close to reprocessed seismic profiles, the cross-sections are also offset short distances along the axial trace of folds at F⁴, G² and G³. Fold plunge is small, and variations in structural style and displacement along strike are also probably minimal between offset cross-section segments. Some mismatch of reflectors, probably due to structural plunge, can be seen at the south end of seismic profile P1192 of Section G (Note 3).

The first thing to note about these sections is that undeformed Beverley Inlet Formation exposed at the west end of Dundas Peninsula overlies an additional 10 km of undeformed Devonian, Silurian, Ordovician and Cambrian(?) strata. A pronounced angular unconformity at 10 km below surface separates flat-lying Lower Cambrian and broadly folded seismic Proterozoic(?). (Proterozoic structure has been described at some length in Chapter 2.)

The first small folds can be seen at depth immediately north of the N. Dundas N-82 well, and the southwestern limit of deformation is close to or at the southwestern limit of the reflectors marking the edge of the lower Bay Fiord evaporites (Section F, Notes 12, 13). The deformation front is also close to the Upper Ordovician through Upper Silurian facies change of Cape Phillips mudrocks and basinal carbonates to platform carbonates of seismic unit OSC (Section F, Notes 2, 7).

Farther north, a train of harmonic, upright, open folds affects the entire stratigraphic section above the

base of the Bay Fiord Formation. Apparent deep structural relief, expressed by gentle warping of sub-Bay Fiord reflectors beneath each anticline (Section F, Note 3), is attributed to velocity pull-up generated by thrust stacking of high-velocity carbonates higher in the section, and for this reason has been filtered out of the structural cross-sections. However, long wavelength folds do occur in the sub-Bay Fiord section north of Liddon Gulf Syncline (Section G, Note 15). These are real structures that cannot be interpreted as geophysical artifacts. These mid-crustal folds are not easily identified on the surface geology map and the associated fold axes do not necessarily coincide with surface fold axes. This is due to the fact that the longer wavelength folds possess a different depth to detachment, and (as shown in Chapter 7) a different tectonic trend. Although horizontal shortening is small, structural relief affects strata down to at least the base of the Cambrian(?) (base of unit sC1).

Considering again the harmonic folds above the base of the Bay Fiord Formation, it is worth noting that anticlines involving upper Bay Fiord through Parry Islands formations are situated spatially above pillow-shaped or welt-shaped structures ("welts") that have developed within the lower Bay Fiord Formation. Likewise, reverse faults and thrusts are mostly found in a subsurface stratigraphic interval below each unfaulted surface anticline and above each welt. The faulted interval is found above the base of the upper (carbonate member of the) Bay Fiord Formation and below one of several levels within the Cape De Bray Formation (Section F, Note 18; Section G, Note 8).

The harmonic character of the fold train above the base of the Bay Fiord evaporites manifests itself in a fairly predictable variation in fold wavelength across the sections. Perpendicular fold wavelength, measured at the level of the Thumb Mountain Formation, increases from about 6 km in the southwest to about 13 km in the northeast. Wavelength appears to be qualitatively proportional to pre-tectonic thickness of salt (compare restored- and deformed-state cross-sections).

Fold amplitude, and the magnitude and complexity of thrust faulting specifically associated with each anticline also increase progressively to the north. Thrusts tend to occur in strata of competent character between the top of the lower Bay Fiord and the Cape De Bray formations, and none are known to reach the surface along these two sections. There is a tendency for thrust splays to reach progressively higher in the stratigraphic pile within more northerly anticlines.

Thrusts are seen only in the Bay Fiord through Cape Phillips interval near the deformation front; others extend upward into the Cape De Bray farther north, and into the lower Weatherall Formation only within the northernmost anticline (Sabine Bay Anticline, Section G, Note 11).

More peculiar is the tendency for thrusts of one vergence to be linked upsection or downsection to conjugate thrusts of opposing vergence. Although individual anticlines may display a preferred sense of asymmetry and fault attitude, thrust vergence varies in a most unsystematic fashion over the length of the two sections. Nevertheless, offsets on thrusts are small. The largest displacement occurs on a north-dipping thrust within Dealy Island Anticline (2.1 km).

In contrast to subsurface anticlines, all synclines are relatively unfaulted features at depth. Thrusts nucleating beneath one anticline are not apparently linked to adjacent anticlines except along the sub-salt décollement.

Consider again the small, faulted anticlines at the southwest end of Section F. The apparent limit of surface folding is marked by the trace of Shellabear Point Syncline (geology map, in pocket). In contrast, subsurface folds and thrusts extend 35 km farther southwest onto the platform. In other words, for the three or four anticline-syncline pairs between Shellabear Point Syncline and the subsurface deformation front, amplitude must decrease upsection to nearly zero at the surface, and the apparent shortening of surface strata is much less than the shortening of clearly folded and thrust faulted strata at depth.

This introduces the more serious of two problems presented by the structural cross-sections. Consider the smaller problem first. Total shortening or maximum tectonic transport distance measured on the Thumb Mountain Formation, (in other words, the palinspastically restored bed length of the formation measured along the line of section (F+G) less the length of the deformed state cross-section; F+G) is 10.6 km (6.2%). In contrast, total shortening of the Eleanor River Formation is nearly negligible (0.2 km). Therefore, if both formations are assumed to be undeformed (autochthonous) in all areas southwest of Cape Providence Anticline (Section F), then a slip differential between the two formations must exist beneath Cape Providence Anticline, and the magnitude of this differential must increase to a maximum at the north end of Section G. The cross-sections assume that this differential is accommodated on a through-going basal detachment situated beneath the lower

(evaporitic) member of the Bay Fiord Formation. However, the question remains, how and where is tectonic transport above the base of the Bay Fiord Formation matched by an equal shortening below the Bay Fiord Formation, or is shortening above the Bay Fiord detachment matched by an equal amount of above-salt extension somewhere north of the line of section. The resolution of this problem is deferred to consideration of adjacent cross-sections that extend farther north, and to discussions relating to the problem in Chapter 6.

The second balancing problem is more serious. Bed length measurements have been determined on the formations within the clastic wedge. Results for combined Sections F and G show that total accumulated shortening of the Hecla Bay Formation (for example) is only 4.6 km (2.8%). However, it has already been shown that the Thumb Mountain Formation has been transported up to 10.6 km along the same sections. The shortening differential is not created by one single structure. The problem, as introduced above, is clearly expressed by the small faulted folds in the foreland that have no structural expression at the surface. The problem only increases through each of the larger folds to the north that are clearly thrust faulted at depth but only gently warped at the surface. For this second balancing problem, either a through-going upper detachment (perhaps within the Cape De Bray Formation) must accommodate the slip differential, or some other solution must be found. For the palinspastically restored sections that accompany each of the structure sections, the formations of the Devonian clastic wedge have been area balanced and restored to an original bed length assumed to equal that of the underlying carbonate section. This balancing method assumes that the two packages have experienced the same amount of shortening and that a significant unrecognized shortening mechanism is to be found in the Devonian succession to account for the $(10.6 - 4.6 =) 6.0$ km shortfall in apparent shortening. This solution does not require a through-going upper detachment. The highly debatable validity of this solution is explored in more detail in Chapter 6.

Section D: Chevalier Bay Syncline (on Viscount Melville Sound) to the west arm of Weatherall Bay (west of Tingmisut Lake)

This cross-section begins within the fold belt of eastern Melville Island and terminates within the faulted area of exposed upper Paleozoic strata on southeastern Sabine Peninsula. The section and all but one

supportive seismic profile are less than 20° removed from perpendicular to structure. Profile P1141 is more oblique to structure. The adjacent part of the structural cross-section is offset parallel to structure along the axial traces of Dealy Island and Beverley Inlet anticlines. As in Sections F and G, changes in structural style and plunge are assumed to be small over the small offset distances. Subsurface depth control is provided by three wells (two shown), one relatively close to the line of section. The borehole not marked (Weatherall O-10) is also close but actually falls on the south end of nearby Section E.

Lower Paleozoic strata within the fold belt resemble those of Sections F and G. There are some critical differences in the Middle Ordovician through Lower Devonian interval. There is no indication of either a southern or northern limit of Bay Fiord evaporites. The basin facies Cape Phillips Formation, which extends off the section to the south, changes facies to Lower Devonian Blue Fiord carbonates within Sabine River Syncline. The Upper Ordovician and Silurian portion of the Cape Phillips extends farther north, changing facies to carbonate (unit OSC) within Burnett Point Syncline.

Structures, also common to Section G, are the three southern anticlines and intervening synclines of Section D. Sabine Bay Anticline (a major structure at the north end of Section G), is a small feature, obvious only at depth beneath Byam River Syncline on the present section.

Folding is mostly restricted to the stratigraphic interval above the Eleanor River Formation at the south end of Section D. Whereas structural relief on the Eleanor River and underlying strata appears first under Liddon Gulf Syncline on Section G, similar structure is not evident south of Rea Point Anticline on Section D (Note 11). However, considerable reverse faulting and at least one phase of normal faulting affect the sub-Bay Fiord section beneath and north of Burnett Point Syncline (Notes 13, 14, 16). These faults displace the entire stratigraphic column down to and below seismic unit sC1.

The Canyon Fiord Formation, preserved in a half-graben structure (Weatherall Depression) at the north end of Section D, is perched above the much larger Spencer Range Anticlinorium. Half-graben boundary faults include the Tingmisut Fault, which is listric in profile and flattens downward and to the south into a tilted portion of the lower Bay Fiord Formation (Note 19). Other bounding structures, including Weatherall Bay and St. Arnaud faults, appear to be

planar conjugates: these are not readily identified on seismic profiles although one other unnamed fault that has been imaged seismically does not appear to reach the surface (Notes 15, 17). Separate extension faults affect the Eleanor River Formation and underlying seismic units. Apparent syntectonic growth occurs in the lower Bay Fiord Formation. These deep structures are, however, considered to be the variable brittle and ductile responses to shallow, younger extensions and not a separate mid-Ordovician phase of deformation.

Wavelengths of folds above the Bay Fiord detachment are regular and harmonic, although overall wavelength (11–20 km) is greater than on Section F. The long wavelength of Burnett Point syncline appears to be qualitatively related to the additional thickness in this area of Silurian and Lower Devonian shelf carbonates that contribute to the widespread rigid beam of above-salt Ordovician carbonates. Amplitude of folds (up to 3.4 km) is also greater than on all folds on the described sections to the west. Amplitude increase is especially evident in Robertson Point and Beverley Inlet anticlines (compare with same on Section G). These increases can be attributed to axial tectonic thickening of the Cape De Bray Formation, and increased displacement on subsurface thrusts. Significant subsurface thrust displacements are seen all along Section D. Four thrusts have displacement in excess of 1.5 km in contrast to Sections F and G, which have only two faults of such magnitude. As on Section G, the largest thrust (3.3 km of horizontal slip) occurs within Beverley Inlet Anticline.

The eastward increase in fold amplitudes and thrust displacements is accompanied by increased complexity of faulting within individual anticlines. For example, three north-vergent footwall splays occur beneath the major south-vergent thrust within Beverley Inlet Anticline. Farther north, stacked conjugate thrusts beneath Rea Point Anticline link up four intermediate detachment levels. Thrusts also reach higher stratigraphic levels than on Sections F and G. Three faults displace Beverley Inlet Formation and four reach the surface beginning north of Rea Point Anticline.

Along-strike changes in structural style within anticlines are paralleled by several changes within synclines. Younger conformable strata as high as the Cape Fortune Member of the Parry Islands Formation appear in the synclines of Section D, although this trend is partly offset at depth by eastward thinning of the Weatherall and Hecla Bay formations. In general, synclines remain relatively uncomplicated features with no linkage of thrusts between anticlines above the lower Bay Fiord Formation. However, parasitic structures not

predictable from the surface flank synclines adjacent to Robertson Point, Rea Point and King Point West anticlines, and the eastern limit of Sabine Bay Anticline (not labelled on Section D) has almost no surface expression beneath Byam River Syncline.

The additional thrust complexity, higher fold amplitudes, and larger thrust displacements on Section D translate into greater total horizontal shortening of all strata above the base of the Bay Fiord Formation. Cumulative shortening of the Thumb Mountain Formation is 19.3 km at the north end of the line of section. This includes 3.5 km of horizontal transport in the foreland carried over from Section G along the axial trace of Chevalier Bay Syncline. Shortening of the Eleanor River Formation (most occurring beneath and north of Burnett Point Syncline) is 5.6 km. This is much greater than that on Section G, but is still insufficient to account for the very large slip differential ($19.3 - 5.6 = 13.7$ km) across the basal Bay Fiord detachment. Again the solution to this first problem, introduced in discussion of the previous sections, must be found farther north, off the line of section.

Bed-length shortening of the Hecla Bay Formation, also much greater than on Sections F and G, is 9.8 km, (including 1.3 km carried over from the foreland). The shortening differential of ($19.3 - 9.8 =$) 9.5 km between the Hecla Bay and Thumb Mountain formations is solved on the restored sections in a manner similar to that of Sections F and G. Nevertheless, the validity of the restoration remains to be established.

Section C: Ross Point (on Viscount Melville Sound) to Tingmisut Lake (near Weatherall Bay)

Major structures on Section C include many of the classic linear anticlines of southeastern Melville Island, a large outlier of Isachsen Formation (Lower Cretaceous), the widest part of Burnett Point Syncline, the easterly ends of Weatherall Depression and Spencer Range Uplift and the Silurian carbonates of Tingmisut Inlier on the west arm of Weatherall Bay.

The southern limit of the Bay Fiord evaporites and Cape Phillips shale is off section to the south (as in Section D). Northward facies change of the Lower Devonian portion of the Cape Phillips to Blue Fiord Formation occurs in the subsurface between Baldwin River and Rea Point anticlines (Section C, Note 6; compare with Section D). The lower part of the Cape Phillips changes to carbonate (Unit OSC) within the north limb of Burnett Point Syncline.

There are many similarities between Sections C and D, including: 1) the large amplitude of the southernmost folds; 2) the increased wavelength of folds at the north end of the section corresponding to a related subsurface increase in thickness of competent shelf-type carbonates in the Middle Ordovician through Lower Devonian interval; 3) the involvement in thrusting of the Eleanor River Formation and underlying Lower Ordovician and Cambrian(?) seismic units at the north end of both sections (Note 14); 4) the spatial association of deep-seated reverse faults and extensional growth faults of presumed mid-Cambrian age (Note 12); 5) the perched half graben of Canyon Fiord Formation on Spencer Range Anticlinorium and kinematically-linked, coeval, deep extension faults affecting Bay Fiord and older strata; and 6) the two significant balancing problems presented by bed length shortening differentials: one across the sub-Bay Fiord basal detachment; and the other between the upper Bay Fiord-Cape Phillips interval and the siliciclastic formations of the Devonian clastic wedge.

The regional easterly plunge of synclines, noted between Sections G and D, also carries over to the present section, with the medial shale of the Consett Head Member preserved in two areas. In contrast, there are no major variations in plunge of anticlines detached on the Bay Fiord evaporites. Easterly changes in fold trend have resulted in the merging of Richardson Point and King Point anticlines and the disappearance of King Point West Syncline. Baldwin River Anticline has also emerged on Section C as a major structure rising to the east out of a parasitic structure situated on the south limb of Sabine River Syncline of Section D. Other faulted contractional parasitic structures have evolved within Liddon Gulf, Mecham River and Byam River synclines.

Vertically linked conjugate thrust systems typify and remain spatially associated with major anticlines detached on the Bay Fiord Formation. Vergence and magnitude of displacement of the major thrusts has varied considerably between Sections C and D, particularly within Robertson Point and Rea Point anticlines. The two largest thrusts are south vergent and display 3.7 and 3.9 km of displacement.

On the present section, contractional features do not affect the Eleanor River and underlying formations south of Richardson Point Anticline. Significant thrust displacements are carried on north-dipping faults beneath Spencer Range Anticlinorium. These faults fail to penetrate through the lower Bay Fiord Formation, and it is presumed that most shortening is carried southward on the sub-Bay Fiord detachment (Note 14).

Magnitude of slip on these deep-seated reverse faults is also related, on both Sections C and D, to the magnitude of uplift and exposure of Lower Devonian carbonates in Spencer Range, and of Silurian carbonates of Tingmisut Inlier (compare Sections C and D). The interpretation of this part of the cross-section emphasizes the continuity of lower Paleozoic structure between the two carbonate inliers situated north and south of Weatherall Bay; a south-vergent, westerly plunging anticlinorium modified by normal faults that are spatially associated with the Canyon Fiord Formation of Weatherall Depression.

Most of the uplift of Spencer Range Anticlinorium must have occurred prior to deposition of the Canyon Fiord Formation, because tilted beds below the sub-Carboniferous angular unconformity would still have been tilted when the unconformity peneplain was in its originally horizontal state. However, the westerly plunge of Spencer Range Anticlinorium, (expressed, for example, by the depth to the Eleanor River Formation along the fold apex) affects all lower Paleozoic and upper Paleozoic formations in the area. The thickness of Canyon Fiord Formation preserved within Weatherall Depression increases to the west between Sections C and D, and several Permian formations appear along the axial trace of the depression between the two sections. Furthermore, marine strata preserved in each of these formations have been uplifted well above sea level in all areas above the anticlinorium. Thus it can be concluded that slip on deep-seated contractional faults, which is held partly responsible for uplift and plunge of Spencer Range Anticlinorium, must have occurred in at least two phases; one prior to the Late Carboniferous, the other since the Permian.

Section B: Headwaters of Byam River to Domett Point (on Weatherall Bay)

Major structures intersected by Section B include Towson Point Anticlinorium, and one of the largest thrusts of southeastern Melville Island, which reaches the surface on the south limb of Baldwin River Anticline.

Depositional facies belts are similar to those of Section C. Between Sections C and B, the Cape Phillips to Blue Fiord facies transition is shifted progressively to the north (Section B, Note 4). On the present section, the transition lies within Sabine River Syncline and, by interpolation, must lie variably in the footwall and hangingwall of subsurface thrusts of Baldwin River Anticline between Sections C and B.

The older Cape Phillips transition to undivided unit OSC lies within Burnett Point Syncline, as it does on Sections C and D.

Differences in fold wavelength between the northern and southern halves of the cross-section were recognized on Sections C and D, and are increasingly obvious on the present section. North of Richardson Point Anticline, the entire Cambrian through Upper Devonian stratigraphic interval (11.5 km thick!) appears nearly undeformed. This is in spite of the fact that the fold belt to the south, half of which underlies Viscount Melville Sound, is roughly 170 km wide and is itself bound on the south side by the autochthonous Arctic Platform. Northward change in structural style on this section and on the previous two sections is qualitatively related to the northerly increased thickness of rigid platform carbonates in the Middle Ordovician through Middle Devonian interval. Such carbonates are 700 m thick beneath Byam River Syncline and 3000 m thick on the north limb of Towson Point Anticlinorium. Also probably contributing to the northerly increase in rigidity of the stratigraphic column and disappearance of harmonic folds is the northerly thinning of ductile Cape De Bray Formation (mudrock) from the base of the Devonian clastic wedge, and its replacement by sandstone of the Weatherall Formation. The net result of these facies changes is a rigid beam of formations at least 5500 m thick (top eroded). The base of the rigid beam is defined by the lower Bay Fiord Formation: a unit that is unchanged with respect to seismic stratigraphic properties (strong bounding impedance contrasts) and structural properties (thickness variations produced by ductile flow). These unchanged features imply that the evaporitic character of the lower Bay Fiord Formation also remains essentially unchanged across and beyond all of Sections B, C and D.

Nevertheless, balancing problems discussed previously still remain. The shortening differential across the sub-Bay Fiord detachment, which has accumulated from the autochthonous foreland by shallow folding and thrusting, is necessarily greatest across the sub-Bay Fiord detachment in areas farthest from the foreland. On the present cross-section, total accumulated tectonic transport of the Thumb Mountain Formation is 28.3 km measured at the north end of the section. This includes 13.6 km carried over from the foreland and Section C along the axial trace of Byam River Syncline. In contrast, the Eleanor River Formation and underlying conformable strata have moved less than 100 m horizontally. In other words, nearly 28.3 km of south-directed horizontal slip has occurred above the sub-Bay Fiord detachment north of Towson Point Anticlinorium.

Other differences between Sections B and C will only be briefly touched upon. The intensity of faulting and the magnitude of sub-Bay Fiord shortening and uplift below and north of Burnett Point Syncline has clearly fallen off dramatically, somewhere west of the present section. This implies that deep structure is probably oblique to the line of section and also oblique to surface structure. The change in deep structure is paralleled by some obvious changes in surface fault patterns between Towson Point Anticlinorium (this section) and Spencer Range Anticlinorium, which is located immediately to the west on Section C. The mix of shallow contraction faults and younger extension faults is common to the hinge region of both structures, both above and below the sub-Bay Fiord detachment. Relative dating of various faults within the Towson structure is hindered by the absence of unconformable upper Paleozoic cover.

In the thin-skinned fold-thrust belt, pop-up structures occur within the bifurcated Richardson Point and King Point East anticlines. Farther south, the shallow portion of the south-vergent Baldwin River Anticline and footwall thrust (detached on the Cape De Bray Formation) rides piggyback on the upright north limb of Rea Point Anticline (compare Section C). Thrust systems at depth are a confusion of five north-vergent imbricates and two hangingwall conjugate thrusts facing two south-vergent imbricates, all riding on at least three salt welts of the lower Bay Fiord Formation. An important feature here, representing a significant departure from all thin-skinned structures to the west, is the major disharmony evident between surface folds and subsurface structure. This is apparently brought about by an upper detachment slip plane in the Cape De Bray Formation that links sub-Cape De Bray structure beneath Rea Point Anticline to shallow thrusts above the Cape De Bray within Baldwin River Anticline. The result is a clear example of a through-going upper detachment linking adjacent anticlines. This linkage also allows some southerly directed slip on the Bay Fiord detachment to be carried back through one syncline on a northerly directed upper detachment.

Section A: Little Point (on Viscount Melville Sound) to Bradford Point (on Byam Martin Channel)

Most major structures are continuous with those seen on Section B, including the eastern end of Towson Point Anticlinorium and the exposed limit of the salt-based fold belt of southeastern Melville Island. One curious surface feature on the line of section is the structurally elevated Birch Point Syncline (with lower

Beverley Inlet Formation preserved along the axial line of the structure).

Depositional facies of Sections B, C and D continue onto A. The Blue Fiord carbonate bank edge crosses the hinge of King Point East Anticline east of Section B, and occurs mostly within King Point East Syncline on the present cross-section (Note 8). The limit of the underlying Silurian portion of the Cape Phillips Formation is also shifted north (Note 7).

The northerly shift of facies belts between Section B and the present section is paralleled by an easterly narrowing of Burnett Point Syncline – a structural response to the thicker Cape De Bray ductile mudrock and correspondingly thinner underlying interval of rigid above-salt carbonates. Also relating to sedimentation patterns is the observed northerly thinning of the entire Devonian clastic wedge against the south-facing limb of Towson Point Anticlinorium. A similar thinning trend northward on Section B points to possible synchronous uplift of and sedimentation on the Towson Point structure.

Deep-seated faults are rare on both Sections A and B. Implied motions are at least in part extensional although regional uplift of the sub-Bay Fiord succession also points to compressive activity in the deformation history. Strike-slip movement on several of the sub-Bay Fiord faults may help to explain these ambiguous structural relations (Section A, Note 14).

Towson Point Anticlinorium features two scales of regional folding. The long-wavelength anticline affects all Cambrian(?) through Devonian strata. The other scale of fold features a shorter-wavelength surface anticline underlain by several north-vergent thrusts detached on the Bay Fiord evaporites and a shallow pop-up structure with three south-dipping splays, and two conjugate splays. Some of these shallow structures are also seen on Section B. However, an axial culmination lies between Sections B and C, and it can be presumed that maximum subsurface thrust displacement occurs about midway between the two sections.

It is also worth noting that the crest of the long-wavelength anticline (as defined by the depth to the top of the Eleanor River Formation) is considerably north of the surface antichinal crest. This type of fold disharmony also occurs beneath Towson Point Anticlinorium of Section B, and beneath Sabine Bay Anticline of Section G.

The most remarkable differences in structural style between Section B and the present section occur within

the thin-skinned portion of the fold belt. Simple harmonic surface folds between Byam River and King Point East synclines are underlain at depth by a complex array of structures including pop-ups, linked evaporite welts of varying size, and numerous splays of mixed vergence (Section A, Note 4). Whereas the surface anticlines generally lie above the structurally highest imbricates, large parasitic features extend under all of the intervening synclines. The elevated condition of Byam River Syncline can be related in part to convergent thrust splays in the Cape De Bray Formation that arch over a completely hidden pop-up structure.

Disharmony of surface and subsurface structure is attributed (as in Section B) to contrasting structural styles above and below an upper detachment (Section A, Notes 12, 13). On the present section, the upper detachment is discontinuously traceable from Byam River Syncline to at least King Point East Anticline. Feasibly, a cross-section could also be drawn that links up a single, common upper detachment in the Cape De Bray Formation traceable from south of Beverley Inlet Anticline to Towson Point Anticlinorium (in the north) and beyond. This hypothetical upper detachment would carry the accumulated differential shortening between the Devonian clastic wedge and the various carbonate formations at depth lying above the base of the Bay Fiord Formation which at the north end of the line of section is $(28.4 - 9.1 =) 19.3$ km. As discussed previously (Sections B through D, and F and G) this is not the model of shortening implied by the restored sections, each of which require that additional mechanisms of transport be found to account for the apparent shortening differential across the Cape De Bray Formation.

Section H: Stony Pass (near Liddon Gulf) to Hecla and Griper Bay (near Nias Point)

Several 6-second unmigrated profiles are available for the northern end of cross-section H but have not been reprocessed for publication. Lower Paleozoic depositional facies are continuous with those seen on Section G. Depositional limits of both the Cape Phillips Formation and the evaporitic member of the Bay Fiord Formation are beyond the northern and southern edges of the cross-section.

Major structures along Section H include various, northwesterly trending linear and periclinal folds, one of which (Dealy Island Anticline) has exposed the Cape De Bray Formation at the surface. Not so easily seen at the surface are longer wavelength folds that buckle the entire lower Paleozoic succession, including the

reflector considered to mark the base of the Cambrian(?) at 10 to 12.5 km below the surface (Section H, Note 11). The crest of the sub-Bay Fiord Anticline is situated almost directly below the crest of Dealy Island Anticline. This relation, however, is undoubtedly a coincidence, because the shorter wavelength folds are clearly detached on the lower Bay Fiord Formation, and the crest of the longer wavelength structure lies under the north limb of Liddon Gulf Syncline on Section G.

Obliquity of long wavelength and shorter wavelength regional-scale folds is also indicated by the gentle sub-Bay Fiord syncline to the north, which lies beneath the south limb of Beverley Inlet Anticline on the present section but beneath Mecham River West Anticline on Section G. Likewise, the reverse fault on the south limb of Nias Point Anticlinorium, which is clearly oblique to the other folds of central Melville Island, is also traceable downsection into the sub-Bay Fiord stratigraphic interval. It will be shown in Chapter 7 that the westward transition at the surface, from linear to periclinal folds, is attributable to the westward introduction of interference cross folds.

The southern edge of the dominant long-wavelength anticline is defined at depth by a Precambrian(?) and/or Cambrian(?) age normal fault that dies out upsection in seismic unit sC3 and that may extend downward into block faulted Precambrian(?) unit sAP (Section H, Note 10). Other small faults within the Cambrian(?) succession (beneath Nias Point Anticlinorium) appear to be detached on the base of seismic unit sC2 and to have also been active during deposition of unit sC3 (Note 8).

Several other structural features peculiar to the thin-skinned folds are worth noting. Many small thrusts above the Bay Fiord Formation die out upsection in the Cape De Bray Formation; for example, pop-up thrusts within Dealy Island and Mecham River West anticlines. However, the high quality of the seismic profiles also permits the recognition of a local detachment within the lower Weatherall Formation of Cape Bounty and Beverley Inlet anticlines (Section H, Note 6). An obvious plane of slip at this height in the stratigraphic section has not been recognized on seismic profiles farther east. This possible oversight may be due entirely to regional variations in seismic data quality (Section C, Note 4).

Finally, a note about variations in horizontal tectonic transport. Foreland shortening (to the south) on the Thumb Mountain Formation is 1.0 km (estimated) and is only 7.5 km at the north end of the line of section. Apparent shortening of the Hecla Bay

Formation is 2.2 km and, for the Eleanor River Formation, is 1.2 km (nearly all of which is carried on the Nias Point Fault).

Section I: Cape Edwards (on Liddon Gulf) to Hecla and Griper Bay (near Hillock Point)

Major structures along the line of section include Nias Point Anticlinorium, Apollo Anticline, Blue Hills Syncline, McCormick Depression, McCormick Inlet Anticlinorium, and other structures in Raglan Range. Subsurface control is provided by the Panarctic Apollo C-73 well (Section I, Note 18), and by Middle Ordovician and younger strata that reach the surface (off the line of section) in McCormick Inlet Anticlinorium.

A key facies change, noted on profiles P1654 and C131X, is the hinterland (northwestern) limit of the bounding reflectors that define the distribution of lower Bay Fiord evaporites (Section I, Notes 9, 13). This transition occurs beneath Apollo Syncline at the south edge of profile P726, and beneath Barry Bay Anticline at the north end of P1654. This east-northeast-trending facies front is somewhat oblique to the long-wavelength surface features of Nias Point Anticlinorium, and also highly oblique to all other surface structures, especially those detached on the evaporites.

The other important seismic stratigraphic feature of the cross-section is the southern limit of unit sC4, and associated faults that were apparently active during deposition of sC4 (Section I, Notes 11, 16; Fig. 30). The thin, onlapping, updip limit of the unit lies approximately under Nias Point Anticlinorium on P1654. However, the greatest thickness of the unit and the greatest concentration of associated faults lies under and north of Blue Hills Syncline. Thrust faults that pass upsection into unit sC4 are only very gently dipping within unit sC4. This feature of seismic unit sC4 provides a viable detachment level for thin-skinned deformation beyond the limits of the Bay Fiord evaporites (Section I, Note 24). Short-wavelength folds of Raglan Range are tentatively detached on the proposed slip plane below sC4, and the magnitude of compressive slip is allowed to accumulate northward on this surface, beyond the hinterland limits of the cross-section. To the south, slip is transferred to the basal Bay Fiord detachment on a thrust ramp believed to exist under Apollo Anticline. Transferred slip between detachments is actually only a few kilometres and total foreland slip on the Bay Fiord detachment is equally small.

Folds developed on the Bay Fiord Formation at the south end of the cross-section are typically low in amplitude and are also greatly reduced in wavelength (compared with sections to the east; Section I, Note 22). Associated thrust faults are simple listric structures with very limited displacement. This simplification of structure nearing the thinned limit of the lower (evaporitic) Bay Fiord Formation is also seen at the foreland limit of the fold belt (Section F). However, style is contrasted with the foreland deformation by the various hinterland links to northerly dipping faults of deeper origin.

Some of these deep-seated faults appear to extend downward into the mid-crust (Section I, Note 17). Included in this latter group is a steep, north-dipping reverse fault under Nias Point Anticlinorium, and another similar set of faults under McCormick Inlet Anticlinorium, that appear to originate from below seismic units sC1B and sC3, respectively. The ultimate maximum depth of detachment, at least for the reverse fault under Nias Point Anticlinorium, and for the unit sC4 growth faults, appears to be above a through-going reflector at about 21 km (Section I, Note 25).

Several faults of McCormick Inlet Anticlinorium originate from below 9 km and extend to surface through unconformable Canyon Fiord Formation. Geological relations over the McCormick Inlet structure indicate that other deep-seated reverse faults, also necessarily linked to the origin of McCormick Inlet Anticlinorium, were mostly active before the erosional event that bevelled the anticlinorium prior to Canyon Fiord deposition.

In spite of complications in the deformation history, shortening is extremely modest at all stratigraphic levels of Section I. The Thumb Mountain Formation has only been shortened by 9.4 km at the north end of the cross-section – this in spite of the fact that the line of section is located above what must be some of the thickest but least deformed lower Paleozoic sections known anywhere in the Arctic Islands (14 km below Blue Hills Syncline).

Section J: Bailey Point (on M'Clure Strait) to Fitzwilliam Strait (near Sandy Point)

Section J is 170.4 km long and spans the entire width of the island on the western peninsulas. Dominant structural features include sublatitudinal faults of the Blue Hills region, Purchase Bay Homocline, asymmetrical and overturned periclinal folds of Canrobert Hills, and Paleozoic deformation beneath thin Mesozoic cover of Sproule Peninsula.

Lower Ordovician through Upper Silurian shale-to-carbonate facies changes occur somewhere in the subsurface between the Kitson River Fault and the south end of the line of section (Section J, Note 4). Thickness variations are poorly constrained as a result of a lack of surface stratigraphic control and a complete absence of seismic reflection data south of Marie Bay. On Sproule Peninsula there are unreprocessed seismic profiles from the 1968–1974 period with a mappable upper Paleozoic and Mesozoic seismic stratigraphy, and windows of higher quality data that reveal a limited lower Paleozoic seismic stratigraphy and general structural features (including mappable fold crests and major thrusts; Section J, Notes 1, 2, 9). Well control on subsurface geology is provided by the Panarctic Marie Bay D-02 and Panarctic Sandy Point L-46 wells near the line of section and by the Panarctic AIEG Depot Island C-44 well located 25 km to the east (not shown).

Insight into subsurface structural features is also provided by unreprocessed seismic profiles of Eglinton Island (40 km west of the mouth of Ibbett Bay; Notes 3, 8) several of which cross the south end of Canrobert Hills Fold Belt and Purchase Bay Homocline beneath Mesozoic cover. Estimated depth to detachment beneath the lower Paleozoic homocline of Eglinton Island is four seconds below surface or 2.75 km (1 s) below the top of the reflection-free unit assumed to be Canrobert Formation. This compares favourably with the depth to an intermediate detachment below Blue Hills Syncline and McCormick Inlet Anticlinorium of Section I; 2.1 to 2.4 km below the top of the Eleanor River Formation within seismic unit sC4. (The Eleanor River is age equivalent to the Canrobert Formation, at least in the upper part). This evidence points to a common through-going detachment beneath the Canrobert Hills Fold Belt situated within seismic unit sC4 at 2.1 to 2.7 km below the top of the Canrobert Formation.

Slip on the sub-Bay Fiord Formation detachment disappears east of Section J along the lateral depositional limit of Bay Fiord evaporites. The preferred interpretation, therefore, is that shortening on Section J has been accomplished by coeval slip on a through-going basal detachment within unit sC4. Southerly directed displacement at the foreland limit of shortening has been carried upward on buried conjugate thrust ramps beneath the Blue Hills fault belt and carried backward through the foreland on an upper detachment situated within the Cape De Bray Formation. Shortening is also greatly dissipated between upper and lower detachments by tight folding

in the Canrobert Hills and by subsurface folding and compressive plateau-type uplift in the Blue Hills belt (Section J, Notes 6, 12). The southern limit of the overturned folds of Canrobert Hills is constrained in the present interpretation to areas north of the lower Paleozoic carbonate-to-shale transition. The effectiveness of the platform carbonates to resist most southerly directed shortening was undoubtedly related to their competent character and great thickness (estimated 3800–4100 m).

Throughout the Canrobert Hills and subsurface Sproule Peninsula, lower Cape De Bray and Blackley formations are preserved as linear erosional remnants within sub-Carboniferous synclines. The Ibbett Bay and upper Canrobert formations are exposed on the sub-Carboniferous unconformity and at the current erosion surface in anticlines. This common depth of pre-Carboniferous erosion of most folds implies a common underlying depth to detachment that is subparallel to the sub-Carboniferous erosion surface. It is also evident that a thick succession of post-Cape De Bray Devonian strata is preserved at the surface in all areas south of Purchase Bay Homocline. A phase of pre-Carboniferous regional-scale uplift, therefore, appears to have affected all areas north of the homocline. Maximum restored structural relief on the homocline is approximately 7 km. The model favoured on Section J (and the one that minimizes the total horizontal shortening) is that compressive slip on several deep-seated reverse faults has offset the mid-Cambrian décollement system and caused regional-scale uplift of Purchase Bay Homocline and all other areas to the north. This model most closely resembles the structural interpretation of McCormick Inlet Anticlinorium and smaller uplifted folds of Raglan Range on Section I, although there are different lower Paleozoic depositional facies involved in the deformation.

On Section I, the deep-seated reverse faults are spatially associated with mid(?)–Cambrian age growth faults. It is therefore also probable that the same system of growth faults may underlie parts of the present section (Note 7). The geographic location of such faults is relatively unconstrained. However, if the growth faults of Section I are assumed to parallel Lower Ordovician and Upper(?) Cambrian isopachs (Fig. 59), then these same growth faults might be expected at depth on Section J, west of the terminated axial trace of Blue Hills Syncline, and north as far as Kitson River Fault.

Unlike Section I, one deep-seated reverse fault (Kitson River Fault) is believed to pass upward through all Cambrian, Ordovician, Silurian, and Lower

Devonian units, eventually flattening into the Cape De Bray detachment beneath Purchase Bay Homocline. Southerly directed slip carried on both the deep-seated reverse fault and the shallow detachment fault is presumed to be balanced by north-directed slip on roof thrusts within the Cape De Bray and lower Weatherall formations. Although the upper detachment fault(s) may develop beneath the Blue Hills, they are only detectable where they exit to surface on the south shore of Ibbett Bay. Other deep-seated reverse faults, mostly lying below the mid-Cambrian detachment, have been inferred from seismic profiles of Sproule Peninsula.

Maximum horizontal shortening determined for the Thumb Mountain Formation and equivalent basin facies strata is 46.3 km (31.4%). This value has been lessened on the structural cross-section by 7.5 km of postorogenic extension. Shortening of the Thumb Mountain Formation south of the Kitson River Fault is 6.2 km (with 1.4 km of later extension on the Murray Inlet Fault and splays). In contrast, the Hecla Bay formation has been shortened by only 1.3 km (and later extended by 1.4 km). The slip differential is carried on the northward-vergent Ibbett Bay Fault within the upper Cape De Bray and lower Weatherall formations. Also contributing to the slip on Ibbett Bay Fault is carried displacement on the Kitson River Fault (7.0 km) which is transferred to the north-vergent detachment in the triangle zone beneath Purchase Bay Homocline.

Most horizontal shortening is documented within basin facies rocks north of Kitson River Fault. Measurements indicate that the Ibbett Bay Formation has been shortened by 40.1 km (38.6%). The increase of thrusting with depth is emphasized on this northern portion of the cross-section. A valid cross-section could also be constructed that accommodates most shortening by different scales of folding.

Also uncertain are the incremental magnitudes of extension and later shortening that affected the Canyon Fiord Formation during the late Paleozoic. Features illustrated on the cross-section (and imaged on unmigrated seismic profiles) of Sproule Peninsula imply that relief on the sub-Carboniferous unconformity may be generated by syndepositional block rotation and extension during Canyon Fiord sediment accumulation. However, structures in Canrobert Hills also include a sub-Upper Permian angular unconformity, a gently folded sub-Carboniferous unconformity, reverse faults and intraformational tectonic folds in Carboniferous strata.

Section E: St. Arnaud Hills to Vesey Hamilton Island

This cross-section extends over the exposed width of the southern Sverdrup Basin from the St. Arnaud Hills on southern Sabine Peninsula to north of Vesey Hamilton Island. Major structures lying on the line of section include Weatherall Depression, Spencer Range Anticlinorium, Drake Point Anticline, and diapirs of northern Sabine Peninsula including Barrow Dome and Vesey Hamilton Salt Wall.

Seismic reflection profiles are generally close to the line of section and have been reprocessed to north of Barrow Dome (Section E, Note 1). At E², the cross-section is offset to the west from the seismic profiles and seismic data are not available over the diapir itself. Numerous 4.0 to 5.5 second unmigrated seismic profiles are available and have been examined for all areas north of Barrow Dome. These unprocessed data were used to determine and plot thickness variations and structures of stratigraphic units adjacent to Vesey Hamilton Salt Wall.

A coherent lower Paleozoic seismic stratigraphy and structure is visible under Carboniferous and younger cover at least as far north as Sherard Bay, and a sub-Carboniferous angular unconformity can be recognized to just south of Panarctic et al. Drake Point D-68 well. Subsurface geology is supported by two boreholes that penetrate the sub-Canyon Fiord unconformity (Dome Panarctic Texex Weatherall O-10 and Panarctic et al. Sherard Bay F-34) and at least five other wells that intersect upper Paleozoic, Triassic and younger strata close to the line of section. The Panarctic Eldridge Bay E-79 well, located 23 km west of the section, projects onto the line of section mid-way between the Sherard F-34 and Weatherall O-10 wells and has penetrated lower Cape Phillips, Thumb Mountain, Bay Fiord and upper Eleanor River formations beneath unconformable Canyon Fiord Formation and younger cover.

Numerous facies transitions occur within upper Paleozoic and Mesozoic strata along the line of section. Featured depositional relations are listed in the marginal notes of Section E (Notes 5-9) and are also noted in the description of formations (Chapter 4). Lower Paleozoic depositional facies are mostly continuous with those of Section D. However, the Cape Phillips Formation is believed to continue north under the Blue Fiord Formation, and shelf carbonates of unit OSC are presumed to exist only east of the line of section. The lower evaporitic Bay Fiord Formation is thin or absent within the Spencer Range Anticlinorium; characteristic bounding reflections are absent north of Tingmisut Fault, and only anhydrite and

carbonate occur within the lower Bay Fiord Formation of the Eldridge Bay E-79 well. The southern updip limit of seismic unit sC₄ occurs at depth within Spencer Range Anticlinorium (Section E, Note 2).

Structural features associated with Spencer Range Anticlinorium are also observed on Section D. The deep-seated faults that are seen to flatten upward into sub-Bay Fiord detachment on the present section also extend downward into the Lower(?) Cambrian unit sC₁ at 10 to 13 km below surface. These faults may continue far to the north beneath the Sverdrup Basin. Some faults, such as Tingmisut Fault and associated splays that offset Carboniferous and Permian strata of Weatherall Depression, are physically linked to the Bay Fiord detachment and to the deep-seated faults beneath Spencer Range Anticlinorium. North of the anticlinorium, other normal faults extend upsection and die out within the Belcher Channel, Sabine Bay, Van Hauen and Troid Fiord formations (Notes 11, 12, 14, 15). Thickening and block rotation of strata across these faults is locally evident at the level of the Canyon Fiord Formation. However, extensional growth is also documented across some faults within formations of Early and Late Permian age. These same faults are associated with the northern depositional limit of the Belcher Channel, Great Bear Cape, Raanes, Sabine Bay, Assistance, Degerbøls and Troid Fiord formations.

Balancing and restoration of lower Paleozoic strata has only been attempted for the southernmost (27 km) part of the cross-section. Bed length measurements indicate that the sub-Bay Fiord interval was shortened by 10.6 km prior to the Late Carboniferous, and then was extended by 3.1 km during the later Paleozoic. Most of the compressive slip is carried to the south on the sub-Bay Fiord detachment and is dissipated by thin-skinned folding and thrusting as is apparent on Sections D, F and G.

Farther north, steeply dipping extension faults occur in the shallow part of the section within Drake Point Anticline. Regional mapping indicates that these faults, which apparently die out upsection in the Christopher Formation, are highly oblique to long-wavelength folds and instead are closely associated with northeasterly striking gabbro dykes and related linear magnetic anomalies (Fig. 177). Gabbro sills and sheets, also associated with dyke emplacement in the Sabine Peninsula region, are readily imaged on seismic profiles and can be seen 1) intruding the Hare Fiord and lower Van Hauen formations within and south of Drake Point Anticline, and 2) intruding upper Van Hauen and Blind Fiord formations in the vicinity of Barrow Dome (Notes 13, 15). The high concentration of sills, typical of the Permian stratigraphic interval of

northern Sabine Peninsula, is probably responsible for poor signal returns from sub-Permian geology. Gabbro ring dykes have also been emplaced into Barrow Dome. Balkwill and Fox (1982) have pointed out that the diapirs must have existed before the emplacement of the gabbro bodies because the gabbro occupies ring fractures that could only have been created during previous phases of halokinetic activity.

Seismic reflection profiles over Vesey Hamilton Salt Wall also yield data concerning timing of movement of this diapir. Stratigraphic thinning of Lower Triassic and younger formations against the diapiric ridge range from 35 to 100 per cent of primary depositional thicknesses as preserved within Murray Harbour Syncline. Off-diapir gravity sliding has further contributed to the syntectonic thinning of the Invincible Point Member of the Christopher Formation. The total thinning of sub-Lower Triassic strata adjacent to Vesey Hamilton Salt Wall remains unknown.

Deep structure of Drake Point Anticline is not revealed by the reflection profiles. Warping associated with the anticline extends downward at least to the seismically-defined base of the Hare Fiord Formation.

Structural domains

General comments

Lower Paleozoic tectonic elements of the Canadian Arctic Islands, northern Yukon and north Greenland are illustrated in Figure 96. Melville Island lies within the Parry Islands and Canrobert Hills fold belts and a northern portion of the undeformed Arctic Platform. The Canrobert Hills Fold Belt continues to the west beneath widespread Carboniferous and younger cover of Eglinton, Prince Patrick and Banks islands. There is every reason to believe that the fold belt must also extend beyond the limits, in these directions, of coherent lower Paleozoic seismic signal.

Although various definitions of structural domains and domain boundaries are possible, the subdivision of the Franklinian Mobile Belt in this account is based on dominant basal detachment level in folding (Fig. 97). Smaller structural regions (subdomains) are defined by the dominant lower Paleozoic depositional facies and the presence or absence of deep-seated folds.

Arctic Platform (structural domain 1)

Description and definition. The Arctic Platform on Melville Island is a lower Paleozoic autochthonous or parautochthonous foreland area displaying little or no

compressive deformation since Precambrian(?) time. The region is underlain by shelf facies Cambrian(?) through Middle Devonian strata and foredeep rocks of Middle and Late Devonian age. The Arctic Platform includes most of Tozer and Thorsteinsson's (1964) Dundas Block and probably also the southernmost part of their Blue Hills Fault Belt. Cretaceous(?) extension faults and related parallel sets of lineaments are mapped in some areas.

Location and distribution. The Arctic Platform underlies western Dundas Peninsula, southern and eastern Viscount Melville Sound, and southeastern M'Clure Strait (Figs. 88, 96); it probably extends onto southwestern Melville Island south of Murray Inlet Fault. This domain is continuous with other portions of the Arctic Platform exposed on southeastern Banks, Victoria, Stefansson and western Prince of Wales islands.

Parry Islands Fold Belt (structural domain 2)

Description and definition. The Parry Islands Fold Belt includes the region of thin-skinned folding and associated thrusting that has developed as a consequence of horizontal compressive slip on a décollement situated below the evaporitic lower member of the Bay Fiord Formation. This includes most of the same region as that of the Parry Islands Fold Belt as proposed and used by Tozer and Thorsteinsson (1964), Thorsteinsson and Tozer (1970), and Fox (1983, 1985). A western part of Parry Islands Fold Belt of the old nomenclature is currently included in Canrobert Hills Fold Belt (Domain 3).

Location and distribution. Parry Islands Fold Belt, as defined herein, underlies all of central and southeastern Melville Island and is also continuous across Byam Martin Channel, Byam Martin Island and Bathurst Island. The domain boundary is defined by the lateral limit of folds lying on the salt-based detachment and by the coincident depositional limit of Bay Fiord evaporites as illustrated on Figure 88 and identified on seismic profiles over Dundas Peninsula (Section F), Apollo Anticline (Section I), and Spencer Range Anticlinorium (Section E).

Lower Ordovician and Cambrian(?) seismic units are undeformed below the thin-skinned salt-based folds in the southeastern part of Parry Islands Fold Belt (Subdomain 2A; Fig. 97). This subdomain was mildly disturbed during the Early(?) Cretaceous by extension faults and probable subsurface dykes (Fig. 177). In contrast, Lower Ordovician and Cambrian(?) seismic units have been broadly folded, tilted and faulted

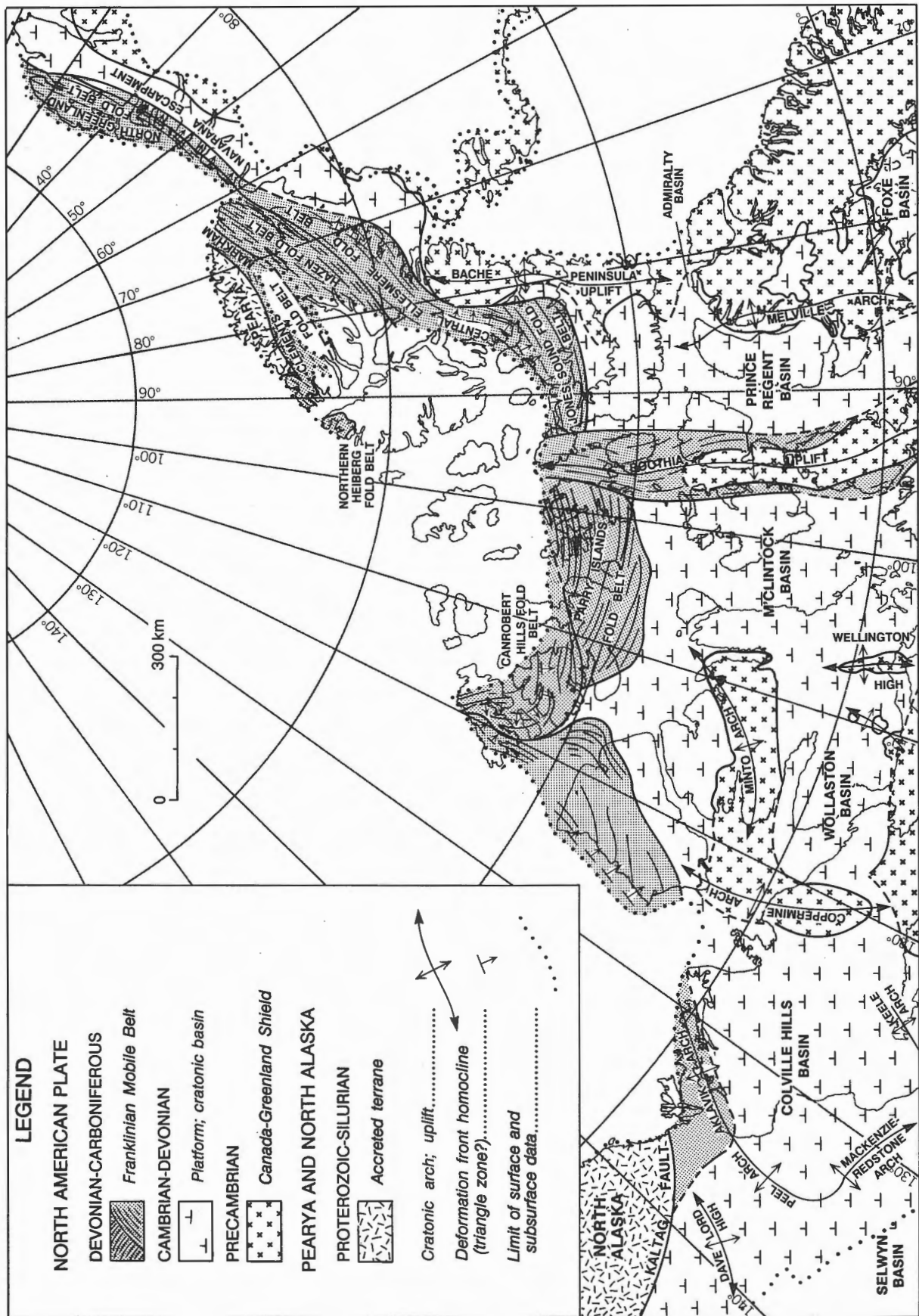


Figure 96. Paleozoic cratonic arches and basins, fold belts, and accreted terranes of northern Yukon, the Canadian Arctic Islands, and northern Greenland.

beneath the detached thin-skinned fold and thrust belt in the northwestern part of Parry Islands Fold Belt (Subdomain 2B; Fig. 97). In Weatherall Bay area, this second subdomain has also been modified by late Paleozoic rifting and younger tectonic phases.

Canrobert Hills Fold Belt (structural domain 3)

Description and definition. Canrobert Hills Fold Belt is a thin-skinned foreland orogen developed on a through-going detachment situated primarily within or near the top of mid-Cambrian(?) seismic unit sC4. Other long-wavelength folds and deep-seated contraction faults also affect sub-middle(?) Cambrian and older strata beneath the unit sC4 detachment. Most of this domain has been modified by separate phases of late Paleozoic rifting and inversion, and Early Cretaceous extension associated with the emplacement of subsurface dykes.

Location and distribution. The Canrobert Hills Fold Belt, as defined herein, underlies Canrobert Hills, Sproule Peninsula and may also underlie all of southwestern Melville Island north of Murray Inlet Fault and Apollo Anticline (Figs. 88, 96).

A southern and southeastern portion of Canrobert Hills Fold Belt (Subdomain 3A) involves lower Paleozoic platform carbonates and the Devonian clastic wedge in the thin-skinned deformation (Figs. 88, 97). This subdomain includes part of Parry Islands Fold Belt and all of Blue Hills Fault Belt as defined and used by Tozer and Thorsteinsson (1964), and Harrison and Bally (1988). The subdomain underlies most of western Melville Island south of the Kitson River Fault. However, the platform carbonate section of the fold belt also lies in the hangingwall of the Kitson River Fault within and north of the Kitson River Inlier. The subdomain is also considered to extend north of the salt-based fold belt beneath thick

upper Paleozoic and younger cover of the Cape Grassy area, Hecla and Griper Bay and central Sabine Peninsula.

In the northwestern part of Canrobert Hills Fold Belt on Melville Island (Subdomain 3B), the thin-skinned deformation above the mid(?) -Cambrian detachment primarily involves lower Paleozoic basin facies mudrocks, chert and resedimented carbonates, and erosional remnants of the basin-fill facies of the Devonian clastic wedge (Figs. 88, 97). This structural subdomain is equivalent to the westernmost portion of Parry Islands Fold Belt of Tozer and Thorsteinsson (1964), Thorsteinsson and Tozer (1970), and Fox (1983, 1985). It is also equivalent to all of the Canrobert Hills Fold Belt of Harrison and Bally (1988), and Trettin (1989). Subdomain 3B lies in the hangingwall of the Kitson River Fault north of Ibbett Bay, and is known to extend beneath all of Sproule Peninsula and northern Eglinton Island.

Deformation phases

Although the Ellesmerian Orogeny (latest Devonian through Early Carboniferous) has produced the dominant orogenic elements of Melville Island, it is clear from the geology map (attached) and supportive structural cross-sections described earlier in this chapter that the style and distribution of Ellesmerian folds and thrusts has been influenced by earlier phases of deformation, and that mid-Paleozoic structure has also been modified by a series of younger tectonic events that span all of late Paleozoic, Mesozoic, and Cenozoic time. These phases of deformation, labelled D1 through D9, are listed with examples in Table 5. Deformation phases D1 and D2 have been considered in Chapters 2 and 3, respectively. The salt-based kinematics of phase 3 deformation is the subject of Chapter 6. Kinematics of later phases are each briefly considered in Chapter 7.

CHAPTER 6

THIN-SKINNED DEFORMATION OF THE SALT-BASED FOLD BELT

General comments

In the previous chapter, two, distinct, mid-Paleozoic (Ellesmerian) orogenic belts on Melville Island, and the tectonic units that each belt contains were delineated.

As well, nine tectonic phases that have influenced and modified the salt-based thin-skinned deformation, were identified (D1 through D9; Table 5).

Tectonostratigraphic units of the salt-based fold belt (Parry Islands Fold Belt), defined in Figure 101, include:

TABLE 5
Deformation phases of the Melville Island region

Phase	Name	Major features	Age
D9	unnamed	regional uplift seismicity	Quaternary
D8	Eurekan Orogeny	periclinal folds strike-slip faults regional uplift	mid-Tertiary
D7	Amerasian Basin rifting	gabbro sheets, dykes normal faults evaporite diapirs	Middle Jurassic–Early Cretaceous
D6	Melvillian Disturbance	rift inversion folds strike-slip faults detachment faults	Early Permian
D5	Sverdrup Basin rifting	half-grabens horsts normal faults growth faults	Carboniferous–Permian
D4	Ellesmerian Orogeny (second phase)	first-order folds strike-slip faults deep-seated reverse faults	Late Devonian–Early Carboniferous
D3	Ellesmerian Orogeny (first phase)	second-order folds conjugate thrusts salt, shale welts detachment faults	Late Devonian–Early Carboniferous
D2	unnamed extension	growth faults block rotation	mid(?)–Cambrian
D1	Franklinian/Mackenzie extensions	regional uplift intrusive sheets basin formation crustal thinning normal(?) faults	Proterozoic(?)

5. An upper rigid layer (URL): Middle and Upper Devonian clastic wedge.
4. An upper ductile layer (UDL): Middle Devonian basin-fill mudrock of the Cape De Bray Formation.
3. A medial rigid beam (MRB): Ordovician through basal Middle Devonian shelf carbonates and coeval basin-facies mudrock.

2. A lower ductile layer (LDL): Middle Ordovician evaporites of lower Bay Fiord Formation.
1. A lower rigid layer (LRL): Cambrian and Lower Ordovician carbonates and related shelf facies seismic units.

Deformation style is dominated by buckling and thrust faulting of the rigid beam, accommodation of room problems in concentric folding by mobility of the two ductile units, and open folding with some minor

faulting of the upper rigid layer. In addition, the lower rigid layer, the detachment beneath the lower ductile layer, and all the overlying tectonic units have been buckled during a second Ellesmerian deformation phase (D4) into long-wavelength folds. At the north and west ends of the imaged fold belt the entire succession has also been shortened by deep-seated reverse faults.

In this chapter, the fundamental problem regarding the shortening differential between the folded surface layers of the Devonian clastic wedge and the more intensely deformed and thrust-faulted carbonate and basinal mudrock formations of the medial rigid beam is reviewed. Possible solutions are presented. The viability of the various models is constrained through a more detailed examination of deformation styles, kinematics and mechanics associated with folding, thrusting and compressive diapiric features above the weak basal layer. From this, a more universal kinematic model is presented that, it is hoped, also provides a solution to the balancing problem.

The balancing problem

Description of the problem

The one structural feature common to the Parry Islands Fold Belt and all thin-skinned fold belts is a through-going basal décollement. Slip across the detachment is zero at the parautochthonous (foreland) limit of thin-skinned deformation. At this limit, all stratigraphic units lie in the order and in the location in which they were deposited. In the hinterland (that is, away from the craton in the direction of the ancient mountain belt), strata below the basal décollement remain relatively undeformed while strata above the detachment surface have been folded and thrust faulted. Palinspastic restoration of these deformed layers to their originally horizontal state reveals that slip across the basal detachment must progressively increase with distance from the deformation front. In the present study, the maximum observable shortening affects competent beds immediately above the lower Bay Fiord evaporites. Within the constraints demanded by numerous migrated seismic profiles, it has been possible to bed-length-balance this shortening (as described in the previous chapter) on at least four horizons within the medial rigid beam including unit tops above 1) the lower and 2) upper members of the Bay Fiord, 3) the Thumb Mountain and 4) the Cape Phillips (or Blue Fiord) formations. To monitor the regional variation in shortening away from the foreland, bed lengths were measured between adjacent

intermediate pin lines on each of ten dip line cross-sections of Melville Island (as reviewed in Chapter 5). Results are summarized on Figure 98.

As well as hinterland increases in shortening at the four stratigraphic levels, shortening also increases along structural trend from west to east as measured near the northern limit of the salt-based décollement. Maximum accumulated subsurface shortening on this décollement is 28.4 km as measured at the north end of Section A. Errors occurring in the determination of these shortening variations are introduced on the southern end of Sections A through D, which do not reach the foreland limit of deformation. For these sections, the foreland shortening is carried over from the combined Sections F and G, which are pinned to the autochthonous Arctic Platform of western Dundas Peninsula.

The balancing problem is evident when formations of the Middle and Upper Devonian clastic wedge are also palinspastically restored to their undeformed state. Results for the ten prepared cross-sections are summarized in Figure 99. General shortening trends are similar to those seen in the medial rigid beam. Shortening accumulates in both the regional stratigraphic dip direction (toward the hinterland) and also along strike from west to east. However, total accumulated shortening of the upper rigid layer is everywhere between 32 and 53 per cent of the bed-parallel shortening measured on the medial rigid beam. As pointed out previously, in discussion of Sections F and G of Chapter 5, this problem does not pertain to just one structure but is a problem evident within most folds. Amplitude and shortening of the simplest thrust-involved subsurface anticlines of Dundas Peninsula gradationally die out upsection and are entirely masked by conformable flat-lying cover of the Devonian clastic wedge. Within the central portion of the fold belt, mostly unfaulted surface folds conformably overlie a complex fold-thrust belt in the beam at depth, with compressive slip on some thrust ramps reaching more than 3 km.

Possible solutions

Solution 1: underthrust wedge (triangle zone)

In this solution (Fig. 100), forward- (cratonward-) directed slip on the basal Bay Fiord detachment is matched by a combination of backward- (hinterland-) directed slip on a through-going upper detachment in the Cape De Bray Formation, and backward-directed slip dissipated by layer-parallel slip and folding in the siliciclastic formations of the clastic wedge.

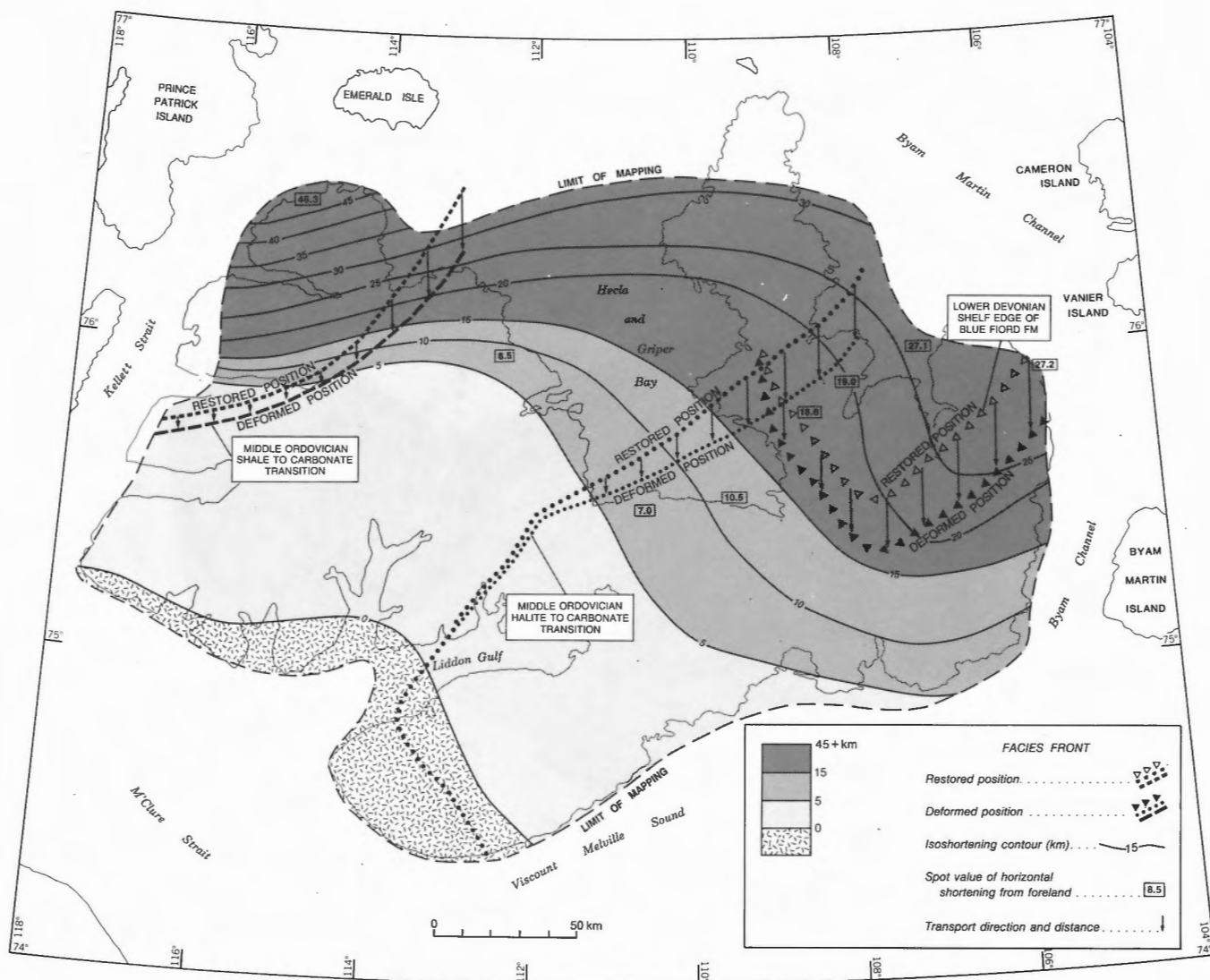


Figure 98. Regional variations in bed-length shortening of the medial rigid beam, as determined on unit tops above the lower and upper members of the Bay Fiord Formation, and the Thumb Mountain and Cape Phillips (or Blue Fiord) formations.

This solution creates a regional-scale structure similar to the triangle zone at the eastern margin of the Canadian Cordillera of southern Alberta (Gordy et al., 1977; Jones, 1982). A comparable structure is McMechan's (1985) "low-taper triangle zone" as first applied to parts of the Cordilleran foothills belt of British Columbia.

The taper in this case refers to the angle of the tectonic wedge created by thrust-faulted strata enveloped by the hinterland dip of the basal detachment and the foreland dip of the upper detachment. For the Alberta foreland wedge, the taper is 16° and the upper detachment is probably eroded to surface 7 km west of the foreland limit of deformation (Gordy et al., 1977). In British Columbia, the taper angle and width (as

taken from cross-sections of McMechan, 1985) is 7° and 65 km, respectively. In contrast, the implied taper angle within the salt-based portion of the Parry Islands Fold Belt is about 1.6° , and the minimum potential taper width for that portion of the fold belt south of the Sverdrup Basin is 173 to 184 km assuming the upper detachment riding in the Cape De Bray Formation exits to surface at the sub-Carboniferous unconformity.

This solution, favoured in the construction of Section J (which does not involve the sub-Bay Fiord detachment), might also be valid for Sections A through I if: 1) the rocks can be proven mechanically capable of producing an underthrust wedge of the dimension indicated above; 2) a through-going

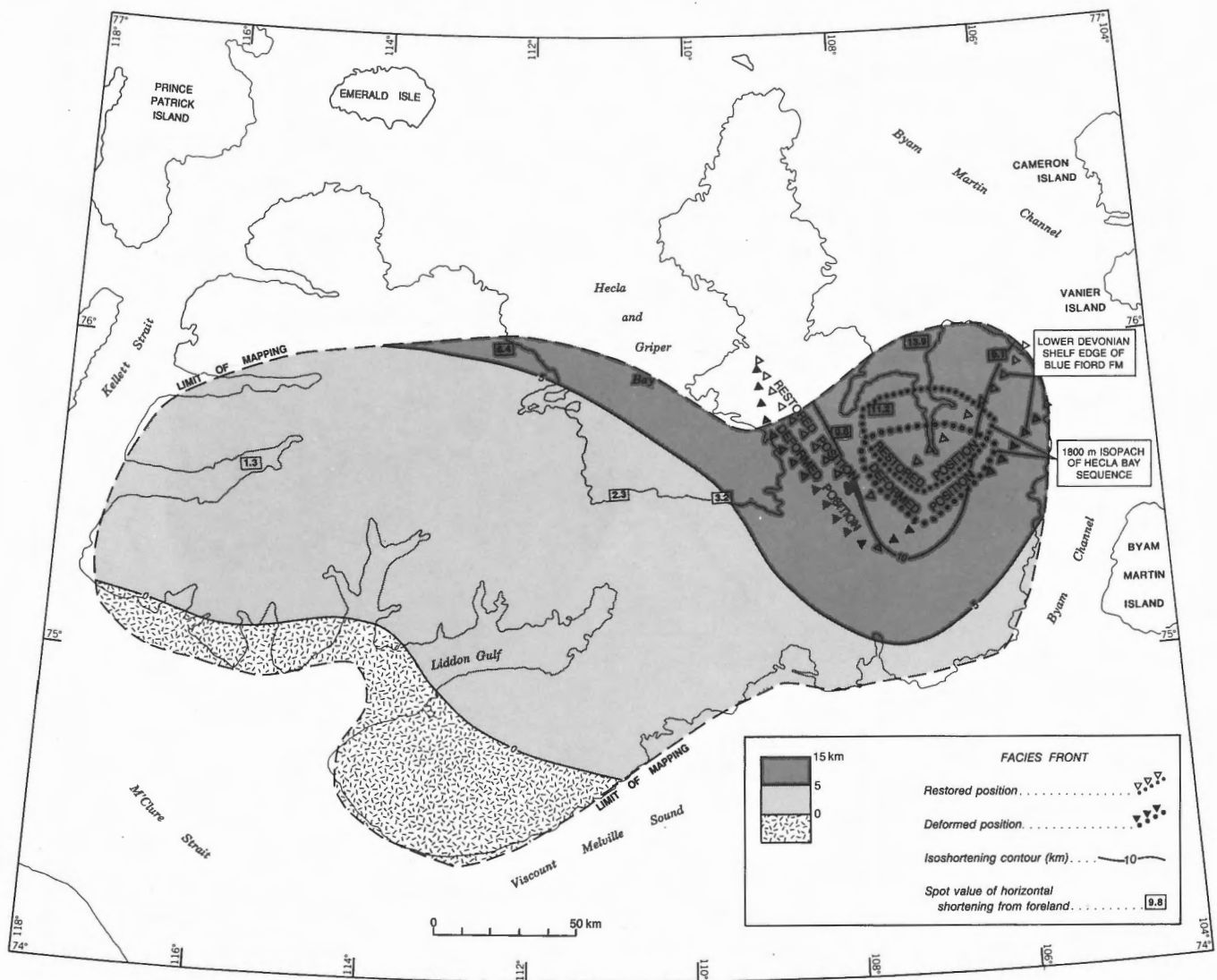


Figure 99. Regional variations in bed-length shortening of the upper rigid layer, as determined on the contact above the Hecla Bay Formation. Location of the depositional minimum (1800 m) isopach of the Hecla Bay Sequence is shown in restored position, as is the restored Blue Fiord depositional shelf edge (as determined and illustrated on Fig. 98). The region of compactional thinning of the Hecla Bay Sequence has been shifted off the Blue Fiord bank in this attempted palinspastic restoration. This would not be the case if the actual horizontal shortening of the Hecla Bay Formation were closer to that of the Blue Fiord and underlying carbonate units.

detachment is discovered in or near the Cape De Bray interval; 3) this detachment can be found to exit through the clastic wedge to surface; and 4) there is no other, less complex solution.

Solution 2: volume redistribution (tectonic thickening)

Implicit in the triangle zone solution are assumptions regarding styles of deformation. Balancing and restoring deformed beds by measuring bed lengths

implies that bedding thickness remains constant in folding and that shortening is only accomplished by a combination of layer-parallel slip and obvious reverse faulting. Given sufficient outcrop, it is possible to document centimetre- or even millimetre-scale deformation. With the aid of a microscope, it is possible to detect much smaller features. The cross-sections in this account were mostly constructed with the aid of low-resolution reflection seismic profiles and 1:60 000-scale aerial photographs. At these scales, the smallest folds are 30 to 50 m in size, and variations in unit thickness of less than 100 m are mostly ignored or undetectable.

It is possible that the concentric style of deformation, which preserves constant bed thickness, does not apply to the Hecla Bay Formation and other siliciclastic units of the Devonian clastic wedge. In this second proposed solution to the balancing problem, there is no through-going upper detachment, and shortening within anticlines at depth is exactly matched by some form of penetrative shortening within surface anticlines; for example, mesoscopic folds and intraformational imbricates in rigid layers and ductile flow of intercalated mudrock.

Volume redistribution is implied by restored Sections A through I; the formations of the clastic wedge have been area balanced and restored to an original bed length that is equivalent to that of the rigid units between the Bay Fiord and Cape De Bray formations. In this type of balancing, cross-sectional areas of units are equal on both deformed- and restored-state cross-sections. The magnitude of tectonic thickening that is required by this solution is generally small (see marginal notes of Sections A through I); 2 to 10 per cent for all but two parts of Sections A and B, where required thickening ranges to about 23 per cent.

The validity of this solution could be tested qualitatively by discovery of contractional deformation features in the clastic wedge too small to take into consideration at the scale of the prepared maps and sections. Convincing proof would also have to show that these features are quantitatively common enough throughout the clastic wedge to produce the desired syntectonic thickness increases.

Solution 3: volume loss (tectonic compaction)

In this solution, the balancing problem is conveniently removed from the system. As in the previous model, there is no through-going upper detachment, and shortening differentials above the basal detachment are solved between one syncline and the next. However, there is no need to invoke an increase in formation thickness during deformation. In the present model, the shortening of the Devonian clastic wedge is accommodated by a combination of loss in sediment volume and conventional folding, either simultaneously or consecutively. To create the differential, the syntectonic volume loss from the clastic wedge must greatly exceed any similar volume loss experienced by the rigid carbonate formations at depth. Outcrop- and microscopic-scale evidence of volume loss includes axial planar cleavage, strain fabrics as preserved in fossils and other primary depositional features, pressure solution on mineral grain surfaces, mineralogical phase changes and increased grain packing density. Evidence of resultant large-scale fluid movements could include regional variations in cementation, fluid overpressuring, mud diapirism, mud volcanoes, and accumulations of hydrocarbons.

It is worth noting in this respect that Engelder (1979) has found evidence for more than 15 per cent layer-parallel shortening in the Devonian clastic wedge of the foreland salt-based fold belt exposed on the Appalachian Plateau of western New York state. This type of shortening is expressed as fold-parallel compressive strain of deformed crinoid ossicles. Strain

MELVILLE ISLAND'S SALT-BASED FOLD BELT

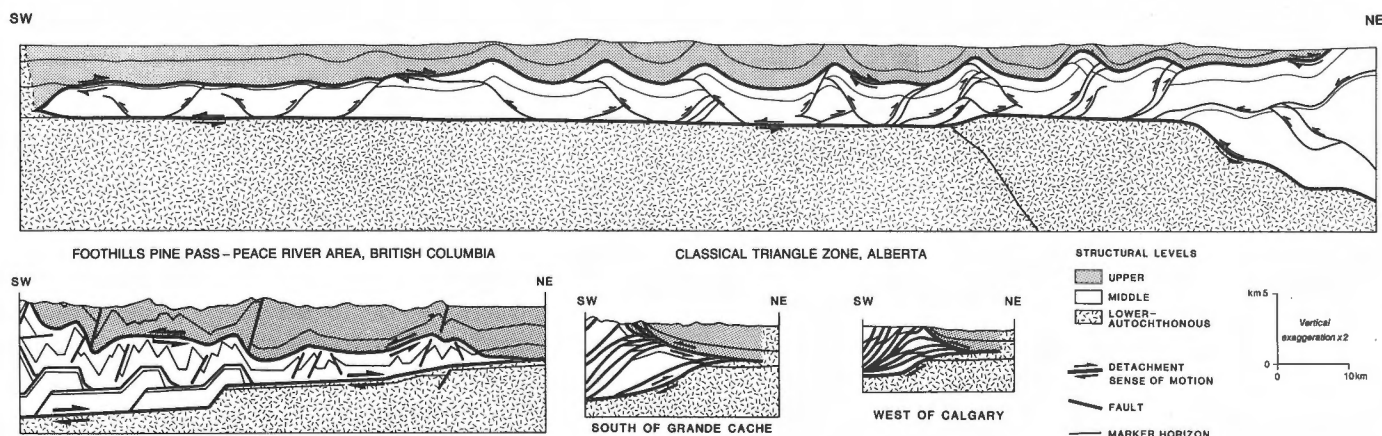


Figure 100. Possible structural geometry of the Parry Islands Fold Belt, compared with similar triangle-zone geometries of the Pine Pass/Peace River area of British Columbia (after McMechan, 1985) and of the Foothills belt near Calgary (after Gordy et al., 1977).

features are believed to result from a combination of mechanical twinning of calcite (to account for 1–5% layer-parallel shortening) and cleavage-forming calcite dissolution from fold-parallel ossicle walls.

Solution 4: syntectonic sedimentation

The fourth solution to the balancing problem requires a different form of sedimentation in the Devonian clastic wedge; one of deposition during folding. In this geological model, later-preserved sands in the middle and upper parts of the clastic wedge are deposited as the harmonic anticlines and synclines are formed. This would be expected to produce thinning and erosion of strata over anticlines. If folding continued after sedimentation then the result would be greatest bed length shortening of the oldest pre-tectonic and syntectonic formations and gradationally less shortening for progressively younger deposits. The shortening differential is presently recognized on bed lengths measured on the upper contact of the Cape De Bray Formation and on all higher units. For this fourth model to be viable, it must be proven that the Cape De Bray and overlying Devonian formations are at least in part syntectonic.

Approach to solutions

In order to constrain these four geological models, the bulk of this chapter will be concerned with a detailed examination of deformation kinematics. The largest kinematic elements to be considered are:

1. The harmonic folds affecting the upper rigid layer.
2. The bi-vergent thrust folds affecting the medial rigid beam.
3. Salt welts and related ductile features of the lower ductile layer (lower Bay Fiord Formation).
4. Semi-ductile features of the upper ductile layer (Cape De Bray Formation).

Folds

Scale and stratigraphic variation of folds

The observed scale of folding ranges from centimetres to tens of kilometres. The relation between scale of folding and stratigraphy is summarized in Figure 101. First-order folds with wavelengths of mostly 30 to 50 km have affected the entire Cambrian through Devonian stratigraphic section. Obvious examples have

been noted on Sections G through I. The kinematic significance of first-order folds is explored in the next chapter.

Second-order folds could also be termed detachment-related folds because of their genetic relation to the thin-skinned deformation process. Included in this category are the large, linear, harmonic folds of eastern Melville and western Bathurst islands developed above the Bay Fiord décollement (wavelength 12–17 km; length locally in excess of 350 km; Fig. 88) and the harmonic folds of the Canrobert Hills region detached within seismic unit sC4 (wavelength 3–9 km).

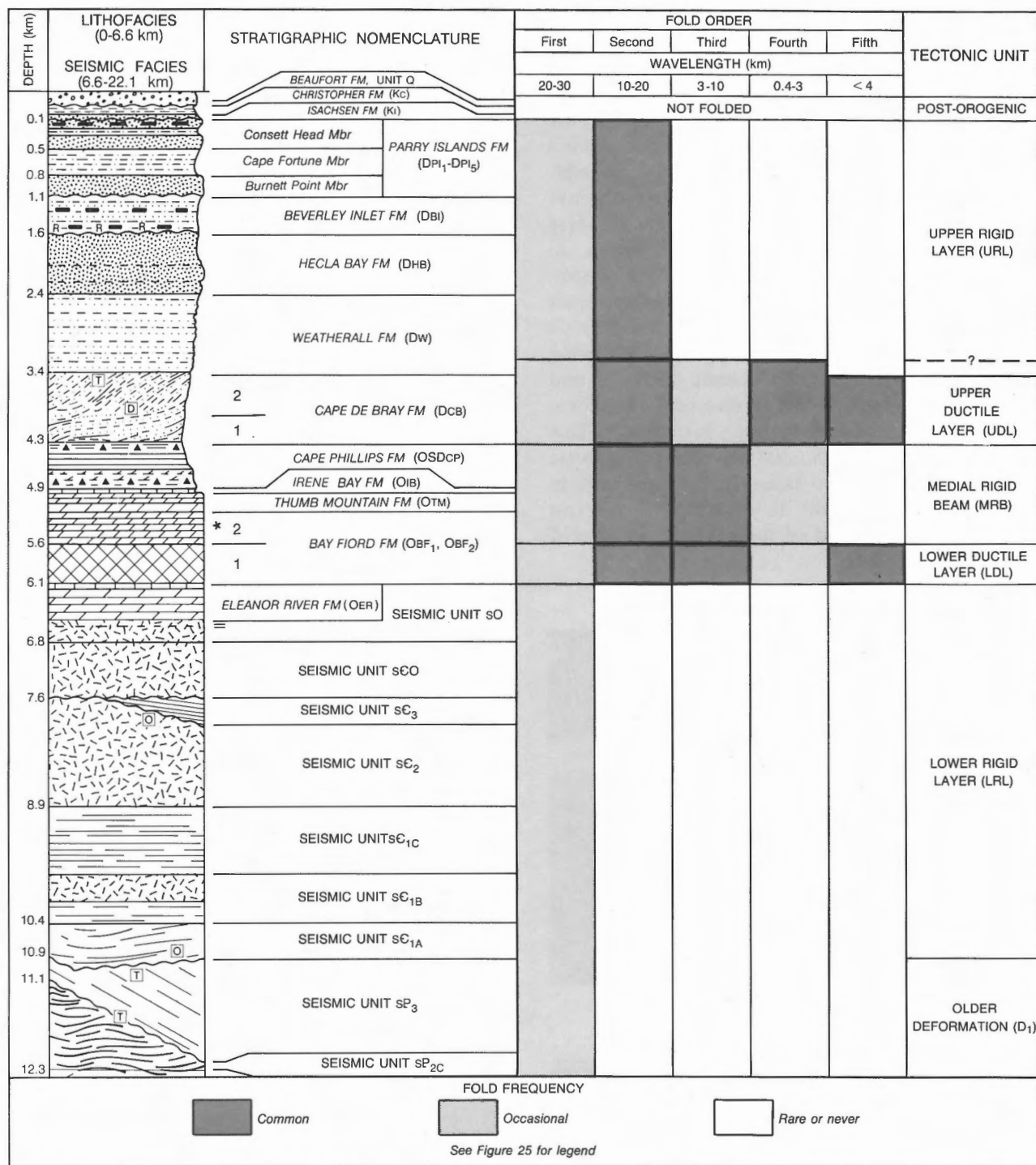
Third-order folds are also mappable at 1:250 000 scale and are either intraformational or limited in stratigraphic height to parts of two conformable formations (wavelength 400 m–2 km). The development of these and all higher order folds is attributed to slip on one of many local intermediate detachment surfaces. In Canrobert Hills Fold Belt, third-order folds are common within the Blackley and Cape De Bray formations of the Canrobert Hills (Fig. 131), and within the lower Weatherall Formation of Purchase Bay Homocline (Fig. 102). In Parry Islands Fold Belt, examples are detected on reflection seismic profiles of Sections C and G.

Fourth- and higher-order folds range downward from outcrop scale to hand specimen size (one centimetre–several hundred metres). Folds of this magnitude are common in the Cape De Bray and lower Weatherall formations, in the Blue Fiord Formation of Towson Point Anticlinorium and in all the basin facies rocks of the Canrobert Hills (Figs. 103B–D, 104B–D, 130, 131). Centimetre-scale folds have also been observed in laminated anhydrite of the lower Bay Fiord Formation (Fig. 143).

Principal tectonic transport directions

The use of mappable fold patterns to determine principal tectonic transport direction in two dimensions was developed initially with the aid of simple lab experiments by Tokuda (1926–27). Results were applied by Norris (1972) to determine a northeast–southwest direction of transport for the arcuate Laramide fold systems of the northeastern margin of the Canadian Cordillera.

Tokuda showed that when flat-lying sheets of plastic paper coated with rice paste were pushed from one end, the applied force created diagnostic fold patterns in the deformed paper. These patterns included



relaying fold bundles in directions perpendicular to the indenting feature, and en echelon bundles in peripheral areas oblique to the applied push. The en echelon arrays were characteristically right-stepping (dextral) to the right of the applied force and sinistral on the left side. Maximum horizontal shortening is also inferred

to occur along a line of section parallel to the direction of applied force where folds are arranged in relaying sets.

The regional map pattern of folds associated with the salt-based décollement in the western Arctic Islands

is illustrated in Figure 88. Over a distance of 470 km, the eastern and southeastern limit of the Ordovician evaporites against coeval carbonates of Boothia Uplift and the Arctic Platform is marked by an array of left-hand en echelon fold terminations. In contrast, the much smaller, southwest-trending belt, which defines the limit of salt against the Arctic Platform of Dundas Peninsula and Viscount Melville Sound, displays right-hand en echelon fold terminations. Between these contrasting foreland limits of the fold belt is an intervening evaporite facies front that has a sub-latitudinal trend. Salt-based folds at the foreland limit in this area are also east-west-trending and display no preferred dextral or sinistral arrangement. Following from the methods suggested by Tokuda (1926-27) and Norris (1972), the implied overall direction of tectonic transport for the salt-based fold belt is southerly. This direction is the one assumed in the palinspastic restoration of depositional facies fronts illustrated in Figures 98 and 99 and is also the direction perpendicular to the trend of the most closely-spaced iso-shortening contours.

Asymmetry of second-order folds

Departures from fold symmetry can be used to determine local transport direction (vergence) of deformed strata, and the dip direction and sense of slip on thrusts that fail to reach the surface. The inclination of axial planes of second-order surface anticlines has been measured and compared to attitudes of spatially associated major reverse faults that occur at the level of the Thumb Mountain Formation and that sole into the sub-Bay Fiord detachment. Results indicate that all surface folds display a high degree of symmetry and that 93 per cent of fold axial planes are inclined to between 80 and 90° (Fig. 105). Facing direction of asymmetrical anticlines is nearly equally split between north-vergent (55%) and south-vergent (45%). High fold symmetry implies an equal development of synthetic and antithetic planes of simple shear during folding and a related tendency for equally abundant forward- and backward-dipping reverse faults at depth. Chapple (1978), and Davis and Engelder (1985, 1987) relate this state of strain in fold and thrust belts to a

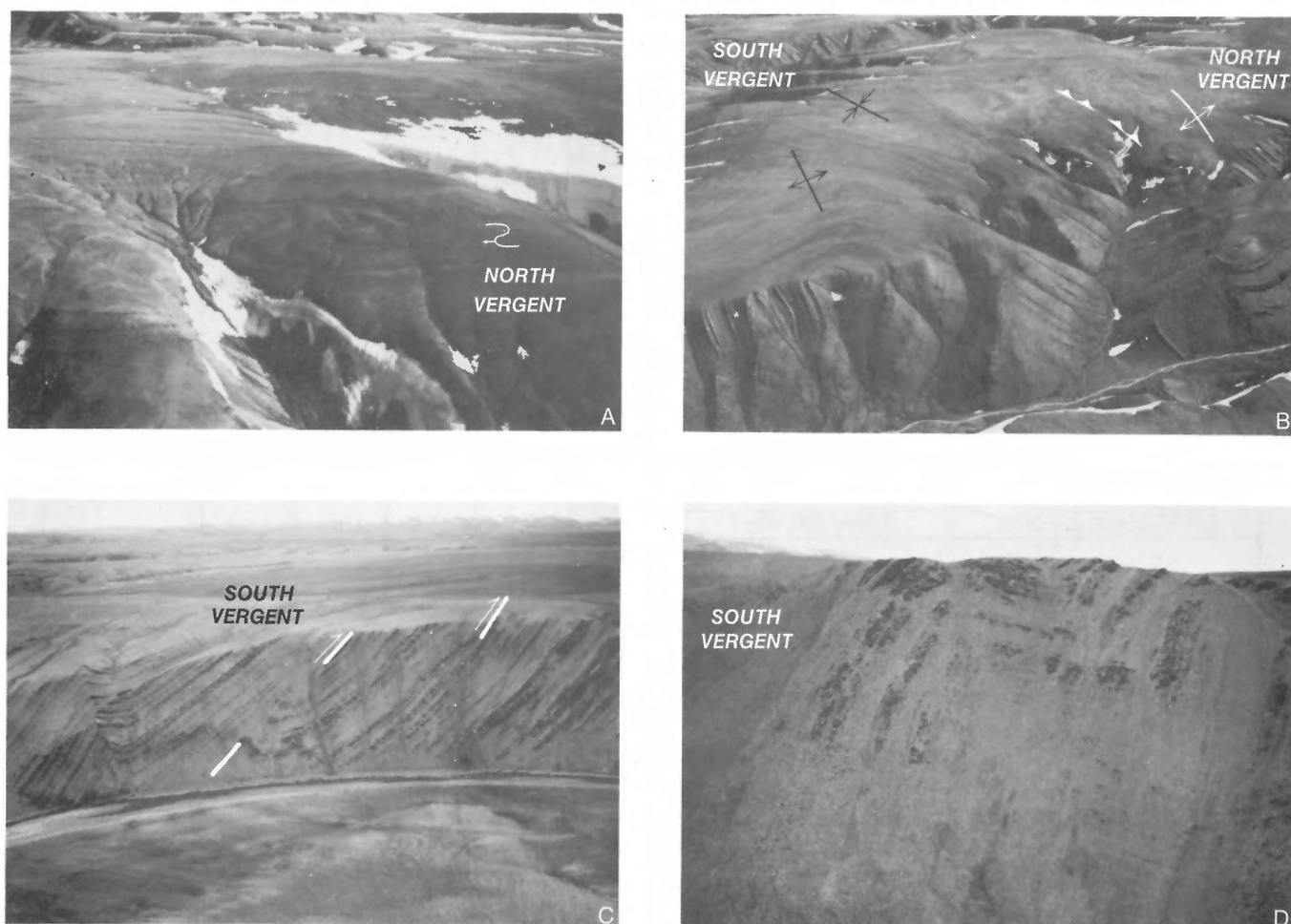


Figure 102. Outcrop-scale structures in the Weatherall Formation, A-D: Purchase Bay Homocline, northwestern Melville Island. Axes of minor folds and faults are indicated. ISPG photos. 2887-11, -13, -28, -29.

shallow-dipping basal décollement of low shear strength. The basal shear strength of the lower Bay Fiord Formation during deformation is calculated later in this chapter.

Fold asymmetry is often used to predict the dip of major subsurface thrusts where detailed seismic and other subsurface structural data are lacking (as is the case for many thrust foldbelts). The second-order surface folds of Parry Islands Fold Belt would be only modestly useful in such an exercise; 32 per cent of the related thrusts have a transport direction opposite that

predicted by surface fold inclination. This unpredictability is due to superposed folding (see Chapter 7) and the ductile behaviour of the Cape De Bray Formation (see below, this chapter).

Figure 105 also features fold and thrust inclination as a function of distance from the southern limit of deformation. A startling revelation of this plot is the tendency for 67 per cent of the folds and 65 per cent of the largest subsurface thrusts to be south-facing at 0 to 100 km from the southern foreland. In contrast,

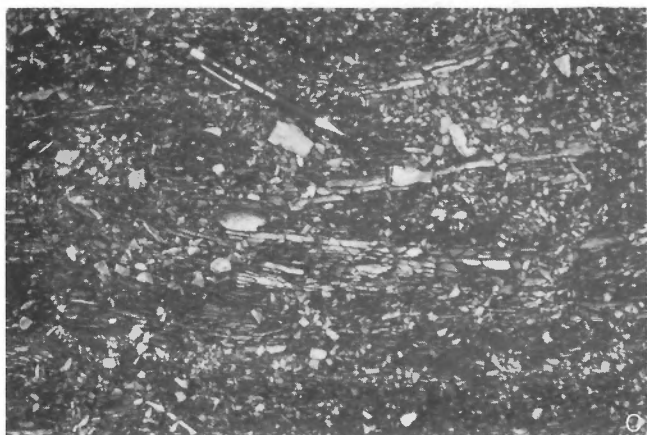
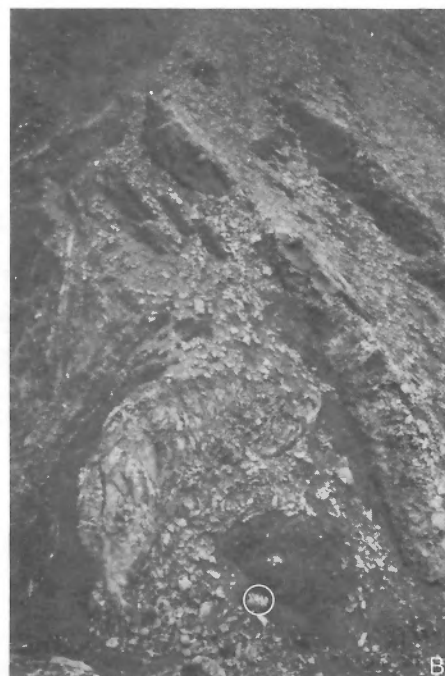


Figure 103. Outcrop-scale structures in the Cape De Bray Formation. **A.** Bedding entirely obliterated by cleavage in typical outcrops southeast of McCormick Inlet. Circled pack-sack for scale in A, B. **B.** Ductile mudrock and boudinaged sandstone bed, head of Ibbett Bay; **C, D.** Tight, small-scale folds in thin bedded, very fine grained sandstone (pencils for scale), head of Ibbett Bay. ISPG photos. 2887-9, -32, -51, 2912-6.

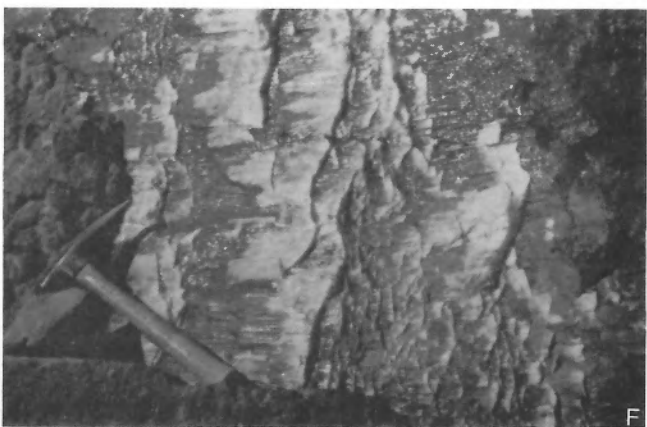
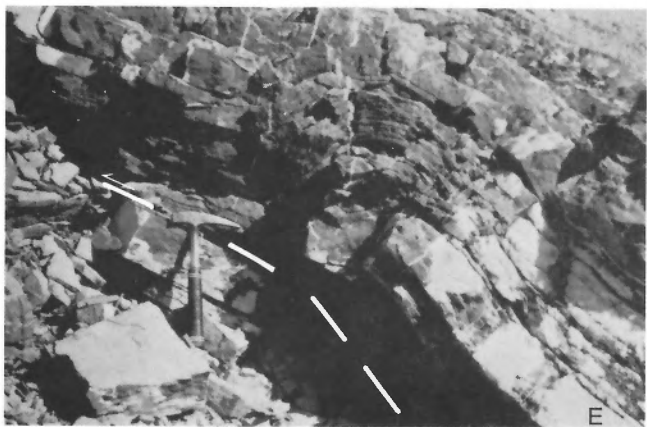
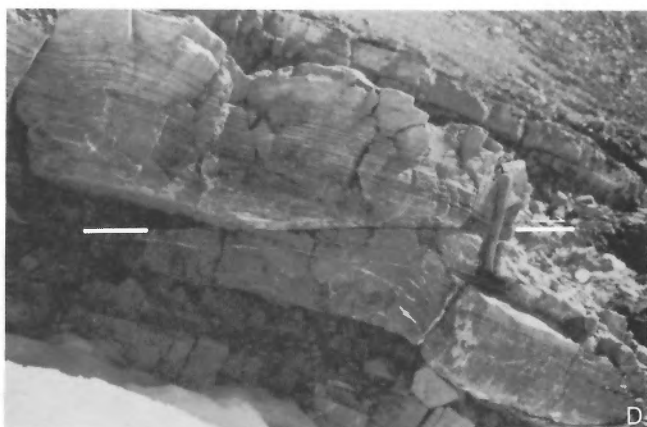
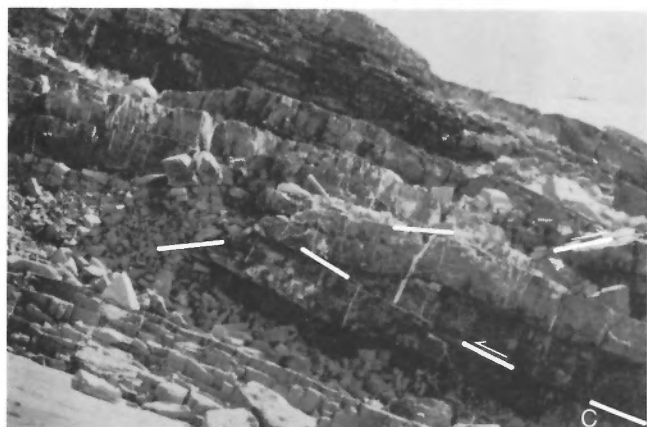
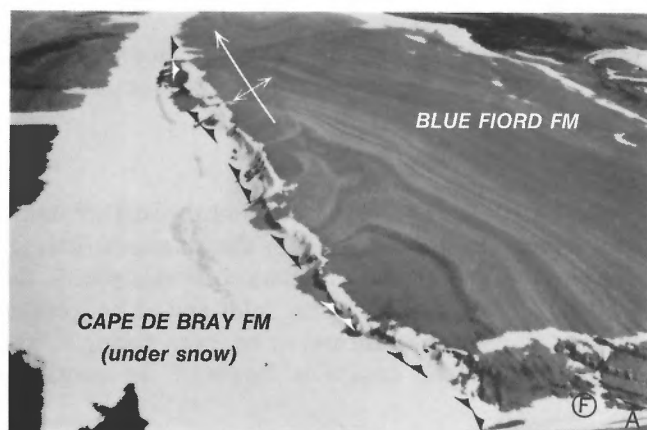


Figure 104. Outcrop-scale structures in the Blue Fiord Formation, Towson Point Anticlinorium (stream section near the S on Fig. 39). **A.** North-vergent thrust and hangingwall anticline. **B.** Minor anticline and north-vergent thrust displacing a calcite vein; minor left-lateral strike-slip fault partly healed with vein calcite (height of section is about 15 m). **C.** Fish-tail thrust faults in veined limestone (hammers for scale in C–F). **D.** Minor thrust and footwall drag anticline in a stromatoporoidal limestone bed. **E.** A tilted, fault-bend fold. **F.** Fault plane slip lineations with steps in accretionary calcite. Movement to the left is assumed to have occurred on this exposed horizontal rock surface. ISPG photos. 2887-5, -14, -19, -20, -24, -57.

70 per cent of the folds and 78 per cent of the related large thrusts are north-vergent at 100 to 200 km from the foreland. Although this pattern is greatly modified

by conjugate faults, the overall pattern is one of an upright fold fan that dies away above the southern and northern limits of the Bay Fiord evaporites.

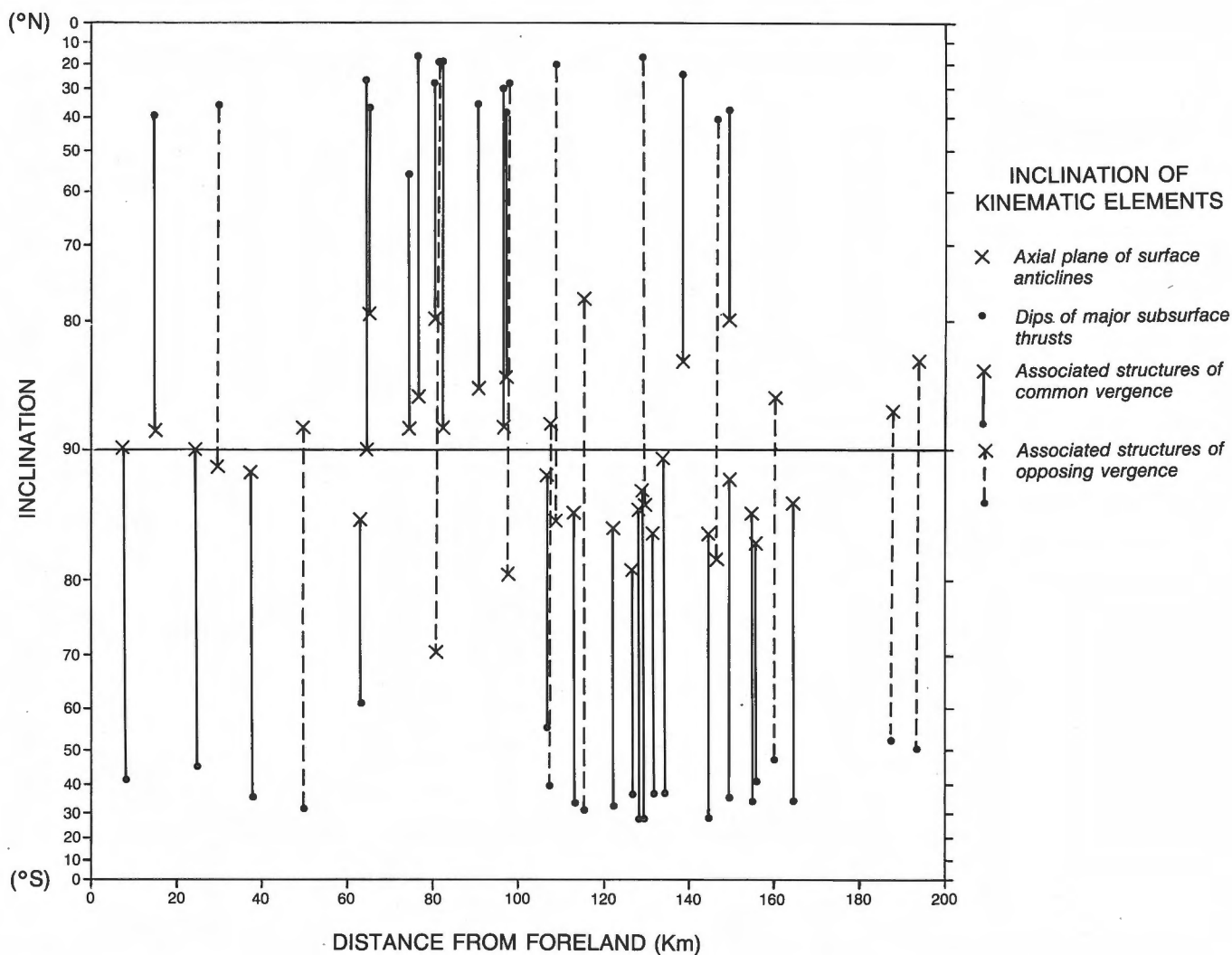


Figure 105. Graph of the axial-plane inclinations of surface anticlines and the dips of associated major subsurface thrusts, plotted as a function of distance from the foreland. At zero to 100 km from the foreland 67 per cent of the surface folds and 65 per cent of the major subsurface thrusts verge toward the south. Between 100 and 200 km from the foreland, 70 per cent of the surface anticlines and 78 per cent of the major subsurface thrusts verge toward the north.

Nonparallel folding in the Devonian clastic wedge

Cross-section constructions and restorations were completed under the assumption that during deformation the siliciclastic formations of the Devonian clastic wedge above the Cape De Bray Formation behaved as a single competent layer, and that bed thickness remained constant during folding. The result of this assumption is a train of concentric folds on each of the cross-sections. However, most rocks do not usually conform to this ideal. Ramsay (1967) showed that most natural folds fall in the realm between truly concentric and truly similar. From this observation he was able to create a widely accepted fold classification based on orthogonal unit thickness measured around fold hinges that are observed in profile.

Unfortunately, it is not possible to reliably determine most thickness variations around fold hinges for most second-order folds of eastern and central Melville Island. The surface expression of these folds is well known from aerial photographs, satellite images, and geological mapping. Fold plunge, determined geometrically on the assumption of concentric style, varies between 0 and 6°. Correct down-plunge projection, however, requires abundant in-place outcrop, which is mostly lacking. Absence of exposed bedrock prohibits a detailed understanding of axial plunge variations caused by inherent ductile properties. This problem is compounded by the poor quality of seismic reflection profiles over steep-limbed anticlines. Where shallow image quality is good (profiles of Sections F, H and I), style of folding in the medial Weatherall through Hecla Bay formations can be seen to be close

to concentric. It is therefore reasonable to assume that concentric folds are dominant everywhere. Small departures from a parallel style identified on seismic profiles could also be attributed to lateral velocity fluctuations, miscorrelation of reflection segments, and primary depositional variation. Nevertheless, there is evidence to indicate that nonparallel folds do exist in the siliciclastic formations of the Devonian clastic wedge: 1) third- and higher-order folds are common in the lower Weatherall Formation of Purchase Bay Homocline; 2) parasitic downward-pointing cusped-shaped synclines that occur at two locations on seismic profile P1763/1193 (Note 1 of Figs. 106, 107; Section H, Note 6) die out gradationally upsection; 3) tectonic thickening of the Weatherall Formation occurs on the south-facing limb of Nias Point Anticlinorium and Barry Bay Anticline (Section I, Note 21); 4) rapid southerly thickening of the Hecla

Bay Formation, possibly of tectonic origin, occurs on the north limb of Richardson Point Anticline (Section C, Note 13) and Baldwin River Anticline of Section A (Fig. 108, Note 7); and 5) three, third-order folds are probably responsible for some near-surface steepening of the limbs of Sabine Bay Anticline (Fig. 109, Note 1; Section G, Note 11). Indirect evidence of nonparallel folding of the Weatherall Formation is provided by the accompanying aerial photograph of Robertson Point Anticline (Fig. 110). The inset enlargement illustrates mesoscopic structural features associated with a room problem in the fold hinge. Minor folds, thrusts, oblique faults and some sinuosity of the fold hinge can be attributed to a nonconcentric, locally ductile style of deformation. It is worth emphasizing that these structures, only a few tens to several hundred metres in size, are too small to be considered in 1:250 000 scale mapping and are also

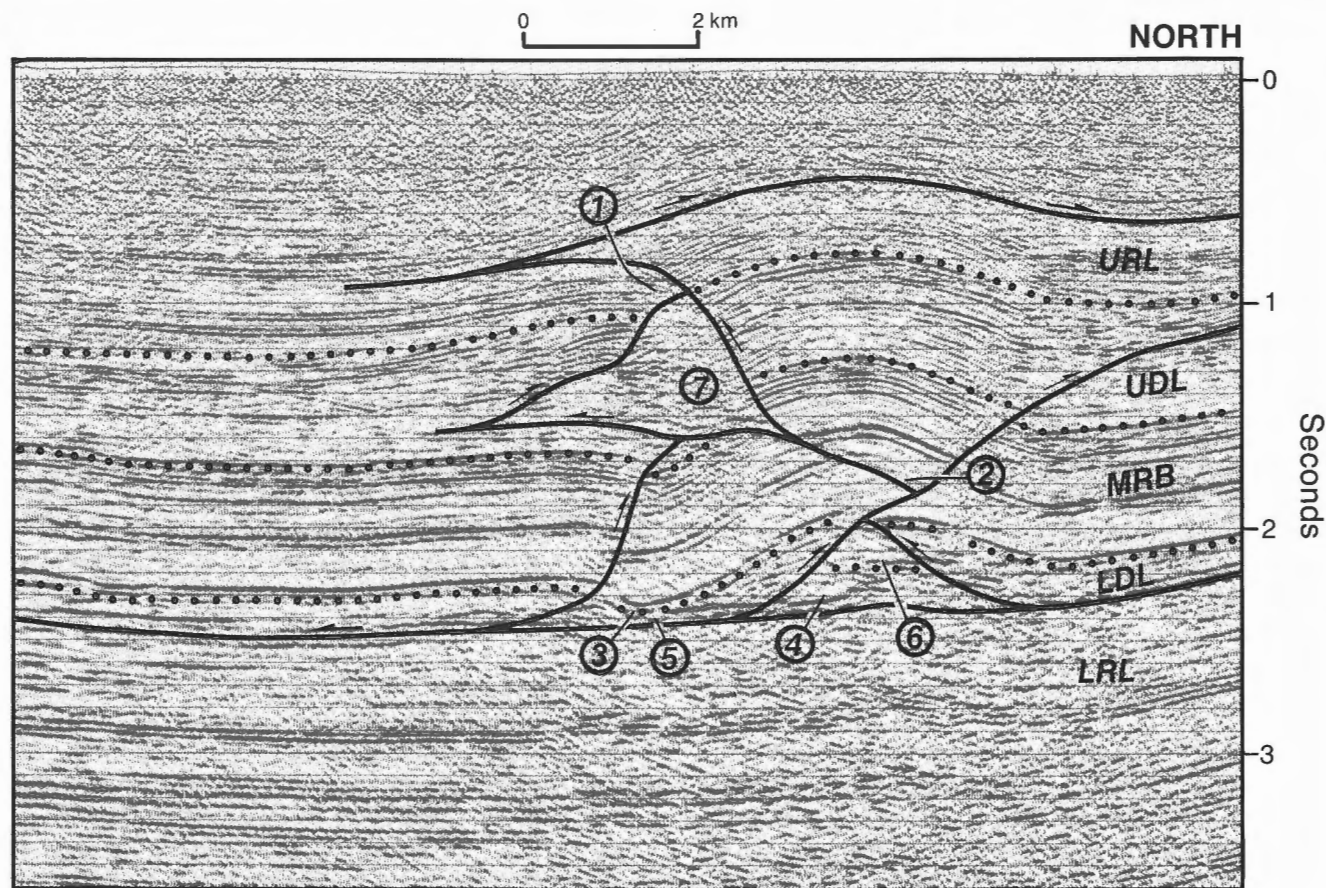


Figure 106. Mechem River West Anticline, on a part of seismic profile P1763/1193, Section H. Component formations of each layer are listed in Figure 101. LRL, lower rigid layer; LDL, lower ductile layer; MRB, medial rigid beam; UDL, upper ductile layer; URL, upper rigid layer; 1, cusped-shaped syncline beneath an upper detachment in the Weatherall Formation; 2, local detachment below the Thumb Mountain Formation; 3, footwall syncline; 4, compound salt well with a faulted small hinge saddle; 5, local evacuation of salt from syncline; 6, a triangular, fault-bounded tectonic fragment of the medial rigid beam is encapsulated by evaporites; 7, tectonic thickening of the Cape De Bray Formation above upward-flattening thrusts emerging from the underlying Cape Phillips Formation.

unlikely to be imaged on reflection seismic profiles. Nevertheless, such structures may have played a significant role in the shortening and deformation history of the clastic wedge, and could account for some of the unrecognized intraformational shortening required by the second of the four possible solutions to the fold belt shortening problem discussed previously in this chapter.

In spite of these observations, there is only sparse field evidence to indicate a non-brittle style of deformation for the Weatherall and younger formations. Features attributed to even modest levels of layer-parallel shortening (such as slaty cleavage or crenulation) are unknown above the Cape De Bray Formation. Primary sedimentary structures including flat lamination, trough and planar cross-stratification, ripple crosslamination, shelly macrofauna and trace fossils are all exceedingly well preserved, even in vertical-dipping beds and in the hinge region of

anticlines. Microscopic fabrics have not been studied. The only exception to the above point is very modest levels of bedding-parallel strain witnessed in crinoid ossicles of the lowermost Weatherall Formation at one locality near the hinge of Dealy Island Anticline.

Faults

Distribution and recognition

Before entering into various aspects of fault kinematics, it is worth reviewing some general features of faults in the Parry Islands Fold Belt. Types include: faults, mostly compressional, that parallel the trends of second-order folds ("fold-parallel faults"); faults, mostly extensional, that are near perpendicular to second-order fold trends ("fold-perpendicular faults"); and various faults that are oblique to second-order fold trends ("fold-oblique faults"). The last two types of

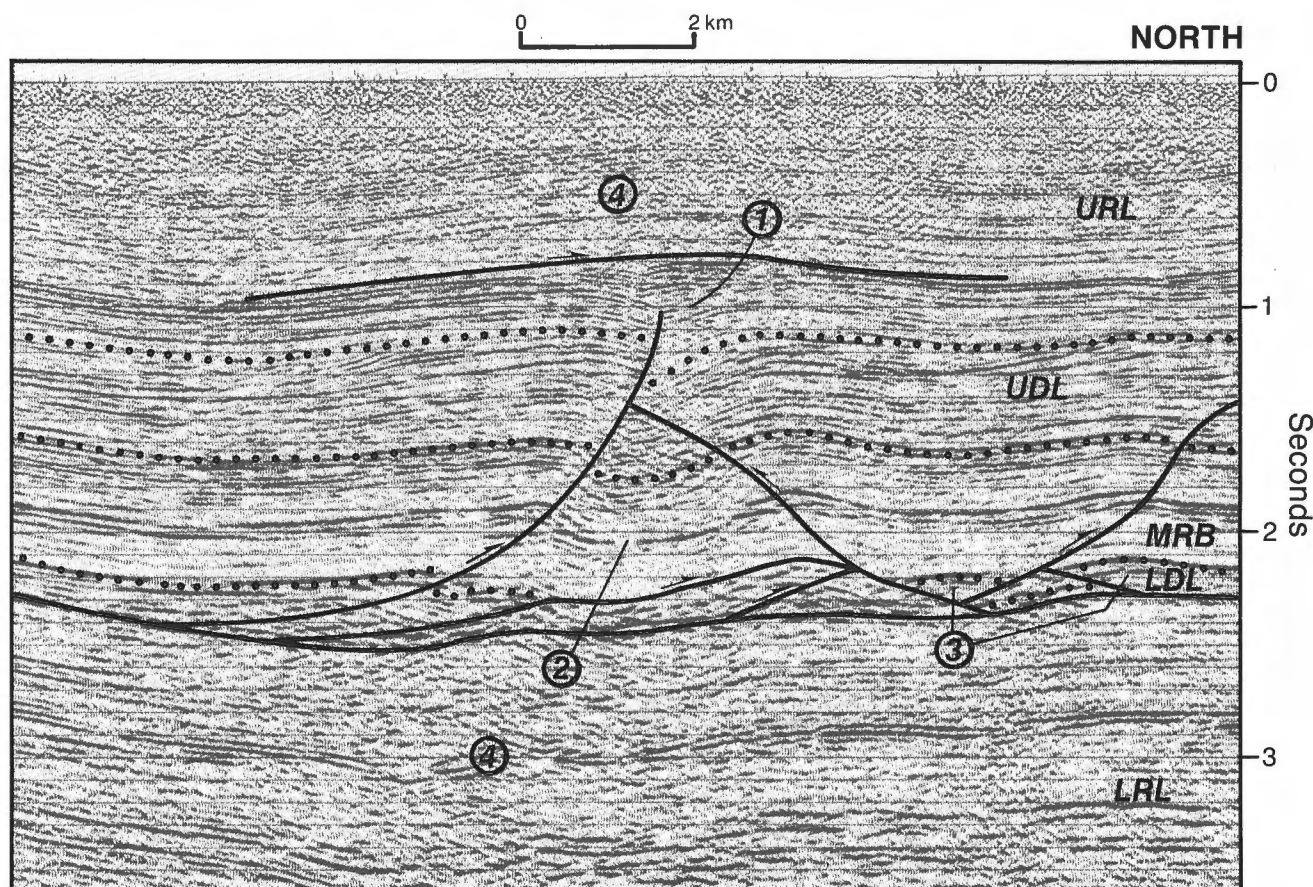


Figure 107. Beverley Inlet Anticline, on a part of seismic profile P1763/1193, Section H. Component formations of each layer are listed in Figure 101. LRL, lower rigid layer; LDL, lower ductile layer; MRB, medial rigid beam; UDL, upper ductile layer; URL, upper rigid layer; 1, cusped syncline beneath an upper detachment in the Weatherall Formation; 2, footwall syncline; 3, parasitic salt welts; 4, the crest of the D3 anticline detached on the Bay Fiord evaporites lies in the axial trough of the deep-seated D4 Liddon Gulf Syncline.

fault are of small consequence in the deformation kinematics of Parry Islands Fold Belt and will therefore be treated first and briefly.

Fold-oblique faults

Fold-oblique faults, common in the Nias Point, Towson Point and Spencer Range structures, are associated with younger phases of deformation as discussed in Chapter 7. Oblique faults within the main portion of the fold belt are rare and limited in displacement. One prominent oblique fault that strikes southeast across Burnett Point Syncline from the west arm of Weatherall Bay can be seen on satellite images.

Indicated offset is right lateral but not more than several hundred metres at any single point. The northeasterly striking sinistral oblique fault that marks the western limit of Birch Point Syncline is probably a thin-skinned tear fault linking west-striking thrusts. Northwest-striking lineaments, marginally oblique to second-order fold trends, define the northeastern limit of Isachsen Formation in the Bridport outlier and both the northeastern and southwestern limits of Isachsen Formation in the Mecham River and Skene Bay outliers. There is no seismic evidence of displacement on these lineaments. Rather, these linear features are considered to be pre-Isachsen escarpments produced by differential erosion of the sub-Lower Cretaceous peneplain surface.

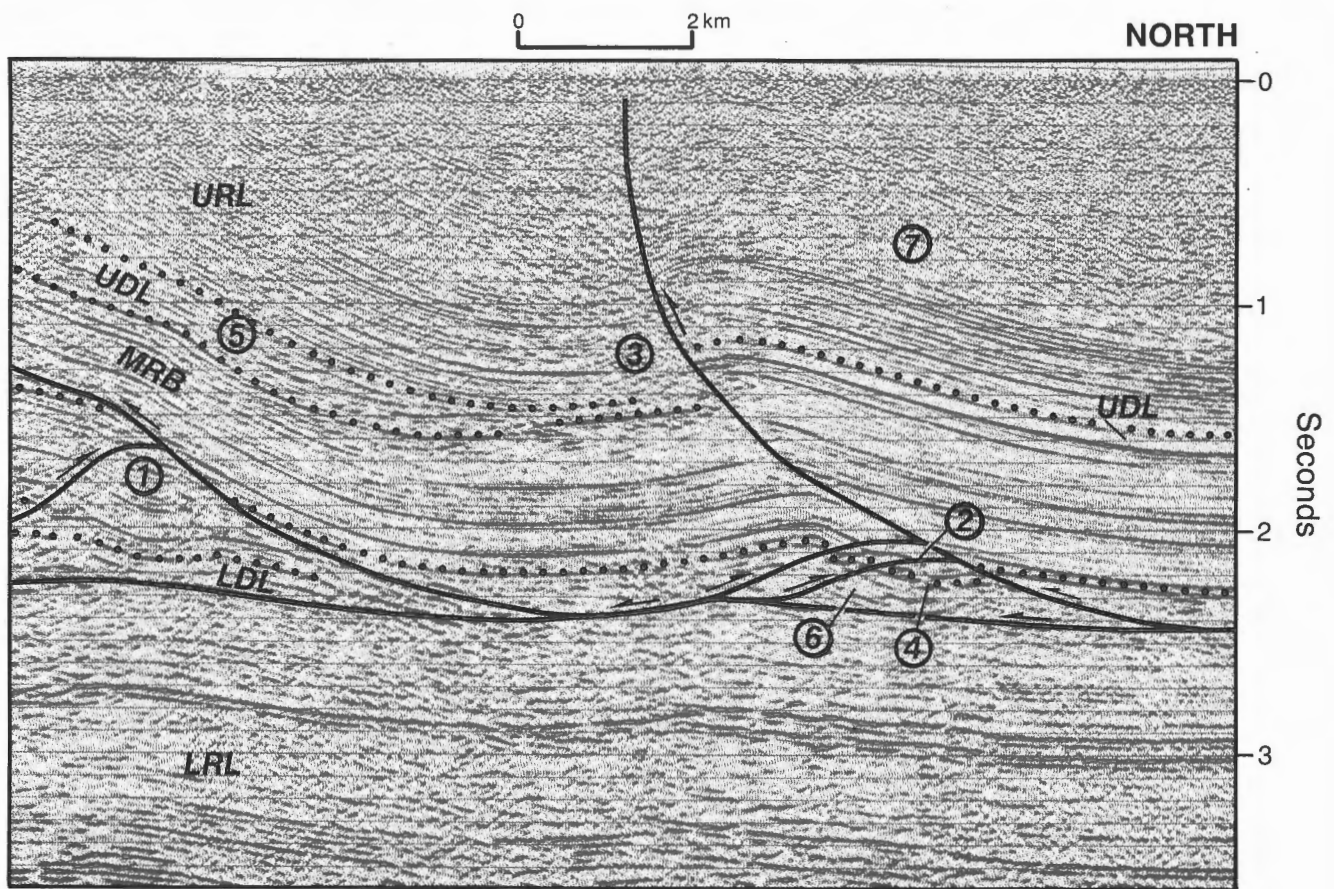


Figure 108. Baldwin River Anticline and the north half of Rea Point Anticline, on a part of seismic profile P2218, Section C. Component formations of each layer are listed in Figure 101. LRL, lower rigid layer; LDL, lower ductile layer; MRB, medial rigid beam; UDL, upper ductile layer; URL, upper rigid layer. There is also a facies transition, southward in the upper part of the beam, from Blue Fiord Formation to upper Cape Phillips Formation. 1, thrust duplication of the medial rigid beam; 2, intermediate detachment in the lower part of the upper Bay Fiord Formation; 3, footwall syncline in the Weatherall Formation; 4, footwall syncline in the lower part of the medial rigid beam; 5, changes in dip of the north-facing fold limb due to thrust wedging at depth; 6, compound anticlinal welt ('Napoleon's Hat'); 7, 20 per cent local thickening indicated for the Hecla Bay Formation from backlimb to hinge of the Baldwin River Anticline.

Fold-perpendicular faults

Fold-perpendicular and near-perpendicular faults are more common than fold-oblique faults. The longest are associated with linear aeromagnetic anomalies interpreted as unroofed gabbro dykes (see Chapter 7). Short-length perpendicular faults, most too small to be mapped and all of unknown dip direction, are exceedingly common along some anticlinal fold hinges (for example, Rea Point Anticline, and the western culmination of Beverley Inlet Anticline). These slip surfaces probably first developed during folding by hinge-parallel extension in areas of either pronounced fold arcuation, in map view, or variations in fold plunge. Perpendicular faults of extensional and wrench tectonic sense are also associated with a southerly jog

in the tectonic trend of Byam River Syncline, where it wraps around the western limit of Consett Head Anticline.

Fold-parallel faults at surface

The most common fault is the fold-parallel type. While some of these may be extensional, the majority are contractional and kinematically related to second-order folds. These reverse faults are common only at the surface between Rea Point and King Point anticlines. One sinuous thrust within Towson Point Anticlinorium places medial Blue Fiord Formation on Cape De Bray Formation. The duplicated section is about 450 m thick (Figs. 39, 104A). Small displacement thrusts are also

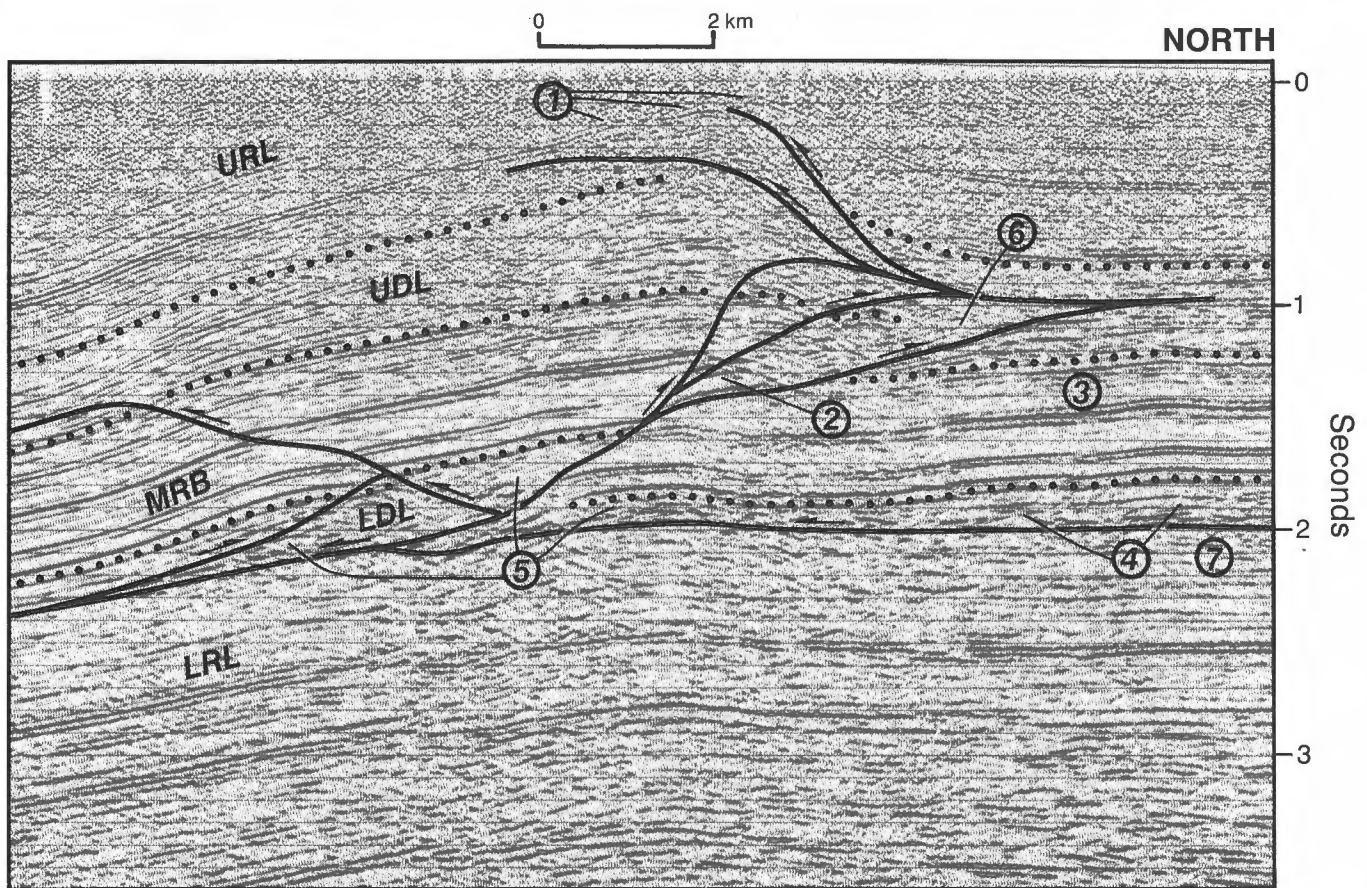


Figure 109. Sabine Bay Anticline, on a part of seismic profile P1192, Section G. Component formations of each layer are listed in Figure 101. LRL, lower rigid layer; LDL, lower ductile layer; MRB, medial rigid beam; UDL, upper ductile layer; URL, upper rigid layer; 1, third-order folds in the Weatherall Formation; 2, reflection from a thrust fault; 3, unfaulted buckles in the medial rigid beam; 4, parasitic salt welts; 5, Sabine Bay Anticline is underlain by a complex anticlinal welt that includes three welt culminations; 6, tectonic thickening of the Cape De Bray Formation above upward-flattening thrusts emerging from the underlying Cape Phillips Formation; 7, the culmination of the first-order anticline, at this location below the Bay Fiord Formation, is 10 km north of the culmination of the second-order anticline at the surface.



Figure 110. Vertical airphoto (with inset) of the Robertson Point Anticline. Mechem River is visible at the bottom. The inset enlargement illustrates mesoscopic structural features associated with a space problem in the fold hinge. Minor folds, thrusts, oblique faults, and some sinuosity of the fold hinge can be attributed to a nonconcentric, locally ductile style of deformation. Dw, Weatherall Formation; DHB, Hecla Bay Formation; DBI, Beverley Inlet Formation; DPI, Parry Islands Formation; KC, Christopher Formation. See also legend, Figure 33. NAPL photos. A16766-87, -89.

associated with third-order folds in the lower Weatherall Formation of Purchase Bay Homocline (Fig. 102C) and fourth-order folds in the Blue Fiord Formation (Figs. 104B-E). Thrusts associated with second-order folds are recognized by either footwall or hangingwall cut-off of strata at small angles to the fault trace (Figs. 53, 110). The maximum thickness of repeated or overlapped surface section is about 1000 m and maximum strike length is 41 km.

Subsurface thrusts

Thrusts are much more numerous in the subsurface. From one to ten synthetic and antithetic thrusts occur beneath every surface anticline. Evidence of thrusts at depth has been acquired from both reflection seismic profiles and exploratory wells. Repeated section occurs in the following boreholes:

1. Panarctic et al. Beverley Inlet G-13. The lower part of the Thumb Mountain Formation has been thrust over the upper Cape De Bray Formation. The repeated section is 1548 m thick.
2. Panarctic et al. Sabine Bay A-07. The basal part of the upper Bay Fiord Formation has been thrust over the lower Cape Phillips Formation (Figs. 7, 109). The repeated interval is about 880 m thick.
3. Texex King Point West B-53. The upper Thumb Mountain Formation has been thrust over the medial Cape Phillips Formation. The repeated section is 344 m thick.
4. Winter Harbour No.1 A-09. The Llandovery portion of the lower Cape Phillips Formation has been tectonically thickened. Tectonic thickness of the formation in the well is 1149 m (primary thickness is about 750 m in this area). Possible intraformational thrusts occur at 3109 and 3400 m below K.B. Faults intersected by cored intervals of the Cape Phillips Formation are associated with minor displacements on tectonic stylolites in argillaceous limestone, incipient cleavage, tectonic breccia and multiple vein sets.

The geophysical evidence for large subsurface thrusts includes: 1) velocity pull-up caused by tectonic duplication of high-velocity strata; 2) duplication of coherent seismic stratigraphic reflectors; and 3) reflections from fault planes. Examples of each are described below.

Velocity anomalies are readily observed on the otherwise subhorizontal Eleanor River Formation and

conformable underlying units. The anomaly is usually a positive deflection (up to 280 ms of velocity pull-up) of the reflectors beneath each anticline. The width of the anomaly is roughly equal to the width of the overlying thrust sheet(s), and the amplitude is proportional to the thickness of repeated high-velocity strata (Bay Fiord through Cape Phillips/Blue Fiord formations) that would otherwise have been occupied by low-velocity strata of the Devonian clastic wedge. Examples are obvious on Section F (Note 3; Fig. 111, Note 1; Fig. 112). The anomaly shape is distinctly cusped and upward pointing at levels below the Eleanor River Formation, and also disrupted by overmigration hyperbolae deeper in the profiles (Fig. 113, Note 1; Section B, Note 2; Section H, Note 2). Extensive tectonic duplication can result in breakup of deep reflectors and complex regional velocity anomalies in what must be undeformed strata (Fig. 114, Note 1; Section A, Note 4). In several cases, velocity pullup is superimposed on actual sub-Bay Fiord structural relief (Fig. 115, Note 1; Section C, Note 5; Section D, Note 11).

Recognition of repeated seismic stratigraphic reflections is the most common form of identification of subsurface thrusts (Fig. 108, Note 1). In each case, flat and concave portions of repeat section are the variety most readily imaged; these are commonly not the structurally highest panels (Fig. 113, Note 2). The width of overlapping section ranges to 3.5 km (on the south-vergent thrust beneath Robertson Point Anticline, Section A). In the extreme case, Bay Fiord evaporites have been thrust over the lowermost Cape De Bray Formation (King Point East Anticline, Section A; Baldwin River Anticline, Section B). Maximum thickness of repeated section is 2200 m.

Actual fault surface image is only apparent where impedance contrasts across such surfaces are large, and the migrated dip of the fault plane is shallow. For example, a weak reflector occurs near the thrust plane where Thumb Mountain Formation has been emplaced over the Cape Phillips Formation (Cape Bounty Anticline, Section H; Sabine Bay Anticline on Section G and Note 2 of Fig. 109; Baldwin River Anticline on Sections B), or where Thumb Mountain lies in tectonic contact with lowermost Cape De Bray Formation (Dealy Island and Beverley Inlet anticlines, Section D).

The distribution of all major thrusts and associated folds at the level of the Thumb Mountain Formation has been compiled from all subsurface data sources (migrated and unmigrated reflection profiles) on Figure 116. This map complements the surface geology map (in pocket) with which numerous similarities in

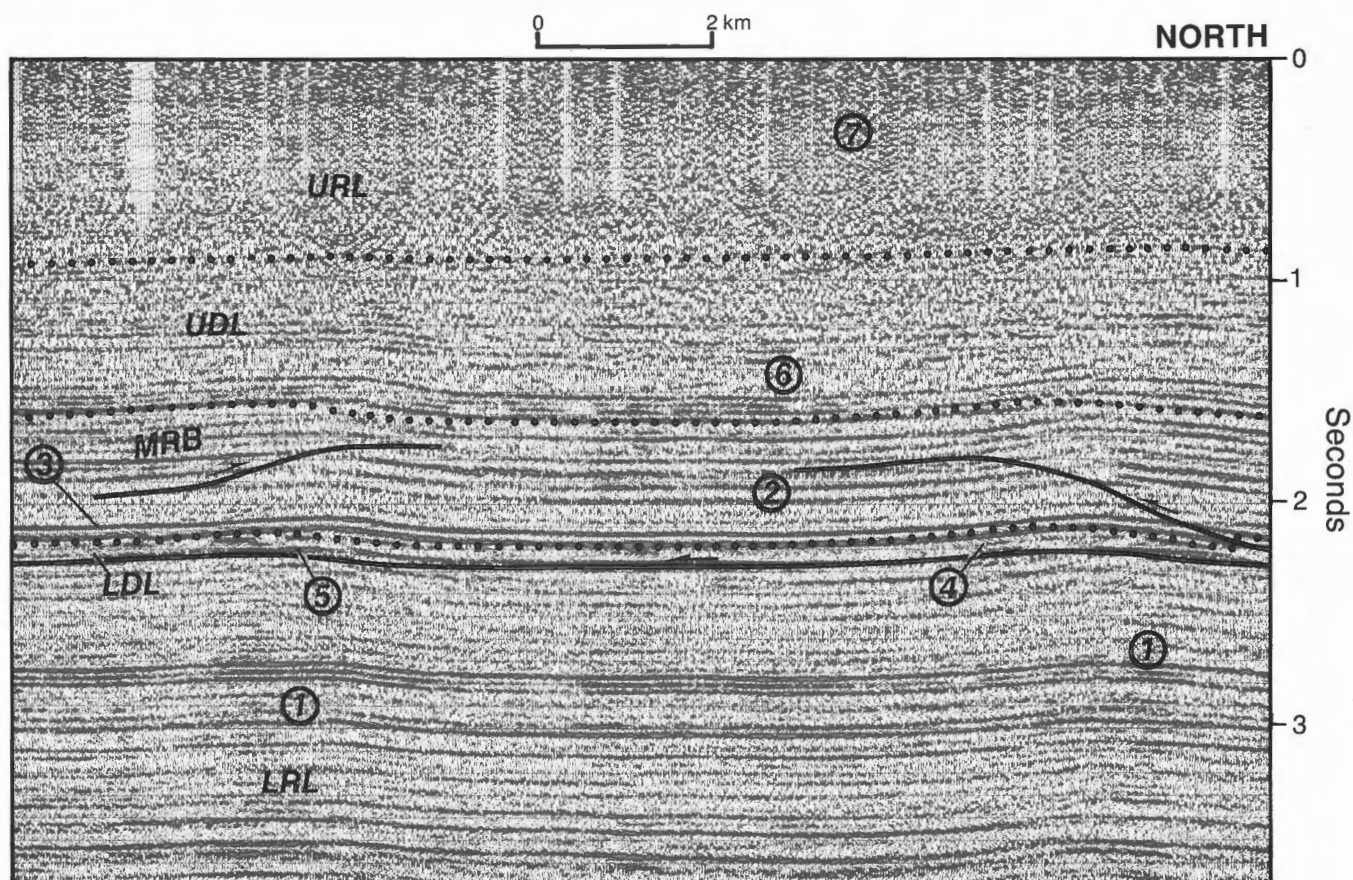


Figure 111. Cape Providence Anticline (left) and a second, unnamed anticline, on a part of seismic profile P1171, Section F. Component formations of each layer are listed in Figure 101. LRL, lower rigid layer; LDL, lower ductile layer; MRB, medial rigid beam; UDL, upper ductile layer; URL, upper rigid layer; 1, velocity pull-up due in part to some thrust duplication in the medial rigid beam; 2, detachment in the Cape Phillips Formation; 3, anticline predates faulting as the lower Bay Fiord Formation has not been offset by the thrust that is evident higher in the medial rigid beam; 4, a simple anticlinal salt welt; 5, a simple anticlinal welt with imbricated internal reflection segments; 6, a synclinal mudrock welt in the Cape De Bray Formation (thinning over the anticline, evident in the lower Cape De Bray, could be due to differential compaction during folding); 7, the amplitudes of subsurface folds decrease upsection and conformable strata are flat-lying at the surface.

tectonic trend can be seen; the southerly facing convex arc of surface folds is coincident with a southerly facing arc of subsurface thrusts. Limits are defined by a coincident change in tectonic trend along the south flank of Nias Point Anticlinorium. However, on Dundas Peninsula, the subsurface thrusts and intervening synclines extend 37 km farther onto the craton (southwest) than corresponding surface folds.

The thin-skinned fabric of the Parry Islands Fold Belt is markedly oblique to regional geophysical anomalies. The regional gravity field is east-trending and of longer wavelength (Fig. 9). Magnetic anomalies are short-wavelength N- through N40°E-trending features superimposed on a low amplitude N70°E-trending regional gradient (Figs. 10, 177). The trend of the structural fabric at the surface and at the Thumb

Mountain level is also in direct contrast with the orientation of some key depositional facies fronts, especially the southern limit of Silurian through basal Middle Devonian carbonates of the Towson Point carbonate platform (Figs. 24, 64) and isopachs defining the trend of the Cambrian(?) and Ordovician shelf margin (Figs. 55, 59, 63). There is some correspondence between the southwestern edge of thin-skinned deformation and the limit of Bay Fiord evaporites and Cape Phillips basinal mudrock and carbonate in the Dundas Peninsula area (compare Figs. 62-64 and 116). However, regional mapping indicates that throughout Viscount Melville Sound these facies limits are east-northeast-trending. In contrast, fold axes are mostly oblique to these facies fronts (compare Figs. 24 and 88). In conclusion, folds and thrusts of Parry Islands Fold Belt have been pushed from the

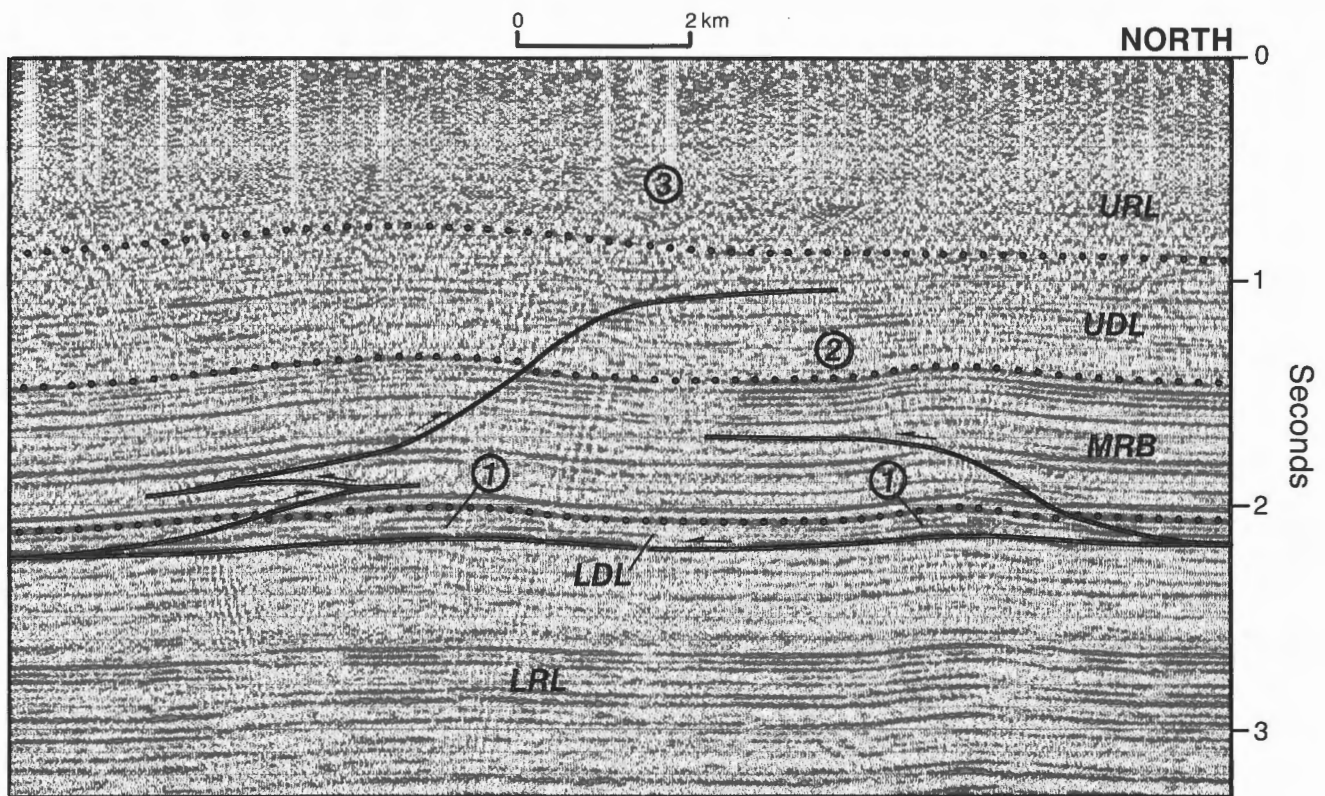


Figure 112. Cape Clarendon Anticline (left) and another (unnamed) anticline, on a part of seismic profile P1171, Section F. Component formations of each layer are listed in Figure 101. LRL, lower rigid layer; LDL, lower ductile layer; MRB, medial rigid beam; UDL, upper ductile layer; URL, upper rigid layer; 1, simple anticlinal wells in lower Bay Fiord evaporites; 2, synclinal mudrock welt in the Cape De Bray Formation (thinning over the anticline, evident in the lower Cape De Bray, could be due to differential compaction during folding); 3, the amplitudes of subsurface folds decrease upsection and conformable strata are flat-lying at the surface.

pre-existing oceanward side of the Franklinian shelf margin and southward toward the craton. Angle of obliquity and sense of convergence for the fold belt as a whole is 25 to 30° and sinistral with respect to the overall trend of the autochthonous lower Paleozoic platform margin.

Nature of vertical linkages

A distinctive feature of the subsurface thrust system is the vertical linkage of short fault segments of contrasting vergence from the base of the Bay Fiord upward through the fractured core of major anticlines. The links consist of thrust ramps and bedding-parallel basal, intermediate and upper detachment surfaces. Basal and upper décollement planes lie, respectively, below the Bay Fiord evaporites and at various levels within the Cape De Bray Formation. Intermediate detachment surfaces are less predictable. Examples can be found within the upper Bay Fiord (Fig. 108, Note 2), at the base of the Thumb Mountain (Fig. 106, Note 2), in the medial Cape Phillips (Fig. 111, Note 2)

and in the Blue Fiord Formation of Richardson Point (Fig. 117, Note 1) and Towson Point (Fig. 39) anticlines.

A range of seven basic structures are sketched in Figure 118 with examples cross-referenced to Sections A through H. Simple thrust systems are developed from the basic structures by an increased number of synthetic and antithetic conjugates as illustrated in Figure 119. Other, more complex thrust systems can be imagined depending on additional variables, such as the upper level of faulting, the point of nucleation of splays off both foreland- and hinterland-vergent major thrusts, and the distribution of conjugates associated with each splay fault. Examples of composite thrust systems include: Sabine Bay Anticline (Fig. 109) on Section G, a hinterland-vergent thrust with hangingwall conjugate and splays linked upward to a foreland-vergent thrust also with splays; Rea Point Anticline on Section B, a hinterland-vergent thrust with zig-zag structures, and conjugates on each imbricate; and Richardson Point Anticline (Fig. 117) on Section A, a hinterland-vergent

NORTH

0 2km

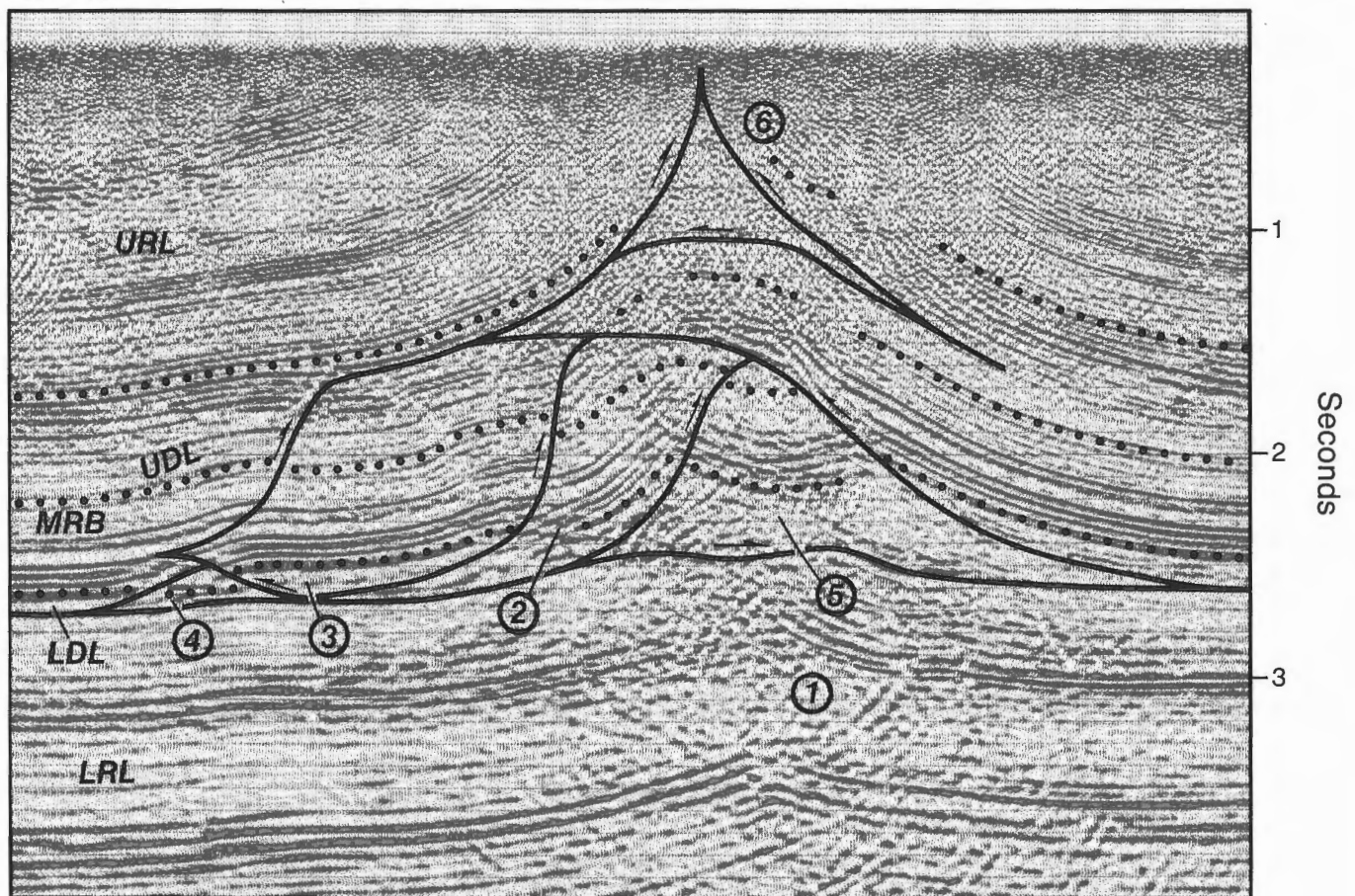


Figure 113. Robertson Point Anticline, on a part of seismic profile P1660, Section C. Component formations of each layer are listed in Figure 101. LRL, lower rigid layer; LDL, lower ductile layer; MRB, medial rigid beam; UDL, upper ductile layer; URL, upper rigid layer; 1, large velocity pull-up attributed to thrust duplication of the medial rigid beam; 2, footwall syncline; 3, salt welt beneath a parasitic anticline; 4, moderate thinning of the lower Bay Fiord Formation from beneath the Mecham River Syncline; 5, the Robertson Point Anticline is underlain by a complex anticlinal salt welt featuring four separate culminations; 6, a simple anticlinal mudrock welt within the Cape De Bray Formation is also indicated by surface structure.

thrust with splays and one hangingwall conjugate also with splays.

Nature of lateral linkages

In thrust belts with a single dominant direction of thrust transport, there are a limited number of displacement transfer mechanisms, including: 1) transfer on a lateral ramp or perpendicular tear fault; 2) en echelon transfer between laterally overlapping thrusts; and 3) relaying transfer. En echelon faults can be either right- or left-handed. In weak detachment systems, the direction of thrust vergence creates an additional variable in transfer mechanism. Some of the possible map patterns are illustrated in Figure 120. It is easy to

see how many of the basic thrust structures of Figure 118 can be generated at different points in the region of transfer between adjacent faults, and how the map pattern in the zone of transfer will vary depending on the depth at which mapping is conducted.

Careful examination of Figure 116 and comparison with the fold-out geology map (in pocket) will reveal that individual surface anticlines are associated with one or more major thrusts at the level of the Thumb Mountain Formation. These thrusts display a variety of lateral transfer mechanisms not readily predicted by surface evidence alone. For example, Beverley Inlet Anticline on Sections A through D is associated at depth with a sinistral en echelon thrust system consisting of one south-vergent thrust linked eastward to

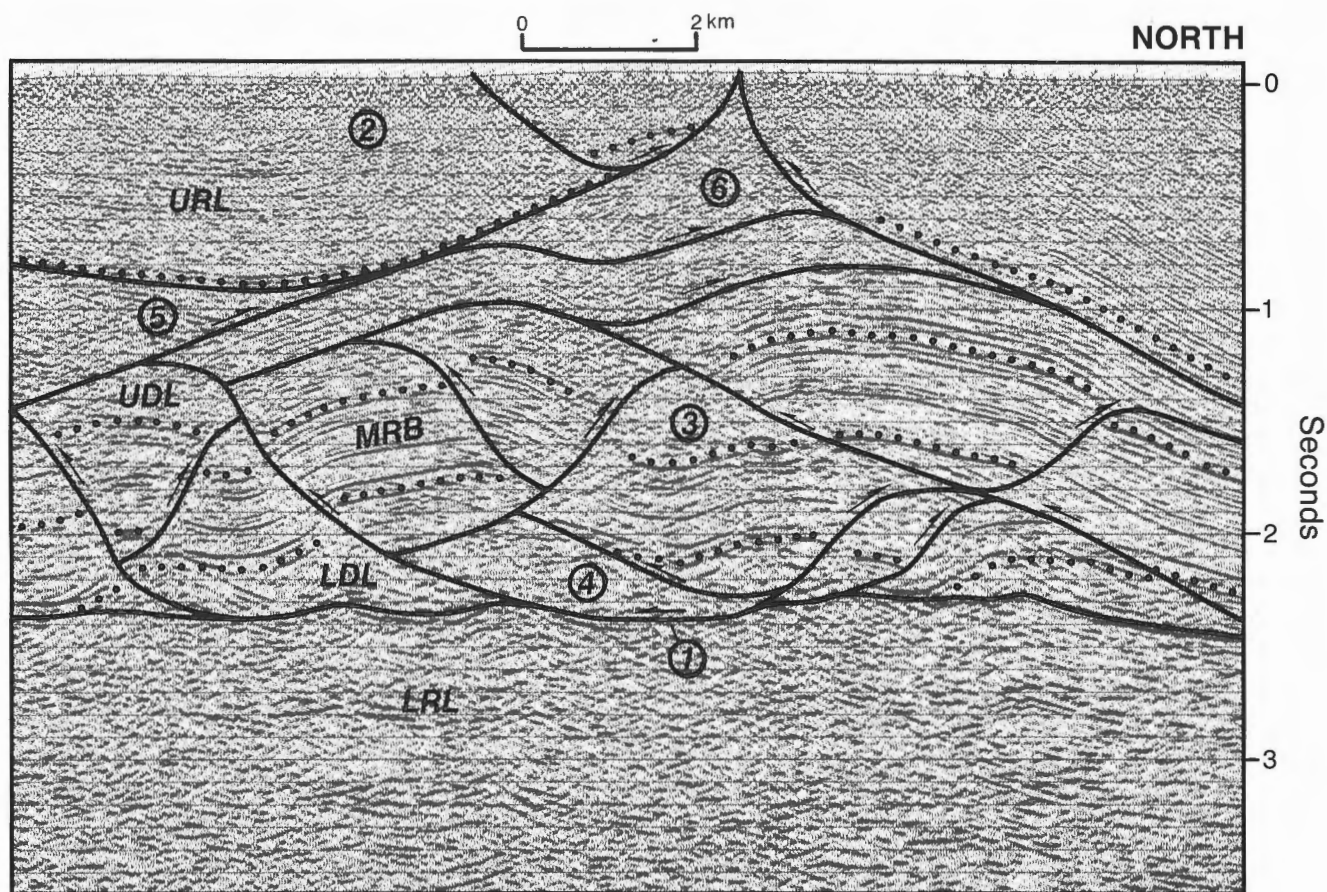


Figure 114. King Point East Anticline and Birch Point Syncline (to left), on a part of seismic profile C75, Section A. Component formations of each layer are listed in Figure 101. LRL, lower rigid layer; LDL, lower ductile layer; MRB, medial rigid beam; UDL, upper ductile layer; URL, upper rigid layer; 1, breakup of the sub-Bay Fiord reflector is due to complex structure and associated velocity anisotropy in the medial rigid beam; 2, Birch Point Syncline is a surface-mappable second-order fold that has been uplifted by complex disharmonic shortening in the medial rigid beam; 3, footwall syncline; 4, King Point East Anticline is underlain by an anticlinal salt welt of the complex type, featuring six separate culminations; 5, tectonic wedging into the Cape De Bray Formation has been facilitated by compressive slip on depositional clinoforms; 6, a simple, anticlinal mudrock welt within the Cape De Bray Formation is also indicated by the surface structure.

two overlapping north-vergent thrusts. Left-handed transfer is also implied by four anticline-syncline pairs of subsurface Dundas Peninsula, which have no surface expression. In contrast, four relaying faults of mixed vergence are associated with Dealy Island Anticline, as is transfer on three major thrusts of opposing transport direction beneath King Point Anticline.

In other places, the suspicion of a linkage between surface folds is supported by more obvious thrust linkages at depth. For example, the thrust pattern and associated magnitudes of fault motion indicate a kinematic link between Robertson Point Anticline and Mecham River West Anticline by left-hand transferred slip on three major thrusts of varying vergence. Similarly, there may be some sinistral transfer of slip

on three thrusts beneath Rea Point and Sabine Bay anticlines. In general, the left-hand sense of transfer of many subsurface thrusts is similar to that of the fold belt as a whole as previously observed.

Spatial relation to folds

As pointed out already, the complexity of subsurface thrust systems within some anticlines is unsuspected from surface evidence alone, and surface fold asymmetry is only modestly successful as an indication of thrust vergence at depth (Fig. 105). Nevertheless, there is some correlation between variations in fold plunge and trend, and locations of transferred motion on major subsurface thrusts. Anticlinal culminations

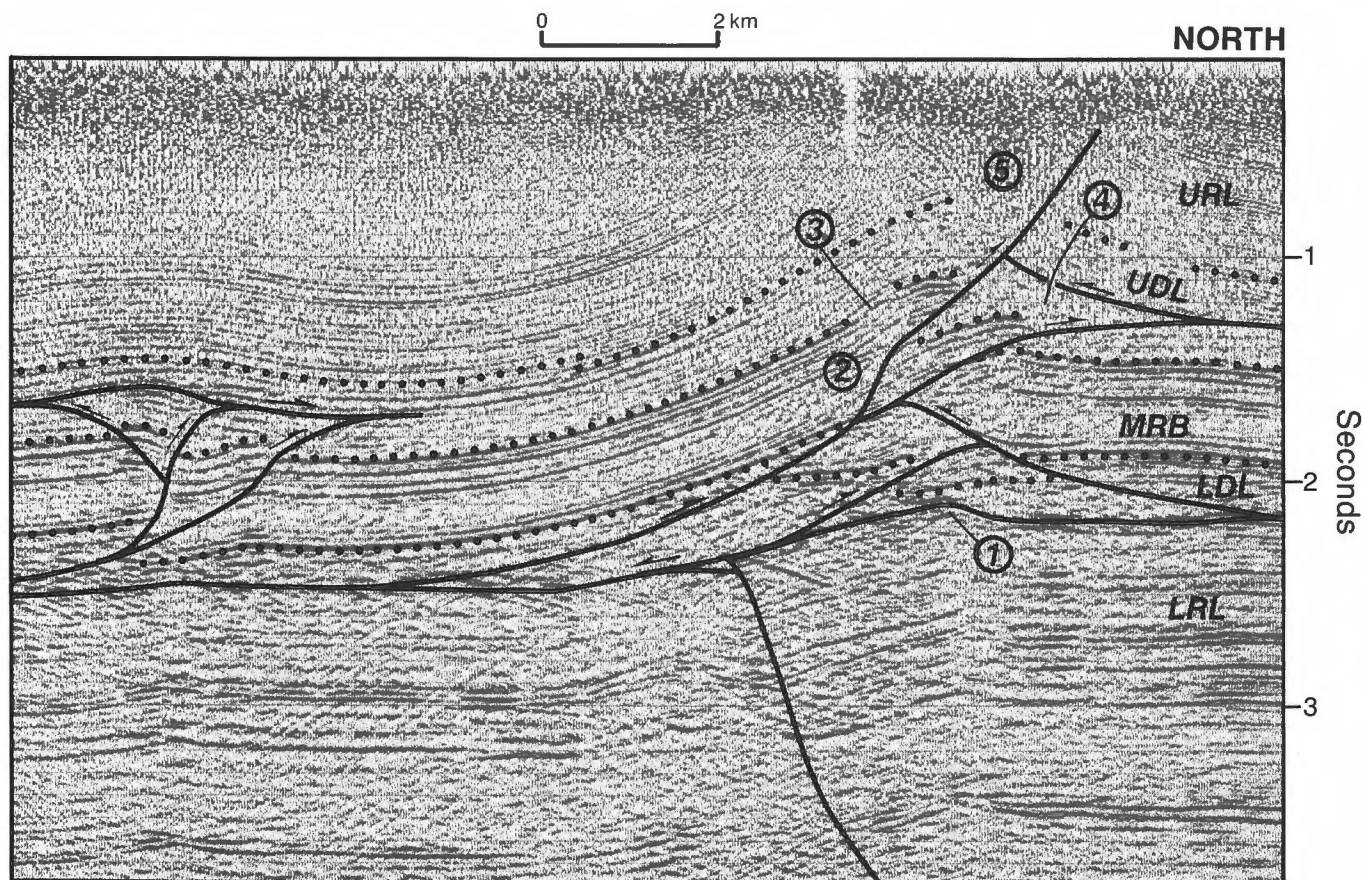


Figure 115. Rea Point Anticline and most of Sabine Bay Anticline (left), on part of seismic profile T8, Section D. Component formations of each layer are listed in Figure 101. LRL, lower rigid layer; LDL, lower ductile layer; MRB, medial rigid beam; UDL, upper ductile layer; URL, upper rigid layer; 1, velocity pull-up superimposed on real sub-Bay Fiord structural relief; 2, fault-bend fold; 3, dip variation in south-facing fold limb due to imbrication and underthrust wedging at depth; 4, tectonic thickening of the Cape De Bray Formation above upward-flattening thrusts emerging from the underlying Cape Phillips Formation; 5, a simple anticlinal mudrock welt within the Cape De Bray Formation, also indicated by surface structure.

are situated vertically above thrusts of large displacement. Examples include Sabine Bay Anticline near Section G, King Point West Anticline on Section D, Robertson Point Anticline on Sections C and D, Baldwin River Anticline of Section B and Consett Head Anticline of Section A. Hinge-line saddles occur above regions of transferred displacement on overlapping subsurface thrusts. Examples include Cape Bounty Anticline between Sections G and H, Robertson Point and Rea Point anticlines between Sections C and D, and King Point and Richardson Point anticlines near Section C. Regions of lateral overlap between thrusts of differing strike direction also occur beneath bends of anticlinal hinge lines. Examples are found along Robertson, Rea and King Point anticlines.

In contrast, bends of synclinal fold axes can mark the termination of subsurface thrusts. Examples

include the east and west ends of Byam River Syncline at the termination of Consett Head and Sabine Bay anticlines, respectively, and Mecham River Syncline at the east and west ends of Mecham River East Anticline. Fold terminations and axial saddles on synclinal hinge lines occur above the convergence of thrusts within adjacent anticlines. This relation occurs along King Point Syncline of Section C. Synclinal depressions commonly occur where there is an absence of structural disturbance at depth: Burnett Point Syncline (Section B); Liddon Gulf Syncline (Section D); and King Point East Syncline (Section A). In some places, synclinal depressions will occur above regions of pronounced structural complexity. The only example of this is Birch Point Syncline (Fig. 114, Note 2; Section A). In this case, uplift of the syncline by disharmonic structure at depth has caused subsequent erosion of the entire Parry Islands Formation and part of the underlying Beverley Inlet Formation.

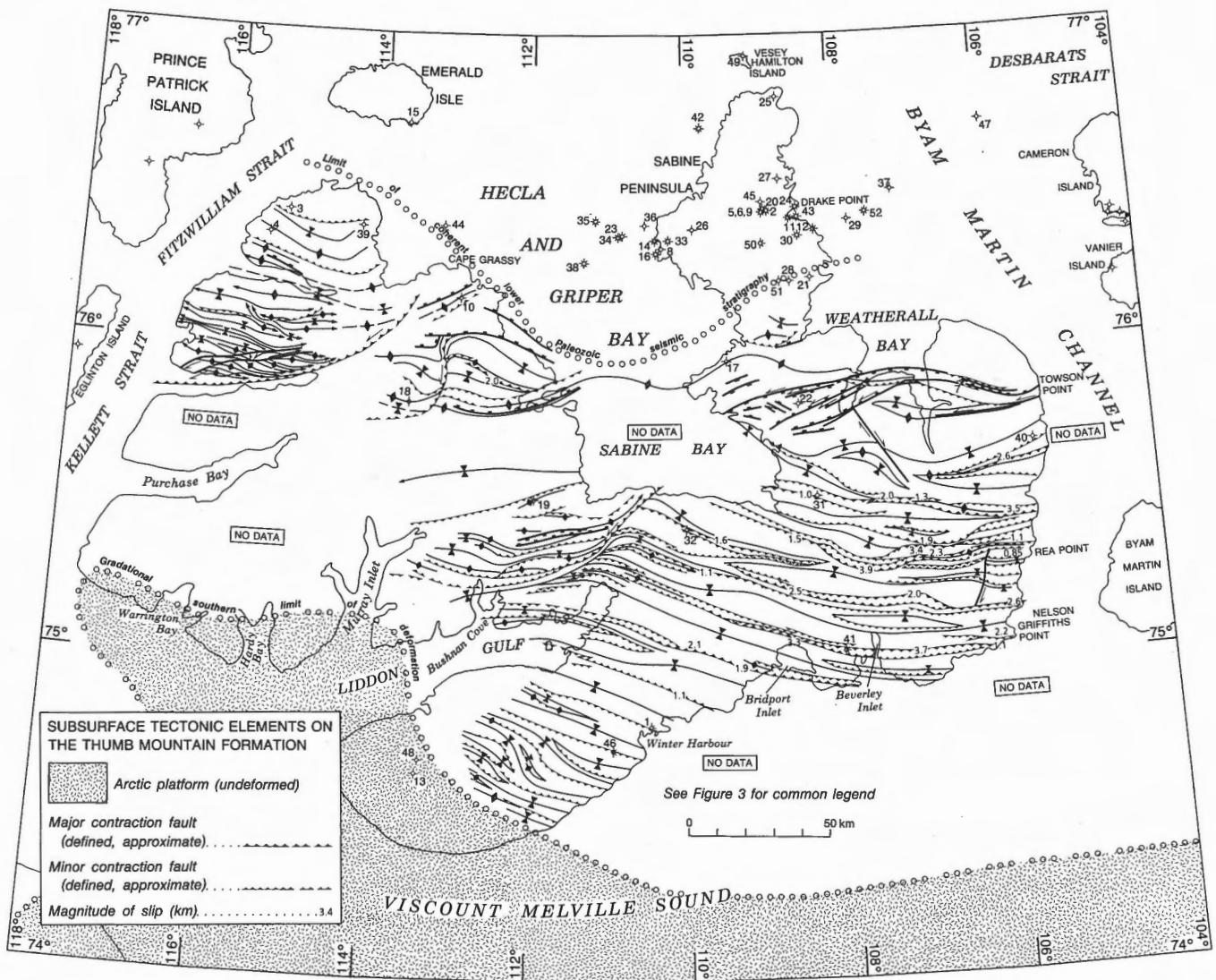


Figure 116. Subsurface conjugate thrusts and other tectonic elements at the level of the Thumb Mountain Formation, Melville Island.

Temporal relation to folds

An important initial consideration in the construction of structural cross-sections is the temporal relation between folding and faulting. This problem has been considered in some detail in the study of high-strength basal detachment thrust foldbelts such as those of the western Canadian Cordillera and Taiwan (Suppe, 1983; Suppe and Chang, 1983; Woodward et al., 1989). In these areas, two thrust-related fold types are recognized: fault-bend folds, and fault propagation folds (Fig. 121). In the first type, slip on a footwall flat-ramp-flat slip surface can exclusively generate a hangingwall fold during contraction. In the second type of structure, rocks first yield to a horizontal compressive stress by folding. Ongoing strain will cause progressive rotation to lower dip angles of the

axial planes. Faulting will only occur at an advanced stage of folding, when simple shear localized on the forelimb reaches the point of brittle failure. The fault will then propagate upward as folding and rotation continue. Although both fold types can arise without appreciable folding of the footwall section (and commonly do so in theoretical considerations of these types of deformation), the occurrence of footwall synclines in natural thrust-fold systems is very common and must indicate that folding has initially preceded thrusting.

It is clear from the seismic profiles and cross-sections of Parry Islands Fold Belt that rheological contrasts between rigid and ductile units has caused early-stage buckling and the development of a train of second-order folds. Thrusts develop in regions where

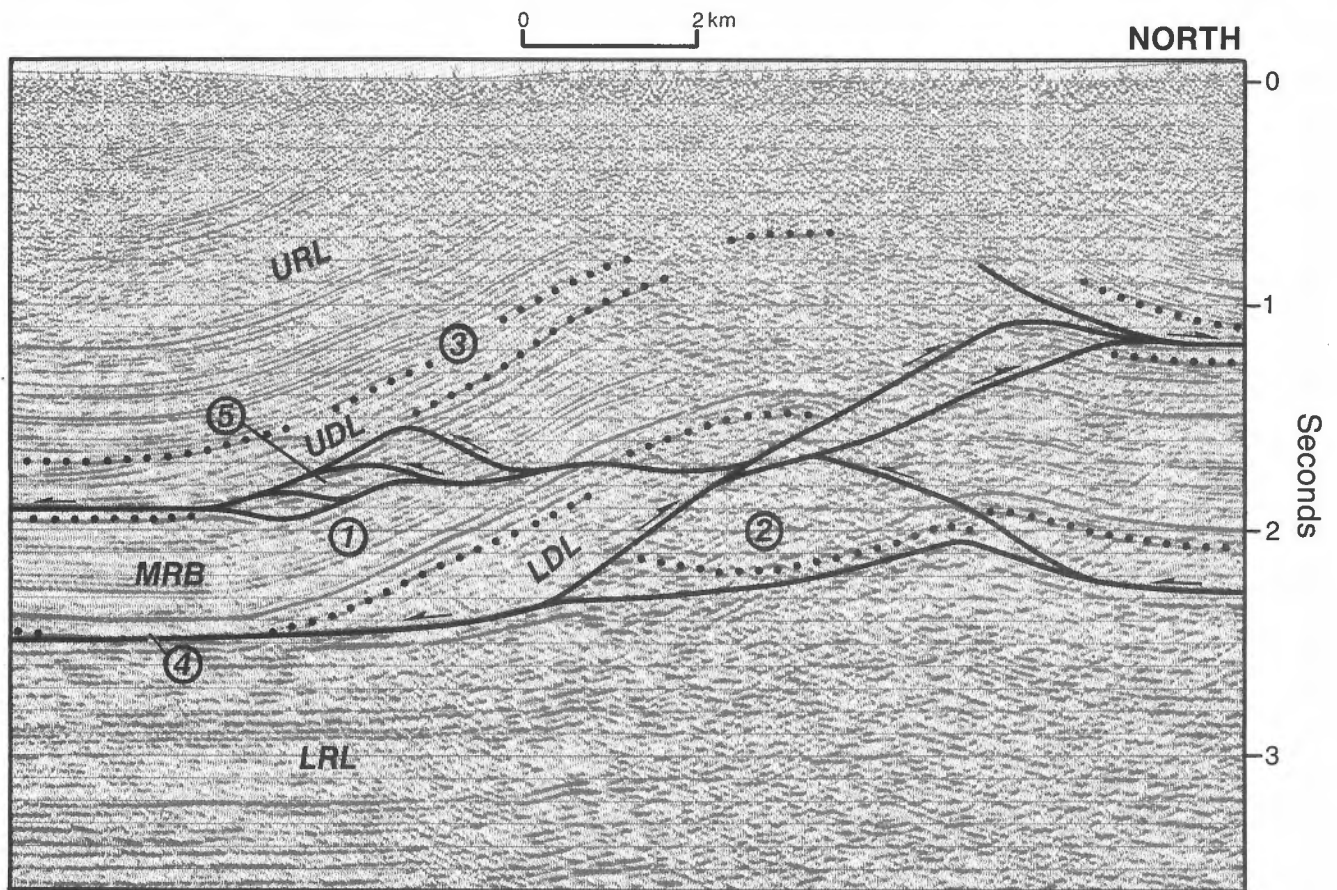


Figure 117. Richardson Point Anticline, on a part of seismic profile C75, Section A. Component formations of each layer are listed in Figure 101. LRL, lower rigid layer; LDL, lower ductile layer; MRB, medial rigid beam; UDL, upper ductile layer; URL, upper rigid layer. The beam also includes the Blue Fiord Formation. 1, intermediate detachment in the Blue Fiord Formation; 2, imperfectly imaged footwall syncline; 3, dip variations on south-facing limb, attributed to underlying thrust ramps and flats; 4, possibly complete evacuation of the lower Bay Fiord Formation from the axis of the King Point East Syncline; 5, local tectonic thickening in the Cape De Bray Formation, where thrust imbricates emerge out of the underlying Blue Fiord Formation.

progressive concentric folding has created room problems, notably, in the hinge region of all second-order anticlines.

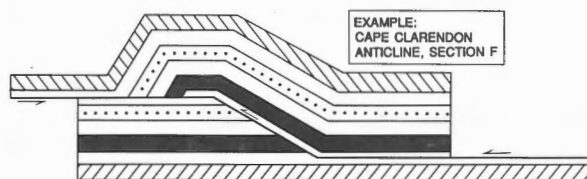
Examples of the pre-fault development of folds is provided at every stratigraphic level above the base of the salt. For the siliciclastic formations of the Devonian clastic wedge, every second-order fold south of Rea Point Anticline has developed without the aid of a footwall ramp. In the case of Richardson Point, King Point, Baldwin River and Rea Point anticlines, associated thrusts have greatest displacement at depth. Slip is observed to decrease upsection along or near fold limb inflections and, in every case, the thrust is matched by a pre-existing footwall syncline (Fig. 108, Note 3; Fig. 117, Note 2; Fig. 122, Note 1).

For the second-order folds of the Bay Fiord through Cape Phillips/Blue Fiord interval, wavelength has been

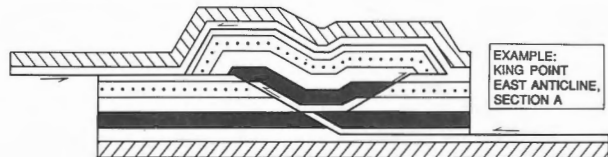
predetermined by ductility contrasts with both the Cape De Bray and evaporitic lower Bay Fiord formations. Evidence for the pre-existence of salt welts and buckle folds is provided by: 1) Cape Providence Anticline (Section F; Fig. 111, Note 3) which, for the medial rigid beam, has been shortened almost exclusively by folding and associated layer-parallel slip; 2) apparently unfaulted parasitic buckle folds such as those peripheral to Sabine Bay (Fig. 109, Note 3) and Beverley Inlet anticlines (Section G, Note 10), to name but a few; and 3) the ubiquitous occurrence of a footwall syncline beneath nearly every single thrust (for example: Figs. 106, Note 3; 107, Note 2; 108, Note 4; 114, Note 3; 122, Note 2; 123, Note 1).

It is also apparent, however, that once developed, a pattern of thrust ramps and flats will cause modifications to evolving fold shape within faulted buckle folds. Examples of flexure influenced by a footwall

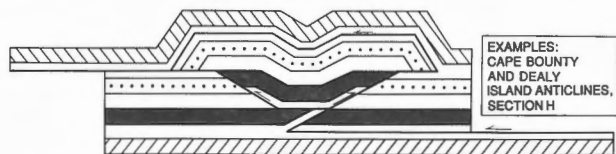
A: FORELAND-VERGENT THRUST



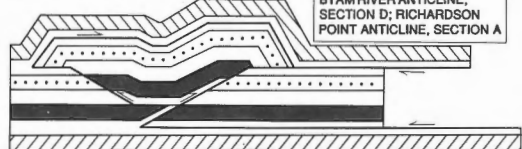
B: FORELAND-VERGENT THRUST WITH HANGING WALL CONJUGATE



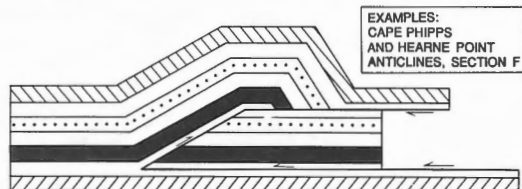
C: "POP-UP" STRUCTURE



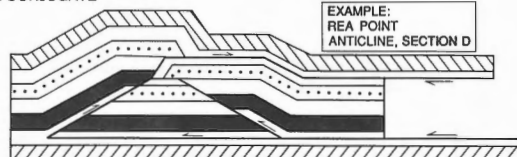
D: HINTERLAND-VERGENT THRUST WITH HANGING WALL CONJUGATE



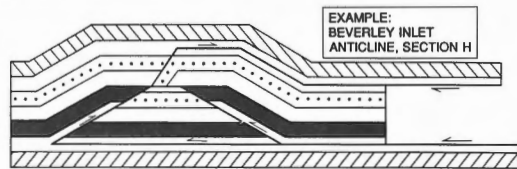
E: HINTERLAND-VERGENT THRUST



F: HINTERLAND-VERGENT THRUST WITH FOOTWALL CONJUGATE



G: "POP-DOWN" STRUCTURE



H: FORELAND-VERGENT THRUST WITH FOOTWALL CONJUGATE

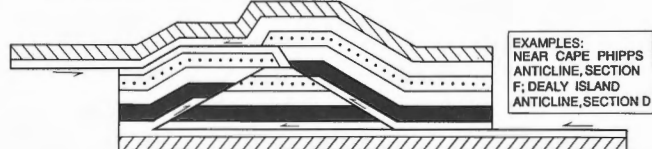


Figure 118. Vertically-linked thrust structures developed on a weak basal decoupling surface, with examples from the Parry Islands fold belt.

flat-ramp-flat geometry include Richardson Point Anticline (Sections A and B; Fig. 117, Note 3), Rea Point Anticline (Sections B, C, and D; Fig. 115, Note 2; Fig. 108, Note 5), Beverley Inlet Anticline (Section C; Fig. 124, Note 1), Robertson Point Anticline (Section D) and Cape Bounty Anticline (Section G). Hangingwall flexure can also arise by underthrust wedging as seen within Rea Point Anticline (Sections C and D; Fig. 115, Note 3), and Beverley Inlet Anticline (Section C; Fig. 124, Note 1). It is also proposed that fold shape may arise from the development of mesoscopic flat-ramp-flat thrust systems within the two apparently ductile layers. The evidence for, and implications of this concept are covered later in the chapter.

Kinematic analysis of conjugate thrusts

Faulting in the medial rigid beam is accomplished by conjugate thrust faulting (Fig. 125A). Following from this, the maximum principal compressive stress axis (σ_1) at the time of initial failure of the beam is situated

parallel to the acute bisectrix of conjugate fault pairs. For thrust conjugates, σ_1 is also nearly horizontal, σ_2 is parallel to the line of intersection of the conjugates and σ_3 is close to vertical (Fig. 125C).

Local attitudes and inferred trends of σ_1 have been obtained from cross-sections and subsurface mapping of the Thumb Mountain Formation. Results are plotted on Fig. 126. From this it can be seen that the trends of σ_1 are generally perpendicular to the map trace of subsurface thrusts. Individual σ_1 determinations plunge both north at up to 17° and south at up to 12° within the salt-based fold belt. There are two apparent populations of σ_1 : a S10–25°W- or N10–25°E-trending set; and a S- (or N-) to S15°E- (or N15°W-) trending set. The first set is prominent between Beverley Inlet and Liddon Gulf and in three other peripheral areas (Towson Point, Raglan Range and Canrobert Hills). The second set is dominant in the eastern part of the island and in the central region north of Liddon Gulf. The south-trending set, north of Liddon Gulf, appears to display an interference pattern that impinges on the S25°W set. The implication of

THRUST SYSTEMS

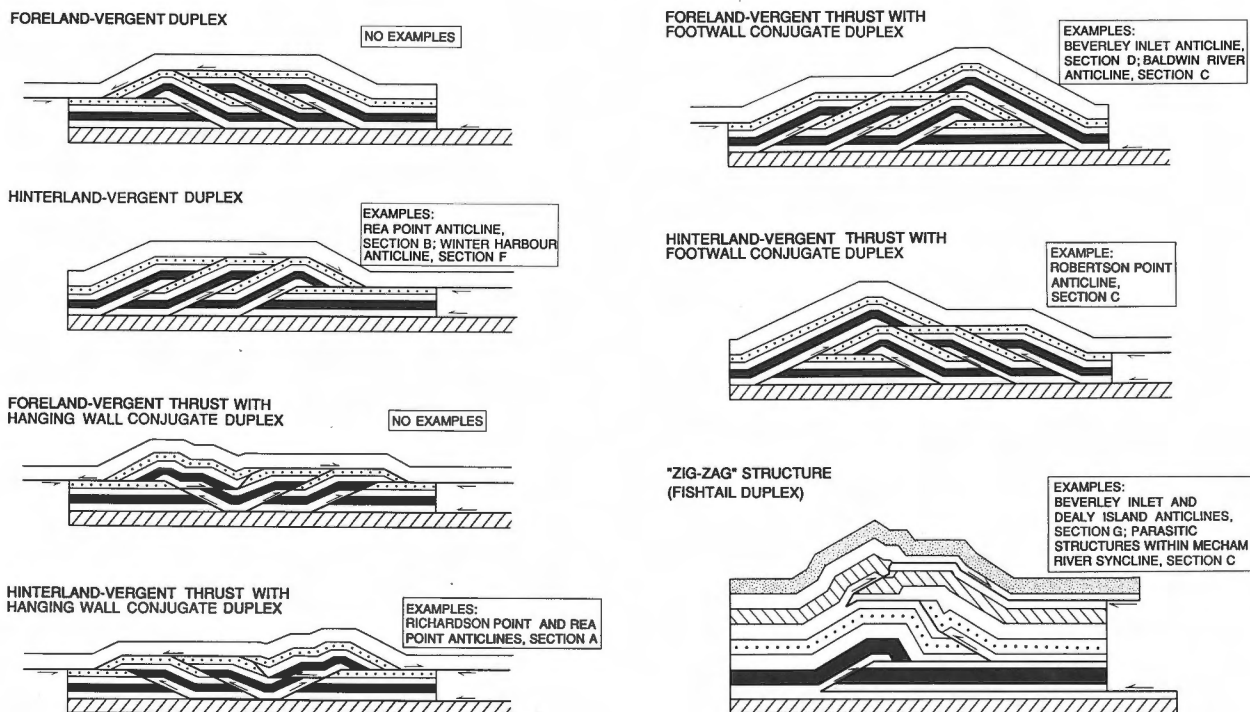


Figure 119. Foreland- and hinterland-vergent hangingwall and footwall duplexes developed on a weak, basal decoupling surface with examples from Parry Islands fold belt.

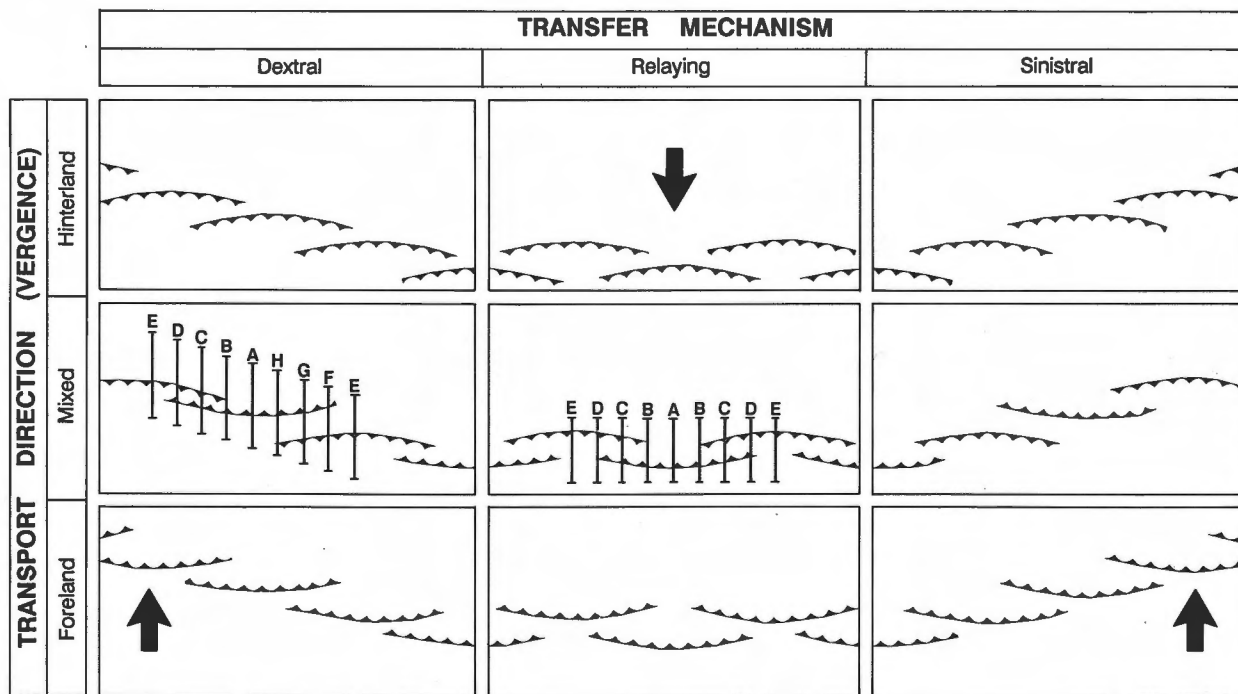
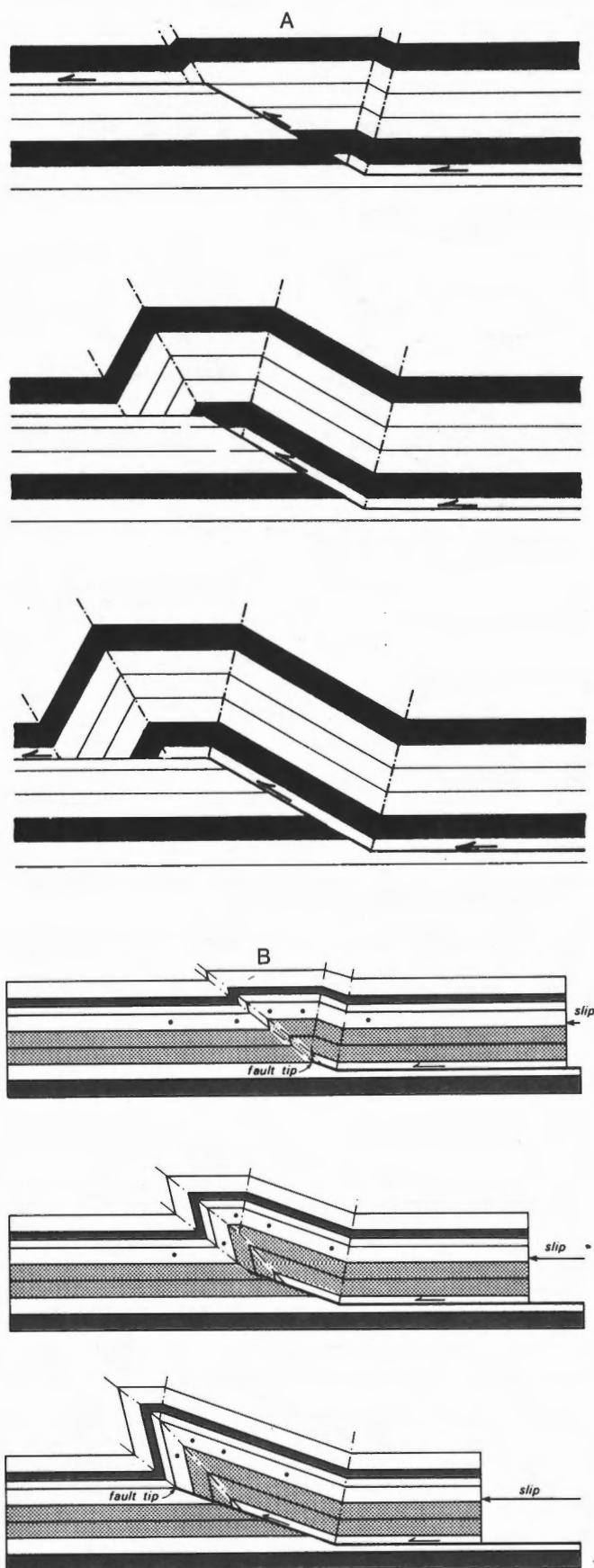


Figure 120. Mechanisms of displacement transfer in weak, basal detachment thrust systems. All nine types of transfer system could exist within a single tectonic re-entrant bound to the left and right by salients. By turning the figure upside down, the thrust systems envelop a salient with re-entrants to the left and right. The direction of tectonic transport is indicated by arrows. Lettered cross-sections refer to fundamental structures illustrated in Figure 118.



this last point is that the S25°W set in the west may predate the southerly set. In contrast, the S10–25°W trends of σ_1 , east of Liddon Gulf, appear to be gradational with the southerly-trending σ_1 values in the eastern part of the island, and there is no convincing reason to believe that this gradational variation does not continue onto the eastern half of the salt-based fold belt of Bathurst Island (Fig. 88). However, the implication of an inferred radial pattern for σ_1 throughout the salt-based fold belt is that principal tectonic transport directions have also been radial. Radial plane strain would create a restoration room problem in the hinterland prior to deformation. An alternative to radial tectonic transport is the possibility of other components of slip within the fold belt, particularly in those parts of the belt that are oblique to the dominant southerly transport direction determined previously in this chapter. These alternative slip directions could include unseen components of left-lateral bedding-parallel or oblique shear within southwest-trending portions of the fold belt, dextral bedding-parallel or oblique shear within northwest-trending portions, and/or components of extension normal to fold axial planes. The maximum amount of required extension is approximately the arc length of the entire fold belt (500 km on Fig. 88) less the straight line distance between the end points of the arc (470 km), or about 30 km (6.4%). Constraints applicable to a resolution of this problem are offered by kinematic analysis of selected areas that expose strata of the medial rigid beam: Towson Point Anticlinorium, which lies near the northern periphery of the salt-based fold belt; and Canrobert Hills region which, although lying beyond the salt-based deformation, has experienced a coeval phase of southerly directed thin-skinned shortening (Fig. 88).

Towson Point Anticlinorium

Kinematic analysis of Towson Point Anticlinorium benefits from a combination of surface geology (Fig. 39), a detailed seismic grid, and mesoscopic kinematic elements. This periclinal anticlinorium is associated with an equal distribution of both southwest- and northeast-vergent parasitic conjugate thrusts of both regional and outcrop scale that together

Figure 121. Temporal relations between folding and faulting: **A.** the fault-bend fold develops as a result of the underlying flat-ramp-flat geometry; **B.** in the fault-propagation fold, the fault develops as a consequence of progressive simple shear on the oversteepened fold limb. (Reproduced from Woodward et al., 1989, after Suppe, 1983.)

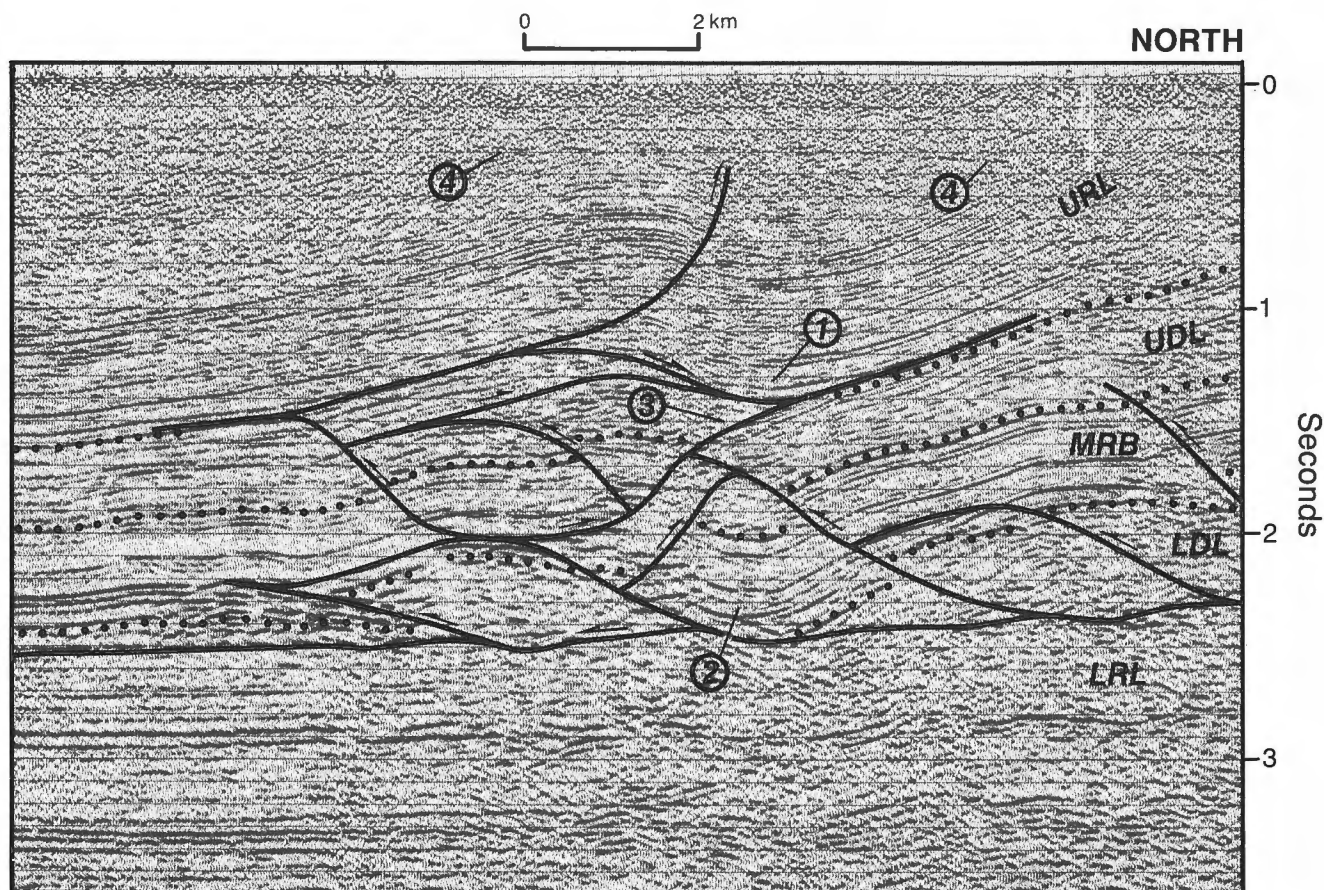


Figure 122. Consett Head Anticline, south limb of Rea Point Anticline (right) and north limb of Byam River Syncline (left), on a part of seismic profile C75, Section A. Component formations of each layer are listed in Figure 101. LRL, lower rigid layer; LDL, lower ductile layer; MRB, medial rigid beam; UDL, upper ductile layer; URL, upper rigid layer; 1, footwall syncline in the Weatherall Formation; 2, footwall syncline in the medial rigid beam; 3, tectonic wedging into the Cape De Bray Formation has been facilitated by compressive slip on depositional clinoforms; 4, possible base of permafrost reflector.

define a subhorizontal S50°W-trending axis for σ_1 and a vertical attitude for σ_3 (Figs. 104, 126, 127). The largest thrust has a sinuous surface trace and places Emsian strata of the medial Blue Fiord Formation on lower Eifelian Cape De Bray Formation (Figs. 39, 104a, geology map (in pocket)). Scatter in trend of slip lineations on fault planes, poles to bedding planes and poles to minor thrusts is attributed to rotation during superimposed second-order concentric folding about the dominant S64°E-trending β -pole for the Towson structure (Fig. 127).

Vein fill of interlocking, nonbanded, coarse crystalline, white calcite occurs in void space up to several tens of centimetres thick in association with Lower Devonian carbonate rocks exposed in the hinge region of the anticlinorium. Calcite veins occupy steep planar tension fractures that crosscut bedding, as well as bedding-parallel tensional space in fold hinge areas (Figs. 104C-E). The crosscutting veins are variably

normal, oblique and subparallel to the regional axial plane of the pericline (Fig. 127A). The vein walls commonly bear evidence of slip, including striated new-growth calcite in asperity pressure shadows (Fig. 104F).

As well as the thrusts and calcite veins, there is a separate set of strike-slip faults, some displaying a sinistral sense of displacement (Fig. 104B). These steeply dipping surfaces are subparallel to mapped and outcrop-scale thrusts, and the trend of second-order folds within the anticlinorium. Striae on strike-slip minor faults (Fig. 127B) fall in a loose cluster about S78°E/27 and possess a consistent southeasterly plunge. Implied principal stress directions at failure for the strike-slip faults, alone, are N67°E for σ_1 and near vertical for σ_2 . Crosscutting relations indicate that some minor thrusts are older than the strike-slip shears; others are younger. The strike-slip faults in the vicinity of Towson Point Anticlinorium occur only

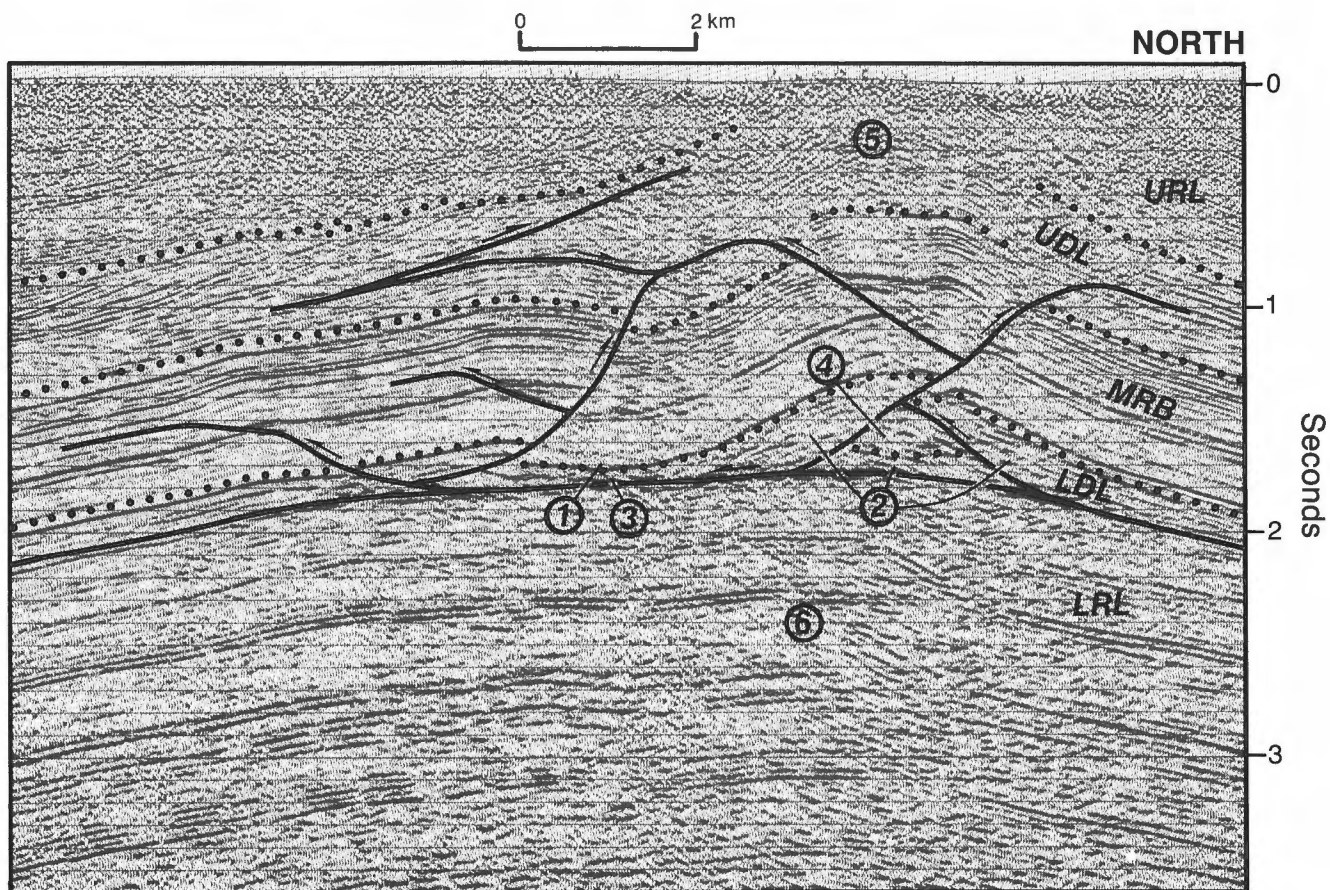


Figure 123. Dealy Island Anticline, on a part of seismic profile P1763/1193, Section H. Component formations of each layer are listed in Figure 101. LRL, lower rigid layer; LDL, lower ductile layer; MRB, medial rigid beam; UDL, upper ductile layer; URL, upper rigid layer; 1, footwall syncline; 2, a compound anticlinal salt welt with a faulted and indistinct hinge saddle; 3, dramatic local thinning of the lower Bay Fiord Formation in a parasitic syncline; 4, a triangular, fault-bounded tectonic fragment of the medial rigid beam is encapsulated by evaporites; 5, some anticlinal hinge thickening of mudrock is indicated for the Cape De Bray Formation; 6, the crest of the surface D3 anticline detached on the Bay Fiord Formation lies nearly directly above the crest of an underlying deep-seated D4 anticline — this relation is strictly coincidental since the two fold trends are oblique to each other.

within the upper panel of strata on seismic profiles P1788/P2227 of Section A and P2061 of Section B, and must be at least locally detached on the through-going sub-Bay Fiord décollement reflector at a depth of 4 to 5 km.

For all the tectonic elements of the Towson structure, σ_1 lies between N67°E and N40°E. The other two principal stress directions alternate between horizontal and vertical. The entire array of mappable faults and folds and the dominant second-order pericline have developed in a left-lateral transpressive shear system traceable over a distance of 100 km from Byam Martin Channel to Tingmisut Lake (Fig. 128). In this interpretation, Towson Point Anticlinorium has formed on a restraining bend in the system and the sublatitudinal faults, mapped both east and west of the pericline, are interpreted as sinistral shears. Lateral

linkage to a coeval first-order sinistral restraining bend pericline (Spencer Range Anticlinorium), the eroded roots of which are preserved on the sub-Canyon Fiord unconformity surface beneath and west of Spencer Range (Fig. 129), is also indicated. The Towson Point and Spencer Range structures have experienced other phases of deformation in late Paleozoic to Tertiary time (Chapter 7).

From these observations and conclusions, the Towson Point structure cannot be considered typical of the other second-order salt-based structures on Melville Island. As well as the complications provided by superimposed deformation phases, σ_1 for the Towson structure is highly oblique to the overall southerly transport direction suggested for the salt-based fold belt, and the sinistral shear sense of sublatitudinal faults is contrary to that proposed in the general

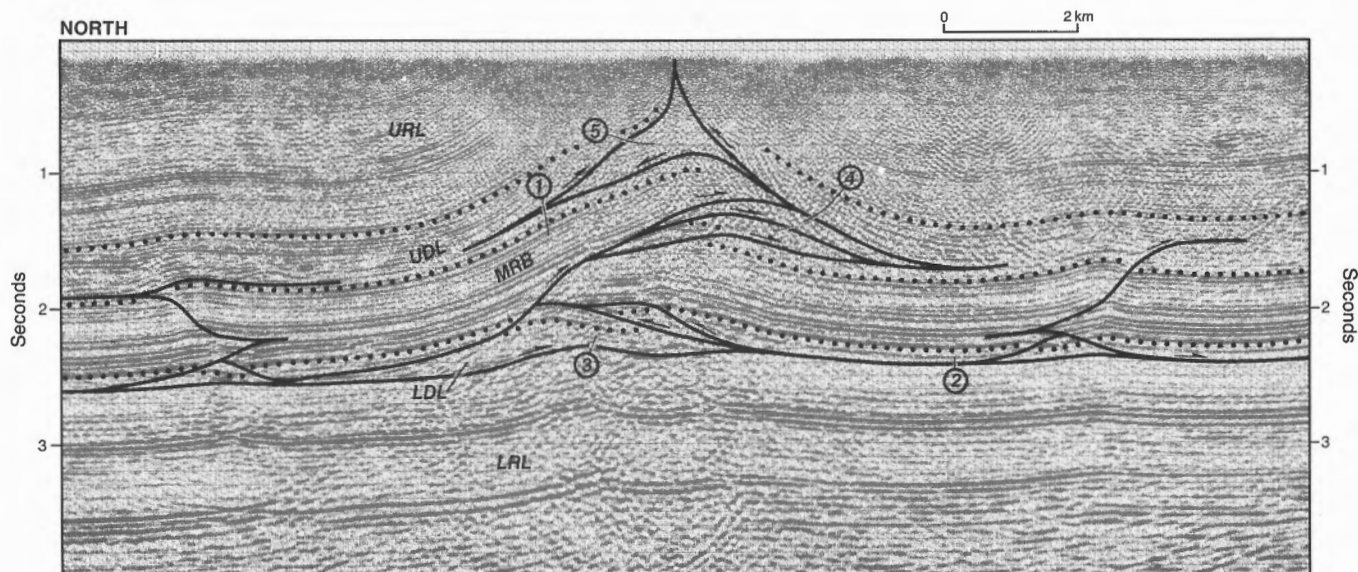


Figure 124. Beverley Inlet Anticline, on a part of seismic profile P1660, Section C. Component formations of each layer are listed in Figure 101. LRL, lower rigid layer; LDL, lower ductile layer; MRB, medial rigid beam; UDL, upper ductile layer; URL, upper rigid layer; 1, change in dip of strata due to underthrust wedging and resultant bends in the underlying roof thrust; 2, moderate thinning of the lower Bay Fiord Formation below Liddon Gulf Syncline; 3, compound anticlinal welt ('Napoleon's Hat'); 4, tectonic thickening of the Cape De Bray Formation above upward-flattening thrusts emerging from the underlying Cape Phillips Formation; 5, a simple anticlinal mudrock welt within the Cape De Bray Formation is also indicated by the surface structure.

kinematic model for regional fold belt arcuation. Nevertheless, these kinematic data confirm that syn-orogenic strike slip and extension has occurred along planes, respectively parallel and normal to the axial plane of at least one second-order salt-based fold.

Canrobert Hills region

The dominant structural fabric of the region is defined by second- and third-order folds (geology map, in pocket). The character and scale of these and other higher order folds are illustrated in Figures 42, 45, 90, 103, 130, and 131. Fold wavelength and amplitude are greatest in the Canrobert and Ibbett Bay formations; the competent equivalent of the medial rigid beam within the salt-based fold belt. Folds have straight limbs, doubly plunging axes and hinges with tight radii of curvature. Hinge thickening of strata is locally apparent and axial parasitic minor folds are common (Figs. 42, 45, 130A, B). Folds are associated with forelimb brecciation, boudinage of competent layers within fissile argillaceous intervals, and forelimb axial planar cleavage (Fig. 130C-E). Measured β -poles to second-, third-, and fourth-order folds plunge at zero to 22° toward N80°W and S80°E (Fig. 132A). Poles to axial planes of second-order folds display a mixed north-northeasterly and south-southwesterly sense of asymmetry.

Third- and fourth-order folds are dominant in the Blackley Formation (Figs. 47, 131B-D), the lower part of the correlative upper ductile layer of the salt-based fold belt. Thinly interbedded sandstone and mudrock has facilitated the development of bedding-parallel shears, intraformational chevrons and similar folds comprising stacked and alternating competent and incompetent thin beds. Hinge collapse features and cleavage development on oversteepened and overturned limbs are also encountered (Figs. 131B, C).

Lower-order folds are generally absent within the Cape De Bray Formation, the upper part of the upper ductile layer of Canrobert Hills. Second- and third-order folds in the underlying Blackley and overlying Weatherall formations die out within this, apparently, most ductile interval (Fig. 103).

Mappable faults of the Canrobert Hills include sets that are mostly normal and parallel to fold trends. The faults that are perpendicular to the regional fold trend are moderate to steeply dipping. Many of these are definitely extensional. Some of the axis-parallel faults are steep and contractional. Hand-specimen-scale contraction faults have developed as a result of oversteepening of folded forelimbs and have also propagated as a consequence of axial space problems developed during concentric folding (Figs. 130C, D). Outcrop-scale, unmineralized, minor slip planes

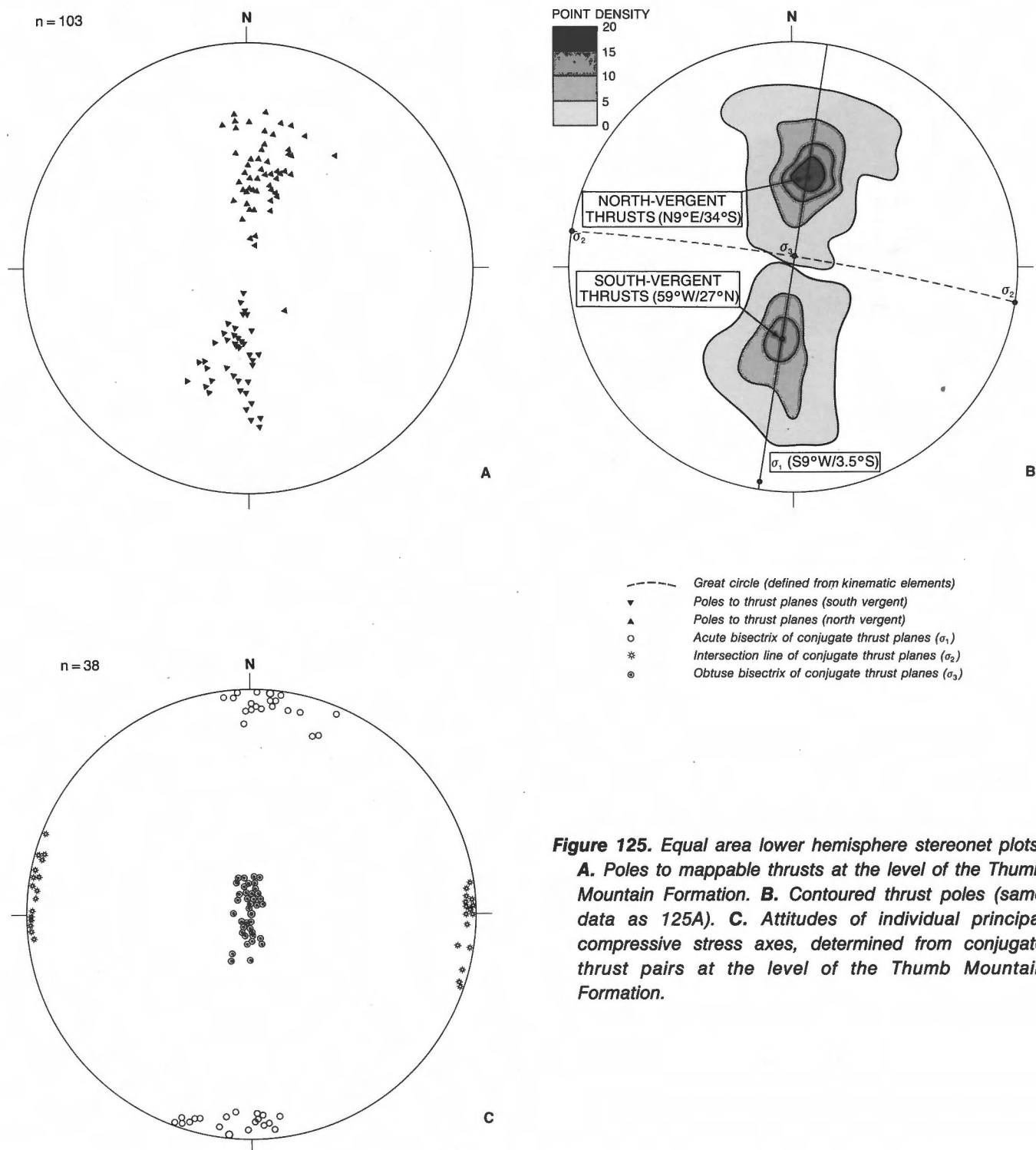


Figure 125. Equal area lower hemisphere stereonet plots. **A.** Poles to mappable thrusts at the level of the Thumb Mountain Formation. **B.** Contoured thrust poles (same data as 125A). **C.** Attitudes of individual principal compressive stress axes, determined from conjugate thrust pairs at the level of the Thumb Mountain Formation.

discovered and measured in the Ibbett Bay Formation tend to parallel the trend of the second-order fold axes, and the poles to these slip planes have roughly the same distribution as the poles to axial planes (Fig. 132B). Slip lineations on fold axis-parallel shears possess a wider scatter (Fig. 132C). Represented here are conjugate thrust lineations, north- and south-plunging lineations with nondiagnostic slip sense and a

separate set of right-lateral and sublatitudinal strike-slip lineations.

Mineralized fractures are common and comprise calcite, or less commonly, dolomite, quartz, and/or barite. Subsidiary fracture fill includes antazonite fluorite, sulphide minerals and bitumen. The smaller veins feature internally unstructured interlocking

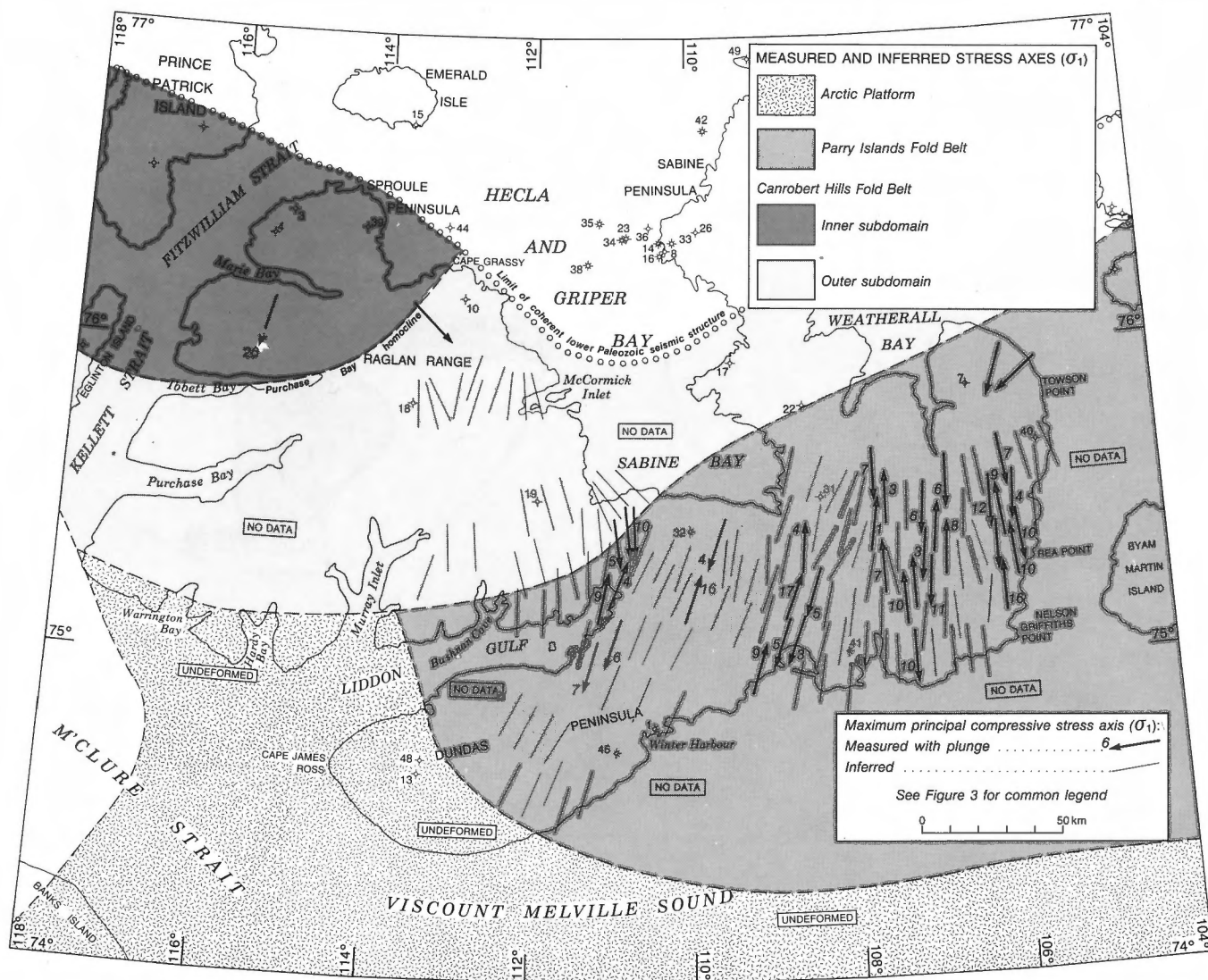


Figure 126. Geographic variation in measured attitudes and inferred trends of the maximum principal compressive stress axis (σ_1), determined from conjugate thrusts at the level of the Thumb Mountain Formation (Fig. 125).

crystalline calcite. These veins occupy hand-specimen-scale axial planar fractures, steeply dipping oblique shears, transverse fractures, bedding-parallel and fault-parallel tensional space, and laminae-parallel axial saddle reef void space (Figs. 130B, C).

Also encountered are giant cross-fibre calcite veins hundreds of metres to over 5 km in length, and up to 17 m wide(!). Some of these are visible on aerial photographs (Fig. 133). These veins, typically found within the Ibbett Bay Formation north of the Nisbet Point Fault, occupy steeply dipping transverse fractures and pre-existing tensional space along transverse faults. Vein walls are sheared, tectonically brecciated or flat but textured with interlocking calcite subhedra.

The veins are made up almost entirely of either fibrous calcite, or calcite euhedra where vein fill has not completely filled vuggy or cavernous void space. Careful examination was made of one 15 m wide vein exposed near Blackley Haven. The calcite cross-fibres are arranged in bands, each with an average thickness of 16 cm and a range of 2 to 42 cm. Band walls are defined by discrete and continuous fracture surfaces along the bases of specific cross-fibre layers. In this and most veins, the calcite bands are parallel to the outer vein walls and to the overall strike of the vein. Noted within one 7 m wide vein, however, are outcrop-scale folds affecting 15 to 20 calcite bands, an axial planar veinlet set that crosscuts the previously folded calcite bands, and a small thrust fault that offsets both the folds and second phase veins.

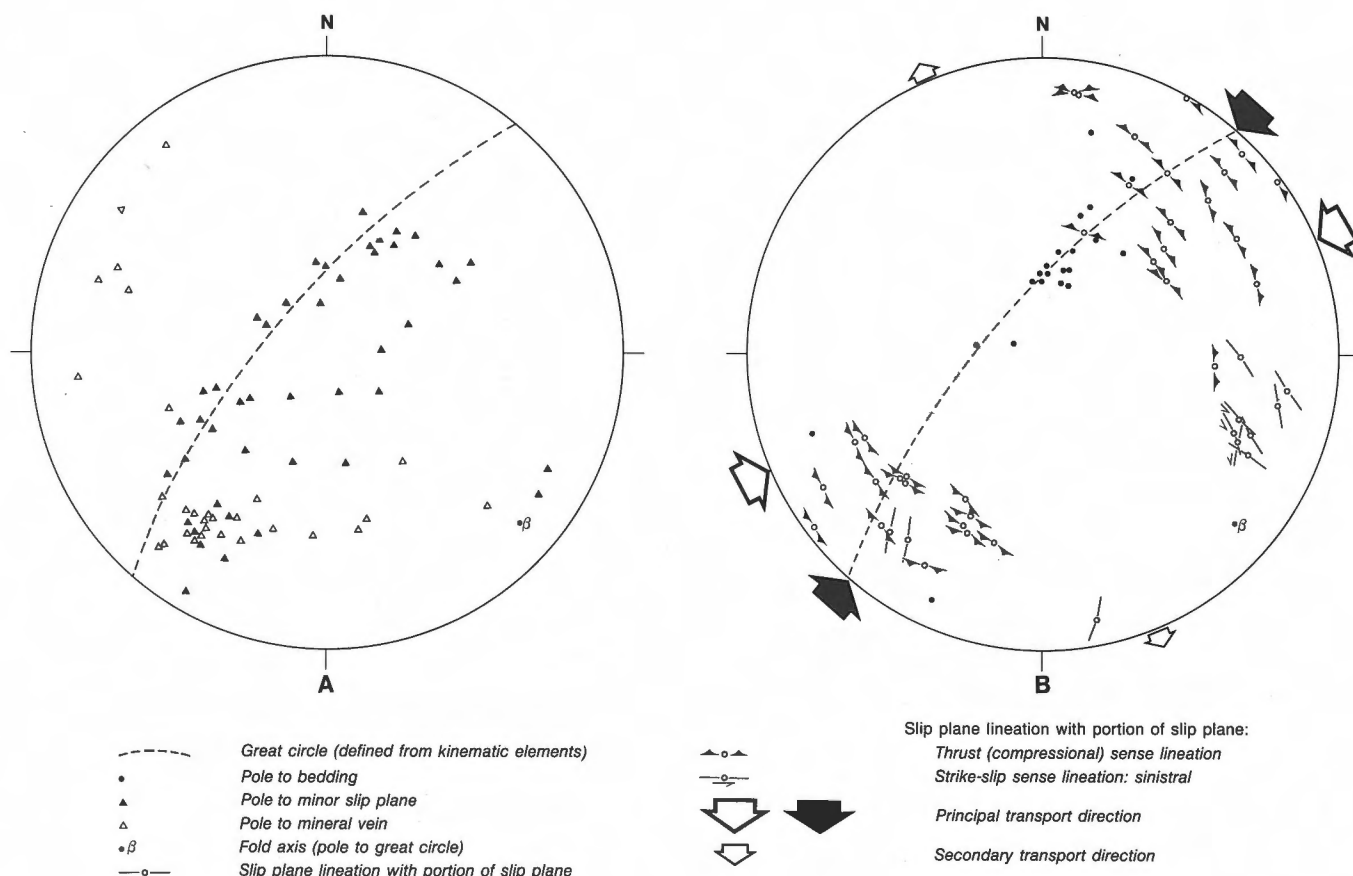


Figure 127. Lower hemisphere equal-area stereonet plots of kinematic indicators for the Towson Point Anticlinorium. The data were mostly collected at the location marked on Figure 39 (near the circled "S" symbol). **A.** Poles to minor slip planes and poles to mineral veins. **B.** Slip plane lineations with portions of associated slip planes, and poles to bedding planes with great circle girdle and implied β -pole. Large black arrows define the approximate direction of tectonic transport (σ_1) implied by the conjugate thrusts. The open arrows are approximate transport directions (σ_2 and σ_3) implied by the easterly-plunging sinistral strike-slip lineations.

Some uncertainty exists in the discrimination of individual band walls, because most bands comprise 5 to 10, yellowish orange, pale yellow, white, grey or black cross-fibre calcite layers and laminae, each 0.5 to 3.0 cm thick. In general, a 15 m wide vein might contain 90 calcite bands and 450 to 900 individual calcite cross-fiber layers. The preferred interpretation is that each of the bands represents a separate tensional and subsequent void-filling event and that a vein with 90 calcite bands may be the preserved record of 90 separate paleoseismic (earthquake) events. An alternative interpretation is that each cross-fiber layer represents a single event and that a wide vein is the accumulated record of hundreds of similar events. Measured poles to these giant calcite veins are plotted in Figure 132B. Vein-wall slip lineations occur in two dominant clusters (Fig. 132D): a shallow southwest-plunging left-lateral set, and a steep, easterly-plunging tensional oblique set.

The kinematic data described from the Canrobert Hills are consistent with three probable stress states, two of which are illustrated on Figure 134. The first embraces the north- and south-vergent conjugate contraction faults, poles to cleavage and poles to axial planes of all major (second-order) and some minor folds, north- and south-plunging thrust lineations, and sublatitudinal β -poles. Implied principal compressive stress directions are approximately S16°W/20° for σ_1 , and near vertical for σ_3 . The range of dip and plunge of planar and linear elements lying in the σ_1 - σ_3 plane is attributed to coeval horizontal rotation about σ_2 during the creation of second-order folds and related transport of hangingwall strata over convex portions of underlying listric thrust faults. The trend of σ_1 is similar to that obtained from western parts of the salt-based fold belt where the associated folds and conjugate thrusts are oblique to the overall southerly direction of tectonic transport (Fig. 126).

Kinematic elements of the second indicated stress state include sinistral (synthetic) shears, cross-fibre calcite dykes and the cluster of contained southwest-plunging sinistral slip lineations. In this state of stress, σ_1 is similar to that of the first-described stress state; σ_2 and σ_3 have switched positions – σ_3 is subhorizontal and situated parallel to unrotated calcite cross-fibres; σ_2 is near vertical (Fig. 134). In other words, kinematic indicators have been created in a sinistral strike-slip setting. The fold-axis-perpendicular, giant cross-fibre calcite veins and other normal faults identified during regional mapping imply a significant component of extension parallel to these fold axes.

It can be imagined that the regional system of folds and thrusts created under the influence of the first stress state and the sinistral shears and giant calcite veins related to the second stress state did not evolve during two independent deformation phases. Rather, there was probably a single deformation phase during which the σ_2 and σ_3 axes alternated between the horizontal and vertical. Likewise, the associated deformation was alternately creating and filling tensional space and slipping on oblique strike-slip faults or deforming the rocks by folding and thrusting.

The third stress state accounts for the steep extensional slip lineations on some calcite vein walls

and also some normal faults mapped perpendicular to second-order fold trends. Implied attitude for σ_1 is near vertical.

In conclusion, the full array of kinematic data from the Canrobert Hills provide strong, albeit indirect, support for the previously stated model accounting for radial patterns of σ_1 and regional arcuation of the salt-based folds. Second-order folds, oblique to the dominant southerly direction of tectonic transport should possess, and in the Canrobert Hills at least are now proven to contain, evidence of additional fold-axis-parallel extension and oblique strike slip.

Mechanical analysis of failure in the beam

Failure of the medial rigid beam of the salt-based fold belt occurs when horizontal stresses are large enough to cause brittle failure in the most competent part of the beam. Failure of less competent portions of the beam will follow directly from this. The relation between fault angle and competence is expressed by the friction coefficient, μ , such that

$$\mu = \tan\phi; 2\theta = 90 + \phi$$

where θ is the angle between σ_1 and the fault plane normal. For horizontal attitudes of σ_1 , higher fault

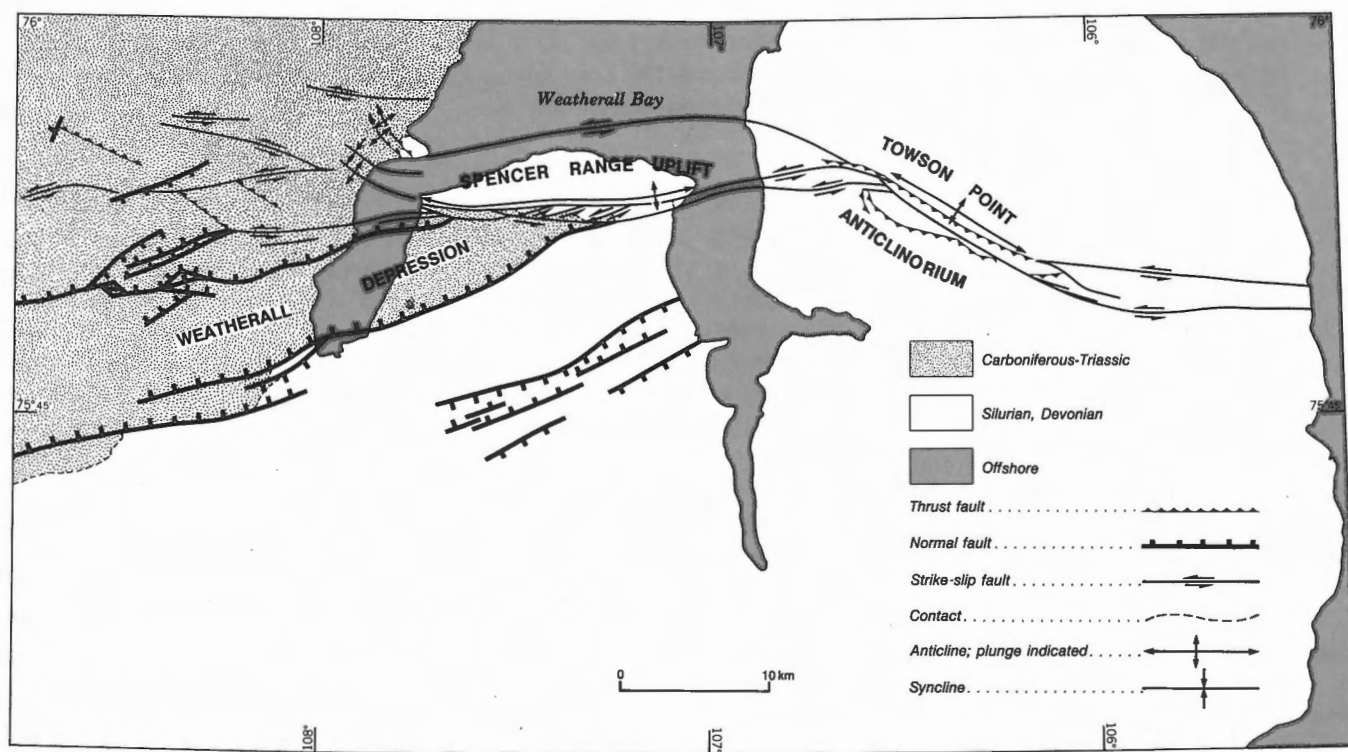


Figure 128. Sinistral strike-slip faults, thrusts, periclineal folds, and related kinematic elements of the Weatherall Bay area.

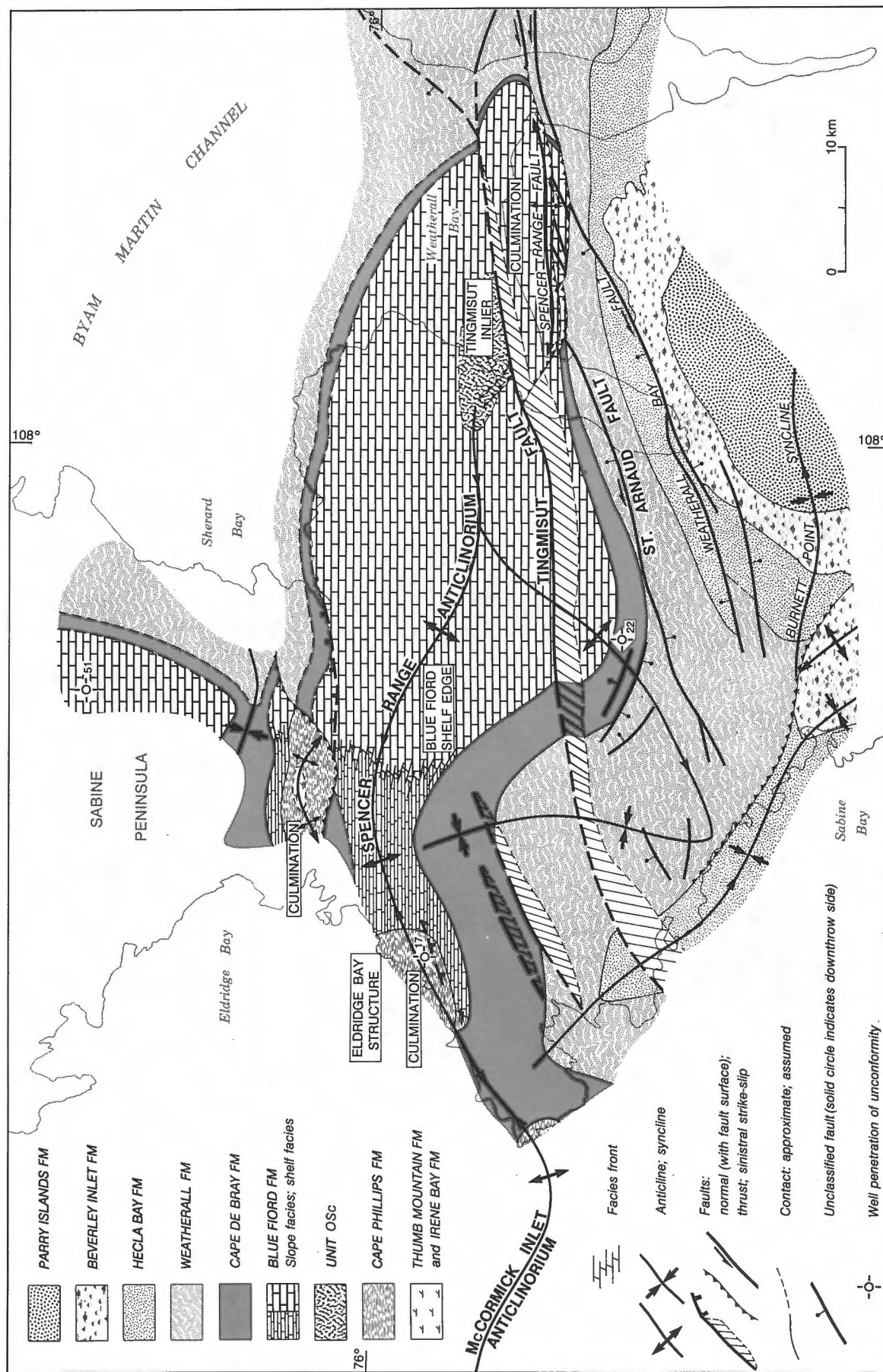


Figure 129. Sub-Middle Carboniferous geology of southern Sabine Peninsula, as defined by subcropping Devonian and older rocks on the sub-Canyon Fiord angular unconformity.

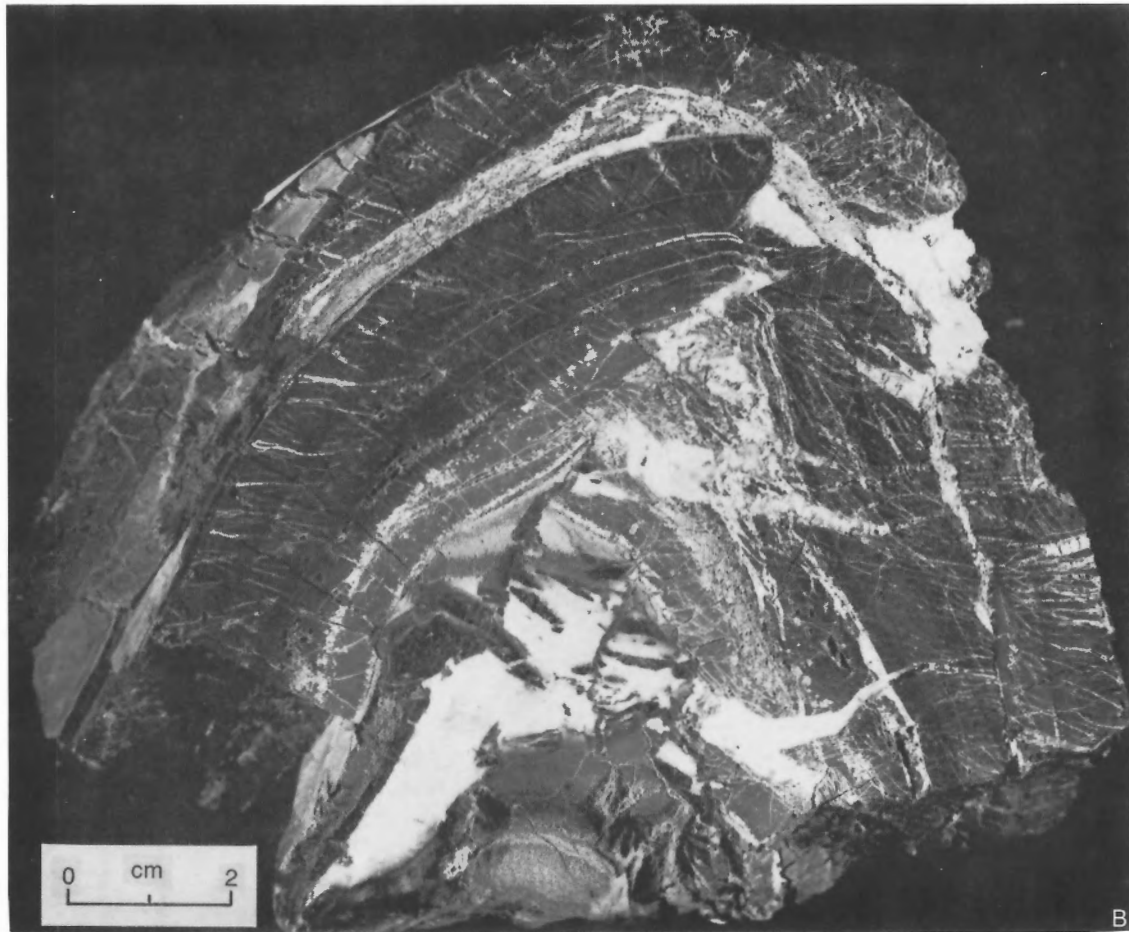
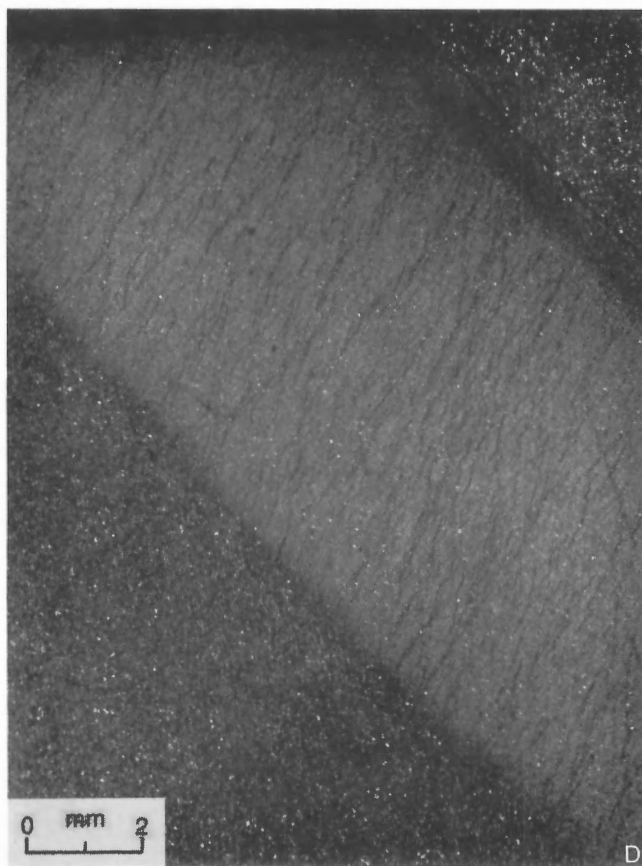


Figure 130. Outcrop- and hand specimen-scale structures in the Canrobert and Ibbett Bay formations. **A.** North-vergent isoclinal minor fold with axial stratal thickening, in the Ibbett Bay Formation argillaceous limestone. **B.** Vein-filled tensional fractures in faulted and brecciated chert of the Ibbett Bay Formation. **C.** Axial planar cleavage and minor faults in an asymmetrical anticline from the Ibbett Bay Formation. **D.** Cleavage refraction in thin beds of the Canrobert Formation; steep cleavage to bedding intersections occur in light coloured dolostone; shallow intersections occur in argillaceous limestone. **E.** Axial planar cleavage normal to compositional lamination in Ibbett Bay argillaceous limestone. ISPG photos. 2887-12, 3029-2, -16, 3874-6, -7.



C



D



E

Figure 130. (cont'd.)



Figure 131. Outcrop-scale structures in the Blackley Formation. **A.** Steep cleavage to bedding intersections on an inverted anticlinal fold limb. Circled knapsack for scale. **B.** Disharmonic folds and perpendicular, north-striking minor faults (width of frame is about 1 km). **C.** South-vergent chevron folds (hillside is about 200 m high). **D.** Intraformational fold closure (width of frame is about 1.5 km). ISPG photos. 2887-33, -49, -50, 2913-11.

angles imply higher friction coefficients and higher bed competence. Qualitative inspection of the cross-sections reveals that the steepest thrust faults occur in the middle part of the rigid beam, in the Thumb Mountain Formation. Lower average fault angles in the overlying Cape Phillips Formation and in the underlying upper Bay Fiord Formation, point to correspondingly lower competence and lower friction coefficients. The steepest average fault angles and related friction coefficients for the most competent part of the beam can also be used to calculate the maximum shear and normal stresses required to cause failure of the beam as a whole.

The mean attitude of north-vergent thrusts with respect to bedding in the Thumb Mountain Formation is 34° based on contouring of 52 stereonet data points (Fig. 125B). Mean dip of south-vergent thrusts in the same formation is 27° (41 data points). The acute bisectrix of these two conjugates defines a mean σ_1 with a bisect angle of 30.5° and $\theta = 59.5^\circ$ ($90 - 30.5^\circ$). This angle implies a specific shear stress (τ) and compressive stress (σ) for failure as provided by the Coulomb (1773) failure criterion for which:

$$\tau = S_0 + \mu P_L$$

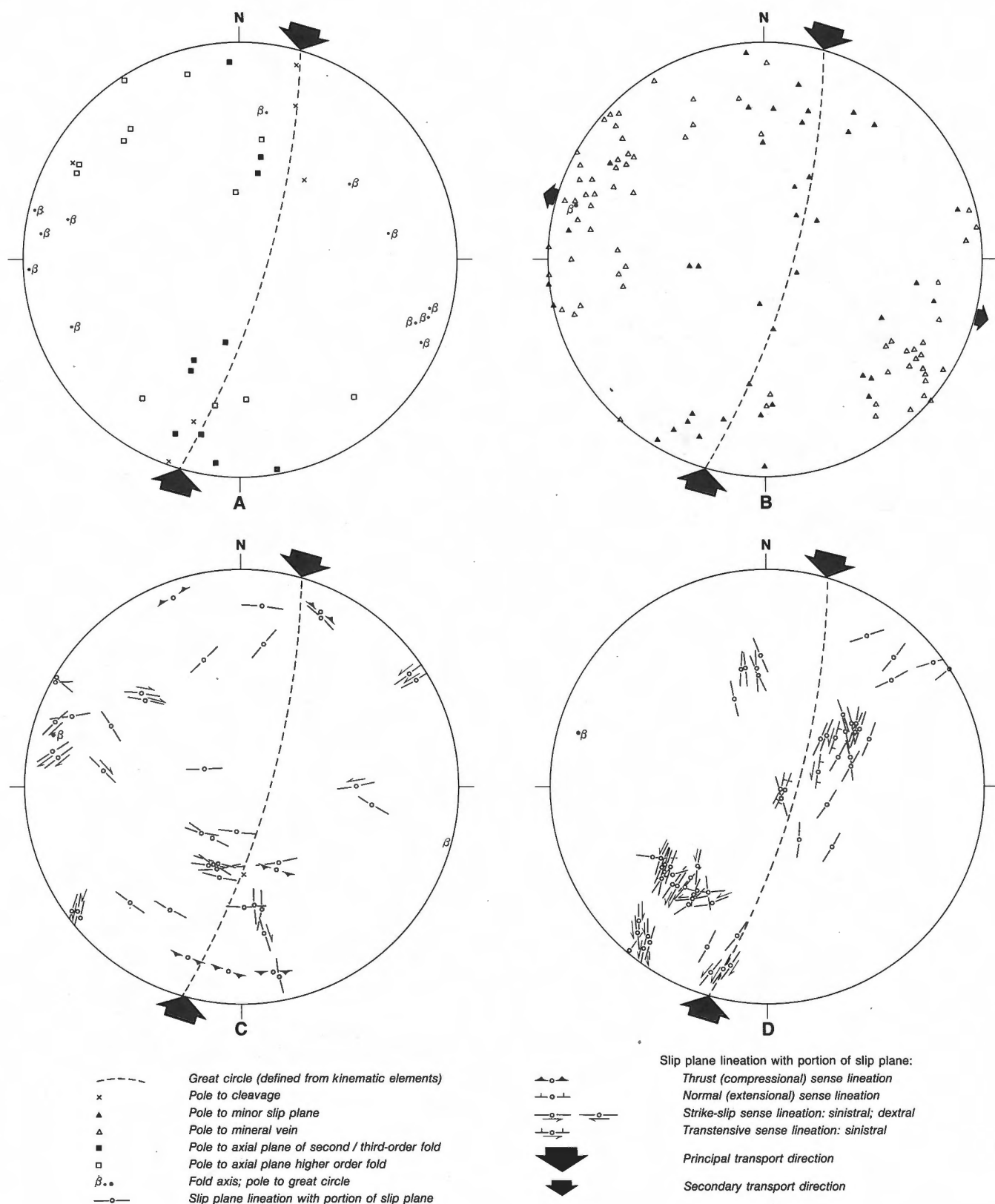


Figure 132. Lower hemisphere equal-area stereonet plots of kinematic indicators collected from numerous scattered field stations in the Canrobert Hills. **A.** Fold axes, and poles to cleavage and axial planes. **B.** Poles to minor fault planes and mineral veins. **C.** Slip lineations with slip sense and parts of the associated fault plane. **D.** Slip lineations measured on cross-fibre calcite vein walls with slip sense and parts of the associated fault plane. The great circle girdle on Figures A, C, and D, and the β -pole marked on C and D are taken from the great circle distribution of poles to unmineralized minor slip planes, and the implied fold axis illustrated in B.



Figure 133. Giant cross-fibre calcite vein within the Ibbett Bay Formation. Vein width is about 3 m. ISPG photo. 2887-41.

where S_0 is the cohesive strength, or shear stress, for failure in the absence of normal stress, μ is the friction coefficient, and P_L is the lithostatic pressure for which:

$$P_L = \rho g Z \approx \sigma_3$$

where ρ is the average density of overburden, g is the acceleration due to gravity, and Z is the depth to detachment at the time of deformation.

Values of S_0 vary with rock type. The full range, derived experimentally, is about 2 to 50 MPa, with the highest cohesion represented by some intrusive rocks and the lowest by poorly consolidated sediment (Handin, 1966; Hoek and Bray, 1981). Most limestones, dolostones and hard sandstones have cohesive strengths between 10 and 30 MPa (Hoek and Bray, 1981). Cohesion of various Arizona Redwall limestones ranges from 13 to 36 MPa (Handin, 1966). A value of 25 MPa is assumed for typically massive-bedded dolostone of the Thumb Mountain Formation in the medial rigid beam.

For θ of 59.5° , the friction coefficient (μ) is 0.55. The density of the 4900 m of preserved overburden has been determined from well logs (2580 kg m^{-3}). Eroded

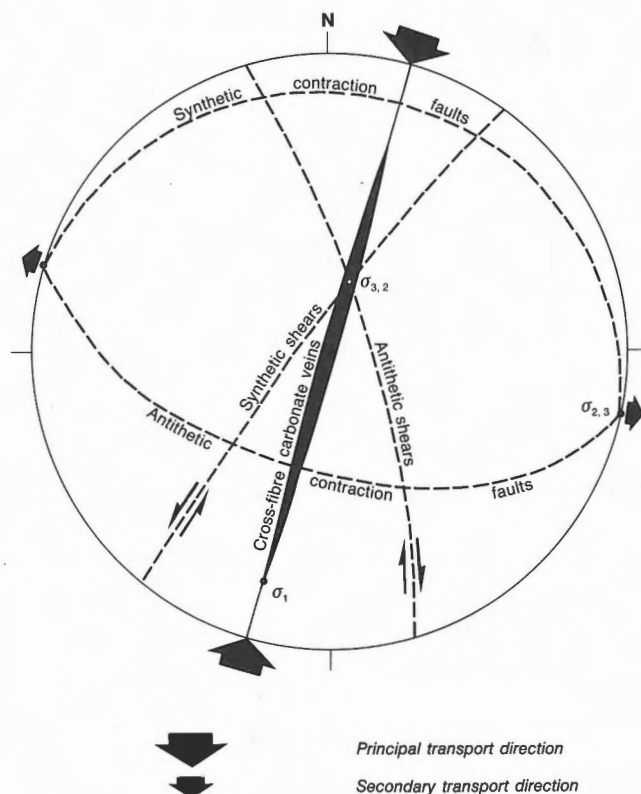


Figure 134. Lower hemisphere equal-area stereonet plot of suggested principal compressive stress axes and associated structures for the two dominant phases of deformation associated with the Ellesmerian Orogeny in the Canrobart Hills fold belt.

overburden, estimated from thermal maturity data to have been about 2700 m thick (Embry, 1988a), is here assigned an assumed density of 2300 kg m^{-3} . Calculated lithostatic pressure at the time of failure in the beam is 169 MPa and the failure shear stress as implied by the Coulomb failure criterion is 118 MPa (Fig. 135). For zero pore fluid pressure, the minimum compressive stress (σ_3) is also approximately equal to $\rho g Z$ and 169 MPa. The maximum compressive stress (σ_1) is related to σ_3 and τ by the following relation (from Ramsay and Huber, 1987):

$$\tau = [(\sigma_1 - \sigma_3)/2]\sin 2\theta$$

or rearranging

$$\sigma_1 = 2\tau \csc 2\theta + \sigma_3$$

The implied maximum compressive normal stress (σ_1) for the Thumb Mountain Formation for failure is 439 MPa.

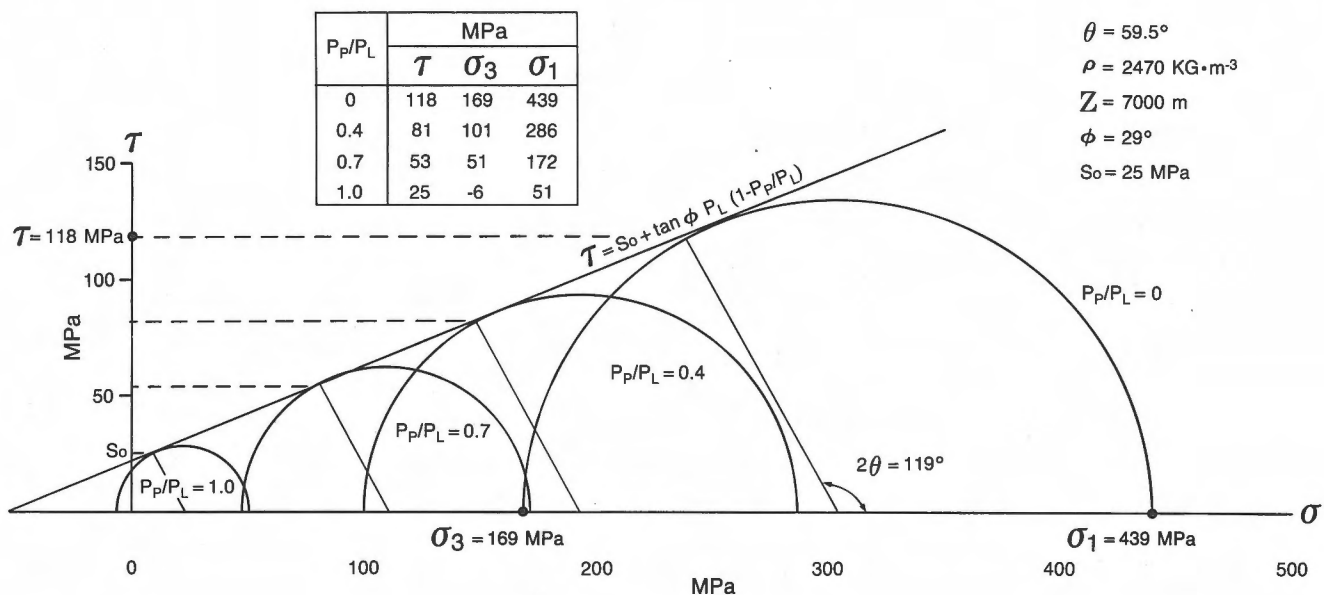


Figure 135. Mohr's circle construction, displaying maximum and minimum normal stresses and shear stresses at various pore-fluid pressures for compressive failure in the beam.

However, Hubbert and Rubey (1959) have shown that shear and normal stresses for failure are universally reduced by elevated pore fluid pressures such that:

$$\tau = S_o + \mu P_L (1 - P_P/P_L)$$

Shear and normal stresses for various fluid pressures are illustrated on the Coulomb failure envelope (Fig. 135). For hydrostatic fluid pressures (P_P/P_L) of 0.4, the shear stress causing failure is reduced to 81 MPa and for overpressured conditions (P_P/P_L of 0.7) is still further reduced to 53 MPa. Flotation of the rock column occurs when the pore fluid pressure is equal to the lithostatic pressure. Under these conditions, the failure shear stress is equal to the maximum cohesive strength of the beam or about 25 MPa.

Contributing to potential synorogenic fluid pressures is the expulsion of lattice-bound water from gypsum during conversion to anhydrite. In triaxial compression tests on Italian alabaster, Heard and Rubey (1966) showed that differential stress resulting in failure was greatly decreased by the gypsum-to-anhydrite phase change. For confining pressures, comparable to those acting on the Thumb Mountain and Bay Fiord formations and at elevated strain rates ($\dot{\epsilon} = 10^{-7} \text{ sec}^{-1}$), dehydration-related stress drop was found to begin at close to 100°C. Heard and Rubey (1966) also predicted that normal geological strain rates would have the effect of further reducing the phase

change temperature. The availability of pore fluids for the beam, derived from the dehydration of gypsum, seems highly likely. Anhydrite, now abundant in the lower part of the Bay Fiord Formation, is also known in accessory amounts in the Thumb Mountain Formation. Maximum paleotemperatures inferred from contained organic matter are about 150°C in the middle part of the beam and 185 to 195°C in the Bay Fiord evaporites (Gentzis, 1990). If these temperatures are the result of sediment burial, then the beam and underlying evaporites would probably have transgressed the gypsum-to-anhydrite reaction temperature during the Late, not latest, Devonian (Skibo et al., 1991).

Also contributing to the concentration of interstitial pore fluid is the second stage dewatering of the rock-forming clay minerals (Burst, 1969). Common very low grade metamorphic reactions generating water in argillaceous rocks are reviewed by Kirsch (1987), and include the conversion of smectite to mixed-layer clays (illite/smectite mixed-layers) at 0.45–0.70% Ro measured on vitrinite (100–140°C), and the conversion of kaolinite to illite at 1.2 to 2.2% Ro (140–275°C).

Shear stress resulting in slip on the basal décollement

Figure 125B demonstrates that for the Thumb Mountain Formation in the medial rigid beam, the

average angles between the north-vergent thrusts and basal detachment and between the south-vergent thrusts and the basal detachment are both similar. This implies that σ_1 , which bisects the acute angle between the two failure planes, is also close to parallel to the basal décollement (Fig. 136A). In fact, the average plunge of σ_1 with respect to the basal detachment is 3.5° in the direction of tectonic transport (perpendicular to the strike of the conjugate thrusts and also to the overall structural trend of the fold belt). Ignoring superimposed deep-seated folds, the present regional dip of the basal detachment varies as follows:

1. 460 m over a distance of 75 km or 0.35° along part of Section A
2. 400 m over 49 km or 0.47° for part of Section B

3. 100 m over 53 km or 0.11° for part of Section F
4. 650 m over 56 km or 0.66° for part of Section G
5. 290 m over 38 km or 0.44° for part of Section H

These data indicate that the dip of the basal décollement is about 0.1° at zero to 50 km from the foreland and 0.4 to 0.6° from 50 to over 125 km. The overall dip of the fold belt measured along the combined Sections F and G is close to 0.4° . The implication is that σ_1 must have plunged, on average at 3.1° (3.5° less 0.4°) toward the south-southwest with respect to the present horizontal peneplain surface. If the plunge of σ_1 were also parallel to the surface topography at the time of deformation, then the thickness of the sedimentary prism eroded off the

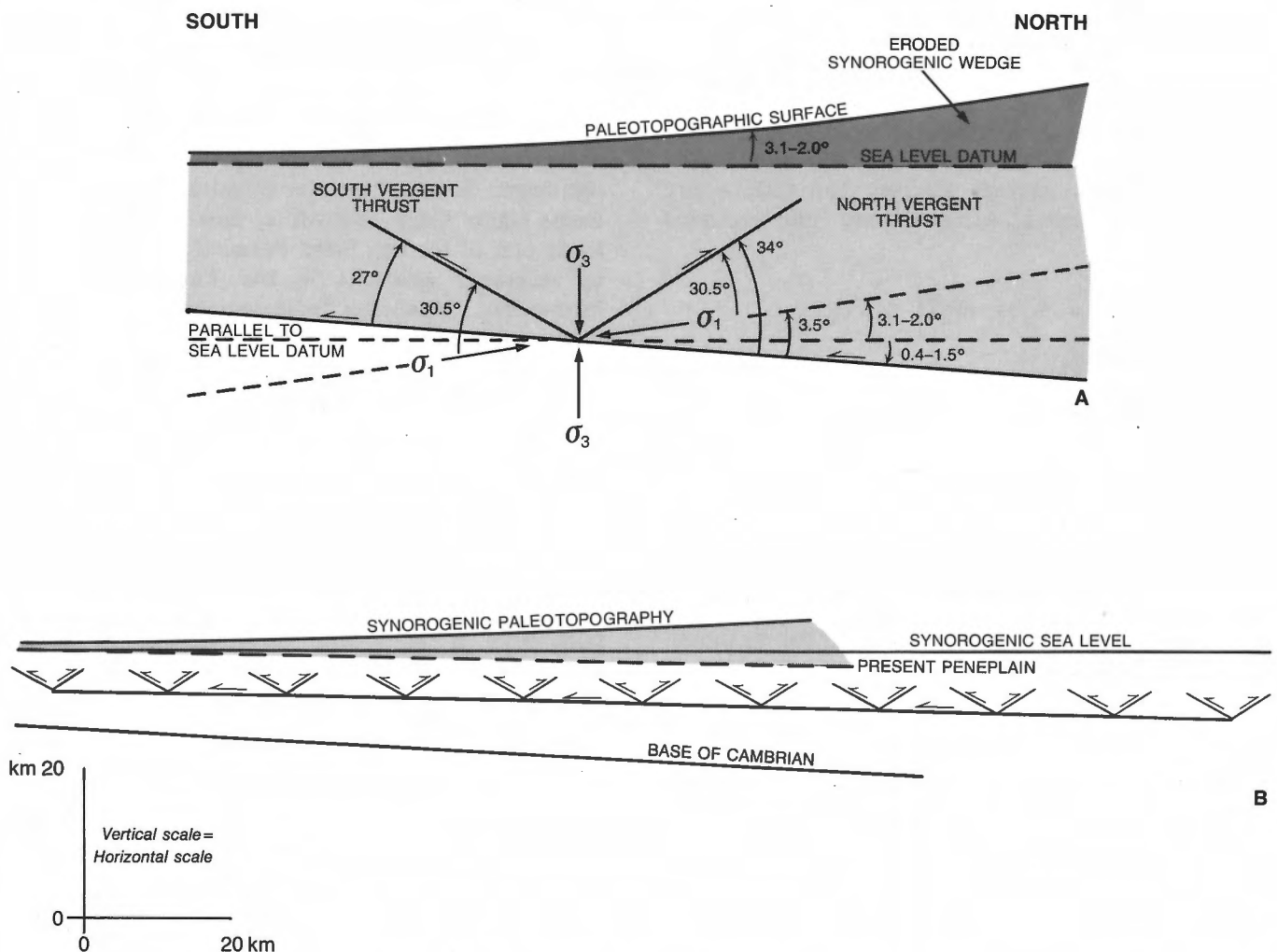


Figure 136. Schematic cross-sections of the salt-based thrust foldbelt and the eroded synorogenic clastic wedge. **A.** Attitudes of the basal décollement, conjugate thrusts in the beam, principal compressive stress axes, and the calculated paleotopographic surface with respect to a present sea-level datum. **B.** Scale model regional representation of structural and sedimentary elements.

modern peneplain would have increased into the hinterland along a surface paleotopographic profile also dipping to the south-southwest at 3.1° (Figs. 136A, B). At distances of 50, 75 and 100 km from the foreland the subaerial wedge would have had thicknesses of (50, 75, 100 $\sin 3.1^\circ =$) 2700, 4000 and 5400 m, respectively. These thicknesses of sediment cover are higher than those implied by thermal maturity data obtained from youngest preorogenic (mid-Famennian) strata in this part of the fold belt; implied thickness of eroded synorogenic post-mid-Famennian and pre-Moscovian cover for central Melville Island at about 100 km from the foreland is estimated to have been 2500 to 3000 m (Embry, 1988a).

An alternative explanation, similar to a general mechanical model proposed by Davis et al. (1983), is that uplift and tilting of proximal sediment cover began in the hinterland. As deformation propagated toward the foreland, the hinterland sediment cover was then repetitively eroded, redeposited, deformed and again uplifted from the migrating deformation front. In this model, the synorogenic sediment prism and associated mountain belt paleotopography maintains a slope of 3.1° , a dip on the basal detachment of 0.4° and a critical taper to maintain failure of 3.5° but a width across tectonic trend that is not greater than about 45 to 55 km. The width maximum is maintained as a result of migration of the foreland toe of the deforming wedge and coeval hinterland erosion, thus preventing any increase in hinterland wedge thickness beyond about 2500 to 3000 m.

Regardless of the significance of the plunge of σ_1 , the basal shear stress (τ_0) for failure is now calculable using the relation of Davis and Engelder (1985, 1987) for which:

$$\alpha + \beta = (\text{approx.}) \frac{\beta + \tau_0 / \rho g Z}{1 + (1 - P_p / P_L) (2 / \csc \phi^{-1})}$$

where $\alpha + \beta$ is the critical wedge taper yielding failure that includes the mean paleotopographic slope of the ancient mountain belt ($\alpha = 3.1^\circ$; 0.054 radians), plus the local dip of the basal detachment measured in the tectonic transport direction ($\beta = 0.4^\circ$; 0.007 radians); ϕ is the internal friction angle of the overlying rock (29°) such that $\tan \phi = \mu = 0.55$. The depth to detachment (Z) at the time of failure is 7900 m. This is the present depth to detachment (5200 m) plus the average thickness of eroded cover as implied by thermal maturity data from youngest preserved preorogenic mid-Famennian strata (2700 m; Embry, 1988a). The density (ρ) of the overburden is

2500 kg m^{-3} as obtained from the weighted average densities of preserved cover (2600 kg m^{-3}) and the since-eroded siliciclastic wedge (estimated 2300 kg m^{-3}).

For zero pore-fluid pressures, calculated basal shear stress causing failure is 33 MPa. For P_p/P_L of 0.4 and 0.7, failure shear stresses are 24 and 17 MPa, respectively. A source of error in these calculations is the dip of the basal detachment. The value adopted for β is the present dip. However, at the time of incipient deformation, the value of β would probably have been greater as a result of the additional load of sediment cover at that time. The dip of the detachment has likely decreased through time as a consequence of isostatic recovery from postorogenic off-loading of synorogenic sediment cover. The effect of a higher β will not change the critical taper ($\alpha + \beta$). It will, however, modestly decrease the basal shear stress for failure. For a critical taper of 3.5° and a hypothetical detachment dip of 1.5° at the time of deformation, the failure shear stress for zero pore-fluid pressure will be reduced by 9 per cent or about 4 MPa.

These calculations indicate that the failure shear strengths for conjugate thrusts in the medial rigid beam are at least 3.6 times the shear strength of the basal décollement for zero pore fluid pressures, and at least 3.2 times stronger for moderately overpressured conditions ($P_p/P_L = 0.7$). In other words, the stresses required to cause brittle failure and sliding on the basal décollement are relatively small compared to the stresses required to cause shortening in the beam by thrust faulting. It is also probably safe to conclude from this that the rate-dependent step in deformation is the rate of brittle failure and shortening in the beam and not the rate of slip on the base. Calculated low basal shear strengths confirm what is already known about the lithology, deformation style and implied mechanical properties of evaporitic rocks lying on the basal décollement. These features are outlined in the following section.

Deformation of the Bay Fiord Formation

Description

In view of the low shear strength of the basal décollement, it is not surprising that evaporites of the lower Bay Fiord Formation, which lie on this detachment, also display widespread evidence of extreme mobility, particularly on reflection seismic profiles, but also in cores of borehole-penetrated intervals. The geophysical response of the unit is displayed by thickness variations that are spatially

associated with folds and thrust faults in the overlying formations, and related to deep-seated faults that originate below the evaporite layer. In both cases, thickness variation has resulted in regions of thinning with respect to primary depositional thickness and other regions of tectonic thickening.

Where structural relief and faulting occurs below the Bay Fiord Formation, deformed-state thickness variation has induced a general reduction of structural relief higher in the section by thickening of the evaporites within synclines and coincident thinning above anticlines. Examples of this phenomena occur beneath Burnett Point Syncline in Sections A through D (Fig. 137, Note 1). The lower Bay Fiord Formation has been thickened most where it occurs in the footwalls of thrust and reverse faults that emerge into the evaporite unit from deeper in the section. Examples are demonstrated on Sections C and D on the south

flank of Spencer Range Anticlinorium, on Section I on the south-facing limb of Nias Point Anticlinorium, and beneath Richardson Point Anticline (Section A; Fig. 117).

More common are evaporite thickness variations that are related to folds detached above the salt layer. In the absence of sub-Bay Fiord structure, thickness variation of the Bay Fiord evaporites has been accomplished so as to reduce to zero the thin-skinned structural relief at the level of the Eleanor River Formation. Thus, tectonic thickening is generally located below surface anticlines and, more specifically, below major and parasitic anticlines, and similarly beneath thrust ramps of the medial rigid beam (Fig. 106, Note 4; Fig. 107, Note 3; Fig. 109, Note 4; Fig. 111, Note 4; Fig. 113, Note 3; Fig. 123, Note 2). Thickened areas of salt in profile are cusped-, lens- or pillow-shaped in the tectonic transport direction

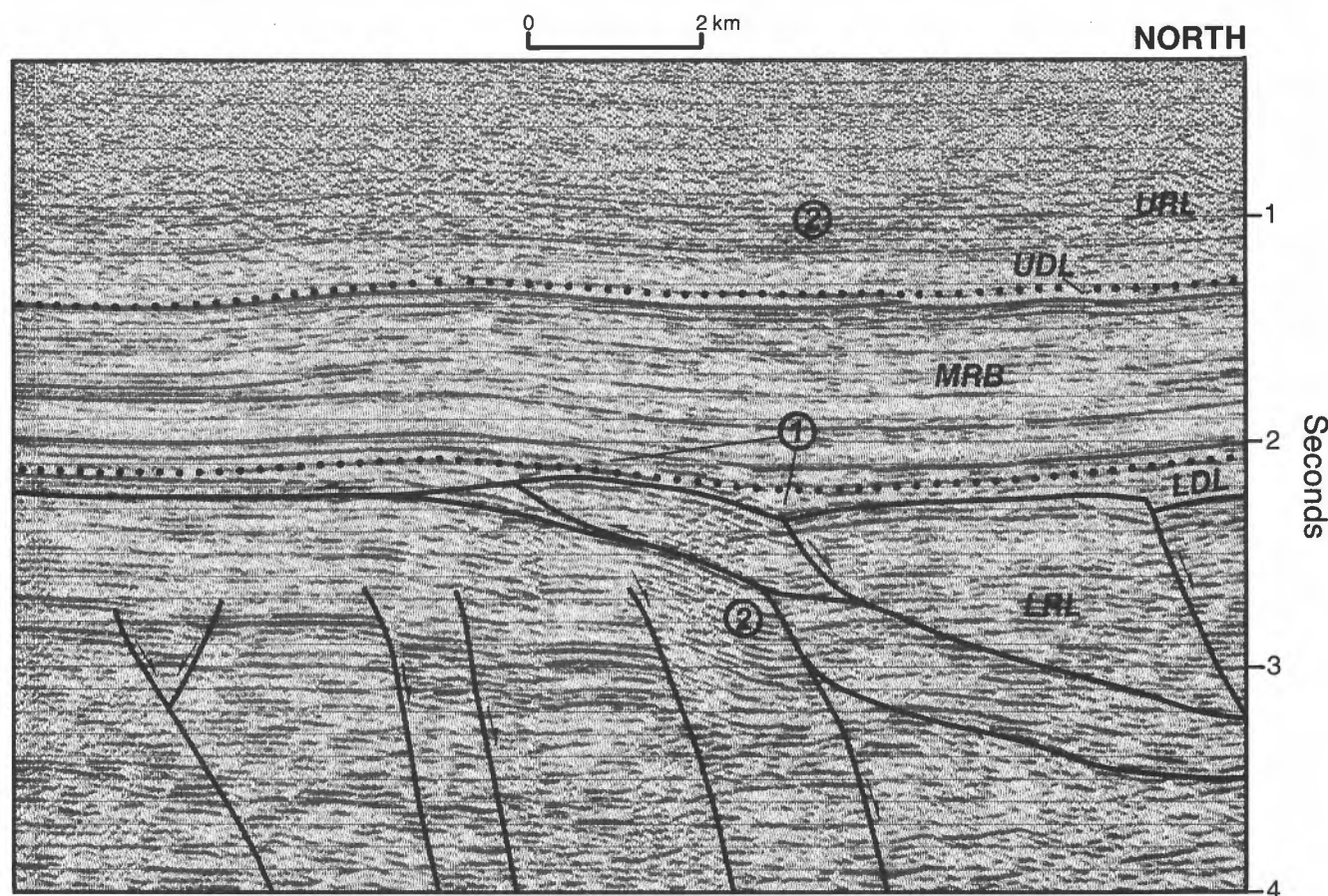


Figure 137. Burnett Point Syncline, on a part of seismic profile T4, Section C. LRL, lower rigid layer; LDL, lower ductile layer; MRB, medial rigid beam; UDL, upper ductile layer; URL, upper rigid layer. The medial rigid beam, in this area, includes the Blue Fiord Formation and, below that, the facies transition from seismic unit OSc southward to the lower Cape Phillips Formation. Other component formations of each layer are listed in Figure 101. 1, synclinal salt welts in the lower Bay Fiord Formation and coincident salt thinning above anticlines; 2, the surface syncline lies nearly directly above the axial line of a heavily faulted D4 syncline below the Bay Fiord décollement.

(parallel to σ_1), but also greatly elongated parallel to σ_2 and the axial trend of second-order anticlines. In a similar way, tectonic thinning of the lower Bay Fiord Formation occurs beneath surface and subsurface synclines. The thinnest salt intervals occur below synclines with the greatest negative structural relief and greatest preserved surface section (Fig. 106, Note 5; Fig. 113, Note 4; Fig. 117, Note 4; Fig. 123, Note 3; Fig. 124, Note 2).

Relative thickness variation of salt in its tectonized state ranges from 8 to 360 per cent of primary depositional thickness. Range of absolute tectonic thickness is from less than 60 m to 2220 m. To isolate the tectonic component of thickness variation of the lower Bay Fiord Formation, a "tectonic thickness parameter" (T') is provided (Fig. 138), representing a minimum and maximum bedding-normal unit thickness in synclines (T'_S) and anticlines (T'_A), respectively, normalized against primary depositional thickness. A value of 0.80 for T'_S means that the tectonic thickness is 80 per cent of the primary thickness. Frequency histograms for variations in tectonic thickness parameters for lower Bay Fiord Formation within synclinal and anticlinal hinge areas are plotted in Figure 138. Although peak frequencies occur at $T' = 0.65$ for synclines and at $T' = 1.12$ for anticlines, there are lesser frequency maxima at $T'_S = 0.35$ and 0.15 and at $T'_A = 2.25$ and 3.40 . There is also a small group of anticlines within which there has been a net tectonic thinning of evaporites ($T'_A < 1.0$) and a larger group of synclines within which there has been a net thickening ($T'_S > 1.0$).

Wells: ductile rock bodies formed in compression

The term "welt" has been previously applied to linear, lens- or cusped-shaped rock bodies formed in compression (Harrison and Bally, 1988). The origin in compression is deemed the fundamental criterion required to distinguish welts from the evaporite pillows and diapirs of other tectonic settings for which gravitational instability and stratigraphic inversion are the fundamental genetic causes and results. The descriptive classification of salt welts (Fig. 139) also recognizes that thickening can occur within deep-seated synclines and in front of deep-seated thrusts that emerge into the ductile layer.

The across-strike termination of an anticlinal welt is identified (in profile) beneath synclines by the tectonic divergence of the flat-lying rigid succession beneath the salt and the tilt due to folding of the medial rigid beam above the salt. The welt is enclosed between two facing sub-syncline divergences. For simple anticline-related welts, tectonic thickening is produced in a single linear cusped zone flanked by thinned evaporites in adjacent synclines (Fig. 111, Notes 4, 5). This type represents not more than 35 per cent of all anticlinal welts. More common (>53%) are compound anticlinal salt welts also referred to as "Napoleon's Hat" structures. The compound welt features two hinge area evaporite-cored culminations and an intervening saddle. The hinge culminations are commonly the locus of thrust ramps that mostly lie in the overlying medial rigid beam. In the case of Cape Phipps Anticline (Fig. 140) only one hinge culmination is faulted and the footwall syncline

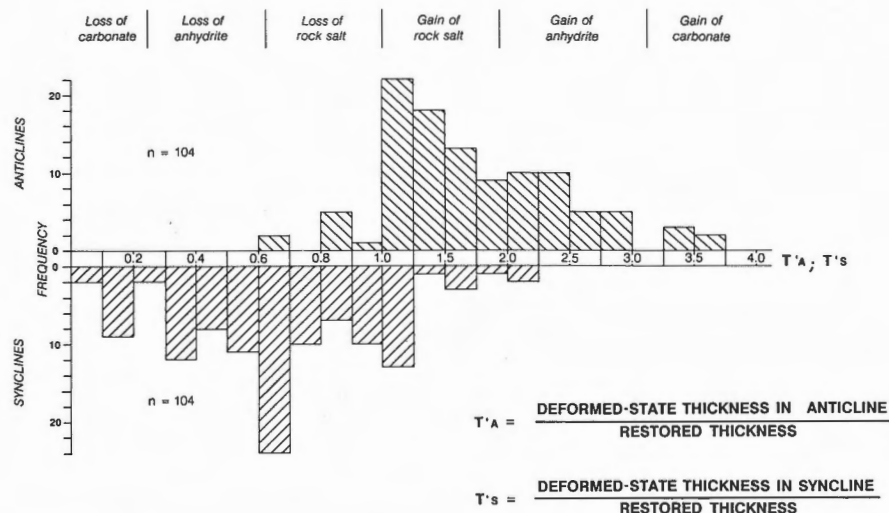


Figure 138. Frequency histogram plot of tectonic thickness parameters (T') for the lower Bay Fiord Formation within anticlinal welts (T'_A) and synclines (T'_S). Frequency peaks are correlated with successive loss or gain of rock salt, anhydrite, and dolostone during horizontal shortening.

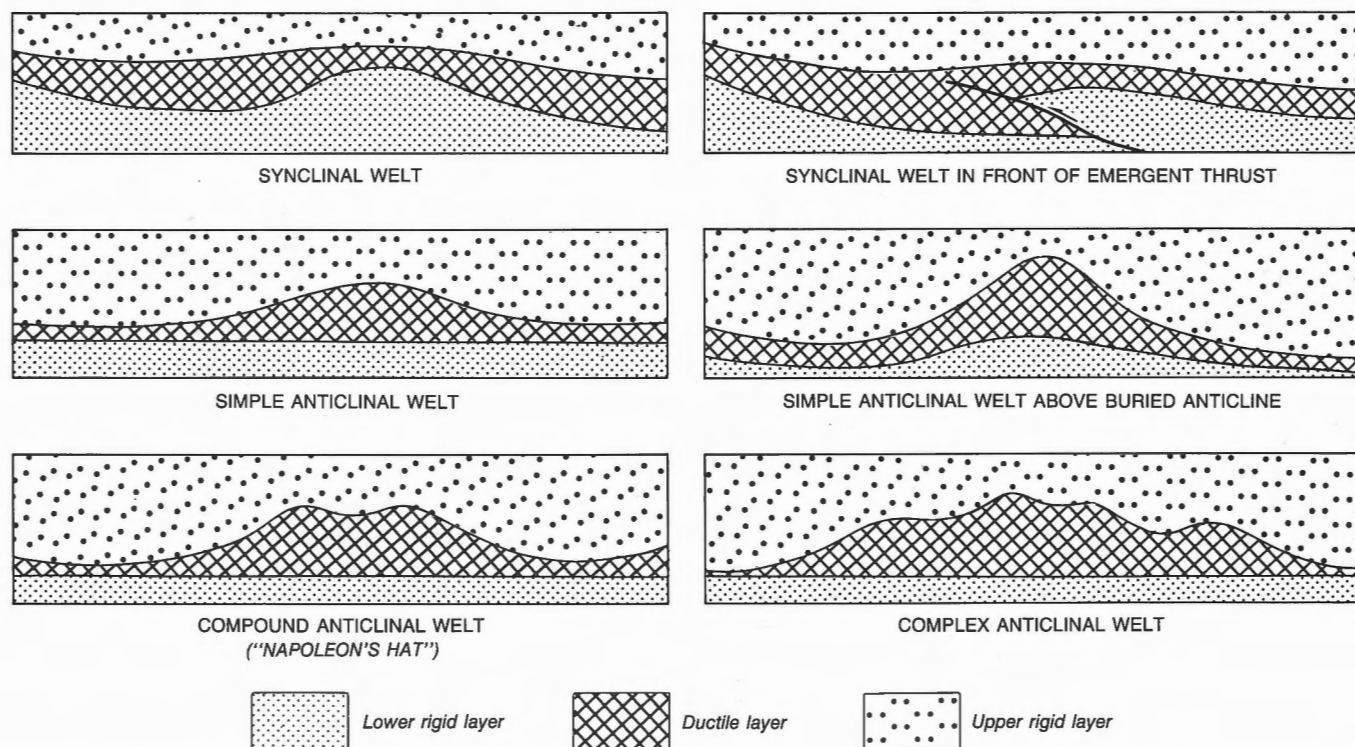


Figure 139. External morphology of salt welts, shale welts and other ductile rock bodies formed during compression.

in the hinge of the compound welt is very small. In most cases both welt culminations are faulted (Fig. 108, Note 6; Fig. 124, Note 3). The hinge thrusts tend to verge toward each other and converge upsection. As a result the intervening saddle is bound by both hinterland- and foreland-vergent thrusts. At an advanced stage of compound welt growth, a triangular fragment of the medial rigid beam within the hinge can become completely encapsulated by lower Bay Fiord Formation – autochthonous evaporites below and transported evaporites lying in the hangingwall of both bounding convergent thrusts (Fig. 141). This appears to have occurred within Dealy Island and Mecham River anticlines of Section H (Fig. 106, Note 6; Fig. 123, Note 4). Second-order anticlines, possessing peripheral third-order parasitic folds, are commonly underlain by complex anticlinal salt welts (12%). These welts possess three, hinge-region evaporite culminations in the case of Sabine Bay Anticline on Section H (Fig. 109, Note 5), four beneath Robertson Point Anticline on Section C (Fig. 113, Note 5), and six beneath King Point East Anticline on Section A (Fig. 114, Note 4).

There is qualitative evidence to indicate that, for limited horizontal shortening in the medial rigid beam (3–5%), the Bay Fiord evaporites occur within low-amplitude simple welts with limited anticlinal

thickening and synclinal thinning, or within compound welts for which only one culmination has experienced brittle failure (examples on Section F). Progressive shortening (10–20%) appears to produce thicker welts of compound type, failure of both hinge culminations and a more complete synclinal evacuation of the evaporite (Section G). For anticlines displaying the greatest shortening (20–35%), underlying evaporites occur within either complex welts or asymmetrical compound welts with encapsulated tectonic fragments of the medial rigid beam (Sections A and B).

The seismically imaged deformation style for the Bay Fiord Formation is complemented by cored intervals through the formation in the Caledonian R. J-34 well drilled on the hinge line of Caledonian River Anticline, southern Bathurst Island (Figs. 142–144). Primary layering is commonly near vertical (within 0–20° of core axes). Competent layers of dolostone have been attenuated along fractures perpendicular to layering, boudinaged parallel to layering, and also tectonically brecciated. Similar structures occur in laminated anhydrite, which also displays a pre-tensile phase of folding and compressive shear. A parasitic similar fold in laminated anhydrite of one sample (Fig. 143) displays local hinge thickening of up to 670 per cent with respect to an adjacent limb. No evidence of a primary depositional fabric remains in

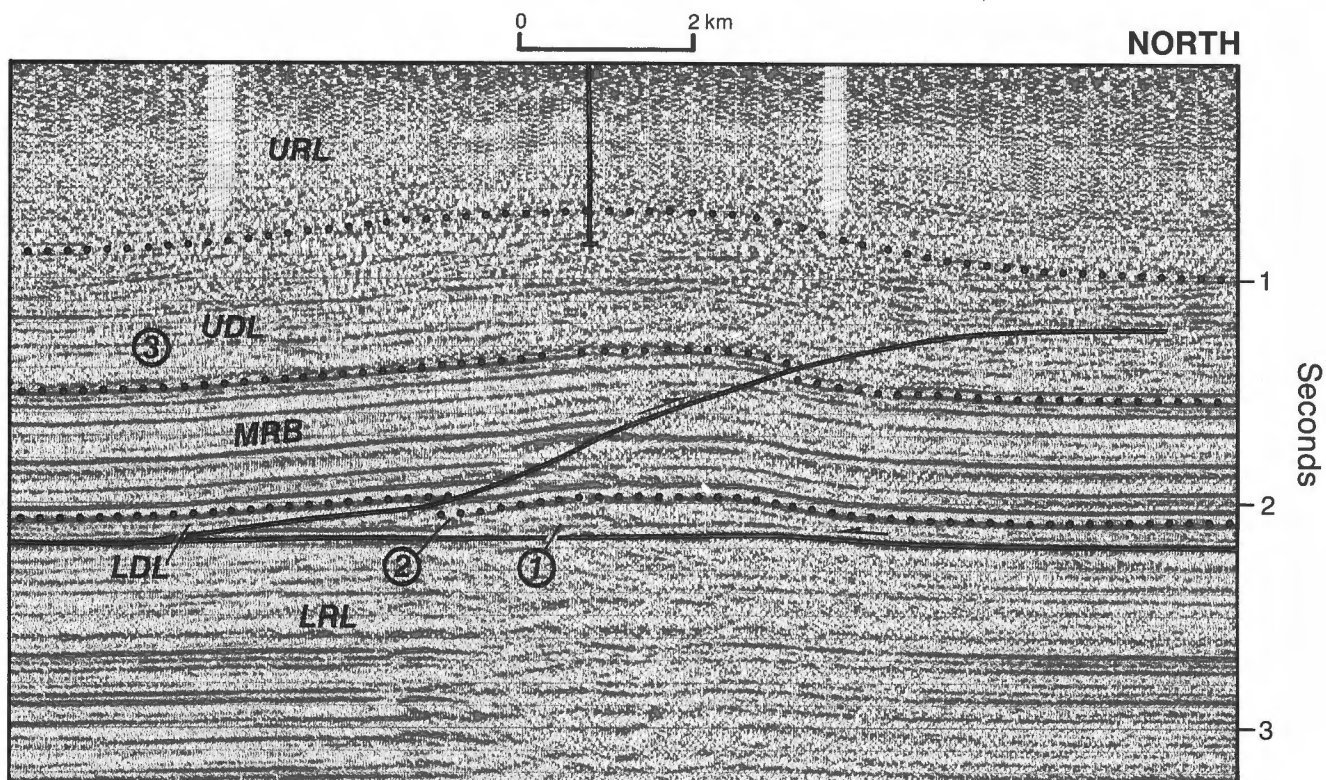


Figure 140. Cape Phipps Anticline, on a part of seismic profile P1171, Section F. Component formations of each layer are listed in Figure 101. LRL, lower rigid layer; LDL, lower ductile layer; MRB, medial rigid beam; UDL, upper ductile layer; URL, upper rigid layer; 1, a compound anticlinal welt with only one faulted culmination; 2, a small footwall syncline within the saddle of the compound anticline welt; 3, the synclinal mudrock welt, especially evident in the lower Cape De Bray Formation, could have been generated in part by differential compaction over the anticline during folding.

Figure 144, which features isolated dolostone breccia fragments entrained and rotated in a ductile halite-anhydrite matrix. Coarsely recrystallized halite (grains to 2.5 cm) fills large tension fractures between breccia fragments (Figs. 142, 144). In a separate sample (Fig. 143), fine crystalline halite fills voids within boudin pressure shadows and within fine tension fractures perpendicular to layering. The magnitude of extension implied by volume of vein fill in the three illustrated samples is estimated to be 15 to 20 per cent.

Various theoretical internal geometries for salt welts are illustrated in Figure 145. The concept of simple welts as comprising an imbricate thrust stack of several competent layers is consistent with the observation that for Cape Providence Anticline (Section F, Note 15; Fig. 111, Note 5) several internal reflection segments appear to be imbricated within the welt. However, imbrication alone fails to explain the tectonic thinning of the lower Bay Fiord evaporites within most synclines. Other structural models applicable to compound

salt welts include box-shaped folds with large conjugate kink bands or transported evaporite layers moulded into ductile folds that decrease in amplitude downward.

These structural models (Figs. 145A–C) each possess features of individual merit but are all rejected because of a failure to take into account the mixture of rock salt (42%), bedded anhydrite (28%) and dolostone (30%) actually encountered in borehole-penetrated sections of the lower Bay Fiord Formation (Fig. 34). The favoured internal structural geometry of a fully evolved salt welt (Fig. 145E), therefore, consists of grossly thickened salt layers that may be completely necked on the limbs and in the synclines. Volumetrically significant salt has also been trapped in large pressure shadows, tension gashes, and in the lower part of some pop-up structures. The anhydrite occurs within variably thickened and thinned ductile folds. At the other competency extreme, the dolostone layers may be thrust duplicated in the anticlinal hinge,

tilted but relatively undeformed on the limbs, and, in the synclines, brecciated and horizontally boudinaged parallel to layering.

Ductility of evaporites

The inferred ductility of the geophysically-imaged evaporites of the lower Bay Fiord Formation is also supported by a well established body of published experimental data on the mechanical properties of mono-mineralic halite, and both naturally- and synthetically-aggregated rock salt. At strain rates ($\dot{\epsilon}$) of 10^{-6} through 10^{-9} sec^{-1} , Carter and Hansen (1983) were able to show that the behaviour of dry, natural rock salt conformed to a steady-state flow equation such that:

$$\dot{\epsilon} = A (\sigma_1 - \sigma_3)^n \exp[-B/RT]$$

where $A = 7.6 \times 10^{-4} \pm 2.8 \times 10^{-3} \text{ sec}^{-1}$, B (the activation energy) $= (66.5 \pm 17.5) \times 10^3 \text{ kJ/mol}$, $\sigma_1 - \sigma_3$ is the stress difference, the constant $n = 4.5 \pm 1.3$, R is the Universal gas constant, and T is the temperature ($^{\circ}\text{K}$).

Extrapolating to geological strain rates of $10^{-14} \text{ sec}^{-1}$ (or about 5 cm/yr. over the 180 km width of the fold belt) and at detachment temperatures of 195°C (25 mK m^{-1} and 7.8 km depth), the implied stress differential required to induce ductile flow in Bay Fiord rock salt is much less than 1 MPa. Anhydrite at these temperatures and strain rates has also been found

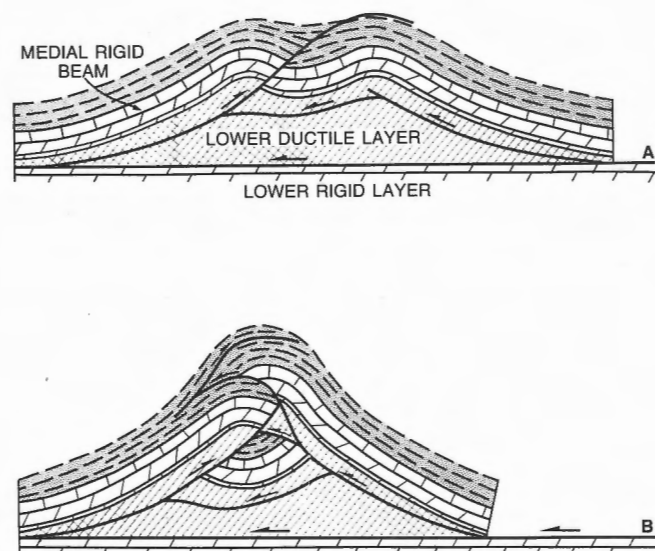


Figure 141. Progressive growth of a compound anticlinal welt. **A.** Convergent thrusting in the hinge of both culminations. **B.** In the advanced stages, there is complete encapsulation by evaporites of a fault-bounded, triangular-shaped tectonic fragment of the medial rigid beam.

to have low strength. In contrast, most other rocks do not become comparably ductile above depths of 15 km (Fig. 146).



Figure 142. Halite vein filling, in core from the lower member of the Bay Fiord Formation, Dominion Explorers Canso et al. Caledonian R. J-34 well, Bathurst Island. ISPG photo. 3104-1.

Since the ductile strength for salt is 1/10th that of anhydrite and several orders of magnitude lower than that of dolostone and most other rocks (as shown in Fig. 146 and as discussed previously), the stress differential required to move rock out of synclines must, intuitively, also increase substantially with progressive sub-syncline thinning and evacuation first of salt, later of anhydrite and finally of dolostone. In addition, fluid dynamic theory predicts that for homogeneous ductile materials sandwiched between

two rigid, parallel and converging plates (such as a synclinal layer of salt between two carbonate formations), the force required to maintain flow will be inversely proportional to the cube of the distance between the plates (Jaeger, 1962, p. 140). This relation is also confirmed by triaxial stress tests on natural rock salt (Carter and Hansen, 1983), which show that initial differential stresses, less than 1 MPa at <1 per cent strain ($T=115^{\circ}\text{C}$), rise to 22 and 27 MPa at 5 and 15 per cent strain, respectively.

Deformation of the Cape De Bray Formation

Description

The style of deformation of the Cape De Bray Formation is documented by field observations at all scales from hand specimen to cliff sections hundreds of metres high (Fig. 48). Additional data have been provided by drill core and seismic reflection profiles. In outcrop, the dominant rock fabric is a bedding-parallel parting, particularly in the upper part of the formation where thin cemented sandstone and siltstone beds cap coarsening-upward, progradational rhythms. In contrast, compositional layering may be entirely absent through many tens of metres of section in the lower part of the formation (Fig. 103A). In these circumstances, the rock fabric includes closely spaced (cm scale) fractures that cause the rock to break into blocky, splintery or cigar-shaped fragments. Rare, thin sandstone beds allow the fracture system to be recognized as an incipient form of axial planar cleavage (Fig. 103B). Deformation fabrics in drill core



Figure 143. Minor folds and boudinage structures in core from the lower member of the Bay Fiord Formation, Dominion Explorers Canso et al. Caledonian R. J-34 well, Bathurst Island. ISPG photo. 3029-13a.



Figure 144. Tectonic breccia in core from the lower member of the Bay Fiord Formation, Dominion Explorers Canso et al. Caledonian R. J-34 well, Bathurst Island. ISPG photo. 3029-12.

also include wavy tabular fragments of intercalated mudrock and very fine grained sandstone with polished and lineated minor slip surfaces spaced at intervals of 2 to 10 cm. Microfolded minor faults have also been

produced by polyphase cross-faulting. Common attitudes of slip surfaces range from subhorizontal to 45° with respect to both core axis and compositional layering.

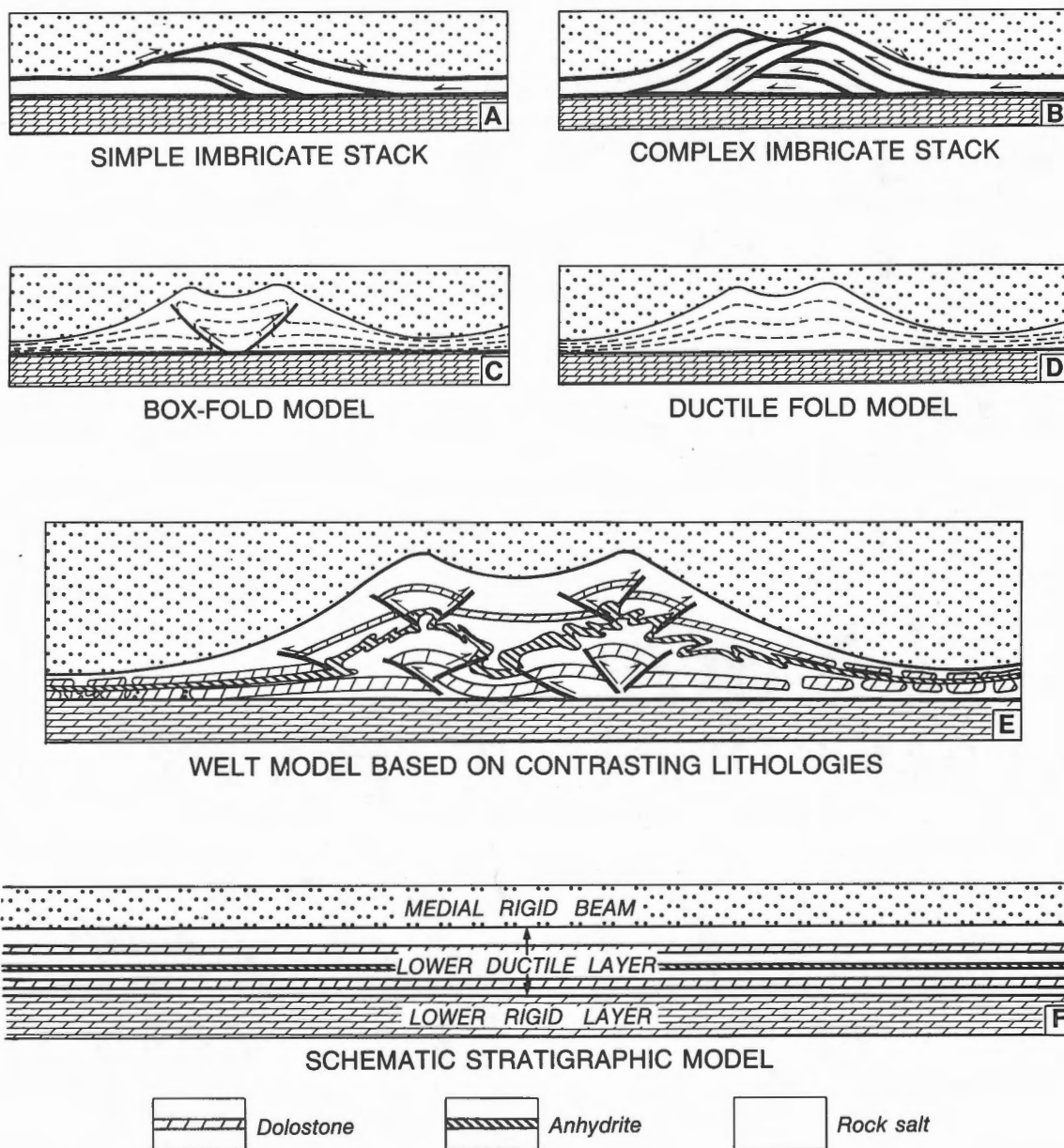


Figure 145. Possible internal geometries of anticlinal salt welts. The favoured model (E) is based on contrasting lithologies within the lower ductile layer, as indicated in exploratory wells that penetrate the lower Bay Fiord Formation.

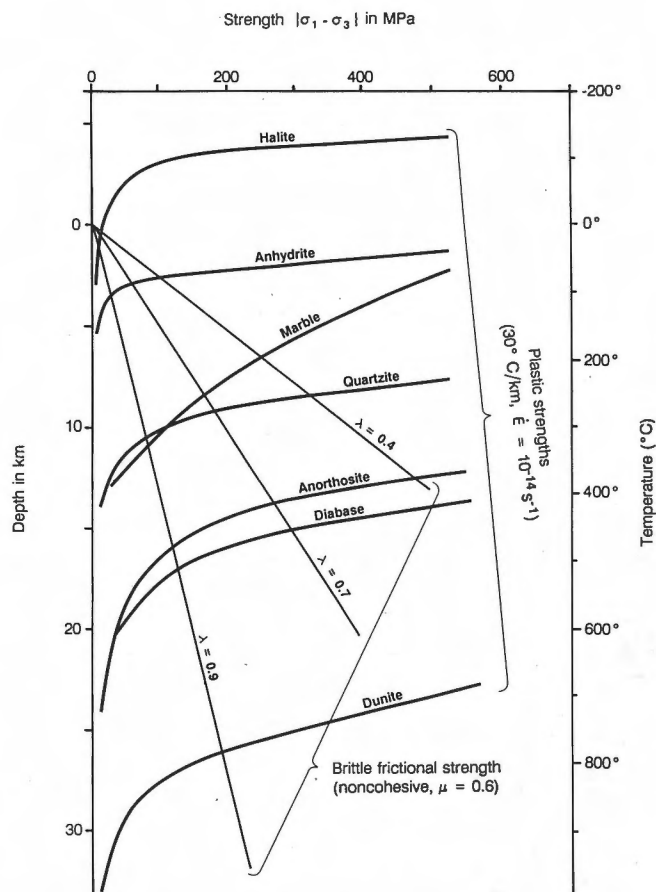


Figure 146. Strengths of salt and other common rock types as a function of depth, temperature, and strain rate. (Redrafted from Davis and Engelder, 1987, and Dahlen, 1990.) The sub-Bay Fiord detachment falls within the ductile field (<1 MPa) at strain rates less than 10^{-13} s^{-1} for anhydrite, and at all strain rates above 10^{-10} s^{-1} for salt.

Various outcrop-scale structures, illustrated in Figure 103, include small, tight, similar folds, boudinaged sandstone beds, and cleaved diapiric mudrock occupying faulted anticlinal hinges. This style is contrasted with that observed in the lower Weatherall Formation (Fig. 102) which features minor thrusts, and chevron and fault propagation folds possessing wavelengths mostly greater than 200 m. The contrast in style and scale of deformation in outcrop is best observed outside the salt-based fold belt within Purchase Bay Homocline on the south side of Ibbett Bay and eastward from the head of Ibbett Bay. Mappable thrusts in the lower Weatherall Formation converge downsection into several ill-defined thrust faults situated within the uppermost Cape De Bray Formation. Mesoscopic folds die out downsection by loss of amplitude; shortening is then presumably accommodated on subparallel slip surfaces in Cape De

Bray mudrock. On the south side of Ibbett Bay, topset beds above depositional clinoforms are also spatially and stratigraphically associated with contractional folds and low-angle thrusts (Fig. 147). Top-truncated slope-facies strata can be misinterpreted as tectonically inclined footwall beds beneath a subhorizontal hangingwall detachment.

Mudrock welts of the Cape De Bray Formation

The apparent primary thickness of the Cape De Bray Formation, imaged on seismic profiles, has remained relatively undisturbed throughout most folded areas. Obvious tectonic disturbance of the formation occurs only on some syncline limbs and within some anticlinal hinges. Mudrock welts are locally developed and are superficially similar to those encountered in the lower Bay Fiord Formation (Fig. 139). Common varieties, in decreasing order of importance, include synclinal welts in front of emergent thrusts, simple anticlinal welts, and synclinal welts.

Tectonic thicknesses of the Cape De Bray Formation range to a maximum of 2200 m or about 300 per cent of the pre-deformational thickness. Clear evidence of tectonic thinning has not been found. The implication of this is that local thickness increase may be due entirely to brittle deformation and internal imbrication, but not ductile flow.

Tectonic thickening of the Cape De Bray Formation is most commonly observed on the limbs of synclines in front of upward-flattening thrusts that emerge from the underlying Cape Phillips and correlative Blue Fiord formations. The seismic expression of this type of welt is observed on the south limbs of Sabine River and Byam River synclines (Section D; Fig. 115, Note 4), on the north limb of Liddon Gulf Syncline (Section I) and on both limbs of Stony Pass Syncline (Sections F and H). Other examples are noted on: Figures 106, Note 7; 109, Note 6; and 124, Note 4. A fine example of the internal geometry of this type of welt occurs on the south limb of Chevalier Bay Syncline (Section G; Fig. 148A). In this case, thickening can be attributed to south-directed wedging of a thrust imbricate into a horizontal bedding plane detachment situated in the middle of the Cape De Bray Formation. At three locations on Section A (Note 12), a combination of bedding plane detachment wedging and ramping appears to have been facilitated by slip on depositional clinoforms (Fig. 114, Note 5; Fig. 122, Note 3; Fig. 148B). Tectonic thickening has also been accomplished in front of a series of four thrust splays that emerge together out of the Blue Fiord Formation on

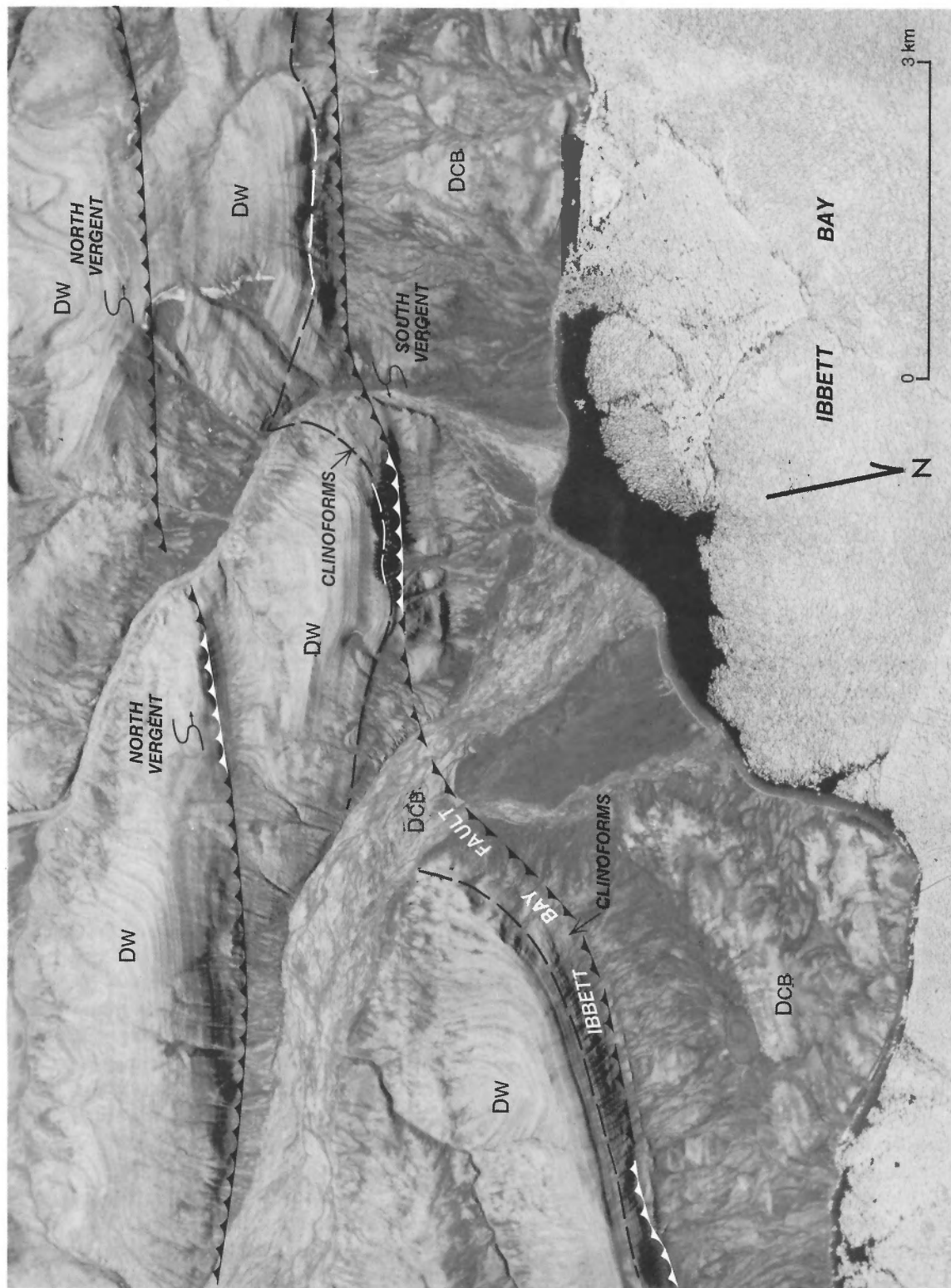


Figure 147. Vertical airphoto of detachment faults, minor folds, and depositional clinoforms of the lower Weatherall and upper Cape De Bray formations, Purchase Bay Homocline. DCB, Cape De Bray Formation; DW, Weatherall Formation. See also legend, Figure 33. NAPL photo. A17719-139.

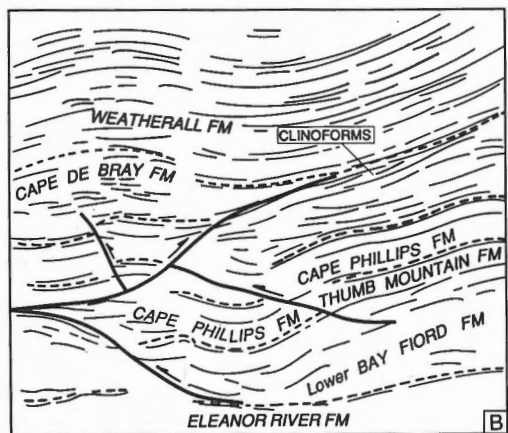
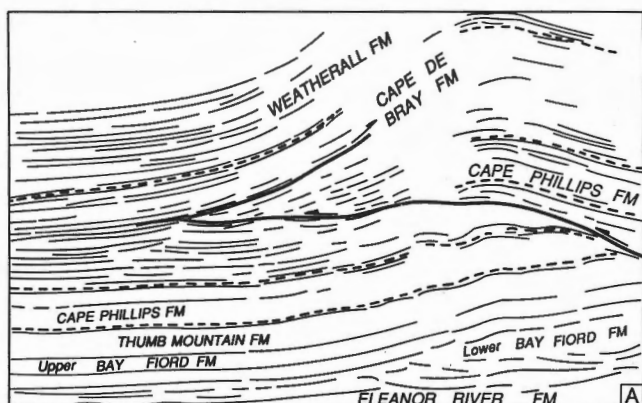


Figure 148. Non-ductile internal geometries of synclinal welts resulting from simple thrust wedging into horizontal (A), and clinoform (B) bedding-plane detachments in the Cape De Bray Formation.

the north limb of King Point East Syncline (Section A; Fig. 117, Note 5). A non-ductile solution to the thickening might involve wedging of an imbricate stack into a single bedding plane detachment. General thickening on Section A also occurs in a disturbed interval of Cape De Bray Formation sandwiched between Birch Point Syncline (above) and seven upward-flattening thrusts of mixed vergence (below).

Simple anticlinal welts of Cape De Bray mudrock have been predicted from bedding attitudes collected at surface from the overlying formations (Figs. 51, 149, 150A). Additional constraints on the external form of these welts are offered by seismic images displayed with Sections A through D. From these data, anticlinal welts in the shallow subsurface are inferred for Beverley Inlet Anticline (Fig. 124, Note 5), Robertson Point Anticline (Fig. 113, Note 6), Rea Point Anticline (Fig. 115, Note 5), King Point East Anticline



Figure 149. Vertical beds in the Weatherall Formation, north limb of Beverley Inlet Anticline, southeastern Melville Island. ISPG photo. 2887-56.

(Section A, only; Fig. 114, Note 6) and Dealy Island Anticline on Section H (Fig. 123, Note 5).

For Beverley Inlet Anticline, the lower surface of the anticlinal welt is defined by subhorizontal and convex reflection segments on the uppermost surface of thrust-duplicated Cape Phillips Formation (Section C). Lateral limits of the welt are marked by downward convergence of top- and base-Cape De Bray reflections to a minimum separation width within adjacent synclines. The implied welt shape in profile is one of an upright triangle with concave sides, cusped upper point and open lower corners. The shape resembles some Bay Fiord salt welts in that the form allows for the correction of a room problem created in the hinge of an overlying downward-tightening concentric fold. Since there is no evidence of thinning of the Cape De Bray Formation in adjacent synclines, an intraformational duplex style of deformation is probably the most likely one to account for the excess thickness of mudrock in the welt (Fig. 150C). Before leaving the Beverley Inlet structure it is worth noting that the depth-to-detachment calculation from a top-Weatherall datum can approximately locate an important shallow detachment level near the top of the Cape De Bray Formation (Figs. 150A, B). However, in the absence of seismic data, this information would be disastrously misleading if it were assumed that the calculated detachment level were also the ultimate depth to the basal décollement.

Least common of the Cape De Bray welts are those found in synclines above folded, but not necessarily thrust-faulted, Cape Phillips Formation of Section F. Demonstrable thickening occurs in the lower Cape De

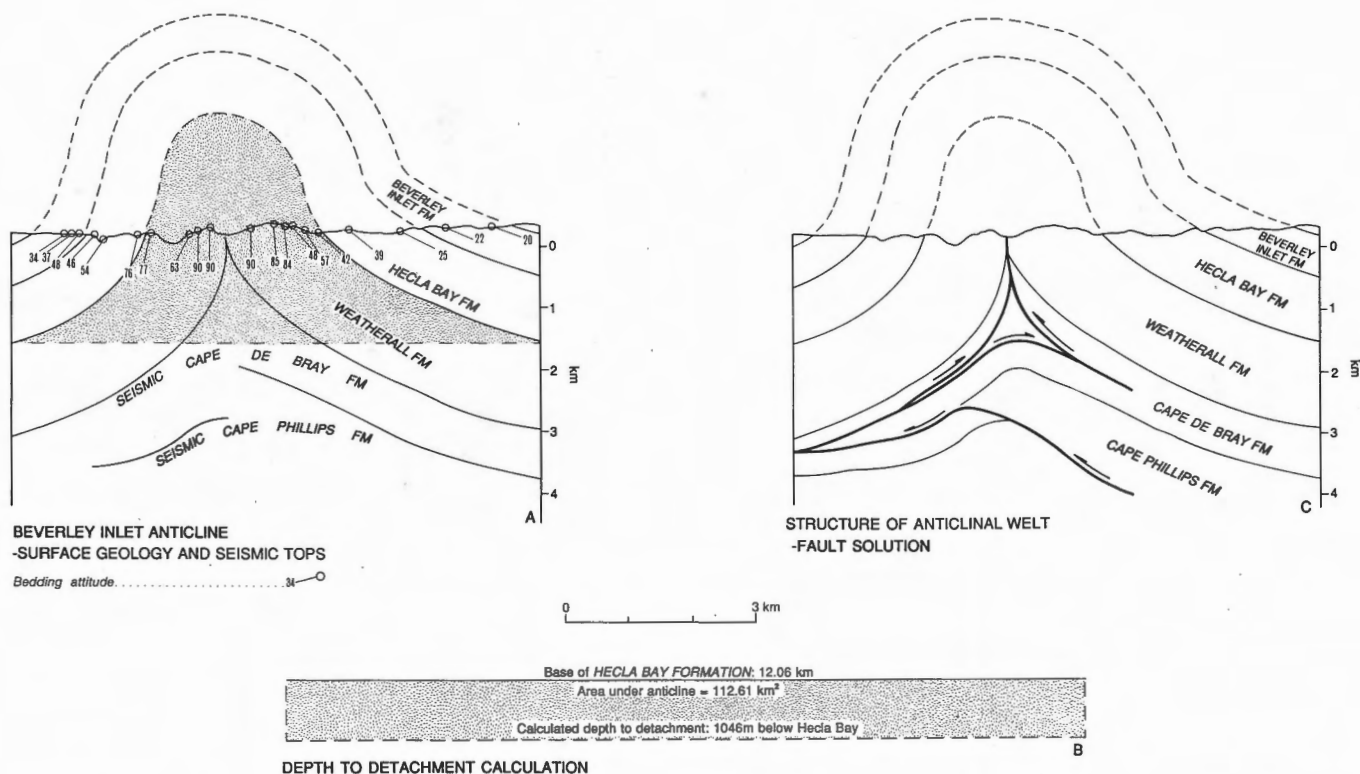


Figure 150. Near-surface structure of the Beverley Inlet Anticline. **A.** Surface geological and seismic reflection data. **B.** Calculated depth to detachment. **C.** A possible internal geometry of the associated anticlinal welt in the Cape De Bray Formation.

Bray Formation (Fig. 111, Note 6; Fig. 112, Note 2; Fig. 140, Note 3). The existence of these very low amplitude and long-wavelength welts is also deduced from the fact that four subsurface anticlines of Dundas Peninsula, clearly definable at the level of the Cape Phillips Formation, become progressively flatter upsection, and are unidentifiable within horizontally bedded surface strata of the Beverley Inlet Formation (Fig. 111, Note 7; Fig. 112, Note 3). These features could be formed by either a tectonic or depositional thickening of the Cape De Bray, Weatherall and/or Hecla Bay formations within synclines. The simplest explanation, however, is that these thickness variations are caused by differential compaction of the Cape De Bray and Devonian clastic formations during folding.

The “life history” of thin-skinned salt-based folds

The fold belt “family”

Every structural cross-section of an orogenic belt represents an accumulation of “snapshots” of a portion of the earth’s crust. Each shot portrays

structural features as they appeared just before the compressive stress was large enough to produce strain and brittle failure. The geophysical images and geological data of the Parry Islands Fold Belt display structures representing a range of strain states. It is reasonable to infer that structures featuring large finite strains and complex styles of deformation have suffered a longer history of infinitesimal strain. If fold and thrust belts evolve by progressive expansion toward the foreland, as originally proposed by Bally et al. (1966), it is reasonable to conclude that the more northerly structures of the Parry Islands Fold Belt were “born” first and began to grow to their present state of finite strain before other structures farther south. The simple structures, situated nearest the southern foreland (on Dundas Peninsula), were last to come into existence and, therefore, represent the embryonic stages of fold formation. This does not imply a strictly sequential growth of individual folds. More realistic, at any point in time, is the simultaneous, tectonically active existence of a family of folds represented by different fold generations. Like any family, each member possesses individual characteristics as well as general features typical of the specific stage of growth. Thus, seven stages are proposed for the “life history”

of the thin-skinned salt-based folds of the Parry Islands Fold Belt (Fig. 151).

Fold belt inception

Style of deformation in the salt-based fold belt has been significantly influenced by deposition and burial of a five-layer sedimentary stack comprising: 1) a thick, lower, rigid layer (3.7–7.5 km thick) of Cambrian(?) and Lower Ordovician shelf sediments; 2) a highly ductile evaporite layer (lower Bay Fiord Formation) composed of interlayered rock salt, anhydrite and dolostone (0.1–0.8 km thick); 3) a medial rigid beam (1.3–3.2 km thick) of shelf dolostones, slope and basin-facies limestone and carbonate-mudrock; 4) a low-strength upper ductile layer (to 1 km) of basin-fill mudrock and siltstone (Cape De Bray Formation); and 5) a shallow, buried, upper rigid layer of deltaic and nonmarine siliciclastic sediments (including at least the preserved upper 1.3–3.2 km of Devonian clastic wedge).

The first fold is created in this deformation history through the application of a small differential shear stress to the basal salt layer leading to ductile failure (Fig. 151A). This could occur when one or more deep-seated contraction faults reach the salt layer on thrust ramps situated near the hinterland (northern) edge of the lower Bay Fiord evaporite facies. Thin-skinned deformation is not yet evident at seismic scale. However, the development of kink bands and outcrop-scale minor faults may occur in the beam and other strain elements in the ductile units and upper rigid layer.

Embryonic folds

Subhorizontal compressive stress is transmitted through the rigid beam during the embryonic stage of deformation (Fig. 151B), leading to the creation of a train of low-amplitude buckles in the beam. The wavelength of the new folds appears to be qualitatively pre-determined by the thickness of the medial rigid beam and its net ductility contrast with the two bounding ductile layers. Salt in the lower ductile layer is simultaneously sucked into anticlines to form simple, short-wavelength welts that resolve initial hinge area room problems. The upper ductile layer (Cape De Bray Formation) compacts differentially over anticlines, and the upper competent (siliciclastic) package remains apparently undeformed although contractional processes involving layer-parallel shortening (tectonic

compaction), and differential compaction are suspected for theoretical reasons.

Birth of folds

The folds are seen to be “born” when embryonic buckles in the most competent layer (Thumb Mountain Formation) of the medial rigid beam experience irreversible brittle failure (Figs. 111, 112, 151C). These first obvious faults nucleate in the hinge areas of some anticlines in order to resolve worsening room problems created by continued shortening. Synclinal evacuation of salt is still far from complete. Failure planes in the competent beam include either one or both upright conjugate shears. Low-amplitude folding begins in the siliciclastic layer.

Juvenile folds

General developments during the “juvenile” stage of folding (Figs. 106, 107, 140, 151D) include full link-up of upper and lower ductile layers, formation of syncline-marginal mudrock welts by intraformational imbrication of the Cape De Bray Formation in front of upward-flattening thrusts, and continued long-wavelength and low-amplitude folding of the clastic wedge. All of the salt may be evacuated from the synclines during this stage. For compound evaporite welts, separate culminations now experience axial brittle failure and the upward propagation of, usually, convergent conjugate thrusts in the overlying medial rigid beam. Many individual characteristics are created in the beam by the varying shapes of footwall cut-offs, occurrence of intermediate detachments, imbrication at different stratigraphic levels, and by antithetic thrusts propagating from various hanging wall and footwall positions.

Mature folds

The salt-based folds reach full maturity (Figs. 113, 115, 123, 124, 151E) in conjunction with a dramatic increase in amplitude of the surface anticline. Cape De Bray mudrock, previously thinned by differential compaction over anticlinal hinges during the embryonic stage, is now transferred to anticlinal hinge areas to resolve room problems created by concentric-style buckling of the clastic wedge. This is accomplished by intraformational duplex thrusting, and results in simple anticlinal welts of brittle-deformed mudrock stacked vertically above Bay Fiord evaporite welts. During the mature stage, all the salt

and most of the anhydrite are evacuated from the synclines, resulting in greatly increased basal shear stress for failure. Preferred vergence of major thrusts within the carbonate beam also produces a tendency toward asymmetrical growth of anticlinal salt welts.

Convergent thrusts propagating above mature, compound welts cause partial or complete encapsulation by evaporites of fault-bounded tectonic fragments of the medial rigid beam (Fig. 141). Parasitic structures at the level of the carbonate beam develop on anticline flanks

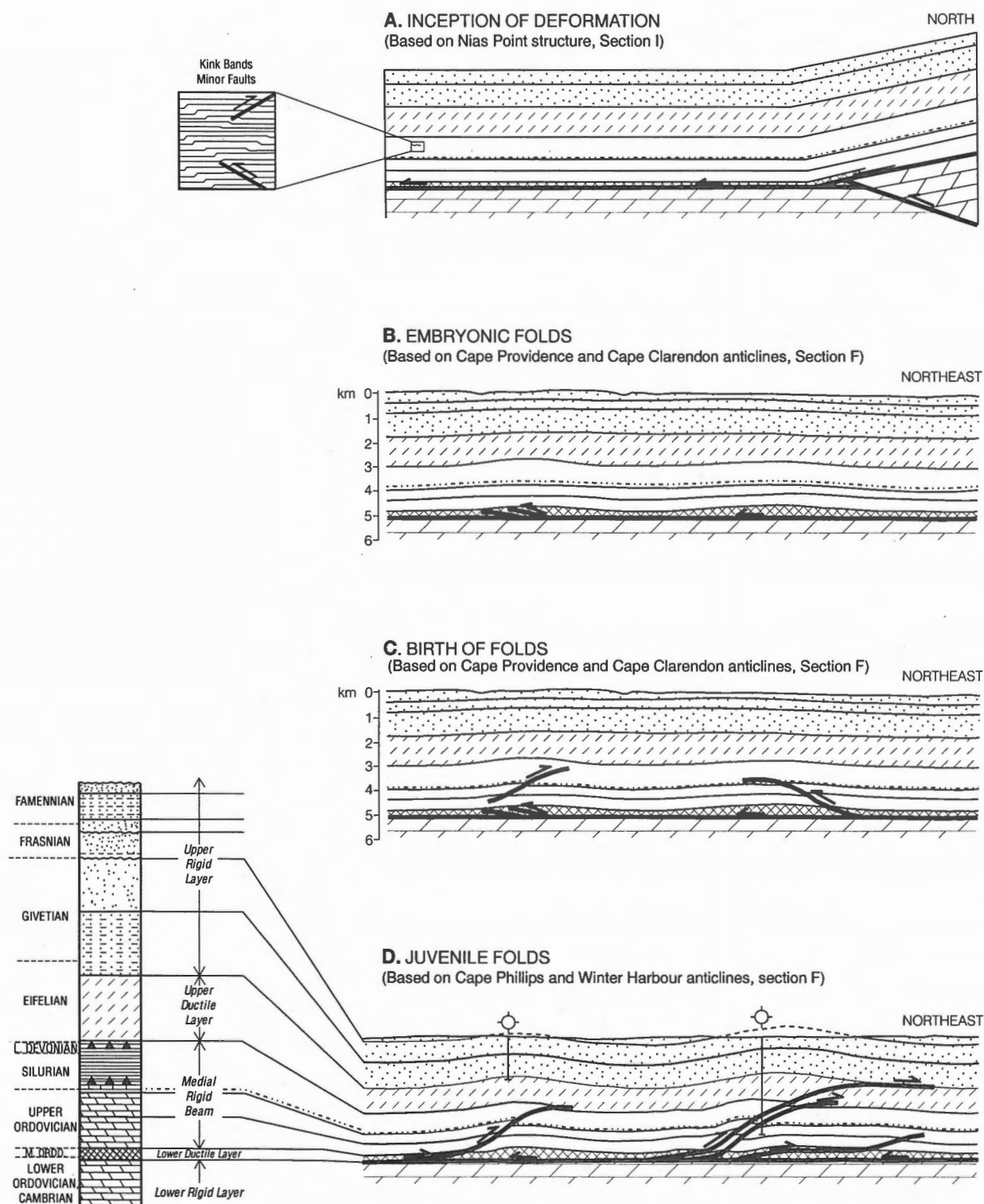


Figure 151. Schematic development of salt-based folds in six stages (A-F).

and also locally below surface synclines by a combination of new welt growth and increased overlap on relaying and en echelon structures. Simple, compound and other parasitic anticlinal salt welts begin to coalesce into complex welts.

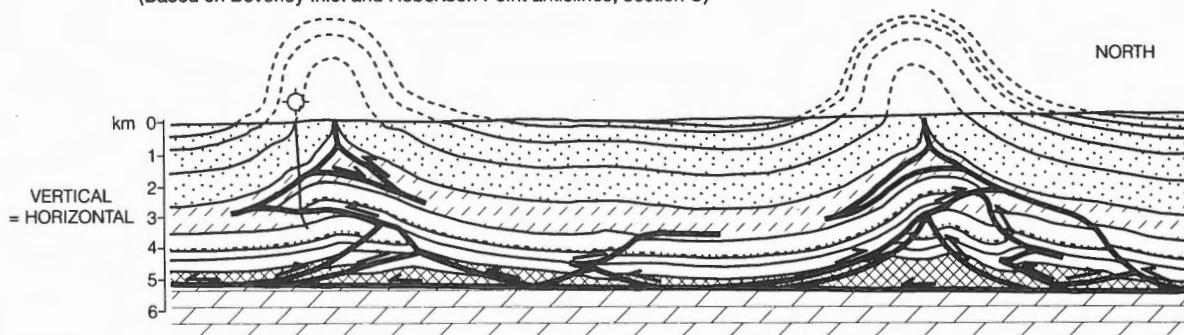
Folds in "old age"

In old age (Figs. 109, 114, 117, 122, 151F), all the salt and anhydrite has been exhausted from beneath the synclines. Dolostone interbeds in the lower ductile layer have been brecciated and boudinaged above the basal detachment as the competent roof of the lower

ductile layer in the syncline approaches the undeformed competent carbonate floor (Eleanor River Formation). Larger displacements are developed on individual thrusts within the medial rigid beam. Parasitic structures are everywhere common beneath both surface anticlines and synclines. The disharmony between surface folds and complex subsurface structure is caused by a completed linkage of upper detachment slip planes beneath synclines and between adjacent anticlines within the upper ductile layer. Buckling of the upper competent layer is replaced by brittle failure of surface anticlines and thrust faulting of siliciclastic formations starting within the lower Weatherall Formation. This is the tectonic response to

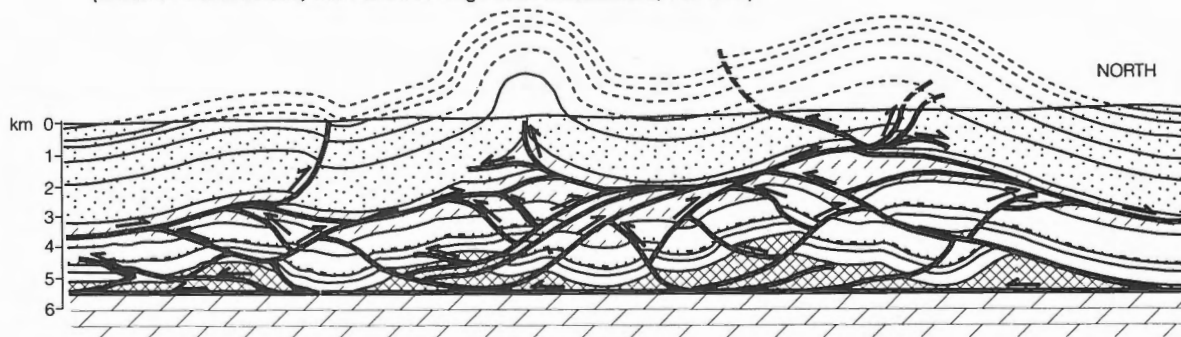
E. MATURE FOLDS

(Based on Beverley Inlet and Robertson Point anticlines, section C)



F. "OLD AGE" FOLDS

(Based on Consett Head, Rea Point and King Point East anticlines, Section A)



DEVONIAN



Upper rigid layer

MIDDLE DEVONIAN



Upper ductile layer

ORDOVICIAN TO DEVONIAN



Medial rigid beam

MIDDLE ORDOVICIAN



Lower ductile layer

CAMBRIAN, ORDOVICIAN



Lower rigid layer

Figure 151. (cont'd.)

severe hinge region problems created within and above the Cape De Bray Formation during the previous, mature stage of deformation.

The end of folding

The end of deformation must occur when available shear stresses are not large enough to cause continued movement of rock out of some synclines. This will happen when the evaporites have been exhausted from the synclines and the medial rigid beam has settled onto the undeformed floor, thus preventing slip on the basal detachment by excessive frictional resistance. Also significantly contributing to the eventual demise of salt-based tectonics are the paleogeographic limits of the Bay Fiord evaporitic facies; continued creation and expansion of the fold belt toward the craton is prevented by the foreland limit of the basal detachment where rock salt and anhydrite undergo a facies change to dolostone.

Discussion

Presentation of data in this chapter was partly undertaken with the expectation that it might provide constraints for a solution to the fundamental problem concerning large apparent differences in surface and subsurface bed-length shortening in the salt-based fold belt. The nature of the problem and the four possible solutions have been fully outlined early on in this chapter. Observations and comments bearing on the problem are found throughout the remainder of the chapter. The following discussion will therefore serve as a summary of the relative merits and deficiencies of each proposed solution.

The triangle zone model (Fig. 100) solves the regional surface and subsurface shortening discrepancy by allowing foreland (south)-directed slip on the sub-Bay Fiord detachment to be partly balanced by hinterland-directed slip on a through-going upper detachment somewhere within the Cape De Bray and lower Weatherall formations. This model, conceptually similar to McMechan's (1985) "low taper triangle zone" would require a taper angle and width of 1.6° and 173 to 184 km, respectively, if applied to Melville Island's salt-based fold belt. This solution may be mechanically feasible given the low basal shear strength for both Bay Fiord salt and Cape De Bray mudrock under suitably high pore-fluid pressures during thrusting. The triangle zone model requires a decoupling of the upper rigid succession from the underlying medial rigid beam during shortening. Considering hinterland structures, within which

differential slip across the upper detachment is greatest, the strata of the upper rigid package would have been folded, unfolded and then folded again repeatedly as the underthrust anticlines and synclines of the medial beam were carried along between bounding detachments.

General features of the fold belt, however, point to a long history of vertically linked slip surfaces through each anticline from the basal detachment through the Cape De Bray Formation and upward to surface. In other words, faulted surface anticlines are commonly situated vertically above subsurface thrusts and faulted anticlines of the medial rigid beam. Part of this vertical linkage is related to facies belts of Blue Fiord Formation and an isopach minima of the Hecla Bay sequence that can be attributed to differential compaction over the underlying carbonate bank. As shown in Figure 99, if actual shortening in the clastic wedge were equal to that in the underlying carbonates, then the region of greatest compaction (1800 m isopach of the Hecla Bay Sequence) would remain vertically above the carbonate bank on both palinspastically restored and present state isopach/facies maps. If the apparent shortening differential were correct and due to accumulated slip on a through-going Cape De Bray detachment, then, in plan view, the compaction-related minimum isopach would be partly displaced off the carbonate bank edge in the palinspastic restoration.

Nevertheless, evidence has been presented that supports the idea of horizontally linked slip surfaces between adjacent anticlines at the level of the Cape De Bray Formation, albeit, only locally (on Sections A and B; Fig. 114) and only during the last two stages of fold development (Fig. 151F). The weight of evidence therefore rules out the existence of a widespread negligible-taper triangle zone as a principal solution to the balancing problem.

The second model invokes equal shortening of the clastic wedge and all other formations above the basal detachment by appealing to unseen mesoscopic and microscopic deformation processes resulting in local or regional tectonic thickening of the clastic wedge prior to or during folding. This is the model applied during the construction of palinspastically restored Sections A through I. The magnitude of required thickening necessary to account for the shortening differential is generally small – 2 to 10 per cent between individual pin lines except on parts of Sections A and B where thickening must rise to 10 to 23 per cent. There is much additional merit in this solution in view of the fact that mesoscopic folds, minor thrusts, and some hinge axial thickening of mudrock interbeds, too small to be taken into account during cross-section construction, have

been identified on aerial photographs and at scattered surface localities in the lower part of the Weatherall Formation. In addition, there are several examples of more regional tectonic thickening of the lower Weatherall Formation on several seismic profiles and, also, two examples of local thickening of the Hecla Bay Formation. A drawback to this solution is that constancy of bed thickness is the general rule in the Devonian clastic wedge. Outcrop- and hand-specimen-scale contractional structures, such as minor thrusts, slip-plane striations, and higher-order folds are unknown, even in vertically dipping strata and in the hinge region of anticlines. Primary sedimentary structures and fine bedding-parallel features such as trace fossils, rip-up clasts, scours, and parallel and ripple crosslaminae are pristinely preserved and ubiquitous in all exposures.

The third model accounts for differences in shortening by geological processes acting on the Devonian clastic wedge that involve volume loss such as tectonic compaction, intraformational fluid loss, and dissolution of silica and redeposition as overgrowths and silica cement. Syntectonic volume loss and resulting cementation of the clastic wedge may explain initial delays in the onset of folding, later delays in rapid amplitude growth of anticlines, and brittle failure of the clastic wedge only during the last stages (Fig. 151). Transfer of fluids during volume loss could also contribute to late rise of pore fluid pressures in the Cape De Bray Formation, thus contributing to the delayed growth of anticlinal mudrock welts. However, there is no significant surface evidence of volume loss in the form of cleavage, vein fill or regional strain variation. Nevertheless, this is the most likely solution in view of the fact that Engelder (1979) has found evidence from strained crinoid ossicles for more than 15 per cent layer-parallel shortening in the Devonian clastic wedge of the salt-based fold belt of the Appalachian Plateau. In this respect, several samples of fossiliferous sandstone from the Weatherall Formation do contain modestly strained crinoid ossicles. Indicated volume losses due to bedding-parallel shortening in these samples are estimated to be about 5 per cent. However, the direction of this type of shortening and the true extent and magnitude of strain in the fold belt remain to be established. Convincing evidence from Melville Island's salt-based fold belt must also establish not only adequate layer-parallel shortening in the clastic wedge, but also quantitatively more shortening of this kind in the wedge than might be proven to exist in the medial rigid beam.

The final model requires overlap in time of clastic wedge sedimentation and some folding. Direct evidence of such processes, none of which have been

documented, could include local variation in attitude and implied direction of sediment transport of clinoforms in Cape De Bray Formation, radial dispersion of younger siliciclastic sediment into synclines, thinning and erosion of units over anticlines, anticline-related unconformities that pass into conformable surfaces in synclines, and symmetrical grading of grain size about fold hinges. By the same token, such features could be quite subtle and the evidence may be either difficult to collect because of rarity of high-quality bedrock exposure or impossible to collect because of the present deep level of erosion over most anticlines. Nevertheless, there is some indirect evidence of folding during sedimentation. Thinning toward the northeast of Beverley Inlet and lower Parry Islands formations (Figs. 72, 74) is spatially associated with long-wavelength folding of the entire Cambrian through Devonian succession of Towson Point and Spencer Range anticlinoria. This regional-scale uplift is caused by contractional slip on faults that flatten into the sub-Bay Fiord detachment (as observed on Sections C, D and E). Accepting the fact that this deep-seated slip must be balanced by folding and thrusting farther south and above the base of the Bay Fiord Formation, then some thin-skinned deformation in Parry Islands Fold Belt may be coeval with deposition of Beverley Inlet and Parry Islands formations in the Frasnian and Famennian.

In conclusion, all four solutions to the regional shortening problem are supported by different aspects of the data, and at the same time, all have drawbacks in terms of identification of associated processes at the mesoscopic scale. The "life history" proposed, above, and in Figure 151 invokes volume redistribution together with some volume loss for the Devonian clastic wedge in the early stages of folding, and the development of a nascent triangle zone in the latest stages by linkage through synclines of an upper detachment plane of slip in the Cape De Bray Formation.

Implications of the fold belt history are potentially farther reaching. Fundamental rules for the relative dating of thrust belts, proposed by Bally et al. (1966), require that thrust faults rooted to a common detachment become progressively younger toward the foreland. Since these shallow detachment faults are themselves commonly observed to be folded in many thin-skinned thrust belts, a second rule was proposed by Bally and associates, that places progressively later slip on progressively deeper detachment surfaces. From these two rules there has arisen the concept of "in-sequence" thrusts (which obey the rules), and "out-of-sequence" thrusts, which are usually considered geological oddities. However, for Parry Islands Fold

Belt, the “out-of-sequence” structure is the rule rather than the exception. Deformation by ductile slip begins in the weakest unit, the lower Bay Fiord Formation. Brittle failure ensues higher in the section, in the medial rigid beam, as a result of a developing anticlinal room problem. Folding and still later faulting of the near-surface clastic wedge occurs only after a period of probable layer-parallel shortening, volume loss and cementation. The failure of Bally et al.’s (1966) second rule for the relative dating of thrusts arises from the

fact that the rule does not take into account: 1) the effects of differential compaction on the style of deformation; 2) movements in and out of the plane of section (orogen-parallel strike-slip); 3) stratigraphic variations in ductility contrast that might influence the timing of the onset of ductile behaviour; 4) depth of burial, which might affect the magnitude of pore fluid pressures; and 5) differences in shear stress required to induce brittle failure and related temporal variation as a result of delayed cementation and compaction.

CHAPTER 7

SUPERIMPOSED DEFORMATION PHASES

Folding of the salt-based décollement system (D4)

Surface expression

Seismic reflection profiles on cross-sections A through E and G through I show deep-seated first-order folds. These have cross-folded second- and higher-order folds detached on the Bay Fiord Formation. Where the two fold sets have differing axial planes, the cross folds cause surface fold interference patterns. Ramsay (1967) has described dome, crescent, mushroom and zigzag fold patterns that result from differing axial plane inclinations and angles of obliquity (Fig. 152). On Melville Island, some isolated domes and basins are formed by a single early Ellesmerian phase of deformation (D3 of Table 5; refer to “Spatial relation to folds”, Chapter 6). More typically, however, late Ellesmerian (D4) axial planes produce a systematic alignment of sets of domes and basins. The locations of D4 fold alignments of Parry Islands Fold Belt (Fig. 153) are based on the mapped distribution of axial culminations, depressions and structural saddles on D3 fold axes (geology map, in pocket). D4 anticlinal hinges are interpreted as passing through domes on D3 anticlines and saddles on D3 synclines. Likewise, D4 synclinal hinges pass through basins on D3 folds and saddles on D3 anticlines. Beyond the region of D4 folds, there is a random pattern of domes, basins and saddles. The line marking the sub-salt deformation front is defined at the surface by the southeasternmost D4 syncline and by saucer-shaped depressions that preserve the youngest foredeep strata (compare Fig. 153 and geology map, in pocket).

Additional cross folds exist beyond the salt-based fold belt and include elliptical, faulted and irregular

periclinal domes and basins of Canrobert Hills (Type A interference structure of Ramsay, 1967; Fig. 152), the crescentic second-order syncline (Type B) structure of central Raglan Range (made up of Raglan Range Syncline, Green Creek Syncline and intervening Raglan Range Anticline), an unnamed crescentic anticline in northeastern Canrobert Hills, and at least one zigzag-shaped (Type C) anticline-syncline pair in the north-central Canrobert Hills. Suggested D4 cross-fold axes are illustrated on Figure 154.

The axial planes of D4 folds are approximately upright, oblique to D3 thin-skinned structures, and

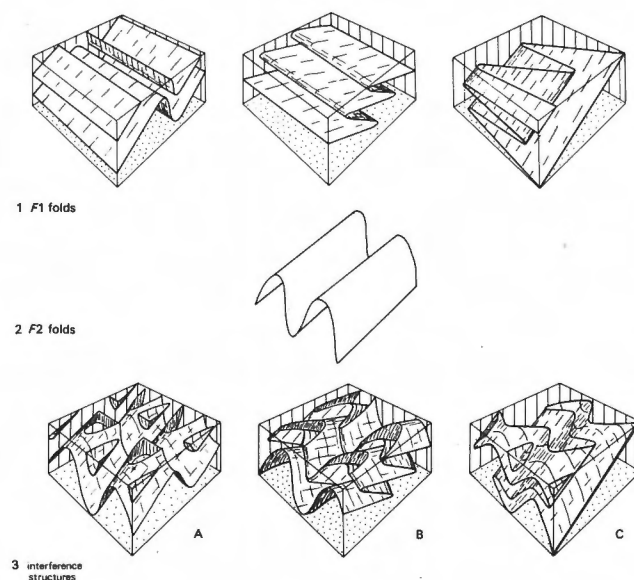


Figure 152. Interference patterns produced by cross-folding. **A.** Domes and basins. **B.** Crescent folds. **C.** Zig-zag folds. (Reproduced from Park, 1983, after Ramsay, 1967.)

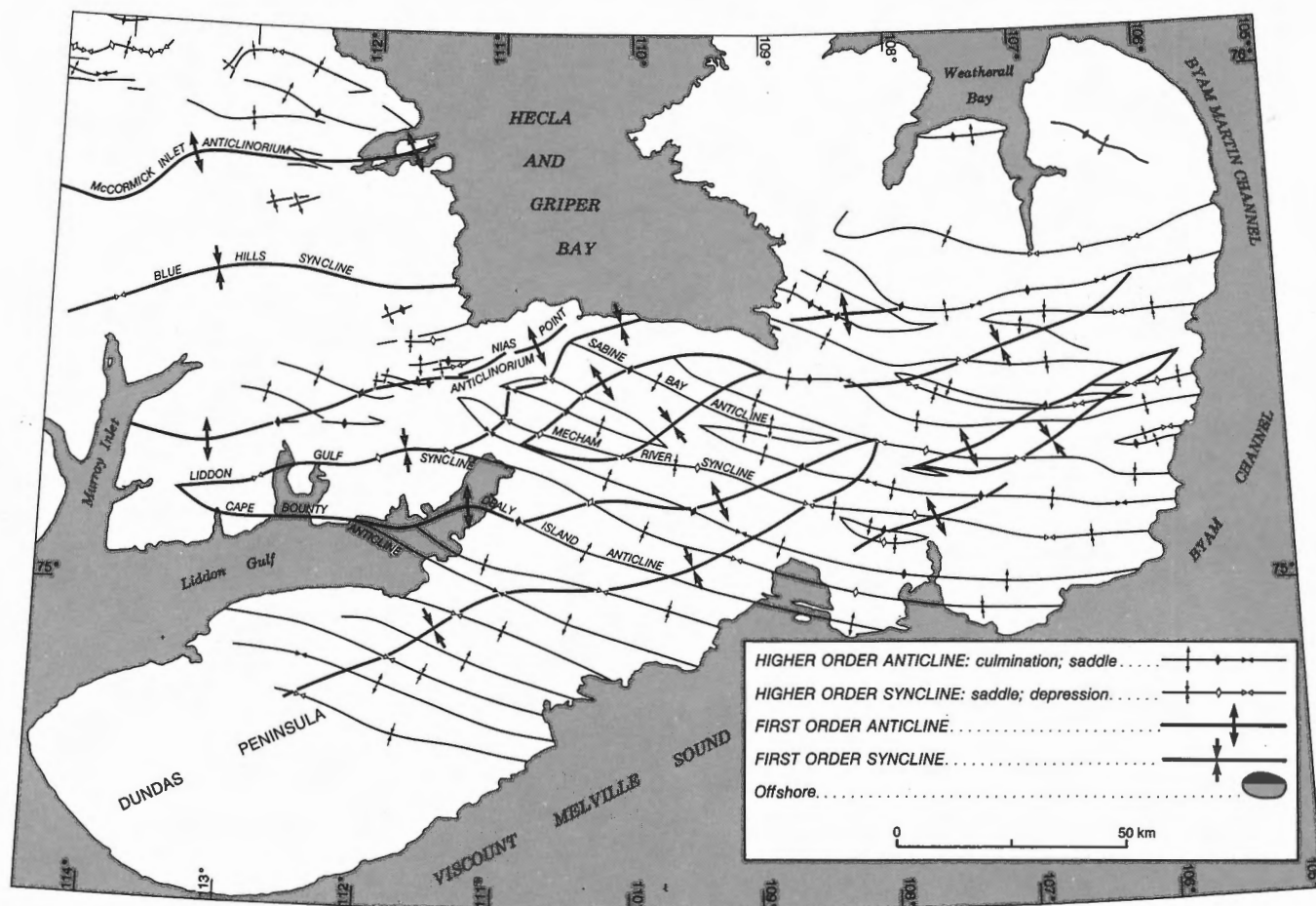


Figure 153. D3 and D4 fold trends of the Parry Islands fold belt, eastern and central Melville Island, as predicted from surface fold interference patterns.

trend N55°E through N70°E. These trends are subparallel to some mappable folds and faults of central Melville Island. Additional parallelism of D4 fold axes with Bouguer gravity anomalies, subsurface isopachs, limits of some depositional facies and deep-seated ancient faults (Fig. 155) implies that reactivation of a deep-seated anisotropy may have played an important part in D4 kinematics.

Structural style of deformed Eleanor River Formation

To test the validity of the interpreted surface fold interference patterns (Figs. 153, 154), a structure contour map in two-way time has been constructed on the seismic top of the Eleanor River Formation (Fig. 156). Data points have been selected in order to avoid residual velocity pull-up created by shallow thin-skinned (D3) structure. Not filtered out of the data is regional velocity pull-up created by the Cape

Phillips to Blue Fiord facies transition (up to 150 ms or 375 m at 5 km s⁻¹). Small errors in horizontal position of data points from unmigrated profiles occur in areas of dipping strata. Correction of these errors, mostly accomplished by contour smoothing, has tightened anticlines and broadened synclines.

Results indicate that the location and trend of the southeastern limit of D4 folding can be related to surface map patterns. Also shown are trends and locations of D4 Chevalier Bay Syncline, D4 Dealy Island Anticline and D4 Nias Point Anticlinorium. For Dealy Island Anticline on Section H (Fig. 123, Note 6), the crest of the D4 anticline is within only one or two kilometres of being vertically below the D3 anticlinal crest at surface. However, close inspection of Figures 153 and 156 indicates the true obliquity of the two fold trends. To emphasize the point, note that the crest of the D3 Beverley Inlet Anticline on Section H (Fig. 107, Note 4) lies within the axial trough of the deep-seated continuation of D4 Liddon Gulf Syncline.

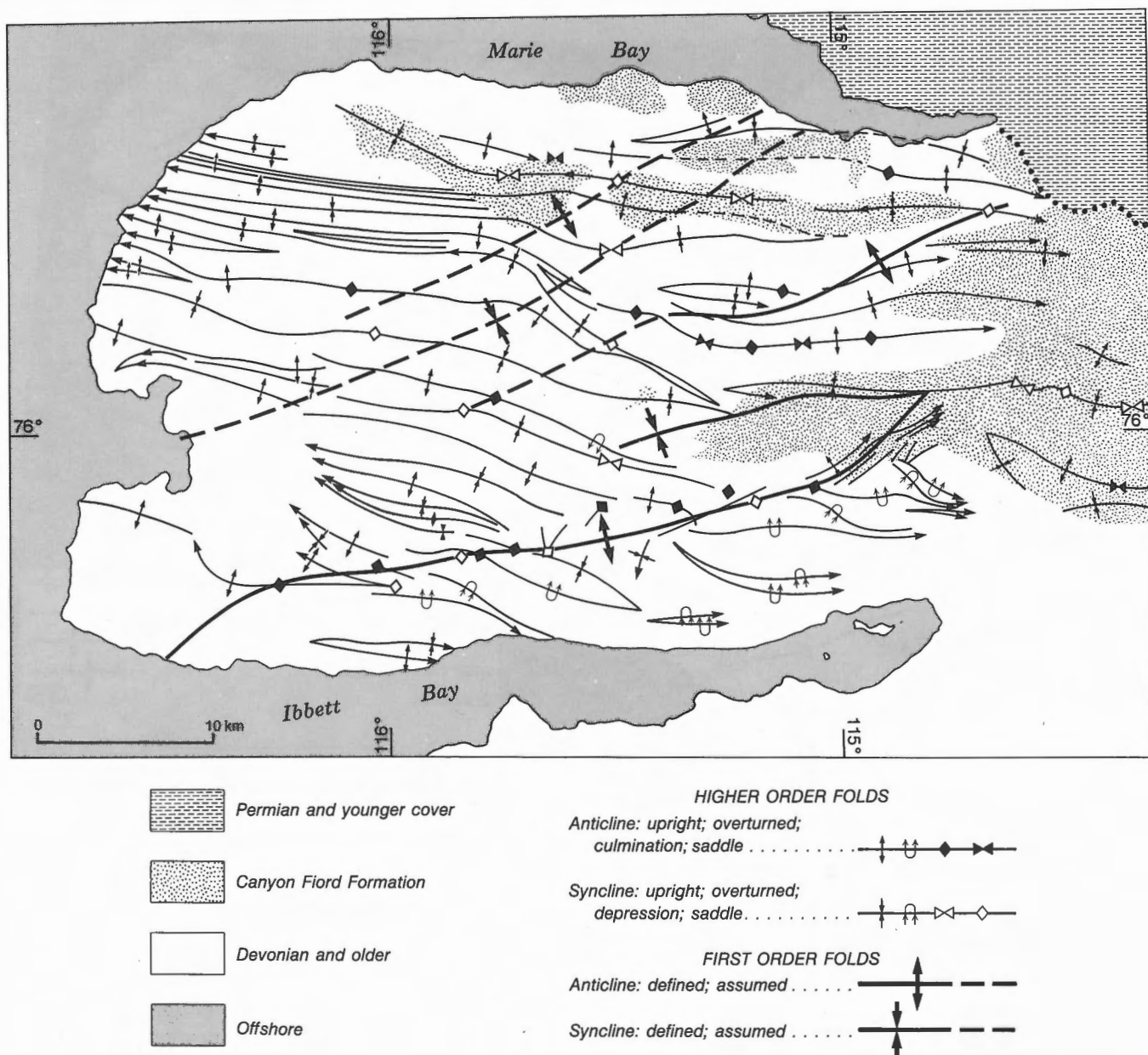


Figure 154. First- and second-order fold trends of the Canrobert Hills region, deduced from surface structural interference patterns.

For Sabine Bay Anticline, the D4 structure is oblique to D3 folds but is east-trending. The fold trends are oblique to each other, and on Section G, the culmination point of the D4 anticline is 10 km north of the point of closure of the D3 anticline at the surface (Fig. 109, Note 7). In the case of Spencer Range Anticlinorium, most D4 structure is hidden by unconformable cover (Fig. 129). The culmination is at or close to the surface near Tingmisut Inlier. Burnett Point Syncline in the west is heavily faulted at the Eleanor River level but is coaxial with the surface D3 syncline east of Weatherall Bay (Fig. 137, Note 2).

Towson Point Anticlinorium has also been coaxially refolded. The deep-seated sub-salt anticlinal hinge is 22 km northeast of the surface culmination.

Subsurface time-structure mapping also permits the recognition of plunge variation on fold axes at the Eleanor River level. The indicated pattern of sub-latitudinal periclinal folds and reverse oblique faults that strike N50–90°E is typical of a structural style developed in a zone of sinistral transpressive deformation. In this system, σ_1 is horizontal and southerly directed; σ_2 is vertical.

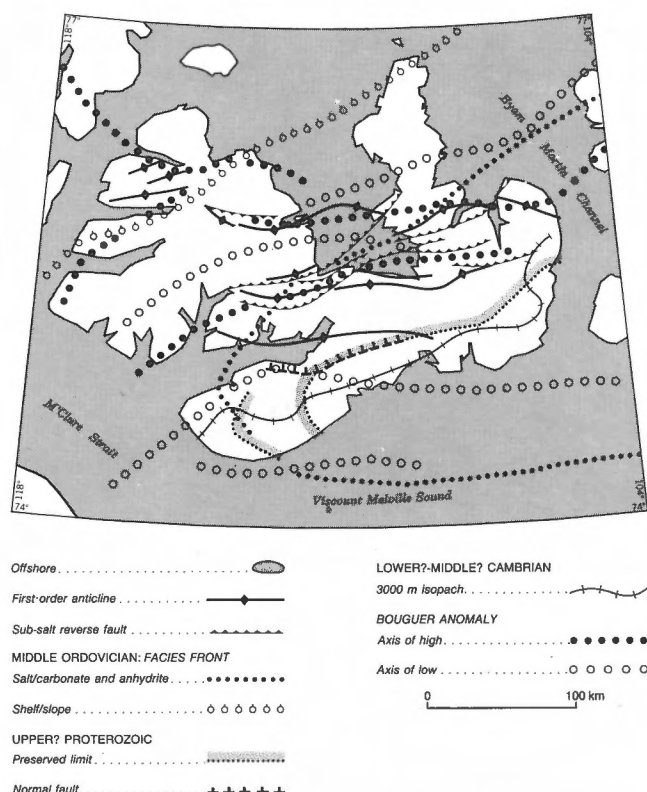


Figure 155. First-order fold axes of the Melville Island region and the trend of selected depositional isopachs, facies belts, low-frequency Bouguer anomalies, and deep-seated D1, D2, and D4 faults.

Kinematic case histories

The fold trend of Dealy Island Anticline, defined at the level of the Eleanor River Formation, lies structurally above an ancient north-dipping normal fault (compare Figs. 18, 155 and 156). A three phase kinematic history is proposed (Fig. 158). North-south extension, during Precambrian(?) phase D1 and mid-Cambrian D2 produced listric faults, block rotation of basement (unit sAP), and accumulation of possible syntectonic rock units. During the subsequent early Ellesmerian (D3) phase, southwest-directed compressive slip and detachment on the lower Bay Fiord Formation produced the thin-skinned structures of Parry Islands Fold Belt. In the late Ellesmerian (D4) phase of deformation, the ancient extension fault was reactivated with a reverse sense of slip. The result is a hangingwall anticline that involves the entire Cambrian through Devonian succession and also obliquely refolds the thin-skinned early Ellesmerian D3 structures. Although a late Ellesmerian age (latest Devonian through Early Carboniferous) is suggested for the deep-seated deformation of Dealy Island Anticline,

possible ages could be latest Devonian through pre-Aptian Early Cretaceous.

Sabine Bay Anticline (Figs. 109, 156) may be another example of a D4 inversion feature perched above Proterozoic (D1) structure. Seismic profiles (Section G) show that the Cambrian(?) and younger section is involved in the D4 refolding phase. However, the deep structural controls have not been imaged.

In the case of Apollo Anticline, the dominant structure is a fault-bend pericline created above a thrust ramp (Section I). The ramp segment links a mid(?)—Cambrian level of detachment, dominant within Canrobert Hills Fold Belt, to the sub-Bay Fiord décollement of the salt-based fold belt. The slip carried on the ramp is equivalent to all thin-skinned shortening over Nias Point Anticlinorium and some additional shortening farther south.

Nias Point Anticlinorium and Spencer Range Anticlinorium are two examples of D4 fault-bend periclines developed above deep-seated, south-directed D4 thrusts (Figs. 129, 157, 163). For both folds, the underlying thrusts reach upward to the sub-Bay Fiord detachment. Timing of the thick-skinned folding appears to have overlapped the thin-skinned D3 phase. The D4 periclines have displaced, tilted and obliquely refolded strata above the Eleanor River Formation. However, some of the slip that helped create the periclines has also been carried southward on the sub-evaporite detachment and is balanced by thin-skinned D3 deformation farther south. Also indicated within both periclines is a subsequent phase of extension which for Spencer Range Anticlinorium is known to have occurred in the mid-Carboniferous during (D5) syntectonic accumulation of the Canyon Fiord Formation.

The axis of Blue Hills Syncline lies above deep-seated D2 extension faults that display growth during accumulation of seismic unit sC4 (Fig. 30). The north limb of the syncline lies in the hangingwall of a thrust that emerges on seismic profiles out of the growth-faulted region and flattens upsection into a detachment near the upper contact of sC4. McCormick Inlet Anticlinorium is a fault-bend fold above the convex ramp segment of this deep-seated thrust. Since the deep-seated slip is carried southward into Apollo Anticline and beyond that is dissipated in thin-skinned shortening above the base of salt detachment, McCormick Inlet Anticlinorium must have been created during foreland D3 of Parry Islands Fold Belt. However, some second-order folds such as Green Creek Syncline, Raglan Range Anticline and Raglan

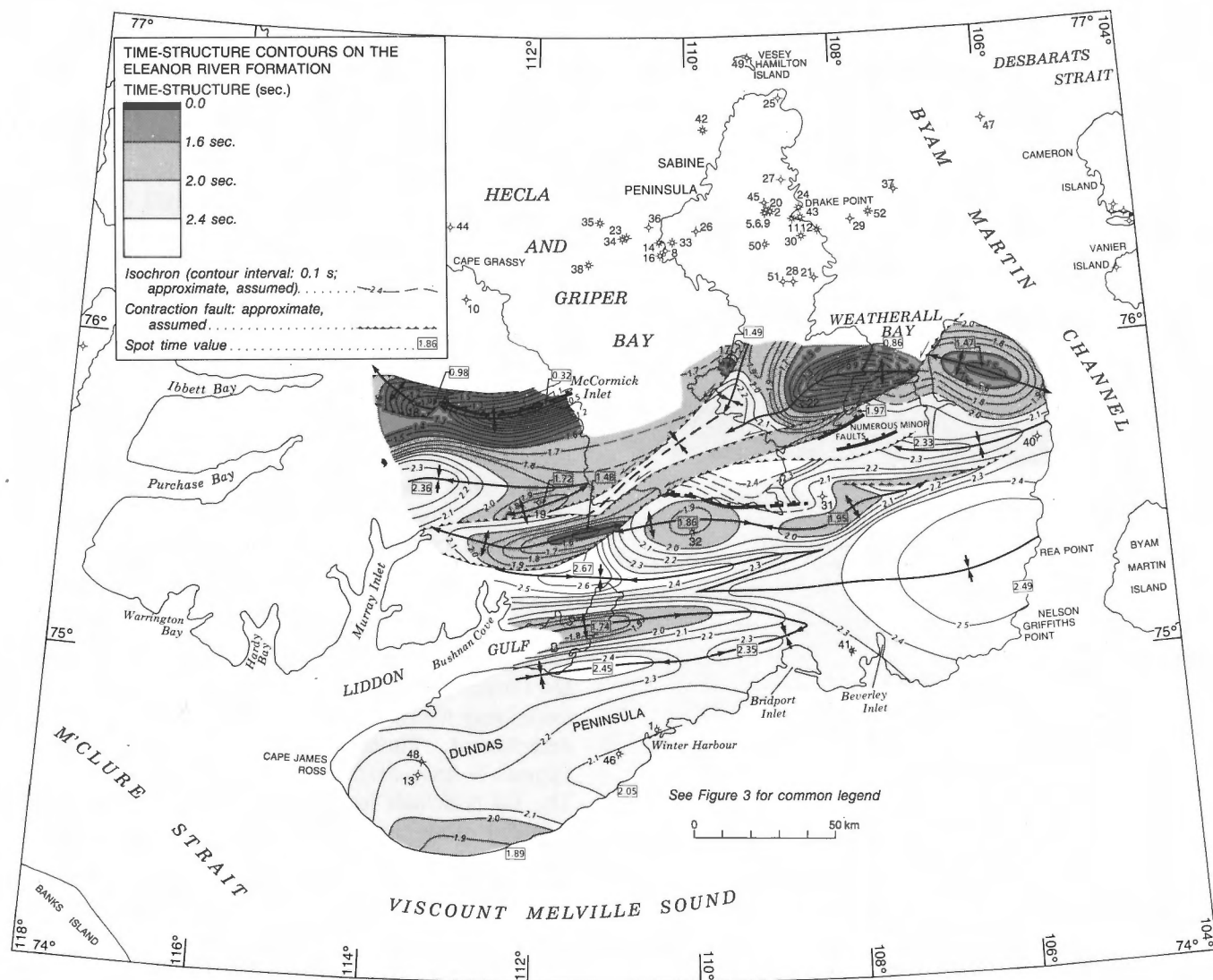


Figure 156. Structure contour map (in two-way travel time) on the seismic stratigraphic top of the Eleanor River Formation, Parry Islands fold belt, and adjacent portions of the Canrobert Hills fold belt, Melville Island.

Range Syncline, which are presumed to be detached on the mid(?)–Cambrian level, have also been refolded about McCormick Inlet Anticlinorium. Therefore, the Raglan Range folds also predate foreland D3 of the salt-based fold belt. The subsequent kinematic history of McCormick Inlet Anticlinorium is considered in a later part of this chapter.

The Kitson River Inlier (Fig. 33) is the exposed portion of a southwest-plunging D4 fold hinge that comprises over 2000 m of Ordovician through Silurian shelf carbonates and up to 1000 m of Devonian basin-plain and basin-fill mudrocks. The fold hinge is faulted on the locally oversteepened southeastern limb against the refolded (D3) Green Creek Syncline to the southeast (Kitson River Fault) and also faulted against the Canyon Fiord Formation of Kitson Depression to

the north. Other curvilinear map-scale and minor faults exposed on the west-facing limb of the inlier hinge bear strike-slip striae, and some are continuous with west-striking (D5 and/or D6) faults situated west of the Kitson River, which also offset the Canyon Fiord Formation. The largest structure in the area is the Kitson River Fault. The surface trace is mappable (in spite of alluvium cover) over a distance of 6 km, contrasting Middle Ordovician through Lower Devonian strata on the upthrown west side, and Middle and Upper Devonian rocks on the east side. Stratigraphic throw decreases progressively from 6 km in the north to less than 1 km where the fault emerges into the Cape De Bray Formation. Southeast-facing asymmetry of the locally overturned anticline in the upthrown block together with similar vergence of the overturned syncline in the downthrown block implies

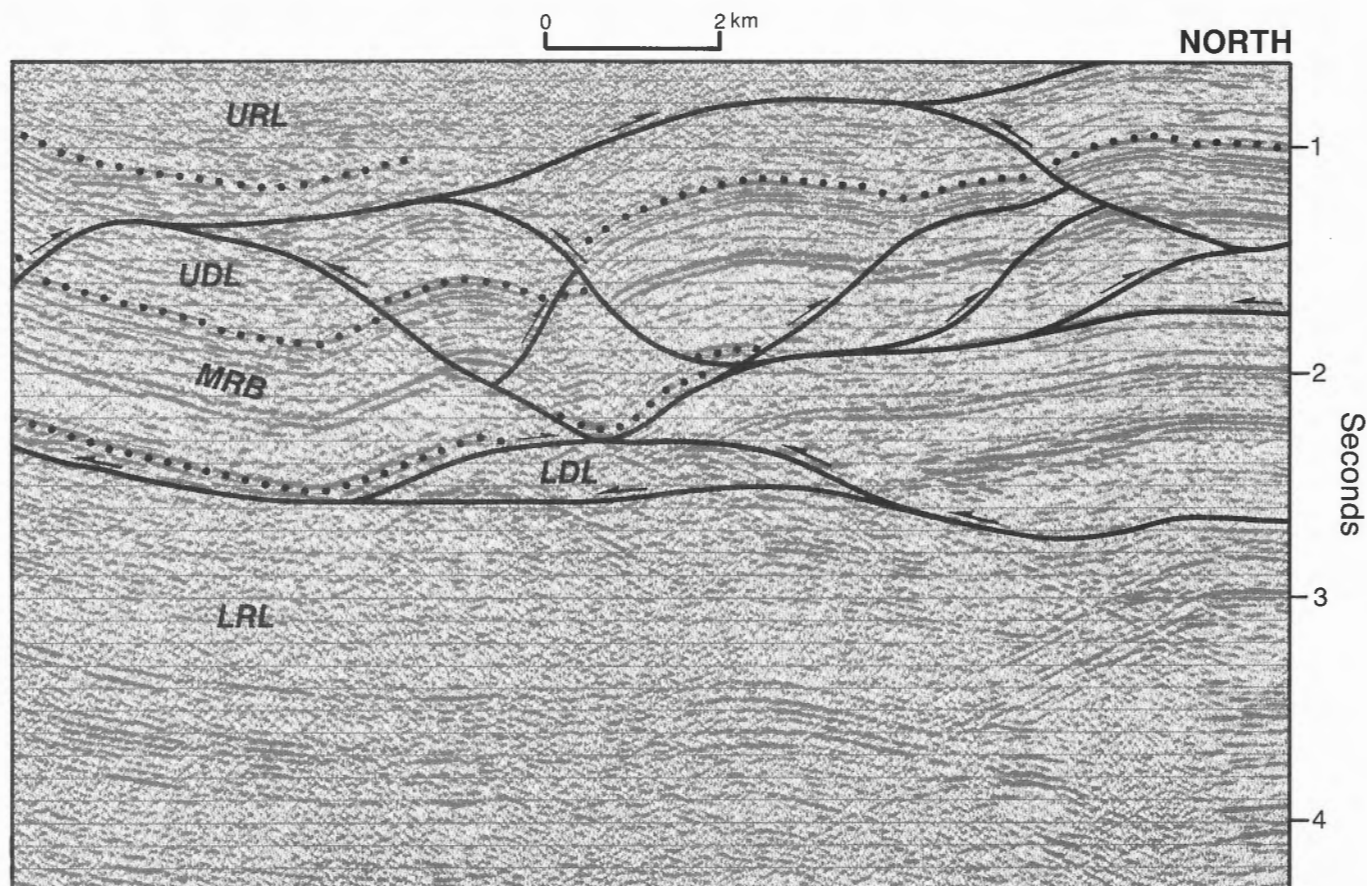


Figure 157. Nias Point Anticlinorium and the north-facing limb of D4 Dealy Island Anticline, on a part of seismic profile P1654, Section I. Component formations of each layer are listed in Figure 101. LRL, lower rigid layer; LDL, lower ductile layer; MRB, medial rigid beam; UDL, upper ductile layer; URL, upper rigid layer.

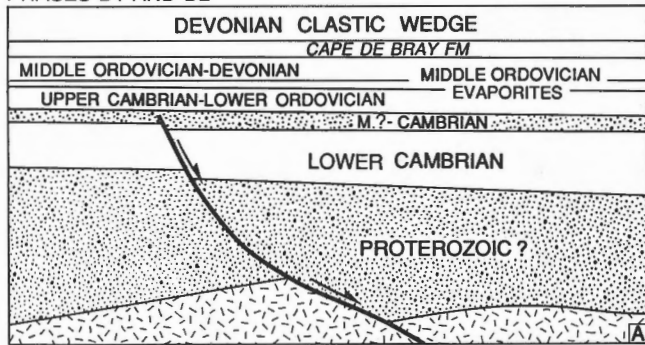
that the Kitson River Fault is northwest-dipping and contractional. This conclusion is supported by minor fault measurements and contained slip lineations that have been collected in the upthrown block and within 10 m of the covered fault trace (Fig. 159A).

Purchase Bay Homocline is a southerly tilted panel of Middle and Upper Devonian strata exposed over a strike length of about 45 km from east of the head of Ibbett Bay to Cape Terrace on the west coast of the island. Maximum structural relief on the homocline is about 7000 m. This includes the structural relief attributed to thin-skinned folding and detachment at the mid-Cambrian level (estimated 2400 m) and the additional structural relief attributed to regional-scale uplift of the entire thin-skinned deformed belt exposed north of Ibbett Bay. The regional uplift is the difference in exposure level between synclines in the uplifted area, which at the highest levels have preserved the lower 200 m of the Cape De Bray Formation, and synclines south of the homocline, which have preserved all of the Cape De Bray, Weatherall, and Hecla Bay formations and up to 750 m of the Beverley Inlet

Formation. Indicated regional uplift of the mid-Cambrian D3 décollement system is approximately 4600 m. The main phase of uplift of the mid-Cambrian décollement system is broadly coeval with phase D4 structures of the salt-based fold belt.

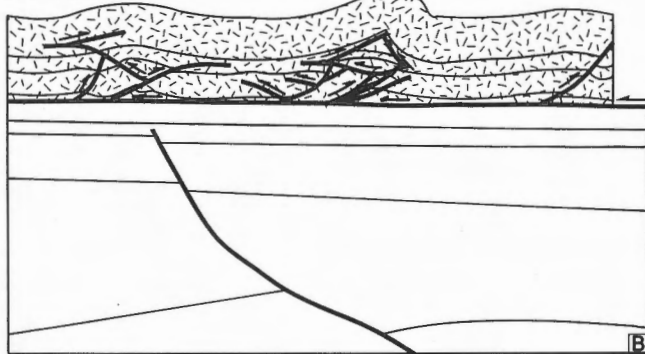
The kinematic model for the Purchase Bay Homocline and Canrobert Hills region during D3 and D4 phases of deformation is illustrated in Figure 160. Decoupling on the mid(?)–Cambrian décollement, during D3, was accompanied by southerly transport of nappe-like folds that included basinal and basin slope facies lower Paleozoic strata. The northeast-trending shelf-to-basin transition may have acted as a buttress defining the southeastern limit of most D3 shortening. The Kitson River Fault and its subsurface continuation beneath Purchase Bay Homocline is considered the oblique lateral ramp linking the mid-Cambrian detachment to the upper detachment located variably in the upper Cape De Bray and lower Weatherall formations. Some tilt on Purchase Bay Homocline was created during D3 deformation by development of a triangle zone, in which south-directed slip on the mid-

PHASES D1 AND D2



PROTEROZOIC? includes both syntectonic and inter-tectonic seismic units (undivided).

PHASE D3



PHASE D4

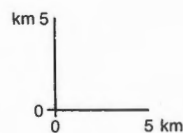
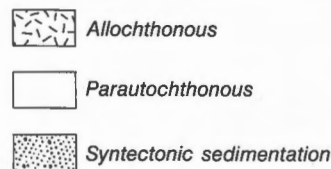
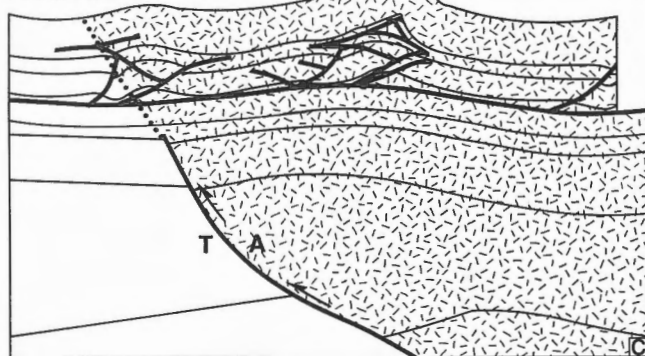


Figure 158. Kinematic history of Dealy Island Anticline (based on the structural style defined on Section H).

Cambrian décollement was balanced by north-directed slip on the oblique upper detachment. The uplift of the mid(?)–Cambrian décollement system is attributed to compressive reactivation of a series of unseen Middle(?) Cambrian (D2) growth faults similar to those imaged beneath Blue Hills Syncline (P1135 of

Section I; Fig. 30). The present geometry of Purchase Bay Homocline and the uplifted décollement system of the Canrobert Hills region has also been affected by Late Carboniferous D5 rifting, Early Permian D6 inversion, and renewed phases of uplift and extension (D7 and D8) in post-Paleozoic time.

Late Paleozoic rifting (D5)

General comments

Indirect evidence of rifting on the site of the ancestral Sverdrup Basin, beginning in the late Viséan and continuing down to the mid-Permian, has been provided by horst- and graben-influenced depositional facies patterns and related sediment dispersal directions (Beauchamp, et al., 1989a; Beauchamp, 1987; Davies and Nassichuk, 1991) and by the pattern of post-rifting thermal subsidence in Triassic and younger rocks (Stephenson et al., 1987). Direct evidence of extension-related growth faulting in the late Paleozoic has been documented by Meneley et al. (1975) from seismic profiles of the Sverdrup Rim, and by Fox (1985) from similar geophysical data of Cameron Island. Rifting in the subsurface of Sabine Peninsula, Melville Island has also been previously suggested by Davies and Nassichuk (1991).

Phase D5 rift-related structures discussed in this chapter are located on Figure 161. The dominant trend of the rift zone is approximately N60–70°E. East and east-southeast trends are also locally important. The regional plunge of the rift zone is toward the east-northeast in the direction of the evaporite diapir belt of northern Sabine Peninsula and offshore Vesey Hamilton Island. The mapped portion of the rift zone includes approximately 12 syntectonic depressions, of which three are exposed at surface and named. There are also eleven uplifts (two exposed and named) over each of which Carboniferous strata are either thin or absent beneath blanketing mid-Permian and younger cover. The terms “depression” and “uplift” are used to designate local sites of sediment accumulation and sediment dispersion, respectively. The upper Paleozoic depressions have generally been formed in extension. In cross-section these small basins are seen to be either simple half-grabens or composite rift-related structures associated with one or several listric faults and other conjugates.

The upper Paleozoic uplifts represent the high side of block-rotated extensional depressions and therefore can be viewed as horst blocks or “half-horsts” paired with adjacent half-grabens. The tectonic history of the uplifts is as complicated as the depressions. In the case

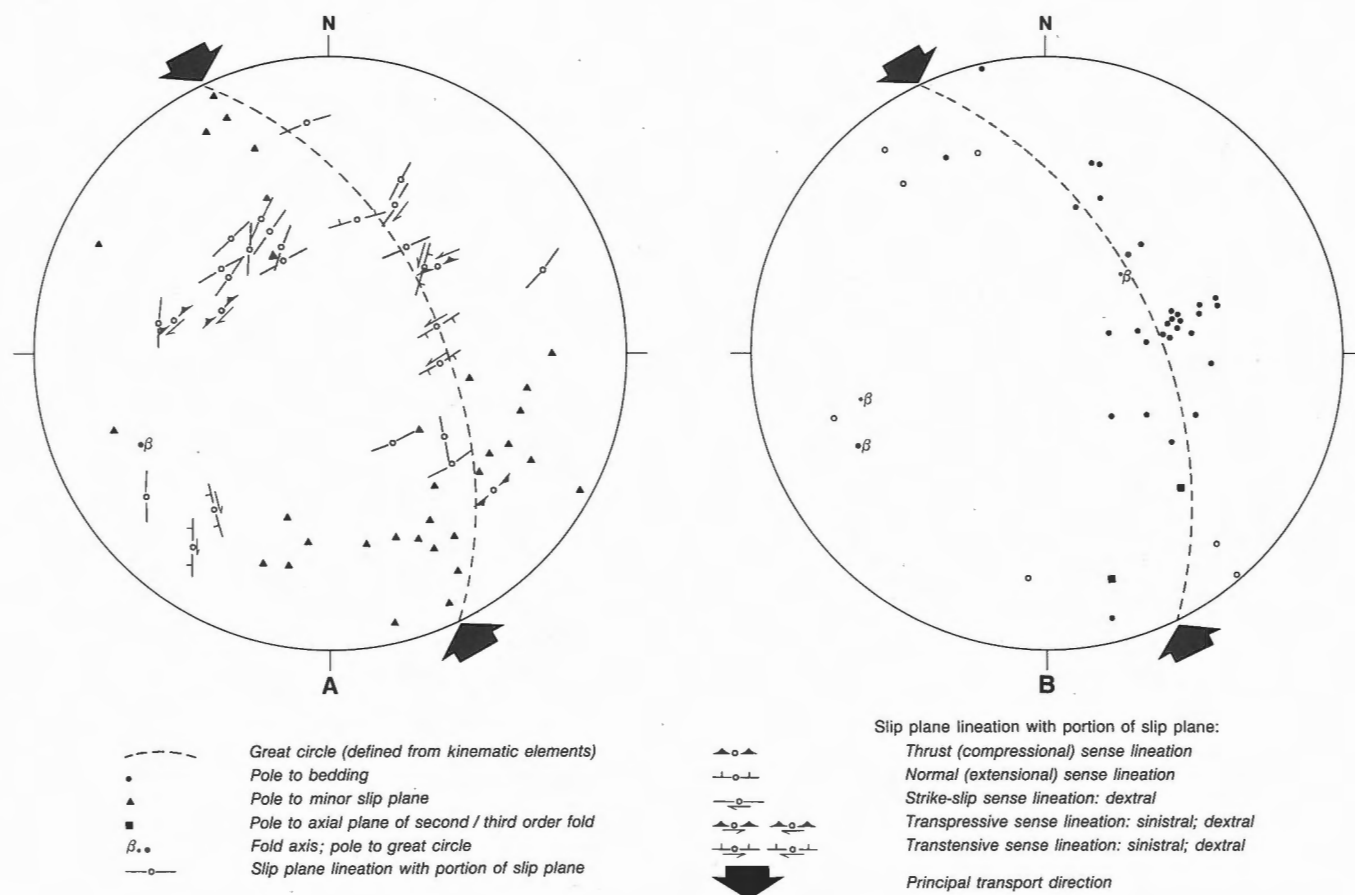


Figure 159. Lower hemisphere equal-area stereonet plot of kinematic data for and principal transport directions of the Kitson River Fault and inlier strata. **A.** Poles to minor slip planes, slip lineations, parts of associated fault planes, and implied direction of tectonic transport for the Kitson River Fault. The great circle girdle and large β -pole is defined by the great circle distribution of bedding plane poles. **B.** Major fold axes (β -poles), poles to bedding planes, poles to axial planes, and implied direction of tectonic transport for folded strata of the Kitson River Inlier.

of Raglan Range Uplift, the second-order folds exposed and mapped at the surface in Devonian and older rocks are related to D3 compressive deformation. Uplift may have begun during D4 and been renewed during the formation of D5 rift depressions to the north and south. However, the present depth of erosion is the sum of these first two uplift phases as well as at least three other possible phases during and since the Permian (D6–D8).

The D5 rifting phase of subsurface northern Sabine Peninsula predates seismic Hare Fiord Formation and is, therefore, probably coeval with accumulation of seismic unit sCGF (Section E) and of Otto Fiord evaporites as exposed in the diapirs (early Serpukhovian through Bashkirian; Nassichuk, 1975; Appendix 4). The main phase of D5 rifting within the region of seismically imaged half-grabens on Figure 161 probably spans the period of deposition of the Canyon Fiord Formation (Baskirian through

Sakmarian; see Chapter 4 and Appendix 4). This is consistent with the timing implied by seismically imaged growth faults on Section E. Late Carboniferous growth (to 1200 m) appears likely across at least four extension faults situated south of Marryatt K-71 of central Sabine Peninsula. Additional growth faulting is indicated in the Lower Permian interval. More specifically, growth is demonstrated on Section E across at least two faults within the Lower Permian (Asselian–Artinskian) Belcher Channel, Raanes and Great Bear Cape formations beneath and south of the K-71 well; across four faults within the Lower Permian (Kungurian–Roadian) of the Sabine Bay and correlative lower Van Hauen formations; and across at least three faults within the Degerbøls and Trolld Fiord formations (Roadian and Wordian). The magnitude of syndepositional slip across individual faults ranges from less than 50 m to about 400 m. The growth faults in and above the Sabine Bay Formation are also coeval with the D6 phase of rift inversion as discussed later in this chapter.

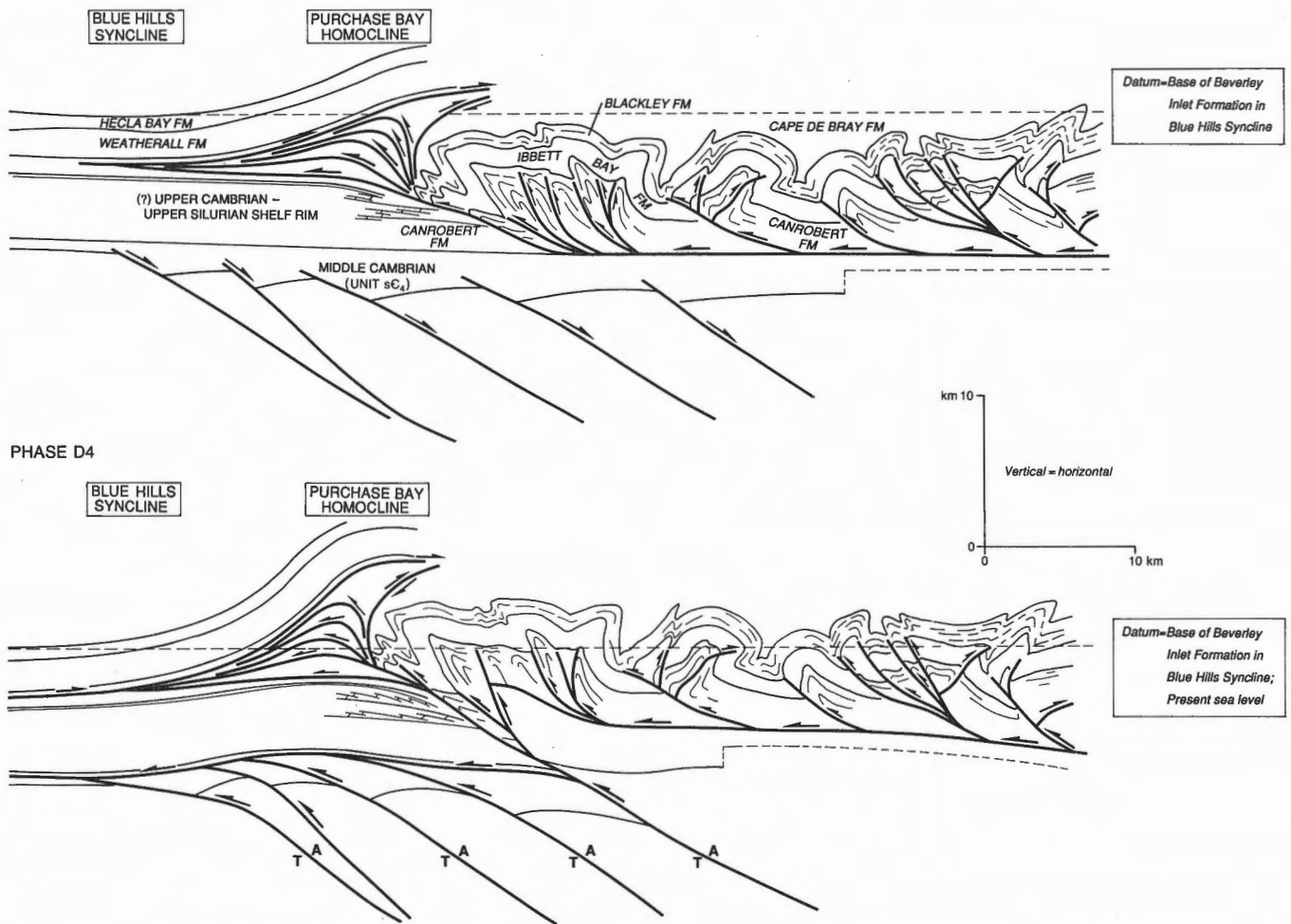


Figure 160. Kinematic model illustrating the development of the Purchase Bay Homocline during two phases of mid-Paleozoic deformation (D3 and D4).

Kinematic case histories

An oblique aerial view of Weatherall Depression and Spencer Range Uplift is shown on Figure 162. Topographic expression across the surface trace of the master listric fault in Spencer Range is due to differential erosion of resistant, footwall, Lower Devonian carbonates and recessive, hangingwall, rift-fill redbeds and conglomerates of the Canyon Fiord Formation. The dominant tilt of the rift fill, measured along two separate ground traverses of the depression, decreases upsection from a maximum of 30°N in the south, to less than 6° near the faulted northern edge of the depression. Tilt of the redbeds is attributed to block rotation on an underlying seismically imaged listric extension fault that flattens to the south (Fig. 163). The direction of rotation is toward S20°E as implied by poles to rift-fill bedding planes (Fig. 164). The seismic profile also shows that systematic variation

in rift-fill bedding attitudes is attributable to syn-tectonic sedimentation. The age of the divergent strata, therefore, dates the motion of the bounding listric fault. Rift-fill Canyon Fiord Formation in the Weatherall Depression is Moscovian through Asselian or early Sakmarian (Tozer and Thorsteinsson, 1964; see also Chapter 4 and Appendix 4).

Rifting has produced large lateral variations in redbed sediment thickness. Pre-Artinskian rift-fill in the central St. Arnaud Hills ranges up to 2200 m. Correlative strata on the upturned edge of Spencer Range Uplift are about 600 m thick. Maximum extensional displacement on Tingmisut Fault is about 2.7 km. Both the preserved rift-fill cover and uplift cover are progressively exposed to the surface toward the east. Windows into the sub-Carboniferous succession occur in northern Spencer Range and in the Tingmisut Inlier. The oldest Carboniferous rift-fill in

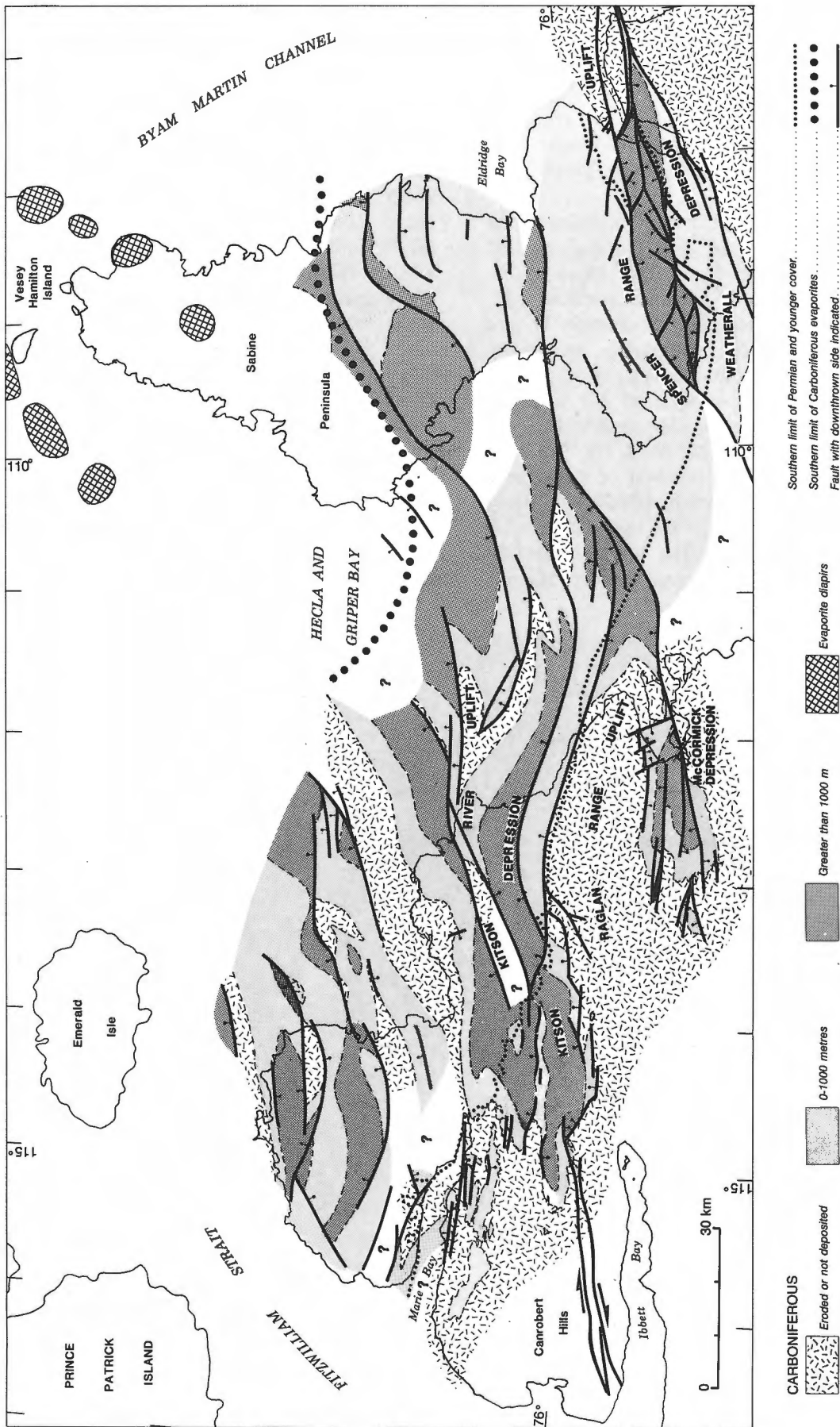


Figure 161. Late Paleozoic rift-related depressions and uplifts of northern Melville Island exposed at the surface and also mapped in the subsurface beneath the widespread Permian cover. Note the regional geological context of this rift-zone on Figure 180.

the keel of the half-graben has been exposed in eastern Spencer Range. Phase D8 tilt toward the west of the half-graben, and adjacent Spencer Range Uplift is also associated with anomalous steep-to-vertical and southwest- or south-dipping bedding attitudes (Fig. 164), minor folds and some superimposed fault plane motion as reviewed in a later part of this chapter.

A kinematic model for the D5 Carboniferous rifting phase of Weatherall Depression and related antecedent deformation is illustrated in Figure 165. Down-to-the-northwest D2 growth faults of mid-Cambrian age, imaged on seismic profile P2185 of Section D, are deemed to be part of the underlying anisotropy influencing all subsequent deformation phases (Fig. 165A). The general nature of D3 and D4 deformation has been treated in Chapter 6 and in part of the present chapter (Figs. 129, 165B, C). The local D4 structure is revealed after removal of subsequent D5 extension. This has been accomplished by restoring the sub-Carboniferous peneplain to its pre-rift horizontal state (Fig. 165C). The angular relation between the peneplain surface and the dip of sub-

unconformity strata has been preserved in the post-D4 pre-rift restoration. Deep-seated, north-dipping reverse faults arising out of the sub-Cambrian are sigmoid in profile and linked upsection to the sub-Middle Ordovician evaporite décollement. Compressive D4 slip on the footwall ramp has created both a large hangingwall anticline (Spencer Range Anticlinorium) and a regional southerly dip expressed at the surface in Upper Devonian and older strata on the foreland-facing limb. Included in this dipping panel is the Middle Ordovician evaporite layer, the underlying décollement, and older Ordovician and Cambrian strata below that.

The spatially associated combination of a highly ductile layer and regional dip of this layer provides a preferred surface for simple shear in extension, and an obvious level of detachment for the southerly flattening listric fault beneath Weatherall Depression. Listric extensional slip, during D5, caused block rotation of: 1) the unconformity (from horizontal to 30°N); 2) hangingwall conjugates (from 60°–90°N); and 3) divergent syntectonic fill (variably 0–30°N).



Figure 162. Oblique aerial view of the Weatherall Depression in Spencer Range. DBF, Blue Fiord Formation; DHB, Hecla Bay Formation; DBI, Beverley Inlet Formation; CPC, Canyon Fiord Formation. ISPG photo. 2899-6.

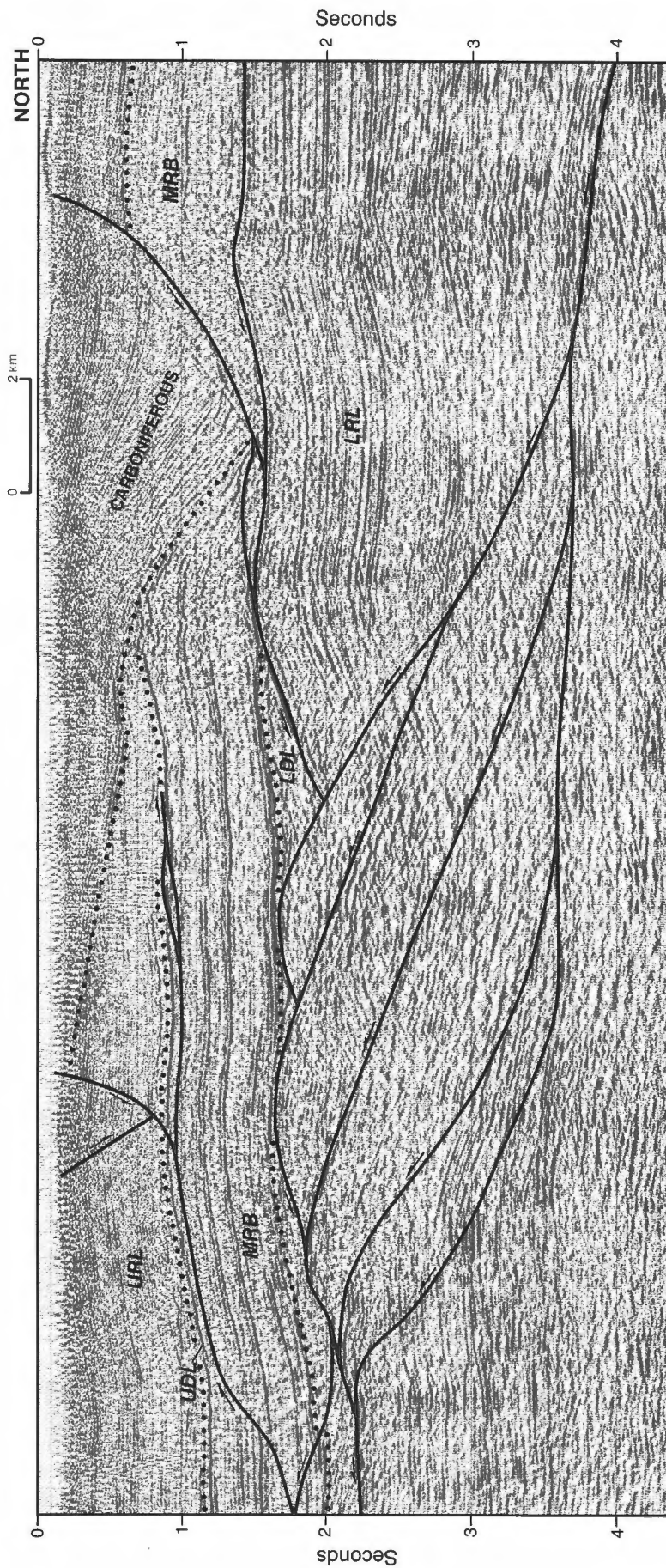


Figure 163. Weatherall Depression and Spencer Range Uplift, on a part of seismic profile P1921, Section E. Component formations of each layer are listed in Figure 101. LRL, lower rigid layer; LDL, lower ductile layer; MRB, medial rigid beam; UDL, upper ductile layer; URL, upper rigid layer. The beam also includes the Blue Fiord Formation. The unit labelled "Carboniferous" includes mostly Canyon Fiord Formation and a veneer of several Permian formations exposed at the surface.

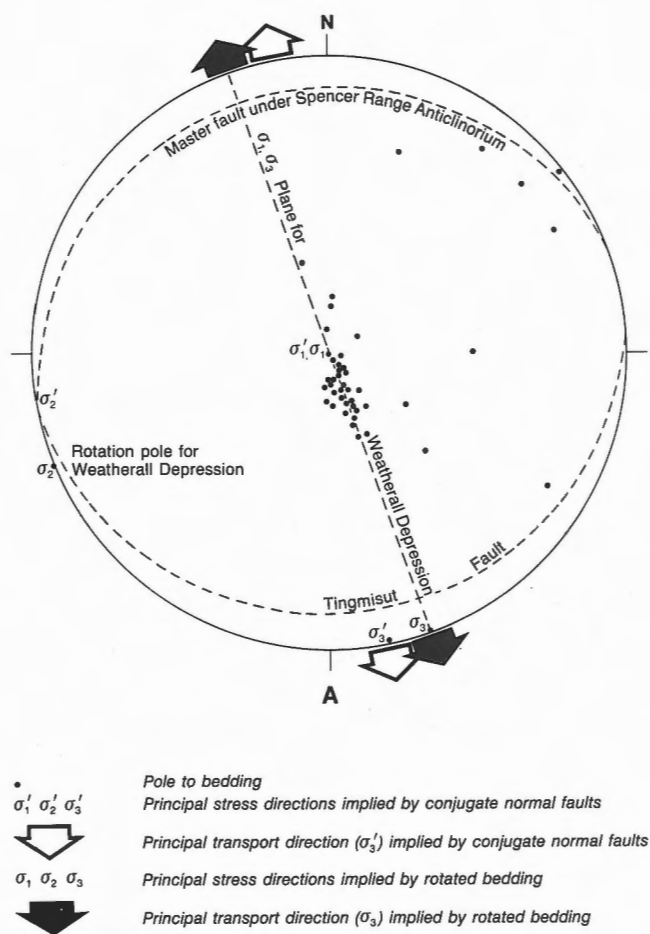


Figure 164. Lower hemisphere equal-area stereonet plot of poles to bedding planes and regional-scale normal faults, principal stress directions, and implied directions of tectonic transport in extension for the upper Paleozoic rocks of southern Sabine Peninsula. The scatter of bedding poles that plunge at steeper angles to the east and northeast are attributed to later sinistral rotation and compressive deformation, probably during the Eurekan Orogeny (phase D8).

This extension also resulted in collapse of the forelimb of the D4 hangingwall anticline. This was probably accomplished by a matching of south-directed extensional slip on the sub-salt detachment with an equal amount of north-directed extensional slip distributed across the deep-seated D5 footwall ramp and associated splays. In other words, there is a wedge-shaped body of rock that, during formation of Weatherall Depression, moved to the north on a through-going sole fault that must have extended beneath the other rift-related structures of the ancestral Sverdrup Basin (Fig. 165D). The direction of extensional transport (σ_3) of the wedge is assumed to

have been subhorizontal, parallel to the bisectrix of the cratonward- and basinward-dipping conjugate shear planes, and toward N10–20°W (Fig. 164).

West of Hecla and Griper Bay, redbeds of McCormick Depression are preserved in a single, large outlier and in at least eight other small, peripheral outliers covering an area of approximately 350 km². Seismic profiles indicate up to 1100 m of preserved Carboniferous section near the centre of the principal outlier. Tozer and Thorsteinsson (1964) were first to suggest that Carboniferous strata preserved south of Raglan Range may have been “deposited within an intermontane basin, with only intermittent and perhaps indirect marine connection with the open sea of the Sverdrup Basin”. This interpretation is now supported with additional observations on regional variations in stratigraphy and coarse-fraction sedimentology. Yellow weathering marine sandstones and crinoidal limestones are represented in a locally mappable marker above basal conglomerate to about 200 m above the base of section along the southern half of the principal inlier west of McCormick Inlet. Northward these strata grade to red and green nonmarine sandstone and tidal-flat-associated mudrock. There is a parallel northward increase in grain size in the upper part of the formation. Fine grained, red weathering sandstones and mudrock are common in southern sections. However, Tozer and Thorsteinsson (1964) have described significant conglomerate intervals in the northern half of the principal inlier. Components of the conglomerate include variably rounded to sub-angular clasts of sandstone ranging to cobble grade. These clasts resemble the Devonian sandstones still exposed to the north in Raglan Range Uplift, the obvious proximal source area for the coarser detrital fraction preserved in McCormick Depression.

The structural features of the depression include sublatitudinal faults, two intra-depressional anticlines, an intervening dish-shaped syncline in the south, and a sublatitudinal half-graben in the north. Minor fault planes in the Canyon Fiord Formation invariably bear strike-slip striae. These small features, together with the post-redded folds and the demonstrable motion on some faults, are tentatively related to the mid-Permian D6 uplift and compressive inversion of the depression. The northern half-graben is probably a relict of the D5 rifting phase that created the depocentre. The proposed kinematic model for McCormick Inlet Depression and Raglan Range Uplift is illustrated in Figure 166. D3 folds of Raglan Range, detached in the mid-Cambrian, have been refolded during D4 by compressive slip on deep-seated reverse faults arising out of the region of D2 growth faulting beneath and north of Blue Hills Syncline (Figs. 166A–C).

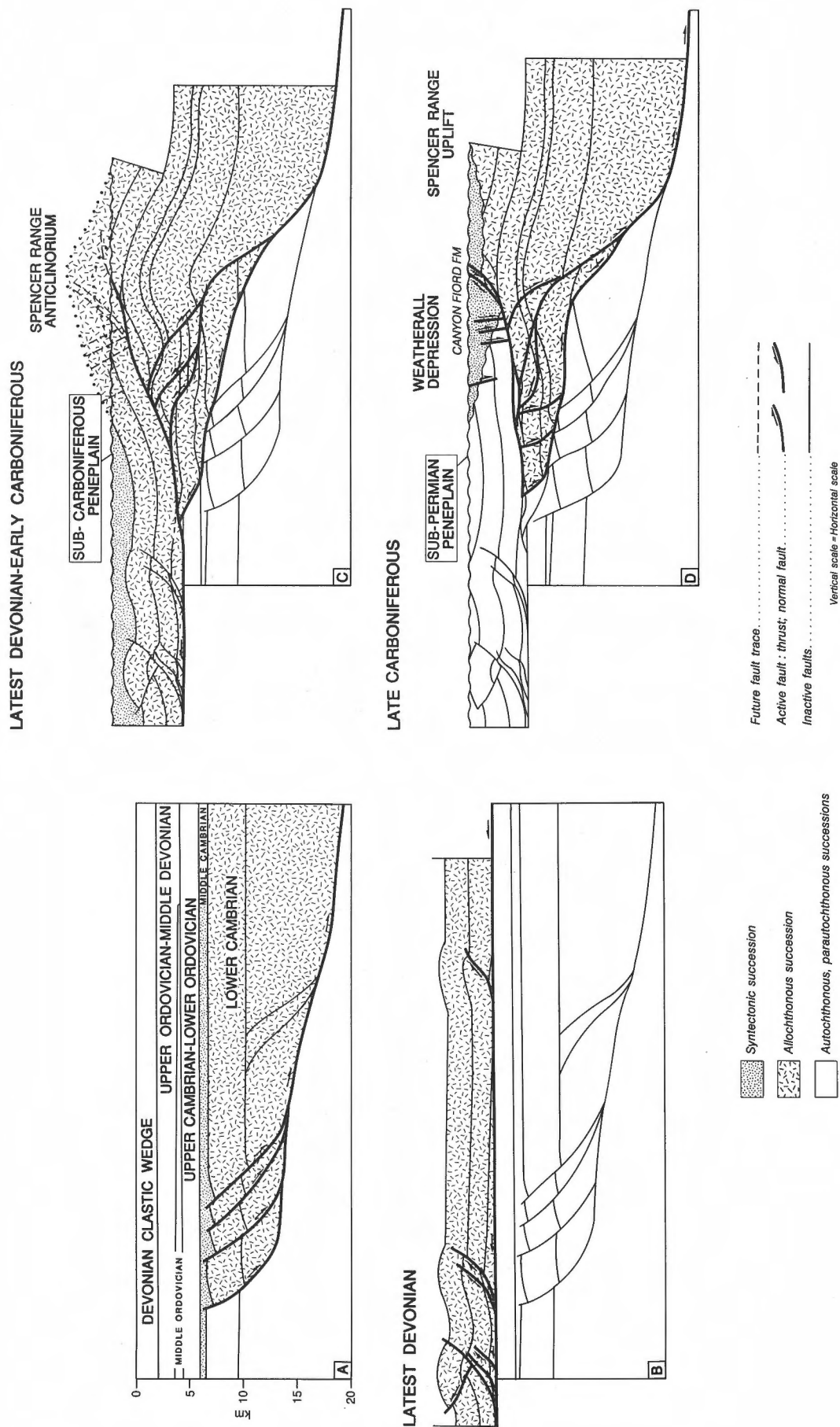


Figure 165. Four-phase kinematic model for the Paleozoic evolution of the Spencer Range Anticlinorium, Spencer Range Uplift and Weatherall Depression.

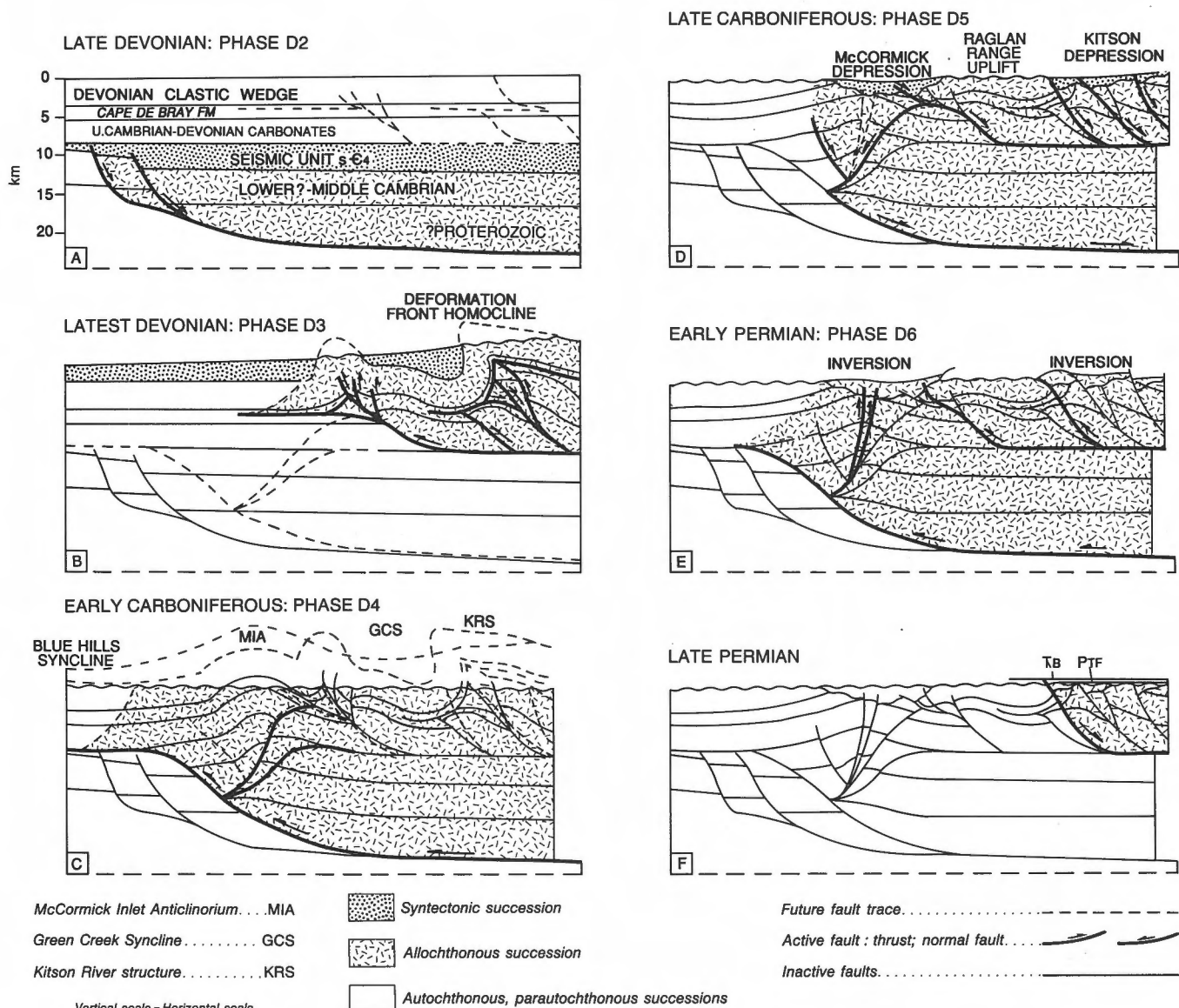


Figure 166. Polyphase Paleozoic kinematic history of McCormick Inlet Anticlinorium and the eastern Raglan Range area.

The restored dips of up to 68° in the Weatherall Formation on the north-dipping limb of McCormick Inlet Anticlinorium also define the maximum dip angle for pre-rift ductile strata in the welt. These previously tilted layers have served as planes of weakness for the propagation of a north-dipping extension fault during the phase D5 development of the half-graben. This is linked to the mid-Cambrian detachment via pre-existing footwall ramps suspected of existing beneath Raglan Range (Fig. 166D). Later events affecting this area and other D5 half-graben sub-basins farther north beneath younger strata are considered in the next part of this chapter.

The Blue Hills structure includes the plateau uplift of southwestern Melville Island lying between Hardy Bay in the south and Blue Hills Fault in the north. Additional tectonic elements include Mt. Joy and Hardy Bay faults, Murray Inlet Fault and the west-trending graben-like structure on its north side (Section J; geology map, in pocket). There are no seismic profiles for this region, and surface kinematic indicators have not been examined. Subsurface interpretation is based on clues from surface mapping and the presumed westward continuation of features identified beneath central Melville Island.

Murray Inlet Fault is considered to be a northward-flattening listric normal fault because the Beverley Inlet Formation, downthrown on the north side, has also experienced northerly directed block rotation consistent with an underlying scoop-shaped extension fault. Blue Hills Fault and the unnamed fault that defines the north side of the east-trending Blue Hills "graben" are considered to be steep reverse faults of opposing vergence. The contractional character of these surfaces is indicated by the local rollover of upthrown strata toward the fault traces. The excess bed length is confirmed when the formation top above the Hecla Bay Formation is restored to its initial pre-deformational state. Compressive slip on the two bounding reverse faults and on others presumed to occur at depth below the Cape De Bray Formation is considered the main cause of regional uplift by at least 1000 m of the central plateau of the Blue Hills structure.

A two-phase evolution, potentially coeval with D3 and D5, is proposed for the Blue Hills structure (Fig. 167). The possible ages of these two tectonic phases are relatively poorly constrained. The earlier compression phase postdates deformed Frasnian (Middle Devonian) strata. The later extensional collapse of this possible low amplitude, bivergent thrust anticline probably predates the peneplain surface (Early Cretaceous) and definitely predates the dissection of the peneplain (Quaternary).

Late Paleozoic inversion structures (D6)

General comments

Tozer and Thorsteinsson (1964) were the first to recognize that Carboniferous strata of Canrobert Hills and McCormick Inlet areas were folded with the lower Paleozoic succession, that this deformation was coaxial with pre-Carboniferous folds, and that the second folding phase (D6 of the present account; Table 5) occurred between the Late Carboniferous and the Permian. Later, Thorsteinsson and Tozer (1970) named this the Melvillian Disturbance and considered the influence of this deformation to extend to southwestern Ellesmere Island, where pre-Late Permian faults have tilted and offset the Canyon Fiord Formation. Mid-Permian deformation is also recorded in the northern Yukon (Bamber and Waterhouse, 1971) and coeval alkalic volcanism is associated with the Essayoo Formation of northern Ellesmere Island (Thorsteinsson, 1974). Other major tectonic elements of the Canadian Arctic region that parallel D6 structures of Melville Island (see Figs. 88, 96), may have been active simultaneously. These regional

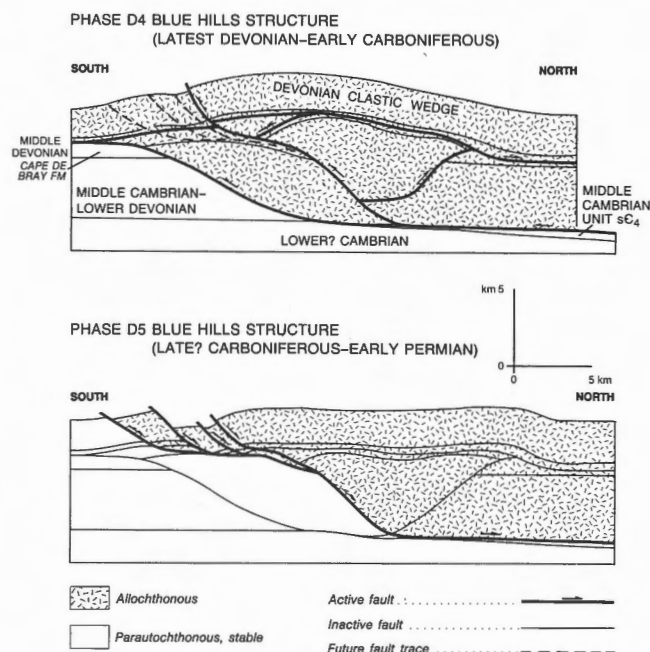


Figure 167. Paleozoic phases of deformation (D4 and D5) deduced for the Blue Hills structure, southwestern Melville Island.

elements include: the ancestral upper Paleozoic Sverdrup Rim, which extends northeast to Axel Heiberg Island; the northeast-trending folded region of Banks and western Prince Patrick islands; Minto Uplift of central Victoria Island; and the Dave Lord High and Aklavik Arch of northern Yukon.

Regardless of the full geographic extent of the Melvillian Disturbance, the occurrence in the Arctic Islands region of mid-Permian folds and related compressive deformation is known with confidence only in the Melville Island area. In the present study it will be shown that the geometry of these compressive structures is consistent with their formation by rift inversion; that is, the compressive reactivation of structures previously created in extension. The fundamental features of D6 shortening are evident in the Canrobert Hills and throughout Kitson Depression, situated north and west of Raglan Range. Regional uplift and some faulting associated with D6 also extend into the northern part of the salt-based fold belt on Sabine Peninsula.

Kitson Depression

Kitson Depression (Fig. 161) is here considered to include a belt of Canyon Fiord outliers extending in outcrop from the eastern slopes of Canrobert Hills to

the west side of Raglan Range. Seismic reflection profiles indicate that the depression is continuous beneath nearly flat-lying Trolld Fiord Formation north and northeast of Raglan Range (Fig. 168A). The southern margin of the depression, north of Raglan Range, is locally exposed along the faulted northern edge of the Kitson River Inlier. The major sub-latitudinal fault on the north side of Kitson River Inlier appears, based on sinuosity of the fault trace around local topographic features, to be a shallow, north-dipping (11°) detachment fault. Hangingwall Canyon Fiord Formation (within Kitson Depression) comprises

proximal conglomerate and breccia with clasts of lower Paleozoic carbonate derived from the adjacent inlier. Similar conglomerates are interstratified with sandstone and thin limestone beds in the exposed part of the depression found west of Raglan Range. These limestones contain Moscovian conodonts, implying approximate synchronicity of D5 rift-related extension and sedimentation with other late Paleozoic depressions of northern Melville Island.

Carboniferous Canyon Fiord beds, exposed north of Raglan Range, have been rotated to the northeast on

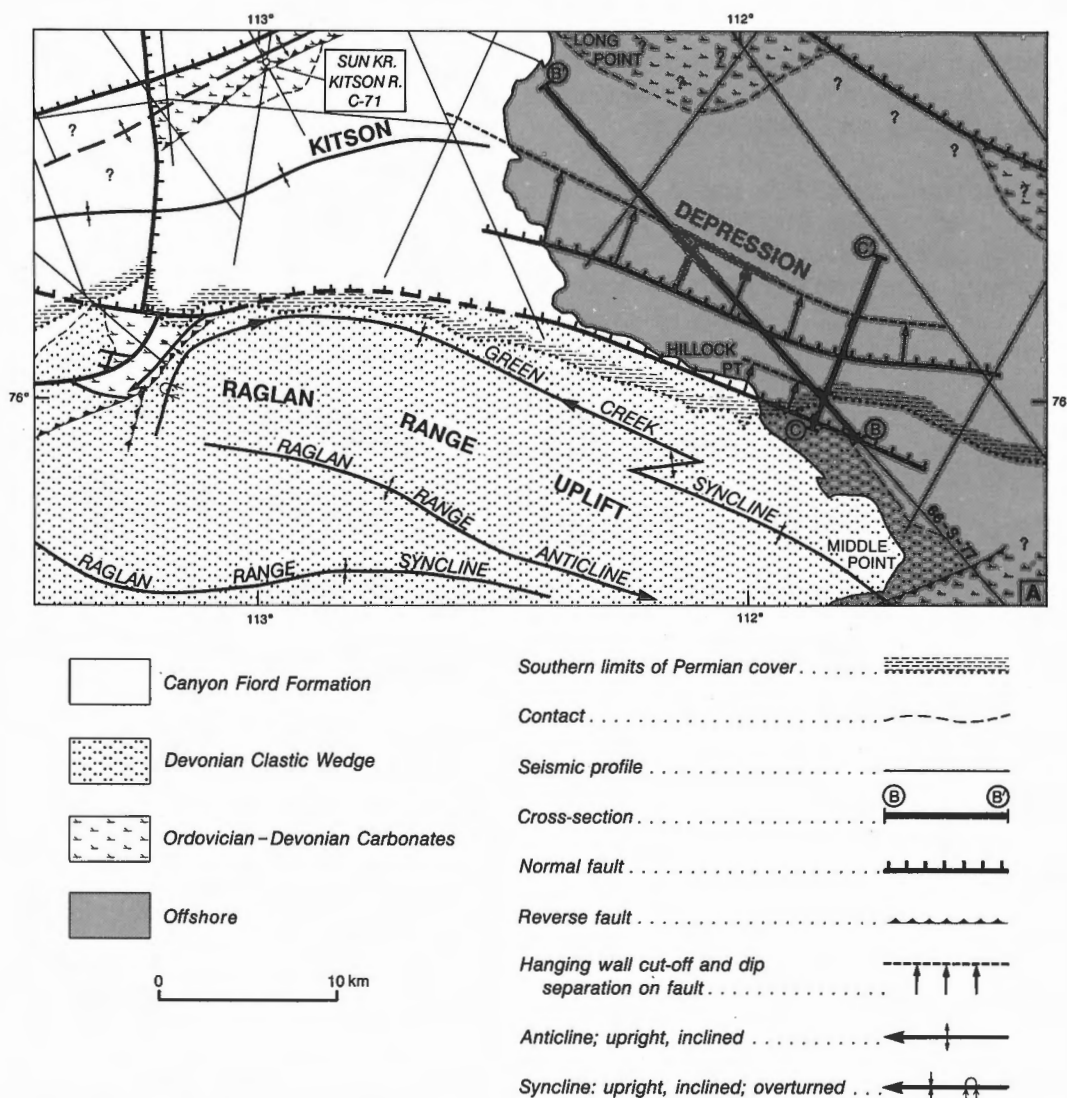


Figure 168. Geology and structure of the Kitson Depression and Raglan Range. **A.** Subsurface geological map of the sub-Permian angular unconformity across Raglan Range and the Kitson Depression. **B.** Line drawing of primary reflections and diffractions along a marine seismic profile across Kitson Depression, offshore Hillock Point area, northern Melville Island. See 168A for location. **C.** Interpreted structural cross-section of Kitson Depression, offshore Hillock Point area, northern Melville Island. See 168A for location.

SEISMIC PROFILE 66-S-77 KITSON DEPRESSION
(OBLIQUE PROFILE)

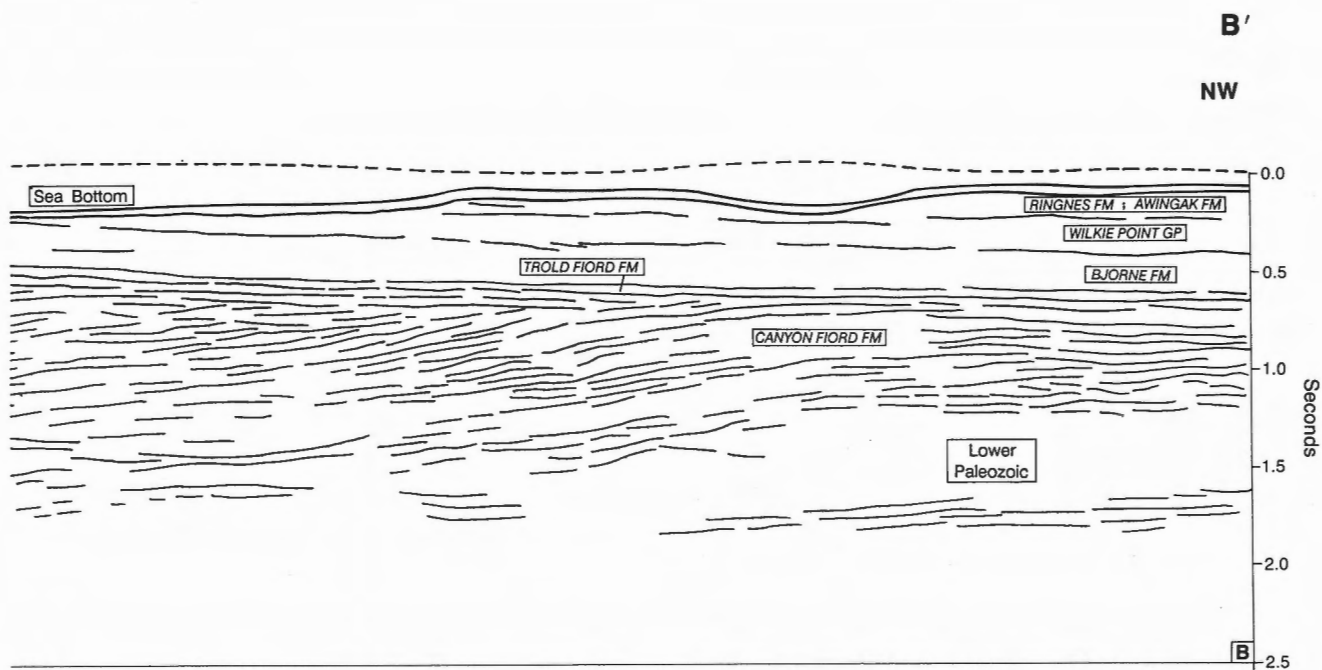
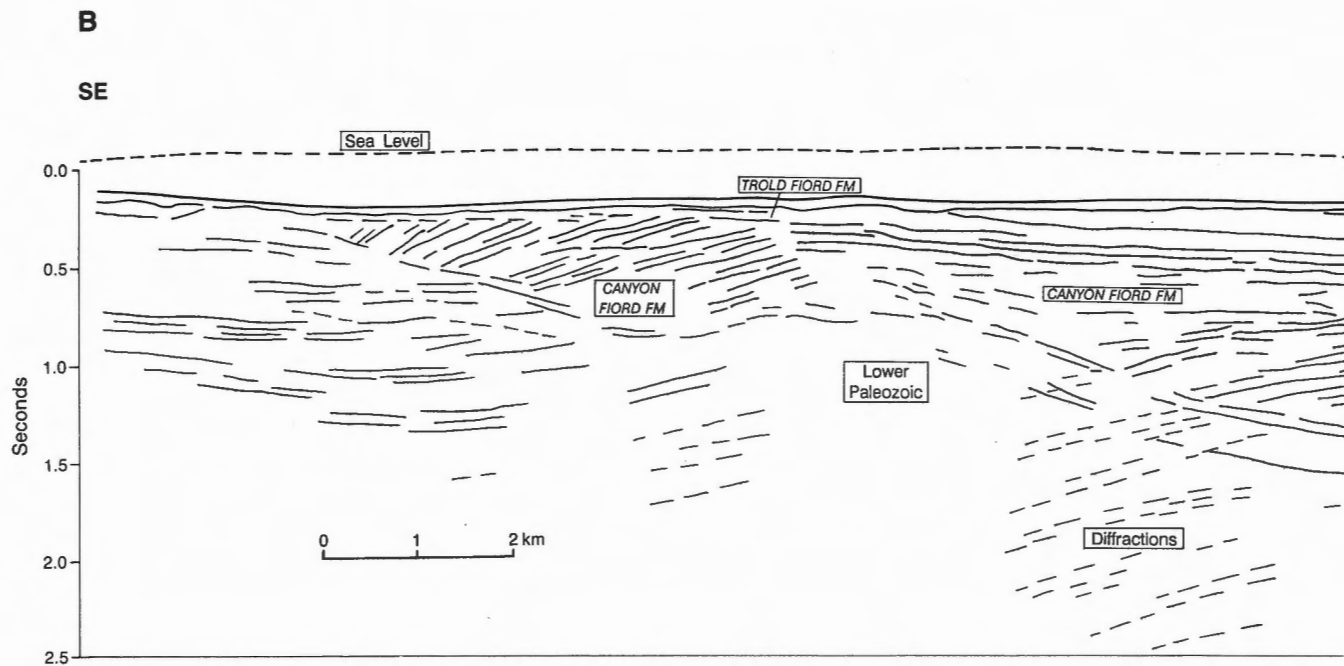


Figure 168. (cont'd.)

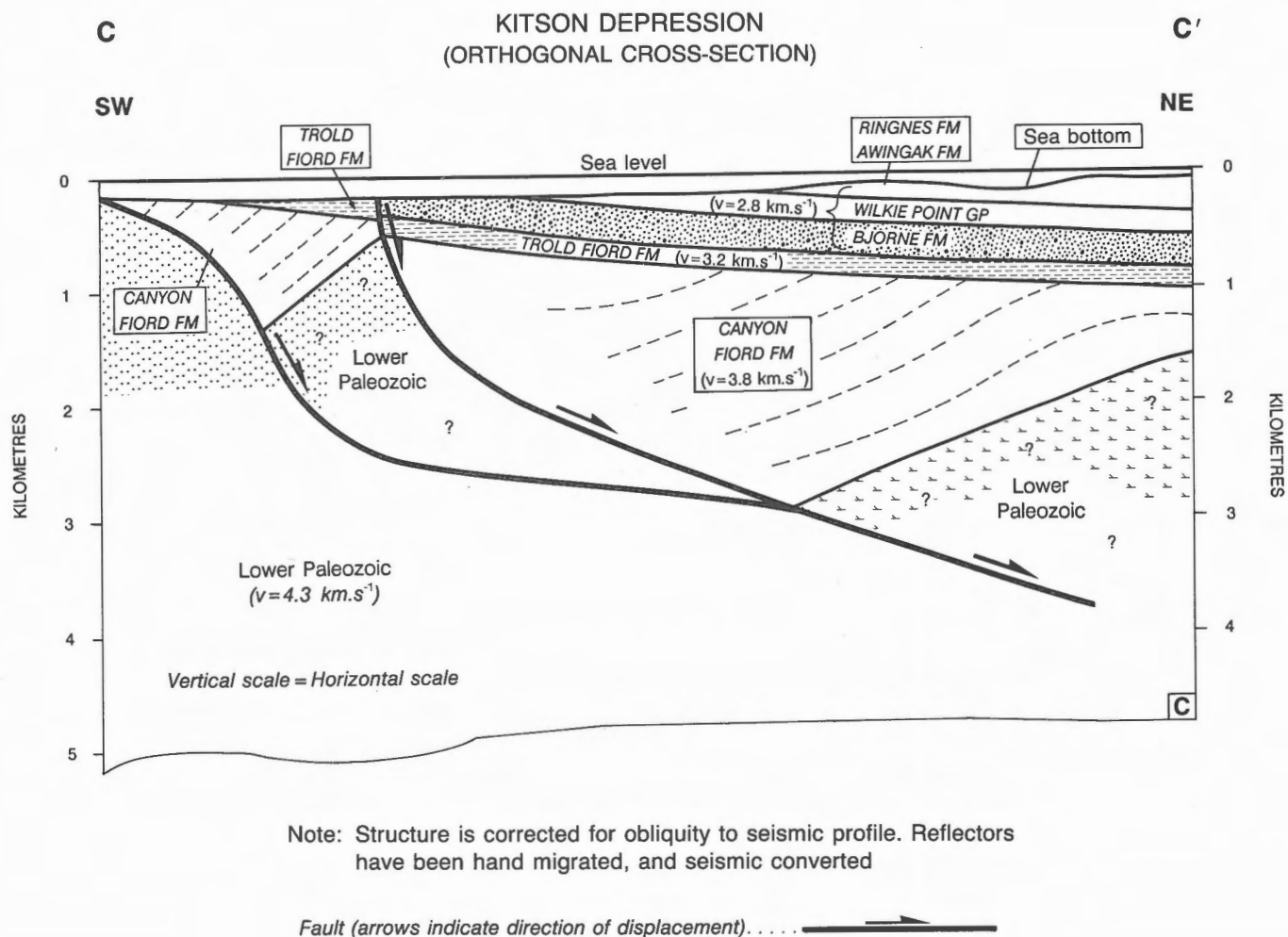


Figure 168. (cont'd.)

the underlying fault plane and now dip at up to 28° southwest against the fault. Trolld Fiord Formation, which lies unconformably on Canyon Fiord strata, has also been downdropped to the north against this fault but is nearly flat lying, as is disconformable cover of Bjorne Formation, which appears to overstep the fault near its western outcrop limit.

The subsurface continuation of Kitson Depression to the north and east lies beneath the outcropping and subcropping Permian through Jurassic succession. Limits of the depression extend beneath the floor of western Hecla and Griper Bay. A half-graben configuration for Kitson Depression is defined by seismic profiles (Figs. 168B, C). Seismic patterns include southerly-divergent internal reflections and an angular unconformity (to 60°) between the Trolld Fiord and Canyon Fiord formations. Preserved stratigraphic section of Canyon Fiord Formation may locally exceed 3200 m. The northern limit of Kitson Depression at the surface is marked by erosionally dissected anticlines

cored by the Ibbett Bay Formation. In the subsurface, the Kitson River C-71 well has drilled the high side of the depression. In this location, Trolld Fiord Formation strata rest unconformably on Silurian shelf carbonates. Elsewhere in the subsurface there is a thin interval of seismic Canyon Fiord Formation lying over the upthrown block.

Based on the evidence presented in Figures 168B and C, it is apparent that Kitson Depression has been formed in extension and that a component of the tilt of the half-graben fill can be attributed to block rotation on two underlying, north-dipping listric faults. Net slip on the two master bounding fault planes is 6.5 km and northeast-directed. The divergence of rift-fill confirms the observations made at the surface that rifting was synchronous with phase D5 uplift and erosion of Raglan Range and also coeval with deposition of proximal Moscovian conglomerates and breccia assigned to Canyon Fiord Formation.

Rift-fill within Kitson Depression has, also, been tilted to at least 60° and these strata have been erosionally truncated by overlapping Troid Fiord Formation. Mappable structures within the depression indicate that the rift-fill experienced a later (D6 phase) compressive deformation. Tectonic elements of the Canyon Fiord Formation that are related to the D6 inversion include anticlines and synclines, reverse faults, detachment faults, strike-slip faults, regional uplift, and erosion of pre-Late Permian and older strata.

D6 folds within the exposed portion of Kitson Depression (Fig. 169) are generally coaxial and continuous with D3 folds beneath the sub-Carboniferous unconformity. This is especially true of two second-order synclines at the western edge of the depression – the D6 synclinal keels defined by the warped unconformity surface overlie tight D3 synclines cored by the Blackley and Cape De Bray formations. Plunge variation on the more continuous D6 synclinal axis links five, saucer-shaped depressions that trend variably N45°E through N90°E between eastern Canrobert Hills and western Raglan Range. This syncline is also probably continuous with the seismically-imaged depocentre line of Kitson Depression north and northeast of Raglan Range. Measured dips of folded strata lie in the 0 to 55° range and are, therefore, also similar to the depth-converted dip of seismically imaged Canyon Fiord strata within the eastern (subsurface) half of the depression.

Other second-order D6 folds are noncoaxial with respect to D3 structures. Examples are found amongst Canyon Fiord outliers south of Marie Bay. These outliers represent the erosional roots of a single, asymmetrical, south-vergent, second-order D6 syncline-anticline pair. The D6 syncline lies variably and obliquely across the truncated roots of six second- and third-order D3 synclines and anticlines. Similarly, a 14 km long portion of the D6 anticlinal axis lies over the southern limb of an underlying D3 anticline.

The relation between D6 faults and D6 folds is complex and not yet entirely understood. The following is a list of brief case histories from localities in the exposed part of Kitson Depression.

A sublatitudinal fault segment in lower Canyon Fiord Formation dies out to the east and west in two oppositely plunging south-facing anticlines (Fig. 169, Note 1). In this case, the fault segment is undoubtedly a south-vergent thrust and the folds are fault-bend hangingwall anticlines.

A sublatitudinal fault segment, with Canyon Fiord Formation faulted against Cape De Bray Formation (to the south), is laterally continuous with a west-plunging anticline in Canyon Fiord strata (Fig. 169, Note 2). Since the fault dips to the north, the simplest kinematic solution, here, is that the Canyon Fiord is in normal fault contact with the Cape De Bray. However, this D5 extension fault was reactivated as a south-vergent D6 thrust to produce the D6 anticline.

A sublatitudinal synclinal fold axis lies parallel to and on the downthrown side of a sinuous fault (Fig. 169, Note 3). Fault sinuosity and the younger-over-older stratigraphic relation implies a normal sense of displacement. The fold axis intersects the sinuous fault toward the west, beyond which the tilt of Canyon Fiord strata is toward the fault. Dip of the fault appears to vary along strike from 0 through 60°N. At one location, 24 km east of the head of Ibbett Bay, hangingwall Canyon Fiord strata are preserved in an erosional remnant (Fig. 169, Note 4; Fig. 170). Strata tilted to 15° in the outlier are truncated downdip by a horizontal fault segment for which the surface trace influenced by topography is generally elliptical in plan view but highly sinuous in detail. The preferred interpretation is that tilt of strata into the sinuous detachment fault is due to block rotation during D5 extension. Where a syncline lies above the fault, the fold is created by D6 compressive slip on the pre-existing D5 extension fault. The syncline is created by folding above a concave portion of the footwall fault. Direction of D6 transport, here, is southerly directed.

Third-order D6 folds, identified on and above the sub-Carboniferous unconformity, lie obliquely across the easterly termination of Nisbet Point Fault (Figs. 171A, B; 172; 173). These folds are also oblique to a sublatitudinal D3 syncline in the Blackley Formation, exposed within the hinge of a D6 anticline, but are subparallel to a D4 anticline identified by culminations and structural saddles on D3 folds of southern Canrobert Hills (compare Figs. 154, 174). strike-slip displacement during D6 is partly inferred from minor fault plane striations peripheral to an exposed and vertical portion of Nisbet Point Fault. This fault extends through southern Canrobert Hills along the hinge of the aforementioned D4 anticline. Magnitude of dextral offset of three D3 synclines and two other D3 anticlines is up to 2.5 km across both Nisbet Point and Hawk Creek faults (total 5 km). The en echelon arrangement of parasitic D6 folds in the Canyon Fiord Formation is also kinematically consistent with the right-lateral sense of displacement on the spatially related faults. The implied direction of tectonic transport is toward the southeast.

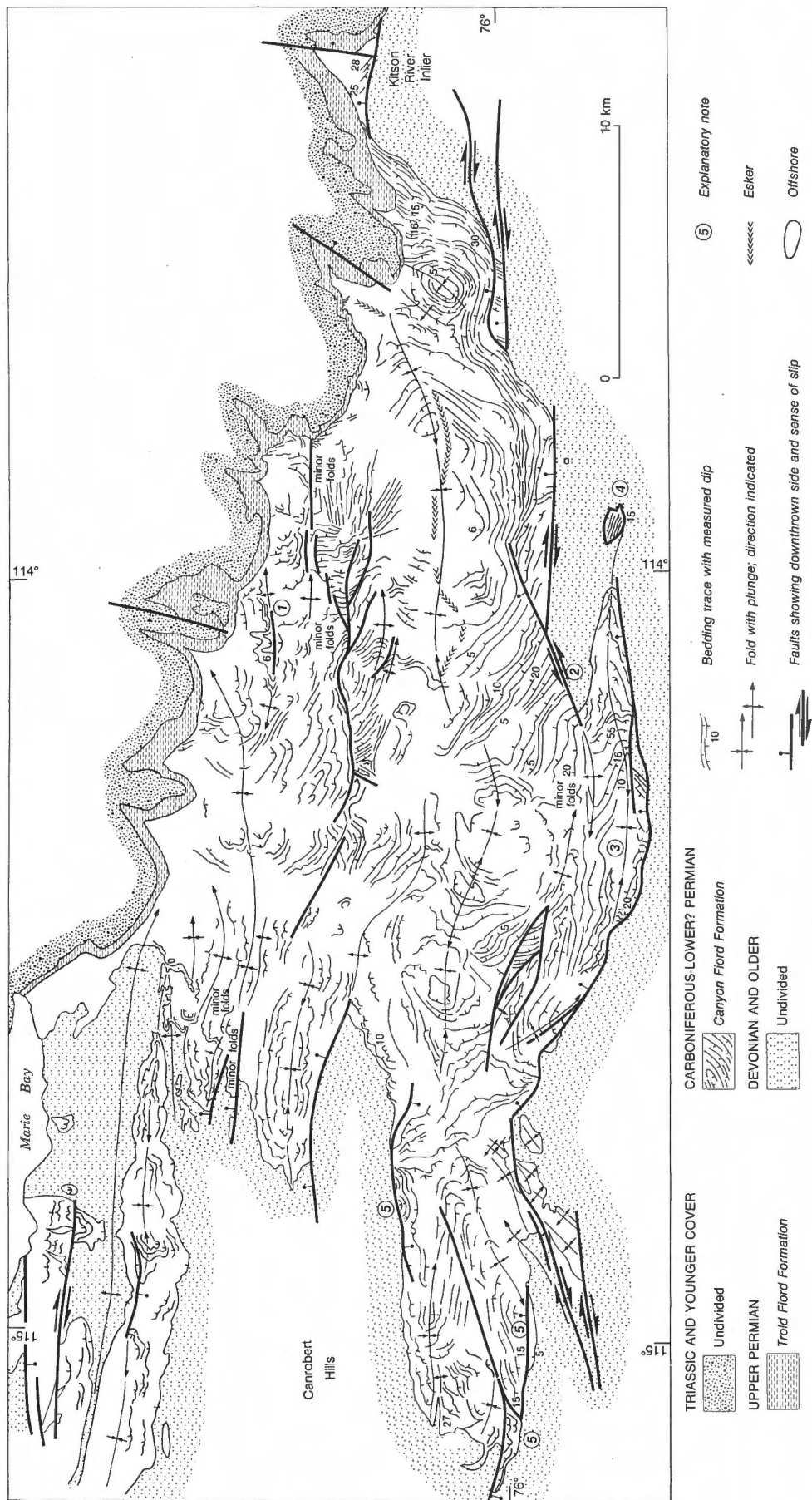


Figure 169. Faults, folds and bedding attitudes of the Kitson Depression, as obtained from field observations and the interpretation of aerial photographs. Surface topographic relief is not significant. 1, a sublatitudinal, and probably reverse, fault segment in the lower Canyon Flord Formation dies out to the east and west in two oppositely plunging south-facing anticlines; 2, a sublatitudinal fault segment, with Canyon Flord Formation faulted against Cape De Bray Formation (to south), is laterally continuous with a west-plunging anticline in Canyon Flord strata; 3, a sublatitudinal synclinal fold axis, parallel to and on the downthrown side of a sinuous fault; 4, tilted Canyon Flord Formation is truncated down dip by a horizontal detachment fault above the Cape De Bray Formation; 5, tilt is attributed to D5 block rotation on the underlying listric extension fault.

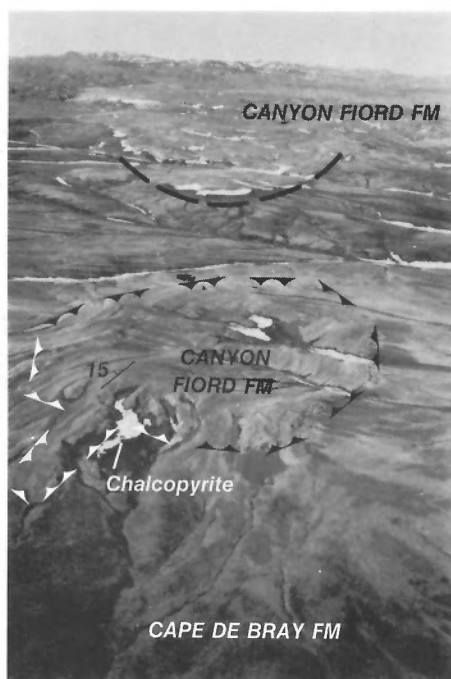


Figure 170. A dipping outlier panel of Canyon Fiord Formation in horizontal tectonic contact with strata of the underlying and older Cape De Bray Formation, 24 km east of the head of Ibbett Bay. Showing of chalcopyrite is "locality 1" in Table 7. ISPG photo. 2912-22.

Regional uplift during D6

The locus of regional D6 uplift is situated to the southwest. On Melville Island, the northeasterly facing direction of the uplifted region is expressed by the southwesterly or westerly increasing depth of erosion of inverted D5 half-grabens preserved beneath the sub-Trold Fiord unconformity (Fig. 161), by the time-transgressive and southwesterly onlap of post-uplift cover (Fig. 175), and by the northeasterly increase in thickness and age range of sediment cover. The local trend of the D6 uplift across Melville Island is approximately N45°W and parallel to facies belts of the Sabine Bay Formation (Fig. 175). The proximal facies of the Sabine Bay on southeastern Sabine Peninsula is rich in variegated chert pebbles recycled from similar chert pebble conglomerates of the Canyon Fiord Formation. Grain size within the Sabine Bay decreases toward the northeast off the uplift. There is a parallel northeastward increase in sediment thickness within the Sabine Bay and a decrease in the eroded or nondeposited section across the sub-Sabine Bay disconformity.

Models of modest and pronounced rift inversion are illustrated in Figure 176. Inversion is responsible for the existence and angularity of the post-inversion unconformity. The magnitude of inversion and the longevity of inversion-related uplift have influenced the depth of erosion of pre-inversion rift fill and the thickness of the subsequent Permian sedimentary section.

Mesozoic tectonics (D7)

General comments

By mid-Carboniferous time most of Melville Island's salt-based fold belt had become a relatively stable part of the North American tectonic plate. Nevertheless, it has been shown in this chapter that dipping surfaces of weakness, notably key levels of detachment in the fold belt, influenced the location and orientation of rift-related depressions and uplifts during the embryonic stage of Sverdrup Basin evolution. Subsequent to late Paleozoic rifting (D5) and Permian rift-inversion (D6), the Sverdrup Basin experienced a prolonged period of thermally-driven subsidence and sedimentation (see Chapter 4, and Stephenson et al., 1987). The tectonic styles resulting from this subsidence are not readily related to the ancient salt-based fold belt. Rather, the increased depth of burial of the fold belt resulting from Sverdrup Basin subsidence has entirely obscured the physical and genetic links between the two structural domains, particularly in the northeastern part of the project area (subsurface Hecla and Griper Bay, northern Sabine Peninsula and Byam Martin Channel).

Other tectonic events and structural styles related to basin evolution in the Mesozoic, phase D7 of the present account (Table 5), have served to further obscure and modify the present structure of the salt-based fold belt. These events include: 1) widespread mafic igneous activity featuring sills, sheets, dykes and related magnetic anomalies; 2) extension faulting; and 3) evaporite diapirism of the northern Sabine Peninsula region.

Mesozoic igneous activity

Surface exposures of gabbro include en echelon dykes, near Tingmisut Lake, ring dykes, and irregular masses within the two onshore evaporite diapirs of northern Sabine Peninsula. Borehole-penetrated intervals of gabbro are listed in Table 4. Radiometric ages, quoted in Chapter 4, lie in the 123 to 152 Ma range (Oxfordian

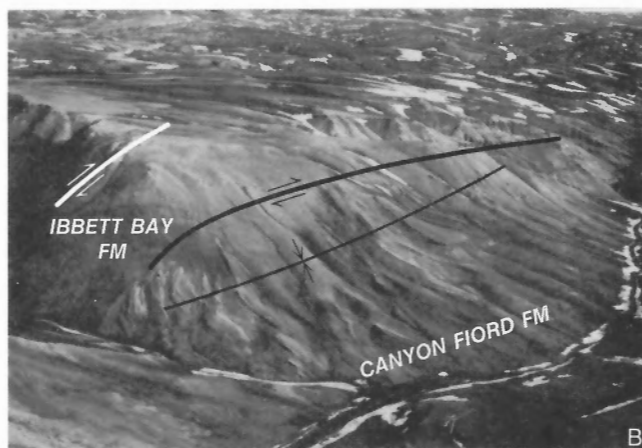
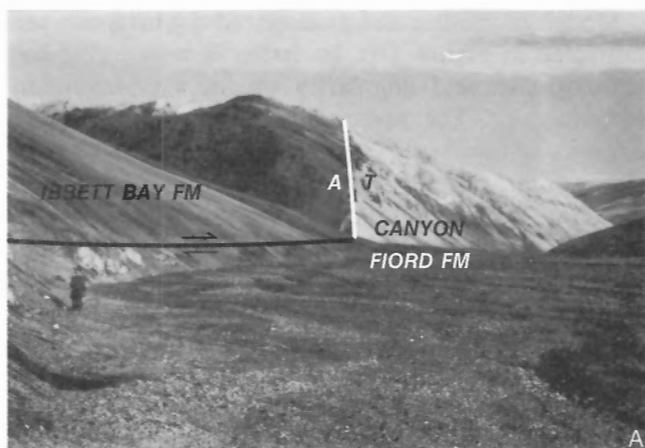


Figure 171. Nisbet Point Fault. **A.** Ground view of Nisbet Point Fault in the Canrobert Hills. ISPG photo. 2887-40. **B.** Aerial view of a third-order syncline in the Canyon Fiord Formation on the south side of Nisbet Point Fault. ISPG photo. 2887-53.

or Volgian through Barremian or Aptian). The surface exposures have a pronounced magnetic signature and are therefore also readily identified on the magnetic maps of the Polar Continental Shelf Project (1965; 1987). The anomalies over the Tingmisut dykes are 200 nT above background and 2 km wide. Weaker magnetic anomalies (10–20 nT and each about 3 km wide) betray the existence of other unroofed gabbro dykes as illustrated on Figure 177. Forsyth et al. (1979) have estimated the depth to the tops of magnetically susceptible bodies to range from the surface down to 2000 m below sea level.

The swarm of magnetic linears trend variably N45°E on southern Sabine Peninsula, N20°E on south-central Melville Island, and due north over Hecla and Griper Bay and western Melville Island. These anomalies extend far to the north of Melville Island and are especially common in the Loughed Island area and in the interisland channels between Borden Island and Isachsen Peninsula of Ellef Ringnes Island (inset, Fig. 177). Implied direction of regional extension is perpendicular to the walls of the dyke swarm or approximately N70–45°W and subhorizontal. This extensional direction, together with the age of the dykes, generally supports the concept that the modern continental margin of the Canadian Arctic Islands facing the Arctic Ocean to the northwest began as a rifted margin in the Early Cretaceous. An equally important facet of the origin of this dyke swarm is the observation of Embry and Osadetz (1988) that the majority of the Cretaceous dykes and sills in the Arctic Islands may be part of a single swarm radiating from a common hot spot situated over northeasternmost Ellesmere Island adjacent to Alpha Ridge.

Balkwill and Fox (1982) suggested that dyke swarm emplacement in the western Arctic Islands may have been influenced by a pre-existing Precambrian basement anisotropy. Dyke trends indeed appear to parallel some Precambrian trends and related potential field anomalies of Victoria Island, the Boothia Uplift region and the northern mainland (compare Figs. 9, 10 and 177). However, it has been shown (*in* Chapters 2 and 3) that Late(?) Proterozoic basins and the Cambro–Ordovician shelf margin situated within the upper 10 to 15 km of the seismically imaged crust beneath the salt-based fold belt have an east-northeasterly trend that is highly oblique to the dyke swarm. If the dyke swarm is somehow related to trends in crystalline basement, these trends must exist below 10 to 15 km and possibly only within seismic Precambrian unit sAP below 20 to 24 km. This possibility is supported by first motion studies on recent earthquakes with foci located beneath Byam Martin Channel; fault planes parallel to and within the dyke swarm magnetic anomalies, at depths of 22–27 km, are still tectonically active (Hasegawa, 1977).

The gabbro bodies intersected in drilling (Table 4) are believed to be sills or shallow-dipping intrusive sheets. Depth of intrusion ranges from 3501 to 4946 m below surface. The strong impedance contrast of these sills against the enclosing strata has also allowed identification of the sills on many seismic profiles of central Sabine Peninsula (Section E; Notes 13, 15). The seismically imaged sills extend downward to at least 6000 m and, along Section E, are not known above 3500 m. Since the magnetically identified subsurface dyke swarm may, according to Forsyth et al. (1979), terminate upward at and above 2000 m, the dykes may



Figure 172. Vertical airphoto of the central parts of the Hawk Creek and Nisbet Point faults (with related structures) in the southern Canrobert Hills. OCR, Canrobert Formation; OSDI, Ibbett Bay Formation; DB, Blackley Formation; DCB, Cape De Bray Formation. See also legend, Figure 33. NAPL photos. A17719-142, -144.

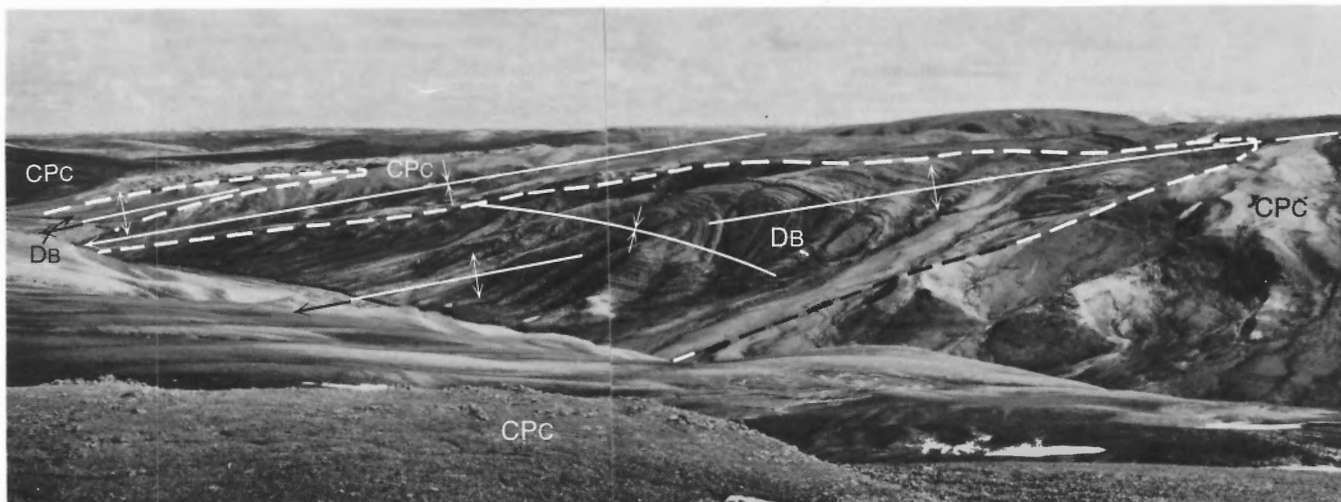


Figure 173. Oblique panoramic view of a D3 syncline in the Blackley Formation, exposed in the hinge region of one of several D6 anticlines defined by the folded sub-Carboniferous angular unconformity. These folds occur at and east of the eastern termination of Nisbet Point Fault, eastern Canrobert Hills. Wavelengths of D6 folds are about 1.2 km. DB, Blackley Formation; CPC, Canyon Fiord Formation. ISPG photos. 2887-46, -47.

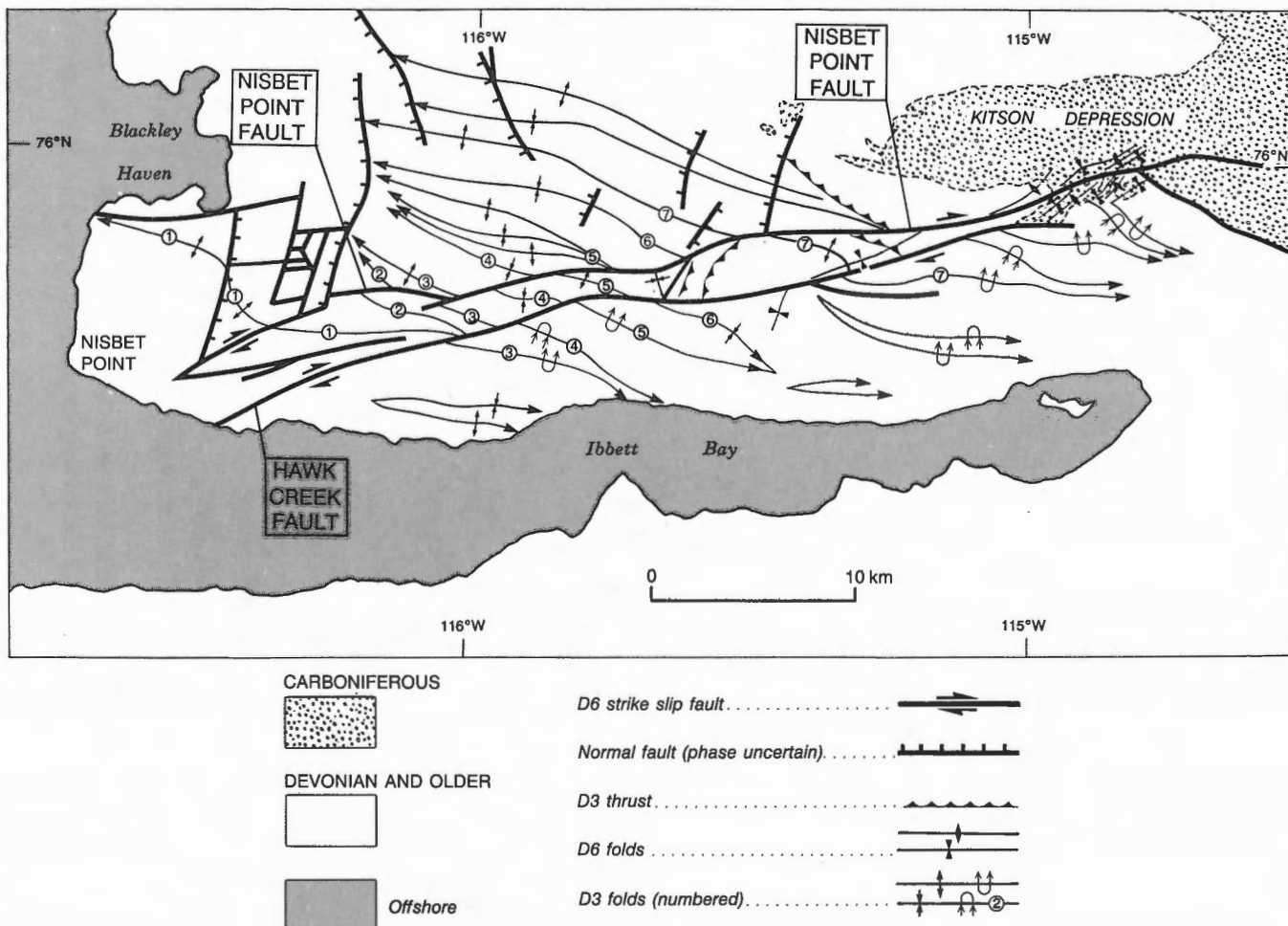


Figure 174. Major tectonic elements of the southern Canrobert Hills region. Numbered second-order D3 folds are offset right-laterally by the Nisbet Point and Hawk Creek faults. Note also the kinematically compatible en echelon D6 minor folds near the eastern termination of Nisbet Point Fault.

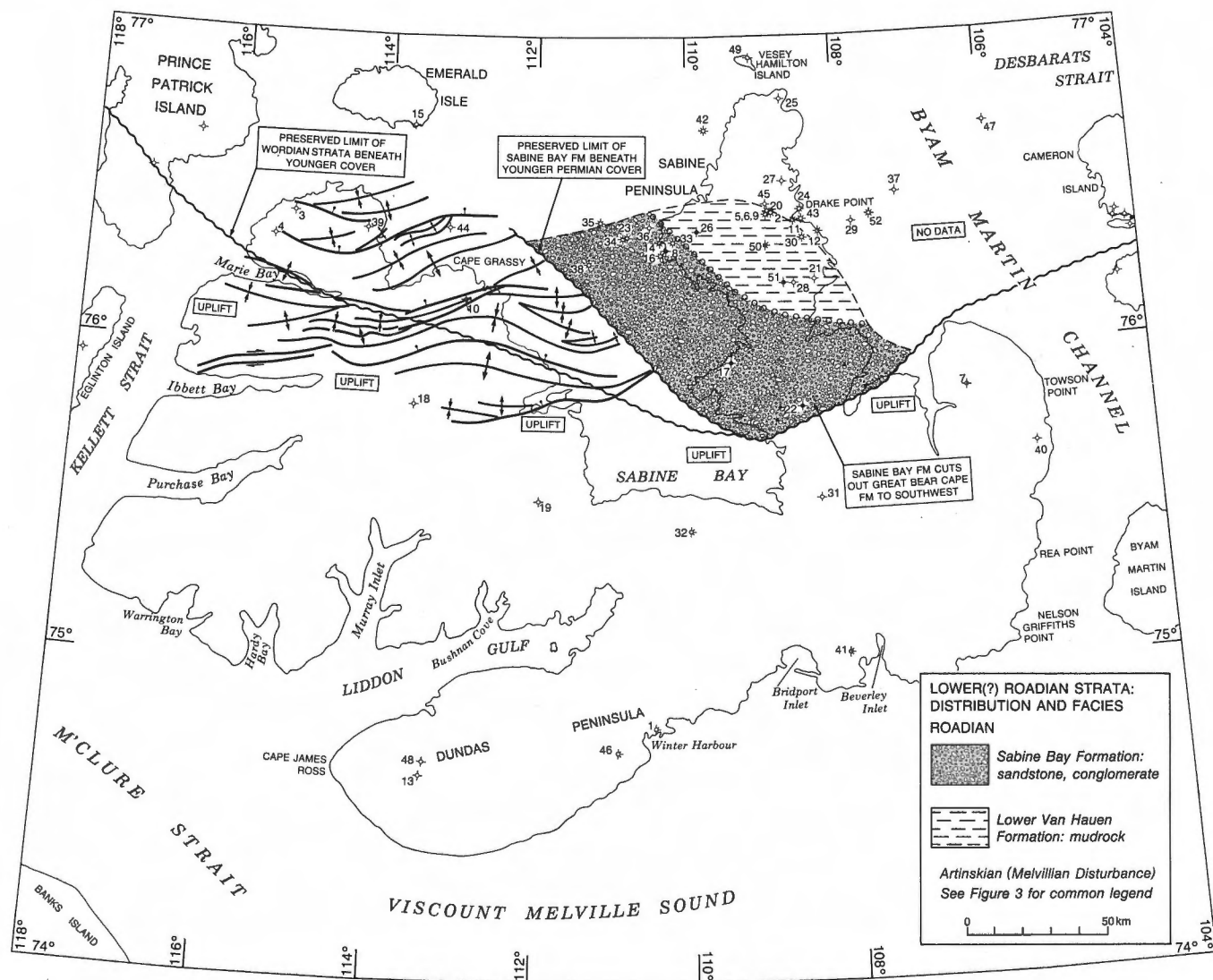


Figure 175. Simplified paleogeographic map and tectonic elements of the Melville Island area for late Early Permian (part of Roadian) time. Facies belts define the northeastern limit of regional-scale uplift and compressive deformation associated with the Melvillian Disturbance (phase D6).

also not feed the sills. Thus, the intrusion of dykes and intrusion of sills might be attributed to two separate magmatic events.

On seismic profiles (Fig. 178), the sills and sheets are observed to intrude Lower and Upper Permian basin facies mudrock, chert and siltstone of the Hare Fiord, Trappers Cove and Van Hauen formations. While the sills appear to follow seismic bedding planes for distances of up to 14 km, the same imaged intrusives also cut upsection at low dip angles ($<30^\circ$). The probable three dimensional shape of individual sheets is that of a circular or elliptical flat-based saucer with upturned distal edges. In some areas of subsurface Sabine Peninsula these gabbro “saucers” appear to be

stacked vertically and also linked at the upturned edges.

Extension faults and lineaments

Single and paired (“keystone graben”) normal faults are identified at the surface across Melville Island (see geology map, in pocket; Figs. 89, 179) and are also common on seismic profiles of Hecla and Griper Bay, central Sabine Peninsula and to the east beneath Byam Martin Channel (Figs. 177, 178; Section E, Note 16). In some instances, keystone faults are parallel and spatially coincident with the trend of individual, dyke-related linear magnetic anomalies.

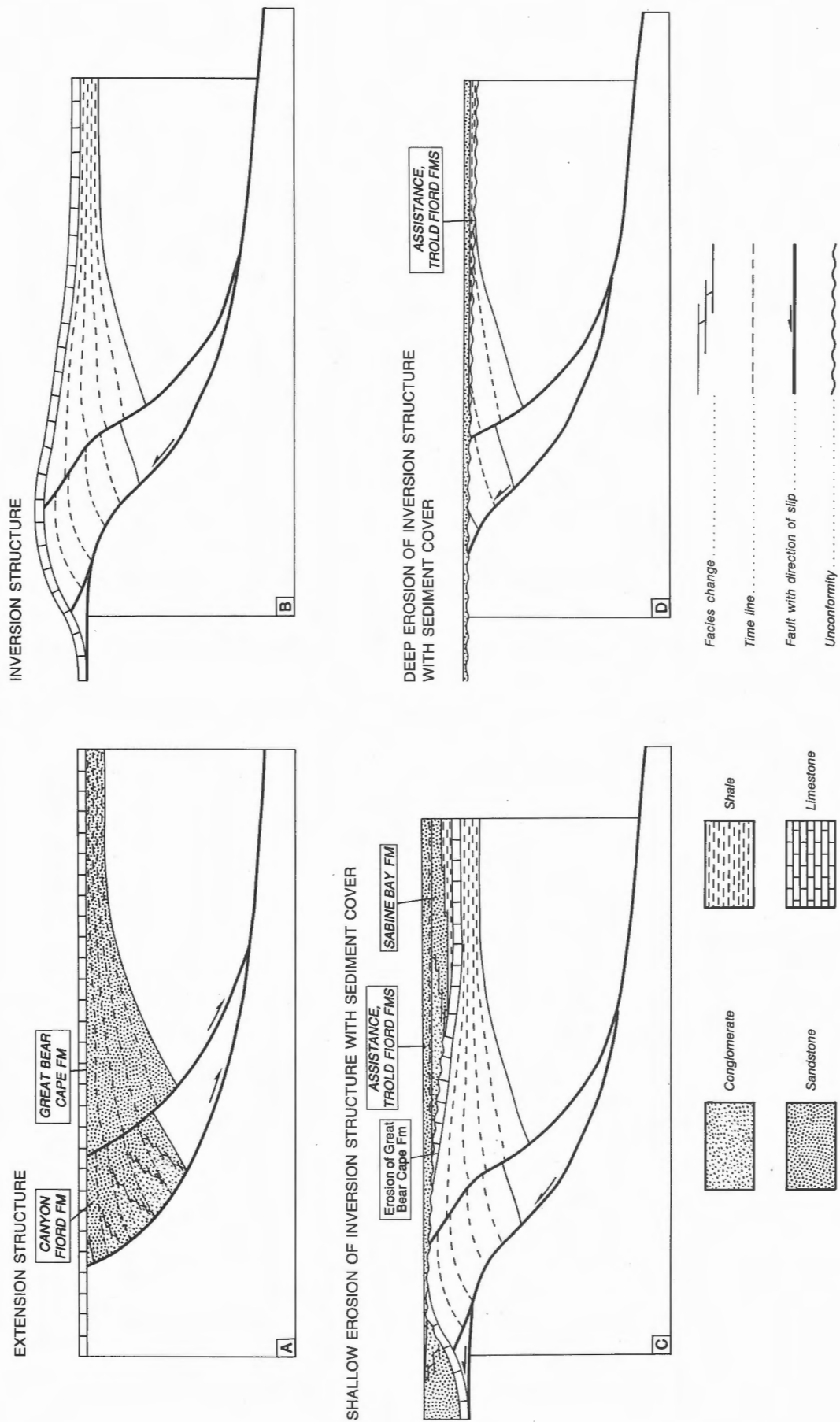


Figure 176. Geological models to account for the sub-Upper Permian angular unconformity of northern Melville Island.

These faults and associated lineaments have been mapped across the peneplained roots of the salt-based fold belt. In several locations, single and paired faults also appear to offset Lower Cretaceous cover (Isachsen and Christopher formations) on the peneplain. Two fault sets in this area are spatially associated with linear magnetic anomalies. The parallelism but noncoincidence of anomalies and surface faults in these cases is attributable to either a westerly dip on the underlying dykes or navigation errors during the original magnetic survey.

West of the salt-based fold belt, north- and north-northeast-striking faults have also been mapped in the Blue Hills and along and parallel to Kellett Strait from Cape Russell to Blackley Haven. The largest onland

structure, situated near the southwestern coast of the island, is the Comfort Cove Fault. This structure defines the eastern limit of Cape Russell Graben. Up to 270 m of Volgian Awingak Formation is locally preserved within the graben. Minimum vertical separation on the bounding faults is about 500 m. Tilt of strata in the graben is to the east, implying block rotation on an underlying westward-flattening listric fault. The normal faults and lineaments of the Comfort Cove and Kellett Strait areas not associated with linear magnetic anomalies are believed to be rift-related extension features peripheral to the much larger Eglinton Graben. Elsewhere, north-striking normal faults near Cape Grassy (northwestern Melville Island) are observed to offset Oxfordian-Kimmeridgian Ringnes Formation and all older strata

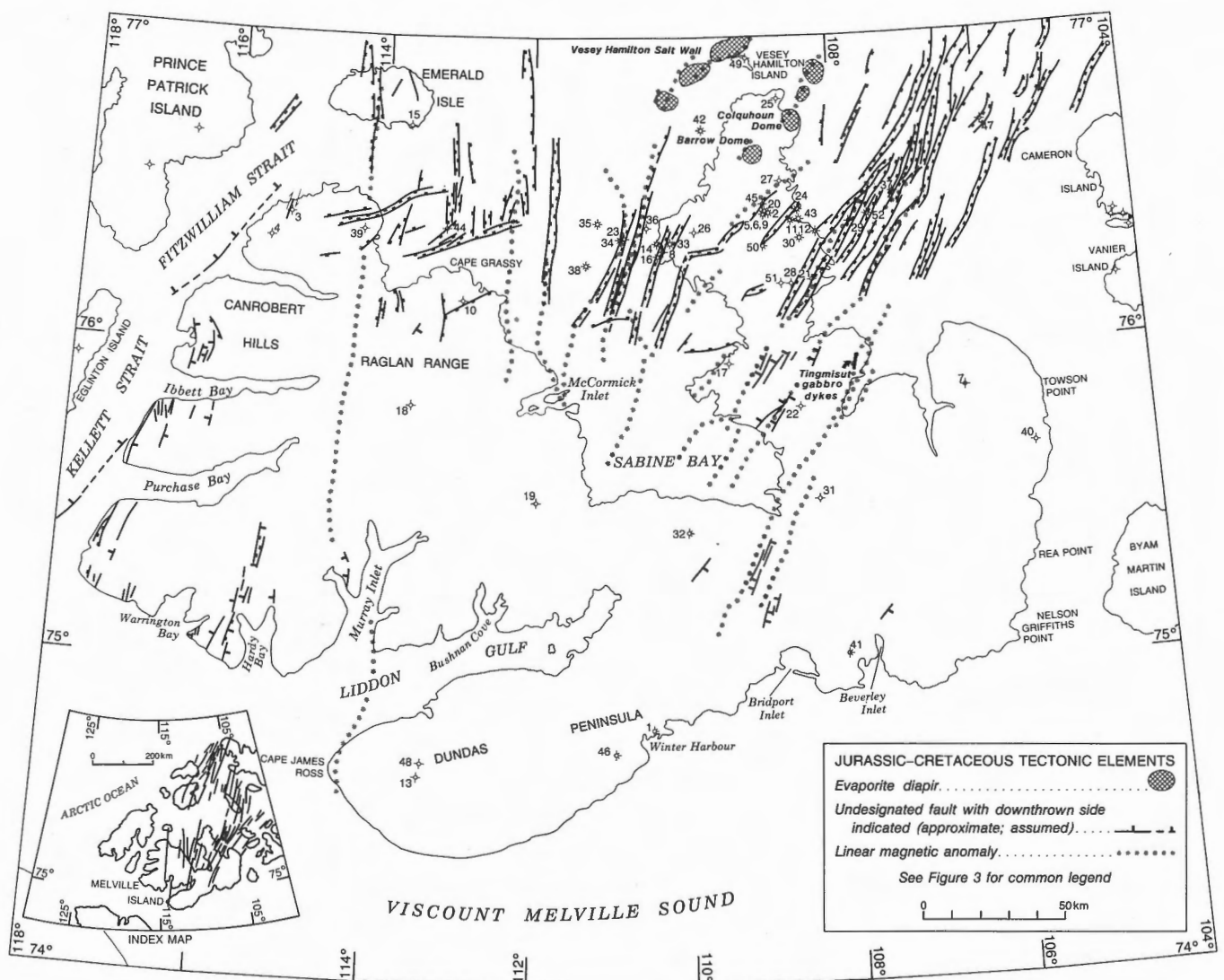


Figure 177. Distribution of Upper Jurassic-Lower Cretaceous gabbro dykes exposed at the surface, single and paired extension faults (keystone grabens), and related linear magnetic anomalies (see also Table 4). Note the full distribution on the inset map of the subsurface dyke swarm in the western Arctic Islands.

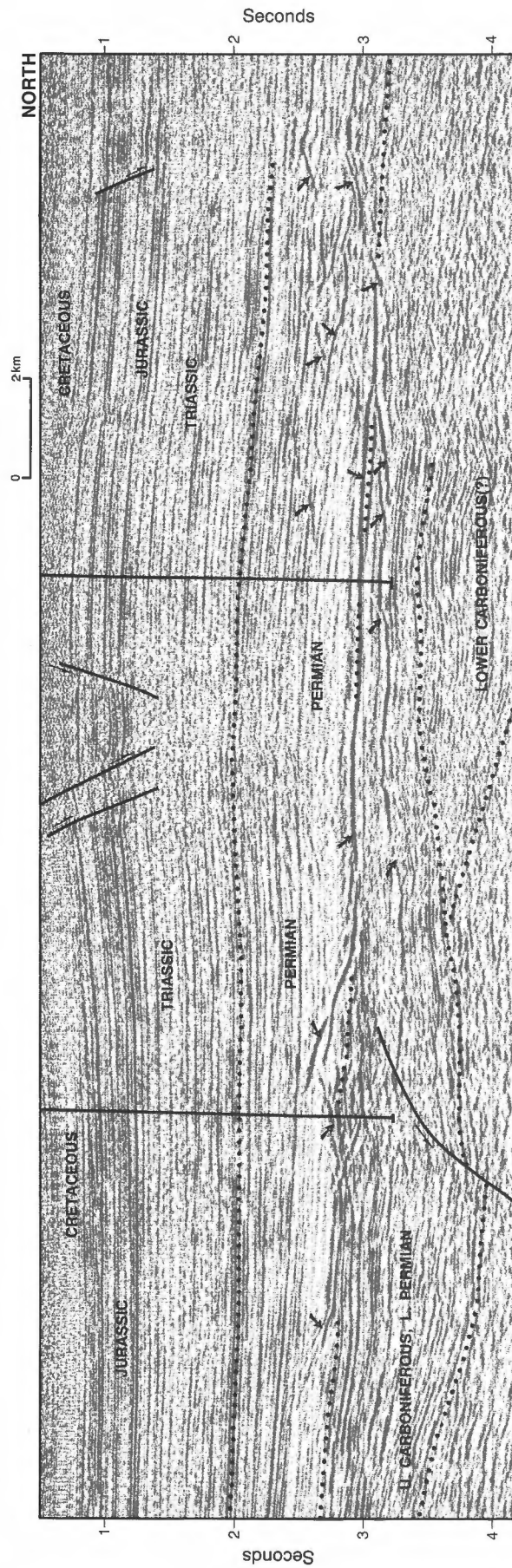


Figure 178. Seismic expression of Upper Jurassic–Lower Cretaceous gabbro sills and sheets (indicated by arrows) emplaced into Permian strata of central Sverdrup Basin. Part of seismic profile P2674, Section E.

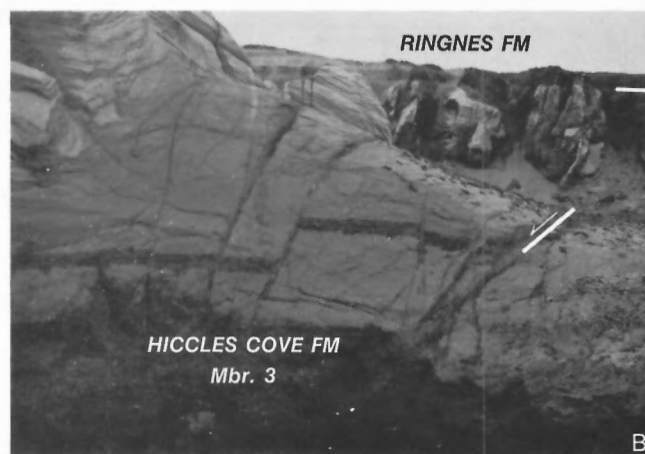


Figure 179. Field photographs of structures in the Hiccles Cove and Ringnes formations. **A.** Northerly striking normal fault (phase D7) displacing Hiccles Cove and Ringnes formations south of Cape Grassy. ISPG photo. 2887-42. **B.** Outcropping major and minor normal faults (phase D7) offsetting uppermost Hiccles Cove Formation south of Cape Grassy. Vertical displacement on the main fault strand, right of centre, is about 30 m and down to the east. ISPG photo. 2887-44.

at the surface (Figs. 179A, B). Other northeasterly striking faults are mapped at the surface in Bjorne and Trolld Fiord formations of southern Sabine Peninsula.

Many faults illustrated on Figure 177, such as those of central Sabine Peninsula and others in marine areas to the east and west, are known only from reflection profiles. Since the faults are commonly arranged in oppositely dipping conjugate pairs, the implied transport direction in extension is readily determined. This direction is subhorizontal, toward N45°W beneath Byam Martin Channel, toward N70°W beneath Hecla and Griper Bay and due west beneath much of western Melville Island. These directions are identical to the extension directions implied by the subsurface dyke swarm.

The conjugate fault pairs form keystone grabens up to 1.5 km apart as measured on the sub-Isachsen disconformity in the Byam Channel region. Downward convergence is implied for inward-dipping pairs. For conjugate slip planes with 60° dips, the line of convergence lies at or above 1300 m as measured downward from the sub-Isachsen level; in other words, within or above the Bjorne Formation at depths of not more than 2500 m below surface. Upsection, the same faults generally die out in the Christopher Formation and are not known at the surface. This indicates that most northeasterly striking faults, like the dykes related to them, may date to the time of deposition of the Christopher Formation with most extensional displacement ending during or prior to the late Early Cretaceous (Albian).

The association of linear magnetic anomalies with these various faults implies a kinematic linkage. Balkwill and Fox (1982) suggested that the shallow emplacement of gabbroic magma should result in the upward flexure of overlying strata. To maintain constant bed length during flexure, the strata are forced to deform by extension, ultimately leading to brittle failure. The shallow keystone faults lying at and above the dykes define the zone of local flexure. The previously stated depth to the line of convergence on conjugate faults may then also represent the depth to the upper surface of the related magnetically susceptible magma body. It is worth noting that the maximum depth to the tops of unroofed dykes determined by Forsyth et al. (1979) from related magnetic anomalies (<2000 m) is in excellent agreement with the depth implied by downward convergence of conjugate normal faults (<2500 m). This agreement lends added support to the proposal that the linear magnetic anomalies may be associated with a young dyke swarm that crosscuts older, seismically imaged gabbro sills and sheets known only at 3500 to 6000 m below surface.

Evaporite diapirs

Meneley et al. (1977) recognized two diapiric provinces in the central Sverdrup Basin and suggested that the distribution of diapirs also reflected the original distribution of Carboniferous evaporites at depth (Fig. 180). The western province extends north from the Drake Point area on northern Sabine Peninsula across Hazen Strait to south of Loughheed and

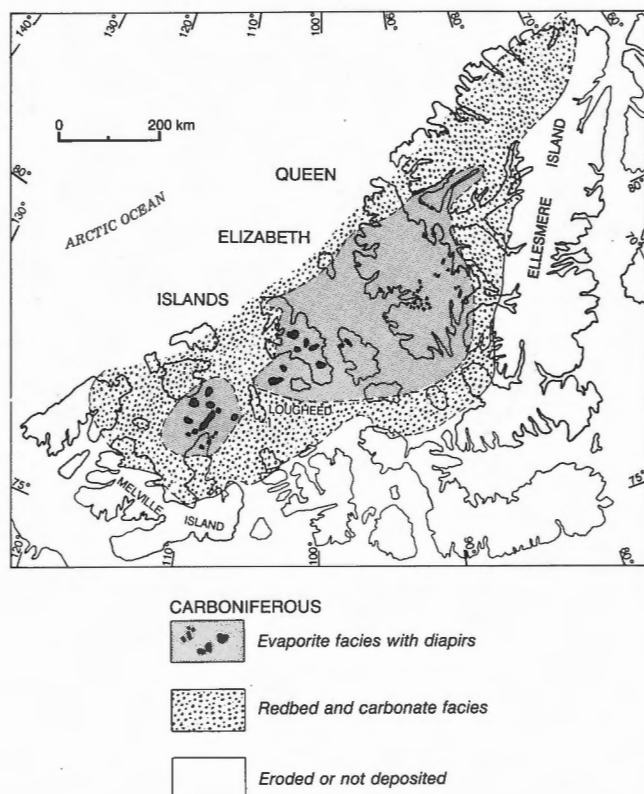


Figure 180. Evaporite diapirs and other piercement structures of the Sverdrup Basin. The western and eastern diapiric provinces are separated by a possible northeast-trending intrabasinal high beneath Lougheed Island. (Adapted from Balkwill and Fox, 1982.)

Mackenzie King islands. This uplifted but only gently folded region includes the two onshore piercement diapirs of northern Sabine Peninsula (Colquhoun and Barrow domes; Fig. 181); seven seismically imaged piercement diapirs and Vesey Hamilton Salt Wall, which subcrop on the sea floor in Hazen Strait; and at least four other diapirs that fail to penetrate sedimentary cover. Apart from the salt wall, the diapirs of the western province are either circular in plan view or slightly elliptical, with the diapir long axes aligned roughly N40°E. The diapirs and salt wall of the western province are also arranged in northeasterly trending rows that parallel the trends of surface gabbro dykes and related linear magnetic anomalies (compare Figs. 177 and 180).

The evaporites of Barrow and Colquhoun domes have intruded the Kanguk Formation and all underlying strata. The Expedition Formation of the Eureka Sound Group has been tilted in the vicinity of the intrusive contacts. Thus, the last stage of diapiric movement is post-Paleocene but also predates

unconformable Quaternary cover. Balkwill and Fox (1982) have also pointed out that for gabbro to intrude ring fractures in the diapirs, the ring fractures must have existed before the magmatic activity. Since the gabbro bodies are radiometrically dated to the Late Jurassic–Early Cretaceous, at least one stage of evaporite diapirism and ring fracture formation must predate this time.

For Vesey Hamilton Salt Wall, thinning of seismically imaged marginal strata against the wall points to a long history of diapirism beginning no later than the Early Triassic. Vesey Hamilton Salt Wall is a N40–50°E-trending diapiric ridge, the upper part of which is defined by marine seismic profiles north and west of Vesey Hamilton Island in Hazen Strait (Fig. 182; Section E). Seismic profiles of this diapiric wall are particularly illuminating because these data permit the identification of movement phases of Otto Fiord evaporites (Fig. 182; Fox, 1983). The upward movement of salt is believed to have had the effect of creating local topographic relief over the rising diapir, leading to deflection of incoming sediment into surrounding rim synclines. Periods of inactivity are equated with erosion and a more even sediment cover over diapirs and within adjacent depressions. In a similar way, the minimum rate of upward movement of salt can also be determined from the difference between sediment unit thickness far from diapiric influence and the unit thickness near the diapir contact expressed in m/m.y.. By examining a series of seismically identifiable stratigraphic units it is possible to track the relative rate of salt movement over time.

The results of this exercise, compiled from all available seismic profiles of southern Vesey Hamilton Salt Wall, are presented in Table 6. The lowest unit for which seismic profiles permit recognition of salt movement is the Bjorne Formation (Lower Triassic). Results, similar to those suggested by Fox (1983), indicate that evaporites were actively rising in Vesey Hamilton Salt Wall during deposition of all units from the Early Triassic through the Early Cretaceous (Albian Christopher Formation). The most rapid rates of evaporite movement correspond to periods of diapir-marginal sediment thinning in the Early Triassic (32–55 m/m.y. during deposition of Bjorne Formation), in the early Albian during a phase of sediment gravity sliding on the flanks of the salt wall (43–72 m/m.y. at the time of the Invincible Point Member) and in the late Albian (16–30 m/m.y. during deposition of the Macdougall Point Member). No salt movement is indicated for the Upper Cretaceous (Hassel and Kanguk formations). However, the evaporites have penetrated through these formations and also the overlying Expedition Formation of the

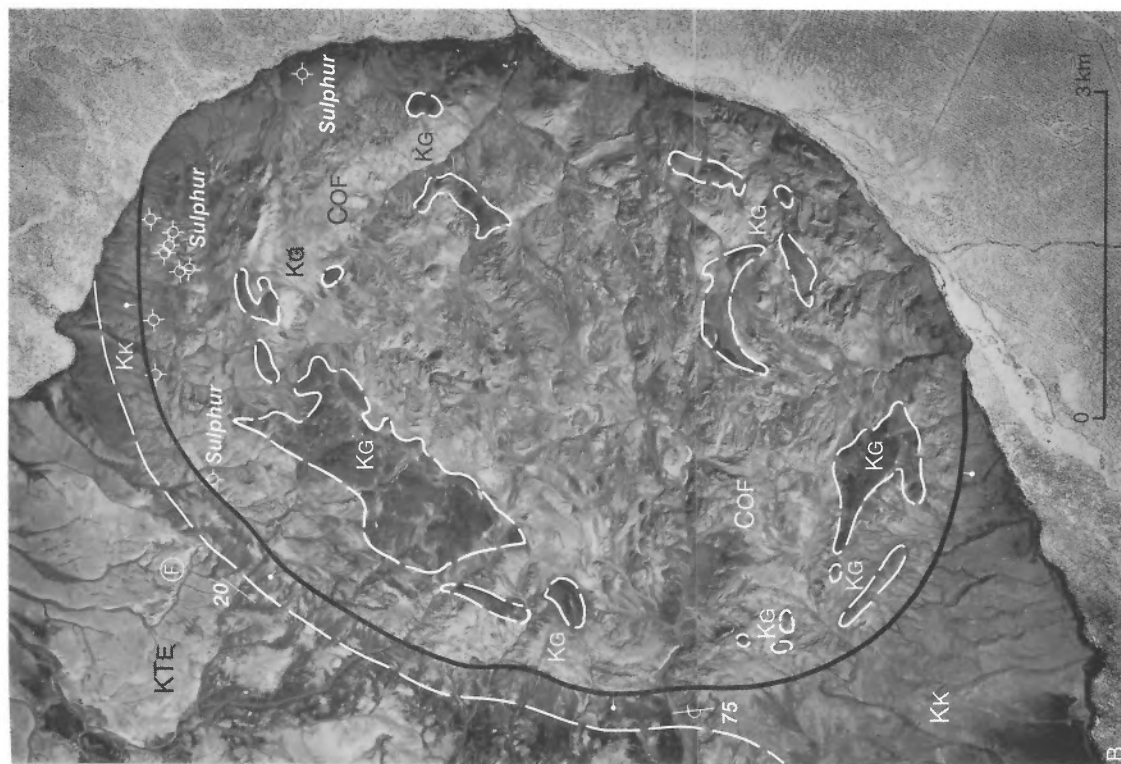
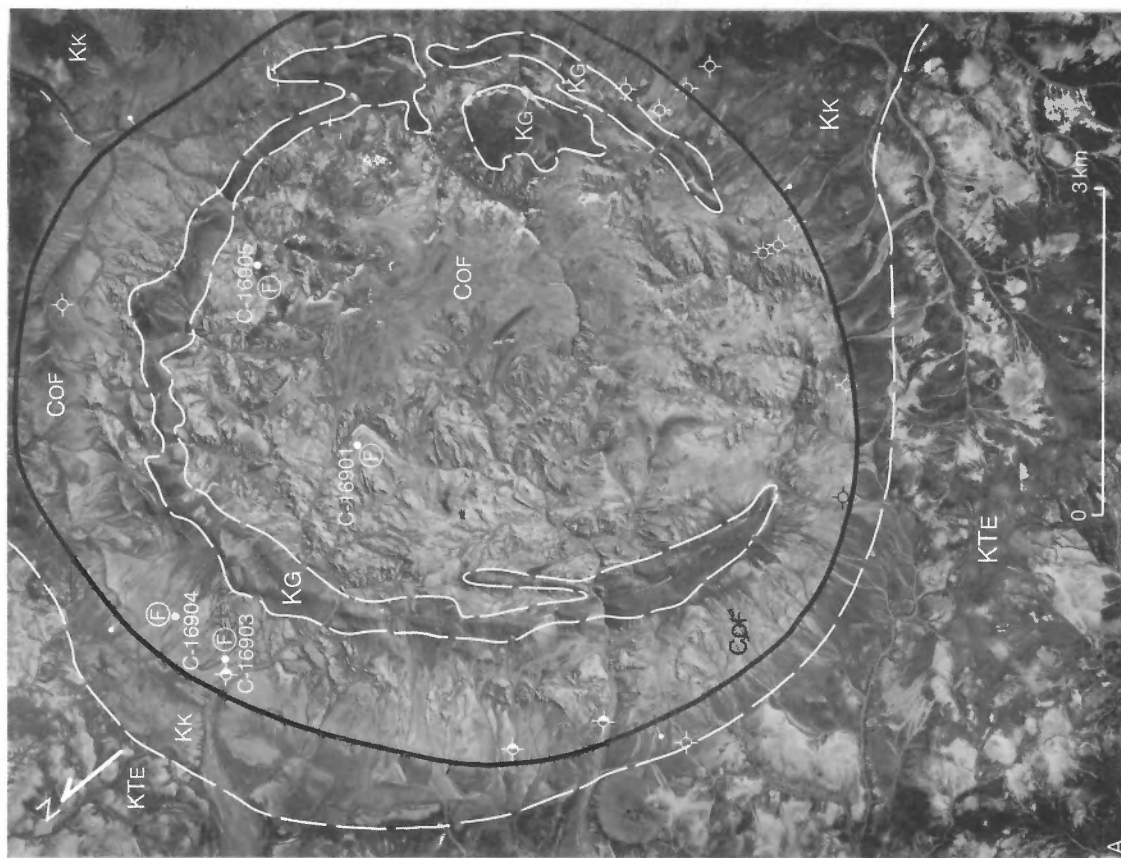


Figure 181. Vertical airphotos of Barrow Dome (A) and Colquhoun Dome (B), illustrating the internal structure, contact relations, distribution of intrusive gabbro bodies (KG), native sulphur and hydrocarbon occurrences (F), and the ammonoid fossil localities of Nassichuk (1975) as listed in Appendix 4. The fossil locality (F) in the Expedition Formation (Fig. 181A; see also Fig. 76) marks the approximate location of the Maastrichtian–Paleocene boundary (as described by Rahmani and Hopkins, 1977). CoF, Otto Fiord Formation; Kk, Kanguk Formation; KTE, Expedition Formation. See also legend, Figure 33, NAPL photos. A16764-20, -44.

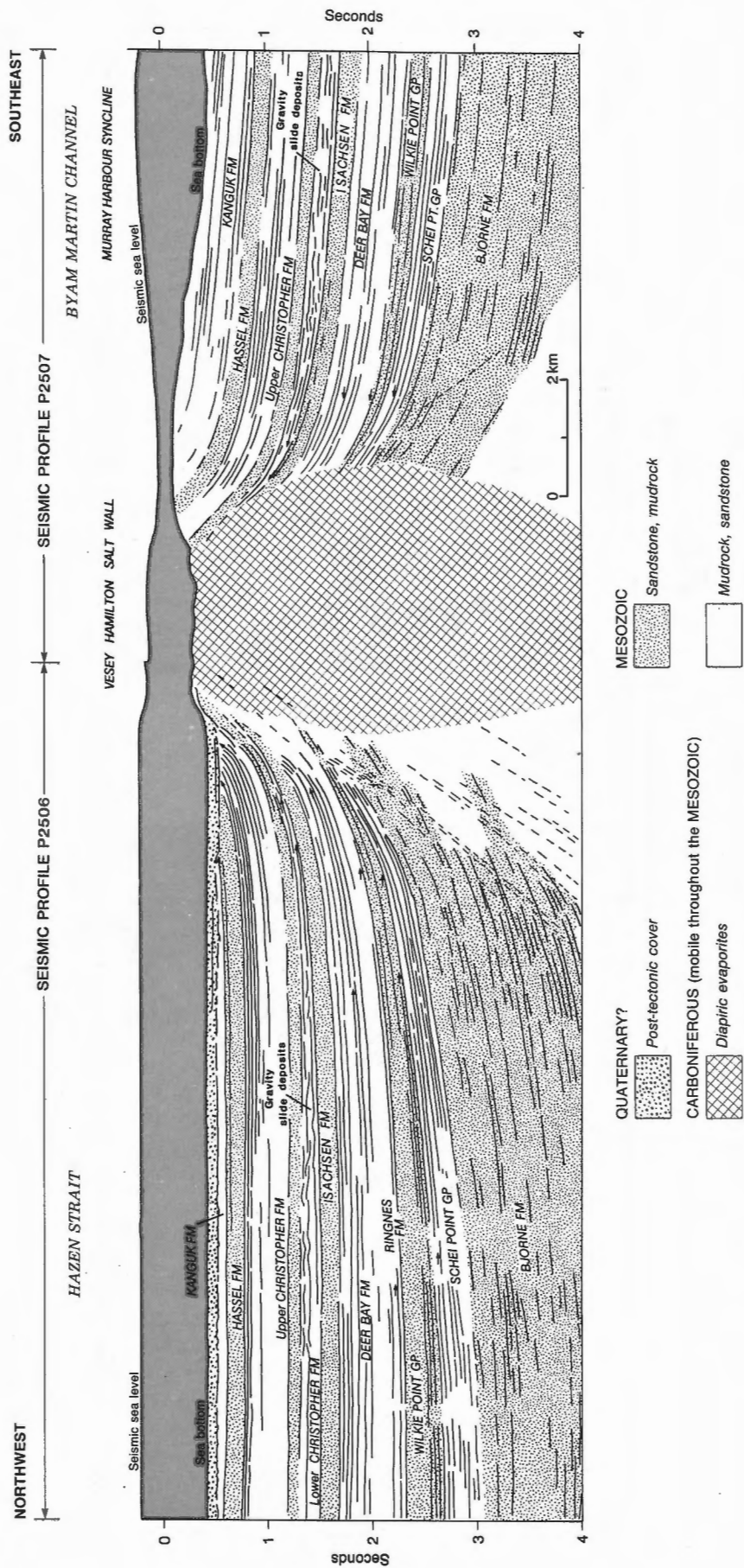


Figure 182. Line drawing of seismic profiles P2506 and P2507 adjacent to Vesey Hamilton Salt Wall.

TABLE 6

Thinning (% of maximum thickness) of seismic stratigraphic units against Vesey Hamilton Salt Wall and calculated minimum rates of diapirism for Early Triassic through Late Cretaceous time

Age	Time span (m.y.)	Formations, units	Velocity (km s ⁻¹)	Minimum thickness (%)	Minimum rise rate (m/m.y.)	Comments
Quaternary, Neogene(?)	23	unit Q, unit(?) TQ _G	2.1	?	low(?) or nil	angular unconformity below Q, TQG(?)
Paleogene(?)	12	Eureka Sound Fm.	2.1	no data	16	min. 1000 m rise of salt in Tertiary
Late Cretaceous	30	Kanguk Fm.	2.1	100%	nil	
Albian	~2	Hassel Fm.	2.1	100%	nil	
Albian	~4	upper Christopher Fm.	2.5	96%	4	
Aptian–Albian	~2	mid-Christopher Fm.	2.5	64%	15	
Aptian	~2	lower Christopher Fm.	2.5	37%	107	gravity sliding on diapir flanks
Barremian–Aptian	~3	Isachsen Fm.	3.5	65%	37	ages of gabbro dykes, sheets
Berriasian–Valanginian	15	Deer Bay Fm.	3.6	42%	21	ages of gabbro dykes, sheets
Late Jurassic	17	Awingak, Ringnes fms.	3.6	50%	18	
Early–Middle Jurassic	40	Wilkie Point Gp.	3.2	31%	7	
Early Jurassic, Late Triassic	30	Heiberg Gp., upper Schei Pt. Gp.	4.3	28%	9	
Middle–Late Triassic	15	lower Schei Point Gp.	4.3	61%	13	
Early Triassic	6	Bjorne, Blind Fiord fms.	3.8	84%	55	

Eureka Sound Group after the Paleocene (965 m in about 42 m.y. or 23 m/m.y.) and prior to erosional dissection and overlap by unconformable Quaternary(?) cover (Fig. 182).

The reason for the Late Cretaceous hiatus in diapirism may be due to a change, beginning in the late Albian, from an extensional to a compressional state of stress within this part of the Sverdrup Basin.

Eurekan Orogeny (D8)

General comments

Phase D8 structures include regional-scale open folds of the Sverdrup Basin exposed on northern Sabine Peninsula, and small folds and associated fault arrays of Sproule and southern Sabine peninsulas that have been at least intermittently active since the previous

compressive deformation (D6; Melvillian Disturbance) of the mid-Permian. Phase D8 predates unconformable Quaternary and Holocene cover and is tentatively associated with the regional influence of the mid-Tertiary Eurekan Orogeny, the effects of which are most clearly observed in the eastern Arctic Islands.

D8 structures situated within or peripheral to Melville Island's salt-based fold belt are located and named on Figure 183. Many of these structures are found either within the Sverdrup Basin or near the contact between the Sverdrup Basin and the exposed portions of the lower Paleozoic fold belts. It is especially worth noting that this young compression-related deformation extends well to the south of the limit of Eurekan deformation indicated on the maps of Trettin (1989) and Okulitch and Trettin (1991).

An additional aspect of D8 tectonics is regional uplift of Lower Cretaceous (Aptian-Albian) marine and nonmarine cover, erosional remnants of which are preserved across the peneplained salt-based fold belt on eastern Melville Island (see Chapter 4 for descriptions of Isachsen and Christopher formations and sections of Chapter 5 for an outline of the pre-Pliocene unconformity). Timing and magnitude of uplift (several hundreds of metres) is expressed by the depth of burial below sea level and subsequent erosional off-loading implied by the difference in thermal maturity between lignite-grade coals and organic matter preserved in the Cretaceous outliers and uncoalified wood recovered from overlying Beaufort Formation (Pliocene?). The D8 phase of uplift should not be confused with the presently elevated condition of the Melville Island topographic surface, which is primarily a neotectonic (D9) feature.

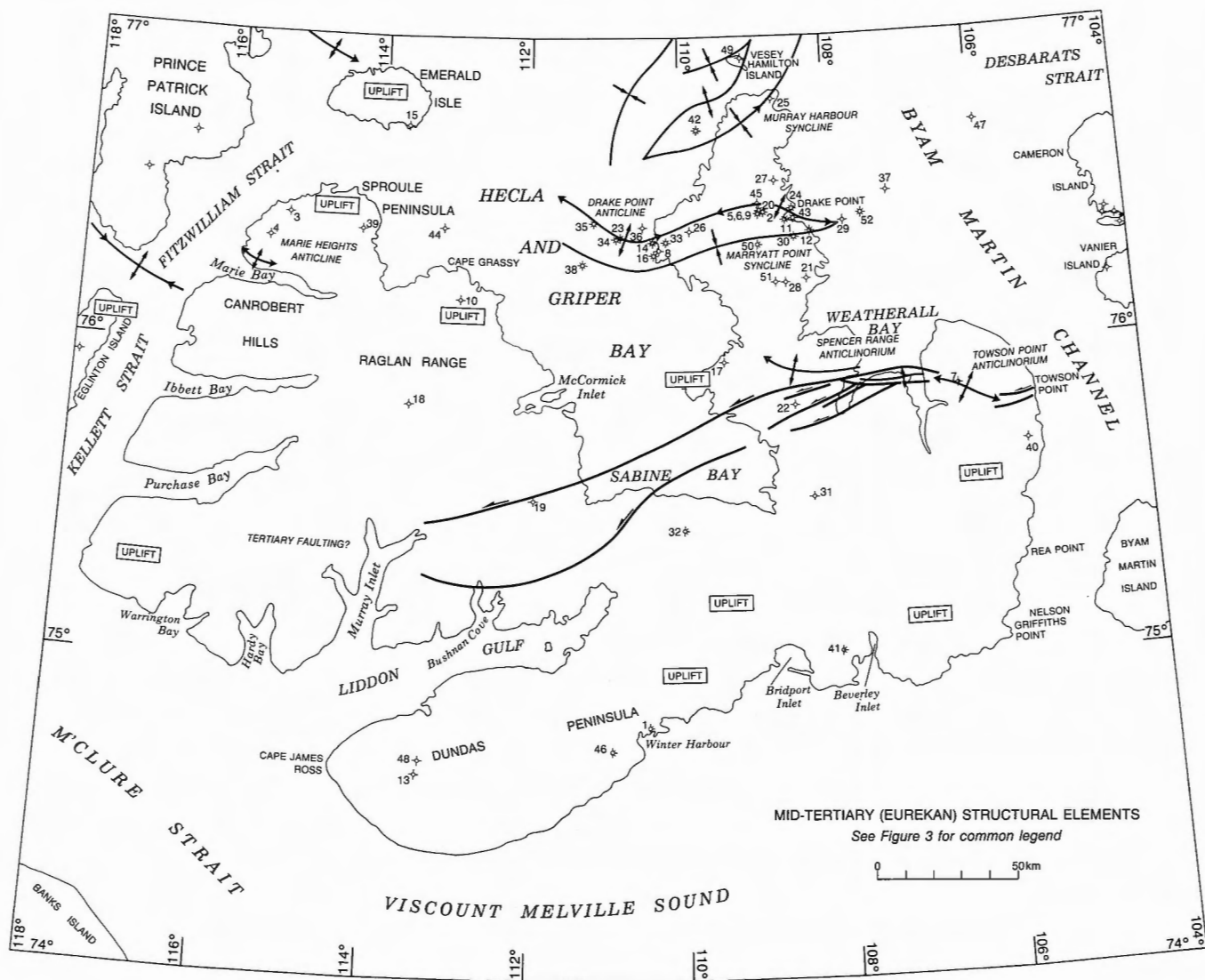


Figure 183. Tectonic elements of the Eurekan Orogeny (phase D8) in the Melville Island area.

Kinematic case histories

Minor faults occurring within cover rocks over Spencer Range Anticlinorium have also displaced the Lower Cretaceous gabbro dykes near Tingmisut Lake. Thus, although this anticlinorium has been affected by phases D2 through D5 and D7, there is evidence for additional deformation, possibly during phase D8. Towson Point Anticlinorium near the northern exposed edge of Melville Island's salt-based fold belt is physically linked to the fault array in Spencer Range and Tingmisut Lake areas and is therefore also considered to be, at least partly, a phase D8 structure.

The entire Towson Point–Spencer Range–Tingmisut Lake–St. Arnaud Hills region is rich in kinematic indicators. Minor shear planes and associated striae are especially common in Lower Devonian and Lower Permian limestones and calcite-cemented Carboniferous conglomerates. Spatially associated west- and northwest-plunging folds are also noted in the Canyon

Fiord, and overlying Permian formations northwest of the Tingmisut Inlier (Fig. 78). D8 minor faults observed within Permian limestones and Cretaceous gabbro dykes exposed near Tingmisut Lake tend to fall into two steeply dipping sets (Figs. 184, 185): a N30°E-striking set parallel to dyke trends with mostly dextral-sense slip lineations (Figs. 184B, 185B); and a steep, east-striking set with sinistral slip sense (Fig. 184B). These indicators are consistent with a set of principal stress axes for which σ_1 is subhorizontal and aligned S60°W, and σ_2 is vertical. This direction for σ_1 is similar to that obtained from kinematic analysis of the Towson Point structure (Chapter 6). Although the Towson Point Anticlinorium is primarily a D3 structure, some of the sinistral restraining bend deformation and many of the minor kinematic elements associated with this structure may have been active during D8 deformation of late Paleozoic and younger cover rocks of southern Sabine Peninsula. The main result of D8 tectonics has been to uplift Weatherall Depression and Spencer Range Uplift and to tilt these structures toward the southwest.

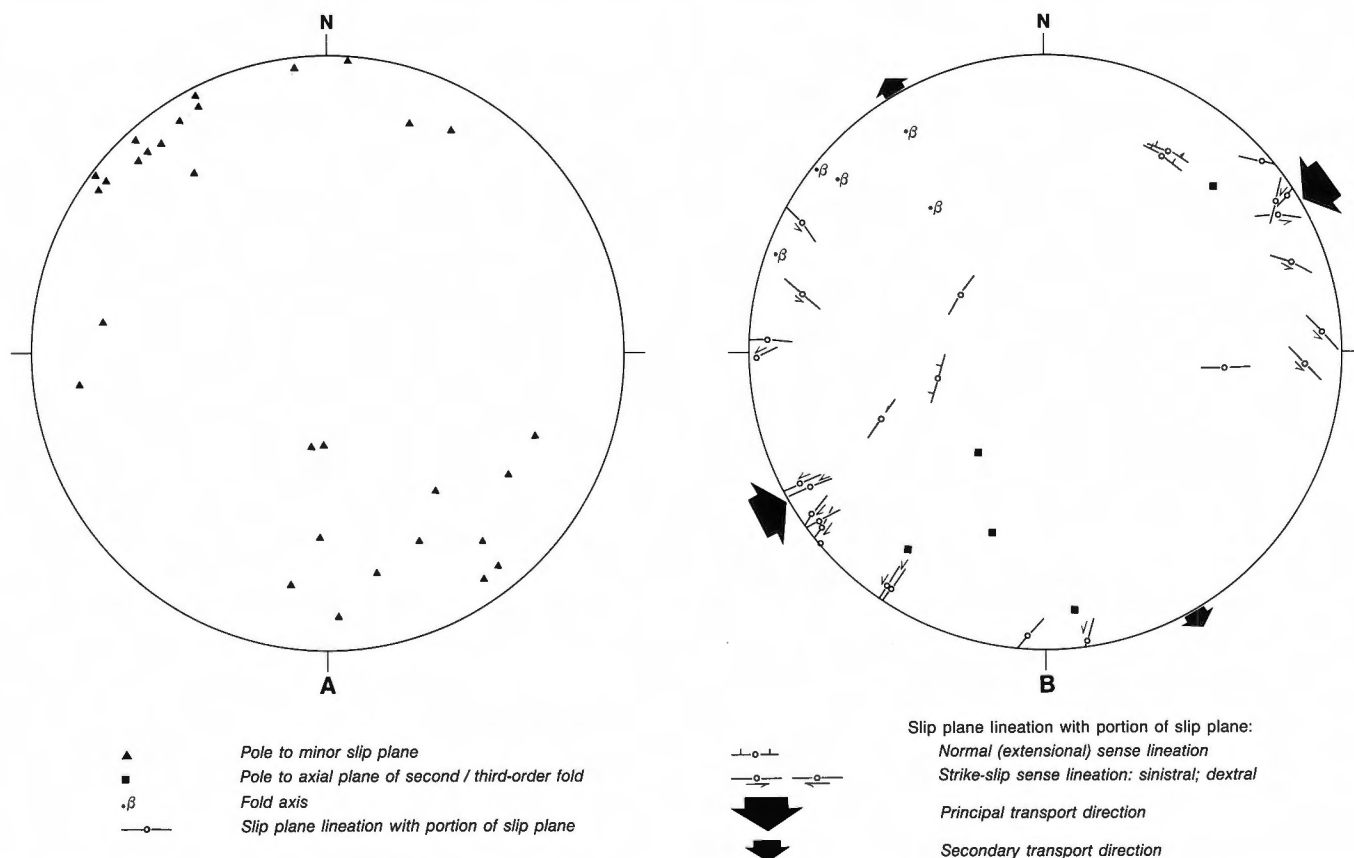


Figure 184. Lower hemisphere equal-area stereonet plots of (D8) kinematic elements and implied tectonic transport directions for deformed Carboniferous and Lower Permian strata of southern Sabine Peninsula and Spencer Range. The principal (σ_1) and secondary (σ_3) tectonic transport directions are those implied by sinistral slip on easterly striking faults, and dextral slip on northerly and northeasterly striking faults. The fold axes and poles to axial planes are also consistent with a southwesterly direction of principal tectonic transport in compression.

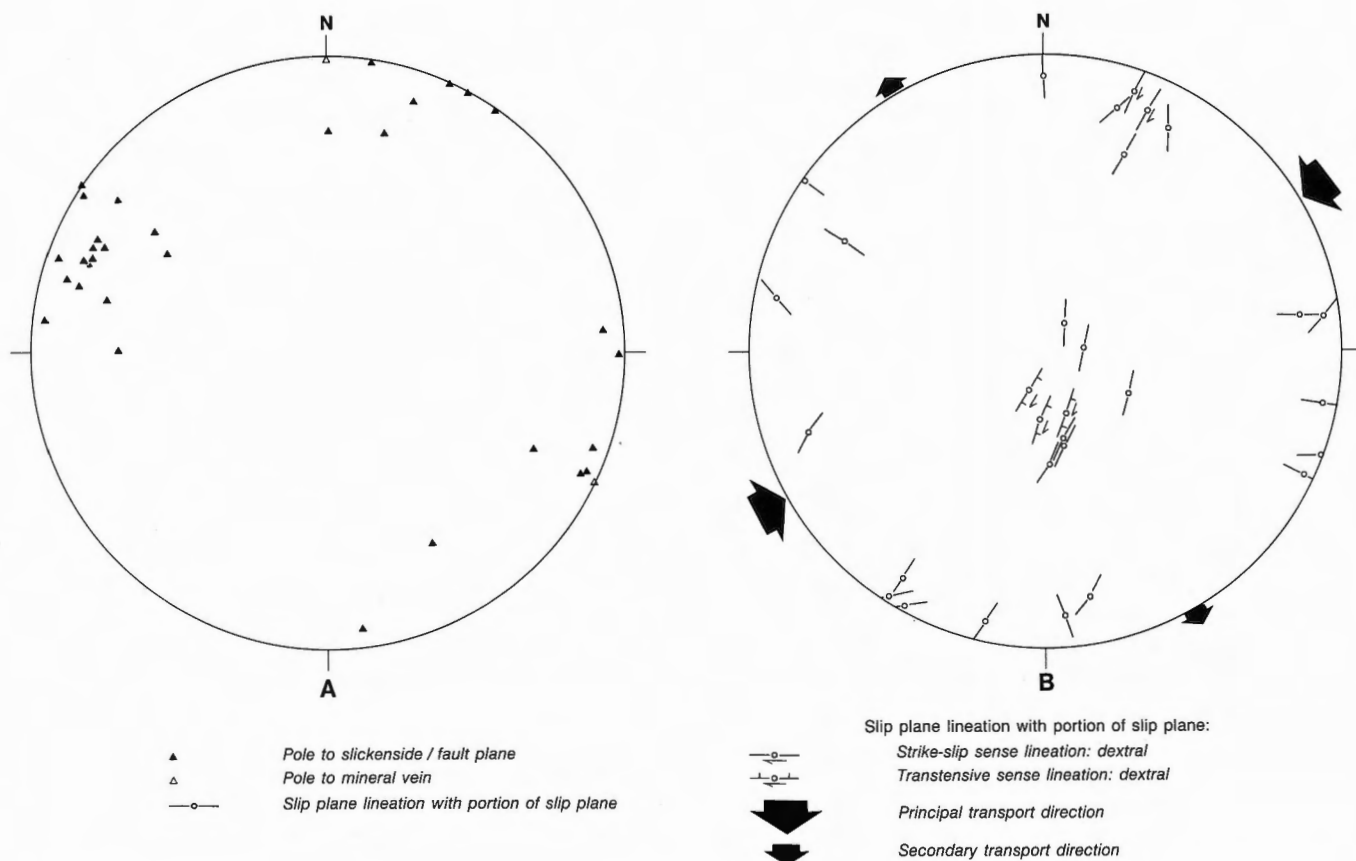


Figure 185. Lower hemisphere equal-area stereonet plots of (D8) kinematic indicators and implied tectonic transport directions for deformed Cretaceous gabbro dykes near Tingmisut Lake. Data have been collected in the vicinity of locations indicated by the letter "S" on Figure 78. The principal (σ_1) and secondary (σ_3) tectonic transport directions are those implied by dextral slip on north-northeasterly striking faults and assumed sinistral slip on easterly striking faults.

Older (D5) block rotation can account for poles to upper Paleozoic bedding scattered along a great circle that trends N20°W (Fig. 164). Other anomalous bedding attitudes, which strike variably north and northwest, and which possess steep and even vertical dips, are considered to be the result of the later phase of tilting and folding. Steep upper Paleozoic bedding is noted, for example, in Spencer Range against regional-scale (Riedel-type) shears and in the folded hangingwall of various faults located north and east of Tingmisut Inlier. Thus, Canyon Fiord strata within Weatherall Depression, previously rotated (to northerly dip angles) on the Bay Fiord detachment during the D5 creation of the depression, are rotated again, this time clockwise, to steeper westerly and southwesterly dip angles (Fig. 164). This final phase of deformation of Spencer Range Anticlinorium is probably post-Early Cretaceous and related to phase D8 (Eurekan) tectonics of the mid-Tertiary since the associated minor faults also displace the Lower Cretaceous gabbro dykes.

However, some of this deformation is post-Carboniferous (post-D5) but pre-dyke emplacement (pre-D7); the aforementioned folds within Canyon Fiord Formation near Tingmisut Inlier are clearly cut by the gabbro dykes (Fig. 78).

Drake Point Anticline is here considered to include the open, upright, anticlinal warp of Paleocene and older rocks partly exposed on northern Sabine Peninsula that contains the Hecla and Drake gas fields. In plan view the axial trace is sublatitudinal in trend with two northwesterly trending jogs situated near Drake and Macdougall points (Fig. 183). Structural culminations occur on each of the N43°W- and N55°W-trending segments, and a structural saddle occurs on the fold hinge midway between the two culminations and halfway across Sabine Peninsula. Seismic profiles (Section E) reveal that strata of the Hare Fiord Formation (Upper Carboniferous-Lower Permian) and all overlying rocks are involved in

folding. There are two possible structural configurations for Drake Point Anticline: 1) the anticline is underlain by a salt welt of Otto Fiord Formation with a subhorizontal base-of-salt detachment; or 2) folding extends downward into Franklinian basement.

Principal compressive stress axes are indicated by the orientation of en echelon culminations on northwest-trending portions of the anticline (Fig. 183). Suggested stress axes are S35–47°W and subhorizontal for σ_1 , near vertical for σ_3 on the restraining bends. These stress directions are similar to those previously determined for the Towson Point structure and the final (D8) phase of deformation on Spencer Range Anticlinorium. The transport direction is consistent with the development of deep-seated reverse faults on northwest-trending fold segments. Also kinematically compatible with these principal stress axes are the preferred alignments of evaporite diapirs in the vertical plane of σ_1 and σ_3 (S45°W). Sinistral faulting along sublatitudinal planes, and dextral slip on both pre-existing gabbro dykes and pre-existing normal faults that strike S20–45°W is also part of this system for which the maximum and intermediate compressive stress axes lie in a vertical, northeasterly striking reference plane. As there is no stratigraphic or structural evidence to indicate that the Drake Point Anticline might have existed before the Eocene, the simplest kinematic model is that this is a transpressive structure created during the Eurekan Orogeny.

The small Marie Heights Anticline, situated along the north shore of Marie Bay, is a pericline affecting Jurassic and older strata most recently during D8. There are also two older angular unconformities in this structure: one above open-folded Carboniferous Canyon Fiord Formation created after D6, and the other above tightly folded Blackley Formation created after D4.

Discussion

The present study extends the region of recognition of Eurekan compressive deformation in the Arctic Islands well to the south of the limits suggested by Trettin (1989) and Okulitch and Trettin (1991). In fact, with the present evidence for long-wavelength folds, regional-scale uplift of Paleocene and older marine strata, and strike-slip faulting across the northern peninsulas of Melville Island and additional compressive deformation within Eglinton Graben, the Eurekan Orogeny is now known to have affected the entire Sverdrup Basin.

The kinematic mechanism for the Eurekan convergence in the Arctic Islands is now partly clarified by the present study. Eurekan dextral strike-slip faults identified by Trettin (1989) and Okulitch and Trettin (1991) on the eastern boundary of the orogen across southeast Ellesmere Island and north Greenland are matched by sinistral strike-slip faults along the southern boundary of the orogen across northern Melville Island (Fig. 186). The kinematic implications are that the southwesterly directed convergence of the stable Greenland and Arctic North American plates was accompanied in the early- to mid-Tertiary by a component of northwesterly directed escape of the intervening orogen.

Recent seismicity and uplift (D9)

Although the Melville Island region is entirely within the stable North American tectonic plate, the region is not entirely aseismic. A large diffuse swarm of low- to moderate-strength earthquakes has been recorded along a N15°E–N30°E-trending zone of weakness located east of Sabine Peninsula in Byam Martin Channel (see Fig. 187). Four earthquakes in this area have registered over 5.0 on the Richter scale. The largest (Richter 5.7) was recorded on Nov. 21, 1972. First motion studies on the four largest events indicate a right-lateral strike-slip mechanism operating along N20°E-through N45°E-striking planes of weakness, and a maximum principal compressive stress direction of N65°E (plunge 5°) and N65°W through N95°W (plunge 35–40°; Hasegawa, 1977). Indicated focal depths are 22 to 27 km. A listing of principal stress directions for the entire Arctic Islands region has been compiled by Adams (1987). Fourteen out of a total of 21 stress measurements indicate a maximum principal compressive stress direction oriented N45°E through N73°E.

Some of these stress directions also lie within the range of those implied by D8 kinematic elements of Towson Point and Spencer Range anticlinoria and Drake Point Anticline. From this observation it could be concluded that some of these large Tertiary structures may be displaying some renewed tectonic activity. This is especially true for Drake Point Anticline, which is situated immediately west of the Byam Martin earthquake swarm.

Regional uplift can be considered an additional aspect of D9 tectonic activity. Average topographic

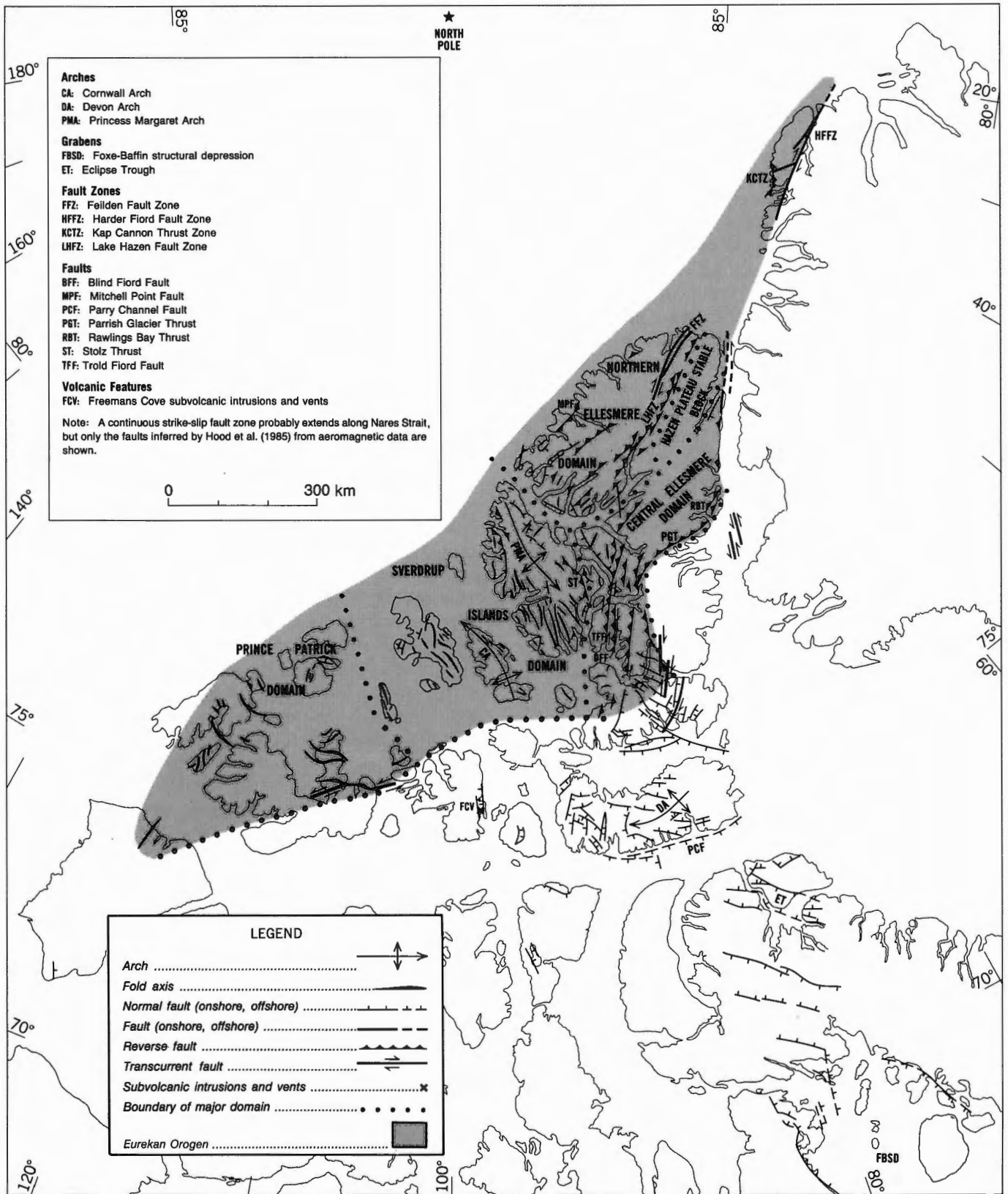


Figure 186. Kinematic elements of the Eurekan Orogen in the Canadian Arctic Islands. (Modified from Okulitch and Trettin, 1991 and Trettin, 1990.)

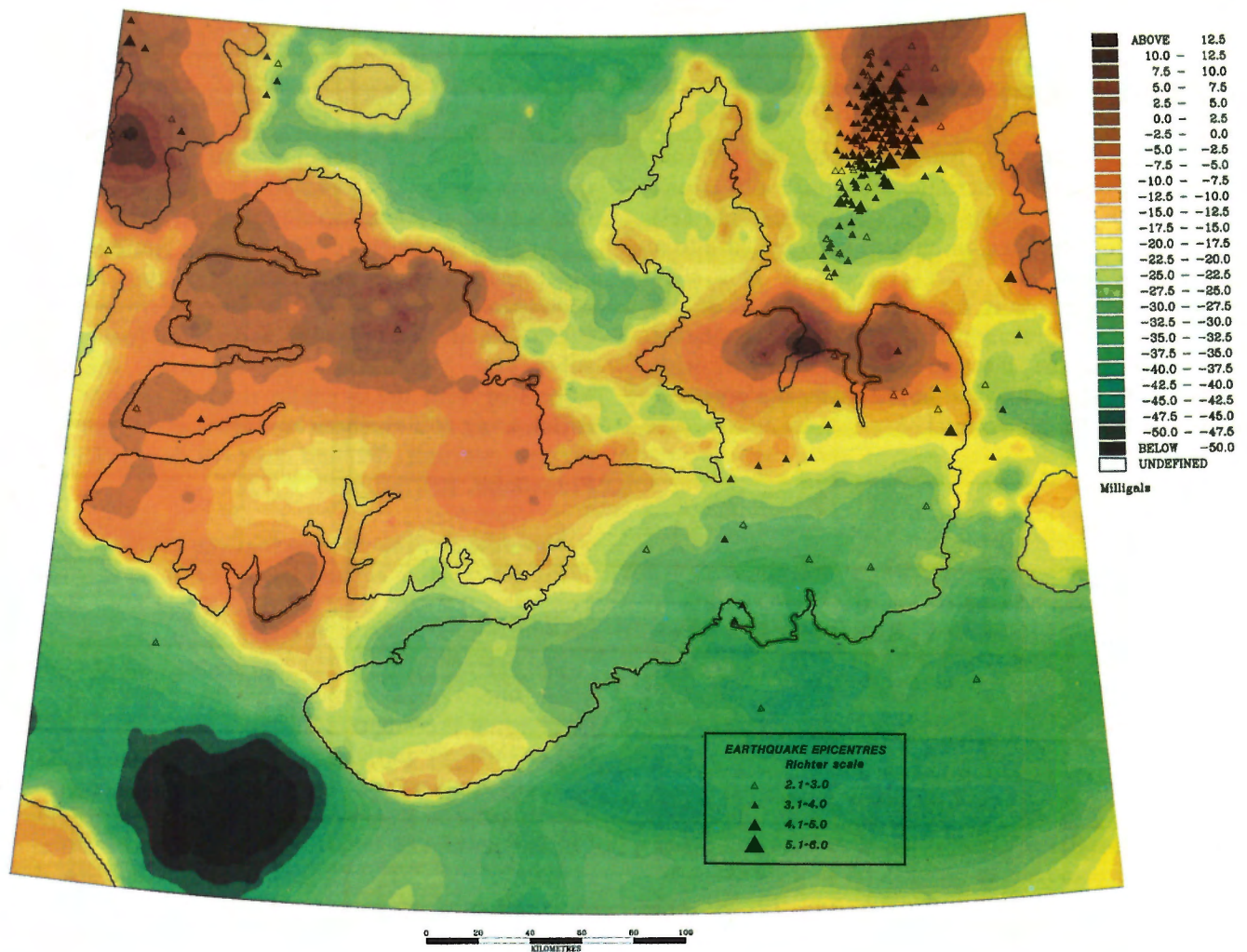


Figure 187. Recent earthquake epicentres (D9) plotted on the Bouguer anomaly for land areas and on the isostatic anomaly for marine areas. Positive gravity anomalies are associated with topographically elevated regions of Plio(?)–Pleistocene (D9) thermal uplift.

relief on Melville Island is expressed by the height of the widely exposed peneplain surface (Figs. 8, 94). This surface ranges from 750 m in the Blue Hills to about 150 m over the eastern part of the salt-based fold belt. Pliocene(?) Beaufort Formation and Early to Middle Pleistocene gravel ridges containing shield-derived erratics, marine bivalve fragments and driftwood have been deposited on this synchronously or subsequently uplifted and dissected peneplain surface of Dundas Peninsula and southeastern Melville Island (see description of units Q and TB in Chapter 4). Thus timing of uplift may be Pliocene, Early Pleistocene and younger. Sobzack and Halpenny (1990) indicated that topography above sea level in the Canadian Arctic

Islands is directly and linearly correlated with isostatic gravity anomalies, implying that relief is relatively young and probably generated by thermal expansion. The uplifted areas, defined by positive gravity anomalies on Figure 187, cannot be explained in terms of a crustal response to glacial-isostatic unloading because depressed areas recovering from glacial loads should presently feature a negative anomaly character. Available data also indicate that Melville Island and the entire western Arctic Islands north of Viscount Melville Sound has always remained peripheral to the North American continental ice sheets and therefore the region has also never been significantly depressed by past glacial loads (Vincent, 1989; Hodgson, 1989).

CHAPTER 8

DISCUSSION AND CONCLUSIONS

Sedimentation patterns, magmatic activity, tectonic styles, and derived tectonic transport directions through time for Melville Island's salt-based fold belt and the surrounding region have been compiled into a simplified correlation chart (Fig. 188). This self-explanatory chart traces the geological history of the area since the Precambrian. The tectonic phases represented on the chart are reviewed below, with special emphasis on regional implications and potential directions for future research.

D1: Precambrian rifting

Possible extension-related features of presumed Proterozoic age (deformation phase 1) include rotated blocks of acoustic basement unit sAP, syntectonic thickness variations in weakly reflective seismic packages (sP1 and sP3) of early(?) Middle Proterozoic and Late(?) Proterozoic ages, respectively, and seismically imaged intrusive sheets emplaced into an intervening package of more uniform thickness tentatively correlated with the upper Middle and lower Upper Proterozoic Shaler Group of Victoria Island. In addition, refraction surveys (Overton, 1972), and gravity models (Sobczak et al., 1986; Sweeney et al., 1986) point to a 50 per cent thinning of the Precambrian crust over a distance of 300 km from the Arctic Platform south of Viscount Melville Sound to central Melville Island.

The present study favours two stages of Precambrian extension: The first stage is coeval with the formation of the lower unreflective succession (unit sP1) and the emplacement of the Mackenzie dyke swarm of the northwestern Canadian shield at 1267 ± 2 Ma (Fig. 21; LeCheminant and Heaman, 1989). The second stage includes rift-related accumulation of the upper unreflective succession (unit sP3), the outpouring of flood basalts of the Natkusiak Formation, and emplacement of the Graveyard Bay and Coronation sheets, and the Hottah, Thule and Franklin dyke swarms, the latter at 723 ± 3 Ma (Fig. 22; Heaman et al., 1990).

The N50–80°E orientations of unit sP3 isopachs and at least one low-angle normal fault (Fig. 18) permits identification of the local direction of transport in extension (N40–10°W). Considering together the

attitude of the two continental-scale dyke swarms and the attitude of the seismically imaged rift zone of Melville Island, the emerging pattern is consistent with the proposal of LeCheminant and Heaman (1989) – that a thermal plume developed under Victoria Island leading to a tectonic plate triple junction. The Mackenzie igneous event led to rifting and later widespread deposition of the Shaler Group and the correlative highly reflective succession (unit sP2) of subsurface Melville Island. Likewise, the plume associated with the Franklin thermal episode led to rifting away of a northern land mass and deposition of the syn-rift unit sP3 and post-rift lower Paleozoic Franklinian succession.

Nevertheless, the concept that the Franklin thermal event led to the accumulation of post-rift Lower Cambrian sedimentation must also take into account the 170 m.y. break in the geological history of the Arctic region between 720 and about 550 Ma. Other great uncertainties remain in the analysis of the deep-seated Precambrian(?) geology of Melville Island. Reflections on seismic profiles lie at the limits of coherent primary data. The existing grid of reprocessed seismic profiles does not permit the closing of loops between correlated reflection segments. Correlation of Precambrian(?) seismic packages with surface rock units situated elsewhere in the Arctic Islands is particularly speculative. The upper unreflective succession, for example, may eventually prove to predate the Shaler Group, and the highly reflective succession could represent a metamorphic suite in crystalline basement. Evidence for northward thinning of the sub-Cambrian(?) crust from Victoria Island to Melville Island is also tenuous. For example, estimates of crustal thickness beneath the Arctic Platform rely entirely on gravity models of the crust beneath Somerset Island, which is situated 350 km to the east.

Also difficult to reconcile in the context of crustal extension are: 1) the apparent local angular unconformity beneath the highly reflective succession; 2) anomalously thick intervals of the highly reflective succession; 3) the Precambrian synclinorium of western

Figure 188. Simplified correlation chart of the Arctic Platform, Franklinian Mobile Belt, and Sverdrup Basin in the Melville Island region, together with major tectonic and magmatic events and possible tectonic transport directions from the Precambrian to the Quaternary.

Dundas Peninsula that affects all seismic successions down to and including sub-Proterozoic acoustic basement; and 4) the widespread angular unconformity beneath Lower(?) Cambrian incised valley fill.

Early(?)–Middle Cambrian thermal subsidence

The most compelling indirect evidence for a Late(?) Proterozoic phase of rifting is the pattern of post-rift thermal subsidence expressed by the logarithmic fall-off of sediment accumulation rate beginning in the Early(?) Cambrian (Fig. 54). Isopachs of trailing margin sedimentation (Fig. 55) also confirm the approximately N65°E orientation of the shelf margin and the N25°W direction of extensional transport and spreading within oceanic realms situated in the northwest. Unconformity-bound seismic sequences involved in the Early(?) and Middle(?) Cambrian interval of basin subsidence have been correlated from an analysis of thickness variation and seismic depositional facies with coeval miogeoclinal formations of Judge Daly Promontory, eastern Ellesmere Island. It is concluded that incised valley-fill seismic unit sC1A at the base of the Cambrian has no outcrop equivalent in the Arctic Islands, and that units sC1B, sC1C, sC2 and sC3 are roughly equivalent to the Kennedy Channel and Ella Bay formations, the Ellesmere Group, and Scoresby Bay formations, respectively.

These conclusions are extremely speculative and potential pitfalls are evident. First, the correlated distance is no less than 1100 km, albeit parallel to a probably common Early Cambrian outer shelf. Second, use of thickness as a factor in correlation requires a confident knowledge of interval velocity. The chosen velocity (5.7 km s⁻¹) is derived from refraction velocities of Overton (1972) estimated on the upper part of the lower Paleozoic carbonate bank succession. If thick clastic rocks underlie carbonates in the Lower Cambrian, then lower interval velocities would be expected. At 5.7 km s⁻¹, the thickest interval assigned to units sC1 through sC3 is 5600 m thick (Fig. 55). At 5.0 km s⁻¹ the same interval is 4900 m thick, and at 4.6 km s⁻¹, 4500 m.

The third potential pitfall lies in the difficulty of local correlation of Lower(?) Cambrian units across deep-seated transpressional faults such as those beneath Nias Point Anticlinorium and Apollo Anticline (Section I, Note 23). This problem is compounded by the absence of tie lines and parallel seismic profiles that might confirm the interpretation of this critical area.

D2: Mid(?)–Cambrian faulting

Normal faulting, block rotation, and syntectonic sedimentation in the mid(?)–Cambrian seismic interval is convincingly illustrated on profile P1135 of Blue Hills Syncline (Section I; Fig. 30). Similar structures can also be interpreted at the limits of seismic resolution on other profiles across the northern part of the island (Sections C, D, G and H).

On profile P1135, the growth-faulted interval lies in seismic unit sC4, a sea-level lowstand depositional unit that is correlated with the lower Cass Fjord Formation. The Cass Fjord of the outer miogeocline is exposed on central Ellesmere Island and is also intersected in the Cornwallis Central Dome well of Cornwallis Island.

A major sequence boundary is identified seismically beneath sC4 and cratonward (beyond the preserved limits of sC4) beneath unit sC0. This same surface is tentatively traceable into the sub-Cass Fjord unconformity, which in the eastern Arctic Islands represents an erosional hiatus that has locally removed the entire underlying Lower Cambrian package. Thus, a sea level minimum in the mid-Cambrian has Arctic Islands-wide significance. Growth faulting at this time is attributed to gravitational sliding induced by instability and erosion of the off-shelf sediment load. Not entirely ruled out, however, is the possibility that mid(?)–Cambrian erosion and faulting is due to thermal uplift and lithospheric extension.

Additional uncertainties lie in the age of specific seismically identified faults apparently active during the mid-Cambrian. On Sections C, D, G and H, the growth-faulted interval is variously placed in either unit sC2 or the lower part of unit sC3. Although timing of growth could vary from one location to another, there are two alternatives to consider. Miscorrelation of reflections is a distinct possibility in these areas. Apparent growth can also be generated by a younger phase of strike-slip faulting. These uncertainties might be resolved through the reprocessing and interpretation of a more complete grid of migrated seismic profiles.

Late(?) Cambrian through Early Ordovician (mid-Arenig) subsidence

The pattern of thermal subsidence typical of the Early(?) Cambrian resumed after the mid(?)–Cambrian sea-level lowstand event. The principal feature of the Late(?) Cambrian and Early Ordovician of Melville Island was stable sedimentation on a slowly subsiding outer shelf ramp. Seismic depositional facies combined

with drill-hole data from the upper part of the package point to shallow-marine carbonate-dominated sediment accumulation for most of the time interval. This embraces seismic units sCO, and sO and correlative carbonate formations of the Franklinian shelf and miogeocline of the eastern and southern Arctic Islands (upper Cass Fjord, Cape Clay, Blaney Bay and Eleanor River formations). Depositional isopachs (Fig. 59) continue to define a north-northeasterly trend for the trailing margin. Sea-level highstand sedimentation during this time caused the shelf edge to prograde out over the pre-existing mid(?)—Cambrian lowstand deposits reaching (by the mid-Arenig), a new position 100 km to the northwest.

The Ordovician intrashelf basin and basin cover

The late Arenig marks another major sea-level lowstand in the depositional history of the Franklinian shelf. The occurrence of quartz sand, preserved in slope deposits of the uppermost Canrobert Formation, testifies to the exposure and erosion of the North American craton at this time. Carbonate debris flows in the Canrobert Formation also point to within-wave-base scouring of the upper basin slope during the sea-level minimum. Overlap of these lowstand deposits by transgressing graptolitic mudrock and radiolarian chert of the deep water basin is coeval with the creation of the intrashelf basin and intervening peritidal carbonate rim. The axial line of the intrashelf basin, and the depositional limits of rock salt and anhydrite that fill the basin possess trends that parallel the underlying Upper(?) Proterozoic faults and rift basins, and isopachs of the Cambrian(?) miogeocline.

Important features of the intrashelf basin fill are the thickness maxima along the downslope (northern) edge of the basin (Fig. 62). Evaporites in the depocentre are over 800 m thick. This thickness is that determined after palinspastic restoration of the salt layer, which has involved the removal of harmonic thickness variations caused by subsequent D3 folding and shortening within and above the salt layer. Less successfully taken into account are tectonic thickness variations induced by sub-salt D4 and younger deep-seated deformation. Nevertheless, it is reasonable to expect that the illustrated restored thickness of evaporites in the intrashelf basin is due to a combination of 1) primary depositional thickness and 2) gravity-induced postdepositional preorogenic downslope creep of salt.

The intrashelf basin disappeared during the Llanvirn as evaporites of the lower Bay Fiord Formation gave

way to less restricted and more widespread shelf carbonate sedimentation of the upper Bay Fiord and Thumb Mountain formations.

The intrashelf embayment

The intrashelf embayment represents an unrestricted marine seaway that flooded both the Late Ordovician shelf rim and the coeval carbonate strata lying above the Middle Ordovician intrashelf basin. The embayment in the Melville Island area forms an arm of the Franklinian deep water basin partly enclosed by shallow-marine carbonate platforms situated over the breached shelf rim. The principal features of the embayment are widespread sediment starvation and progressive deepening and widening from the Ashgill, when it was created, through to the early Eifelian, when it was progressively filled with foredeep mudrock. The carbonate banks on the shelf rim and on the edge of the southern shelf display a pattern of upward and outward growth during sea-level highstand cycles, alternating with periods of exposure and transgressive flooding.

The concept favoured in the present account is that flooding events in the history of the intrashelf basin are linked to sinistral plate convergence and discrete phases of sediment and tectonic loading of distant segments of the contiguous shelf beginning in North Greenland in the early Late Llandovery (Higgins, et al., 1991).

The Devonian foredeep

By latest Emsian or earliest Eifelian time, south-westerly prograding orogen-derived siliciclastic sediment gravity flows, filling the Franklinian deep water basin, had reached the base of slope of the shelf rim platform of northwestern Melville Island (Figs. 68, 69). A separate foredeep sediment lobe invaded the intrashelf embayment from the northeast in the early Eifelian, initially following the bottom contours of the embayment around the southern flank of Towson Point carbonate platform. A third lobe, prograding from the north in deep water, eventually flooded the western flank of the Towson Point platform, simultaneously overlapping the carbonate platform toward the east and prograding into the embayment over the slope and rise of the carbonate bank to the west. By the middle Eifelian, the three siliciclastic sediment lobes had coalesced into a single south-westerly prograding delta front.

The direction of filling of the intrashelf embayment is readily defined by the attitudes of seismically imaged clinoforms (Fig. 68). These clinoform trends serve to place a lower age limit on the onset of folding in the salt-based fold belt. If the folds had already existed during progradation of the foredeep mudrock, then the submarine topography between the folds would have influenced the direction of sediment flow. In fact, the trends of foredeep clinoforms are all subparallel to each other and oblique to fold trends. It can be concluded from this that folding of the foredeep succession began not before the late Eifelian. Other geological models could invoke the onset of folding beginning either during the latest Givetian or during the late Frasnian–early Famennian. There is, however, no clear evidence for convergence of stratal reflections over most anticlines and thus no direct evidence of widespread folding during deposition of the preserved portion of the Devonian clastic wedge.

A significant unresolved question remains concerning the provenance of sand contained in the Devonian clastic wedge. For the Upper Devonian Beverley Inlet and Parry Islands sequences, the abundance of chert in the package testifies to uplift of the lower Paleozoic deep water basin in the north and erosion of rocks similar to the Ibbett Bay Formation (Embry and Klován, 1976). However, the Middle Devonian Hecla Bay Sequence actually displays the highest sediment accumulation rate (Fig. 54). It is the source of sand in the contained formations that remains uncertain. Provenance could be characterized and potentially identified through the analysis and absolute dating of the heavy mineral fraction.

D3: first phase of the Ellesmerian Orogeny

Biostratigraphic data obtained from latest preorogenic and earliest postorogenic strata allows the Ellesmerian Orogeny of Melville Island to occur anytime between the late (not latest) Famennian and the Bashkirian: a time span of about 40 m.y. However, at strain rates of 1 to 5 cm yr.⁻¹ the entire exposed portion of the fold belt could be created in only a 2.5 to 0.5 m.y. time interval. This means that the Ellesmerian Orogeny could have occurred entirely within the late Famennian after deposition of the Parry Islands sequence. The reasons for the short deformation interval are twofold. First, maximum horizontal shortening is only 28.4 km over the 180 km width of the belt (13.6%). Second, high strain rates are predicted for salt-based orogens like the Parry Islands Fold Belt, for which basal slip is aided by the very low shear strength of salt.

Deformation on salt is considered the main reason for the distinctive structural style of the region. This style is created by three rigid tectonic units (the Cambrian(?)–Lower Ordovician miogeoclinal wedge, the Middle Ordovician–lower Middle Devonian carbonate beam, and the siliciclastic formations of the Devonian clastic wedge), and two intervening ductile layers (the evaporites of the Ordovician lower Bay Fiord Formation, and the basin-fill mudrocks of the Middle Devonian Cape De Bray Formation). The lower rigid layer formed a stable surface for sliding below the lower ductile layer. Horizontal stresses, however, were transmitted through the medial rigid beam and buckling and faulting began in the beam. Room problems created by concentric folding can be resolved by ductile flow of salt in anticlinal hinge areas to create compressive stratiform salt welts. Theory also predicts that the south-directed, near-horizontal shear stress, and near-horizontal dip of the basal detachment are responsible for the equal occurrence of north- and south-vergent thrusts in the rigid beam. These thrusts are arranged in relaying and sinistral en echelon sets beneath each surface anticline. In addition, thrusts of one vergence are linked up- and downsection to thrusts of opposing vergence.

Sets of conjugate thrusts in the medial rigid beam have been used to determine local transport directions and implied axes of maximum horizontal compressive stress. Together with kinematic study of minor structures of the Towson Point Anticlinorium and Canrobert Hills area, results indicate that arcuation of the fold belt and subsurface thrust system has been accomplished by a combination of radially transported thrusting and minor components of oblique slip, and extension on normal faults and cross-fibre calcite veins that are perpendicular to the fold belt.

While thrusts are dominant in the medial rigid beam, long-wavelength folds are the only common form of shortening in the upper rigid package mostly exposed at surface. This constitutes a fundamental problem in the understanding of Melville Island's salt-based fold belt. The horizontal shortening of the upper rigid package is apparently only 32–53 per cent of the shortening in the medial rigid beam. The preferred solution to this problem involves a combination of tectonic compaction and tectonic thickening of the Devonian clastic wedge in the early stages of deformation and the initiation of a low-taper triangle zone enveloping the rigid beam in the later stages. However, the confirmation of these ideas requires proof of both volumetrically adequate and widespread bedding-parallel strain in the Devonian clastic wedge and the existence of related mesoscopic and microscopic deformation fabrics.

The style of structures created above the lower ductile layer is apparently unrelated to depositional facies changes. Indeed, the tectonic fabric of the fold belt is oblique to nearly all facies fronts and related potential field geophysical anomalies. Although the deformation ends at the limit of the evaporitic facies of the Bay Fiord Formation, the folds generally terminate in a sinistral en echelon pattern against the facies transition (Fig. 88). For other facies, such as the Lower Devonian carbonate bank of the Towson Point platform, the sinuous bank edge is situated variably within the footwall and hangingwall of at least four major sublatitudinal thrusts. In contrast, the wavelength and amplitude of folds above the salt layer are at least qualitatively related to thickness of the two ductile layers and the thickness of the medial rigid beam. Quantitative analysis of these relations, employing the techniques of Ramberg (1959, 1970), is considered beyond the scope of the present study but may prove a useful avenue for future research.

D4: second phase of the Ellesmerian Orogeny

Deep-seated folds oblique to the trend of the salt-based folds and thrusts are identified by surface map patterns and also mapped on seismic profiles at the level of the Eleanor River Formation. They affect the entire Cambrian(?) through Devonian succession. This deformation partly overlaps and is partly younger than the above-salt D3 structures. A sinistral transpressive tectonic setting is indicated that includes south-directed first-order (long wavelength) sublatitudinal periclinal folds and an oblique set of faults that strike N50–90°E. The oblique faults are subparallel to potential field anomalies, isopachs, and related anisotropic features created on the upper(?) Proterozoic through Ordovician, rifted and trailing margin in the Melville Island-area.

In the grander frame of reference, the southerly principal transport direction for both D3 and D4 phases of the Ellesmerian Orogeny is oblique to the northeasterly trend of the lower Paleozoic trailing margin in the Arctic Islands. This confirms the observations from the stratigraphic record of Silurian and Devonian orogen-derived siliciclastic rocks, that the Ellesmerian Orogeny was the last of a series of sinistral transpressive deformations resulting from the oblique convergence of a northern landmass with ancestral North America. Although zones of potential strike-slip deformation have been identified (along the north margin of the Ordovician intrashelf basin and along the south margin of the coeval deep water basin) magnitudes of lateral offset do not appear to be large.

D5: Sverdrup Basin rifting

Regional mapping points to the existence of twelve syntectonic depressions and eleven uplifts in the Carboniferous rift belt of the ancestral Sverdrup Basin throughout the northern Melville Island area (Fig. 161). Gravitational slip on pre-existing north-dipping and also south-dipping Ellesmerian thrusts and other inclined planes of weakness, (notably situated in the Cape De Bray and Bay Fiord formations on the limbs of first-order Ellesmerian anticlines), have facilitated the development of these half-grabens and horst-related structures. Graben-fill Canyon Fiord Formation displays seismic and sedimentological evidence for syntectonic sediment accumulation and growth faulting during Late Carboniferous (Bashkirian) through Early Permian (Sakmarian–Artinskian) time.

The evaporites contained within the diapirs of northern Sabine Peninsula and adjacent marine areas also probably accumulated in a rift-related setting. Evaporite deposition, dated by contained ammonoids (Nassichuk, 1970; Appendix 4) and, by inference, the related extensional deformation, occurred in the Serphukhovian and Bashkirian.

D6: rift inversion (the Melvillian Disturbance)

The D5 half-grabens that formed during the previous deformation phase were partly inverted during the mid-Permian (Kungurian–Roadian) Melvillian Disturbance. Effects of the D6 disturbance are most obvious in the Canrobert Hills and are manifested by structures involving the Canyon Fiord and underlying formations, all of which are truncated by a widespread sub-Trold Fiord Formation (sub-Wordian) angular unconformity. Mesoscopic features include coaxially refolded first- and second-order Ellesmerian folds, new third-order folds, detachment faults, reverse faults, and dextral strike-slip faults that parallel the N50–80°E anisotropy of the Upper(?) Proterozoic (D1) rift zone and the lower Paleozoic miogeocline of subsurface Melville Island. Kinematic indicators suggest a southerly through southeasterly direction of compressive tectonic transport during D6. The effects of the disturbance are also indicated over the hinge of Spencer Range Anticlinorium on Sabine Peninsula by the unconformity above the Great Bear Cape Formation (upper Artinskian), by the distribution of the syntectonic clastic wedge of the Sabine Bay Formation which fringes the region of Melvillian (D6) deformation to the northeast, and by growth faults that die out in the Sabine Bay and lower van Hauen formations.

Considering the overall pattern of mid-Permian inversion tectonics across northern Melville Island, the degree of uplift and shortening associated with the D6 inversion event decreases progressively from west to east. At the eastern edge of the belt on southeastern Sabine Peninsula, breaks in sedimentation through the mid-Permian are not manifested by obvious tectonic activity. In contrast, mid-Permian uplift and inversion-related shortening at the far western edge of the deformed belt in western Canrobert Hills has caused complete erosion of the entire Upper Carboniferous and Lower(?) Permian rift-associated redbed succession.

On a more regional scale, the northeasterly-trending folds of Banks Island and Minto Uplift may also have been generated during the D6 Melvillian Disturbance (Figs. 88, 96).

D7: the Mesozoic igneous event

The end of the Melvillian Disturbance marks the onset of passive sediment accumulation in Sverdrup Basin. Nevertheless, minor growth faulting identified on seismic profiles continued locally along the basin margin down through the Late Permian (Wordian). Related and subsequent sediment loading caused gravitational instability and diapiric rise of (Carboniferous) Otto Fiord evaporites beginning probably during the Permian and certainly no later than the Early Triassic. Diapirism continued to the end of a period of rapid gravitational inversion in the late Early Cretaceous (Aptian). Sand was derived primarily from the southern margins of the basin between the Permian and the early Middle Jurassic. After the Aalenian, provenance of sand was from the west and southwest (Harrison et al., 1988). The post-Aalenian Middle Jurassic marks the onset of D7 rifting along planes of weakness that are marginally oblique and parallel to the modern continental margin west of Prince Patrick and Banks islands, respectively. Evaporite diapirism and rifting also overlap the period of emplacement of a N- through N45°E-trending subsurface swarm of gabbro dykes, and related linear magnetic anomalies and either coeval or older sills and sheets dated radiometrically to between 152 ± 6 (Volgian) and 123 ± 6 Ma (Aptian). The dyke swarm has been emplaced into the Sverdrup Basin succession and both Canrobert and Parry Islands fold belts. The shallow manifestation of the swarm is a parallel system of keystone grabens. The indicated transport direction in extension is perpendicular to the plane of the dykes, or roughly N70–45°W and subhorizontal.

The age of the dyke swarm and the age of the associated extension faulting are critical to the understanding of the timing of rifting and spreading within Amerasian Basin. Evidence from the present study suggests that the local termination of magmatic activity and extension-related diapirism in the Aptian–Albian marks the onset of spreading within the Amerasian Basin. Basaltic volcanism, however, continued throughout the later Early Cretaceous and Late Cretaceous in the northern Arctic Islands (Embry and Osadetz, 1988). Concern has also been raised by Embry (pers. comm., 1988) as to the reliability of radiometric ages determined by Balkwill and Fox (1982) and quoted in the present work. The determination of precise U–Pb ages for the dykes and subsurface sills of the western Arctic Islands should be considered an important direction of future study.

D8: the Eurekan Orogeny

The post-Aptian Cretaceous was a period of apparent tectonic stability and passive sedimentation over dormant Otto Fiord diapirs. A final phase of diapiric activity probably coincided with the development of other structures created during or subsequent to the Eurekan Orogeny (Eocene–Oligocene). Tectonism within the salt-based fold belt during D8 is limited to several hundred metres of uplift as implied by the estimated thickness of off-loaded cover on lignite-grade coal and organic matter within the post-peneplain Lower Cretaceous strata of the Isachsen and Christopher formations.

Low-amplitude buckling, tilting and some faulting during D8 is recognized, however, in the northern part of the salt-based fold belt and within the southern Sverdrup Basin. Kinematic elements of Towson Point and Spencer Range anticlinoria and Drake Point Anticline are consistent with a sinistral transpressive setting for which the principal D8 transport direction in compression is subhorizontal and varies locally between S35°W and S60°W. The main kinematic features of the Eurekan Orogeny in the western Sverdrup Basin and Parry Islands Fold Belt are: northwesterly trending periclinal; dextral planes of slip along pre-existing D7 keystone faults and D7 gabbro dyke walls; and westerly striking sinistral faults that are parallel to and that may also have reactivated Ellesmerian (D3 and D4) thrusts and late Paleozoic (D5) extension faults. These structures and transport directions are consistent with the theory reviewed by Trettin (1989) that the Eurekan Orogeny resulted from the northeast–southwest convergence and counter-clockwise rotation of the ancestral Greenland tectonic

plate with respect to the Arctic Islands portion of the North American plate during the coeval early- to mid-Tertiary spreading within Labrador and Baffin Bay basins. The Greenland-North American convergence has resulted in a partial tectonic "extrusion" of the Eurekan Orogen toward the northwest.

D9: Neotectonic activity

Recent earthquakes, most of which are scattered along a N15-30°E within-plate zone of crustal weakness at 22 to 27 km beneath Byam Martin Channel, have ranged

in magnitude to 5.7 on the Richter scale. First motion studies by Hasegawa (1977) define a dextral sense of slip along the zone and a southeasterly direction of tectonic transport in compression. These and other stress indicators collected from boreholes by Adams (1987) indicate that the currently active principal stress directions are not unlike those determined for the (phase D8) Eurekan Orogeny. The Arctic Islands, including Melville Island's salt-based fold belt, has also experienced a Pliocene(?) and younger D9 phase of thermal uplift as implied by the linear correlation of isostatic gravity anomalies and topographic relief (Sobzack and Halpenny, 1990).

CHAPTER 9

ECONOMIC GEOLOGY

Economic minerals

Occurrences

Mineral occurrences of economic interest on Melville Island, listed in Table 7 and located on Figure 189, include base metal minerals of copper, lead, and zinc, and the industrial minerals fluorite, barite, hydroxypapatite (in phosphorite), and native sulphur. Thick and widespread accumulations of bedded and tectonized rock salt (halite) also exist in the subsurface.

Locality 1

Copper mineralization occurs in a fault bounded outlier of the Canyon Fiord Formation at an occurrence situated 24.7 km east-northeast of the head of Ibbett Bay (Table 7, loc. 1; Fig. 170). The outlier, measuring 1.5 km by 1 km, comprises interbedded red and yellowish weathering coarse pebbly sandstone, chert pebble conglomerate and lesser limestone. These Carboniferous strata dip to the south at 15° and are truncated down-dip by a horizontal detachment fault above older Cape De Bray Formation. The copper occurrence is situated at the east end of the outlier. The mineralization was discovered in a muddy talus apron immediately downslope from the weathered bedrock source. Concentration of copper sulphides is highest in a sandstone layer conformably underlying limestone and immediately above the faulted base. The principal mineral showing is 30 cm thick and has been uncovered

in a shallow trench 10 m in length. Here, the unconsolidated sandstone is impregnated with an intense malachite and azurite stain that originates from nodules of calcite and copper sulphide-cemented sandstone up to 15 cm in diameter. The stratiform nature of the mineralization is indicated by the additional occurrence of outcropping, bedding-parallel disseminated copper sulphides and mineralized float along strike and above the fault for several tens of metres to the west of the principal showing. Economic copper minerals identified in hand specimen and confirmed by X-ray diffraction analysis include chalcopyrite (12-50%), cuprite (13-15%) and malachite (2-3%). Additional visible copper minerals include azurite, native copper and possible chalcocite. Mineral concentrations are based on measurements of diffraction peak heights from five separate sulphide-bearing nodules. The total of all copper minerals does not exceed 50 per cent in any one nodule. Chalcopyrite is probably the primary copper mineral in the occurrence. The other minerals undoubtedly originate from supergene enrichment during the present period of bedrock exposure and weathering.

The close spatial association of the highest grade mineralization and the outlier-bounding fault points to a possible genetic relation between faulting and the postdepositional transport of metal-bearing brines. The specific site of the occurrence is also probably linked to zones of high intergranular porosity in the sandstone and a potential brine trap provided by the overlying limestone. Other occurrences in the area seem likely as malachite and azurite-bearing pebbles are encountered in float elsewhere in the outlier.

TABLE 7
Base metal and related economic mineral occurrences

Locality	Elements	Minerals	Host Fm./Mbr.	NTS, UTM	Lat./long.
1	Cu	chalcopyrite cuprite native copper malachite azurite	CPc	88H, VV421250E 8432400N	75°57'33"N 113°54'45"W
2	Ba	barite	OTM	78G, VV476300E 8419100N	75°51'20"N 111°52'10"W
3	Cu	malachite	OIB1	88G, NQ513000E 8426250N	75°55'10"N 116°31'20"W
4	Cu, P	malachite azurite apatite	OIB2	88G, NQ518200E 8429600N	75°57'00"N 116°19'45"W
5	Zn, Pb, F	sphalerite galena cerussite fluorite	SDIB5	89B, NQ521400E 8452900N	76°09'37"N 116°11'40"W
6	F	fluorite	CPc	88H, NQ555120E 8434250N	75°59'07"N 114°57'45"W
7	Ba	barite	SDIB5	88H, NQ554900E 8434400N	75°59'10"N 114°58'00"W
8	Pb	galena	OSc	78H, DQ425200E 8427200N	75°55'N 107°45'W
9	S	native sulphur	COF	79B, WA562700E 8521700N	76°45'49"N 108°33'57"W
10	S	native sulphur	COF	Barrow Dome area	

Locality 2

Coarse honey-yellow and white barite spar occurs within a tongue of the Allen Bay Formation in cliff exposures along the west coast of Middle Island in McCormick Inlet (Table 7, loc. 2). The yellow barite variety (up to 61%) occurs with calcite (39%) in a 20 cm thick zone exposed near the base of the coastal cliffs over a length of 2 m. The host rock is brecciated dark brown dolostone with up to 25 per cent sparry calcite void fill. The dolostone also contains nodules to two centimetres of a chalky white variety of chert. Corals, nautiloids and other marine macrofauna

typical of the Arctic Upper Ordovician occur stratigraphically and immediately below the barite occurrence. Smaller veins of white barite spar are found throughout the cliffs, both within the Allen Bay Formation and in the lower part of the Cape Phillips Formation. Along strike to the east, on the upland plateau surface, there are zones up to several tens of metres in diameter within the upper part of the Thumb Mountain composed of coarse-crystalline white dolomite and solution breccia.

The Cape Phillips Formation and the carbonates of the Allen Bay and Thumb Mountain formations are

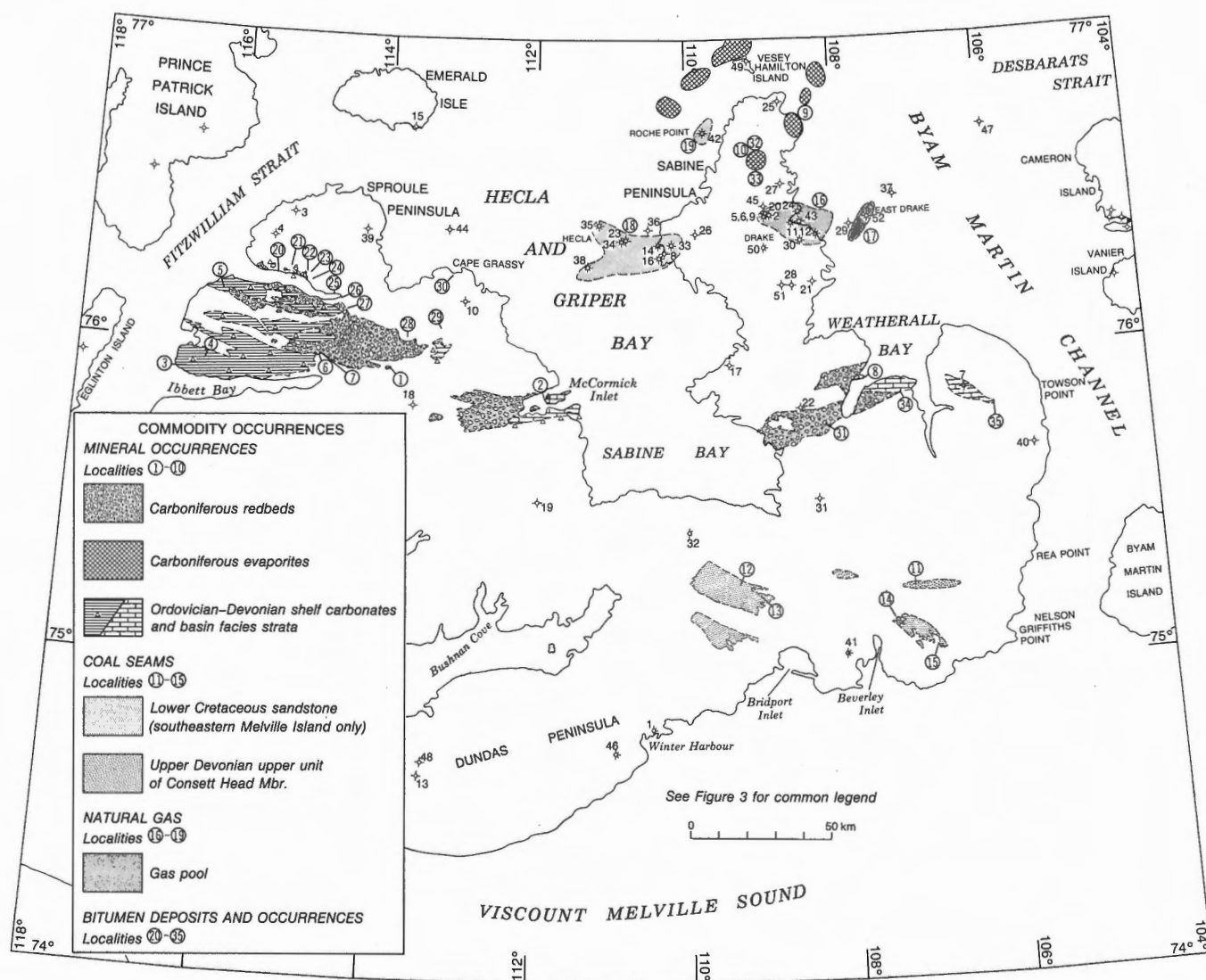


Figure 189. Commodity occurrences map of Melville Island. Numbered occurrences are cross-referenced to Tables 7 and 9 through 11.

both deeply altered and stained red by hematite across Middle Island and throughout the McCormick Inlet area. The alteration is found immediately downsection from the sub-Carboniferous angular unconformity beneath the Canyon Fiord Formation. The occurrence of vein and replacement barite, secondary dolomite, and solution breccia may be genetically related to the development of cavernous porosity and subsequent brine migration on and immediately below the unconformity surface.

Locality 3

Scattered small occurrences of malachite alteration occur throughout cliff exposures of Ibbett Bay and Canrobert formations situated along the south shore of

Blackley Haven. A separate small occurrence is found 6.0 km upstream on the banks of a tributary that empties into Kellet Strait near Nisbet Point (Table 7, loc. 3). The host rock is black, laminated, radiolarian dolomitic chert of the chert member (Middle Ordovician). Malachite occurs in a riverbank cliff exposure of chert over a distance of only a few tens of centimetres. The copper bloom appears to be related to weathering of an unknown primary copper mineral within a parting of carbonaceous chert.

Locality 4

Malachite spotting, pyritization and other alteration minerals are associated with bedded phosphorite and chert in a fault-bounded outlier of the lower black

shale member of the Ibbett Bay Formation 4.5 km southeast of the closest part of Blackley Haven (Table 7, loc. 4). Collophane is the principal mineral of economic interest in this locality. X-ray diffraction and chemical analyses indicate that the principal phosphorous mineral is hydroxyapatite (Table 8). The analyzed phosphorite samples also contain quartz vugs, microscopic quartz and anomalous concentrations of zinc and lead.

Phosphorite occurs throughout the outlier in an area measuring approximately 1200 m by 540 m. The

phosphorite is intercalated with chert in thin beds, thick laminae, blebs and fracture fillings, all making up 10 to 40 per cent of the rock volume. Colour ranges from black through shades of grey to chalky white. Chert interbeds are shades of grey, pale greyish green and black. The chert-phosphorite deposit is 60 to 80 m thick at the north end of the outlier. Graptolites collected from talus are Late Ordovician and also early Llandovery in age. The south end of the deposit has been deeply dissected by stream erosion and only the lower 20 m or less are still preserved. Grade appears to be highest in the lower 10 m of the lower black shale member immediately above a tectonically brecciated and pyritized facies of the underlying dolostone member of the Ibbett Bay Formation. Phosphorite disappears at about 60 to 80 m above the base of the deposit where the rocks grade upward into intercalated black chert with carbonaceous shale partings.

TABLE 8
Chemical analyses of Ordovician hydroxyapatite phosphorite, locality 4, southwestern Canrobert Hills

Major elements	C-133825-1	C-133825-2
SiO ₂	3.29	36.64
TiO ₂	0.01	0.11
Al ₂ O ₃	0.70	3.57
Fe ₂ O ₃	0.27	0.30
MgO	0.09	0.15
CaO	55.33	32.72
Na ₂ O	0.01	0.00
K ₂ O	0.39	3.00
P ₂ O ₅	37.48	22.15
MnO	0.00	0.00
LOI	2.30	1.15
Total	99.87	99.79
Minor elements (ppm)		
Pb	555	505
Zn	4763	2747
Cu	28	26
Ni	62	64
Mn	67	64
Cr	43	49
Zr	0	26
Y	30	29
Sr	176	112
Rb	0	19
Ba	352	689
Rh	0	0
X-ray diffraction analysis		
Hydroxyapatite	92%	42%
Quartz	8%	50%
Feldspar	0%	8%
Total	100%	100%

Limonitic staining and pyritic breccia are common both beneath the deposit and along bounding and internal faults. Immediately north of the deposit, a northerly-striking boundary fault is occupied by a giant cross-fibre calcite vein system up to 30 or 40 m wide. This fault and several other westerly-striking faults both within and bounding the phosphorite deposit are also associated with malachite spotting and scattered occurrences of aluminite (Al₂(SO₄)·OH₄·7H₂O). The latter mineral occurs as reniform nodules and concretions weathering out of chert-phosphorite talus. Individual masses range from 1 to 50 cm. Aluminite has a low specific gravity and in the smaller masses has either a boney or earthy white lustre. The larger pure masses are translucent white, pale yellow or bluish black and possess a radiating and densely-packed fibrous internal fabric. According to Palache et al. (1951), aluminite usually occurs in marls and is derived from the alteration of pyrite or marcasite and aluminous silicate minerals.

Locality 5

In a separate locality, sphalerite and galena occur in a zone of intense brecciation, calcite veining, and limonitic alteration in the upper black shale member of the Ibbett Bay Formation (Table 7, loc. 5). The mineralization is found in low-relief stream bank exposures 3.3 km southeast of Fitzwilliam Strait near the mouth of Marie Bay. Local bedding attitudes within the black platy to fissile mudrock dip to the north at less than 5°. However, depositional layering near the mineralization is greatly disturbed by brecciation and carbonate veining for a distance of 400 m along the stream bank and inland to the east for 240 m. Sulphide mineralization is exposed in fractured outcrop and felsenmeer rubble. An earthy, micro-

crystalline, honey-coloured variety of sphalerite (10–28% in some veins) is the dominant sulphide mineral. It occurs in banded, laminated and encrusting veins up to 70 cm thick. Associated minerals include fine crystalline calcite (36–47%), colourless, light green and antazomite varieties of fluorite (35–42%), galena (0–10%), minor quartz, kaolinite, pyrite and cerussite. The calcite is white, translucent and coarsely crystalline where it lines and fills drusy cavities and second-generation centimetre-scale veinlets. Individual calcite fibres are also found embedded in the sphalerite. Although this locality is probably not far below the sub-Carboniferous unconformity, the nearest area of altered red-weathering rock is actually composed of rock fulgurite (lightening-fused Ibbett Bay mudrock) and bocanne (mudrock of brick-like consistency that has been subjected to incineration of the flammable components; see also fold out legend, in pocket, Note 6).

Other localities

Several other small mineral occurrences are worth noting. Vein fill within and adjacent to the Nisbet Point Fault includes barite, fluorite and ubiquitous calcite (Fig. 171; Table 7, locs. 6, 7). The fluorite occurs sparingly with secondary calcite spar in the matrix of tectonically brecciated Canyon Fiord Formation. The barite has been noted in veins (to 10 cm thick) within the upper black shale member of the Ibbett Bay Formation. Also noteworthy is the widespread occurrence throughout the Canrobert Hills region of hydrozincite blooms on fracture planes within Ibbett Bay mudrock.

At the east end of the island, there has been a report of scattered galena cubes within fine crystalline Silurian dolostones of the Tingmisut Inlier (Fig. 78; Table 7, loc. 8). The size and significance of this occurrence is unknown.

On northern Sabine Peninsula, occurrences of native sulphur have been reported by King Resources Limited, both in outcrops and drill core of Carboniferous limestone and breccia within Colquhoun and Barrow domes (Fig. 181; Table 7, locs. 9 and 10, respectively). Assayed concentrations of native sulphur reported by King Resources range up to 5.3 per cent in porous Carboniferous limestone outcrops of Colquhoun Dome (loc. 9). Four drill holes have penetrated similar limestones with up to 3.2 per cent sulphur in intervals that range from 3 to 6 m in thickness.

Diapiric rock salt has been intersected between 3936.1 and 4461.2 m below K.B. in the lower Bay

Fiord Formation of the Panarctic et al. Sabine Bay A-07 well of central Melville Island (Fig. 34). Salt, representing 42 per cent of the lower Bay Fiord Formation, occurs with minor intercalated shale partings and dolomite and is the dominant lithology in discreet bedsets up to 45 m thick. The evaporitic facies of the Bay Fiord Formation underlies an 82 300 km² area of the Parry Islands including the offshore (Fig. 88) and is present at depths ranging from 3400 to 5500 m beneath the surface of Melville Island. The contained volume of onshore rock salt of Melville Island, measured from Figures 34 and 62, is estimated to be approximately 42 km³ or 90 billion tonnes. In addition to halite, up to 2 per cent sylvite has been reported by Mayr (1980) from the lower Bay Fiord Formation in the Caledonian River J-34 well of Bathurst Island. Potential therefore exists for sizeable deposits of potassium chloride and related potassic minerals. Additional shallow rock salt of Carboniferous age probably occurs within Barrow and Colquhoun domes of northern Sabine Peninsula.

Exploration potential

The above mineral occurrences indicate that the economic mineral potential of the Melville Island region is not entirely insignificant. Although all occurrences are small and few in number, these showings are guides to the possible discovery of larger base metal and industrial mineral concentrations. Mineralization and associated altered or brecciated bedrock is spatially related to either the sub-Carboniferous unconformity or faults that offset the unconformity surface. Eight out of ten showings are situated either within Canyon Fiord redbeds or within lower Paleozoic shelf carbonates and basin-facies black mudrocks that subcrop on the sub-Carboniferous unconformity. There is no indication of base metal potential in the various formations of the Devonian clastic wedge. Therefore most exploration can be limited to the Canyon Fiord Formation, the five inliers of Ordovician to Devonian shelf-type carbonates, and the region of Ibbett Formation that is exposed throughout the Canrobert Hills and along the north shore of Marie Bay. Three ore deposit types could exist within this belt: 1) carbonate-hosted Mississippi Valley-type lead-zinc (Anderson and Macqueen, 1982); 2) stratiform sedimentary-type lead-zinc in Ibbett Bay mudrocks (Morganti, 1981); and 3) sedimentary-type copper (Morganti, 1981) associated with redbeds of the Canyon Fiord Formation.

The greatest potential for Mississippi Valley-type ores exists within the Thumb Mountain Formation of the Middle Island and McCormick Inlet areas. The

possibility of pre-ore cavernous porosity is provided on and beneath the sub-Carboniferous erosion surface. Channelways for potential metal-bearing brines may include deep-seated sublatitudinal faults that lie along the hinge of McCormick Inlet Anticlinorium.

The exploration potential for stratiform sedimentary-type ore deposits is noteworthy insofar as the extent of favourable geology in the Canrobert Hills region is considerable and the critical base-of-slope depositional setting exists at a number of stratigraphic levels spanning Early Ordovician through latest Early Devonian time. Although the short list of mineral occurrences includes only one minute showing of stratiform sulphide, the existence of hydrozincite blooms on shale partings and the discovery of epigenetic lead, zinc, copper and barium minerals in Ibbett Bay mudrock testifies to the presence, at some point in time, of metal-bearing brines. Also curious and perhaps significant from an exploration standpoint is the coexistence of base metal elements with phosphorite in locality 4.

The same can be said of the potential for stratiform copper in Canyon Fiord redbeds. Known copper occurrences are associated with the replacement of porous sandstone by cupriferous brines. However, the ultimate source of these metals may yet be found in stratiform accumulations situated elsewhere in the upper Paleozoic outcrop belt.

Coal

Significant coal occurrences on Melville Island are found in rocks of Late Devonian and Early Cretaceous age (Table 9). The oldest preserved coal seams occur in the Middle Devonian clastic wedge. Embry and Klován (1976) report seams up to 25 cm thick within thin mudrock intervals of the Hecla Bay Formation. Coal is also reported in minor amounts from the Weatherall Formation. However, detrital grains of coal and minute plant fragments are far more usual. Upper Devonian coal seams up to 30 cm in thickness are common in both the Beverley Inlet and Parry Islands formations. The thickest seams are found in the middle to upper (not uppermost) Famennian upper sandstone unit of the Consett Head Member of the Parry Islands Formation within Byam River Syncline. At one occurrence, situated 23.5 km northeast of the head of Beverley Inlet (Table 9, loc. 11), a single seam has been discovered that measures up to 5 m in thickness. This coal is ranked as high-volatile bituminous B and, within the seam, is relatively free of mudrock partings and other detrital impurities. The coal-bearing strata, high in the Consett Head Member of the Parry Islands Formation, underlie much of the eastern end of Byam River Syncline: an area measuring about 50 km². Although continuity of occurrence is indicated within the limits of the syncline, lateral continuity of thickness is unknown. Nevertheless, there exists here the potential for a high-grade thermal resource measuring tens and perhaps hundreds of millions of tonnes.

TABLE 9
Coal deposits and major occurrences

Locality	Coal rank	Host Fm./Mbr.	NTS, UTM	Lat./long.
11	high-vol. bituminous	DPI5	78H, DP437900E 8353100N	75°15'25"N 107°11'50"W
12	lignite	KI	78G, WU547100 8353800N	75°15'55"N 109°20'10"W
13	lignite	KI	78G, WU552100E 8351300N	75°14'40"N 109°09'45"W
14	lignite	KI	78H, DP429700E 8341600N	75°09'05"N 107°27'50"W
15	lignite	KI	78H, DP443800E 8332800N	75°04'40"N 106°57'20"W

Coal is uncommon in the upper Paleozoic succession. Coaly sand and detrital coal layers up to 10 cm thick have been noted in the lower part of the Sabine Bay Formation on southern Sabine Peninsula. Coal partings are also intercalated with fine grained sand and mudrock in the Assistance Formation.

Coaly sand and sandy redeposited coal layers to 30 cm thick occur in most Mesozoic and Tertiary siliciclastic formations on Melville Island including the Bjorne, upper Hiccles Cove, Awingak, Isachsen, Hassel and Expedition formations. The thickest and most extensive coal is found in two of the three outliers of Lower Cretaceous Isachsen Formation on south-eastern Melville Island. Two distinct seams identified on Mecham River have excellent lateral continuity over an area of at least 200 km² (Table 9, locs. 12, 13). Seam thickness ranges from 1 to 2.5 m. However, coal rank is in the lignite range and appears to be of fairly low quality as a result of intercalated mud and fine grained sand. Similar or lower quality coal of comparable thickness underlies an area of 80 km² east and northeast of Beverley Inlet within Skene Bay outlier (Figs. 93 and 94; Table 9, locs. 14, 15). The occurrence of coal within Bridport outlier is much more limited.

Oil and gas

Gas pools and occurrences

Substantial proven and probable reserves of methane gas and natural gas condensate have been established

by exploratory drilling within Triassic rocks and especially within Lower Jurassic strata of Sabine Peninsula and adjacent offshore areas (Table 10; Waylett, 1979, 1990).

The largest of these reservoirs, discovered in 1969, is the Drake gas pool (Fig. 189; Table 10, loc. 16). Gas has accumulated within the eastern structural culmination on Drake Point Anticline and underlies an area of about 418 km² centred 8.3 km southwest of Drake Point. Reservoirs occur in porous sandstone intervals of the Maclean Strait Formation (Lower Jurassic) and Intrepid Inlet Member of the lower Jameson Bay Formation (Early Jurassic).

The East Drake pool (Table 10, loc. 17) lies within a faulted 100 km² area beneath western Byam Martin Channel centred at a location 16.9 km east-southeast of Drake Point. The East Drake pool is a continuation of the same structural closure on Drake Point Anticline. The two pools are separated by a narrow graben bound on one side by a northeasterly striking normal fault. Additional barren graben structures occur within the East Drake pool (Waylett, 1990). Proven and probable reserves for the combined Drake and East Drake pools are 0.15 TCM (5.37 TCF) of gas and natural gas liquids.

The Hecla gas field, first encountered by exploratory drilling in 1972 (Fig. 189; Table 10, loc. 18), is situated within the faulted western culmination of Drake Point Anticline and underlies a 360 km² area centred in the offshore 13.3 km southwest of Macdougall Point. Gas-bearing intervals have been

TABLE 10
Natural gas pools

Locality	Pool name	Vol. (TCM)	NTS, UTM	Lat./long.
16	Drake	0.15	79B, WV559750 8484000N	76°25'40"N 108°42'55"W
17	East Drake	0.15	79A, DQ426300E 8485100N	76°25'50"N 107°42'05"W
18	Hecla	0.10	79B, WV504400E 8474900N	76°21'30"N 110°50'00"W
19	Roche Point	0.012	79B, WA531300E 8514450N	76°42'35"N 109°46'15"W

discovered in the Schei Point Group (Middle and Upper Triassic) and in the Maclean Strait Formation (Lower Jurassic). Small quantities of viscous crude oil have also been encountered in the deeper strata. Proven and probable reserves include 176×10^6 barrels of oil and 0.10 TCM (3.58 TCF) of dry gas and condensate.

The Roche Point gas field, discovered in 1978 (Table 10, loc. 19), lies on the flanks of a separate smaller culmination that probably represents closure above an unroofed salt diapir. There are two sandstone reservoirs in the Triassic. Proven and probable reserves are 12 BCM (0.43 TCF) of combined gas and condensate.

The lower Paleozoic succession has proven to be gas prone but unproductive so far. Very modest gas flows have been detected from delta-front sandstones of the Hecla Bay Formation in the Winter Harbour No. 1 and Hearne F-85 wells. Indications of gas have also been found in the Bay Fiord Formation of the Sabine Bay A-07 well and in the Thumb Mountain Formation of the Beverley Inlet G-13 well.

Oil seeps, bitumen deposits and occurrences

Bitumen deposits and other surface showings occur in rocks of Early Devonian, Early and Middle Carboniferous, Early Triassic and Early Cretaceous age (Table 11).

Bitumen occurrences, described by Trettin and Hills (1966), are extensively exposed in the upper part of the Bjerne Formation in the outcrop belt of that unit between Marie Heights and Kitson River (Table 11, locs. 20-29). Trettin and Hills recognized 10 bitumen deposits in this belt that, within 45 m of surface, are estimated to contain 75-100 million barrels of oil. The bitumen in surface showings, greatly oxidized and otherwise modified by weathering, possesses gravities ranging from 6.5° to -0.8° API.

The deposits are considered to be unroofed oil fields. Trettin and Hills (1966) estimate original gravity of the oils to have been $26-27^\circ$ API prior to unroofing. This is not inconsistent with their model, which suggests that far-travelled oil has been trapped at the southern updip limit of porous Lower Triassic sands beneath an impervious cap of Lower and Middle Jurassic mudrock (Jameson Bay Formation). Additional structural controls include northerly striking normal faults that may have helped create channelways for fluid migration and also may have influenced local lateral limits of deposit size (Trettin and Hills, 1966).

A separate occurrence of live oil (Table 11, loc. 30) occurs 21.7 km southwest of Cape Grassy in a 3 m thick porous sandstone interval within the Lower Cretaceous Isachsen Formation (Tozer and Thorsteinsson, 1964). Mudrock and lignite also occur in the exposure and one mudrock layer has formed an impervious seal above the bitumen-saturated sand.

On southern Sabine Peninsula, a significant showing of oxidized live oil occurs in the lower part of the Canyon Fiord Formation. The seep is found in the southeastern St. Arnaud Hills, 7.1 km southwest of the west arm of Weatherall Bay (Table 11, loc. 31). Oil is seeping out of an interval of coarse grained quartz sandstones transitional upsection into variegated chert pebble conglomerate. The upper limit of the showing is defined by calcite-cemented zones in the conglomerate. This showing is perplexing, because all nonmarine, marine shelf and basin facies rocks of Middle Carboniferous through Early Permian age have low organic carbon contents and low oil source potential (Powell, 1978). For this reason, the oil showing in the Canyon Fiord Formation is believed to have migrated from lower Paleozoic source beds. However, elsewhere in the Arctic Islands, the Lower Carboniferous (upper Viséan) Emma Fiord Formation is known to be an excellent oil source rock (Davies and Nassichuk, 1988). The existence of these source beds beneath Middle Carboniferous and younger cover of the southwestern Sverdrup Basin should not be discounted.

Flow and related indications of oil, seepage of H_2S , and up to 5 per cent native sulphur have also been reported by King Resources Limited from short test wells penetrating Carboniferous limestones and gypsum of Barrow and Colquhoun domes (Fig. 181; Table 11, locs. 32, 33; see also Table 7, locs. 9, 10). In the case of Barrow Dome, gas and oil shows extend out into mudrocks and sandstones of the Kanguk and Hassel formations beyond the diapir contact.

In the lower Paleozoic succession, bitumen-lined fractures are abundant in the uppermost Blue Fiord Formation at two separate localities (Table 11, locs. 34, 35): one in eastern Spencer Range 1200 m southwest of the west arm of Weatherall Bay and 700 m south of the Spencer Range Fault; the other in an upthrown fault block at the east end of Towson Point Anticlinorium 17.8 km southwest of Towson Point (Fig. 39). Oil staining and bitumen has also been noted in undivided Lower Devonian and Silurian(?) carbonates intersected in the Towson Point F-63 well. The reservoir potential of the Blue Fiord Formation has been realized on Cameron Island. Panarctic Oils Limited is currently producing high API (42°) crude from cavernous Blue Fiord limestones situated beneath a Middle Devonian mudrock seal.

TABLE 11
Bitumen deposits and occurrences

Locality	Deposit name, host	Vol. (bar.)	NTS, UTM	Lat./long.
20	1, TB	0.3–2.5x10 ⁷	89A, NQ541000E 8462400N	76°14'25"N 115°27'00"W
21	2, TB	2x10 ³	89A, NQ547300E 8462750N	76°14'35"N 115°13'00"W
22	3a, TB	1.4x10 ⁶	89A, NQ550500E 8460700N	76°13'25"N 115°06'20"W
23	3b, TB	small	89A, NQ551700E 8463400N	76°14'50"N 115°03'00"W
24	3c, TB	3x10 ⁶	89A, NQ552900E 8460900N	76°13'25"N 115°01'00"W
25	4a, TB	2x10 ³	89A, NQ561100E 8455750N	76°10'35"N 114°42'30"W
26	4b, TB	unknown	89A, NQ565500E 8455900N	76°10'30"N 114°33'00"W
27	4c, TB	2–5x10 ⁷	89A, NQ565900E 8451300N	76°08'00"N 114°32'30"W
28	5, TB	<1x10 ⁵	89A, VV426500E 8442900N	76°03'25"N 113°44'00"W
29	6, TB	2x10 ⁷	89A, VV438400E 8446600N	76°05'40"N 113°18'00"W
30	KI	unknown	89A, VV444400E 8463700N	76°14'53"N 113°05'45"W
31	CPc	unknown	78G, WV575600E 8411500N	75°46'20"N 108°15'45"W
32	COF	unknown	79B, WA Barrow Dome area	
33	COF	unknown	79B, WA Barrow Dome area	
34	DBF	unknown	78H, DQ442100E 8422550N	75°52'45"N 107°07'45"W
35	DBF	unknown	78H, DQ470550E 8416200N	75°49'50"N 106°04'45"W

Source beds

Geographic and stratigraphic variations in organic carbon content and source bed potential have been assessed by Henao-Londoño (1977) and Powell (1978). In the lower Paleozoic of the Melville Island region, organic carbon is highest in the Kitson and Cape Phillips formations (1.5–7%). These formations are also prone to high gas yields within overmature intervals of the Sabine Bay A-07, Apollo C-73,

Dundas C-80 and Zeus F-11 wells. Source potential is recognized as being particularly high where these formations lie within the mature zone of hydrocarbon generation. This is especially true of the subsurface Weatherall Bay, Sabine Peninsula and Towson Point areas, where thermal maturity levels are lower than in the southern and western parts of the island. The Kitson and upper Cape Phillips formations of Melville Island and the correlative "Eids Formation" of Bathurst Island (Kerr, 1974) are the probable

hydrocarbon source beds for oils trapped in the Blue Fiord Formation on Cameron Island.

The Devonian clastic wedge spans the mature zone of oil generation throughout large areas of Melville Island. Organic carbon contents are uniformly low (0.3–0.7%) in the Weatherall and Cape De Bray formations and must be very low in the Hecla Bay and younger clastic formations. Widespread kaolinitic cementation of Devonian sandstones also appears to preclude the potential for local stratigraphic traps. Much work still needs to be done to establish the relative timing of deformation, fluid migration, hydrocarbon accumulation and cementation within the clastic wedge.

Source beds in the Sverdrup Basin include lacustrine mudrock of the Emma Fiord Formation (which is unknown in the western Arctic Islands), and mudrocks in the Schei Point Group. Middle and Upper Triassic mudrocks are also recognized as the principal source for migrated hydrocarbons trapped in Triassic and Jurassic reservoirs of southwestern Sverdrup Basin.

Exploration targets

Major tested and untested oil and gas exploration targets in the Melville Island region are briefly described below.

Stratigraphic traps

1. Oil and gas in biostromal carbonate buildups or oolitic carbonate sand shoals in Silurian carbonates. Unproductive test wells include Dundas C-80, N. Dundas N-82, Zeus F-11, and Kitson River C-71. The Zeus and Kitson wells have also been drilled on potential structural traps.
2. Oil and gas in cavernous and related bank and bank-edge porosity within Lower and Middle Devonian Blue Fiord limestones. Unproductive test wells include: Richardson G-12, King Point B-53, and Weatherall O-10. The King Point well has also been drilled on a potential structural trap.
3. Natural gas in delta-front sandstone porosity within the Middle Devonian Hecla Bay Formation. Indications of gas have been found in the Winter Harbour No.1 and Hearne F-85 wells. These wells may also have been drilled near the apices of structural culminations.

4. Hydrocarbons in carbonate bank-edge porosity within Lower Permian (Artinskian) limestones. Unproductive test wells include Marryatt K-71 and Chads Creek B-64. The Chads Creek well has also been drilled on a structural culmination.
5. Hydrocarbons in carbonate bank-edge porosity within the Upper Permian (Wordian) Degerbøls Formation. Unproductive test wells include Hecla J-60 and Sherard F-34. The Hecla well has also been drilled on a structural culmination.
6. Gas, condensate and oil occupying sandstone porosity within various Triassic and Jurassic formations near preserved limits beneath younger cover on the Sverdrup Basin margin. There are ten unroofed bitumen deposits in this setting north of Marie Bay (Table 11). Productive wells have also delineated the Hecla, Drake and East Drake gas pools within structural culminations (Table 10).

Structural traps

1. Deformation phase D3 culminations within the salt-based fold belt. Very modestly productive or unproductive wells include Winter Harbour No. 1, Beverley Inlet G-13 and Hearne F-85. For the Winter Harbour and Hearne Point anticlines, the culmination points may actually lie in offshore areas southeast of the well sites.
2. Structural culminations produced by D3 and D4 interference cross-folding within the salt-based fold belt. The Sabine Bay A-07 well was unproductive.
3. Structural culminations produced by D3 and/or D4 folding within the Canrobert Hills Fold Belt. Unproductive wells include Apollo C-73 and Zeus F-11.
4. On or adjacent to structural highs or horst blocks within the upper Paleozoic rift belt. Unproductive wells include Kitson River C-71, Sandy Point L-46 and Marie Bay D-02.
5. Sinistral transpressive D8 culminations within the salt-based fold belt. The Towson Point F-63 well was unproductive.
6. Sinistral transpressive D8 culminations modified by faulting within Sverdrup Basin. These types of structure are host to the Hecla, Drake and East Drake gas fields.

7. Closure above unroofed evaporite diapirs. The productive Roche Point J-43 well has tested the Roche Point gas field on the flanks of a probable unroofed diapir.
8. Hydrocarbons trapped in strata beneath allochthonous Otto Fiord evaporites peripheral to diapirs. Short test wells have been drilled for sulphur in this setting on the flanks of Barrow Dome. Hydrocarbon shows occur both in Carboniferous carbonates of the diapir and in Upper Cretaceous sandstones trapped beneath the evaporites.
9. Local closure of uncertain origin within Sverdrup Basin. Unproductive wells include Emerald K-33, and Eldridge Bay E-79.

Untested traps

1. The extensive Lower Devonian shelf edge of the Blue Fiord Formation believed to exist beneath Middle Devonian and younger cover of Viscount Melville Sound remains untested. This belt is probably continuous from tested but unproductive well sites on northeastern Banks Island to southwestern Bathurst Island, and over this distance must possess a minimum strike length of 470 km. A potential seal is provided by mudrock of the Cape De Bray Formation, which on seismic profiles is seen to overstep the Blue Fiord Formation.
2. Silurian shelf carbonates capped by Kitson Formation mudrock have been traced across Dundas Peninsula and have been tested in the Dundas and N. Dundas N-82 wells. Untested parts of the Silurian shelf edge probably underlie Liddon Gulf, southwestern Melville Island south of the Zeus F-11 well and a 480 km stretch of subsurface Viscount Melville Sound between Dundas Peninsula and western Cornwallis Island.
3. There are at least 20 untested first- and second-order D3 and D4 culminations within the onland part of Melville Island's salt-based fold belt. There are at least an additional 12 and possibly twice this many untested second-order D3 culminations in the offshore portion of the fold belt beneath northern Viscount Melville Sound. Thirteen culminations are counted on the foreland side of the Hearne F-85 well of Hearne Point Anticline in areas where overburden thickness and probable thermal maturity levels are anticipated to be less

than in the internal portions of the fold belt. Potential traps could include Silurian through Middle Devonian shelf-edge carbonate porosity and cavernous porosity, and Middle and Upper Devonian sandstone porosity in the foredeep clastic wedge.

4. Many potential structural traps for natural gas exist within the salt-based fold belt apart from the obvious surface culminations. For example, numerous smaller culminations must exist within parasitic anticlines on the flanks of second-order surface folds. Other potential traps may be situated within local- or regional-scale triangle zone structures similar to those featured on Figures 100, 118, 119 and 160. Within the salt-based fold belt, secondary porosity resulting from tectonic brecciation of shelf and shelf-edge carbonates may exist beneath either Cape De Bray mudrock or thrust-faulted hanging wall Bay Fiord evaporites.
5. Potential exists for oil and gas within inverted upper Paleozoic half-grabens situated beneath flat-lying Permian and younger cover of Sproule Peninsula, northwestern Melville Island and Hecla and Griper Bay (Fig. 161). Porosity could be provided by uncemented sandstones and conglomerates. Potential seals could include cementation gradients in the graben-fill or post-inversion Permian mudrocks.
6. Many potential stratigraphic traps exist in the Mesozoic section along the southern margin of Sverdrup Basin. Most of these features are extremely subtle on seismic profiles but, nevertheless, are suspected to exist from detailed studies of basin margin stratigraphy (Embry, 1983; 1984a, b; 1985a; 1991b; 1993). Most large structural traps in the Mesozoic have been tested at least within the Melville Island area. However, much untested potential is recognized for oil and gas accumulations within porous Mesozoic sandstones beneath allochthonous evaporites on the flanks of Barrow and Colquhoun domes and related piercement structures in the offshore.

ACKNOWLEDGMENTS

The fieldwork for this report was conducted during the summers of 1984 and 1985. Field activities were undertaken from base camps near Nias Point on the south shore of Hecla and Griper Bay (lat. 75°33'12"N; long. 110°25'W) in 1984, and from a site near the head

of Ibbett Bay (lat. 75°53'50"N; long. 114°28'W) in 1985. Fuel and camp supplies were transported by de Havilland Twin Otter aircraft operated by Bradley Air Services Ltd. out of Resolute. Access to field locations was made possible by a Bell 206B Jet Ranger helicopter contracted from the Polar Continental Shelf Project for the duration of the field operations. Co-operative research activities, involving as many as fifteen scientists, were supervised by R.L. Christie. Results have been published separately (Christie and McMillan, 1993). Support personnel in the field party included: geological assistants M.J. Robson, J. Bracken, S. Fuelgen, K. Higgins, T. Cross, L. Haid, R. McIntosh, D. Christensen, and B. Lawson; aircrew G. Dionne and engineers K. Mahoney, S. Long, and D. Tranelis; camp manager D. Diduck; and cook L. Journault. Panarctic Oils Limited is gratefully acknowledged for periodic use of the Rea Point base camp and airfield in support of some field activities in 1985 and as a route of access for personnel and supplies from southern Canada.

The author is also indebted to Panarctic Oils Limited, Texaco Canada Resources, and Chevron Canada Limited for permission to acquire copies of original seismic field tapes and operator's reports, and to publish the stacked and migrated profiles. Reprocessing was undertaken at Western Geophysical under the supervision of F.W. Nicholson and his associates and at Veritas Limited with the help of E. Roebroek, Z. Berkes and A.N. Kanasewich (University of Alberta, Edmonton). Some redisplayed data have been obtained through the additional assistance of H. Geiger, C. Vasuvedeyan, and F.W. Cook of the LITHOPROBE lab, University of Calgary, Alberta. Potential-field maps and earthquake epicentres, featured on Figures 9, 10 and 187, have been obtained with the help of R.J. Wetmiller of the Geophysics division of the Geological Survey of Canada in Ottawa.

Significant improvements to the manuscript have been made possible through the critical reviews of: A.W. Bally, H.G. Avé Lallemant, and M. Talwani of Rice University, Houston; B. Beauchamp, T. de Freitas, A.F. Embry, L.S. Lane, B.C. MacLean, R. Thorsteinsson, H.P. Trettin, and especially D.G. Cook, of the Institute of Sedimentary and Petroleum Geology, Calgary; and J.G. Fyles of the Terrain Sciences Division of the Geological Survey of Canada. Previously unpublished paleontological determinations (Appendix 4) have been submitted by seventeen contributing authors. Special thanks are extended to T.A. Brent for his substantial offshore and subsurface mapping efforts in the southern Sverdrup Basin region and for comments on base of permafrost

phenomena (Figs. 4, 5). Thermal maturity data presented in Chapter 1 have been provided by F. Goodarzi (GSC) and T. Gentzis (Alberta Research Council).

Drafting of text figures was accomplished with the help of J. Kortenschyl, C. Dornan and D.J. Walter. Maps and cross-sections were completed by S.D. Orzeck, and the cartography staff of the ISPG. Other important contributions have been made by B.C. Rutley and W.B. Sharman (photography), G.N. Edwards and L.J. Wardle (photomechanical services), J.M. Monro (editing), and B.P.L. Chiang, P. Greener and Lisa Cheung (typesetting and layout).

As well as the Geological Survey of Canada, indirect financial support was provided by the Department of Geology and Geophysics at Rice University, Houston in 1986 and 1987.

REFERENCES

- Adams, J.**
1987: Canadian crustal stress data - a compilation to 1987. Geological Survey of Canada, Open File 1622, 130 p.
- Aitken, J.D.**
1991: Cambrian and Lower Ordovician-Sauk sequence. *In* Sedimentary cover of the craton, D.F. Stott and J.D. Aitken (eds.). Geological Survey of Canada, Geology of Canada, v. 5 (also, Geological Society of America, Geology of North America, v. D-1).
- Aitken, J.D. and Stott, D.F. (compilers)**
1991: Geotectonic correlation chart. *In* Sedimentary cover of the craton, D.F. Stott and J.D. Aitken (eds.). Geological Survey of Canada, Geology of Canada, v. 5 (also, Geological Society of America, Geology of North America, v. D-1).
- Anderson, G.M. and Macqueen, R.W.**
1982: Mississippi Valley-type lead-zinc deposits. *Geoscience Canada*, v. 9, p. 108-117.
- Armstrong, J.E.**
1947: The Arctic Archipelago. *In* Geology and economic minerals of Canada. Canada Geological Survey, Economic Geology Series, no. 1, 3rd ed., chapter 8, p. 311-324.
- Balkwill, H.R.**
1978: Evolution of Sverdrup Basin, Arctic Canada. *American Association of Petroleum Geologists, Bulletin*, v. 62, p. 1004-1028.
1983: Geology of Amund Ringnes, Cornwall, and Haig-Thomas islands, District of Franklin. Geological Survey of Canada, Memoir 390, 76 p.
- Balkwill, H.R. and Fox, F.G.**
1982: Incipient rift zone, western Sverdrup Basin. *In* Arctic Geology and Geophysics, A.F. Embry and H.R. Balkwill

(eds.). Canadian Society of Petroleum Geologists, Memoir 8, p. 171-187.

Balkwill, H.R., Wilson, D.G., and Wall, J.H.

1977: Ringnes Formation (Upper Jurassic), Sverdrup Basin, Canadian Arctic Archipelago. *Bulletin of Canadian Petroleum Geology*, v. 25, p. 1115-1144.

Bally, A.W., Gordey, P.L., and Stewart, G.A.

1966: Structure, seismic data, and orogenic evolution of the southern Canadian Rocky Mountains. *Bulletin of Canadian Petroleum Geology*, v. 14, p. 337-381.

Bamber, E.W. and Waterhouse, J.B.

1971: Carboniferous and Permian stratigraphy and paleontology, northern Yukon Territory, Canada. *Bulletin of Canadian Petroleum Geology*, v. 19, no. 1, p. 29-250.

Baragar, W.R.A. and Donaldson, J.A.

1973: Coppermine and Dismal Lakes areas. Geological Survey of Canada, Paper 71-39, 20 p.

Barendregt, R.W. and Vincent, J-S.

1990: Late Cenozoic paleomagnetic record of Duck Hawk Bluffs, Banks Island, Canadian Arctic Archipelago. *Canadian Journal of Earth Sciences*, v. 27, p. 124-130.

Barnes, C.R.

1973: Ordovician conodont biostratigraphy of the Canadian Arctic. In *Geological Association of Canada-Canadian Society of Petroleum Geologists, Proceedings of the Symposium on the Geology of the Canadian Arctic*, J.D. Aitken and D.J. Glass (eds.). Saskatoon, May 1973, p. 221-240.

Barnes, C.R. and Uyeno, T.T.

1974: Ordovician to Silurian assemblages. In *Biostratigraphic determinations of fossils from the subsurface of the Northwest Territories and Yukon Territories*. Geological Survey of Canada, Paper 74-11, p. 26-27.

Barnett, D.M., Edlund, S.A., Dredge, L.A., Thomas, D.C., and Prevett, L.S.

1975: Terrain classification and evaluation, Melville Island, Northwest Territories. Geological Survey of Canada, Open File 252, 747 p.

Baxendale, L.R.

1972: Final geophysical report for Magnorth Exploration Management Ltd. on the 1972 marine seismic program, Viscount Melville Sound, Arctic Islands. Canadian Oil and Gas Lands Administration, assessment report 693-09-10-32.

Beauchamp, B.

1987: Stratigraphy and facies analysis of the Upper Carboniferous to Lower Permian Canyon Fiord, Belcher Channel and Nansen formations, southwestern Ellesmere Island. Unpublished Ph.D. thesis, University of Calgary, 370 p.

Beauchamp, B. and Henderson, C.M.

1994: Stratigraphy and sedimentation of the Raanes, Great Bear Cape and Trappers Cove formations; three new Lower Permian units of the Sverdrup Basin, Canadian Arctic. *Bulletin of Canadian Petroleum Geology*.

Beauchamp, B., Harrison, J.C., and Henderson, C.M.

1989a: Upper Paleozoic stratigraphy and basin analysis of the Sverdrup Basin, Canadian Arctic Archipelago: Part 1, time frame and tectonic evolution. In *Current Research, Part G. Geological Survey of Canada, Paper 89-1G*, p. 105-113.

1989b: Upper Paleozoic stratigraphy and basin analysis of the Sverdrup Basin, Canadian Arctic Archipelago: Part 2, transgressive-regressive sequences. In *Current Research, Part G. Geological Survey of Canada, Paper 89-1G*, p. 115-124.

Beauchamp, M.

1974: Elf Oil Exploration and Production Canada Ltd. interpretation report on reflection seismograph surveys on Banks Island. Canadian Oil and Gas Lands Administration, assessment report 581-06-09-130.

Belcher, Sir E.

1855: The Last of the Arctic Voyages, being a Narrative of the Expedition in H.M.S. *Assistance* in Search of Sir John Franklin, during the years 1852-53-54, 2 vols; London, Lovell Reeve.

Bentham, R.

1936: Geology. In *Humphreys, Noel, et al., Oxford University Ellesmere Land expedition*. *Geographical Journal*, v. 87, appendix 1, p. 427-431.

1941: Structure and glaciers of southern Ellesmere Island. *Geographical Journal*, v. 97, p. 36-45.

Bergquist, R.

1966: Micropaleontology of the Mesozoic rocks of northern Alaska: Exploration of Naval Petroleum Reserve no. 4 and adjacent areas, northern Alaska, 1944-53, pt. 2, regional studies. United States Geological Survey, Professional Paper 302-D, p. i-vi, 93-227.

Bernier, J.E.

1909: Report on the Dominion Government Expedition to the Arctic Islands and Hudson Strait on board D.G.S. *Arctic* (1906-1907). Ottawa, Government Printing Bureau.

1910: Report on the Dominion Government Expedition to the Arctic Islands and Hudson Strait on board D.G.S. *Arctic* (1908-1909). Government Printing Bureau, Ottawa, 529 p.

1911: Report on the Dominion Government Expedition to the Northern Waters and the Arctic Archipelago of the D.G.S. *Arctic* in 1910. Government Printing Bureau, Ottawa, 74 p.

British Parliamentary Papers

1855: Further papers relative to the recent Arctic Expeditions in search of Sir John Franklin and the crews of H.M.S. *Erebus* and *Terror*; London, Eyre and Spottiswoode, for H.M. Stationery Office.

Burst, J.F.

1969: Diagenesis of Gulf Coast clayey sediments and its possible relation to petroleum migration. *American Association of Petroleum Geologists, Bulletin*, v. 53, no. 1, p. 73-93.

Campbell, F.H.A.

1979: Stratigraphy and sedimentation in the Helikian Elu Basin and Hiukitak Platform, Bathurst Inlet-Melville Sound, Northwest Territories. Geological Survey of Canada, Paper 79-8, 18 p.

1981: Stratigraphy and tectono-depositional relationships of the Proterozoic rocks of the Hadley Bay area, northern Victoria Island, District of Franklin. *In* Current Research, Part A. Geological Survey of Canada, Paper 81-1A, p. 15-22.

Carter, N.L. and Hansen, F.D.

1983: Creep of rocksalt. *Tectonophysics*, v. 92, p. 275-333.

Chapple, W.M.

1978: Mechanics of thin-skinned fold-and-thrust belts. Geological Society of America, *Bulletin*, v. 89, p. 1189-1198.

Chatterton, B.D.E.

1974: Middle Devonian conodonts from the Harrogate Formation, Southeastern British Columbia. *Canadian Journal of Earth Sciences*, v. 11, p. 1461-1484.

Christie, R.L.

1964: Diabase-gabbro sills and related rocks of Banks and Victoria Islands, Arctic Archipelago. Geological Survey of Canada, *Bulletin* 105, 13 p.

Christie, R.L. and McMillan, N.J.

1993: The Geology of Melville Island, Arctic Canada. Geological Survey of Canada, *Bulletin* 450.

Coulomb, C.A.

1773: Sur une application des regles de maximus et minimis a quelques problems de statique relatifs a l'architecture. Academie Royale des Sciences, *Memoires de Mathematique et de Physique par divers savans*, v. 7, p. 343-382.

Cowie, J.W. and Bassett, M.G. (compilers)

1989: 1989 global stratigraphic chart with geochronometric and magnetostratigraphic calibration. *Episodes*, v. 12, no. 2, p. 79-83 (with supplement).

Crickmay, C.H.

1960: The older Devonian faunas of the Northwest Territories. Evelyn de Mille Books, Calgary, 21 p.

1966: Devonian time in western Canada. Evelyn de Mille Books, Calgary, 38 p.

Dahlen, F.A.

1990: Critical taper model of fold-and-thrust belts and accretionary wedges. *Annual Review of Earth and Planetary Sciences*, v. 18, p. 55-99.

Davies, E.H.

1983: The dinoflagellate Oppel-zonation of the Jurassic-Lower Cretaceous sequence in the Sverdrup Basin, Arctic Canada. Geological Survey of Canada, *Bulletin* 359, 59 p.

1985: Dinoflagellate cyst occurrences of the Jurassic-Lower Cretaceous sequence in the Sverdrup Basin, Arctic Canada. Geological Survey of Canada, Open File 1153, 28 p.

Davies, G.R.

1975: Hoodoo L-41; Diapiric halite facies of the Otto Fiord Formation in the Sverdrup Basin, Arctic Archipelago. *In* Report of Activities, Part C. Geological Survey of Canada, Paper 75-1C, p. 23-29.

Davies, G.R. and Nassichuk, W.W.

1991: Carboniferous to Permian geology of the Sverdrup Basin, Canadian Arctic Archipelago. *In* Innuition Orogen and Arctic Platform: Canada and Greenland. Geological Survey of Canada, *Geology of Canada No. 3*. (also, *The Geology of North America*, Geological Society of America, v. E.)

1988: An Early Carboniferous (Viséan) lacustrine oil shale in the Canadian Arctic Archipelago. *American Association of Petroleum Geologists, Bulletin*, v. 72, p. 8-20.

Davis, D.M. and Engelder, T.

1985: The role of salt in fold-and-thrust belts. *Tectonophysics*, v. 119, p. 67-88.

1987: Thin-skinned deformation over salt. *In* *Dynamical Geology of Salt-related Structures*, I. Lerche and J.J. O'Brien (eds.). Academic Press, New York, p. 301-337.

Davis, D.M., Suppe, J., and Dahlen, F.A.

1983: Mechanics of fold-and-thrust belts. *Journal of Geophysical Research*, v. 88, p. 1153-1172.

De Paor, D.G., Bradley, D.C., Eisenstadt, G., and Phillips, S.M.

1989: The Arctic Eureka orogen: A most unusual fold-and-thrust belt. Geological Association of America, *Bulletin*, v. 101, p. 952-967.

Dix, C.H.

1955: Seismic velocities from surface measurements. *Geophysics*, v. 20, p. 68-86.

Dostal, J., Baragar, W.R.A., and Dupuy, C.

1986: Petrogenesis of the Natkusiak continental basalts, Victoria Island, Northwest Territories, Canada. *Canadian Journal of Earth Sciences*, v. 23, p. 622-632.

Daae, H.D. and Rutgers, A.T.C.

1975: Geological history of the Northwest Passage. *Bulletin of Canadian Petroleum Geology*, v. 23, p. 84-108.

Dunbar, M. and Greenaway, K.R.

1956: Arctic Canada from the Air. Canada, Defense Research Board, Queen's Printer, Ottawa, 541 p.

Dyke, A.S. and Prest, V.K.

1987: Late Wisconsinan and Holocene history of the Laurentide ice sheet. *Géographie Physique et Quaternaire*, v. XLI, no. 2, p. 237-263.

Eardley, A.J.

1948: Ancient Arctica. *Journal of Geology*, v. 56, p. 490-436.

1951: Structural geology of North America. Harper Brothers, New York, 743 p.

Eldlund, S.A.

1982: Vegetation of Melville Island, District of Franklin, Northwest Territories. Geological Survey of Canada, Open File 852, scale 1:250,000.

Elias, R.J.

- 1981: Solitary rugose corals of the Selkirk Member, Red River Formation (late Middle or Upper Ordovician), southern Manitoba. Geological Survey of Canada, Bulletin 344, 53 p.

Embry, A.E.

- 1982: The Upper Triassic-Lower Jurassic Heiberg deltaic complex of the Sverdrup Basin. *In* Arctic Geology and Geophysics, A.F. Embry and H.R. Balkwill (eds.). Canadian Society of Petroleum Geologists, Memoir 8, p. 189-217.
- 1983: The Heiberg Group, western Sverdrup Basin, Arctic Islands. *In* Current Research, Part B. Geological Survey of Canada, Paper 83-1B, p. 381-389.
- 1984a: The Schei Point and Blaa Mountain groups (Middle-Upper Triassic) Sverdrup Basin, Canadian Arctic Archipelago. *In* Current Research, Part B. Geological Survey of Canada, Paper 84-1B, p. 327-336.
- 1984b: The Wilkie Point Group (Lower-Upper Jurassic), Sverdrup Basin, Arctic Islands. *In* Current Research, Part B. Geological Survey of Canada, Paper 84-1B, p. 299-308.
- 1984c: Stratigraphic subdivision of the Roche Point, Hoyle Bay and Barrow formations (Schei Point Group), western Sverdrup Basin, Arctic islands. *In* Current Research, Part B. Geological Survey of Canada, Paper 84-1B, p. 327-336.
- 1985a: New stratigraphic units, Middle Jurassic to lowermost Cretaceous succession, Arctic Islands. *In* Current Research, Part B. Geological Survey of Canada, Paper 85-1B, p. 269-276.
- 1985b: Stratigraphic subdivision of the Isachsen and Christopher formations (Lower Cretaceous), Arctic Islands. *In* Current Research, Part B. Geological Survey of Canada, Paper 85-1B, p. 239-246.
- 1986: Stratigraphic subdivision of the Blind Fiord and Bjorne formations (Lower Triassic), Sverdrup Basin, Arctic Islands. *In* Current Research, Part B. Geological Survey of Canada, Paper 86-1B, p. 329-340.
- 1988a: Middle-Upper Devonian sedimentation in the Canadian Arctic Islands and the Ellesmerian Orogeny. *In* Proceedings of the Second International Symposium on the Devonian, N.J. McMillan, A.F. Embry, and D. Glass (eds.). Canadian Society of Petroleum Geologists, Memoir 14, p. 15-28.
- 1988b: Triassic sea-level changes: evidence from the Canadian Arctic Archipelago. *In* Sea-Level Changes - An Integrated Approach. Society of Economic Paleontologists and Mineralogists, Special Publication No. 42, p. 249-259.
- 1990: Geological and geophysical evidence in support of the hypothesis of anticlockwise rotation of northern Alaska. *Marine Geology*, v. 93, p. 317-330.
- 1991a: Middle-Upper Devonian clastic wedge of the Arctic Islands, Chapter 10. *In* Innuitian Orogen and Arctic Platform: Canada and Greenland. Geological Survey of

Canada, Geology of Canada, no. 3 (also, Geological Society of America, The Geology of North America, v. E).

- 1991b: Mesozoic history of the Arctic islands. *In* Innuitian Orogen and Arctic Platform: Canada and Greenland. Geological Survey of Canada, Geology of Canada No. 3. (also, The Geology of North America, Geological Society of America, v. E.).
- 1993: Jurassic-Lowermost Cretaceous stratigraphy, Melville Island area. *In* The Geology of Melville Island, R.L. Christie and N.J. McMillan (eds.). Geological Survey of Canada, Bulletin 450.

Embry, A.F. and Klován, J.E.

- 1976: The Middle-Upper Devonian clastic wedge of the Franklinian Geosyncline. *Bulletin of Canadian Petroleum Geology*, v. 24, p. 485-639.

Embry, A.F. and Osadetz, K.G.

- 1988: Stratigraphy and tectonic significance of Cretaceous volcanism in the Queen Elizabeth Islands, Canadian Arctic Archipelago. *Canadian Journal of Earth Sciences*, v. 25, p. 1209-1219.

Engelder, T.

- 1979: Mechanisms for strain within the Upper Devonian clastic sequence of the Appalachian Plateau, western New York. *American Journal of Science*, v. 279, p. 527-542.

Ethington, R.L. and Clark, D.L.

- 1971: Lower Ordovician conodonts in North America. *In* Symposium on conodont biostratigraphy, W.C. Sweet and S.M. Bergstrom (eds.). Geological Society of America, Memoir 127, p. 63-82.

Fahrig, W.F.

- 1987: The tectonic settings of continental mafic dyke swarms: failed arm and early passive margin. *In* Mafic dyke swarms, H.C. Halls and W.F. Fahrig (eds.). Geological Association of Canada, Special Paper 34, p. 331-348.

Fahrig, W.F. and West, T.D.

- 1986: Diabase dyke swarms of the Canadian Shield. Geological Survey of Canada, Map 1627A (scale 1:4,873,900).

Fielden, H.E. and de Rance, C.E.

- 1878: Geology of the coasts of the Arctic lands visited by the late British expedition under Captain Sir George Nares, R.N., K.C.B., F.R.S. *The Quarterly Journal of the Geological Society of London*, v. 34, p. 556-567.

Forsyth, D.A., Mair, J.A., and Fraser, I.

- 1979: Crustal structure of the Sverdrup Basin. *Canadian Journal of Earth Sciences*, v. 16, p. 1581-1598.

Fortier, Y.O., McNair, A.H., and Thorsteinsson, R.

- 1954: Geology and Petroleum Possibilities in Canadian Arctic Islands. *American Association of Petroleum Geologists, Bulletin*, v. 38, no. 10, p. 2075-2109.

Fortier, Y.O. and Thorsteinsson, R.

- 1953: The Parry Islands Fold Belt in the Canadian Arctic Archipelago. *American Journal of Science*, v. 251, p. 259-267.

- Fox, F.G.**
1983: Structure sections across Parry Islands Foldbelt and Vesey Hamilton Salt Wall, Arctic Archipelago. *In* Seismic expression of structure styles, v. 3, A.W. Bally (ed.). American Association of Petroleum Geologists, Studies in Geology Series, no. 15, p. 3.4.1.54 to 3.4.1.72.
- 1985: Structural geology of the Parry Islands Fold Belt. *Bulletin of Canadian Petroleum Geology*, v. 33, no. 3, p. 306-340.
- Fox, F.G., and Densmore, A.A.**
1992: The pre-late Middle Devonian rocks of Melville Island, Queen Elizabeth Islands, Arctic Canada. *Geological Survey of Canada, Paper 91-16*, 18 p.
- Frebold, H.**
1960: The Jurassic faunas of the Canadian Arctic, Lower Jurassic and lowermost Middle Jurassic ammonites. *Geological Survey of Canada, Bulletin 59*, 33 p., 15 pls.
- 1975: The Jurassic faunas of the Canadian Arctic, Lower Jurassic ammonites, biostratigraphy and correlations. *Geological Survey of Canada, Bulletin 243*, 24 p., 5 pls.
- Funder, S., Abrahamsen, N., Bennike, O., and Feyling-Hanssen, R.W.**
1985: Forested Arctic: evidence from North Greenland. *Geology*, v. 13, p. 542-546.
- Gentzis, T.**
1990: Regional maturity and source-rock potential of Paleozoic and Mesozoic strata, Melville Island, Arctic Canada. Unpub. Ph.D Thesis, University of Newcastle-upon-Tyne, UK.
- Geological Survey of Canada**
1987: Magnetic anomaly map of Canada, fifth edition. *Geological Survey of Canada, Map 1255A*, scale 1:5 000 000.
- Goodarzi, F., Harrison, J.C., and Wall, J.H.**
1993: Stratigraphy and petrology of Lower Cretaceous coal, southeastern Melville Island, District of Franklin, Northwest Territories, Canada. *In* The Geology of Melville Island, R.L. Christie and N.J. McMillan (eds.). *Geological Survey of Canada, Bulletin 450*.
- Goodbody, Q.H.**
1988: Devonian Shelf Systems on Melville Island, Canadian High Arctic. *In* Proceedings of the Second International Symposium on the Devonian, N.J. McMillan, A.F. Embry, and D. Glass (eds.). *Canadian Society of Petroleum Geologists, Memoir 14*, v. 2, p. 29-52.
- 1989: Stratigraphy of the Lower to Middle Devonian Bird Fiord Formation, Canadian Arctic Archipelago. *Bulletin of Canadian Petroleum Geology*, v. 37, p. 48-82.
- 1993: Lower and middle Paleozoic stratigraphy of Melville Island. *In* The Geology of Melville Island, R.L. Christie and N.J. McMillan (eds.). *Geological Survey of Canada, Bulletin 450*.
- Gordy, P.L., Frey, F.R., and Norris, D.K.**
1977: Geological guide for the Canadian Society of Petroleum Geologists, and 1977 Waterton-Glacier Park Field Conference. *Canadian Society of Petroleum Geologists, Calgary*, 93 p.
- Greenaway, K.R. and Colthorpe, S.E.**
1948: An aerial reconnaissance of Arctic North America, Ottawa, Joint Intelligence Bureau.
- Handin, J.**
1966: Strength and ductility. *In* Handbook of physical constants, S.P. Clark (ed.). *Geological Society of America, Memoir 97*, p. 223-290.
- Haq, B.U., Hardenbohl, J., and Vail, P.R.**
1988: Mesozoic and Cenozoic chronostratigraphy and cycles of sea-level change. *In* Sea-level Changes-An Integrated Approach (C.K. Wilgus, B.S. Hastings, C.A. Ross, H.W. Posamentier, J. Van Wagoner, and C.G. St. C. Kendall). *Society of Economic Paleontologists and Mineralogists, Special Publication No. 42*, p. 71-108.
- Harker, P. and Thorsteinsson, R.**
1960: Permian rocks and faunas of Grinnell Peninsula, Arctic Archipelago. *Geological Survey of Canada, Memoir 309*, 145 p.
- Harland, W.B., Armstrong, R.L., Cox, A.V., Craig, L.E., Smith, A.G., and Smith, D.G.**
1989: A Geologic Time Scale 1989. *Cambridge University Press, Cambridge, U.K.*, 131 p.
- Harrison, J.C.**
1991: Geology, seismic profiles and structural cross-sections, Melville Island, N.W.T. *Geological Survey of Canada, Open File 2335*, (13 oversized sheets).
- 1993: The structural geology of Melville Island. *In* The Geology of Melville Island, R.L. Christie and N.J. McMillan (eds.). *Geological Survey of Canada, Bulletin 450*.
- Harrison, J.C. and Bally, A.W.**
1988: Cross-sections of the Parry Islands Fold Belt on Melville Island. *Bulletin of Canadian Petroleum Geology*, v. 36, p. 311-332.
- Harrison, J.C. and Brent, T.**
1991: Late Devonian-Early Carboniferous deformation, Prince Patrick and Banks islands; Chapter 12H. *In* Innuitian Orogen and Arctic Platform: Canada and Greenland. *Geological Survey of Canada, Geology of Canada*, no. 3 (also, *Geological Society of America, The Geology of North America*, v. E.).
- Harrison, J.C., Embry, A.F., and Poulton, P.**
1988: Field observations of the structural and depositional history of Prince Patrick Island and adjacent areas, Canadian Arctic Islands. *In* Current Research, Part D. *Geological Survey of Canada, Paper 88-1A*, p. 41-50.
- Harrison, J.C., Fox, F.G., and Okulitch, A.V.**
1991: Late Devonian-Early Carboniferous deformation of the Parry Islands and Canrobert fold belts, Chapter 12G. *In* Innuitian Orogen and Arctic Platform: Canada and Greenland. *Geological Survey of Canada, Geology of Canada*, no. 3 (also, *Geological Society of America, The Geology of North America*, v. E.).

- Harrison, J.C., Goodbody, Q.H., and Christie, R.L.**
1985: Stratigraphic and structural studies on Melville Island, District of Franklin. *In* Current Research, Part A. Geological Survey of Canada, Paper 85-1A, p. 629-637.
- Hasegawa, W.W.**
1977: Focal parameters of four Sverdrup Basin, Arctic Canada, earthquakes in November and December of 1972. *Canadian Journal of Earth Sciences*, v. 4, p. 2481-2494.
- Hea, J.P., Arcuri, J., Campbell, G.R., Fraser, I., Fuglem, M.O., O'Bertos, J.J., Smith, D.R., and Zayat, M.**
1980: Post-Ellesmerian basins of Arctic Canada: their depocentres, rates of sedimentation and petroleum potential. *In* Facts and principles of world petroleum occurrence, A.D. Miall, (ed.). Canadian Society of Petroleum Geologists, Memoir 6, p. 447-463.
- Heaman, L.M., LeCheminant, A.N., and Rainbird, R.H.**
1990: A U-Pb Baddeleyite study of Franklin igneous events, Canada. Geological Association of Canada-Mineralogical Association of Canada, Joint Annual Meeting, Program and Abstracts.
- Heard, H.C. and Rubey, W.W.**
1966: Tectonic implications of gypsum dehydration. *Geological Society of America, Bulletin*, v. 77, no. 7, p. 741-760.
- Henao-Londoño, D.**
1977: A preliminary geochemical evaluation of the Arctic Islands. *Bulletin of Canadian Petroleum Geology*, v. 25; no. 5, p. 1059-1084.
- Henderson, C.M.**
1988: Conodont paleontology and biostratigraphy of the Upper Carboniferous to Lower Permian Canyon Fiord, Belcher Channel, Nansen, unnamed, and Van Hauen formations, Canadian Arctic Archipelago. Unpublished Ph.D. thesis (December, 1988), University of Calgary, 20 pl., 287 p.
- Heywood, W.W.**
1957: Isachsen area, Ellef Ringnes Island, District of Franklin, Northwest Territories. Geological Survey of Canada, Paper 56-8, 36 p.
- Higgins, A.K.**
1986: Geology of central and eastern North Greenland. *In* Developments in Greenland Geology, F. Kalsbeek and W.S. Watt (eds.). Grønlands Geologiske Undersøgelse, Rapport Nr. 128, p. 37-54.
- Higgins, A.K., Friderichsen, J.D., and Thyrted, T.**
1981: Precambrian metamorphic complexes in the East Greenland Caledonides (72°-74°N) - their relationship to the Eleanore Bay Group, and Caledonian orogenesis. Grønlands Geologiske Undersøgelse, Rapport Nr. 104, p. 5-46.
- Higgins, A.K., Ineson, J.R., Peel, J.S., Surlyk, F., and Sønnerholm, M.**
1991: Lower Paleozoic Franklinian Basin of North Greenland. *In* Sedimentary Basins of North Greenland, J.S. Peel and M. Sønnerholm (eds.). Grønlands Geologiske Undersøgelse, Rapport Nr. 160, p. 71-140.
- Hodgson, D.A.**
1989: Quaternary stratigraphy and chronology (Queen Elizabeth Islands). *In* Chapter 6 of Quaternary Geology of Canada and Greenland, R.J. Fulton (ed.). Geological Survey of Canada, Geology of Canada, no. 1 (also, Geological Society of America, The Geology of North America, v. K-1), p. 452-459.
- Hodgson, D.A., Vincent, J.S., and Fyles, J.G.**
1984: Quaternary geology of central Melville Island, Northwest Territories. Geological Survey of Canada, Paper 83-16, 25 p.
- Hoek, E. and Bray, J.W.**
1981: Rock Slope Engineering. The Institute of Mining and Metallurgy, London, 3rd. ed., 358 p.
- Hoffman, P.F.**
1987: Continental transform tectonics: Great Slave Lake shear zone (ca. 1.9 Ga), northwest Canada. *Geology*, v. 15, no. 9, p. 785-788.
- 1989: Precambrian geology and tectonic history of North America. *In* The Geology of North America - An overview, A.W. Bally and A.R. Palmer (eds.). Geological Society of America, The Geology of North America, v. A, p. 447-509.
- Hoffman, P.F., Tirrul, R., Grotzinger, J.P., Lucas, S.B., and Eriksson, K.A.**
1984: The externides of Wopmay Orogen, Takijuk Lake and Kikerk Lake map areas, District of Mackenzie. *In* Current Research, Part A. Geological Survey of Canada, Paper 84-1A, p. 383-395.
- Hubbert, M.K. and Rubey, W.W.**
1959: Role of fluid pressure in the mechanics of overthrust faulting. 1. Mechanics of fluid-filled solids and its applications to overthrust faulting. *Geological Society of America, Bulletin*, v. 70, p. 115-166.
- Jackson, G.D. and Ianelli, T.R.**
1981: Rift-related cyclic sedimentation in the Neohelikian Borden Basin, northern Baffin Island. *In* Proterozoic Basins of Canada. Paper 81-10, p. 269-302.
- Jaeger, H.**
1979: Devonian Graptolithina. *In* The Devonian System, M.R. House (ed.). Paleontology, Special Paper no. 23, p. 335-339.
- Jaeger, J.C.**
1962: Elasticity, fracture and flow with engineering and geological applications, 2nd edition. Methuen and Co., London, 208 p.
- Jeletzky, J.A.**
1984: Jurassic-Cretaceous biochronology and paleogeography of North America. Geological Association of Canada, Special Paper no. 27, p. 175-256.
- Johannessen, E.P. and Embry, A.F.**
1989: Sequence correlation: Upper Triassic to Lower Jurassic succession, Canadian and Norwegian Arctic. *In* Correlation in Hydrocarbon Exploration. Norwegian Petroleum Society, Graham and Trotman, London, p. 155-170.

- Jones, G.H.**
1981: Economic development - Oil and Gas. *In* A Century of Canada's Arctic Islands, 1880-1980, M. Zaslow (ed.). The Royal Society of Canada, p. 221-230.
- Jones, P.B.**
1982: Oil and gas beneath east-dipping underthrust faults in the Alberta Foothills. *In* Geological studies of the Cordilleran thrust belt, R.B. Powers (ed.). Rocky Mountain Association of Geologists, Denver, Colorado, v. 1, p. 61-74.
- Kanasewich, E.R. and Berkes, Z.**
1988: Reprocessed and interpreted seismic reflection data from the Arctic Platform, Parry Islands Fold Belt, and the Sverdrup Basin of eastern Melville Island, Canadian Arctic Islands: a study of geophysical data acquired by industry within portions of NTS 78F, 78G, 79B and 88E. Geological Survey of Canada, Open File 1818, 230 p.
1990: Seismic structure of the Proterozoic on Melville Island, Canadian Arctic Archipelago. *Marine Geology*, v. 93.
- Kerr, J.W.**
1967: Stratigraphy of central and eastern Ellesmere Island, Arctic Canada. Part I. Proterozoic and Cambrian. Geological Survey of Canada, Paper 67-27, Part I, 63 p.
1968: Stratigraphy of central and eastern Ellesmere Island, Arctic Canada. Part II. Ordovician. Geological Survey of Canada, Paper 67-27, Part II, 67 p.
1974: Geology of the Bathurst Island group and Byam Martin Island, Arctic Canada (Operation Bathurst Island). Geological Survey of Canada, Memoir 378, 152 p.
1975: Cape Storm Formation - a new Silurian unit in the Canadian Arctic. *Bulletin of Canadian Petroleum Geology*, v. 23, p. 67-83.
- Kirsch, H.J.**
1987: Correlation between indicators of very low-grade metamorphism. *In* Low Temperature Metamorphism, M. Frey (ed.). Blackie and Son, London, p. 227-300.
- Klapper, G.**
1969: Lower Devonian conodont sequence, Royal Creek, Yukon Territory, and Devon Island, Canada. *Journal of Paleontology*, v. 43, p. 1-27.
- Klapper, G. and Johnson, J.G.**
1980: Endemism and dispersal of Devonian conodonts. *Journal of Paleontology*, v. 54, p. 400-455.
- König, C.**
1824: Rock Specimens. *In* A Supplement to the Appendix of Captain Parry's voyage for the discovery of a northwest passage, in the years 1819-1820, London, J. Murray (ed.). p. 247-257.
- Lane, H.R. and Ormiston, A.R.**
1979: Siluro-Devonian biostratigraphy of the Salmontrout River area, east-central Alaska. *Geological Paleontology*, v. 13, p. 39-96.
- Larner, K., Gibson, B., and Chambers, R.**
1983: Imaging beneath complex structure. *In* Seismic Expression of Structural Styles, v. 1, A.W. Bally (ed.). American Association of Petroleum Geologists, Studies in Geology Series, no. 15, p. 26-39.
- LeCheminant, A.N. and Heaman, L.M.**
1989: Mackenzie igneous events, Canada: Middle Proterozoic hotspot magmatism associated with ocean opening. *Earth and Planetary Science Letters*, v. 96, p. 38-48.
- Lenz, A.C.**
1990: Ludlow and Pridoli (Upper Silurian) graptolite biostratigraphy of the central Arctic Islands: a preliminary report. *Canadian Journal of Earth Sciences*, v. 27, p. 1074-1083.
- Lenz, A.C. and Borré, D.J.**
1993: A note on graptolite correlation of the Canrobert and Ibbett Bay formations, Nisbet Point, northwestern Melville Island. *In* The Geology of Melville Island, R.L. Christie and N.J. McMillan (eds.). Geological Survey of Canada, Bulletin 450.
- Lenz, A.C. and Melchin, M.J.**
1990: Wenlock (Silurian) graptolite biostratigraphy of the Cape Phillips Formation, Canadian Arctic Islands. *Canadian Journal of Earth Sciences*, v. 27, p. 1-13.
- Liebe, R.M.**
1962: Conodonts from the Alexandrian and Niagaran Series (Silurian) of the Illinois Basin. Unpublished Ph.D. dissertation, State University, Iowa, 162 p., pls. 1-3.
- Long, D.G.F.**
1989a: Kennedy Channel Formation: key to the early history of the Franklinian continental margin, central eastern Ellesmere Island, Arctic Canada. *Canadian Journal of Earth Sciences*, v. 26, p. 1147-59.
1989b: Ella Bay Formation: Early Cambrian shelf differentiation in the Franklinian basin, central eastern Ellesmere Island, Arctic Canada. *Canadian Journal of Earth Science*, v. 26, p. 2621-2635.
- Majid, A.H.**
1989: Sequence stratigraphy, lithostratigraphy, and hydrocarbon potential of the subsurface upper Paleozoic section of Sabine Peninsula, Melville Island, Canadian Arctic Archipelago. *In* Current Research, Part G. Geological Survey of Canada, Paper 89-1G, p. 167-176.
- Mamet, B.L., Farmer, J.D., Fischer, R., and Reed, W.E.**
1993: Biostratigraphy of the Ebbadalen Formation (Bashkirian, Carboniferous) at Odelfjellet, central Spitsbergen. *Compte Rendu XII International Congress of Carboniferous Stratigraphy and Geology*, Buenos Aires, 1992, v. 1.
- Matthews, J.V., Ovenden, L.E., and Fyles, J.G.**
1987: Plant and insect fossils from the late Tertiary Beaufort Formation on Prince Patrick Island, N.W.T. *In* Canada's missing dimension; science and history in the Canadian Arctic Islands, C.R. Harington (ed.). p. 105-139.

- Mayr, U.**
1978: Stratigraphy and correlation of lower Paleozoic formations, subsurface of Cornwallis, Devon, Somerset, and Russell islands, Canadian Arctic Archipelago. Geological Survey of Canada, Bulletin 276, 55 p.
- 1980: Stratigraphy and correlation of lower Paleozoic formations, subsurface of Bathurst Island and adjacent smaller islands, Canadian Arctic Archipelago. Geological Survey of Canada, Bulletin, v. 306, 52 p.
- Mayr, U., Uyeno, T.T., Tipnis, R.S., and Barnes, C.R.**
1980: Subsurface stratigraphy and conodont zonation of the lower Paleozoic succession, Arctic Platform, in southern Arctic Archipelago. In Current Research, Part A. Geological Survey of Canada, Paper 80-1A, p. 209-215.
- McCracken, A.D.**
1985: Middle Ordovician to Silurian (Wenlock) conodont taxonomy and biostratigraphy from basal strata of the Road River Formation in the Richardson Mountains, northern Yukon Territory. Ph.D. Thesis, The University of Western Ontario, London, Ontario.
- McGhee, R.**
1978: Canadian Arctic Prehistory. Van Nostrand Reinhold Ltd., Toronto, for the National Museum of Man, 128 p.
- McIntyre, D.J.**
1989: Paleocene palynoflora from northern Somerset Island, District of Franklin, N.W.T. In Current Research, Part G. Geological Survey of Canada, Paper 89-1G, p. 191-197.
- McIntyre, D.J. and Ricketts, B.D.**
1989: New palynological data from Cornwall Arch, Cornwall and Amund Ringnes islands, District of Franklin, N.W.T. In Current Research, Part G. Geological Survey of Canada, Paper 89-1G, p. 199-202.
- M'Clintock, Sir Francis Leopold**
1857: Reminiscences of Arctic Ice Travel in Search of Sir John Franklin and his Companions. Journal of the Royal Society, Dublin, v. 1, p. 183-280.
- McGregor, D.C.**
1993: Palynological correlation of Middle and Upper Devonian rocks of Melville Island, Arctic Canada. In The Geology of Melville Island, R.L. Christie and N.J. McMillan (eds.). Geological Survey of Canada, Bulletin 450.
- McGregor, D.C. and Camfield, M.**
1982: Middle Devonian miospores from the Cape de Bray, Weatherall, and Hecla Bay formations of northeastern Melville Island. Geological Survey of Canada, Bulletin 348, 105 p., 18 pls.
- McGregor, D.C. and Uyeno, T.T.**
1972: Devonian spores and conodonts of Melville and Bathurst islands, District of Franklin. Geological Survey of Canada, Paper 71-13, 37 p.
- McLaren, D.J.**
1963: Goose Fiord to Bjorne Peninsula. In Geology of the north-central part of the Arctic Archipelago, Northwest Territories (Operation Franklin), Y.O. Fortier et al. (ed.). Geological Survey of Canada, Memoir 320, p. 310-338.
- McMechan, M.E.**
1985: Low-taper triangle-zone geometry: an interpretation for the Rocky Mountain foothills, Pine Pass-Peace River area, British Columbia. Bulletin of Canadian Petroleum Geology, v. 33, p. 31-38.
- Melchin, M.J.**
1987: Late Ordovician and Early Silurian graptolites, Cape Phillips Formation, Canadian Arctic Archipelago. Ph.D. Thesis, The University of Western Ontario, London, Ontario.
- 1989: Llandovery graptolite biostratigraphy and paleobiogeography, Cape Phillips Formation, Canadian Arctic Islands. Canadian Journal of Earth Sciences, v. 26, p. 1726-1746.
- Meneley, R.A., Henao, D., and Merritt, R.**
1975: The northwest margin of the Sverdrup Basin. In Canada's continental margins and offshore petroleum exploration, C.J. Yorath, E.R. Parker and D.J. Glass (eds.). Canadian Society of Petroleum Geologists, Memoir 4, p. 531-544.
- Miall, A.D.**
1986: The Eureka Sound Group (Upper Cretaceous-Oligocene), Canadian Arctic Islands. Bulletin of Canadian Petroleum Geology, v. 34, p. 240-270.
- Mitchum, R.M. and Vail, P.R.**
1977: Seismic stratigraphic interpretation procedure. In Seismic stratigraphy - applications to hydrocarbon exploration, C.E. Payton (ed.). American Association of Petroleum Geologists, Memoir 26, p. 135-144.
- Montadert, L., Roberts, D.G., de Charpal, O., and Guennoc, P.**
1979: Rifting and subsidence of the northern continental margin of the Bay of Biscay. In Initial reports of the Deep-Sea Drilling Project, L. Montadert and D.G. Roberts (eds.). U.S. Govt. Printing Office, Washington, D.C., p. 1025-1060.
- Morganti, J.**
1981: Sedimentary-type stratiform ore deposits: some models and a new classification. Geoscience Canada, v. 8, p. 65-75.
- Mossop, G.D.**
1979: The evaporites of the Baumann Fiord Formation, Ellesmere Island, Arctic Canada. Geological Survey of Canada, Bulletin 298, 52 p.
- Murphy, M.A. and Berry, W.B.N.**
1983: Early Devonian conodont-graptolite collation and correlations with brachiopod and coral zones, central Nevada. American Association of Petroleum Geologists, Bulletin, v. 67, p. 371-379.
- Murphy, M.A., Matti, J.C., and Walliser, O.H.**
1981: Biostratigraphy and evolution of the *Ozarkodina remscheidensis-Eognathodus sulcatus* lineage (Lower Devonian) in Germany and central Nevada. Journal of Paleontology, v. 55, p. 747-772.
- Nassichuk, W.W.**
1965: Pennsylvanian and Permian rocks in the Parry Islands Group, Canadian Arctic Archipelago. In Report of

- Activities. Geological Survey of Canada, Report of Activities, Paper 65-1, p. 9-12.
- 1970: Permian ammonoids from Devon and Melville Islands, Canadian Arctic Archipelago. *Journal of Paleontology*, v. 44, no. 1, p. 77-97.
- 1975: Carboniferous ammonoids and stratigraphy in the Canadian Arctic Archipelago. Geological Survey of Canada, Bulletin 237, 240 p.
- Nassichuk, W.W. and Davies, G.R.**
- 1980: Stratigraphy and sedimentation of the Otto Fiord Formation. Geological Survey of Canada, Bulletin 286, 87 p.
- Nassichuk, W.W., Furnish, W.M., and Glenister, B.F.**
- 1965: The Permian ammonoids of Arctic Canada. Geological Survey of Canada, Bulletin 131, 72 p.
- Nassichuk, W.W. and Wilde, G.L.**
- 1977: Permian fusulinaceans and stratigraphy at Blind Fiord, southwestern Ellesmere Island. Geological Survey of Canada, Bulletin, 59 p.
- Nielsen, T.F.D.**
- 1987: Mafic dyke swarms in Greenland: A review. *In* Mafic dyke swarms, H.C. Halls and W.F. Fahrig (eds.). Geological Association of Canada, Special Paper 34, p. 349-360.
- Norlands Petroleum Ltd.**
- 1974: Interpretation of seismic reflection data conducted on Magnorth Petroleum Ltd. acreage, Viscount Melville Sound, District of Franklin, N.W.T. for Norlands Petroleum Ltd. Canadian Oil and Gas Lands Administration, assessment report 511-09-09-014.
- 1976: Interpretation of seismic reflection data conducted on Magnorth Petroleum Ltd. acreage, Wellington Channel, Viscount Melville Sound, and M'Clure Strait, District of Franklin, N.W.T. for Norlands Petroleum Ltd. Canadian Oil and Gas Lands Administration, assessment report 511-09-10-017.
- Norris, A.W.**
- 1985: Stratigraphy of Devonian outcrop belts in northern Yukon Territory and northwestern District of Mackenzie (Operation Porcupine Area). Geological Survey of Canada, Memoir 410, 81 p.
- Norris, D.K.**
- 1972: En echelon folding in the Northern Cordillera of Canada. *Bulletin of Canadian Petroleum Geology*, v. 20, p. 634-642.
- Nowlan, G.S.**
- 1976: Late Cambrian to Late Ordovician conodont evolution and biostratigraphy of the Franklinian Miogeosyncline, Eastern Canadian Arctic Islands. Unpublished Ph.D. thesis, University of Waterloo, Waterloo, Ontario, 591 p.
- 1985: Late Cambrian and Early Ordovician conodonts from the Franklinian Miogeosyncline, Canadian Arctic Islands. *Journal of Paleontology*, v. 59, p. 96-122.
- Okulitch, A.V. and Trettin, H.P.**
- 1991: Cretaceous-Early Tertiary deformation, Arctic Islands, chapter 17. *In* Inuitian Orogen and Arctic Platform: Canada and Greenland, H.P. Trettin (ed.). Geological Survey of Canada, Geology of Canada No. 3 (also, Geological Society of America, The Geology of North America, v. E).
- Osborn, S.**
- 1857: The Discovery of the North-West Passage by H.M.S. *Investigator*, Captain R. M'Clure, 1850, 1851, 1852, 1853, 1854 (Second Edn.), London, Longmans Green, 405 p.
- Overton, A.**
- 1972: Seismic refraction surveys, western Queen Elizabeth Islands and Polar continental margin. *Canadian Journal of Earth Sciences*, v. 7, p. 346-365.
- 1982: Seismic reconnaissance profiles across the Sverdrup Basin, Canadian Arctic Islands. *In* Current Research, Part B. Geological Survey of Canada, Paper 82-1B, p. 139-145.
- Palache, C., Berman, H., and Frondel, C.**
- 1951: Dana's system of mineralogy. Seventh edition, vol. II, John Wiley and Sons, New York, 1124 p.
- Palmer, A.R. (compiler)**
- 1983: The Decade of North American Geology geologic time scale. *Geology*, v. 11, p. 503-504.
- Panarctic Oils Limited**
- 1986: Annual Report of Panarctic Oils Limited, Calgary, 7 p.
- Park, R.G.**
- 1983: Foundations of Structural Geology. Blackie, New York, 135 p.
- Parry, Sir W.E.**
- 1821: Journal of a Voyage for the Discovery of a North-West Passage from the Atlantic to the Pacific performed in the years 1819-1820 in H.M.S. *Hecla* and *Griper*; London, John Murray.
- Pedder, A.E.H.**
- 1975: Revised megafossil zonation of Middle and lowest Upper Devonian strata, central Mackenzie Valley. *In* Report of Activities, Part A. Geological Survey of Canada, Paper 75-1A, p. 571-576.
- Pieuchot, M. and Sercel**
- 1984: Seismic Instrumentation, volume 2. *In* Handbook of Geophysical Exploration: Section I, Seismic Exploration. Geophysical Press, London, 375 p.
- Polar Continental Shelf Project**
- 1965: Aeromagnetic maps of Melville Island, District of Franklin, Scale 1:126 720. Geological Survey of Canada, geophysical maps 3442G-3455G.
- 1987: Aeromagnetic maps of Melville Island, District of Franklin, Northwest Territories, Scale 1:125,000. Geological Survey of Canada, geophysical maps 9707G-9722G.

- Pollock, C.A., Rexroad, C.B., and Nicoll, R.S.**
1970: Lower Silurian conodonts from northern Michigan and Ontario. *Journal of Paleontology*, v. 44, no. 4, p. 743-764, pls. 111-114.
- Poulton, T.P.**
1993: Jurassic stratigraphy and fossil occurrences - Melville, Prince Patrick and Borden islands. *In* The Geology of Melville Island, R.L. Christie and N.J. McMillan (eds.). Geological Survey of Canada, Bulletin 450.
- Powell, T.G.**
1978: An assessment of the hydrocarbon source rock potential of the Canadian Arctic Islands. Geological Survey of Canada, Paper 78-12, 82 p.
- Rahmani, R.A. and Hopkins, W.S., Jr.**
1977: Geological and palynological interpretation of Eureka Sound Formation on Sabine Peninsula, northern Melville Island, District of Franklin. *In* Report of Activities, Part B. Geological Survey of Canada, Paper 77-1B, p. 185-189.
- Ramberg, H.**
1959: Evolution of pygmatic folding. *Norsk Geologisk Tidsskrift*, v. 39, p. 99-151.
1970: Folding of compressed multilayers in the field of gravity II. numerical examples. *Physics of the Earth and Planetary Interiors*, v. 4, p. 83-120.
- Ramsay, J.G.**
1967: Folding and fracturing of rocks. McGraw Hill, New York, 568 p.
- Ramsay, J.G. and Huber, M.I.**
1987: The techniques of modern structural geology, volume 2: folds and fractures. Academic Press, London, 393 p.
- Richardson, J.B. and McGregor, D.C.**
1986: Silurian and Devonian spore zones of the Old Red Sandstone continent and adjacent regions. Geological Survey of Canada, Bulletin 364, 79 p.
- Ricketts, B.D.**
1986: New formations in the Eureka Sound Group. *In* Current Research, Part B. Geological Survey of Canada, Paper 86-1B, p. 363-404.
1991: Delta evolution in the Eureka Sound Group, western Axel Heiberg Island: the transition from wave-dominated to fluvial-dominated deltas. Geological Survey of Canada, Bulletin 402, 72 p.
- Riediger, R.L. and Harrison, J.C.**
1993: The Upper Carboniferous and Lower Permian Canyon Fiord Formation, Melville Island. *In* The Geology of Melville Island, R.L. Christie and N.J. McMillan (eds.). Geological Survey of Canada, Bulletin 450.
- Sandberg, C.A. and Dressen, R.**
1984: Late Devonian icriodontid biofacies models and alternate shallow-water conodont zonation. Geological Society of America, Special Paper 196, p. 143-178.
- Sartenaer, P.**
1969: Late Upper Devonian (Famennian) rhynchonellid brachiopods from western Canada. Geological Survey of Canada, Bulletin 169, 269 p.
- Schei, Per**
1903: Summary of geological results. *Geographical Journal*, v. 22, p. 56-65.
1904: Preliminary account of the geological investigations made during the Second Norwegian polar expedition in the Fram. *In* Sverdrup, Otta, New land; four years in the Arctic regions. v. 2, p. 455-466.
- Skibo, D.N., Harrison, C., Gentzis, T., and Goodarzi, F.**
1991: Organic maturity/time-temperature models of the Ellesmerian (Paleozoic) Orogeny, Melville Island, Northwest Territories. *In* Current Research, Part E. Geological Survey of Canada, Paper 91-1E, p. 165-175.
- Sobczak, L.W. and Halpenny, J.F.**
1990: Gravity anomaly maps of the Arctic. *Marine Geology*, v. 93, p. 15-41.
- Sobczak, L.W. and Overton, A.**
1984: Shallow and deep crustal structure of the western Sverdrup Basin, Arctic Canada. *Canadian Journal of Earth Sciences*, v. 21, p. 902-919.
- Sobczak, L.W., Mayr, U., and Sweeney, J.F.**
1986: Crustal section across the polar continent-ocean transition in Canada. *Canadian Journal of Earth Sciences*, v. 23, p. 608-621.
- Souther, J.G.**
1963: Geological traverse across Axel Heiberg Island from Buchanan Lake to Strand Fiord. *In* Geology of the north-central part of the Arctic Archipelago, N.W.T. (Operation Franklin), Y.O. Fortier (ed.). Geological Survey of Canada, Memoir 320, p. 426-448.
- Stefansson, V.**
1921: The friendly Arctic: the story of five years in polar regions. New York, Macmillan.
- Stephenson, R.A., Embry, A.F., Nakiboglu, S.M., and Hastaoglu, M.A.**
1987: Rift-initiated Permian to Early Cretaceous subsidence of the Sverdrup Basin. *In* Sedimentary basins and basin-forming mechanisms, C. Beaumont and A.J. Tankard (eds.). Canadian Society of Petroleum Geologists, Memoir 12, p. 213-231.
- Stewart, W.D.**
1987: Late Proterozoic to early Tertiary stratigraphy of Somerset Island and northern Boothia Peninsula, District of Franklin, N.W.T. Geological Survey of Canada, Paper 83-26, 78 p.
- Stuart-Smith, S.J.H. and Wennekers, J.H.N.**
1979: Geology and hydrocarbon discoveries of Canadian Arctic Islands. *Bulletin of the American Association of Petroleum Geologists*, v. 61, p. 1-27.
- Suneby, L.B. and Hills, L.V.**
1988: Palynological zonation of the Heiberg Formation (Triassic-Jurassic), eastern Sverdrup Basin, Arctic

Canada. Bulletin of Canadian Petroleum Geology, v. 36, p. 347-361.

Suppe, J.

1983: Geometry and kinematics of fault-bend folding. *American Journal of Science*, v. 283, p. 684-721.

Suppe, J. and Chang, Y.L.

1983: Kink method applied to structural interpretation of seismic sections, western Taiwan. *Petroleum Geology of Taiwan*, v. 19, p. 29-49.

Surlyk, F. and Ineson, J.R.

1987: Aspects of Franklinian shelf, slope and trough evolution and stratigraphy in North Greenland. *Grønlands Geologiske Undersølgelse, Rapport Nr. 133*, p. 41-58.

Sweet, W.C., Ethington, R.L., and Barnes, C.R.

1971: North American Middle and Upper Ordovician conodont faunas. In *Symposium on conodont biostratigraphy*, W.C. Sweet and S.M. Bergström (eds.). Geological Society of America, Memoir 127, p. 163-193.

Sweeney, J.F., Balkwill, H.R., Franklin, R., Mayr, U., McGrath, P., Snow, E., Sobczak, L.W., Wetmiller, R.J., and Panarctic Oils Ltd.

1986: G. Somerset Island to Canada Basin. Geological Society of America, Centennial Continent/Ocean Transect #11.

Taylor, A.

1964: Geographical discovery and exploration in the Queen Elizabeth Islands. Geographical Branch, Memoir 3, Mines and Technical Surveys, Ottawa, 172 p.

Tappan, H.

1955: Foraminifera from the Arctic Slope of Alaska: pt. 2, Jurassic foraminifera. United States Geological Survey, Professional Paper 236-B, p. 21-90.

Telford, W.M., Geldart, L.P., Sheriff, R.E., and Keys, D.A.

1976: *Applied Geophysics*. Cambridge University Press, Cambridge, U.K., 860 p.

Texaco Canada Resources Ltd.

1983: Melville Island - Northwest Territories, Canada: Line No. 7. In *Seismic expression of structural styles*, v. 3, A.W. Bally (ed.). American Association of Petroleum Geologists, p. 3.4.1-73 to 3.4.1-78.

Thorsteinsson, R.

1958: Cornwallis and Little Cornwallis islands, District of Franklin, Northwest Territories. Geological Survey of Canada, Memoir 294 (1959), 134 p.

1963: Geology of the north-central part of the Arctic Archipelago, Northwest Territories (Operation Franklin), Prince Alfred Bay, Y.O. Fortier et al. (ed.). Geological Survey of Canada, Memoir 320, 671 p.

1974: Carboniferous and Permian stratigraphy of Axel Heiberg Island and western Ellesmere Island, Canadian Arctic Archipelago. Geological Survey of Canada, Bulletin 224, 115 p.

1988: Geology of Cornwallis Island and neighbouring smaller islands, Canadian Arctic Archipelago, District of

Franklin, Northwest Territories. Geological Survey of Canada, Map 1626A (scale 1:250 000).

Thorsteinsson, R. and Fortier, Y.O.

1954: Report of progress on the geology of Cornwallis Island, Arctic Archipelago, Northwest Territories. Geological Survey of Canada, Paper 53-24, 25 p.

Thorsteinsson, R. and Kerr, J. Wm.

1968: Cornwallis Island and adjacent smaller islands, Canadian Arctic Archipelago. Geological Survey of Canada, Paper 67-64, 16 p.

Thorsteinsson, R. and Mayr, U.

1987: The sedimentary rocks of Devon Island, Canadian Arctic Archipelago. Geological Survey of Canada, Memoir 411, 182 p.

Thorsteinsson, R. and Tozer, E.T.

1957: Geological investigations in Ellesmere and Axel Heiberg Islands, 1956. *Arctic (Journal of the Arctic Institute of North America)*, v. 10, no. 1, p. 2-31.

1960: Summary account of structural history of the Canadian Arctic Archipelago since Precambrian time. Geological Survey of Canada, Paper 60-7, 25 p.

1962: Banks, Victoria, and Stefansson islands, Arctic Archipelago. Geological Survey of Canada, Memoir 330, 83 p.

1970: Geology of the Arctic Archipelago. In *Geology and Economic Minerals of Canada*, R.J.W. Douglas (ed.). Geological Survey of Canada, Economic Geology Report no. 1, p. 547-590.

Thorsteinsson, R. and Uyeno, T.T.

1980: Stratigraphy and conodonts of Upper Silurian and Lower Devonian rocks in the environs of the Boothia Uplift, Canadian Arctic Archipelago; Part 1, Contributions to stratigraphy by R. Thorsteinsson with contributions by T.T. Uyeno. Geological Survey of Canada, Bulletin 292, 75 p.

Tissot, B.P. and Welte, D.H.

1984: *Petroleum Formation and Occurrence*. 2nd ed. Springer-Verlag, Berlin, 699 p.

Tokuda, S.P.

1926-27: On the en echelon structure of the Japanese Archipelago. *Japanese Journal of Geology and Geography*, v. 5, p. 41-76.

Tozer, E.T.

1956: Geological reconnaissance, Prince Patrick, Eglinton, and western Melville islands, Arctic Archipelago, Northwest Territories. Geological Survey of Canada, Paper 55-5, 32 p.

1961: Triassic stratigraphy and faunas, Queen Elizabeth Islands, Arctic Archipelago. Geological Survey of Canada, Memoir 316, 184 p.

1963a: Southeastern Sabine Peninsula, Melville Island. In *Geology of the north-central part of the Arctic Archipelago, Northwest Territories (Operation Franklin)*. Geological Survey of Canada, Memoir 320, p. 645-655.

- 1963b: Mesozoic and Tertiary stratigraphy. *In* Geology of the north-central part of the Arctic Archipelago, Northwest Territories (Operation Franklin). Geological Survey of Canada, Memoir 320, p. 74-95.
- 1965: Lower Triassic stages and ammonoid zones of Arctic Canada. Geological Survey of Canada, Paper 65-12, 14 p.
- Tozer, E.T. and Thorsteinsson, R.**
- 1964: Western Queen Elizabeth Islands, Arctic Archipelago. Geological Survey of Canada, Memoir 332, 242 p.
- Trettin, H.P.**
- 1969: Lower Paleozoic sediments of northwestern Baffin island, District of Franklin. Geological Survey of Canada, Bulletin 157, 70 p.
- 1989: The Arctic Islands. *In* The Geology of North America - An overview, A.W. Bally and A.R. Palmer (eds.). Geological Society of America, The Geology of North America, v. A, p. 349-370.
- 1991: Inuitian Orogen and Arctic Platform: Canada and Greenland, H.P. Trettin (ed.). Geological Survey of Canada, Geology of Canada No. 3 (also, Geological Society of America. The Geology of North America, v. E).
- Trettin, H.P. (compiler)**
- 1972: The Inuitian Province. *In* Variations in Tectonic Styles in Canada, R.A. Price and R.J.W. Douglas (eds.). Geological Association of Canada, Special Paper No. 11, p. 83-179.
- 1990: Geotectonic correlation chart; Figure 4, Sheet 1. *In* Inuitian Orogen and Arctic Platform: Canada and Greenland, H.P. Trettin (ed.). Geological Survey of Canada, Geology of Canada No. 3 (also, Geological Society of America. The Geology of North America, v. E).
- Trettin, H.P. and Hills, L.V.**
- 1966: Lower Triassic tar sands of northwestern Melville Island, Arctic Archipelago. Geological Survey of Canada, Paper 66-34, 122 p.
- Trettin, H.P., Mayr, U., Long, G.D.F., and Packard, J.J.**
- 1991: Cambrian to Early Devonian deposition, Arctic Islands. *In* Inuitian Orogen and Arctic Platform: Canada and Greenland, H.P. Trettin (ed.). Geological Survey of Canada, Geology of Canada No. 3 (also, Geological Society of America, The Geology of North America, v. E).
- Troelsen, J.C.**
- 1950: Contributions to the Geology of Northwest Greenland, Ellesmere and Axel Heiberg Islands. Meddeleser om Grønland, v. 147, no. 7.
- Tucker, R.D., Krogh, T.E., Ross, R.J., Jr., and Williams, S.H.**
- 1990: Time-scale calibration by high-precision U-Pb zircon dating of interstratified volcanic ashes in the Ordovician and Lower Silurian stratotypes of Britain. *Earth and Planetary Science Letters*, v. 100, p. 51-58.
- Turner, S.**
- 1982: Middle Palaeozoic elasmobranch remains from Australia. *Journal of Vertebrate Paleontology*, v. 2, p. 117-131.
- Utting, J.**
- 1985: Preliminary results of palynological studies of the Permian and lowermost Triassic sediments, Sabine Peninsula, Melville Island, Canadian Arctic Archipelago. *In* Current Research, Part B. Geological Survey of Canada, Paper 85-1B, p. 231-238.
- 1989: Preliminary palynological zonation of surface and subsurface Carboniferous, Permian and lowest Triassic rocks, Sverdrup Basin, Canadian Arctic Archipelago. *In* Current Research, Part G. Geological Survey of Canada, Paper 89-1G, p. 233-240.
- Utting, J., Goodarzi, F., Dougherty, B.J., and Henderson, C.M.**
- 1989a: Thermal maturity of Carboniferous and Permian rocks of the Sverdrup Basin, Canadian Arctic Archipelago. Geological Survey of Canada, Paper 89-19, 20 p.
- Utting, J., Jachowicz, M., and Jachowicz, A.**
- 1989b: Palynology of the Lower Carboniferous Emma Fiord Formation of Devon, Axel Heiberg, and Ellesmere islands, Canadian Arctic Archipelago. *In* Contributions to Canadian Paleontology. Geological Survey of Canada, Bulletin 396, p. 145-171.
- Uyeno, T.T.**
- 1990: Biostratigraphy and conodont faunas of Upper Ordovician through Middle Devonian rocks, eastern Arctic Archipelago. Geological Survey of Canada, Bulletin 401, 211 p.
- 1981: Systematic study of conodonts. *In* Stratigraphy and conodonts of Upper Silurian and Lower Devonian rocks in the environs of the Boothia Uplift, Canadian Arctic Archipelago, R. Thorsteinsson and T.T. Uyeno (eds.). Geological Survey of Canada, Bulletin 292, Part II, p. 39-75.
- 1975: Devonian assemblages (conodonts), Dome et al. Weatherall O-10 well. *In* Biostratigraphic determinations from the subsurface of the districts of Franklin and Mackenzie and the Yukon Territory. Geological Survey of Canada, Paper 75-10, p. 14.
- Vail, P.R.**
- 1987: Seismic stratigraphy interpretation using sequence stratigraphy. *In* Atlas of Seismic Stratigraphy, volume 1, A.W. Bally, (ed.). American Association of Petroleum Geologists, Studies in Geology, no. 27, p. 1-10.
- van der Houwen, P.J. and Schwartz, R.A.**
- 1983: Final geophysical report I-448 on northeast Banks Island for Panarctic Oils Ltd. Canadian Oil and Gas Lands Administration, assessment report 624-06-09-271.
- Van Wagoner, J.C., Mitchum, R.M., Posamentier, H.W., and Vail, P.R.**
- 1987: Part 2: Key definitions of sequence stratigraphy. *In* Atlas of Seismic Stratigraphy, volume 1, A.W. Bally, (ed.). American Association of Petroleum Geologists, Studies in Geology, no. 27, p. 11-14.

Van Wagoner, J.C., Posamentier, H.W., Mitchum, R.M., Vail, P.R., Sarg, J.F., Loutit, T.S., and Hardenbol, J.

- 1988: An overview of the fundamentals of sequence stratigraphy and key definitions. *In* Sea-Level Changes - An Integrated Approach, (C.K. Wilgus, B.S. Hastings, C.A. Ross, H.W. Posamentier, J. Van Wagoner, and C.G. St. C. Kendall). Society of Economic Paleontologists and Mineralogists, Special Publication No. 42, p. 39-45.

Vincent, J-S.

- 1989: Quaternary geology of the northern Interior Plains. *In* Chapter 2 of Quaternary Geology of Canada and Greenland, R.J. Fulton (ed.). Geological Survey of Canada, Geology of Canada, no. 1 (also, Geological Society of America, The Geology of North America, v. K-1), p. 100-137.

Wall, J.H.

- 1983: Jurassic and Cretaceous foraminiferal biostratigraphy in the eastern Sverdrup Basin, Canadian Arctic Archipelago. *Bulletin of Canadian Petroleum Geology*, v. 31, no. 4, p. 246-281.

Walliser, O.H.

- 1964: Conodonten des Silurs. *Abhandlungen des Hessischen Landesamtes für Bodenforschungen*, Heft 41, 106 p., 32 pls.

Waylett, D.C.

- 1979: Natural gas in the Arctic Islands - discovered reserves and future potential. *Journal of Petroleum Geology*, v. 1, no. 3, p. 21-34.

- 1990: Drake Point Gas Field, Canadian Arctic Islands. *In* Structural traps; I. Tectonic fold traps, E.A. Beaumont and N.H. Foster (eds.). American Association of Petroleum Geology, Treatise of Petroleum Geology, Atlas of Oil and Gas Fields A-016, p. 77-102.

Winkler, H.G.F.

- 1976: *Petrogenesis of Metamorphic Rocks*. 4th ed. Springer-Verlag, Berlin, 334 p.

Woodward, N.B., Boyer, S.E., and Suppe, J.

- 1989: Balanced geological cross-sections: an essential technique in geological research and exploration. American Geophysical Union, Short Course in Geology, v. 6, 132 p.

Young, G.M.

- 1981: The Amundsen Embayment, Northwest Territories; relevance to the upper Proterozoic evolution of North America. *In* Proterozoic Basins of Canada, F.H. Campbell (ed.). Geological Survey of Canada, Paper 81-10, p. 203-218.

Yilmaz, O.

- 1987: *Seismic Data Processing*. Society of Exploration Geophysicists, Tulsa, OK, 526 p.

Zaslow, M.

- 1981: A century of Canada's Arctic Islands - 1880-1980. The Royal Society of Canada, 358 p.

APPENDICES 1-4

APPENDIX 1

Acquisition parameters for reprocessed seismic data

Accompanying notes (keyed to bracketed superscript numbers in the tables on the following pages)

1. GD1 = gelatin-type dynamite ("GEOGEL").
2. GD2 = gelatin-type dynamite ("NITROPEL").
3. DFS-3, 4, 5 are made by Texas Instruments of Houston, Texas.
4. The alias filter is a high-cut band-pass filter that passes on all frequencies below 124 HZ (in this case) for future processing.
5. For line TPC4, a low-cut filter was also applied during the recording stage.
6. L2 and L10 models are made by Mark Products Inc. of Houston, Texas.
7. Each receiving station includes an array of 9 or 12 geophones arranged in a line (9IL and 12IL, respectively) normally parallel to the seismic survey line.
8. 9/11 = 9 geophones in a liner array that is 11 m long.
9. Spread type 1: symmetrical split-dip spread with a shotpoint gap.
10. Spread type 2: asymmetrical split-dip spread without a shotpoint gap. The shothole is at geophone 25.

LINE	DATE	SOURCE			
		Source type	Source interval (m)	Shothole depth (m)	Charge size (kg)
Panarctic data					
P726	03/72	GD1 ⁽¹⁾	268	22	34
P872	10/72	GD1	268	18	40
P1135	04/73	GD1	268	18	36.2
P1137	03/73	GD1	268	18	36
P1147	03/73	GD1	268	19	32
P1192	11/73	GD1	268	24	36
P1193	11/73	GD1	268	18	22.6
P1654	03/75	GD1	300	22	22.6
P1660	07/75	GD1	268	20	22.6
P1662	06/75	GD1	268	18	22.6
P1662A	06/75	GD1	268	18	22.6
P1763	03/75	GD1	268	18	22.6
P1788	05/75	GD1	268	22	22.6
P1830	02/75	GD1	268	22	22.6
P2061	04/76	GD1	268	18	22.6
P2185	05/76	GD1	201	18	22.6
P2186	05/76	GD1	201	18	22.6
P2189	05/76	GD1	201	18	22.6
P2218	03/77	GD1	300	19	22.6
P2219	03/77	GD1	300	20	22.6
P2227	03/77	GD1	300	40	22.6
Chevron data					
C75	11/72	GD1	268	25	36.2
C131X	03/72	GD1	268	27	36.3
Texaco data					
T4	04/73	GD2 ⁽²⁾	268	27	34

LINE	RECORDING INSTRUMENTS				
	Make/model	Record length (sec)	Alias filter (hz)	No. of channels	Sample interval (msec)
Panarctic data					
P726	DFS-4 ⁽³⁾	6 ⁽¹⁾	124 ⁽⁴⁾	48	2
P872	DFS-3	6	124	48	2
P1135	DFS-3	8	124	48	2
P1137	DFS-3	8	124	48	2
P1147	DFS-3	8	124	48	2
P1192	DFS-3	8	124	48	2
P1193	DFS-3	8	124	48	2
P1654	DFS-3	8	124	48	2
P1660	DFS-3	8	124	48	2
P1662	DFS-3	8	124	48	2
P1662A	DFS-3	8	124	48	2
P1763	DFS-3	8	124	48	2
P1788	DFS-3	8	124	48	2
P1830	DFS-3	8	124	48	2
P2061	DFS-4	8	124	48	2
P2185	DFS-4	8	124	48	2
P2186	DFS-4	8	124	48	2
P2189	DFS-4	8	124	48	2
P2218	DFS-5	8	124	96	2
P2219	DFS-5	8	124	96	2
P2227	DFS-5	8	124	96	2
Chevron data					
C75	DFS-4	6	124	48	2
C131X	DFS-4	6	124	48	2
Texaco data					
T4	DFS-4	6	124 ⁽⁵⁾	48	2

LINE	RECEIVERS				
	Geophone type	Array type	Group interval (m)	Average % coverage	Array length
Panarctic data					
P726		12IL	67	600	
P872	L10 8HZ ⁽⁶⁾	12IL ⁽⁷⁾	67	600	
P1135	L2 14HZ	9IL ⁽⁷⁾	67	600	9/11 ⁽⁸⁾
P1137	L2 14HZ	9IL	67	600	9/11
P1147	L2 14HZ	9IL	67	600	9/11
P1192	L2 14HZ	9IL	67	600	9/11
P1193	L10 14HZ	9IL	67	600	9/11
P1654	L10 14HZ	9IL	50	600	9/11
P1660	L10 14HZ	9IL	67	600	9/11
P1662	L10 14HZ	9IL	67	600	9/11
P1662A	L10 14HZ	9IL	67	600	9/11
P1763	L10 14HZ	9IL	67	600	9/11
P1788	L10 14HZ	9IL	67	600	9/11
P1830	L10 14HZ	9IL	67	600	9/11
P2061	L10 14HZ	9IL	67	600	9/11
P2185	L10 14HZ	9IL	67	800	9/11
P2186	L10 14HZ	9IL	67	600	9/11
P2189	L10 14HZ	9IL	67	800	9/11
P2218	L10 14HZ	9IL	50	800	9/11
P2219	L10 14HZ	9IL	50	800	9/11
P2227	L10 14HZ	9IL	50	800	9/11
Chevron data					
C75	L2 14HZ	9IL	67	600	9/11
C131X	L2 14HZ	9IL	67	600	9/11
Texaco data					
T4	L2 14HZ	9IL	67	600	9/11

LINE	SPREAD GEOMETRY					
	Type	Min. offset (m)	Max. offset (m)	Line length (km)	SP range	Direction
Panarctic data						
P726	2	0	1608	14	2600-7644	S
P872	1 ⁽⁹⁾	134	1675	34	1169-1290	NW
P1135	2 ⁽¹⁰⁾	0	1608	28	0-396	S
P1137	2	0	1608	21	-12-283	S
P1147	1	67	1608	15	0-216	S
P1192	1	134	1675	28	0-396	S
P1193	1	134	1675	22	0-192	S
P1654	1	100	1250	29	0-406	S
P1660	1	134	1675	39	0-600	S
P1662	1	134	1675	19	0-268	S
P1662A	1	134	1675	10	-2-142	S
P1763	1	134	1675	53	0-752	S
P1788	1	134	1675	16	4-228	NE
P1830	1	134	1675	19	0-270	S
P2061	1	134	1675	22	0-314	N
P2185	1	134	1675	32	0-453	N
P2186	1	134	1675	10	0-144	N
P2189	1	134	1765	28	0-390	S
P2218	1	50	2400	19	0-354	S
P2219	1	50	2400	34	1-642	N
P2227	1	50	2400	12	0-222	N
Chevron data						
C75	1	134	1675	59	180-412	N
C131X	1	134	1608	20	291-360	S
Texaco data						
T4	1	67	1608	40	54-144	S

APPENDIX 2

Other sources for reprocessed seismic profiles
(reprocessed by and acquired from E.R. Kanasewich,
University of Alberta, Edmonton)

Panarctic lines

P1138*	P1139	P1140*	P1141*
P1168*	P1169	P1171*	P1179
P1180*	P1190	P1762*	P1768
P1770	P1862	P1920	P1921*
P2144	P2145	P2146	P2674*

Texaco lines

T2
T7*
T8*

All the above lines have been reinterpreted. Lines marked with an asterisk (*) have also been redisplayed on Sections D through G. For a listing of acquisition and processing parameters, and an alternative interpretation of the data, the reader is directed to Kanasewich and Berkes (1988; 1990).

APPENDIX 3

Reprocessing sequence and parameters

Preprocessing

1. Data Retrieval and Copy
Field tapes, operator's reports and surveyor's reports were retrieved from Panarctic, Chevron and Texaco files and copied.
2. Demultiplex
Time samples for each channel were resorted and reassembled.
3. Tape Format Conversion
SEGA or SEG Y format tapes were converted to Western Geophysical internal Code 4 format.
4. Assignment of specifications
Datum elevation = sea level
Replacement velocity for data above sea level = 3.65 km s^{-1}
Reprocessing sample interval = 4 ms
5. Trace editing
Deletion of dead or anomalous traces.
6. Recording phase compensation
A wavelet was designed and applied to each trace to remove phase distortion induced by geophone and/or recording instruments.

7. Line geometry input

A database was created containing a full description of all shot and receiver coordinates including elevation data.

8. Field (elevation) statics

Time adjustments were calculated and applied to each trace in order to normalize all measured travel times to a common datum elevation (sea level).

9. Amplitude recovery

A gain was applied that increases as a function of increasing travel time on each trace to compensate for progressive loss of signal associated with spherical (wavefront) divergence.

10. Low-cut filter

Frequencies above 10 hz were passed on for further processing.

Shot-ordered processing

11. Surgical mute

Removal of spontaneous noise bursts. This coherent noise is attributed to permafrost fracture ("ice-breaks") occurring after ignition of the dynamite source. Removal is 80% successful.

12. FK filter

Removal of much linear coherent noise was accomplished by transposing shot-ordered data to the fk (frequency and wave number) domain where a fan filter was designed and applied. Optimal design fan passes on for further processing all data in the -5 ms/tr to +9 ms/tr range.

13. Prewhitening

Uniform addition of an element (.1%) of white noise was applied prior to deconvolution to increase the sensitivity of the deconvolution filters.

14. Gapped deconvolution

Significant broadening of bandwidth of the stacked data and reduction of reverberations was achieved by test and application of Wiener-Levinson minimum phase inverse filters. The four filters, each with 25% overlap and applied successively over the length of each trace, possess a 150 ms operator length and a 24 ms prediction length.

15. RMS amplitude AGC (Automatic Gain Control)

A root mean square calculation of amplitude was computed on input traces over specified gate lengths.

A gain factor was then applied to each sample to normalize amplitudes of output traces.

Normalized amplitude = 2000

16. Sort to CDP (CMP) gathers
Shot-ordered traces were resorted into CDP (Common Depth Point) gathers for further processing. (CDP is synonymous with CMP = Common Mid Point and CDF = Common Depth Field).

CDP - Ordered Processing

17. Velocity analysis
Velocity analyses were conducted at average 2 line km intervals.
For each analysis an optimal time-variant velocity function was designed from seven test functions applied to 1) a group of 21 adjacent stacked traces, and 2) four adjacent CDP gathers.

18. Normal Move-out (NMO)
A hyperbolic-type correction was applied to traces in each gather. The magnitude of this velocity-dependent correction is directly proportional to offset and inversely proportional to arrival time. Chosen velocities were based on lateral interpolation of optimal velocity functions as determined by previous analyses.

19. Automatic statics
A Western Geophysical-designed, Gauss-Siedel-type, automatic surface consistent static correction was applied.
This adjustment, applied to traces within NMO-corrected gathers, creates small time shifts (0 to ± 12 ms), which can improve lateral consistency of reflections.

20. Near-surface mute
Excessive, shallow low-frequency noise at long offsets, created in part by post-NMO stretch of far offset traces, was deleted using a time-variant mute function.
Mute design - offset 550 m, time 0 ms
offset 620 m, time 280 ms
offset 950 m, time 480 ms
offset 1800 m, time 800 ms

21. Trim statics
This automated post-NMO residual static correction involves cross-correlation of mid-point traces between groups of five adjacent CDP gathers. The resulting time adjustment applied uniformly to all traces in each gather is small (0 to ± 16 ms). Corrections were calculated within a moving 3 s gate.

22. Stack
Traces were summed in each CDP gather to create an average 6 or 8 fold redundancy of coherent energy.

Post-stack processing

23. Band-Pass Filters
Time-variant zero phase filters were designed and applied to stacked section
- | Design - time | 0 to 1900 ms | 2200 to end of records |
|---------------|--------------|------------------------|
| low-cut | 10 hz | 10 hz |
| slope | 12 db/oct | 12 db/oct |
| high-cut | 60 db | 40 hz |
| slope | 50 db/oct | 50 db/oct |

24. Gain
An RMS-type amplitude gain was calculated by dividing the input trace into gates. The amplitude of each sample was squared, a mean of these values was calculated and the square root was taken. This is the RMS amplitude for that gate (RMS_1). The ratio of the desired RMS amplitude (RMS_2) to the existing value is the scaler to apply at the centre of the gate ($scaler = RMS_2 / RMS_1$). Window length is 50-600 ms.

25. Merge
Seismic profiles were merged where possible to achieve longer, more regional scale sections. Traces near the merge location from each profile were mixed (or blended) together to ensure a smooth transition from one profile segment to the next.
Blend width = 10 tr
Blended surveys = P1662 and P1662A
P1788 and P2227
P2186, TPC4 and P2218
T75 and part of P1662A

26. Migration velocity tests
Stacked partial sections were experimentally migrated using velocities of 5%, 10% and 20% below the previously selected stacking velocity functions.

27. Migration
Stacks and merged stacks were time migrated by the finite difference technique using previously selected optimal migration velocities.

Display

28. Full section display

Large-scale normal and reverse polarity film and print copies of stacked sections and migrated sections were produced that are suitable for interpretation.

Horizontal scale was designed to equal vertical scale for interval velocities of 5.25 or 5.5 km s⁻¹ (see below)

Vertical exaggeration (vert./horiz.) for various interval velocities (V_{int}):

V_{int} (km s ⁻¹)	Vert./horiz.*	Vert./horiz.#
3.0	1.83	1.74
3.5	1.56	1.49
4.0	1.37	1.31
4.5	1.22	1.16
5.0	1.10	1.05
5.5	1.00	0.95
6.0	0.91	0.87
6.5	0.84	0.80

Horizontal scales: *11.8 tr cm⁻¹ at 33 m tr⁻¹
#15.1 tr cm⁻¹ at 25 m tr⁻¹

Vertical scale of 6.93 cm s⁻¹

Type of display: wiggle trace, variable area with 12 db plotting gain and 100 ms horizontal timing lines. The profile defining the applied static correction was placed on the top of the data thus defining a pseudo-topographic surface.

29. Reduced section display

Copies of the migrated section designed for publishing quality output were produced at a reduced scale and with slightly modified display parameters.

Darkness of sections was found to be excessive for greatly reduced copies of the seismic data. To correct for this, a 2 to 1 sum of the migrated traces was performed before plotting. This procedure halves the number of traces and the effective stack fold, and lightens the profiles with a variable area plot.

Scale: horizontal = vertical for interval velocity of 5.25 or 5.5 km s⁻¹ (as in table above).

Type of display: variable area trace with 12 db plotting gain and 1000 ms timing lines. The static correction profile was placed on the top of the data thus defining a pseudo-topographic surface.

APPENDIX 4

Paleontology Reports

Unless otherwise stated, the following paleontology reports have been compiled from unpublished internal reports held in the curation files of the Institute of Sedimentary and Petroleum Geology, Calgary.

Franklinian Succession (Ordovician through Devonian)

Intrashelf Basin and Embayment

Eleanor River Formation	300
(A.D. McCracken, T.T. Uyeno and C.R. Barnes)	
Bay Fiord Formation	300
(C.R. Barnes, A.D. McCracken, and T.T. Uyeno)	
Thumb Mountain Formation	301
(A.D. McCracken)	
Irene Bay Formation	302
(A.D. McCracken, and B.S. Norford)	
Cape Phillips Formation	302
(A. Lenz, A.D. McCracken, B.S. Norford, A.W. Norris, and T.T. Uyeno)	

Southern Shelf and Shelf Rim

Allen Bay Formation	304
(A.D. McCracken, and T.T. Uyeno and C.R. Barnes)	
Cape Storm Formation	305
(A.D. McCracken)	
Douro Formation	305
(A.D. McCracken)	
Barlow Inlet Formation	306
(A.D. McCracken, and T.T. Uyeno)	
Kitson Formation	306
(T.T. Uyeno)	

Towson Point Carbonate Platform

Blue Fiord Formation	308
(T.T. Uyeno)	

Deep water basin

Canrobert Formation	309
(A. Lenz and D.J. Borré, A.D. McCracken, and B.S. Norford)	
Ibbett Bay Formation, Chert member	309
(A. Lenz and D.J. Borré, and B.S. Norford)	
Ibbett Bay Formation, Dolostone member	310
(A.D. McCracken, and G.S. Nowlan)	
Ibbett Bay Formation, Lower black shale member	311
(A.D. McCracken, and B.S. Norford)	
Ibbett Bay Formation, Brown mudrock member	312
A.D. McCracken, and B.S. Norford)	
Ibbett Bay Formation, Upper black shale member	312
(A. Lenz, A.D. McCracken, and B.S. Norford)	

Devonian Clastic Wedge

Blackley Formation	313
(D.C. McGregor)	
Cape De Bray Formation	314
(A.W. Norris)	
Weatherall Formation	314
(A.W. Norris, and T.T. Uyeno)	
Hecla Bay Formation	316
(A.W. Norris)	
Beverley Inlet Formation	317
(A.W. Norris)	
Parry Islands Formation	318
(A.C. Higgins, D.C. McGregor, A.W. Norris, S. Turner and T.T. Uyeno)	

Sverdrup Basin Succession (Carboniferous through Paleocene)

Upper Paleozoic

Otto Fiord Formation	320
(W.W. Nassichuk)	
Canyon Fiord Formation	320
(C.M. Henderson, B.L. Mamet, S. Pinard, and J. Utting)	

Belcher Channel Formation	322	Hiccles Cove Formation	325
(B.L. Mamet)		(T.P. Poulton, and E.H. Davies)	
Great Bear Cape Formation	322	Ringnes Formation	326
(C.M. Henderson)		(J.H. Wall)	
Sabine Bay Formation	323	Awingak Formation	327
(W.W. Nassichuk)		(J.A. Jeletzky, and T.P. Poulton)	
Assistance Formation	323	Deer Bay Formation	327
(W.W. Nassichuk)		(J.H. Wall)	
Degerbøls Formation	323	Isachsen Formation	328
(C.M. Henderson, and B.L. Mamet)		(J.H. Wall)	
Trold Fiord Formation	324	Christopher Formation	329
(C.M. Henderson, and J. Utting)		(J.H. Wall)	
<i>Mesozoic and Cenozoic</i>		Kanguk Formation	330
Lougheed Island Formation	324	(J.H. Wall)	
(H. Frebold)		Expedition Formation	330
Jameson Bay Formation	324	Strand Bay Formation	330
(T.P. Poulton, and J.H. Wall)		(J.H. Wall, and D.J. McIntyre)	
McConnell Island Formation	325		
(T. Tozer and R. Thorsteinsson)			

FRANKLINIAN SUCCESSION (ORDOVICIAN THROUGH DEVONIAN)

INTRASHELF BASIN AND EMBAYMENT

ELEANOR RIVER FORMATION (OER)

Kitson River C-71 well

A.D. McCracken

GSC loc. C-51897. 2752-2754 m (9030-9037') below K.B.;
436-438 m below upper contact

Chosonodina herfurthi (Müller) [1]

Drepanodus? sp. [2]

indeterminate acantiodontiform elements [22]

Age: Early Ordovician; probably middle to late
Tremadoc

Remarks. *Chosonodina herfurthi* is a middle to late Tremadoc species found in fauna C of Ethington and Clark (1971). The strata were questionably identified as Eleanor River (Early-earliest Middle Ordovician; Barnes, 1973).

(Published report of C.R. Barnes and T.T. Uyeno, 1974)

GSC loc. C-23943. 2752-2754 m (9030-9037') below K.B.;
436-438 m below upper contact

Acodus oneotensis (transition series)

Chosonodina herfurthi (Müller)

Paltodus cf. *P. variabilis* (Furnish)

Scandodus cf. *S. furnishi* (Lindström)

Scolopodus quadraplicatus (Branson and Mehl)

Age: Early Ordovician; Tremadoc to mid-Arenig

Remarks (C.R. Barnes). *Chosonodina herfurthi* appears to have a relatively short stratigraphic range, corresponding to that of Fauna C of Ethington and Clark (1971, p. 72). Most of the other form species are common in Fauna D of those authors and are present in the Marathon Formation of Colorado, in the lower Arbuckle Group of Oklahoma, and in the Oneota Formation of the Upper Mississippi Valley. A Canadian (Tremadoc to mid-Arenig) age is indicated.

BAY FIORD FORMATION (OBF)

Kitson River Inlier Section (76°02'20"N, 113°13'W)

A.D. McCracken

GSC loc. C-134242. 768 m below upper contact

Indeterminate blade fragment [1]

Age: probably Middle Ordovician

Remarks. Denticulation on this fragment is like that in elements of *Appalachignathus*.

GSC loc. C-134245. 447.5 m below upper contact

cf. *Glyptotoconus quadraplicatus* (Branson and Mehl) [3]

Age: probably Early to Middle Ordovician

GSC loc. C-134248. 16 m below upper contact

Semiacontiodus cf. *S. cordis* (Hamar)? [2]

indeterminate drepanodontiform element [1]

indeterminate ?leptochirognathiform element [1]

Age: probably Middle Ordovician

Remarks. *Semiacontiodus* cf. *S. cordis* occurs in the lower and middle Table Head Formation of Newfoundland (Llanvirn: Middle Ordovician).

Kitson River C-71 well

Published report of C.R. Barnes and T.T. Uyeno, 1974

GSC loc. C-23942. 1726-1732 m (5664-5683'); est. 241-
247 m below upper contact

Prioniodus sp. A of Sweet et al., 1971

indeterminate simple cone

Age: early Middle Ordovician; Chazyan

Remarks. The form species *Prioniodus* sp. A (Sweet et al., 1971, Pl. 1, figs. 26, 28) is present in Fauna 4 of Sweet et al. (1971) and also is known from the upper Ship Point Formation of the Fox Basin and probably also from the lower Bay Fiord Formation on Bathurst Island.

GSC loc. C-7682. 1527-1542 m (5011-5062'); est. 42-57 m
below upper contact

Microcoelodus sp. (probably n. sp.)

M. unicornis? of Branson and Mehl, 1933

M. cf. *M. gracilis* (Branson and Mehl)

Age: Middle Ordovician; Porterfieldian

Remarks (T.T. Uyeno). Probably corresponding to Fauna 5 of Sweet et al. (1971) of Porterfieldian age.

A.D. McCracken

GSC loc. C-51897. 1726-1732 m (5669-5683'); est. 241-
247 m below upper contact

Drepanodus? sp. [2]

Erisomodus sp. [3]

indeterminate hyaline cordylodontiform element [1]

Age: probably Middle Ordovician

Remarks. The strata were questionably logged as Bay Fiord Formation (Middle Ordovician). *Drepanodus* is not diagnostic (range is Ordovician); *Ersomodus* is a Middle Ordovician genus. The strata could be reassigned to the Thumb Mountain Formation (lower part is Middle Ordovician; Barnes, 1973).

THUMB MOUNTAIN FORMATION (OTM)

King Point West B-53 well

A.D. McCracken

GSC loc. C-53200. 3012–3019 m (9882–9906.5'); est. 236–243 m below top of formation

Curtognathus sp.

Age: probably Middle Ordovician

Remarks. *Curtognathus* is a Middle Ordovician genus. This stratigraphic level was originally logged as Irene Bay Formation; however the Irene Bay is Late, not Middle Ordovician. The lower part of the Thumb Mountain Formation is Middle Ordovician; the upper part of this formation is Late Ordovician. The underlying Bay Fiord Formation is also Middle Ordovician (Barnes, 1973).

Kitson River Inlier Section (76°02'20"N, 113°14'W)

A.D. McCracken

GSC loc. C-134249. 895 m above base of section; est. 127 m above base of formation (Unit 2 of Goodbody, 1993)

Erraticodon? sp. [13]

cf. *Glyptoconus quadraplicatus* (Branson and Mehl) [17]

Multiositodus subdenticulatus Cullison [176]

indeterminate hyaline elements [2]

indeterminate prioniodontiform element [1]

Age: probably Middle Ordovician; late Whiterockian to early Mohawkian

Remarks. *Erraticodon* is a Middle Ordovician genus. *Glyptoconus* ranges from Early Ordovician to Middle Ordovician (Llanvirn); *G. quadraplicatus* is an Early Ordovician (Canadian) species. *Multiositodus subdenticulatus* is found in rocks of late Whiterockian–early Mohawkian (Middle Ordovician) age.

GSC loc. C-134253. 1160 m above base of section; est. 4.0 m below upper contact with overlying Irene Bay Formation

cf. *Panderodus feulneri* (Glenister) [1]

Panderodus gracilis (Branson and Mehl) [2]

indeterminate element [1]

Age: probably Middle Ordovician to Middle Devonian

Middle Island Section (75°51'30"N, 111°53'10"W)

A.D. McCracken

GSC loc. C-134190. Coastal cliffs on west end of Middle Island; 40 m below upper contact; 1.0 m above base of section (base of formation not exposed)

Drepanoistodus suberectus (Branson and Mehl) [5]

Panderodus feulneri (Glenister) [5]

Panderodus gracilis (Branson and Mehl) [5]

Panderodus cf. *P. liratus* Nowlan and Barnes? [1]

Plegagnathus dartoni (Stone and Furnish) [1]

Age: probably Late Ordovician; latest Edenian to Gamachian

Remarks. *Drepanoistodus suberectus* and *Panderodus gracilis* are long-ranging species; *Panderodus feulneri* ranges from at least Edenian to Gamachian, and forms similar to this species are present in the Silurian. *Panderodus liratus* sensu stricto occurs in the upper Richmondian–Gamachian. The probable age assignment is based on *Plegagnathus dartoni* sensu lato.

GSC loc. C-134191. 19.2 m below upper contact and 21.8 m above base of section

Drepanoistodus suberectus (Branson and Mehl) [1]

Panderodus feulneri (Glenister) [1]

Panderodus gracilis (Branson and Mehl) [9]

Age: probably Late Ordovician; middle Maysvillian to Gamachian

Remarks. Unsorted elements (approximately 220) include *Amorphognathus ordovicianus* Branson and Mehl. Occurrence of *Amorphognathus ordovicianus* indicates the middle Maysvillian–Gamachian *A. ordovicianus* Zone. Barnes (1973) does not report this index species from the Thumb Mountain Formation of Bathurst Island. However, Nowlan (1976) found *A. ordovicianus* in uppermost strata of the Thumb Mountain Formation on Devon and Hoved islands.

GSC loc. C-134202. 3.8 m below upper contact and 37.2 m above base of section

Amorphognathus ordovicianus Branson and Mehl [1]

Belodina sp. [1]

Panderodus gracilis (Branson and Mehl) [21]

Panderodus spp. [4]

Paroistodus? sp. [1]

Pseudobelodina? sp. [1]

Walliserodus amplissimus (Serpagli) [3]

indeterminate oistodontiform element [1]

Age: probably Late Ordovician; middle Maysvillian–Gamachian; *A. ordovicianus* Zone

IRENE BAY FORMATION (OIB)

Kitson River Inlier Section (76°02'20"N, 113°14'W)

B.S. Norford

GSC loc. C-134254. 1165 m above base of section, 1 m above base of formation

Bighornia sp.

Calapoecia 2 spp.

Catenipora 2 spp.

Crenulites cf. *C. magnus* Flower

Grewingia cf. *G. robusta* (Whiteaves)

Sarcinula sp.

Age: late Middle Ordovician; latest Caradoc to earliest Ashgill, Red River Fauna

A.D. McCracken

GSC loc. C-134255. 1165 m above base of section, 1 m above base of formation

cf. *Panderodus feulneri* (Glenister) [2]

Age: probably Middle Ordovician-Middle Devonian

CAPE PHILLIPS FORMATION (OSDCP)

Middle Island Section (75°51'30"N, 111°53'10"W)

A.D. McCracken

GSC loc. C-134203. 0.4 m above base of formation; 33.6 m below top of unit 1

Amorphognathus ordovicianus (Branson and Mehl) [8]

Belodina aff. *B. arca* (Sweet) [1]

Drepanostodus suberectus (Branson and Mehl) [1]

Panderodus gracilis (Branson and Mehl) [15]

Paroistodus? mutatus (Branson and Mehl) [1]

Pseudobelodina? dispansa (Glenister) [4]

indeterminate panderodontiform [2]

Age: Late Ordovician; probably middle Maysvillian-Gamachian; *A. ordovicianus* Zone

GSC loc. C-134204. 9.0 above base of formation; 25 m below top of unit 1

Amorphognathus ordovicianus (Branson and Mehl) [138]

Belodina sp. [24]

Coelocerodontus trigonius Ethington [2]

Drepanostodus suberectus (Branson and Mehl) [75]

Panderodus gracilis (Branson and Mehl) [178]

Panderodus liratus Nowlan and Barnes? [49]

Panderodus spp. [40]

Paroistodus? mutatus (Branson and Mehl) [88]

?*Plectodina* sp. [3]

Plegagnathus dartoni (Stone and Furnish) [2]

Pseudobelodina? dispansa (Glenister) [15]

Pseudooneotodus beckamanni (Bischoff and Sannemann) [3]

Pseudooneotodus mitratus Moskalenko [1]

Walliserodus amplissimus (Serpagli) [4]

indeterminate elements [6]

Age: Late Ordovician; probably middle Maysvillian-Gamachian; *A. ordovicianus* Zone

GSC loc. C-134208. 31.2 m above base of formation; 2.8 m below top of unit 1

Amorphognathus ordovicianus (Branson and Mehl) [349]

Belodina confluens Sweet [18]

Besselodus sp. [21]

?*Decoriconus costulatus* (Rexroad) [1]

Drepanostodus suberectus (Branson and Mehl) [22]

Panderodus feulneri (Glenister) [3]

Panderodus gibber Nowlan and Barnes [2]

Panderodus spp. [130]

Paroistodus? mutatus (Branson and Mehl) [129]

Protopanderodus insculptus (Branson and Mehl) [18]

Pseudobelodina? dispansa (Glenister) [10]

?*Pseudooneotodus beckamanni* (Bischoff and Sannemann) [1]

Pseudooneotodus mitratus (Moskalenko) [4]

?*Walliserodus* sp. [7]

indeterminate blade [3]

Age: probably late Ordovician; middle Maysvillian-Gamachian; *A. ordovicianus* Zone

Remarks. *Panderodus* spp. includes *P. feulneri*, *P. gibber* and *P. gracilis*. Fauna is typical of those from the Irene Bay Formation in other localities (Bathurst Island: Barnes, 1973; Cornwallis Island; McCracken, unpublished collections).

GSC loc. C-134211. 47.0 m above base of formation; 10 m above base of unit 2

Juanognathus? sp. [3]

Panderodus gracilis (Branson and Mehl) [9]

Panderodus aff. *P. gracilis* (Branson and Mehl) [4]

Plectodina tenuis (Branson and Mehl) [2]

Walliserodus amplissimus (Serpagli) [31]

Age: probably Late Ordovician

Remarks. *Plectodina tenuis* ranges from middle Kirkfieldian to Richmondian; *Walliserodus amplissimus* occurs in the *A. ordovicianus* Zone, but its lower limit may not yet be known. Systemic boundary based on conodonts lies within the 6.4 m interval between this sample and sample C-134193 (i.e., within 47.0-53.4 m).

GSC loc. C-134193. 53.4 m above base of formation; 19.6 m above base of unit 2 and 17.4 m below unit 3

Aspelundia fluegeli (Walliser) [7]

Panderodus gracilis (Branson and Mehl) [4]

Pterospirifer celloni (Walliser) [5]

Walliserodus curvatus (Branson and Branson) [6]

Age: Early Silurian; probably late Llandovery; *P. celloni* Zone

Remarks. *Walliserodus curvatus* occurs in *O.?* *nathani*-*I. inconstans* zones (early-late Llandovery). *Aspelundia fluegeli* is found in the *P. celloni* and *P. amorphognathoides* zones (late Llandovery-earliest Wenlock); Uyeno (in Barnes and Uyeno, 1974) reports *Oulodus?* (= *Aspelundia*) *fluegeli* and *O.?* cf. *O.?* *fluegeli* from older strata (early-middle Llandovery). *Pterospathodus celloni* is the nominate species of a late Llandovery conodont zone.

B.S. Norford

GSC loc. C-134196. 71 m above base of formation

Cyrtograptus sakmaricus Koren

Monograptus spp.

M. ex gr. M. spiralis (Geinitz)

Age: Early Silurian; latest Llandovery; *C. sakmaricus*-*laqueus* Zone

GSC loc. C-134195. 72 m above base of formation; 1 m above base of unit 3

Monograptus spp.

M. ex gr. M. spiralis (Geinitz)

Age: Early Silurian; late Llandovery; *M. turriculatus* Zone to *C. sakmaricus*-*laqueus* Zone

GSC loc. C-134198. 79.9 m above base of formation; 8.9 m above base of unit 3

Cyrtograptus sakmaricus Koren

Monograptus spp.

Age: Early Silurian; probably latest Llandovery; *C. sakmaricus*-*laqueus* Zone.

A. Lenz

81.5 m above base of formation; est. 10.5 m above base of unit 3 (stratigraphic separation of this locality and C-134198 is only approximate)

Monograptus aff. *M. riccartonensis* Lapworth

Age: Early Silurian; early? Wenlock

82.5 m above base of formation; est. 11.5 m above base of unit 3

Monograptus aff. *M. riccartonensis* Lapworth

Cyrtograptus perneri Bouček

87.0 m above base of formation; est. 16.0 m above base of unit 3

C. cf. C. perneri Bouček

M. cf. M. priodon (Bronn)

M. flumendosae Gortani

90.0 m above base of formation; est. 19.0 m above base of unit 3

C. multiramis Törnquist

C. cf. C. ellesi Gortani

M. flemengii (Salter)

Plectograptus (*Sokolovograptus*) *textor* Bouček and Munch

M. flumendosae Gortani

Remarks. Indicated age of collections at 82.5 to 90.0 m is Early Silurian, approximately middle Wenlock.

97.5 m above base of formation; est. 26.5 m above base of unit 3

C. hamatus Bailly

M. cf. M. flemengii (Salter)

M. flumendosae Gortani

98.0 m above base of formation; est. 27.0 m above base of unit 3

C. cf. C. multiramis Törnquist

C. sp.

M. cf. M. flemengii (Salter)

M. flumendosae Gortani

100.0 m above base of formation; est. 29.0 m above base of unit 3

C. radians Törnquist

C. cf. C. lundgreni Tullberg

M. priodon (Bronn)

M. aff. M. probosciformis Bouček

Remarks. Indicated age of collections at 97.5 to 100.0 m is approximately late Wenlock.

Tozer and Thorsteinsson (1964) also report *M. testis* (Barrande) (late Wenlock), *M. nilssoni* Perner (early Ludlow), and *M. ultimus* (Barrande) (early Pridoli) from the lower 200 m of unit 3. Lenz (1990) also reports *L. progenitor* from 122.5 m above base of the formation.

Section Southwest of McCormick Inlet (75°47'10"N, 112°21'W)

A.W. Norris

GSC loc. C-140031. stream section located 4.5 km SW of head of McCormick Inlet; est. 173 m below top of formation; est. 63.0 m below top of unit 3

monograptid

Monograptus yukonensis Jackson and Lenz

cf. *Diploctenus mutabilis* Lütke

Metastyliolina sp.

Striatostyliolina sp.

Styliolina sp.

Age: Early Devonian; Pragian; *M. yukonensis* Zone

GSC loc. C-140032. est. 173.5 m below top of formation;
est. 63.5 m below top of unit 3

cf. *Nowakia acuaria* (Richter)

Striatostyliolina sp.

Age: Early Devonian; Pragina; *N. acuaria* dacryoconarid zone

T.T. Uyeno

GSC loc. C-128734. est. 60–112 m below top of formation;
within uppermost metre of unit 3

Polygnathus costatus partitus Klapper, Ziegler and Mashkova

P. costatus cf. *costatus* Klapper

P. linguiformis bultyncki Weddige

P. robusticostatus Bischoff and Ziegler

Age: Middle Devonian; early Eifelian; *costatus* Zone, lower part

In addition to the above collections, Melchin (1987), who has measured the Middle Island section independently, reports *turriculatus* Zone graptolite fauna at approximately 55 m above (our) base of formation, *griestionensis* Zone fauna at about 60 m above base, and *sakmaricus* Zone fauna from 6 horizons at about 70 to 86.5 m above (our) base of formation.

In summary, the age ranges of the various units of the Cape Phillips Formation are:

Unit 4: early to middle? Eifelian

Unit 3: *sakmaricus* graptolite zone of latest Llandovery to *costatus* conodont zone of early Eifelian

Unit 2: *ordovicianus* conodont zone of Ashgill to latest Llandovery

Unit 1: within *ordovicianus* Zone of Ashgill

SOUTHERN SHELF AND SHELF RIM

ALLEN BAY FORMATION (OSAB)

Kitson River Inlier Section (76°02'20"N, 113°15'W)

A.D. McCracken

GSC loc. C-134260. 2 m above base of member 2 and 227 m above base of formation

Ozarkodina confluens (Branson and Mehl)? [3]

Ozarkodina excavata excavata (Branson and Mehl) [4]

cf. *Panderodus feulneri* (Glenister) [13]

Panderodus gracilis (Branson and Mehl) [13]

Panderodus recurvatus (Rhodes)? [9]

Panderodus spasovi Drygant? *sensu* Barrick [2]

indeterminate zygnathiform fragment [1]

indeterminate element

Age: Early Silurian; probably Llandovery–early Wenlock

Remarks. *Ozarkodina confluens*: middle Ludlow–Pridoli, possibly as old as early Wenlock, as young as Early Devonian. *Panderodus spasovi* Drygant? *sensu* Barrick occurs in the *P. amorphognathoides* Zone (late Llandovery–earliest Wenlock).

GSC loc. C-134265. 51 m above base of member 2 and 276 m above base of formation

Spathognathodus manitoulinensis Rexroad et al. s.f. [1]
indeterminate blade fragment [1]

Age: probably Early Silurian; possibly Llandovery

Remarks. Few *spathognathodiform* elements have a deflected blade like the element comparable to *Spathognathodus manitoulinensis* s.f. This form species occurs in the early Llandovery of North America. *Spathognathodus abruptus* Aldridge s.f. is found at about the same interval in Britain. Somewhat similar elements, which may be a different species than the element in this sample, are found in C-129533 and C-129548.

Kitson River C-71 well

Published report of C.R. Barnes and T.T. Uyeno, 1974

GSC locs. C-7683 to C-7692. Depth 924.6–934.5 m, est. 295.5–305.4 m above base of formation

Panderodus simplex (Branson and Mehl)

P. unicastatus unicastatus (Branson and Mehl)

P. gracilis (Branson and Mehl)

Spathognathodus? sp. (fragmentary)

Ozarkodina cf. *O. typica* Branson and Mehl (juvenile form)

Neoprioniodus sp. (probably conspecific with that of Pl. 2, fig. 14 of Liebe, 1962)

Trichonodella sp.

Lonchodina cf. *L. detorta* Walliser (juvenile form)

Age: probably Early Silurian

Remarks (T.T. Uyeno). The general aspect is Silurian. Juvenile forms resembling *Lonchodina detorta* and *Ozarkodina typica* are present and these species are restricted to the Silurian in the Carnic Alps and in the midwestern United States. The presence of Liebe's (1962) *Neoprioniodus* sp. is difficult to assess accurately at this time without access to his dissertation, but his species has been reported from the Alexandrian and Niagaran Series of the Illinois Basin. Pollock et al. (1970) erected a new zone, *Panderodus simplex* Assemblage Zone, which corresponds to the lower part of Walliser's (1964) Bereich I (= lower part of Llandovery). It is characterized by the general paucity of conodonts, the only common species being *Panderodus simplex* and *P.*

unicostatus. Because no diagnostic Ordovician nor younger Silurian conodonts are present, the present fauna is assigned tentatively to the *P. simplex* Assemblage Zone and, therefore, tentatively dated as Early Silurian (early part of Llandovery).

CAPE STORM FORMATION (SCS)

Kitson River Inlier Section (76°02'20"N, 113°15'W)
A.D. McCracken

GSC loc. C-134277. 2 m above base of formation

cf. *Lonchodina detorta* Walliser s.f. [1]
cf. *Panderodus feulneri* (Glenister) [5]
Panderodus gracilis (Branson and Mehl) [1]
Panderodus recurvatus (Rhodes) [1]
indeterminate coniform element A [1]
Age: Late Silurian; middle Ludlow-Pridoli

Remarks. *Lonchodina detorta* s.f. occurs in *P. siluricus*-*O. eosteinhornensis* zones (middle Ludlow-Pridoli).

Kitson River Inlier Southeast Section (76°00'20"N, 113°13'30"W)

GSC loc. C-129525. 50 m below top of formation

cf. *Ozarkodina* aff. *O. polinclinata* (Nicoll and Rexroad) [4]
Panderodus gracilis (Branson and Mehl) [2]
cf. *Panderodus recurvatus* (Rhodes) [1]
indeterminate element [1]
Age: probably Early Silurian; middle Llandovery-early Wenlock

Remarks. *Panderodus recurvatus* occurs in the *I. discreta*-*I. deflecta* to *P. amorphognathoides* zones (early Llandovery-earliest Wenlock); however, this age limit may not be reliable. *Ozarkodina* aff. *O. polinclinata* (also in C-129527) is present in unpublished collections (ADM) from the Yukon in what is probably the *P. celloni* Zone (middle-late Llandovery). Similar species are *O.* aff. *O. polinclinata* and *O. borenlundi* Aldridge from the *P. celloni* Zone of Greenland. *Ozarkodina polinclinata* (*sensu stricto*) in Oklahoma is found in *P. celloni*-*P. amorphognathoides* zones (middle Llandovery-earliest Wenlock).

DOURO FORMATION (SD)

Kitson River Inlier Section (76°02'20"N, 113°15'W)
A.D. McCracken

GSC loc. C-129506. 7.5 m below stratigraphic top of section in overturned beds

Ligonodina elegans Walliser s.f.? [3]
cf. *Lonchodina greilingi* Walliser s.f. [3]

cf. *Lonchodina walliseri* Zeigler s.f. [5]
Ozarkodina confluens (Branson and Mehl) [3]
indeterminate plectospathodiform element [1]
indeterminate platform A sp. A fragments [6]
indeterminate b element (?*Oulodus*) [3]
indeterminate synprioniodiniform element (?*Oulodus*) [2]
indeterminate ozarkodiniform element [2]
indeterminate spathognathodiform element [1]
indeterminate f or g element (?*Oulodus*) [1]
indeterminate f or g element (?*Ozarkodina*) [2]
indeterminate element [1]

Age: Silurian; probably early Wenlock-Pridoli

Remarks. Indeterminate platform A sp. A is an association of at least three elements: scyphiodiform platform, oulodiform?, and eoligonodiniform. All have an unusual denticulation consisting of small denticles arranged in rows of two or three oblique to the axis of the processes. Its identity and age are unknown. *Ligonodina elegans* s.f. ranges from the *O. crista* to *O. eosteinhornensis* zones (late Ludlow-early Pridoli). *Lonchodina greilingi* s.f. (some forms are part of early Ludlow *Kockelella variabilis* Walliser): *K. patula* Zone (early Wenlock) to Early Devonian; *L. walliseri* s.f.: *O. sagitta* Zone (late Wenlock to Early Devonian); *Ozarkodina confluens*: middle Ludlow-Pridoli; possibly as old as early Wenlock, as young as Early Devonian.

GSC loc. C-129508. 15.0 m below stratigraphic top of section in overturned beds

cf. *Ligonodina elegans* Walliser s.f. [1]
Ozarkodina confluens (Branson and Mehl) [3]
indeterminate platform A sp. A fragment [1]
Age: Late Silurian; probably middle Ludlow-early Pridoli

Remarks. *Ozarkodina confluens* is comparable to the "gamma type" found in the *P. siluricus*-*P. index* zones.

GSC loc. C-129510. 35.0 m below stratigraphic top of section in overturned beds

cf. *Hindeodella equidentata* Rhodes s.f. [1]
cf. *Ligonidina silurica* Branson and Mehl s.f. [1]
cf. *Lonchodina greilingi* Walliser s.f. [1]
Ozarkodina? sp. [2]
cf. *Synprioniodina silurica* Walliser s.f. [5]
indeterminate platform A sp. A fragment [1]
Age: probably early Wenlock to early Devonian

Remarks. *Hindeodella equidentata* s.f. and *Ligonidina silurica* s.f. are found in the *O. sagitta* Zone (late Wenlock to Early Devonian). Some workers include *H. equidentata* s.f. as a junior synonym of *Ozarkodina excavata excavata* (Branson and Mehl), a long-ranging species (Early Silurian-Early Devonian). *Lonchodina greilingi* Walliser s.f. suggests a probable age of early Wenlock to Early Devonian.

GSC loc. C-129511. 45.0 m below stratigraphic top of section in overturned beds

Ozarkodina confluens (Branson and Mehl)? [7]
indeterminate oligonodiniiform elements [3]
indeterminate plectospathodiform elements [3]
indeterminate ?priniidiniiform fragment [1]

Age: Late Silurian; probably middle Ludlow-Pridoli;
possibly as old as early Wenlock, as young as Early Devonian

Remarks. One spathognathodiform element of *Ozarkodina confluens*? suggests *Spathognathodus primus primus* (Branson and Mehl) s.f. *sensu* Helfrich (1975; *O. sagitta*-lower *O. eosteinhornensis* zones; late Wenlock-early Pridoli). Another compares with the "delta-type" of spathognathodiform element of *O. confluens* (*P. index*-lower *O. eosteinhornensis* zones; early Pridoli).

BARLOW INLET FORMATION (SBI)

Kitson River Inlier Section (76°02'20"N, 113°17'W)
A.D. McCracken

GSC loc. C-134081. est. 70-80 m below upper contact of formation

cf. *Ligonodina elegans* Walliser s.f. [1]
cf. *Ligonodina* c.f. *L. salopia* Rhodes *sensu* Walliser s.f. [1]
Panderodus sp. [2]
indeterminate platform A sp. A [1]
indeterminate platform A sp. A fragment [1]
Age: Silurian; probably Wenlock-Pridoli

Remarks. Indeterminate platform A sp. A is discussed under C-129506. Its identity and age are unknown. *Ligonodina elegans* s.f. has a range of late Ludlow-early Pridoli. *Ligonodina* cf. *L. salopia* s.f. occurs in the *O. sagitta* Zone (late Wenlock to Early Devonian).

T.T. Uyeno

GSC loc. C-128702. 15 m below upper exposed limit of the formation (est. <20 m below covered upper contact)

Oulodus sp.
Ozarkodina excavata excavata (Branson and Mehl)
cf. Apparatus B of Uyeno (1981)
Age: probably Silurian or Early Devonian; Wenlock to *dehiscens* Zone; possibly Late Silurian

Remarks. Apparatus B was reported from the uppermost part of the Douro Formation, and the lower member of the Peel Sound Formation (Uyeno, 1981).

GSC loc. C-128701. 5 m below upper exposed limit of the formation (est. <10 m below covered upper contact)

Ozarkodina excavata excavata (Branson and Mehl)
Panderodus sp.
cf. Apparatus B of Uyeno (1981)
Age: Silurian to Early Devonian; Wenlock to *dehiscens* Zone

Kitson River Inlier Southeast
A.D. McCracken

GSC loc. C-129547. (76°00'10"N, 113°15'30"W); est. 150 m below top of formation (spot sample)

?*Oulodus* sp. [7]
Panderodus gracilis (Branson and Mehl) [4]
Apparatus A. Uyeno [7]
indeterminate coniform fragment [1]
Age: Silurian; probably Ludlow

Remarks. Apparatus A. Uyeno (1981) occurs in the Cape Storm Formation, with *Ozarkodina confluens* (Branson and Mehl), on Cornwallis Island. Thorsteinsson and Uyeno (1980) indicate that the Cape Storm Formation on Ellesmere Island is Llandovery-Ludlow; elsewhere it is early to late Ludlow.

Dundas C-80 well
A.D. McCracken

GSC loc. C-53056. Cored interval at 2897-2901 m (9504-9519') below K.B.; 14-18 m below upper contact

Panderodus gracilis (Branson and Mehl) [19]
indeterminate neoprioniodiniiform element [1]
Age: probably Silurian

KITSON FORMATION (DK)

The following biostratigraphic data are compiled from 5 incomplete sections; four located on the west side of Kitson River inlier, and one located on a stream bank on the southwest corner of the inlier. Locations include:

Section K1: west side of inlier (76°01'50"N, 113°17'30"W)
Section K2: 150 m north of section K1
Section K3: SW corner of inlier (76°00'15"N, 113°21'10"W)
Section K4: 380 m north of section K1
Section K5: 185 m west of section K1

Kitson River Inlier Section
T.T. Uyeno

GSC loc. C-134060. Section K1; 5.8 m below top of lower member and <6 m above base of formation

Icriodus sp. (2 small, fragmented I elements)
Ozarkodina remscheidensis remscheidensis (Ziegler)
Pedavis cf. *P. biexoramux* (Murphy and Matti)
Pelekygnathus? sp.

Age: Early Devonian; Lochkovian; probably *eurekaensis* Zone

GSC loc. C-134061. Section K1; 2.6 m below top of lower member

Icriodus woschmidtii Ziegler

Ozarkodina remscheidensis remscheidensis (Ziegler)

Age: Early Devonian; *hesperius* to *eurekaensis* zones (probably *eurekaensis* Zone by stratigraphic position)

GSC loc. C-134074. Section K2; 2.5 m below top of lower member

Ozarkodina remscheidensis remscheidensis (Ziegler)

O. remscheidensis (Ziegler) subsp. indet.

Pandorinellina cf. *P. optima* (Moskalenko)

Age: Early Devonian; Lochkovian; probably *delta* Zone

GSC loc. C-134075. Section K2; 0.8 m below top of lower member

Amydrotaxis cf. *A. johnsoni* of Klapper (1969)

Ancyrodelloides omus Murphy and Matti transitional to *A. transitans* (Bischoff and Sannemann) of Murphy and Matti (1983)

A. cf. *A. eleanorae* (Lane and Ormiston) (fragmentary Pa)

Age: Early Devonian; Lochkovian; probably *delta* Zone

GSC loc. C-134064. Section K1; 0.4 m above base of upper member

Ancyrodelloides cf. *A. eleanorae* (Lane and Ormiston)

Eognathodus sulcatus Philip, *iota* morph of Murphy et al. (1981)

Age: Early Devonian; Lochkovian to Pragian; *sulcatus* Zone

GSC loc. C-134076. Section K2; 3.0 m above base of upper member

Ancyrodelloides cf. *A. eleanorae* (Lane and Ormiston)

Eognathodus sulcatus juliae Lane and Ormiston

Age: Early Devonian; Lochkovian to Pragian; *sulcatus* Zone

GSC loc. C-134111. Section K3; 4.0 m above base of upper member

Ozarkodina cf. *O. eberleini* Savage

Age: Early Devonian; Lochkovian to Pragian; possibly *sulcatus* to *kindlei* zones

GSC loc. C-134078. Section K2; 8.5 m above base of upper member

Pandorinellina steinhornensis praeoptima (Mashkova) of Lane and Ormiston (1979)

Polygnathus pireneae Boersma

Age: Early Devonian; Pragian to Emsian; *kindlei* to *dehiscens* zones

GSC loc. C-128698. Section K4; est. 11.5 m above base of upper member

Eognathodus sulcatus kindlei (Lane and Ormiston)

Pandorinellina steinhornensis cf. *miae* (Bultynck)

Pedavis sp. indet. (single fragmentary I element)

Polygnathus cf. *P. pireneae* Boersma (small, fragmentary Pa)

Age: Early Devonian; Emsian; *dehiscens* Zone

GSC loc. C-134112. Section K3; 13 m above base of upper member

Pandorinellina exigua philipi (Klapper)

Polygnathus dehiscens Philip and Jackson

Age: Early Devonian; Emsian; *dehiscens* Zone

Remarks. All specimens extremely malformed and recrystallized.

GSC loc. C-128695. Section K4; est. 20 m above base of upper member

Icriodus trojani Johnson and Klapper

Pandorinellina exigua philipi (Klapper)

P. steinhornensis (Ziegler)

Polygnathus dehiscens Philip and Jackson

P. pireneae Boersma

Age: Early Devonian; Emsian; *dehiscens* Zone

GSC loc. C-128694. Section K4; est. 27.5 m above base of upper member

Icriodus trojani Johnson and Klapper

Pandorinellina exigua (Philip)

P. steinhornensis cf. *miae* (Bultynck)

Polygnathus dehiscens Philip and Jackson

P. dehiscens transitional to *P. gronbergi* Klapper and Johnson

P. gronbergi Klapper and Johnson

Age: Early Devonian; Emsian; *gronbergi* Zone

GSC loc. C-134069. Section K4; 12 m below top of formation

Panderodus sp.

Pandorinellina expansa Uyeno and Mason

Polygnathus linguiformis bultyncki Weddige

Age: Early to Middle Devonian; Emsian to Eifelian;
serotinus to *costatus* zones

GSC loc. C-134072. Section K4; 1.0 m below top of formation

Polygnathus costatus partitus Klapper, Ziegler and Mashkova

P. linguiformis bultyncki Weddige

Age: Early to Middle Devonian; Emsian to Eifelian;
patulus to *costatus* zones

The lower member of the Kitson Formation includes strata of middle Lochkovian age. The thin covered interval low in the lower member could conceivably include strata of late Ludlovian to middle Lochkovian age. Only 1.2 m of strata separate the highest occurrence of *delta* in the lower member and the lowest occurrence of *sulcatus* in the upper member. The intervening *pesavis* Zone strata are either highly condensed or the zone fauna are missing for paleoecological reasons. The adjacent *delta* and *sulcatus* zones are well-defined and cosmopolitan, whereas the *pesavis* Zone requires clearer definition (Murphy et al., 1981, p. 752). The upper member of the Kitson Formation has a latest Lochkovian or Pragian to early Eifelian age range.

TOWSON POINT CARBONATE PLATFORM

BLUE FIORD FORMATION (DBF)

Weatherall 0-10 well

Published report of *T.T. Uyeno*, 1975

GSC loc. C-30171. 1990.3-2057.4 m (6530-6750'); est. 0.3-67 m below upper contact of member 1

Pandorinellina exigua philipi (Klapper)

Polygnathus pirenege Boersma

Belodella sp.

Neopanderodus? sp.

Age: Early Devonian; Emsian; *dehiscens* to *gronbergi* zones

Remarks. Weight of sample was 1217 gm. Because the sample consisted of cuttings, the above age is the minimum for the interval sampled. Conodonts of this age have been found in the middle part of the Stuart Bay Formation on northeastern Bathurst Island (McGregor and Uyeno, 1972).

Towson Point Section (75°52'N, 106°18'W)

T.T. Uyeno

GSC loc. C-129587. On southerly flowing stream situated 23.3 km west of Towson Point; est. 60 m below top of member 1; 385 m below top of formation

Polygnathus inversus Klapper and Johnson

P. inversus transitional to *P. serotinus* Telford

Steptotaxis glenisteri (Klapper)

Age: Early Devonian; Emsian; *inversus* Zone

GSC loc. C-129591. Est. 20 m below top of member 1; 345 m below top of formation

Pandorinellina expansa Uyeno and Mason

Polygnathus inversus Klapper and Johnson

Steptotaxis glenisteri (Klapper)

Age: Early Devonian; Emsian; *inversus* Zone

GSC loc. C-129602. Est. 10 m above base of member 2; 315 m below top of formation

Pandorinellina expansa Uyeno and Mason

Age: early to Middle Devonian; Emsian to Eifelian;
inversus to *costatus* zones

GSC loc. C-129613. Est. 25 m below upper contact of member 2; 140 m below top of formation

Pandorinellina expansa Uyeno and Mason
unassigned simple cones

Age: Early to Middle Devonian; Emsian to Eifelian;
inversus to *costatus* zones

GSC loc. C-129627. Est. 10-20 m below upper contact of formation

Icriodus cf. *I. werneri* Weddige

Pelekygnathus sp.

Polygnathus linguiformis cf. *bultyncki* Weddige

Age: Early to Middle Devonian; Emsian to Eifelian;
probably *serotinus* to *costatus* zones, possibly
patulus Zone (based on the similarity of the
icriodontan element)

Sherard Bay F-34 well

T.T. Uyeno

GSC loc. C-16559. 5437-5441 m

Belodella sp.

Panderodus spp.

Pandorinellina exigua exigua (Philip)

Polygnathus inversus Klapper and Johnson

Steptotaxis glenisteri (Klapper)

indet. spathognathodontan element
P. expansa Uyeno and Mason
indet. spathognathodontan element
Age: Early Devonian; Emsian; *inversus* Zone

Remarks. The presence of *Pandorinellina expansa* suggests that this interval is probably from the upper part of the *inversus* Zone.

The Blue Fiord Formation on nearby Cameron Island ranges into the early Eifelian *costatus* Zone (Mayr, 1980).

DEEP WATER BASIN

CANROBERT FORMATION (OCR)

Giddy River Section, northeastern Canrobert Hills
(75°59'00"N, 115°12'W)

B.S. Norford

GSC loc. C-131006. On north-flowing stream situated 10.7 km north of Ibbett Bay; collection from talus

Adelograptus cf. *A. antiquus* (Hall)
A. aff. *A. clarki* (Hall)
Clonograptus spp.
Dictyonema sp.
? *Kiaerograptus* cf. ? *K. pritchardi* (Hall)
Tetragraptus sp.
Age: Early Ordovician; late Tremadoc; *antiquus* Zone

Central Canrobert Hills Section (75°58'30"N, 115°48'00"W)
A.D. McCracken

GSC loc. C-140143. On north-flowing stream situated 8.0 km north of Ibbett Bay; 180.0 m below top of formation

Acodus? sp. [3]
Drepanoistodus forceps (Lindström)? [7]
Glyptoconus? sp. [10]
Oistodus? sp. [1]
Paroistodus parallelus (Pander)? [1]
indeterminate ?drepanodontiform element [6]
Age: probably Early Ordovician

Remarks. *Drepanoistodus forceps* is found in early middle to middle Arenig; *Paroistodus parallelus* occurs in early to early middle Arenig. The genus *Glyptoconus* has a range of Early-Middle Ordovician.

GSC loc. C-140146. 10.0 m below top of formation

Acodus? sp. [9]
Drepanodus arcuatus Pander [9]
cf. *Eoneoprioniodus bialatus* (Mound) [10]
Paracordylodus gracilis (Lindström) [18]
Paroistodus parallelus (Pander)? [1]
Prioniodus elegans Pander [21]
Scalpellodus? sp. [3]

Scolopodus? sp. fragments [4]
indeterminate ?drepanodontiform element [6]
Age: probably Early Ordovician; early Arenig

Remarks. *Drepanodus arcuatus* is an Early-Middle Ordovician species. The genus *Eoneoprioniodus* occurs in Early-Middle Ordovician. *Paracordylodus gracilis* and *Prioniodus elegans* occur in the early Arenig *P. elegans* Zone.

Nisbet Point Section (75°55'N, 116°34'W)

A. Lenz and D.J. Borré

GSC loc. C-131009. 5.7 km northeast and upstream from Nisbet Point; uppermost 3 m of Canrobert Formation

Didymograptus deflexus Harris
D. extensus (Hall) (sensu lato)
Tetragraptus quadribrachiatus (Hall)
T. serra (Brogniart)
T. cf. bigsbyi (Hall)
T. cf. taraxacum Ruedemann
Isograptus sp.
I. caduceus australis Cooper
I. victoriae maximodivergens Harris
Pseudisograptus dumosus
P. manubriatus (T.S. Hall) (sensu lato)
? *Pseudotrigonograptus ensiformis* (Hall)
Dichograptus octobrachiatus (Hall)
? *Cardiograptus morsus* Hall and Keble
Phyllograptus sp.
Skiagraptus gnomonicus Harris
Kinnegraptus sp.
? *Kinnegraptus* cf. *gracilis* Chen
Age: Early Ordovician; late Arenig; *I. victoriae* Zone;
Oncograptus subzone

Remarks. The genera *Isograptus*, *Pseudisograptus* and *Tetragraptus* are very common and make up more than 50% of the fauna.

IBBETT BAY FORMATION, CHERT MEMBER (OIB1)

Nisbet Point Section (75°55'N, 116°34'W)

A. Lenz and D.J. Borré

GSC loc. C-131010. See C-131009 for locality data; talus from basal 12 m of member

Amplexograptus cf. *coelatus* Lapworth
? *Dichograptus*
Cardiograptus crawfordi sp. Harris
Dichograptus sp.
Glossograptus hincksii (Hopkinson)
Isograptus caduceus (Salter) sensu lato
I. caduceus australis Cooper
Loganograptus logani Hall
Paraglossograptus aff. *tentaculatus* (Hall)
Phyllograptus sp.
Tetragraptus cf. *acanthanotus* Gurley
T. cf. pendens Elles

Tylograptus sp.
Undulograptus austrodentatus (Harris and Keble)
Age: early Middle Ordovician; early Llanvirn;
tentaculatus Zone

Central Canrobert Hills Section (75°58'30"N, 115°48'W)
B.S. Norford

GSC loc. C-140149. 22 m above base of member

inarticulate brachiopod
Clonograptus sp.
Didymograptus cf. *D. extensus* (Hall)
D. cf. *D. deflexus* (Harris)
Isograptus cf. *I. caduceus australis* (Cooper)
I. cf. *I. victoriae victoriae* (Harris)
Oncograptus sp.
Phyllograptus sp.
Tetragraptus sp.
Pseudotrigranograptus ensiformis (Hall)
graptoloid genus 1 cf. sp. 3 of Cooper, 1979
Age: Early Ordovician; *I. victoriae* Zone; *Oncograptus*
subzone

GSC loc. C-140150. 48.5 m above base of member

Caryocaris sp.
Climacograptus sp.
? *Clonograptus* sp.
Didymograptus cf. *D. extensus* (Hall)
Holmograptus sp.
? *Tetragraptus* sp.
biserial graptolite
Age: early Middle Ordovician; Llanvirn; *tentaculatus*
Zone

GSC loc. C-140151. 51 m above base of member

? *Climacograptus* sp.
Glossograptus sp.
Glyptograptus sp.
goniograptid (?)
Isograptus sp.
Paraglossograptus tentaculatus (Hall)
Phyllograptus sp.
Tetragraptus sp.
T. cf. *T. pendens* Elles
Tristichiograptus sp.
Tylograptus sp.
Age: early Middle Ordovician; Llanvirn; *tentaculatus*
Zone

GSC loc. C-140152. 74 m above base of member

Caryocaris sp.
? *Cryptograptus* sp.
Glossograptus sp.
Glyptograptus sp.

goniograptid (?)
? *Leptograptus* sp.
Tetragraptus sp.
Age: Middle Ordovician; Llandeilo to early Caradoc;
probably *gracilis-bicornis* Zone

IBBETT BAY FORMATION, DOLOSTONE MEMBER
(O1B2)

Giddy River Section, northeastern Canrobert Hills
(75°59'00"N, 115°12'W)
G.S. Nowlan

GSC loc. C-130651. 264 m below top of member

Belodella n. sp. Barnes and Poplawski, 1973 [2]
Coelocerodontus trigonius (Sweet and Bergström) [1]
Drepanoistodus sp. [1]
Periodon sp. [5]
Pteracontiodus? sp. [4]
Scandodus sp. [1]
indeterminate dichognathiform elements [1]
indeterminate oistodiform elements [8]
indeterminate protopanderodiform elements [5]
indeterminate simple cone elements [8]
Ptiloncodus simplex (Harris) [4]
Age: early Middle Ordovician

Remarks. Most of the specimens are so poorly preserved as to be unidentifiable at the specific level. Bases of specimens are generally well preserved, but cusps are completely recrystallized and details are obliterated. The conodont assemblage is suggestive of a Middle Ordovician age. The non-conodont, hook-shaped microfossil *Ptiloncodus simplex* is known elsewhere only from strata of latest Canadian to Whiterockian age.

GSC loc. C-130701. 147.5 m below top of member

Belodella jemtlandica (Löfgren) [10]
Drepanoistodus sp. [7]
? *Panderodus* sp. [1]
Phragmodus sp. [5]
Trigonodus sp. [2]
Ptiloncodus simplex (Harris) [4]
Age: early Middle Ordovician; Whiterockian-Chazyan?

GSC loc. C-130702. 119 m below top of member

Belodella jemtlandica (Löfgren) [6]
Coelocerodontus? sp. [1]
Drepanoistodus sp. [5]
Panderodus? sp. [3]
Periodon aculeatus (Hadding) [5]
Phragmodus flexuosus Mosakalenko [9]
Protopanderodus sp. [3]
indeterminate oistodiform element [1]
indeterminate scandodiform element [1]

hyaline ramiform fragments [2]
Age: early Middle Ordovician; Chazyan

Remarks. Assigned age is based on the presence of *Phragmodus flexuosus*.

Central Canrobert Hills Section (75°58'30"N, 115°48'00"W)
A.D. McCracken

GSC loc. C-140154. 83.0 m above base of member

Ansella? sp. [11]
Drepanoistodus basiovalis (Sergeeva)? [10]
Eoneoprioniodus bilongatus (Harris)? [7]
Erraticodon n. sp. [3]
cf. *Panderodus gibber* Nowlan and Barnes [3]
Periodon aculeatus (Hadding) [8]
Protopanderodus cf. *P. varicostatus* (Sweet and Bergström) [1]
Ptiloncodus simplex (Harris) [2]
Walliserodus ethingtoni (Fahraeus) [6]
indeterminate apparatus A [8]
indeterminate oistodontiform element [1]
Age: Middle Ordovician; probably Llanvirn-Llandeilo

Remarks. Ranges are as follows: *Drepanoistodus basiovalis* (middle Arenig-middle Llanvirn); *Eoneoprioniodus bilongatus* (Middle Ordovician); *Erraticodon* (Middle Ordovician); *Periodon aculeatus* (latest Arenig or earliest Llanvirn-latest Llandeilo); *Protopanderodus* cf. *P. varicostatus* (late Arenig-Llanvirn, ?Llandeilo); *Walliserodus ethingtoni* (early Llanvirn-Llandeilo).

IBBETT BAY FORMATION, LOWER BLACK SHALE MEMBER (OS1B3)

Central Canrobert Hills Section (75°58'30"N, 115°48'00"W)
B.S. Norford

GSC loc. C-140156. Base of member

?*Climacograptus* sp.
Dicellograptus sp.
Orthograptus cf. *O. truncatus* (Lapworth)
Age: late Middle or Late Ordovician; late Caradoc to Ashgill

Giddy River Section (75°59'00"N, 115°12'W)
B.S. Norford

GSC loc. C-131199. 24.0 m above base of member

Climacograptus sp.
Dicellograptus sp.
Glyptograptus cf. *G. tenuissimus* Ross and Berry
Orthograptus sp.
Age: Middle Ordovician; Caradoc; high *gracilis-bicornis* Zone to *quadrimumcronatus* Zone

GSC loc. C-131003. 87.5 m above base of member

Climacograptus sp.
?*Glyptograptus* sp.
Monograptus gregarius arcuatus Obut and Sobolevskaya
Orthograptus sp.
Age: Early Silurian; early Llandovery; probably *cyphus* Zone

Eastern Canrobert Hills Section (75°56'N, 114°54'W)
B.S. Norford

GSC loc. C-122752. About 55–60 m above base of member and 217 m below top of member

Glyptograptus cf. *G. venustus venustus* (Legrand), or possibly *G. ex gr. G. persculptus* (Salter)
Age: latest Ordovician or earliest Silurian; late Ashgill or earliest Llandovery (studied by A.C. Lenz)

GSC locs. C-122751 and C-122753. About 155–160 m above base of member and 114–118 m below top of member

Climacograptus sp.
Lagarograptus cf. *L. inexpeditus* Obut and Sobolevskaya
Monograptus aff. *M. communis* Lapworth
Monograptus sp.
Rastrites sp.
Age: Early Silurian; middle Llandovery; *C. gregarius* Zone to *M. sedgwicki* Zone

GSC loc. C-122754. About 190 m above base of member and 84 m below top of member

Climacograptus sp.
Monograptus sp.
M. aff. M. sidjachenkoi (Obut and Sobolevskaya)
Petalograptus sp.
Age: Early Silurian; middle Llandovery; *C. gregarius* Zone to *M. sedgwicki* Zone

Southeastern Canrobert Hills Section (75°55'20"N, 115°17'30"W)

A.D. McCracken

GSC loc. C-140114. On south-flowing stream, 3.4 km north of Ibbett Bay; 133.2 m above base of member

cf. *Dapsilodus sparsus* Barrick? [58a]
Distomodus staurognathoides (Walliser) [2]
Aspelundia fluegeli (Walliser) [12]
Oulodus sp. [3]
Panderodus gracilis (Branson and Mehl) [9]
Walliserodus blackstonensis A McCracken [5]
Age: Early Silurian; probably late Llandovery

Remarks. *Dapsilodus sparsus* occurs in middle Wenlock; the Melville species also has similarities to *Dapsilodus?* sp. B McCracken (1985). This unnamed species, and the rest of the

species listed above, occur in a late Llandovery fauna in the northern Yukon. This Yukon fauna is associated with graptolites of the *M. turriculatus* Zone; *Distomodus staurognathoides* and *Aspelundia fluegeli* have a range of late Llandovery–earliest Wenlock. *Panderodus gracilis* is long ranging: Middle Ordovician–Middle Devonian.

B.S. Norford

GSC loc. C-140116. 139.7 m above base of member

Monograptus 2 spp.

M. cf. *M. marri* Perner

M. exiguus primulus (Bouček and Přibyl)

?*Pseudoplegmagraptus* sp.

Age: Early Silurian; late Llandovery; *turriculatus* Zone

Nisbet Point Section (75°54'25"N, 116°37'W)

B.S. Norford

GSC loc. C-133810. Stream bank 3.4 km east of Nisbet Point; 50 m below upper contact of member

sponge spicules

radiolarians

Climacograptus sp.

Dimorphograptus confertus swanstoni Lapworth

"*Monograptus*" spp.

?*Orthograptus* sp.

Age: Early Silurian; early Llandovery; probably *acinaces* Zone

GSC loc. C-133811. 25–30 m below upper contact

Monograptus spp.

M. cf. *M. falx* (Suess)

M. ex gr. *M. priodon* (Bronn)

M. ex gr. *M. spiralis* (Geinitz)

Retiolites geinitzianus angustidens (Elles and Wood)

Age: Early Silurian; late Llandovery; *spiralis* Zone

**IBBETT BAY FORMATION,
BROWN MUDROCK MEMBER (S1B4)**

Nisbet Point Section (75°54'25"N, 116°37'30"W)

B.S. Norford

GSC loc. C-133813. Stream bank at 3.0 km east of Nisbet Point; 8–10 m above base of member

radiolarians

Bohemograptus bohemicus tenuis (Bouček)

Monograptus sp.

?*Plectograptus* sp.

?*Saetograptus* sp.

Age: Late Silurian; Ludlow; *fritschii linearis* Zone

GSC loc. C-133814. 15–20 above base of member

Bohemograptus bohemicus tenuis (Bouček)

Pristiograptus cf. *P. dubius* (Suess)

Saetograptus cf. *S. leintwardinensis* (Hopkinson)

Age: Late Silurian; Ludlow; *fritschii linearis* Zone

Giddy River Section (75°59'00"N, 115°12'W)

GSC loc. C-131174. 13.5 m below top of member

Bohemograptus bohemicus cf. *B. bohemicus tenuis* (Bouček)

Age: Late Silurian; Ludlow

Southeastern Canrobert Hills Section (75°55'20"N, 115°17'30"W)

A.D. McCracken

GSC loc. C-140119. 38.5 m above base of member

Panderodus gracilis (Branson and Mehl) [4]

?*Oulodus* sp. [1]

Ozarkodina confluens (Branson and Mehl)? [3]

Ozarkodina excavata excavata (Branson and Mehl) [5]

Age: probably early Wenlock–early Devonian

Remarks. *Ozarkodina confluens* occurs in middle Ludlow–Pridoli; the range may be as much as early Wenlock–early Devonian. *Ozarkodina excavata excavata* ranges from Early Silurian to Early Devonian.

**IBBETT BAY FORMATION, UPPER BLACK SHALE
MEMBER (SD1B5)**

Southeastern Canrobert Hills Section (75°55'20"N, 115°17'30"W)

B.S. Norford

GSC loc. C-140127. 282.1 m above base of member

Monograptus cf. ex gr. *M. yukonensis* Jackson and Lenz

Age: probably Early Devonian; probably Pragian

A.D. McCracken

GSC loc. C-140130. 30.0 m below top of formation

Belodella sp. [17]

Ozarkodina sp. [2]

Panderodus spp. [26]

Panderodus? sp. [2]

Polygnathus linguiformis linguiformis (Hinde) [169]

Polygnathus sp. [2]

indeterminate coniform elements [7]

indeterminate eoligonodiniiform elements [3]

indeterminate neoproniodiniiform elements [2]

Age: latest Early to Middle Devonian; late Emsian-Givetian

Monograptus cf. *M. bouceki* Přibyl
Age: Late Silurian; Pridoli

Eastern Canrobert Hills Section (75°56'N, 114°54'W)
B.S. Norford

GSC locs. C-122759 and C-122760. About 21 and 25 m above base of member; 689 and 685 m below top of formation

Bohemograptus cf. *B. bohemicus* (Barrande)
Monograptus sp.

Saetograptus fritschii (Perner)
S. cf. *S. leintwardinensis* (Hopkinson)

Age: Late Silurian, Ludlow, possibly *S. leintwardinensis primus* Zone

GSC loc. C-122774. About 50 m above base of member and 660 m below top of formation

Bohemograptus bohemicus (Barrande)
Monograptus sp.

Age: Late Silurian, Ludlow

GSC locs. C-122776 and C-122777. About 80 and 99 m above base of member; 630 and 611 m below top of formation

Monograptus cf. *M. formosus* Bouček
M. aff. *M. kosoviensis* Bouček
M. sp.

Age: Late Silurian, probably early Pridoli, probably *M. formosus* Zone or *M. ultimus* Zone

GSC loc. C-122778. About 408 m above base of member and 202 m below top of formation

arthropod fragment
Monograptus yukonensis Jackson and Lenz
Age: Early Devonian, Pragian, *M. yukonensis* Zone

GSC loc. C-122783. About 461 m above base of member and 152 m below top of formation

arthropod fragment
Monograptus yukonensis Jackson and Lenz
Age: Early Devonian, Pragian, *M. yukonensis* Zone

Giddy River Section (75°59'00"N, 115°12'W)
A. Lenz

GSC loc. C-131179. 54.4 m above base of member

Saetograptus cf. *S. willowensis* (Berry and Murphy)
Age: Late Silurian; Pridoli(?)

B.S. Norford

GSC loc. C-131187. 123 m above base of member

A. Lenz

GSC locs. C-131193 and C-131194. 255.2 and 299.5 m above base of member 5

Monograptus yukonensis (Jackson and Lenz)
Age: Early Devonian; Pragian

DEVONIAN CLASTIC WEDGE

BLACKLEY FORMATION (DB)

Except for carbonized spores, the Blackley Formation is generally devoid of biostratigraphically useful material. Scolecodonts, plant fragments and rare chitinozoans are the only other fossils found to date.

Southern Canrobert Hills Section (75°54'20"N, 115°42'45"W)

D.C. McGregor

GSC loc. C-140173. On south-flowing stream, 0-1.5 km north of Ibbett Bay; 112 m above base of formation

Age: Early to Middle Devonian; late Emsian or possibly early Eifelian

Remarks. The sample contains plant fragments, scolecodonts and spores. The spores are carbonized and poorly preserved. Only a few specimens were identifiable: *Apiculatasporites microconus* (Richardson) McGregor and Camfield, *Apiculiretusispora* sp., and *Dictyotriletes emsiensis* (Allen) McGregor. The co-occurrence of *A. microconus* and *Dictyotriletes emsiensis* suggests an age range of late early Emsian to late Emsian. *D. emsiensis* is not known to range above the Emsian in other sedimentary basins, but in the Arctic Islands its stratigraphic range is poorly known, and it does occur rarely (reworked?) in rocks thought to be early Eifelian. Therefore, the age determination should not be regarded as conclusive. The presence of scolecodonts indicates that the depositional environment was marine.

GSC loc. C-140182. 487 m above base of formation

?*Apiculatasporites microconus* (Richardson) McGregor and Camfield
?*A. perpusillus* (Naumova) McGregor
?*Apiculiretusispora densiconata* (Tiwari and Schaarschmidt)
Convolutispora? spp. (3 species)
Diatomozonotriletes franklinii (McGregor and Camfield)
Dictyotriletes emsiensis? (Allen) McGregor
Lophotriletes devonicus (Naumova ex Chibrikova) McGregor and Camfield
Verrucosisporites scurrus (Naumova) McGregor and Camfield

Age: Middle Devonian; Eifelian; possibly middle Eifelian

Remarks. The sample contains spores, scolecodonts, and rare fragments of chitinozoans, all of which are strongly carbonized. The latter two signify a marine depositional site, but are not useful for determining the age of the sample. The spores are more useful, and indicate Eifelian, possibly about mid-Eifelian age.

The youngest conodonts from the underlying Ibbett Bay formation are not older than late Emsian.

CAPE DE BRAY FORMATION (DCB)

Weatherall Bay Area

The Cape De Bray Formation in the Weatherall Bay area is entirely early Eifelian in age as is indicated by the occurrence of *costatus* Zone conodonts in the underlying Blue Fiord Formation of nearby Cameron Island (Mayr et al., 1980) and a probably *costatus* Zone assemblage in the lower part of the overlying Weatherall Formation. The palynomorph assemblage of the Cape De Bray Formation in this area is typical of the *velatas-langii* spore zone of the early Eifelian (McGregor, 1993).

McCormick Inlet Section (75°46'00"N, 112°19'00"W)

A.W. Norris

GSC loc. C-140008. 5.7 km southwest of head of McCormick Inlet; 210 m above the base of the formation

Strophodonta sp.

Warrenella sp. cf. *W. praekirki* Johnson

Buchiola sp.

echinoderm ossicle

Dechenella cf. *D. franklini* (Ormiston, 1967)

Age: Middle Devonian; Eifelian

Liddon Gulf-Dealy Island Anticline Section (75°08'00"N, 110°43'30"W)

A.W. Norris

GSC locs. C-130073, C-130064. Isolated outcrops immediately below the upper contact with the Weatherall Formation

C-130064:

cf. *Spinulicosta stainbrookii* Crickmay, 1960

Eoschuchertella sp.

Desquamatia sp. cf. *D. aperanta* (Crickmay, 1960)

Spinatrypa sp.

Age: Middle Devonian; Eifelian; *adoceta* or *dysmorphostrota* Zone

C-130073:

Spinulicosta sp.

Spinatrypa (*Spinatrypa*) *coriacea* Crickmay, 1960

undet. pelecypod

Age: Middle Devonian; late Eifelian; *dysmorphostrota* Zone

In the McCormick Inlet and Liddon Gulf areas, the Cape De Bray Formation ranges from within or above the *costatus* Zone at the base to the *dysmorphostrota* brachiopod zone (approximately *kockelianus* conodont zone) of the late Eifelian at the top. The lower age limit is constrained by the occurrence of *costatus* Zone fauna in the upper part of the Cape Phillips Formation near McCormick Inlet. The upper age limit of the Cape De Bray Formation is also constrained by the occurrence in the lower part of the Weatherall Formation of a conodont assemblage assigned to the *costatus* to *kockelianus* zones. The Cape De Bray Formation in this area also contains a diverse palynomorph assemblage that falls entirely within the lower *devonicus-naumovae* spore zone: middle to late Eifelian (McGregor, 1993).

Canrobert Hills and Ibbett Bay areas

The likely age of the Cape De Bray Formation in the western part of Melville Island ranges from mid-Eifelian to late Eifelian or possibly early Givetian. The lower age limit is constrained by a mid-Eifelian palynomorph assemblage from the underlying Blackley Formation. The upper age limit is constrained by the occurrence in the lower part of the overlying Weatherall Formation of *dysmorphostrota* Zone brachiopods, and a conodont assemblage ranging from *costatus* Zone to *kockelianus* Zone (middle Eifelian). The Cape De Bray Formation also has a diverse palynomorph assemblage assigned to the upper *devonicus-naumovae* spore zone of early Givetian age (McGregor, 1993).

WEATHERALL FORMATION (DW)

Towson Point Section (75°50'40"N, 106°17'30"W)

T.T. Uyeno

GSC loc. 83287. On southerly flowing stream situated 23.0 km west-southwest of Towson Point; 169.2 m above base of formation

Icriodus sp.

Polygnathus costatus cf. *costatus* Klapper

P. costatus cf. *partitus* Klapper, Ziegler and Mashkova

P. linguiformis cf. *bultyncki* Weddige

Age: probably early Middle Devonian; Eifelian; probably *costatus* Zone

GSC loc. 83288. 312.1 m above base of formation

Polygnathus parawebbi Chatterton

Age: Middle Devonian; Eifelian to Givetian; *australis* Zone to Lower *varcus* subzone

The Weatherall Formation in the Weatherall Bay area contains a diverse palynomorph assemblage that ranges from the base to the top of the *devonicus-naumovae* palynomorph zone (late early Eifelian to early Givetian).

Beverley Inlet Section 1 (75°01'00"N, 106°53'W)

T.T. Uyeno (conodonts), *A.W. Norris* (macrofauna)

GSC loc. C-129368. Stream section located 22.3 km east of Beverley Inlet; 137.7 m above base of section; probably not more than 200 m above base of formation

Conodont assemblage:

Icriodus 'expansa' Branson and Mehl of Chatterton (1979)

I. cf. I. norfordi Chatterton

Polygnathus linguiformis linguiformis Hinde gamma morphotype of Bultynck (1970)

Age: Middle Devonian; Eifelian; *australis* to *ensensis* zones

Macrofauna:

Coenites sp.

Echinocoelia sp.

Emanuella sp.

undet. small, spirally coiled gastropod

echinoderm ossicle with single axial canal

five-sided echinoderm ossicle with single axial canal

undet. trilobite fragments

carbonized plant stem tissue

fish bone fragment

Age: Middle Devonian; probably Eifelian

Beverley Inlet Section 2 (75°10'45"N, 107°23'W)

T.T. Uyeno

GSC loc. 83278. Stream section located 13.3 km northeast of head of Beverley Inlet; 686 m above base of section; approximately 160 m below top of formation

Polygnathus parawebbi Chatterton

Icriodus stelcki Chatterton

Age: Middle Devonian; mid-Eifelian to Eifelian/Givetian boundary; probably *australis* to *ensensis* zones

Remarks. The above species were previously reported from the Harrogate Formation of southeastern British Columbia (Chatterton, 1974). Chatterton, however, was only able to give a general age for the fauna, of Eifelian (probably middle to late) rather than Givetian. Subsequently, *Polygnathus angusticostatus* Wittekindt was recovered from the formation (Uyeno, unpublished data), and this species, together with *Polygnathus parawebbi*, indicate the age cited above.

The Weatherall Formation in this area also contains a diverse palynomorph assemblage that ranges to the top of the *devonicus-naumovae* Zone (McGregor, 1993).

Liddon Gulf-Dealy Island Anticline Section (75°08'20"N, 110°42'00"W)

A.W. Norris

GSC locs. C-130075, C-130076. Base of formation

cf. *Spinatrypa* (*Spinatrypa*) *coriacea* Crickmay, 1960

Spinulicosta stainbrookii Crickmay, 1960

Carinatrypa dysmorphostrota (Crickmay, 1960)

cf. *Desquamatia aperanta* (Crickmay, 1960)

undet. gastropod - very small form

pelecypod(?) fragment

Age: Middle Devonian; late Eifelian; *dysmorphostrota* Zone

GSC loc. C-130080. 42 m above base of formation

Spinulicosta sp. cf. *S. stainbrookii* (Crickmay, 1960)

Desquamatia sp.

Age: Middle Devonian; late Eifelian; *dysmorphostrota* Zone of Pedder (1975)

McCormick Inlet Section (75°44'30"N, 112°25'00"W)

T.T. Uyeno

GSC loc. C-140193. 22.0 m above base of section

Conodonts:

Icriodus stelcki Chatterton

Polygnathus parawebbi Chatterton

Age: Middle Devonian; Eifelian; approximately *costatus* to *kockelianus* zones

Remarks. This faunule is similar to that described from the Harrogate Formation of southeastern British Columbia (Chatterton, 1974).

GSC loc. C-140197. 830.0 m above base of section

Conodonts:

Icriodus cf. *I. angustus* Stewart and Sweet

Polygnathus parawebbi Chatterton

Age: Middle Devonian; ?Eifelian; *australis* Zone to Lower *varcus* subzone; possibly *australis* to *kockelianus* zones

According to McGregor (1993) the palynomorph assemblage in the Weatherall Formation in this area ranges from the medial *devonicus-naumovae* Zone at the base (late Eifelian) to the medial *lemurata-magnificus* Zone (middle Givetian) at the top.

South of Ibbett Bay (75°47'30"N, 116°13'W)

T.T. Uyeno (conodonts), *A.W. Norris* (macrofauna)

GSC loc. C-129651. 2.4 km south of Ibbett Bay on north-flowing stream; 315.0 m above base of section

Conodont fauna:

Icriodus cf. *I. angustus* Stewart and Sweet

I. cf. I. norfordi Chatterton

I. stelcki Chatterton

Age: Middle Devonian; Eifelian; approximately *costatus* to *kockelianus* zones

Macrofauna:

Alveolites sp.

aulopodid

Coenites sp.

Hexagonaria sp.

Utaratuia sp.

Desquamatia sp.

Carinatripa dysmorphostrota (Crickmay, 1960)

cf. *Spinatripa coriacea* Crickmay, 1960

Cyrtina n. sp.

echinoderm ossicle with single axial canal

Age: Middle Devonian; late Eifelian; *dysmorphostrota*

Zone of Crickmay (1960)

GSC loc. C-133789. (75°48'20"N, 115°35'W). Isolated outcrop 4.6 km south of Ibbett Bay; approximately 1215 m below top of formation

Conodont fauna:

Icriodus sp. indet.

Polygnathus cf. *P. parawebbi* Chatterton (single small Pa element)

Age: Middle Devonian; Eifelian to Givetian; probably *australis* Zone to Lower *varcus* subzone

A.W. Norris

GSC locs. C-130116, C-130117, C-130122, C-130124. (75°53'N, 114°48'W); faunal assemblage from a single outcrop 1.0 km southeast of head of Ibbett Bay

C-130116:

cf. *Gypidula* sp.

cf. *Ladogioides pax* McLaren, 1962

cf. *Platyterorhynchus russelli* (McLaren, 1962)

productellid

cf. *Cypricardella* sp.

undet. pelecypod casts

undet. trilobite fragments

Age: Middle Devonian; late Givetian; *impennis* Zone of Crickmay (1966); within conodont lowermost *asymmetricus* Zone

C-130117:

undet. cup coral

cf. *Spinulicosta stainbrooki* Crickmay, 1960

cf. *Spinatripa (Spinatripa) coriacea* Crickmay, 1960

small echinoderm ossicle with single axial canal

large diameter echinoderm ossicle with single axial canal

undet. pelecypod cast

Dechenella (Dechenella) sp.

Age: Middle Devonian; late Eifelian; *dysmorphostrota* Zone of Pedder (1975)

C-130122:

undet. cup coral fragment

Spinulicosta sp.

Desquamatia sp. cf. *D. aperanta* (Crickmay, 1960)

Spinatripa (Spinatripa) coriacea (Crickmay, 1960)

cf. *Cornellites* sp.

large diameter echinoderm ossicle with single axial canal

Age: Middle Devonian; Eifelian; mixture of *adoceta* and *dysmorphostrota* zone elements

C-130124:

cf. *Nervostrophia* sp.

cf. *Eoschuchertella* sp.

Spinulicosta stainbrooki (Crickmay, 1960)

Desquamatia aperanta (Crickmay, 1960)

Spinatripa sp.

Philoxene sp.

orthoconic cephalopod

Age: Middle Devonian; Eifelian; mixture of *adoceta* and *dysmorphostrota* zone elements

GSC locs. C-130113, C-130114. (75°54'30"N, 114°28'W); faunal assemblage from a single outcrop on a ridge 8.4 km east of the head of Ibbett Bay

C-130113:

undet. cup coral fragment

Coenites sp.

cf. *Spinatripa (Spinatripa) coriacea* Crickmay, 1960 fragment

cf. *Loxonema* sp.

cf. *Nuculoidea corbuliformis* (Hall and Whitfield)

cf. *Leiopteria* sp.

Dechenella sp. fragments

undet. trilobite fragments

Spirophyton? sp. spirally shaped trace fossil

rectilinear trace fossil markings

Age: Middle Devonian; Eifelian; *dysmorphostrota* Zone of Pedder (1975)

C-130114:

Spinulicosta n. sp.

Desquamatia aperanta (Crickmay, 1960)

Spinatripa (Spinatripa) sp. cf. *S. (S.) coriacea* Crickmay, 1960

Age: Middle Devonian; Eifelian; mixture of *adoceta* and *dysmorphostrota* zone elements

McGregor (1993) reports that the palynomorph assemblage in the Weatherall Formation of the Ibbett Bay area ranges from high in the *devonicus-naumovae* Zone (early Givetian) at the base to medial *lemurata-magnificus* Zone (middle Givetian) at the top. At the west end of the island, the top of the Weatherall Formation extends into the *optivus-triangularatus* Zone (late Givetian).

HECLA BAY FORMATION (DHB)

The Hecla Bay Formation of eastern Melville Island is generally devoid of marine fauna. The following sparse and long-ranging faunal assemblages were collected from the Hecla Bay Formation in the western part of the island where nonmarine and brackish marine rocks are interstratified.

A.W. Norris

Kelly Point Area (75°24'10"N, 117°26'30"W)

GSC loc. C-137957, C-137960. Coastal section 8.5 km southwest of Kelly Point, western Melville Island; composite sample from a 22.5 m interval at 91 to 113.5 m above base

Barroisella sp. – abundant
cf. *Nuculoidea* sp.

Age: Middle and early Late Devonian (based on range of *N. corbuliformis*)

Ibbett Bay-South Shore Area (75°47'35"N, 115°01'W)

GSC loc. C-130143. Isolated outcrop

Spinatrypa sp.
cf. *Cypricardina* sp.
Bellerophon sp.

Age: Early to early Late Devonian (based on range of *Spinatrypa*)

Purchase Bay Area (75°42'30"N, 115°03'00"W)

GSC loc. C-137252. Head of Purchase Bay, north shore; 283–283.5 m above base

Lingula sp. – numerous
Age: not determined; a long-ranging form

GSC loc. C-137257. 342.7 m above base

Lingula sp.
plant tissue impressions
Age: not determined

Murray Inlet Area (75°21'30"N, 114°45'00"W)

GSC loc. C-129497. Canyon section located 18.0 km northwest of Mt. Joy; 83.6 m above base

cf. *Barroisella* sp.
plant tissue
Age: not determined

The age of the Hecla Bay Formation is constrained to some extent by the occurrence of *australis* Zone to Lower *varcus* subzone (late Eifelian to Early Givetian) conodonts high in the underlying Weatherall Formation of central and western Melville Island, and by the existence of a late Givetian to early Frasnian macrofaunal assemblage in the overlying Beverley Inlet Formation.

The Hecla Bay Formation contains everywhere a diverse assemblage of palynomorphs (McGregor, 1993; McGregor

and Camfield, 1982). In the Weatherall Bay area, the formation ranges from basal *lemurata-magnificus* Zone (early Givetian) at the base to upper *optimus-triangulatus* Zone (latest Givetian or earliest Frasnian) at the top. In the central part of the island as far west as Ibbett and Purchase bays, the lower contact falls within the medial or upper parts of the *lemurata-magnificus* Zone. At Cape Terrace on the west end of the island, where the formation is only about 200 m thick, the palynomorph assemblage falls entirely within the *optimus-triangulatus* Zone. In all of these areas, the top of the Hecla Bay Formation, believed to be stratigraphically on or near a regional disconformity, is high in the *optimus-triangulatus* Zone (near the Givetian-Frasnian or Middle Devonian-Upper Devonian boundary).

BEVERLEY INLET FORMATION (DBI)

A.W. Norris

Cape Cyclops Section 1, southwestern Melville Island
(75°07'40"N, 116°46'30"W)

GSC loc. C-137875. In coastal cliffs; 1.5 km northwest of Cape Cyclops; 50 m above base of section; base of formation not exposed

Schizophoria sp.
Eleutherokomma sp. cf. *E. impennis* (Crickmay)
Actinopteria sp. cf. *A. boydi* (Conrad)
carbonized plant tissue
Age: Middle Devonian; latest Givetian; *impennis* Zone of Crickmay (1966); (within Lowermost *asymmetricus* Zone)

GSC loc. C-137878. 101.2 m above base of section

Allanella allani (Warren, 1944)
cf. *Spathella typica* (Hall)
trace fossil markings
Age: Late Devonian; early Frasnian; *Allanella allani* Zone of Crickmay (1966); (within Middle *asymmetricus* Zone)

Cape Cyclops, Section 2 (75°10'00"N, 117°09'30"W)

GSC loc. C-137909. In coastal cliff section 15.2 km northwest of Cape Cyclops; 208 m above base of section; base of formation not exposed

Atryparia sp.
Spinatrypa albertensis (Warren, 1944)
Eleutherokomma sp. cf. *E. hamiltonensis* (Crickmay, 1950)
large echinoderm ossicle with single axial canal
plant stem tissue
Age: Late Devonian; early Frasnian; *Allanella allani* Zone of Crickmay (1966), (within Middle *asymmetricus* Zone)

Cape Victoria area, southwestern Melville Island
(75°01'10"N, 115°57'30"W)

GSC loc. C-137845. High in coastal cliffs 10.0 km southeast of Cape Victoria; 462 m above base of section; base of formation not exposed

Schizophoria sp. cf. *S. lata* (Stainbrook, 1940)

Eleutherokomma sp. cf. *E. impennis* (Crickmay, 1963)

Age: Middle Devonian; latest Givetian; *impennis* Zone of Crickmay (1966), (=Lowermost *asymmetricus* Zone)

The Beverley Inlet Formation also contains a number of crossopterygian fish remains (Tozer and Thorsteinsson, 1964). A layer of phosphatic sandstone containing numerous such fragments and impressions was discovered in an isolated stream bank exposure northeast of Ross Point.

The Beverley Inlet Formation contains everywhere a diverse palynomorph assemblage that ranges from the base to the upper part of the *ovalis-bulliferus* Zone of the Frasnian (McGregor, 1993). Contained macrofauna are apparently latest Givetian through early Frasnian in age.

PARRY ISLANDS FORMATION, BURNETT POINT MEMBER (DP11)

The Burnett Point Member contains a diverse palynomorph assemblage assigned to the uppermost part of the *ovalis-bulliferus* Zone (Frasnian) and lower *torquata-gracilis* Zone (Frasnian and Famennian) (McGregor, 1993).

PARRY ISLANDS FORMATION, CAPE FORTUNE MEMBER (DP12)

Beverley Inlet Area (75°08'50"N, 107°32'W)

A.C. Higgins

GSC loc. C-128762. 7.8 km upstream and northeast of the head of Beverley Inlet on a small ridge; 60 m above base of member

Icriodus cornutus (Sannemann)

Pelekysgnathus inclinatus (Thomas)

Polygnathus nodocostatus (Branson and Mehl)

Palmatolepis triangularis (Sannemann)

Age: Late Devonian; early Famennian; Lower-Middle *crepida* Zone

Remarks. This fauna is a mixture of shallow-water "icriodids" and pelekysgnathids, and deeper water palmatolepids. The stratigraphic ranges of the shallow-water species have recently been described by Sandberg and Dressen (1984) from Belgium and the United States. Their importance is known in terms of the standard conodont zones, which are based on deep water faunas. "*Icriodus*" *cornutus* Zone. *Pelekysgnathus inclinatus* ranges from the base of the Lower *crepida* Zone into the Upper *praesulcata*

Zone or Middle "*Icriodus*" *cornutus* Zone to Upper "*Icriodus*" *costatus* Zone.

The *triangularis* Zone, which was named after the deep-water element, *Palmatolepis triangularis*, spans the Frasnian/Famennian boundary but does range upward into the succeeding Middle *crepida* Zone. The presence of *Palmatolepis triangularis* is not inconsistent with a *crepida* Zone age.

S. Turner

GSC loc. C-128762. Location as described above

chondrichthyan teeth

Phoebodus sp. nov. cf. *P. sp.* A Ginter, 1991

Phoebodus sp.

Stethacanthus sp. cf. Turner, 1982, Ginter, 1991

Protacodus sp.

chondrichthyan scales

Protacodus sp. cf. *P. wellsii* Gross, 1973

ctenacanth scales

stethacanthid scales

crossopterygians

onychodontid teeth

onychodontid lepidotrichia?

dipnoans

lungfish vomerine teeth

acanthodian? teeth

paleoniscoid teeth

paleoniscoid scales

paleoniscoid lepidotrichia

There are over 200 specimens in this sample of teeth derived from *Phoebodus* sp. nov. cf. *P. sp.* A of Ginter, 1991. This species has been previously reported from the upper Frasnian to lower Famennian of the south Urals, Moravia and the Holy Cross Mountains of central Poland. A second possible *Phoebodus* sp. possesses shorter, coarsely striated cusps. The *Protacodus* teeth occur in smaller numbers but are comparable to material described from both Europe and by Turner (1982) from the *marginifera* zone of Australia.

Published report of *D.C. McGregor* and *T.T. Uyeno*, 1972

GSC loc. 83281. Located near loc. C-128762 (above); 250(?) m below exposed top of formation (in Cape Fortune Member?)

Icriodus costatus (Thomas)

Polygnathus sp.

Age: late Late Devonian; late Famennian

Remarks. *Icriodus costatus* is wide ranging in nearshore depositional environments of the late Famennian (Sandberg and Dressen, 1984).

Baldwin River Area – eastern Melville Island
(75°33'00"N, 106°32'30"W)

GSC loc. C-128894. Stream bank section on northerly flowing portion of Baldwin River; 198 m above base of member

Lingula sp.
Rhysochonetes sp.
Sinotectirostrum sp.
Cyrtiopsis sp.
Age: Late Devonian; Famennian

Mecham River Area (75°11'40"N, 108°47'30"W)

GSC loc. C-128898. South bank of Mecham River, 13.3 km north of Bridport Inlet; 14 m above base of member

Orbiculoidea sp.
Ptychomalotoechia summa Sartenaer, 1969
Cyrtiopsis sp.
undet. bryozoan
Age: Late Devonian; late Famennian; *Gastrodetoechia*
Zone of Sartenaer (1969)

GSC loc. C-128899. Same location as C-128898; 15 m above base of member

Lingula sp.
cf. *Rhysochonetes* sp.
Productella sp.
Sinotectirostrum saxirubrum (Sartenaer, 1969)
cf. *Cyrtiopsis prepta* (Crickmay, 1952)
gastropod
Age: Late Devonian; Famennian; upper *Basilicorhynchus* to lower *Gastrodetoechia* zones of Sartenaer (1969)

The Cape Fortune Member also contains a diverse palynomorph assemblage assigned to the *torquata-gracilis* Zone of the Famennian (McGregor, 1993).

PARRY ISLANDS FORMATION, CONSETT HEAD MEMBER (DP13)

Spencer Range Area (75°45'00"N, 107°40'00"W)
D.C. McGregor

GSC loc. C-133753. 7.7 km upstream and southeast of head of west arm, Weatherall Bay; isolated outcrop

Ancyrospora ampulla Owens
A. magnifica Owens
Cyrtospora cristifera (Luber) van der Swan
Geminospira lemura Balme
Hymenozonotriletes anthoideus Sennova

Hystricosporites spp. (3 species)
Lophozonotriletes macrogrumosus Kedo
Age: Late Devonian; Famennian; *torquata-gracilis*
Zone

Remarks. There are several new species in this sample. Until their stratigraphic ranges have been determined, the sample cannot be dated more precisely than early or middle Famennian on this evidence.

PARRY ISLANDS FORMATION, CONSETT HEAD MEMBER (DP14)

Sabine River Area (75°17'10"N, 108°12'40"W)
D.C. McGregor

GSC loc. C-133770. 28.2 km northeast of Bridport Inlet on the north bank of Sabine River; isolated sample from medial mudrock interval

Cornispora monocornata Nazarenko
C. varicornata Staplin and Jansonius
Cyrtospora cristifera (Luber) van der Zwan
Hymenozonotriletes anthoideus Sennova
Age: Late Devonian; Famennian

Remarks. This assemblage contains relatively few species. Its age is defined by the known stratigraphic range of *Cornispora varicornata*, (early but not earliest Famennian to early late Famennian). Spores are well preserved.

PARRY ISLANDS FORMATION, CONSETT HEAD MEMBER (DP15)

Sabine River Area (75°15'20"N, 107°10'30"W)
D.C. McGregor

GSC locs. C-133775, C-133776, C-133778. 23.4 km northeast of Beverley Inlet near the Sabine River; samples collected from a 4 m thick coal seam in the upper sandstone interval of the member

Cornispora monocornata Nazarenko
C. varicornata Staplin and Jansonius
Cyrtospora cristifera (Luber) van der Zwan
Knoxisporites dedaleus (Naumova) Streel
cf. *Geminospira lemura* Balme
Hymenozonotriletes anthoideus Sennova
cf. *Hymenozonotriletes anthoideus* Sennova
H. parvimammatus (Naumova) Kedo
H. varius Naumova
cf. *Knoxisporites dedaleus* (Naumova) Streel
Lophozonotriletes curvatus Naumova
L. macrogrumosus Kedo
? *Spelaeotriletes microgranulatus* Byvsheva
Vallatisporites spp. (2 species)
Age: Late Devonian; middle Famennian

Remarks. Several new species are present.

SVERDRUP BASIN SUCCESSION (CARBONIFEROUS THROUGH PALEOCENE)

UPPER PALEOZOIC

OTTO FIORD FORMATION (COF)

Barrow Dome

Published report of *W.W. Nassichuk*, 1975

GSC loc. C-16904. 3.2 km north of the centre of Barrow Dome (76°36'15"N, 109°02'30"W)

Cravenoceras tozeri Nassichuk

Age: Early Carboniferous; Chesteran (early Namurian, E₂, = early Serpukhovian)

GSC loc. C-16901. 1.0 km northeast of the centre of Barrow Dome (76°38'N, 109°01'30"W)

Bilinguites canadensis Nassichuk

Bisatoceras hoeni Nassichuk

Age: Early Carboniferous; Halian (late Namurian, R₂ or G₁, = early Bashkirian)

GSC loc. C-16903. 3.2 km north of the centre of Barrow Dome (76°39'15"N, 109°03'W)

Branneroceras branneri Smith

Branneroceras hillsi Nassichuk

Branneroceras sp.

Bisatoceras renni Nassichuk

Gastrioceras melvillensis Nassichuk

Gastrioceras sp.

Syngastrioceras oblatum Miller and Moore

Age: Late Carboniferous; Bloydian (Westphalian-A = Kayalian to late Bashkirian)

GSC loc. C-16905. 2.1 km northeast of the centre of Barrow Dome (76°38'N, 108°58'30"W)

Branneroceras branneri Smith

Branneroceras nicholasi Nassichuk

Melvilloceras sabinensis Nassichuk

Age: Late Carboniferous; Bloydian (Westphalian-A = Kayalian to late Bashkirian)

CANYON FIORD FORMATION (CPC)

Sabine Peninsula

B.L. Mamet

Sherard F-34 well. 5090.0 m below K.B.; est. 168 m above base of formation

apterrinellids

Biseriella sp.

Calcitornella sp.

Calcivertella sp.

Eotuberitina sp.

Globivalvulina moderata Reitlinger

cf. *Lipinella* sp.

Neoarchediscus regularis Suleimanov

Planospirodiscus sp.

Pseudoglomospira sp.

Age: Late Carboniferous; Bashkirian

McCormick Inlet

S. Pinard

GSC loc. C-134149. Stream bank section 16.0 km west of McCormick Inlet; 207.4 m above base of formation (75°47'00"N, 112°48'W)

Biseriella sp.

Endothyra sp.

Globivalvulina sp.

Endothyra cf. *obsoleta* Rauzer-Chernousova (1948)

Tetrataxis sp.

Tuberitina sp.

Fasciella sp.

Age: Late Carboniferous; Bashkirian or younger

C.M. Henderson

GSC loc. C-134149. Geographic locality information as described above; 207.4 m above base of formation

Adetognathus lautus 3 Pa

Idiognathodus sinuosis 2 Pa

Streptognathodus sp. indet. 1 Pa fragment

Diplognathodus orphanus 1 Pa

D. cf. *coloradoensis* 6 Pa

indet. ramiforms

Age: Late Carboniferous; early Mosovian (Zone C4 of Henderson, 1988)

Kitson River

S. Pinard

GSC loc. C-134090. 7.5 km west of Raglan Range and 1.5 km west of the Kitson River; near top of lower clastic member; 120.0 m above base of formation (76°01'30"N, 113°28'30"W)

apterrinellids

Biseriella sp.

Bradyina sp.

Earlandia sp.

Eostaffella sp.?

Globivalvulina cf. *G. bulloides* (Brady, 1976)

Globivalvulina sp. cf. *G. "nassichuki"* (unpub., n. sp.)

paleotextularids

Tetrataxis sp.

Endothyra sp.

Stacheinid sp.

red algae

Age: Late Carboniferous; Moscovian

GSC loc. C-134089. Location as in C-134090; 78.0 m above base of the formation

Bradyina sp.

Endothyra sp.

apterrinellids

Globivalvulina cf. *G. bulloides* (Brady, 1876)

Globivalvulina sp.

Ozawainella sp.?

Climacammina sp.

Tetrataxis of the group *T. conica* Ehrenberg (1854)
emend. von Möller (1879)

Tetrataxis sp.

T. of the group *T. paraminima* Vissarionova (1948)

Eoschubertella sp.

Komia sp.

Ungdarella sp.

Stacheine sp.

Age: Late Carboniferous; Moscovian

C.M. Henderson

GSC loc. C-134101. 8.0 km west of Raglan Range; within upper beds of upper clastic member; 494 m above base of formation (76°01'20"N, 113°33'W)

Adetognathus lautus 3 Pa

Streptognathodus sp. indet. 1 Pa fragment

Age: Late Carboniferous to Early Permian; Moscovian to Asselian (Zone C4-P2 of Henderson, 1988).

Possibly a more restricted range of Gzhelian-early Asselian (Zone C6b-P2)

Remarks. The sample is definitely not younger than early Asselian. The *Streptognathodus* specimen is not *S. oppletus*, but rather is more consistent with *S. elegantulus*; however, it is too fragmentary for identification. The more restricted range above is based on possibility of *elegantulus* identification.

Weatherall Bay

J. Utting

GSC loc. C-128743. 9.5 km west of the head of the west arm of Weatherall Bay in St. Arnaud Hills; 14.5 m below the top of the formation (75°49'45"N, 108°22'W)

Apiculatisporis sp.

Cordaitina sp.

Hamiapollentius sp.

Latosporites sp.

Protohaploxylinus limpidus (Balme and Hennelly) Balme

P. perfectus (Naumova) Samoilovich

P. spp.

Vittatina minima Jansonius

V. striata Luber

V cf. *V. simplex* Jansonius

unidentified alete genus

Age: Early Permian; late Asselian and/or early Sakmarian

Tozer and Thorsteinsson (1964) also report Moscovian fusulinids and middle Late Carboniferous brachiopods from the lower part of the Canyon Fiord Formation.

Eastern Canrobert Hills

B.L. Mamet

GSC loc. C-134215. 16.2 km north of the head of Ibbett Bay; a silty alga-sponge ball pelletoidal grainstone with brachiopod, bivalve, gastropod and echinoderm fragments collected at 2.5 m above base of formation in the lower clastic member (76°02'30"N, 114°42'20"W)

Anthracooporellopsis sp.

Asteroarchaediscus sp.

Bradyina sp.

Climacammina sp.

Cuneiphyucus sp.

Donezella sp.

Endothyra sp.

Eostaffella sp.

Pseudoendothyra sp.

Pseudostaffella sp. cf. *P. antiqua* (Dutkevitch)

Age: Late Carboniferous; early or middle Bashkirian, foraminiferal Zone 20 or 21 (Mamet et al., 1993 and references contained therein)

GSC loc. C-134217. Location as in C-134215; a sandy pelletoidal grainstone collected at 13.3 m above base of formation in the lower clastic member

apterrinellids

Asteroarchaediscus sp.

Archaeolithophylum sp.

Beresella? sp.

Biseriella sp.

Bradyina sp.

Donezella sp.

Endothyra sp.

Eostaffella sp.

Globivalvulina sp.

Neoarchaediscus sp.

Planospirodiscus sp.

Pseudostaffella sp. cf. *P. antiqua* (Dutkevitch)

Ungdarella sp.

Age: Late Carboniferous; early or middle Bashkirian, Zone 20 or 21

Remarks. *Asteroarchaediscus* sp. is extremely abundant. *Ungdarella* sp. is abundant and *Globivalvulina* sp. features a thin diaphanotheca.

GSC loc. C-134218. Location as in C-134217; a *Donezella-Ungdarella* boundstone collected at 29.8 m above base of formation in the lower clastic member

Anthracooporellopsis sp.
Asteroarchaediscus sp.
Biseriella sp.
Bradyina sp.
Climacammina sp.
Cuneiphycus sp.
Donezella sp.
Endothyra sp.
Globivalvulina sp. cf. *G. bulloides* (Brady)
Insolentitheca sp.
Komia sp.
Neoarchaediscus sp.
Ozawainella sp.
Planoendothyra sp.
Planospirodiscus sp.
Profusulinella? sp.
Pseudostaffella sp. cf. *P. antiqua* (Duktevitich)
Tetrataxis sp.
Ungdarella sp.

Age: Late Carboniferous; late Bashkirian, Zone 22

Remarks. *Asteroarchaediscus* sp. is very abundant.

GSC locs. C-134219, C-134220. Location as in C-134217; a skeletal wackestone with echinoid spines, fusulinids and brachiopod and bivalve fragments collected at 67.4 m above base of formation in the middle limestone member.

apterrinellids
Apterrinella sp.
Beresella sp.
Biseriella sp.
Cuneiphycus sp.
Globivalvulina bulloides (Brady)
Globivalvulina "nassichuki" (unpub., n. sp.)
Globivalvulina sp.
Neostaffella sp.
Pseudostaffella sp.
Tetrataxis sp.
Ungdarella sp.

Age: Late Carboniferous; mid-Moscovian, undetermined zone

C.M. Henderson

GSC loc. C-134116. Isolated locality high in the preserved portion of the upper clastic member; 18.6 km south of head of Marie Bay (76°00'20"N, 114°31'10"W)

Adtognathus lautus 4 Pa (2s, 1d)
Diplognathodus aff. *coloradoensis* 4 Pa
indet. fragment [1]

Age: Late Carboniferous; early Moscovian; Zone C4 of Henderson, 1988

Remarks. The specimens of *D. coloradoensis* are identical to those in sample C-134149. These specimens are different from type *coloradoensis* and may represent a separate subspecies. No ramiforms present in this sample.

BELCHER CHANNEL FORMATION (PBC)

B.L. Mamet

Sherard F-34 well. 4071.4 m below K.B.; est. 339 m above base of formation

apterrinellids
Calcitornella sp.
cf. *Ellesmerella*? sp.
Globivalvulina sp.
porcellaneous forams
Schwagerina sp.
Syzrania sp.

Age: Early Permian; Asselian or Sakmarian

Sherard F-34 well. 4116.4 m below K.B.; est. 294 m above base of formation

Ammoverbella sp.
apterrinellids
Calcivertella sp.
Globivalvulina sp.
Schwagerina sp.
Syzrania sp.
Tuberitina sp.
Tubiphytes sp.

Age: Early Permian; Asselian or Sakmarian

GREAT BEAR CAPE FORMATION (PG)

Weatherall Bay
C.M. Henderson

GSC loc. C-126004. Section in small gorge 0.6 km north of Tingmisut Lake; 21.2 m above base of formation (75°57'00"N, 107°53'30"W)

over 300 fragmented conodonts, indet. ramiforms very abundant

Neostreptognathodus ruzhencevi 21 elements
Ellisonia sp.
Sweetognathus aff. *bogoslovskajae* 4 elements
fish teeth
shark dermal denticles

Age: Early Permian; Baigendzhinian; Zone 9 of Henderson, 1988

GSC loc. C-126021. Section on Hiccles Creek; 4.2 m above base of section (base of formation not exposed) (75°56'40"N, 107°59'40"W)

Neogondolella bisselli 1 Pa element
Neostreptognathodus pequopensis 8 Pa elements

Ellisonia sp.

indeterminate ramiforms

Age: Early Permian; Baigendzhinian; Zone 8a of Henderson, 1988

GSC loc. C-126026. Location as in C-126004; 2.0 m above base of formation

Neostreptognathodus pequopensis 7 Pa elements

Sweetognathus whitei 2 Pa elements

ramiform elements 10

Age: Early Permian; early Baigendzhinian; zones 7 to 8a of Henderson, 1988

C.M. Henderson

GSC loc. C-134024. 1.7 km east of the west arm of Weatherall Bay in western Spencer Range; 0.2 m above base of formation (75°52'50"N, 107°40'30"W)

Neostreptognathodus pnavi 33 elements

N. pequopensis 9 elements

Ellisonia sp. +100 fragments

Merrillina cf. *M. oertlii* 4 elements

fish teeth and shark dermal denticles

Age: Early Permian; middle Artinskian

St. Arnaud Hills

GSC loc. C-133763. 8.6 km northeast of closest part of Sabine Bay in southwestern St. Arnaud Hills; 0.5 m above base of formation (75°45'05"N, 108°38'W)

Neostreptognathodus pequopensis 37 elements

N. tschuvashovi? 1 element

Merrillina cf. *M. oertlii* 2 elements

Ellisonia sp. +150 fragments

Age: Early Permian; early Artinskian

SABINE BAY FORMATION (PSB)

Weatherall Bay

Published report of *W.W. Nassichuk*, 1970

GSC loc. 67255. Hiccles Creek area, southeastern Sabine Peninsula; 6 m above base of formation (75°57'N, 107°58'W)

Sverdrupites sp.

ASSISTANCE FORMATION (PA)

Published report of *W.W. Nassichuk*, 1970

Weatherall Bay

GSC loc. C-462. On ridge 400 m east of Hiccles Creek; 3 m above base of formation (75°58'30"N, 107°56'W)

Daubichites fortieri (Harker)

St. Arnaud Hills

GSC loc. C-1930. 9.4 km northeast of closest part of Sabine Bay; 6 m below top of formation (75°47'10"N; 108°44'W); correct location confirmed by *W.W. Nassichuk*, pers. comm., 1989

Sverdrupites amundseni Nassichuk

Daubichites fortieri? (Harker)

Helicoprion sp.

Age: Early Permian; Roadian

Remarks. The Assistance Formation is correlated with the Meade Peak Member of the Phosphoria Formation in Idaho (Nassichuk, 1970) and with the Road Canyon Formation of west Texas (Nassichuk, Furnish, and Glenister, 1965).

DEGERBÖLS FORMATION (PD)

Weatherall Bay

C.M. Henderson

GSC loc. C-126003. Section on ridge near Hiccles Creek, southeastern Sabine Peninsula; 0.8 m above base of section, base of formation not exposed (75°57'40"N, 108°10'00"W)

Neogondolella spp. 5 fragments

2 indet. ramiforms

Age: Permian; late Roadian to early Wordian; late Roadian, suggested by *N. phosphoriensis*

Remarks. One posterior fragment appears to be an advanced *N. idahoensis* and may be referred to *N. phosphoriensis*. Another fragment has an asymmetrical posterior similar to basal Trolld Fiord specimens from Hamilton Peninsula, southwestern Ellesmere Island (*N. sp. A* of Henderson, 1981).

Other fauna collected from this section at 3.0–8.5 m above the base of section (3 samples) include:

Neogondolella sp.

Ellisonia?

indet. ramiform elements

fish teeth

one biserial foram steinkern

Sabine Peninsula

B.L. Mamet

Sherard Bay F-34 well. 2667–2667.5 m below K.B.; est. 333 m above base of formation

Geinitzina sp.

Langella sp.

Nodosaria sp.

Fronicularia sp.

Rectoglandulina sp.

Other fauna include bryozoa, sponge spicules, trilobites, brachiopods, echinoderms and bivalves

Age: Early Permian; Artinskian (or slightly younger)

Remarks. Presence of *Langella-Rectoglandulina* is characteristic of that level.

TROLD FIORD FORMATION (PTF)

C.M. Henderson

Weatherall Bay

GSC loc. C-114937. 7.5 km south of Sherard Bay on Hiccles Creek; 18.0 m above base of section, low in the formation; base of formation not exposed (75°00'00"N, 108°10'00"W)

Neogondolella phosphoriensis 8 specimens, growth series
?Xaniognathus sp. Ph and S elements
indet. ramiform M element

Age: Late Permian; Wordian; middle(?) Wordian

GSC loc. C-114938. Same location as C-114937; 14.0 m above base of section

Neogondolella phosphoriensis subsp. A 35 fragments
Age: late Permian; Wordian

J. Utting

Green Creek Section

GSC loc. C-134170, 1, 2, 7, 9 and C-134180. Section on banks of north-flowing stream on north flank of Raglan Range; 5.8 km southeast of Hillock Point; this stream is labelled Green Creek on NTS 88H, but is mislabelled on 89A (76°99'49"N, 112°17'W)

Remarks. Permian mudrocks from this section contain a diverse assemblage of striate and non-striate disaccate pollen and trilete spores, and acritarchs similar to those obtained elsewhere from the Trolld Fiord Formation (Wordian).

MESOZOIC AND CENOZOIC

LOUGHEED ISLAND FORMATION (JL)

Published reports of *H. Frebold*, 1960, 1975

Sproule Peninsula

GSC loc. 35323 (Fossil locality 89 of Tozer and Thorsteinsson, 1964; also Frebold, 1960; Poulton, 1993). 17.5 km west of the head of Marie Bay on the north shore (76°14'40"N, 115°13'W)

Echioceras sp.

Age: Early Jurassic; late Sinemurian

Remarks. The late Sinemurian ammonoid *Echioceras aklavikense* was also collected on Melville Island by J.C. Sproule and Associates in 1963. No location was provided (Frebold, 1975).

JAMESON BAY FORMATION (JJB)

J.H. Wall

Sproule Peninsula

GSC loc. C-80416. Marie Heights (76°15'N, 115°10'W); 65 m above base of formation

Foraminifera:

Saccamina sp. - 1 small

Hippocrepina spp. - 2 species with total of 3 specimens

Haplophragmoides barrowensis Tappan

Flabellamina sp. 1 of Wall 1983

Triplasia kingakensis Loeblich and Tappan

Gastropoda:

one relatively high-spired conch

Age: Early Jurassic; Toarcian; equivalent to the *Flabellamina* sp. 1 assemblage interval in the eastern Sverdrup Basin (Wall 1983, p. 256)

Remarks. *T. kingakensis*, a species related to *Flabellamina* sp. 1, was reported by Tappan (1955, p. 46) to have a very short vertical range in the lower Toarcian part of the Kingak Shale in Alaska.

GSC loc. C-80425. Same location as C-80416; 92 m above base of formation

Foraminifera:

Ammodiscus sp. cf. *A. asper* (Terquem)

A. sp.

Haplophragmoides sp. - spp., nondescript

Trochammina sp. cf. *T.* sp. 1 of Wall 1983 from the Jaeger Member of the Savik Formation on southern Axel Heiberg Island - 1-3 specimens

T. sp. - 1 small

Age: Middle Jurassic; Aalenian; equivalent to the *Ammodiscus* sp. cf. *A. asper* assemblage interval in the eastern Sverdrup Basin (Wall 1983, p. 256)

Sproule Peninsula

Many of the listed localities, below, were collected and identified by T.P. Poulton. A full listing of Jurassic macrofauna localities in the western Arctic Islands can be found in Poulton (1993).

GSC loc. C-107898. 6.4 km west of the head of Marie Bay, north shore (76°11'N, 114°51'30"W)

Amaltheus stokesi (Sowerby)

Age: Early Jurassic; late Pliensbachian

GSC loc. C-127417. 4.7 km north of Marie Bay near Marie Heights (76°16'46"N, 115°42'W)

Pseudolioceras compactile (Simpson)
P. spitsbergense Frebold

GSC loc. C-127403. 5.6 km west of head of Marie Bay, north shore (76°12'10"N, 114°44'30"W)

Pseudolioceras compactile (Simpson) or *P. spitsbergense* Frebold

Remarks. Indicated age of the fauna at the above two localities is Early Jurassic; Toarcian.

GSC loc. C-127408. 8 km west of the head of Marie Bay, north shore (76°13'20"N, 114°53'30"W)

Leioceras opalinum (Reinecke)
Pseudolioceras(?) sp.

GSC loc. C-127421. 4.7 km north of Marie Bay near Marie Heights (76°16'40"N, 115°42'W)

Leioceras opalinum (Reinecke)
Pseudolioceras(?) sp.

Remarks. Indicated age of the fauna in the above two localities is Middle Jurassic; early Aalenian.

East Kitson River

GSC locs. C-127429-32. 3.6 km upstream from confluence with the Kitson River (76°06'N, 112°58'W)

Leioceras opalinum (Reinecke)
Age: Middle Jurassic; early Aalenian

Sabine Peninsula

GSC locs. C-80372, C-80380, C-80383. Uncertain localities east of Eldridge Bay (collections of A.F. Embry)

Pseudolioceras mcIntocki (Haughton)
Age: Middle Jurassic; Aalenian

McCONNELL ISLAND FORMATION (JMI)

Sproule Peninsula

GSC loc. 37020. Two localities near Marie Heights; lower member of the formation (fossil localities 99 and 100 of Tozer and Thorsteinsson, 1964; 76°17'20"N, 115°44'W and 76°15'50"N, 115°36'W, respectively)

Arkelloceras mclearnii Frebold
Inoceramus sp.
Age: Middle Jurassic; early Bajocian

HICCLES COVER FORMATION (JHC) **T.P. Poulton**

East Kitson River

GSC loc. C-133972. On ridge south of East Kitson River, 4.5 km above confluence with Kitson River (76°05'50"N, 113°00'W); sample from middle member, 5 m above base of formation (in this area, the middle member of the Hiccles Cove Formation disconformably overlies the Sandy Point Formation)

Cadoceras sp.
Age: Middle Jurassic; probably early Callovian or possibly late Bathonian

E.H. Davies

GSC loc. C-133971. Same location as C-133972, above; 1.0 m above base of formation

Dinoflagellates:

Atopodinium prostratum Drugg
Caddasphaera halosa (Filatoff) Fenton et al.
Ctenodinium rotundatum Dodekova
Ellipsoidictyum cinctum Klement
Escharisphaeridia rudis Davies
Gonglyodinium hocneratum Fenton et al.
Gonyaulacysta adecta Sarjeant
Hystrihogonyaulax cladophora (Deflandre) Stover Evitt
Kylindracysta sp.
Kylindracysta spinosa Fenton et al.
Lithodinia jurassica (questionably present) Eisenack
Pareodinia ceratophora

Miospores:

Alisporites bilateralis Rouse
Cerebropollenites macroverrucosus (Thiegart) Schulz
Lycopodiumsporites austroclavitudites (Cookson) Potonié
Osmundacidites wellmannii Couper
Perinopollenites elatoides Couper
Pityosporites dividius (Bolchovitina) Pocock
Taxodiaceapollenites hiatus (Potonié) Kemp
Age: Middle Jurassic; late Bathonian; Oppel-zone F to lower Oppel-zone G of E.H. Davies (1983)

Sproule Peninsula

GSC loc. C-133961. Stream bank section on northerly flowing tributary 8.7 km north of closest part of Marie Bay; sample from middle member (76°18'20"N, 115°07'W)

Dinoflagellates:

Fromea irregularis Courtinat

Dictyopyxidina areolata (Cookson and Eisenack) Eisenack and Kjellström
Gonglyodinium sp.
Hystrihogonyaulax serrata (Cookson and Eisenack) Stover and Evitt
Scriniocassis dictyotas (Cookson and Eisenack) Beju
Sentusidinium asymmetrum (Fenton et al.) Lentin and Williams

Miospores:

Cerebropollenites macroverrucosus (Thiegart) Schulz
Deltoidospora hallii Miner
Lycopodiumsporites austroclavitudites (Cookson) Potonié
Osmundacidites wellmannii Couper
Stereisporites clavus (Balme) Dettmann
Taxodiaceapollenites hiatus (Potonié) Kemp
Todisporites minor Couper
 Age: Middle Jurassic; late Bathonian to early Callovian; Oppel-zone G

Remarks. *H. serrata* has been found to range into the basal portion of Oppel-zone H of E.H. Davies (1983).

RINGNES FORMATION (JR)

J.H. Wall

Sabine Peninsula

GSC loc. C-133851. Small exposure 6.1 km east of Eldridge Bay (76°02'20"N, 109°02'W); 0.5 m above base of exposure

Foraminifera:

Haplophragmoides sp. 1 of Wall 1983 – abundant

Botanical entities:

megaspores and algal(?) cysts
 Age: Late Jurassic; Oxfordian–Kimmeridgian

Remarks. Assigned age is based on the occurrence of the foraminifer in what was formerly called the upper member of the Savik Formation (= Ringnes Formation in Embry's, 1985a, nomenclature) and the overlying Awingak Formation in the Buchanan Lake section, eastern Axel Heiberg Island.

Cape Grassy (Kitson River Area)

GSC loc. C-134291. Small hill located 13.3 km southwest of Cape Grassy near 478' ± benchmark; 4.8 m above base of formation (76°10'10"N, 113°12'W)

Foraminifera:

Ammodiscus thomsi Chameny – one large distorted specimen plus probable fragment
A. sp., a much smaller form
Reophax spp., coarse grained – two species with total of three specimens
Haplophragmoides sp. 1 of Wall 1983 – dominant
H. spp.
Ammobaculites spp. – two species with one specimen each

Trochammina sp.

Gaudryina(?) sp., very small

Age: Late Jurassic; Oxfordian – Kimmeridgian

Remarks. Assigned age is based on recorded ranges of *A. thomsi* and *H.* sp. 1 of Wall (1983) in Buchanan Lake area, eastern Axel Heiberg Island.

GSC loc. C-134293. Same section as C-134291 above; 10.8 m above base of formation

Foraminifera:

Ammodiscus thomsi Chameny – fragments
A. sp., small
Glomospirella sp. 174 of Brooke and Braun 1981 – prominent
Haplophragmoides spp.
Recurvoides sp. cf. *R. disputabilis* Dain
R. spp.
Ammobaculites sp. – 1
Pseudobolivina sp., small
Trochammina annae Levina
T. canningensis Tappan
Verneuilina anglica Cushman – 2
Verneulinoides graciosus Kosyrev
 Age: Late Jurassic; Kimmeridgian to early Volgian

Remarks. Assigned age is based mainly on presence of *G.* sp. 174 and apparent entry of *V. anglica* from comparison with eastern Axel Heiberg Island section.

GSC loc. C-134295. Same section as C-134291 above; 16.8 m above base of formation

Foraminifera:

Ammodiscus sp. cf. *A. orbis* Lalicker – 2–3 small specimens
A. spp., with much size variation
Arenoturrisspirillina jeletzkyi Chameny – although the specimens are much smaller than those in the Buchanan Lake section, they appear to belong to this species
A. waltoni Chameny – 2 reported from the Portlandian of the Richardson Mountains
Glomospirella sp. 174 of Brooke and Braun 1981 – prominent
Lituotuba sp., small – 1
Haplophragmoides sp. cf. *H. canui* Cushman
H. sp., evolute, multichambered, as in the Ringnes of the Sproule Peninsula
Recurvoides sublustris Dain
R. spp.
Trochaminoides sp. = *Evolutinella* sp. of Wall (1983) from the upper part of the Awingak Formation in the Buchanan Lake section
Ammobaculites spp.
Pseudobolivina sp.
Trochammina canningensis Tappan
T. sp. cf. *T. kondaensis* Levina

T. spp.

Verneuillina anglica Cushman – well established

Age: Late Jurassic; Kimmeridgian to early Volgian

AWINGAK FORMATION (JA)

Southwestern Melville Island

T.P. Poulton

GSC loc. C-133861. 2.0 km southeast of Cape Russell on the crest of a coastal cliff (75°14'25"N, 117°37'20"W); collections from 0–2.0 m above base of formation (formation disconformably overlies the Beverley Inlet Formation at this locality)

Astarte sp.

Meleagrinella sp.

Idonearca(?) sp.

Gresslya(?) sp.

other bivalves, indet.

gastropods, indet.

belemnites, poorly preserved small fragments

Age: Late Jurassic; Volgian

Remarks. The fauna are consistent with others in the area that are of Volgian age.

GSC loc. C-137941. Fault-bounded outlier located 3.5 km northeast of Comfort Cove (75°21'20"N, 117°28'30"W)

Pleuromya spp.

Buchia spp.

Modiolus sp. aff. *M. czekanowskii* Lahusen

Mytilus(?) sp. aff. *M. taimyricus* Zakharov

Homomya sp.

Mclearnia sp.

Idonearca(?) sp.

Astarte sp.

other bivalves, indet.

gastropods, indet.

rhynchonellid brachiopods, indet.

terebratulid brachiopods, indet.

vertebrate bone fragments

Age: Late Jurassic; Volgian

Remarks. Assigned age is indicated by presence of *Buchia* and *Mclearnia*.

J.A. Jeletzky

GSC loc. C-137941. Location as above

Buchia russiensis (Pavlow, 1907) s. lato (= *Buchia piochii* (Gabb) s. lato of previous fossil reports) (prevalent)

Buchia aff. *fischeriana* (d'Orbigny, 1845) (less common)

Buchia ex aff. *mosquensis* (von Buch, 1843) (fairly rare)

Buchia ex aff. *terebratuloides* (Lahusen, 1888) (rare)

Pleuromya sp. indet. (solitary specimen)

Inoceramus (s. lato) sp. indet. (rare)

generically indeterminate terebratulid brachiopod (solitary specimen)

Age: Late Jurassic; upper part of Lower Volgian

Remarks. Some part of intercontinental *Buchia russiensis* Zone, upper part of the Lower Tithonian (= Lower Volgian) stage of the international standard. See Jeletzky (1984) for further details. In Sverdrup Basin, *Buchia russiensis* Zone normally occurs in the topmost part of the Awingak Formation and its equivalent.

East Kitson River

T.P. Poulton

GSC loc. C-127435. 3.6 km upstream from confluence with the Kitson River, section on north bank; 2–8 m above base of formation (76°06'30"N, 112°59'10"W)

Buchia fischeriana (d'Orbigny)

Dentalium sp.

Age: Late Jurassic; Volgian

DEER BAY FORMATION (JD)

Sproule Peninsula

J.H. Wall

GSC loc. C-128829. 8.6 km southeast and upstream from Sandy Point, section on north bank; 6 m below top of formation (76°23'40"N, 115°20'30"W)

Foraminifera:

Ammodiscus orbis Lalicker – 1 specimen, plus possibly 2 others

A. sp.-spp., features obscured by numerous adherent grains

Haplophragmoides sp.-spp., with many adherent grains

Ammobaculites spp., with many specimens consisting largely of coiled portions

Orientalia sp. 2 of Wall 1983

Marginulina or *Saracenaria* sp., incomplete – 1

Eoguttulina sp.

Guttulina sp. ex gr. *G. alexandrae* Dain – 1

Age: probably Late Jurassic; Late Volgian, but may be slightly younger

Remarks. Assemblage lacks any proven index forms although the range of *Orientalia* sp. 2 is not known to extend into the Berriasian–Valanginian portion of the Deer Bay Formation elsewhere in the Sverdrup Basin.

Cape Grassy, Kitson River Area

J.H. Wall

GSC loc. C-134300. 8.9 m above base of formation

Foraminifera:

Saccamina sp. - 1
Ammodiscus sp. cf. *A. orbis* Lalicker
Scherchorella sp. - 2
Haplophragmoides spp., including some fairly large forms
Ammobaculites spp. - forms consisting mainly of coiled portions - ex gr. *A. suprajurassicus* (Schwager)
Haplophragmium sp. cf. *H. pokrovkaensis* Kosyrev
Pseudobolivina sp. - 1
Trochammina sp. cf. *T. elevata* Kosyrev
T. spp.
Verneuilina anglica Cushman
Age: Late Jurassic; Volgian

Remarks. Age assignment based on partial resemblance to the *Arenoturrispirillina jeletzkyi* assemblage from the lower part of the Deer Bay Formation in the Buchanan Lake section, eastern Axel Heiberg Island.

ISACHSEN FORMATION (KI)

Sabine Peninsula

J.H. Wall

GSC loc. C-53316. Est. 7.5 km west-northwest of closest part of Eldridge Bay; Rondon Member at 125 m above base of section (76°14'N, 109°00'W)

Miliammina awunensis Tappan
M. ischnia Tappan
Psamminopelta bowsheri Tappan
Haplophragmoides sp. - 3 specimens
Verneuilinoides neocomiensis (Myatliuk)
Age: Early Cretaceous; late Barremian to early Aptian

Remarks. The fauna is basically equivalent to the *V. neocomiensis* assemblage of the Rondon Member in the eastern Sverdrup Basin (Wall, 1983, p. 261).

GSC loc. C-53319. Same locality as C-53316, above; Rondon Member at 159 m above base of section

Foraminifera (strong development):

Saccamina spp. - 3 specimens
Ammodiscus sp. cf. *A. rotalarius* Loeblich and Tappan - 1
A. sp. - 1
Miliammina awunensis Tappan
M. ischnia Tappan - includes forms referred to *M.* sp. 1 of Wall (1983)
M. manitobensis Wickenden
M. sproulei Nauss
Psamminopelta bowsheri Tappan - prominent
P. subcircularis Tappan
P.(?) sp. 1 of Wall (1983)
Haplophragmoides sp. cf. *H. sluzari* Mellon and Wall
Evolutinella sp., very small - 1
Ammobaculites sp. - 1 specimen plus a fragment of another or of a *Reophax*

Ammomarginulina sp. - 1
Trochammina sp. - 1
Uvigerinammina sp. - 1
Verneuilinoides neocomiensis (Myatliuk) - prominent

Ostracoda:

Haplocytheridea(?) sp. - 1 very small carapace
genus-genera unidentified - 1 small and 1 large carapace
Age: Early Cretaceous; probably late Barremian to early Aptian

Remarks. Fauna are equivalent to the *V. neocomiensis* assemblage of the Rondon Member in the eastern Sverdrup Basin.

Southeastern Melville Island

J.H. Wall

GSC loc. C-128653. 26.5 km northwest of closest part of Bridport Inlet on southeast bank of northeasterly flowing portion of Mecham River, stream bank section; composite sample from 4.4-8.0 m above base of section (75°16'00"N, 109°20'30"W)

Foraminifera:

Miliammina awunensis Tappan
M. manitobensis Wickenden
Psamminopelta bowsheri Tappan
Verneuilinoides neocomiensis (Myatliuk)
Age: Early Cretaceous; stage indeterminate; between Barremian and Albian

Remarks. Assemblage is similar to that obtained from the Rondon Member of the Isachsen Formation in the Sverdrup Basin.

GSC loc. C-128768. Section at 9.3 km northeast of head of Beverley Inlet; upland outlier 0.95 km southwest of major river; 18.0-20.0 m from base of formation (75°09'20"N, 107°28'W)

Miliammina ischnia Tappan - 1
Haplophragmoides(?) sp., thin, poorly preserved test - 2
Trochammina(?) sp., thin, poorly preserved test - 2
Gaudryina sp.
Uvigerinammina(?) sp., thin, compressed test - 2
Verneuilinoides sp. cf. *V. neocomiensis* (Myatliuk), poorly preserved
Age: Early Cretaceous; stage indeterminate; probably Aptian to Albian

Remarks. This fauna is not typical of that found in the Rondon Member of the Isachsen, which usually consists of large populations of *Miliammina* and *Verneuilinoides*. Neither can it be readily identified with any Christopher assemblage, although the general composition suggests closer affinity with the fauna of the Christopher than that of the Isachsen.

CHRISTOPHER FORMATION (KC)

J.H. Wall

Kitson River

GSC loc. C-128718. 4.4 km southeast of Cape Grassy near crest of hill at 90 m (300') above sea level; 1.0 m above base of formation (76°14'20"N, 112°56'W)

Foraminifera:

- Hippocrepina barksdalei* (Tappan) - 2
- H.*(?) sp. 1 of Wall (1983) - 2
- Saccamina* spp. - 2 small species with total of 3 specimens
- Ammodiscus* sp.-spp. - 3 specimens
- Miliammina awunensis* Tappan
- M. ischnia* Tappan - includes forms referred to *M.* sp. 1 of Wall (1983)
- M. manitobensis* Wickenden
- M. sproulei* Nauss
- Psammminopelta bowsheri* Tappan
- P. subcircularis* Tappan
- P.*(?) sp. 1 of Wall (1983)
- Reophax* spp. - 2 species with total of 4 specimens
- Haplophragmoides* sp. cf. *H. gigas minor* Nauss
- H. sluzari* Mellon and Wall
- H.* sp.
- Trochammina rainwateri* Cushman and Applin
- T.* sp.
- Gaudryina* sp.
- Uvigerinammina* sp. cf. *U. manitobensis* (Wickenden) - 1 compressed specimen
- Verneuilinoides neocomiensis* (Myatliuk)
- Eoguttulina* sp. - 1

Ostracoda:

- Haplocytheridea*(?) sp. - 1 very small carapace
- 2 genera unidentified - of questionable origin - some carapaces are badly weathered and may be nonmarine post-Cretaceous forms not belonging to the original assemblage
- Age: Early Cretaceous; Barremian to Albian; probably late Aptian to Early Albian

Southeastern Melville Island

GSC loc. C-128706. 30.8 km northwest of closest part of Bridport Inlet on southeast bank of northeasterly-flowing portion of major tributary of Mecham River; stream bank section; 0.2 m above base of formation (75°15'05"N, 109°40'W)

Foraminifera:

- Hippocrepina barksdalei* (Tappan) - 2
- Saccamina lathrami* Tappan
- S.* sp.
- Miliammina ischnia* Tappan - prominent
- M. manitobensis* Wickenden
- M. sproulei* Nauss
- Psammminopelta bowsheri* Tappan

P. subcircularis Tappan - 2

Haplophragmoides collyra Nauss

H. sp. cf. *H. gigas minor* Nauss - prominent

Trochammina rainwateri Cushman and Applin

T. sp.

Verneuilinoides neocomiensis (Myatliuk)

Age: Early Cretaceous; Barremian to Albian; probably late Aptian to Early Albian

Remarks. Fauna are similar to those of GSC loc. C-128718 (Kitson River, Cape Grassy).

GSC loc. C-128746. 34.4 km northwest of closest part of Bridport Inlet on south rim of hill at 210 m (700') above sea level; 60.0 m from base of formation (75°15'40"N, 109°46'W)

Foraminifera:

- Miliammina awunensis* Tappan
- M. ischnia* Tappan
- M.* sp. cf. *M. sproulei* Nauss - 2
- Psammminopelta bowsheri* Tappan
- P. subcircularis* Tappan
- Haplophragmoides* sp.
- Trochammina* sp. - 2
- Siphotextularia*(?) *rayi* Tappan - 1
- Verneuilinoides* sp., small, poorly preserved, may be immature specimens of *V. neocomiensis* (Myatliuk) - 3
- Astacolus* sp., poorly preserved - 1

Ostracoda:

- Haplocytheridea*(?) sp. - 1 free left valve

Bivalvia (Pelecypoda):

- genus unknown - shell fragments
- Age: Early Cretaceous; late Aptian(?) to Early Albian

Remarks. The general appearance of the foraminiferal fauna, including the occurrence of *Siphotextularia*(?) *rayi* and the calcareous *Astacolus*, combined with the presence of the ostracode *Haplocytheridea*(?) suggest equivalence with the *Quadrinophina albertensis* assemblage of Early Albian age in the lower Christopher Formation of the eastern Sverdrup Basin.

GSC loc. C-128866. 29.3 km upstream and northwest of Nelson Griffiths Point; on south bank of tributary (75°13'30"N, 106°48'W)

Foraminifera:

- Miliammina* transitional to *Psammminopelta* sp.
- Haplophragmoides* spp.
- Ammobaculites* spp. - 2 species with 1 specimen each
- Bivalvia (Pelecypoda): 1 shell fragment
- Age: Cretaceous; stage indeterminate; possibly Albian

Remarks. This sample was collected from a cryogenically disturbed embankment of dark coloured mud with embedded glacial erratics. The mud layer, up to 10 m thick, lies

unconformably on folded and peneplained Devonian strata. The identified fauna may be derived from the Christopher Formation, but is reasonably well preserved and not obviously recycled.

KANGUK FORMATION (KK)

Sabine Peninsula

J.H. Wall

GSC loc. C-128849. 20.7 km east-northeast of Chads Point; 3.2 m above base of upper member (76°16'35"N, 109°11'30"W)

Foraminifera:

Trochammina sp.
Gaudryina(?) sp., poorly preserved

Radiolaria:

Cenosphaera (?) sp.
Stylosphaera (*Stylosphaera*) sp.
Stauracontium(?) sp.
Spongodiscus (*Spongodiscus*) *impressus* Lipman
S. (S.) sp. cf. *S.* (S.) *renillaeformis* Campbell and Clark
Stylospongia (*Stylostrochiscus*) sp.
Dictyomitra (*Dictyomitrella*) sp.

Ostracoda:

genus or genera indeterminate – 2 severely weathered carapaces plus partial specimens

Pisces:

vertebra fragment

Algal(?) cysts:

assorted fusiform to subovate shapes
Age: Late Cretaceous; probably post-Turonian and pre-late Campanian

Remarks. Similar assemblages have been observed by the writer in the Kanguk Formation of the Sverdrup Basin and Bylot Island as well as in an outlier on Devon Island. Wall (1983, fig. 18 and p. 265) has recorded radiolarians and algal(?) cysts in the lower beds of the Kanguk Formation from the eastern part of the Sverdrup Basin. In northern Alaska, a similar assemblage of radiolarians from the Barrow Trail Member of the Schrader Bluff Formation was broadly dated as middle Senonian (possibly Santonian-early Campanian) by Bergquist (1966, p. 181).

GSC loc. C-128851. Same section as C-128849, above; 28.5 m above base of upper member

Radiolaria:

Cenosphaera(?) sp.
Spongodiscus (*Spongodiscus*) sp.
Stylospongia (*Stylostrochiscus*) sp.
Dictyomitra (*Dictyomitrella*) sp.

Diatomacea:

Actinopterychus sp. cf. *A. tenuis* Strelnikova – 2
Lepidodiscus(?) sp.

Age: Late Cretaceous; Campanian; probably late Campanian or near boundary of early and late Campanian

Remarks. These diatoms are recorded from the upper part of the Kanguk Formation in the eastern Sverdrup Basin, which is considered to be Late Campanian on the basis of both its diatom and foraminiferal content (Wall, 1983, p. 265).

EXPEDITION FORMATION (KTE)

Sabine Peninsula

Based on assemblages of palynomorphs collected from two sections located near the faulted western contact of Colquhoun Dome, Rahmani and Hopkins (1977) place the Maastrichtian-Paleocene boundary in a nonmarine sandstone interval at approximately 15 m above the base of the formation. The base of the Paleocene is marked by the disappearance of nine Maastrichtian pollen microflora, and by the increased occurrence of *Alnus*, *Carya*, *Carpinus* and *Pterocarya*.

STRAND BAY FORMATION (TSB)

Sabine Peninsula

J.H. Wall

GSC locs. C-133837, C-133838, C-133839, and C-133842. Stream bank section located 4.8 km south-southwest of Murray Harbour, northern Sabine Peninsula; the following is a composite faunal list from four samples collected at 4.1, 6.1, 8.1, and 16.1 m above the base of the formation (76°46'40"N, 108°56'30"W)

Heterostomella(?) sp. (1 specimen)
Trochammina sp. (2 specimens)
Haplophragmoides sp. (1 distorted specimen)
Haplophragmoides spp. (3 specimens)
Eponides(?) sp. (1 small, poorly preserved specimen)
Pullenia(?) sp. (1 poorly preserved specimen)
Trochammina sp. cf. *T.* sp. 3400 MacNeil (1 small, distorted specimen)
Cyclammina(?) sp. or *Haplophragmoides*(?) sp. (fragment)
Age: possibly Paleocene

Remarks. *Trochammina* sp. 3400 of MacNeil occurs in the Ministicog Member of the Moose Channel Formation of the Mackenzie Delta area. *Cyclammina* sp. occurs in the Paleocene section of central Ellesmere Island and the Mackenzie Delta.

GSC locs. C-133835 through C-133844. Same geographic location as GSC loc. C-133837 (above); composite microfloral list from 0-23 m above the base of the formation. The samples, covering 23 m of section, yielded similar microfloral assemblages dominated by pollen of *Pinus* and *Picea* type and contain abundant angiosperm pollen. Reworked Late Cretaceous dinoflagellates and pollen are consistently present.

The angiosperm pollen types present include:

Acer sp.

Alnus sp. (abundant)

Betula sp.

Caryapollenites imparalis Nichols and Ott

Caryapollenties inelegans Nichols and Ott

Cercidiphyllum sp.

ericaceae (*Ericipites* type)

Momipites actinus Nichols and Ott

Momipites anellus Nichols and Ott

Momipites wyomingensis Nichols and Ott

Paraalnipollenites alternipours (Simpson) Srivastava

Triporopollenites spp.

Trudopollis barentsii Manum

Age: Paleocene; probably Late Paleocene

Remarks. The pollen floras recorded from this section on Melville Island clearly indicate a Paleocene age. *Trudopollis barentsii* and the species of *Caryapollenites* and *Momipites* noted occur only in the Paleocene. *Paraalnipollenites alterniporus* is most common in the Paleocene as also are the forms of *Triporopollenites* seen here. A late Paleocene age is indicated by the presence of the juglandaceous species *Momipites actinus*, *M. anellus*, *M. wyomingensis*, *Caryapollenites imparalis* and *C. inelegans*. The pollen floras of the section are similar to late Paleocene assemblages recorded from northern Somerset Island (McIntyre, 1989) and Strand Fiord, Axel Heiberg Island (McIntyre, *in* Ricketts, 1991).

